DISPLAY COPY ONLY

OIL-IN-ICE FATE AND BEHAVIOUR

a subsection of the

Behaviour of Oil SpillS (BOSS) Project

Literature Summary Addendum
to December 1992 Draft Report

by

B. P. Hollebone
and
Delmar N.S. Permann

November, 1996

Scientific Advisor
Merv Fingas

Emergencies Science Division
Environmental Technology Centre
Environmental Technology Advancement Directorate
Environmental Protection Service
Environment Canada
Ottawa, Ontario, Canada

draft

DISPLAY COPY ONLY

Table of Contents

Free, A.P., J.C. Cox, and L.A. Schultz, *Laboratory Studies of Oil Spill Behaviour in Broken Ice Fields* 1

Tebeau, P.A., T.M. Meehan and S.A. Saepoff, *A Laboratory Study of Oil Spreading Under Arctic Conditions* 22

Uzuner, M.S., F.B. Weiskopf, J.C. Cox and L.A. Schultz, *Transport of Oil Under Smooth Ice* 35

Rosenegger, L.W., *The Movement of Oil Under Sea Ice* 47

McMinn, T.J., *Crude Oil Behaviour on Arctic Winter Ice* 59

Dome Petroleum Ltd., *Oil and Gas Under Sea Ice* 72

C-CORE (Centre for Cold Ocean Resources Engineering), *An Oilspill in Pack Ice* 86

Wilson, D.G. and D. Mackay, *The Behaviour of Oil in Freezing Situations* 94

Liukkonen, S., R. Koskivaara, J. Rytkonen and K. Lampela, "Adhesion of Oil to Plastic, Stainless Steel and Ice" 108

Kawamura, P., D. Mackay and M. Goral, *Spreading of Chemicals on Ice and Snow* 111

Fay, J.A., and D.P. Hoult, *Physical Processes in the Spread of Oil on a Water Surface* 129

Fay, J.A., *The Spread of Oil Slicks on a Calm Sea* 138

Glaeser, LTJG J.L., and LCDR G.P. Vance, *A Study of the Behaviour of Oil Spills in the Arctic* 157

Comfort, G. and F. Purves, "An Investigation of the Behaviour of Crude Oil Spilled Under Multi-Year Ice at Griper Bay", ... 168

Chen, E.C., C.K. Overall, and C.R. Phillips, "Spreading of Crude Oil on an Ice Surface" . . . 191

Chen, E.C., B.E. Keevil, and R.O. Ramseier, *Behaviour of Oil Spilled in Ice-Covered Rivers* 197

Cox, J.C., and L. A. Schultz, "The Transport and Behaviour of Oil Spilled Under Ice" 208

Cammaert, A.B., *Oil and Gas Under Ice Laboratory Study* 225

Draft

120Am

Malcolm, J.D. and A.B. Cammaert, "Transport and Deposition of Oil and Gas Under Sea Ice" 233

Deslauriers, P.C., S. Martin, B. Morson, and B. Baxter, *The Physical and Chemical Behavior of the Bouchard #65 Oil Spill in the Ice Covered Waters of Buzzards Bay.* 241

Nelson, W. G., and A. Allen, "Oil Migration and Modification Processes in Solid Sea Ice" . 278

MacNeil, M.R., and R.H. Goodman, *Oil Motion during Lead Closure* 287

Martin, S., "A Field Study of Brine Drainage and Oil Entrainment in First-Year Sea Ice" . . . 292

NORCOR Engineering and Research Ltd., *The Interaction of Crude Oil with Arctic Sea Ice* 302

Richardson, P., "ABSORB Tests Oil/Ice Interaction" 357

Reimer, E.M., "Anticipated Oil Dispersion Rates in Pack Ice" 358

Mackay, D., M. Medir, and D. Thorton, "Interfacial Behaviour of Oil Under Ice" 360

Goodman, R.H., A.G. Holoboff, T.W. Daley, P. Waddell, L.D. Murdock, and M. Fingas, "A Technique for the Measurement of Under-Ice Roughness to Determine Oil Storage Volumes" 363

Welsh, J.P., O.M. Lissaer, G.L. Hufford, T.S. Ellis, B.D. Thompson, L.D. Farmer, and R.R. Hiltabrand, "Some Dynamics of Spilled Oil in a Fractured Ice Field in Buzzards Bay, Massachusetts" 367

Sayed, M., and S. Loset, "Laboratory Experiments of Oil Spreading in Brash Ice" 369

Sayed, M., L.S. Kotlyar, and B.D. Sparks, "Spreading of Crude Petroleum in Brash Ice; Effects of Oil's Physical Properties and Water Current" 379

Puskas, J.K., and E.A. McBean, "The Transport of Crude Oil Under Saline Ice" 390

Puskas, J.K., and E.A. McBean, and N. Kouwen, "Behaviour and Transport of Oil Under Smooth Ice" 398

Moige, M. and A.S. Telford, "Oil in Moving Pack Ice-Laboratory Study" 409

Malcolm, J.D. and C. Dutton, "The Interfacial Tension and Contact Angle of Crude Oil Under Ice" 413

Draft

DISPLAY COPY ONLY

Kovacs, A., "Sea Ice Thickness Profiling and Under-Ice Oil Entrapment" 418

Keevil, B.E. and R. Ramseier, "Behaviour of Oil Spilled Under Floating Ice" 425

Greene, G.D., P.J. Leinonen and D. Mackay, "An Exploratory Study of the Behaviour of Crude Oil Spills Under Ice" 431

Deslauriers, P.C., "Observations of Oil Behaviour in Ice Floes and the 1977 Ethel H Spill" .. 436

Vandermeulen, J.H., B. Amero and T.P. Ahern, "Physical Weathering of Kurdistan Oil: Droplet Formation and Effect on Shore-Ice Melting" 438

Topham, D.R. and P.R. Bishnoi, "Deep Water Blowouts" 442

Topham, D.R., "The Disposition of Gas/Oil Mixtures Trapped Under Ice" 449

Thomas, D.R. and R.S. Pritchard, "Oil Movement in the Ice Covered Beaufort and Chukchi Seas" 459

Purves, F., *The Interaction of Crude Oil and Natural Gas With Laboratory-Grown Saline Ice* 464

Scott, B.F. and R.M. Chatterjee, *Behaviour of Oil Under Canadian Climatic Conditions: Part 1. Oil on Water Under Ice-Forming Conditions* 469

Moir, J. and Y. Lau, *Some Observations of Oil Slick Containment by Simulated Ice Ridge Keels* 485

McMinn, T.J. and P.C. Golden, "Behavioral Characteristics and Cleanup Techniques of North Slope Crude Oil in an Arctic Environment" 488

Martin, S., P. Kauffman and P.E. Welander, "A Laboratory Study of the Dispersion of Crude Oil Within Sea Ice Grown in a Wave Field" 500

Chen, E.C., *Arctic Winter Oil Spill Test* 509

Oil-in-Ice Bibliography B-1

Draft

A.P. Free, J.C. Cox, and L.A. Schultz, *Laboratory Studies of Oil Spill Behaviour in Broken Ice Fields,* DTCG39-80-C-80138, United States Coast Guard, Washington, D.C., 58 p., 1981.

This work has also been reported in (in summary, for ice pack studies only):

A.P. Free, J.C. Cox, and L.A. Schultz, "Laboratory Studies of Oil Spill Behaviour in Broken Ice Fields", in *Proceedings of the Fifth Arctic Marine Oilspill Program Technical Seminar*, Environment Canada, Ottawa, Ontario, pp 3-14, 1982.

Summary

"The study consisted of three separate... analyses: oil flow through a single narrow gap; oil spilled in a restrained field of broken ice; and oil spilled in an unrestrained field of broken ice. The project included both analytical and laboratory studies of the oil/ice interaction phenomena. The laboratory studies were conducted at low temperatures with fresh water ice in ARCTEC's glass-walled Ice Flume."

Several environmental conditions were investigated: ice size, ice coverage, and current and wind velocities. Three oils were used in the experiments: low, medium, and high viscosity.

"Quantitative relationships that were developed as a result of this study are intended to characterize the short-term behaviour of oil spilled in broken ice.... The only limitation of the results is that test conditions allowed only one-dimensional flow. The spreading phenomena for two dimensional conditions could be significantly different. The application of these results is therefore limited to leads, ship channels or other locations where one-dimensional flow can be assumed to exist."

[From the AMOP conference proceedings:]

"The oil spread rate in a one-dimensional broken ice channel can be subdivided into two components: oil seepage through the broken ice pack and oil spreading due to movement of the ice. Equations have been written which give the oil spread rate for both of these components. Oil seepage through the gaps in a broken ice field generally occurs at a slow rate, especially for the heavier oils, where the seepage was not noticeable during the experimental program. The major cause of this slow seepage rate is the hydrostatic pressure of the oil against the ice, keeping the broken ice field tightly packed. Oil spreading behind a moving broken ice pack was the more significant component of the oil spreading. Until the oil slick thickness decreased below a threshold-value, the oil pushed the ice pack at a higher velocity than would have been induced by currents or winds alone. This allowed the oil slick to spread in the open water left behind the ice pack. As the oil slick thickness decreased, the ice velocity also decreased until, at very small thicknesses, the ice velocity was dictated by the current or wind velocity."

Objective

This study examines the short-term behaviour of oil spilled in or near a field of broken ice. A model of oil flow through ice gaps was evaluated in terms of the parameters of gap width, ice coverage, water and wind current velocities, and oil type.

Theory

Oil Seepage through Ice Gaps

The authors developed a theory to determine the minimum ice gap through which oil would flow, and for gap widths greater than the minimum, to determine the oil flow rate through the gap as a function of the oil properties and physical conditions.

Minimum Gap Width for Oil Seepage

Two competing forces determine oil motion through a gap. The driving force is the hydrostatic gravitational force, F_g. The authors use a function of the oil slick thickness, δ, and density differential between water and oil, ρ_{water}-ρ_{oil}, as originally described by Hoult, 1969:

$$F_g = \int_0^{\delta} (\rho_{water}-\rho_{oil}) g h \, dh = \frac{1}{2} (\rho_{water}-\rho_{oil}) g \delta^2 .^{*} \tag{3.1}$$

Capillary tension caused by interfacial tensions on both sides of the gap resists the flow of oil through an ice gap (Sowers and Sowers, 1970):

$$F_c = \frac{2\sigma_i(\cos\alpha)\delta}{w}, \tag{3.3}$$

where σ_i is the oil-ice interfacial tension, α is the oil-on-ice contact angle, δ is the slick width, as above, and w is the gap between ice floes. The minimum gap occurs when the driving and resistive forces are just balanced, $F_c = F_g$. Equating Equations (3.1) and (3.3) gives:

$$w = \frac{4\sigma_i \cos\alpha}{(\rho_{water}-\rho_{oil}) g \delta}. \tag{3.4}$$

Rate of Oil Seepage Through an Ice Gap

For gaps larger than the minimum necessary for oil seepage to start, the velocity of the oil flow is governed by the gravitational force on the head of oil, the shear strength of the oil, the friction along the sides of the gap, as well as any shear stresses due to wind or water current. The gravitational spreading force, as given by the authors in Equation (3.1), is a function of the oil

---

*Expressions (3.1) and (3.4) are incorrect. This appears to have been due to a misreading of Equations 9 through 11 of Hoult, 1969. See discussion in BOSS Critique section of this review.

density, ρ_{oil}, and the thickness of the oil pool, δ. The resistive shear forces are a function of the oil viscosity, μ_{oil}. The frictional forces in the gap are proportional to the gap width, w. The driving force of the wind or current is a function of the density of the driving medium, ρ_D, and its velocity, v_D (Hoult, 1972). The authors express the velocity of the oil flow through the gap as a function of these variables:

$$\phi(v_{oil}, v_D, \delta, w, g, \mu_{oil}, \rho_{oil}, \rho_D) = 0. \tag{3.5}$$

In non-dimensional form, Equation (3.5) is:

$$\phi\left(\frac{v_{oil}}{v_D}, \frac{\delta}{w}, \frac{\rho_{oil}}{\rho_D}, Re, Fr^2\right) = 0, \tag{3.7}$$

where Re, the Reynolds Number, has the form $\rho_D w v_D/\mu_{oil}$ and Fr, the Froude Number, has the form v_D^2/gw.

The Reynolds Number expresses the ratio of the gravitational driving force to the viscous resistive force in the oil. The Froude Number expresses the ratio of the gravitational driving force to the resistive capillary force of passing through the gap. The ratio of the oil to the driving fluid densities reflects the shear stresses exerted on a given oil by the driving fluid.

The authors state that, in general, the functional relationship of Equation (3.7) can be expressed as:

$$\frac{v_{oil}}{v_D} = a_1\left(\frac{\delta}{w}\right)^{a_2}\left(\frac{\rho_{oil}}{\rho_{Water}}\right)^{a_3} Re^{a_4}\,(Fr^2)^{a_5} + a_6. \tag{C.4}$$

Holding the oil-slick-thickness-to-gap ratio (δ/w) constant gives the expression:

$$\frac{v_{oil}}{v_D} = a_7\left(\frac{\rho_{oil}}{\rho_{Water}}\right)^{a_3} Re^{a_4}\,(Fr^2)^{a_5} + a_6. \tag{C.5}$$

The authors state that single gap experiments determined that a_3, a_4, and a_5 were independent of oil type and had values of 1.0, 1.0, and -1.0, respectively. Note that these experiments are not presented in the study, nor are they given a reference. However, the values of a_3, a_4, and a_5 must be assumed for the following equations, which are tested experimentally, to hold. Substituting the exponents yields:

$$\frac{v_{oil}}{v_D} = K_1\left(\frac{Re}{Fr^2}\right)\left(\frac{\rho_{oil}}{\rho_D}\right) + K_2, \tag{3.8}$$

where K_1 [$= a_7\ (\delta/w)^{a_2}$] is dependent on the slick-thickness-to-gap ratio and oil properties, and K_2 ($=a_6$) is dependent on the oil properties only.

Oil Spreading in a Field of Broken Ice

The authors assume that oil spilled in a broken ice pack will spread by two methods. Seepage will occur through gaps in the broken ice pack, and oil will also spread behind the ice pack as the pack moves due to current and wind.

Oil Seepage Through a Field of Broken Ice

Seepage of oil through broken ice is similar to the one-dimensional case developed in Equations (3.5) to (3.8). In an ice field, however, the gap sizes are highly variable and must be described by some kind of statistical average. Also, the oil path through the field is twisted and convoluted, which increases the friction between oil and ice.

The gap spacing in an ice field depends on the coverage of the area by blocks of ice. A fractional concentration, c, can be defined as:

$$c = \frac{A_i}{A} = \frac{d^2}{(d+b)^2}, \tag{3.9}$$

where, A_i is the area covered by ice, A is the total area, d is the average block area, and b is the gap between each ice block. This gap width, b, is a function of the size of the ice blocks and the concentration of the ice pack. The authors describe it as a characteristic field dimension and remark that it is analogous for ice field spreading to the one-dimensional gap width, w, used for the single gap-spreading model of Equations (3.1) to (3.4). Rearranging Equation (3.9) to solve for b, gives:

$$b = d\left(\frac{1}{\sqrt{c}} - 1\right), \tag{3.10}$$

where d is a weighted average of the block areas.

It is convenient to write the flow rate of oil through a broken ice field per unit width, q, as a function of the thickness of the oil slick, δ, and the characteristic dimension of the ice field, b. The authors represent this relationship as:

$$\frac{q^2}{gb^3} = K_3\left(\frac{\delta}{b}\right)^{K_4}, \tag{3.12}$$

where g is the gravitational acceleration constant and K_3 and K_4 are constants.

Although the thickness of the oil slick is often comparable to the dimensions of the ice block, the authors remark that the oil layer seeping through the ice field is much thinner than the ice. Ice blocks can be considered as large-scale roughness elements in the oil flow channel. Also, the authors claim that a boundary layer forms between the (deep) water current and the underside of the ice packs. This boundary layer is stationary with respect to the ice field and "insulates" the spreading oil from the shear force of the moving water. Thus, the authors state that Equation (3.12) should apply to both calm and moving water.

Oil Spreading with a Moving Field of Broken Ice

As well as seepage of oil through an ice field, the authors examined the overall movement of the ice pack with respect to oil, current, and wind forces. They state that the two main driving forces for pack movement are the shear force of water currents or wind and the gravitational spreading force exerted by the oil slick itself. The resistive forces to pack movement include the inertia of the ice blocks and water drag on the ice.

Equation (3.1) implies that the gravitational force is proportional to the square of the slick thickness, δ. The ice inertia depends on the amount of ice and can be supposed to be a function of the length of the ice field, L. Assuming a constant ice block roughness, drag is a function of ice thickness per unit width, t. For a given wind or water current velocity, the authors express the ice field velocity, v_i, as:

$$v_i = K_5(\frac{\delta^2}{tL}) + K_6, \tag{3.13}$$

where K_5 and K_6 are experimentally determined constants.

Experimental

Oil Properties

As recommended by the ASTM F-20 committee, the authors used low viscosity, medium viscosity, and high viscosity oils. Some physical properties of each are given in Table 4.1.

Table 4.1 Test Oil Properties

	Density (g/cm^3)	Viscosity (poise)	Pour Point (°C)	Interfacial Tension (g/sec)	Contact Angle (°)
Number 2[a]	0.857	0.07	-18	18.0	20
SAE 10W	0.880	3.54	-29	23.2	30
SAE 40W	0.901	37.5	-13	26.9	40

[a] The authors refer to this as diesel fuel throughout the report.

Before each test was conducted, oil properties were measured daily to ensure the consistency of the samples and to ensure that aging had not taken place. Oils were stored at -2 to 0°C. Oil densities were measured by a gravity scale hydrometer, in accordance with ASTM specification E100-66. Oil viscosities were measured on a Brookfield Model LVT Synchrolectric Viscometer and were in accordance with ASTM specification D 2983-72. Surface tensions were measured by a Fisher Model 20 Surface Tensiometer, a torsion-type balance, which met ASTM specifications B-971 and D-1331.

Apparatus Used for Tests (from Appendix A)

The ice field experiments were performed in a glass-walled ice flume (see Figure A.1). The flume was 13.7 m long, 0.94 m wide, and 0.61 m deep. Maximum water depth in the flume was 46 cm, with a water flow rate of 140 L/s. The current in the flume was measured by an annubar flow sensor in parallel with two "eagle eye" flow sensors. The annubar was considered to measure currents to within 1% of the true value and had measurement variability of less than 0.1%. The "eagle eye" flow sensors were accurate to 1.5% of their full scales, ±1.1 and ±3.8 L/s.

To simulate wind conditions, a wind tunnel was built over the flume. Wind speeds of up to 550 cm/s were possible over 46 cm of water in the flume. Wind speed was measured by a rotating anemometer installed at the end of the tunnel, in the centre of the airstream.

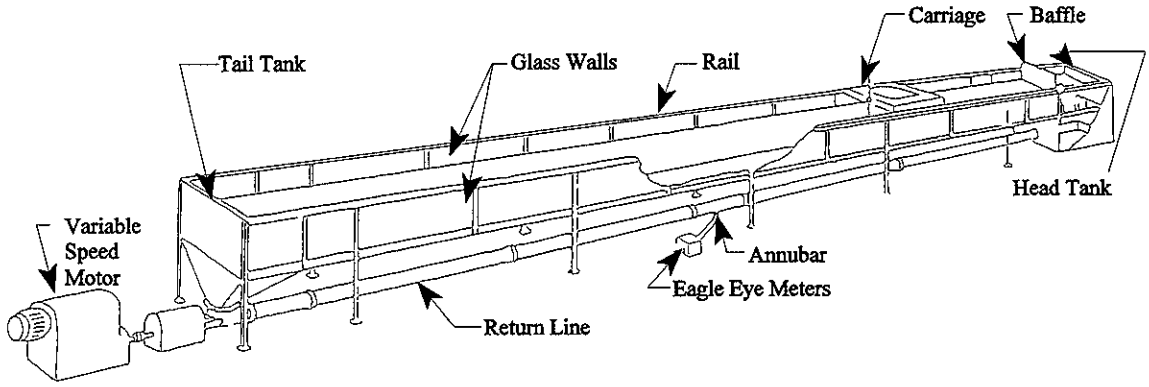

Figure A.1 Insulated Glass-Walled Ice Flume

The carriage arrangement of the ice flume is shown in Figure A.2. A Milliken camera mounted on the carriage took overhead movies of the advancing oil and ice. In addition, by aligning a pointer bar attached to the carriage with the leading edge of the ice field or oil slick, the velocity of the ice field or oil slick was measured. The velocity of the carriage was recorded by a DC generator attached to one of the carriage wheels. The generator voltage output, proportional to the carriage velocity, was plotted on a strip chart recorder.

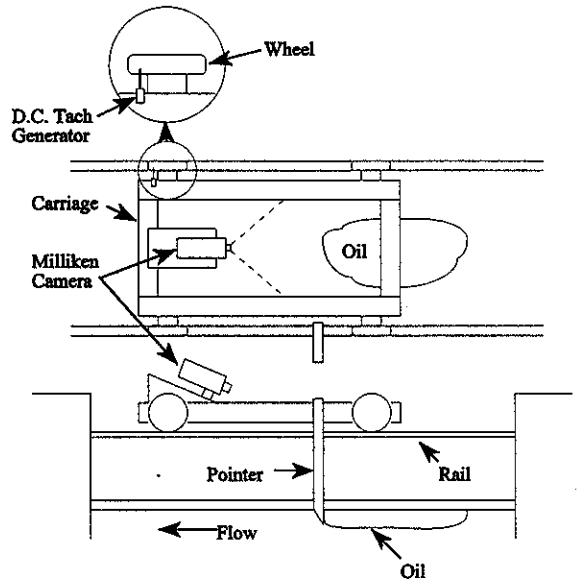

Figure A.2 ARCTEC Ice Flume Carriage Arrangement

Oil Seepage-Single Ice Gap Experiments

Oil flow rates through a single gap were measured through an opening of known size between two ice blocks. The instrument consisted of an oil reservoir and two 46-cm long steel boxes on which the ice blocks could be grown. This was placed in the ice flume with dry ice packed in the boxes. After ice had grown in the gap between the boxes, a gap of the desired width was cut with a saw. Water velocities were varied from 0 to 28 cm/s and wind tunnel velocities from 0 to 10 scale m/s.

Oil was released from the upstream reservoir. The oil thickness was measured with a ruler before release. Oil velocity through the gap was measured by timing small tracers of oil on the surface as they travelled a known distance. The oil reservoir thickness was measured several times during each test. Flow rate was calculated from the change in thickness of the reservoir with time.

All three oils were tested. Water current and wind velocities were used to drive the oil through the gap. Gaps tested ranged from the minimum width that would allow flow, to almost open water conditions, or very wide gaps.

Oil-Free Broken Ice Field Tests

These tests were conducted to provide a control or baseline data for the ice flume. In each test, ice blocks were packed tightly in a random field with barriers both upstream and downstream. The water current and winds were turned on and the barriers removed. The velocity of the front of the ice field was measured by the carriage arrangement, downstream from the ice front. Velocities of the middle and end of the field were determined by the movement of dyed marker blocks. Movie films and still photographs were taken before, during, and after each test.

Cubic ice blocks, with sides measuring 3.25 in (82.5 mm) and 6.5 in (152.5 mm) were used to simulate broken ice fields. Experiments were conducted with both a single size of block and a mixture of the two sizes. Four water currents were used, from 0 to 27 cm/s. Wind velocities of 0 to 10 scale m/s were tested.

Oil Seepage Through a Restrained Field of Broken Ice

In these tests, oil was introduced to an ice field that was restrained by a wide weave mesh. Ice concentrations were 23 to 80%. Initially, an oil reservoir approximately as thick as the ice was built up behind a baffle, upstream from the ice. The water and wind currents were turned on and the baffle removed between ice and oil. Reservoir thickness was measured as a function of time.

The time of the first appearance of oil (if any) on the downstream side of the ice field was also noted. If the oil did not penetrate the ice field, the times to reach equilibrium and final slick height were recorded. Movie films and still photographs were taken before, during, and after each test. Ice block size, water currents, and wind speed were varied as in the tests of oil-free broken ice.

Oil Spreading in an Unrestrained Field of Broken Ice

The final series of tests were set up initially much like the restrained ice field trials but with baffles at both ends of the ice. At the beginning of the experiment, wind and water currents were turned on and the baffles removed. The pointer bar on the carriage was used to track the velocity of the ice front. The location of the oil front and the back of the ice field were recorded at intervals and movies and still photographs were taken before, during, and after the tests. The size of the ice blocks and air and water speeds were varied as in the other two ice field trials.

Ice Field Concentration

The authors determined the ice field concentration, c, using Equation (5.1):

$$c = \frac{nd^2}{WL}, \tag{5.1}$$

where n is the number of ice blocks, d is the dimension of the ice cube blocks, W is the block width, and L is the length of the ice field [compare with Equation (3.9)]. The authors note that, due to packing considerations, the practical maximum concentrations were 0.80 to 0.85 for the small blocks (3.25 in, 82.5 mm) and 0.85 to 0.90 for the larger blocks (6.5 in, 152.5 mm).

Scaling Considerations

When testing with two different types of fluids, and particularly when trying to use prototype fluids, scaling can pose insurmountable problems. The authors therefore decided to perform the entire test program at full scale. The authors remark that previously, Cox *et al.*, 1980 found that the water currents were at full scale and matched field conditions. The scaling of wind speeds in the tunnel was unknown, however. To determine the wind-scaling factor, the authors examined the shear forces exerted by the wind on the ice blocks. In general, the shear force, τ_s, exerted by a moving fluid on a surface is:

$$\tau_s = a\rho_f v_f^2, \tag{4.1}$$

where a is a roughness coefficient, ρ_f is the fluid density, and v_f is the velocities.

The authors state that a is equal to $f/8$ where f is the friction factor. The authors estimated f to be 0.046 for model wind speeds of 20 ft/s over ice blocks in the ARCTEC ice flume. The authors write the shear force of the wind on the model as:

$$\tau_{s\text{MODEL}} = \frac{f_{\text{MODEL}}}{8}\rho_{\text{AIR}} v_{\text{MODEL}}^2. \tag{4.3}$$

In measurements on real ice packs, the roughness coefficient [C_{10}, equivalent to a in Equation (4.1)] is reported to range from 0.0010 to 0.0023 for wind speeds measured at a height of 10 m (Arya, 1979). The authors give the wind shear in real conditions as:

$$\tau_{s\,\mathrm{FIELD}} = C_{10}\rho_{\mathrm{AIR}}v_{\mathrm{FIELD}}^{2}. \tag{4.4}$$

Equating the shear forces, $\tau_{s\,\mathrm{MODEL}}$ and $\tau_{s\,\mathrm{FIELD}}$, gives the model-to-field-scale factor:

$$\frac{v_{\mathrm{FIELD}}}{v_{\mathrm{MODEL}}} = \left(\frac{f_{\mathrm{MODEL}}}{8C_{10}}\right)^{\frac{1}{2}}. \tag{4.6}$$

Assuming a value of the field roughness factor, C_{10}, of 0.002, the authors give the ratio of model to real wind speeds as 1:1.7, i.e., a scale wind speed of 100 cm/s is comparable to a real wind speed of 170 cm/s (just over 3 knots).

Results

Single Gap Results: Minimum Gap Width for Oil Seepage

The authors evaluated the limiting flow of oil through a gap (w) for a series of oil reservoir thicknesses (δ) for each of the three oils given in Table 4.1. Their results are shown in Figure 6.1. The authors note that there is not very good agreement between the test results and the curves plotted using Equation (3.4). See the discussion of this in the BOSS Critique section of this review.

The predictions of Equation (3.4) using the data given in Table 4.1 are shown on Figure 6.1 as solid curves for each of the three oils. The curve calculated for the SAE 10W oil in preparation for this review is very similar to that given by the authors. However, the present calculations are 120 and 80% of the authors' original results (to within 1%) for the diesel fuel and SAE 40W oil, respectively. The reason for this discrepancy is unclear.

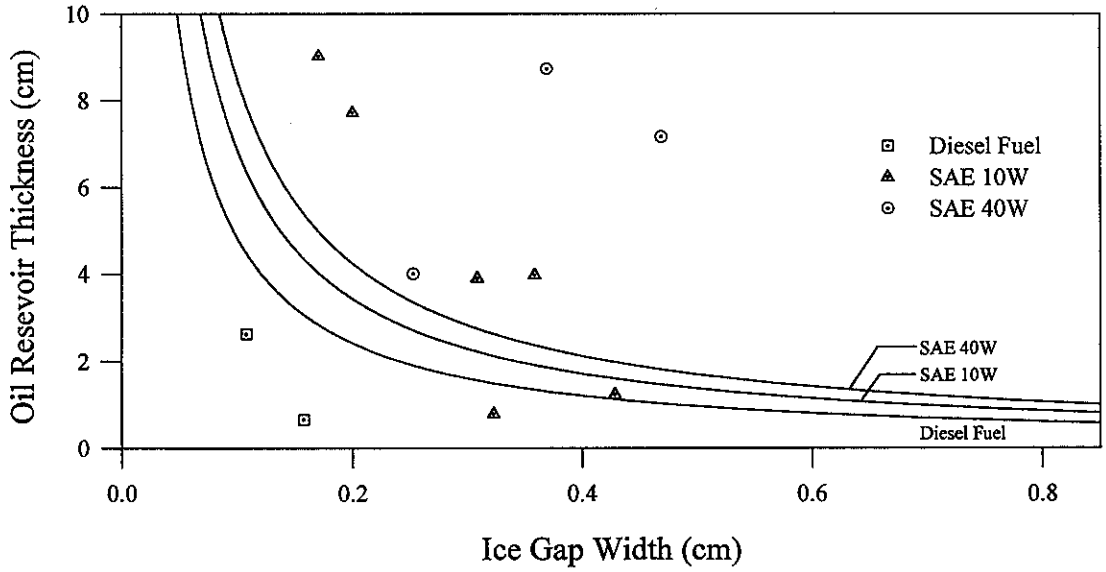

Figure 6.1 Threshold of Motion - Reservoir Thickness *vs* Single Gap Width

Single Gap Results: Rate of Oil Seepage Through an Ice Gap

Equation (3.8) gives a general result for oil flow though a gap above the minimum gap width. Several experiments were carried out for various slick thicknesses, gap widths, and driving velocities. The oil velocity data is plotted for a series of slick-thickness-to-gap-width ratios for all three oils in Figures 6.6 to 6.8. The authors remark that there appears to be a linear relationship between the relative oil velocity [v_{oil}/v_D] and the representative terms for each of the forces acting on the oil, as described by Equation (3.8). Note that the regression slopes shown in Figure 6.6 in the present review, for the SAE 10W oil, differ by as much as 30% from the values given by the authors. The authors' regressions do not seem to correspond to any reasonable statistical fit of the data on Figure 6.6, and were probably estimated visually. However, the slopes given by the authors in Figures 6.7 and 6.8 are within 5% of the linear regression results.

The authors note that the regular progression of slopes in Figures 6.6 to 6.8 for increasing slick-thickness-to-gap-width ratio suggests a relatively simple relationship between the two quantities. The authors' regression slopes are plotted against the ratio of oil thickness to gap width in Figures 6.9, 6.10, and 6.11. The parameters used to plot the exponential fits on Figures 6.9 to 6.11 were taken from Equations (6.1) to (6.3). Note that, on the original figures, curves are drawn through the data that do not have the form of an exponential function (in fact, the functions appear to be logarithmic). The authors used these relationships to determine the functionality of the relative velocities, from Equation (C.4):

Diesel Fuel:
$$\frac{v_o}{v_D} = 3.4\times10^{-5}\left(\frac{\delta}{w}\right)^{0.81}\left(\frac{Re}{Fr^2}\right)\left(\frac{\rho_o}{\rho_D}\right)+0.015, \tag{6.1}$$

SAE 10W:
$$\frac{v_o}{v_D} = 8.9\times10^{-4}\left(\frac{\delta}{w}\right)^{0.78}\left(\frac{Re}{Fr^2}\right)\left(\frac{\rho_o}{\rho_D}\right)+4.9\times10^{-4}, \tag{6.2}$$

SAE 40W:
$$\frac{v_o}{v_D} = 3.4\times10^{-3}\left(\frac{\delta}{w}\right)^{0.45}\left(\frac{Re}{Fr^2}\right)\left(\frac{\rho_o}{\rho_D}\right)+2.8\times10^{-3}. \tag{6.3}$$

When dimensionalized by substitution for the physical constants and known oil properties, the authors give these equations as:

Diesel Fuel:
$$v_{oil} = 0.41\,\delta^{0.81}w^{1.19}+0.015v_D, \tag{6.4}$$

SAE 10W:
$$v_{oil} = 0.22\,\delta^{0.78}w^{1.22}+4.9\times10^{-4}v_D, \tag{6.5}$$

SAE 40W:
$$v_{oil} = 0.081\,\delta^{0.45}w^{1.55}+2.8\times10^{-3}v_D, \tag{6.6}$$

where v_{oil} and v_D are measured in cm/s and δ and w are measured in centimetres.

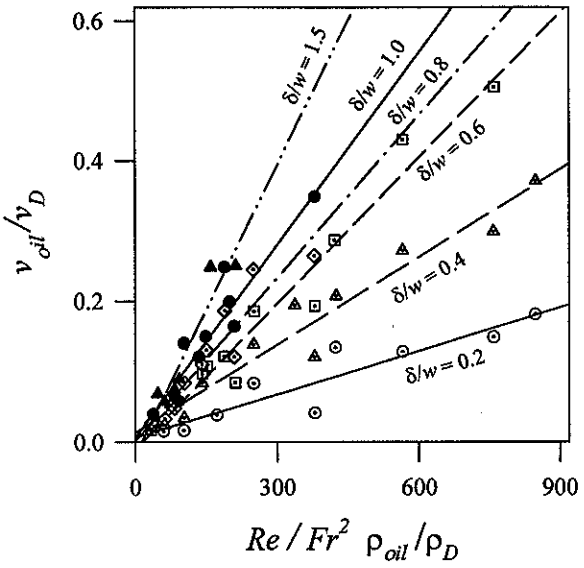

Figure 6.6 SAE 10W: Single Ice Gap Tests: Relative Oil Velocity *vs* Driving Force

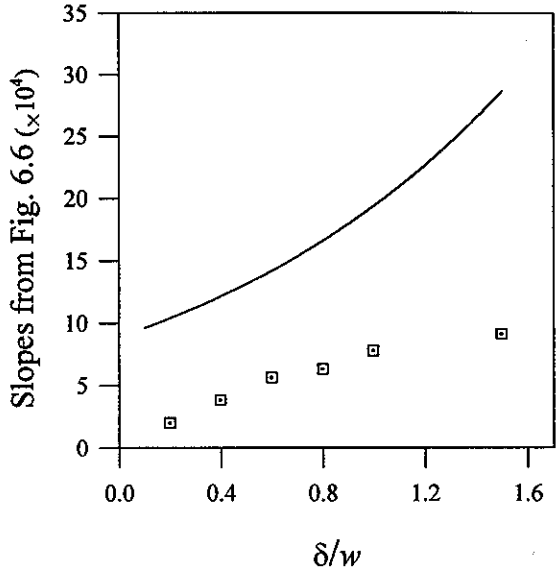

Figure 6.9 SAE 10W: Slope of Relative Velocity Equations *vs* Slick Thickness

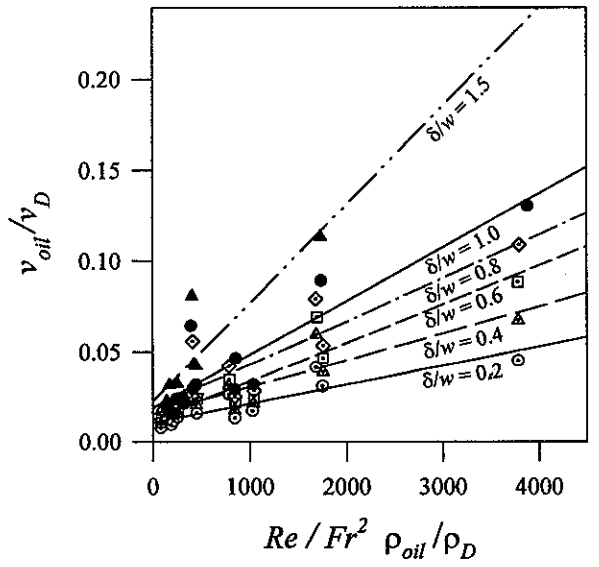

Figure 6.7 Diesel Oil: Single Ice Gap Relative Oil Velocity *vs* Driving Force

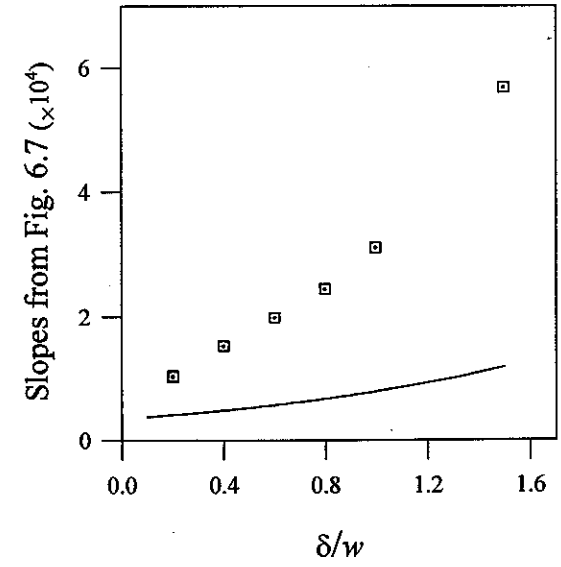

Figure 6.10 Diesel Fuel: Slope of Relative Oil Velocity Equations *vs* Slick Thickness

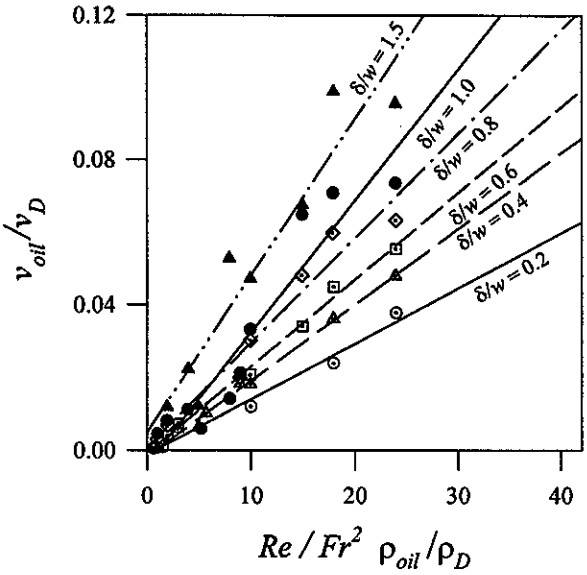

Figure 6.8 SAE 40W: Single Ice Gap Relative Velocity *vs* Driving Force

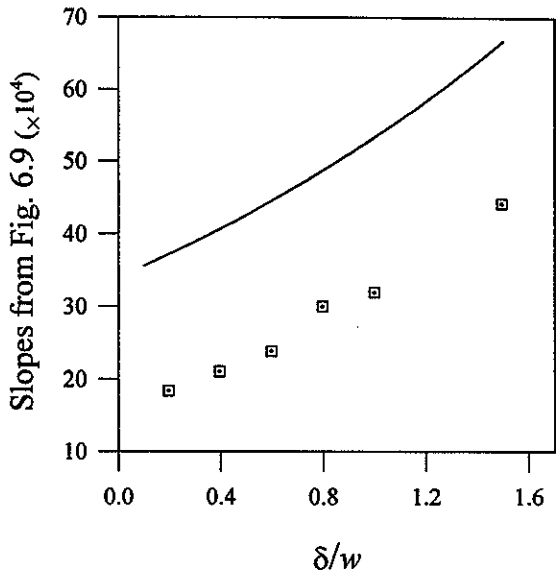

Figure 6.11 SAE 40W: Slope of Relative Oil Velocity Equations *vs* Slick Thickness

Oil Spreading in a Field of Broken Ice

The authors classify oil entrapment in ice fields into three categories: total containment, non-containment, and virtual containment. Total containment is the state in which all of the spilled oil remains trapped in the ice field, unable to flow through the ice gaps adjacent to the slick. The thickness of the oil slick contained behind the ice is much greater than the equilibrium thickness that the oil would have spread to on open water. Non-containment occurs when the ice gives little or no resistance to the flow of oil. The oil spreads at a rate nearly equal to the open water spreading rate. The thickness of the oil slick quickly approaches the open water equilibrium thickness. Virtual containment is the intermediate state, which occurs when the major portion of the oil spill volume is contained in the gaps in the ice field and only a small amount of oil seeps through the ice field into the open water. As with total containment, the oil reservoir constrained by the ice is considerably thicker with virtual containment than it would be in ice-free conditions.

The authors state that the gravitational spreading force is the main factor, and determines which of these three states will result when oil is spilled in an ice field. They claim that the gravitational force is a function of only the height of the oil surface above the water surface and the oil density (see the discussion in the BOSS Critique of this review). They note that this force is exerted on any ice block encountered by the spreading oil slick. It then pushes the block in the direction in which the oil is spreading, and this tends to compact an ice field to its maximum concentration. Even with initial ice concentrations as low as 23%, in tests in a restrained ice field, the authors found that oil was completely or virtually contained in almost all cases. In tests on an unrestrained ice field, the presence of large amounts of oil significantly reduced the spreading of

the ice pack. In addition, the velocity of the unrestrained ice pack was usually greater than that of the water.

The unrestrained ice packs resisted this oil gravitational force as a result of shear at the ice-water interface, shear along the sides of the flume, and inter-block friction in the ice pack. The authors state that typically the oil had to be 1 to 2 cm deep to overcome this resistance (the thickness is a function of oil density, weight of the ice, and the draft of the blocks). Pools of oil that were less than 1 to 2 cm thick reduced the velocity of the ice pack relative to the velocity of the oil-free ice field.

The authors found that ice could become insulated from the water current by the ice blocks, trapped downstream from "a large roughness element," i.e., a partially submerged ice block. In an ice field, with a large number of "roughness elements," it was found that the seepage from a layer of oil trapped in the ice did not depend on the water velocity. However, the thickness of the layer that was isolated from the water current was found to be a function of water velocity.

The mechanics for wind effects were found to be very similar to those for water currents. The authors found, however, that the shear stresses of the wind on the oil and the ice floes were very much less than the shear stresses of the water. Because of this, only a restricted set of wind tests were carried out.

Oil Seepage Through a Restrained Field of Broken Ice

As previously described, when oil was released upstream from a restrained ice field, regardless of the initial ice concentration, the oil pushed the ice blocks against the barrier forming "a compact high concentration ice field." At this high ice concentration, the gaps between the ice were small enough that the SAE 40W and SAE 10W oils were totally contained in the reservoir behind the ice. Only the diesel fuel was able to flow through the gaps in the ice field. The authors proposed that the oil flow through the restrained ice pack could be modeled by Equation (3.12):

$$\frac{q^2}{gb^3} = K_3\left(\frac{\delta}{b}\right)^{K_4}, \tag{3.12}$$

where the characteristic length, b, is given by Equation (3.10) and is related to the dimensions of the ice blocks, d, and the inverse square root of the ice pack concentration, c. The 3.25 in (82.5 mm) blocks were found to have maximum concentrations of 0.8 to 0.85, which results in characteristic lengths of 0.97 cm and 0.70 cm, respectively. The 6.5 in (152.5 mm) blocks had characteristic lengths of 1.40 cm to 0.90 cm for ice concentrations of 0.85 to 0.90. The authors remark that, as b is not a measure of the actual gaps that would exist in a randomly packed ice field, the oil flow rate through the ice did not directly vary with b, and the larger blocks did not

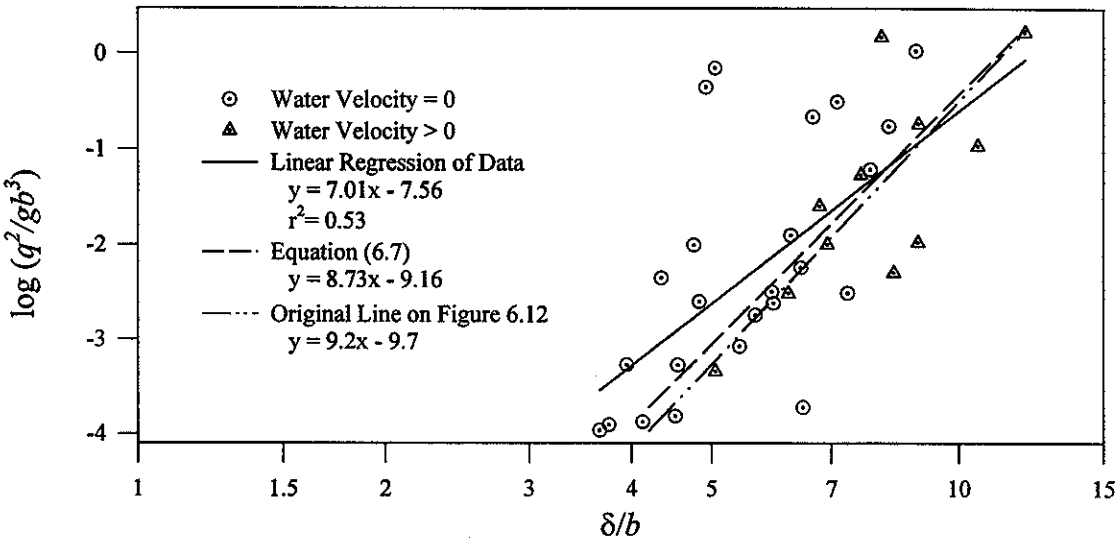

Figure 6.12 Oil Seepage Rate Through Broken Ice: Diesel Fuel

necessarily allow higher oil seepage rates than small blocks.

In Figure 6.12, the authors' data for diesel fuel seepage in the restrained ice field tests is plotted in the non-dimensional form of Equation (3.12). The authors report that the best fit line is:

$$\frac{q^2}{gb^3} = 6.92\times10^{-10}\left(\frac{\delta}{b}\right)^{8.73}. \tag{6.7}$$

However, as can be seen on the reproduction of Figure 6.12, the best fit line appears to be:

$$\frac{q^2}{gb^3} = 2.75\times10^{-8}\left(\frac{\delta}{b}\right)^{7.01}.$$

Note also that the authors' "best fit" numbers from Equation (6.7) (the dashed line on Figure 6.12) do not agree with the "regression line" (the dash-dot-dot line) that was plotted on the original figure. The authors note that the water current has no apparent effect on the results and thus conclude that the ice blocks masked the water current from the oil slick. In fully dimensionalized form, Equation (6.7) (in inches) is:

$$q = 2.63\times10^{-5}\frac{\delta^{4.37}}{b^{8.73}}. \tag{6.8}$$

The authors report a value of 2.74×10^{-5} as the pre-exponential factor in Equation (6.8), but this appears to be incorrect, given Equation (6.7). However, again,

$$q = 1.66\times10^{-4}\frac{\delta^{3.51}}{b^{2.01}}$$

would appear to be what is suggested from the authors' own data.

Figure 6.13 in this review shows q as a function of δ for various values of b. The solid lines are the original predictions, and the dashed lines show the regression performed in this review.

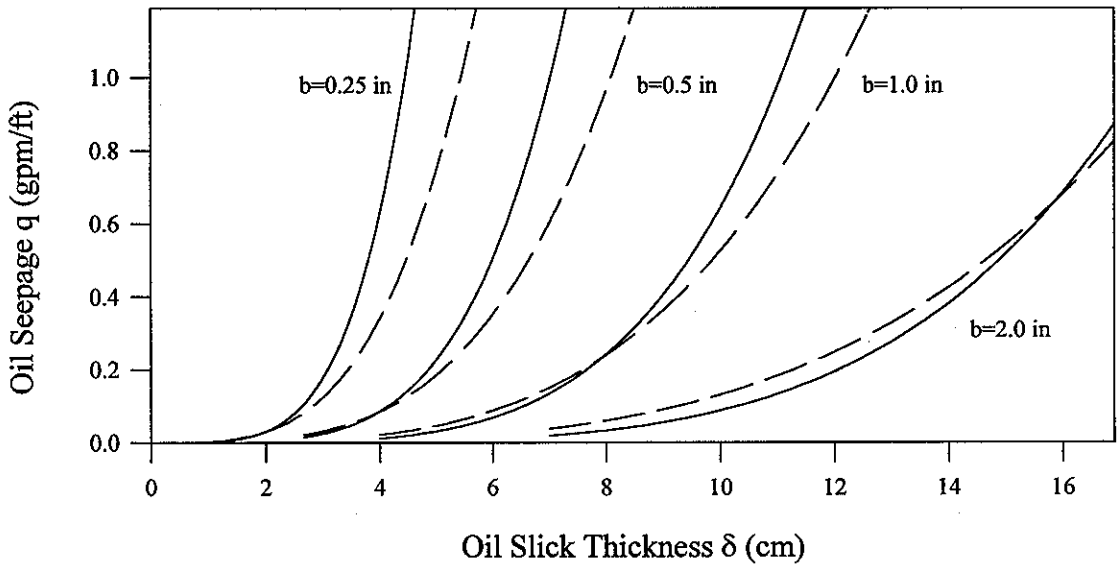

Figure 6.13 Flow Rate Through Broken Ice *vs* Oil Slick Thickness—Diesel Fuel

Oil Interaction with a Moving Ice Field

The authors remark that when oil from a thick reservoir was released into an unrestrained broken ice field, the oil pushed the ice pack downstream. The authors attribute this to the gravitational spreading force of the oil on the ice field. At the same time, small amounts of oil seeped into the broken ice field similar to the results observed in the restrained ice field experiments. The authors conclude that the spreading rate of the oil is equal to the sum of the velocity of the ice field in front of the oil, and the seepage rate of the oil through the ice field.

Data were gathered for several water velocities and the diesel fuel and SAE 10W oil. The tests were conducted with the large and small ice blocks, both separately and together. These results are shown in Figures 6.14 for the diesel fuel and Figure 6.15 for the SAE 10W oil. The authors also note that, at small values of δ^2/tL (i.e., for thin oil slicks), Equation (3.13) no longer applies because the gravitational spreading force becomes much less significant than the driving force due to the water current. As the water shear forces become more important, the ice velocity decreases to the oil-free ice velocity.

The authors report the relationships for diesel fuel, apparently taken from "best fits" of the data in Figure 6.14, as:

$$v_i = 489\frac{\delta^2}{tL} + 5.35 \qquad \text{for } v_w = 0 \qquad [y=751x + 3.93,\ r^2=0.870], \qquad (6.9a)$$

$$v_i = 1546\frac{\delta^2}{tL} + 9.05 \qquad \text{for } v_w = 10.6 \text{ cm/s} \qquad [y=1742x + 8.34,\ r^2=0.944], \qquad (6.9b)$$

$$v_i = 2021\frac{\delta^2}{tL} + 12.9 \qquad \text{for } v_w = 16.7 \text{ cm/s}^* \qquad [y=2064x + 12.8,\ r^2=0.992], \qquad (6.9c)$$

$$v_i = 3002\frac{\delta^2}{tL} + 13.4 \qquad \text{for } v_w = 22.9 \text{ cm/s} \qquad [y=3104x + 13.0,\ r^2=0.973], \qquad (6.9d)$$

where v_i is in units of cm/s and δ, t, and L are in centimetres. Note that the regression values obtained in the present review are given in the square brackets on the right. The authors then plot the slopes and intercepts of Equations (6.9a) to (6.9d) as a function of water current, v_w on Figure 6.16. The equations of the fit lines are given as:

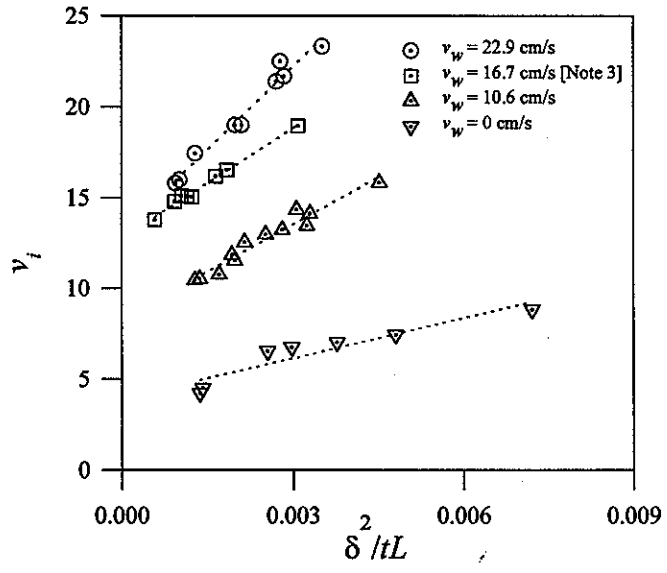

Figure 6.14 Ice Pack Velocity *vs* Relative Oil Thickness Driven By Current: Diesel Fuel

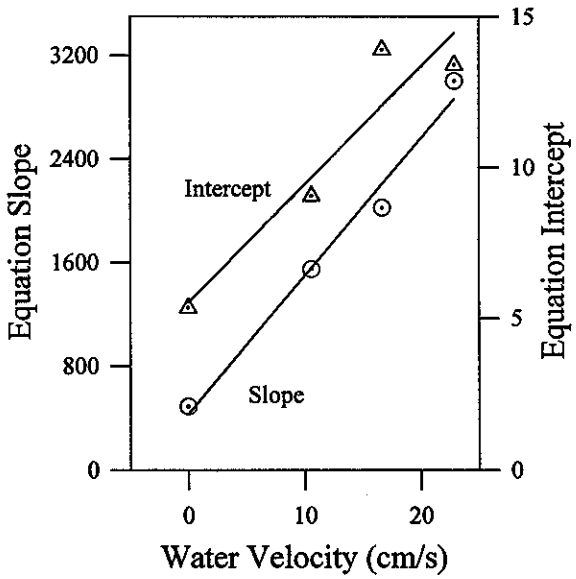

Figure 6.16 v_w *vs* Equation Slope and Intercept for Diesel fuel

* On Figure 6.14, this was originally reported as 16.9 cm/s.

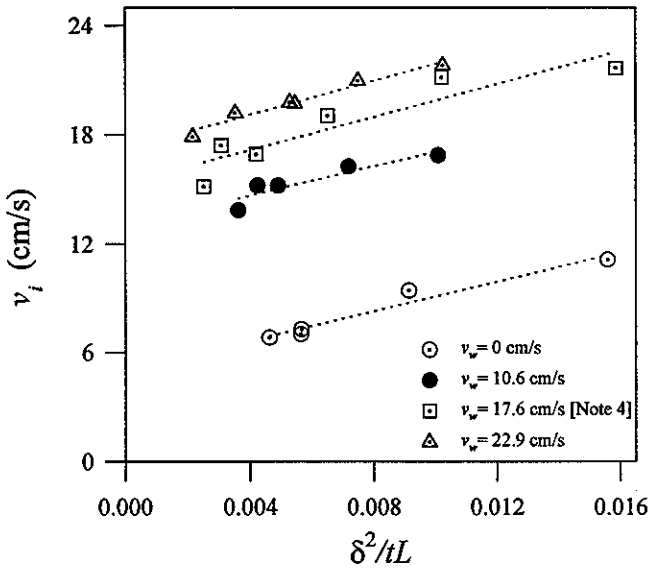

Figure 6.15 Ice Pack Velocity *vs* Relative Oil Thickness Driven by Current: SAE 10W Oil

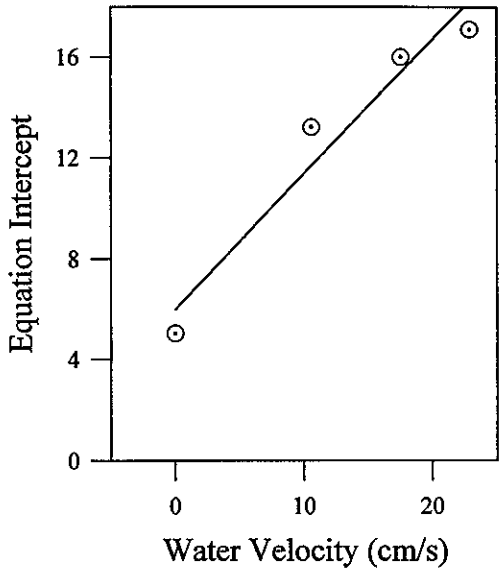

Figure 6.17 v_w *vs* Equation Intercept for SAE 10W Oil

Equation Slope = $106\ v_w + 433$ [y=106x + 4.33, r^2=0.982] (6.10)

Equation Intercept = $0.376\ v_w + 5.44$ [y=5.52x + 0.39, r^2=0.897] (6.11)

Combining Equations (6.9a) to (6.11), the authors give an expression for the velocity of a broken ice pack, behind which a quantity of diesel fuel has been spilled:

$$v_i = (106\frac{\delta^2}{tL}+0.376)v_w+433\frac{\delta^2}{tL}+5.44 \qquad (6.12)$$

in cgs units. The authors state that this equation is valid only for $\delta^2/tL \geq 1.75\times10^{-3}$.

Similarly for the SAE 10W oil, from Figure 6.15:

$$v_i = 414\frac{\delta^2}{tL}+5.04 \quad \text{for } v_w = 0 \quad [y=405x + 5.04, r^2=0.955], \qquad (6.13a)$$

$$v_i = 387\frac{\delta^2}{tL}+13.2 \quad \text{for } v_w = 10.6 \text{ cm/s} \quad [y=400x + 13.0, r^2=0.847], \qquad (6.13b)$$

$$v_i = 401\frac{\delta^2}{tL}+16.0 \quad \text{for } v_w = 17.6 \text{ cm/s}^* \quad [y=453x + 15.3, r^2=0.842], \qquad (6.13c)$$

---

* On Figure 6.15, this was originally reported as 16.7 cm/s.

$$v_i = 365\frac{\delta^2}{tL} + 17.1 \qquad \text{for } v_w = 22.9 \text{ cm/s} \qquad [y=469x + 17.2,\ r^2=0.967], \qquad (6.13d)$$

where v_i is in units of cm/s and δ, t, and L are in centimetres. The authors assumed that the slopes in Equations (6.13a) to (6.13d) were independent of the water velocity. The intercepts were plotted as a function of water velocity in Figure 6.17 giving:

$$\text{Equation Intercept} = 0.540\, v_w + 6.40 \qquad [y=0.555x + 6.00,\ r^2=0.945] \qquad (6.14)$$

The final equation for SAE 10W oil is given as:

$$v_i = 0.504 v_w + 392\frac{\delta^2}{tL} + 6.04, \qquad (6.15)$$

where all quantities are in cgs units, for oil slicks with thicknesses: $\delta^2/tL \geq 4\times10^{-3}$.

The authors also conducted tests, at several wind velocities, of unrestrained ice fields contaminated with diesel fuel. These results are shown in Figure 6.18. The authors remark that the wind has much less influence on oil drift than does water current. Little effect was observed for the wind tunnel velocities below 575 cm/s, which corresponds to a 19 knot, full-scale wind. The authors conclude that this implies that the roughness coefficient between the air and the ice is considerably less than that between water and ice.

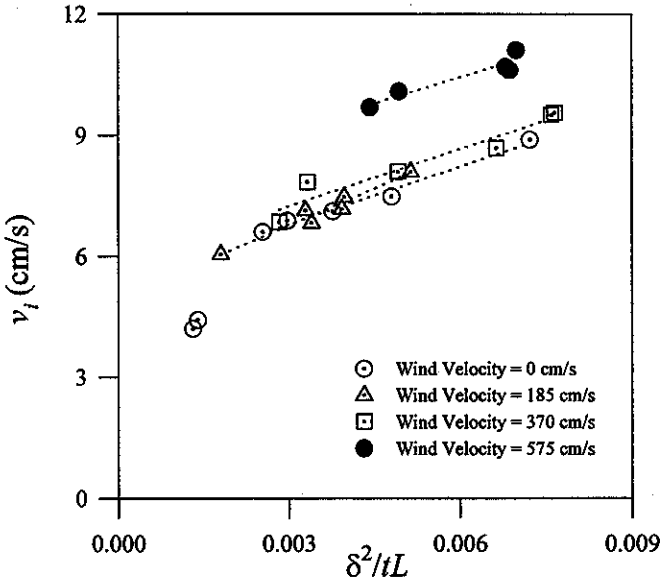

Figure 6.18 Ice Pack Velocity *vs* Relative Oil Thickness Driven By Wind: Diesel Fuel

The relationships between ice velocity and δ^2/tL for diesel fuel at a constant wind velocity are:

$$v_i = 489\frac{\delta^2}{tL} + 5.35 \qquad \text{for } v_{wind} = 0 \qquad [y=476x + 5.37,\ r^2=0.984], \qquad (6.16a)$$

$$v_i = 586\frac{\delta^2}{tL} + 5.06 \qquad \text{for } v_{wind} = 185 \text{ cm/s} \qquad [y=430x + 7.85,\ r^2=0.902], \qquad (6.16b)$$

$$v_i = 464\frac{\delta^2}{tL} + 5.92 \qquad \text{for } v_{wind} = 370 \text{ cm/s} \qquad [y=471x + 5.84,\ r^2=0.926], \qquad (6.16c)$$

$$v_i = 386\frac{\delta^2}{tL} + 8.24 \qquad \text{for } v_{wind} = 575 \text{ cm/s} \qquad [y=610x + 4.94,\ r^2=0.953], \qquad (6.16d)$$

using cgs units. The authors note that there seems to be little correlation between the wind velocity and the slopes or intercepts of Equations (6.16a) to (6.16d). The wind did not appear to exert a significant force on the ice field at speeds below approximately 500 cm/s (or 16.4 knots, full-scale). The authors remark, however, that wind may play a significant role when $\delta^2/tL < 0.004$. The expression for ice velocity is given as:

$$v_i = 533\frac{\delta^2}{tL} + 5.32, \tag{6.17}$$

in cgs units. Note that this equation corresponds to Equation (6.12) for the case $v_w = 0$. Comparing Equations (6.12) and (6.17), there must have been an error of at least 20 to 25% in the slopes determined in this study. The authors note that they could not investigate higher wind speed due to equipment limitations.

BOSS Critique

The authors present an empirical set of relationships for the movement of oil through pack ice. While quite detailed, however, their work has two significant flaws. Firstly, the authors do not appear to have used linear regressions to derive their parameters but instead seem to have used a visual "best fit" of the plotted data. While this can give reasonable results, it can also result in significant differences from the mechanical linear regression values. Where possible, the linear regression results are shown in the results section in square brackets to the right of the authors' results.

The second problem is considerably more serious and, unfortunately, impossible to correct. Note that the expression used for the hydrostatic gravitational spreading force on the right-hand side of Equation (3.1) evaluates as force over length, not force. The correct expression for the force at the foot of the oil slick has the form: $F_p \propto \Delta\rho g\delta^2\sqrt{A}$ (Hoult, 1972), where A is the surface area of a cylindrical slick of height δ. The outward "push" of the oil at the base of the slick depends not only on the slick thickness but also on its size. A larger slick should have a greater hydrostatic force at its boundary than a smaller one. Expression (3.1) indicates otherwise. The correct formulation for Equation (3.4) adjusted for slick volume is:

$$w = \frac{4\sigma_i \cos\alpha}{(\rho_{water}-\rho_{oil})g\delta\sqrt{A}}.$$

Similarly, the functional relationships developed from Equation (3.5), which include Equations (3.8), (3.12), and (3.13), should all have an additional dependency on $\sqrt{A}$. If the reservoir area, A, (or equivalently, volume, assuming a constant reservoir size) was held constant during the flow tests, then it is possible that the experimental data would be correct, uniformly scaled by some function of $\sqrt{A}$. This was probably the case, as it would appear that roughly the same amount of oil was used in each test. However, inconsistent initial volumes in the reservoir are probably the major source of variability in the data plotted on Figure 6.1 and a major source of error in the rest of the study. By comparing Equations (6.16a) to (6.16c), (6.17), and (6.12) (with v_w=0), it can be

seen that the error in the slope and the intercept of the δ^2/tL terms is at least 20%. The authors do not report the volumes of oil spilled, the reservoir sizes, or whether care was taken in each run to ensure that these conditions were kept fixed. Therefore, it is impossible to fully evaluate their results.

Consequently, the results of this study should not be used in any quantitative way to predict spill behaviour. However, the authors do describe some significant features of the behaviour of oil spills in linear breaks in pack ice. Oil slicks, when greater than their equilibrium thickness and presumably only in the inertial spreading regime, will cause loose ice packs to condense and can push ice packs at velocities greater than the water current. Also, water currents will affect ice drift but not the seepage rate of oil from pack ice. It was also found that winds have very little effect on either the ice velocity or the rate of oil seepage.

P.A. Tebeau, T.M. Meehan, and S.A. Saepoff, *A Laboratory Study of Oil Spreading Under Arctic Conditions,* Unpublished Report, United States Coast Guard, Groton, Connecticut, 58 p, 1984

Summary

A series of laboratory experiments were conducted to investigate the spreading of oil in ice packs. Both the flow of oil through a gap of known width and the oil spreading in an ice field were investigated.

Final area and equilibrium thickness of spilled oil in open water are not significantly affected by temperature unless the oil is close to its pour point. These terminal properties are controlled primarily by interfacial tensions at the spill perimeter, which are largely insensitive to temperature. At or below the pour point, the oil solidifies and the final thickness and area are then determined by the internal rheological properties of the oil.

The open water tests conducted by the authors were inconclusive and did not agree with the Fay-Hoult spreading model. They speculate that the size of the tank caused scaling effects, altering the surface tensions at the edge of the spreading slicks. They further caution that laboratory examinations of oil spills in which interfacial tension is an important factor may lead to inaccurate predictions when applied to real-world spills.

The spreading rate and final spill size for No. 2 fuel oil were found to be insensitive to the concentration of broken ice. Prudhoe Bay crude and No. 4 oils were either virtually or totally contained by an ice field. In general, it was found that the ice confined oil to an area smaller than the final area of a spill on open water.

The authors conclude that, for slush or brash ice, larboratory experiments are directly comparable to field spills. For larger ice fields, however, the thickness values reported may not be accurate, due to local damming of the oil, or release into an open water area in leads.

The authors were unable to satisfactorily model the flow of oil through gaps in an ice field. For thick oil slicks and narrow gaps, the formula proposed by Free *et al.*, 1981 [Equation (8)] was found to be effective, while for thin slicks in wide gaps, the authors' own formula [Equation (23)] was more successful. Intermediate gap widths were not well described by either method.

The authors' experiments on oil spreading rates in broken ice and seepage rates through broken ice were inconclusive. In particular, the spreading of the No. 2 heating oil did not depend on ice concentration, which was not predicted by the Fay-Hoult type spreading models evaluated in the work. In addition, the authors found that the two heavier oils spread in the gravity-viscous regime and could be analytically described with confidence. They caution, however, that it would be extremely difficult to extrapolate from their model to accurately predict the spreading rate through the interconnecting channels in a broken ice field.

Objective

The objectives of the study were to investigate the variation in small-scale oil spreading behaviour in open water as a function of the oil/water temperature and the physical properties of the oil; to evaluate the expression for terminal spreading thickness of Langmuir, 1938, [Equation(7)]; and to evaluate the Fay-Hoult spreading equations for oil in a broken ice field and assess the applicability of these results to field situations. Specifically, the experiments focused on the variation in spreading rate and equilibrium thickness as a function of oil volume, oil physical properties, and the gap spacing of the ice field.

Theory

For the oil spreading experiments in open water, the authors used the Fay-Hoult spreading equations as described by Hoult, 1972 as their basic model:

Gravity-Inertia:
$$r \sim \left(\frac{\rho_w}{\pi\rho_o}\right)^{1/4} (\Delta g V)^{1/4}\, t^{1/2}, \tag{3}$$

Gravity-Viscous:
$$r \sim \left(\frac{1}{\pi^2}\, g\, \frac{\Delta V^2}{\nu^{1/2}}\, t^{3/2}\right)^{1/6}, \tag{4}$$

Surface Tension-Viscous:
$$r \sim \sqrt{2}\left(\frac{\sigma^2 t^3}{\rho_w \nu}\right)^{1/4}, \tag{5}$$

where r is the 2D-symmetric spill radius, Δ is the relative difference in density between oil and water $[(\rho_w - \rho_o)/\rho_o]$, ρ_w is the density of water, σ is the oil/water interfacial tension, g is the acceleration due to gravity, ν is the kinematic viscosity of water, V is the total volume of oil spilled, and t is the time from the start of spreading.

The final spill thickness is governed by the spreading coefficient, $S_{o/w}$, which is defined by:

$$S_{o/w} = \sigma_w - (\sigma_o + \sigma_{o/w}). \tag{6}$$

If $S_{o/w}$ is positive, then an oil slick will form a molecular monolayer film. If $S_{o/w}$ is negative, that is, the surface tension of the film retards the spreading of the oil slick, then the slick thickness at equilibrium, h_e, is given by:

$$h_e^2 = -\frac{2S_{o/w}}{\Delta g \rho_o}. \tag{7}$$

The authors wished to investigate Equation (7) in the context of the results of the open water work of Fazal and Milgram, 1977, which showed (for four different crude oils) that oil slicks fractionated as spreading proceeded. Also, other studies (Deslauriers *et al.*, 1977, Glaeser and Vance, 1971, Schultz, 1976) reported that both monolayers and thick terminal slicks had been observed in field trials.

The authors also proposed to investigate the flow of oil through gaps between ice blocks or floes. Free *et al.*, 1981 reported a formula for the minimum gap width between ice flows to initiate oil seepage through the gap as a function of the slick thickness. The authors rearrange this as the minimum slick thickness, h_e, required to initiate flow through a gap of width, w:

$$h_e = -\frac{4\sigma_{o/w}\cos\alpha_{o/w}}{(\rho_w - \rho_o)w}, \tag{8}$$

where $\sigma_{o/w}$ is the oil/water interfacial tension, $\alpha_{o/w}$ is the oil/water contact angle, and ρ_w and ρ_o are the water and oil densities, respectively.

Equation (8) assumes that oil flows through a narrow ice gap, treating the motion as capillary flow. To simulate the conditions of larger ice gaps and thinner oil slicks, the authors propose a different formulation for oil gap flow based on flow through a water-filled channel with ice on the sides. The hydrostatic driving force is the same used by Free *et al.*, 1981:

$$F_g = 1/2\rho_o g w h^2, \tag{17}$$

where h is the thickness of the oil, while the interfacial tension forces that resist spreading are made up of the oil/water surface tension across the gap and the oil/ice surface tension up the sides of the ice walls:

$$F_s = \sigma_{rw} w + \sigma_{ri} 2h, \tag{18}$$

where σ_{rw} is the resultant oil/water interfacial tension and σ_{ri} is the resultant oil/ice interfacial tension. The authors argue that, in most situations, the ice surfaces will be wetted, thus σ_{ri} can be replaced by σ_{rw}. In addition, σ_{rw} is:

$$\sigma_{rw} = \sigma_{o/w}(1 - \cos\theta).^* \tag{20}$$

The force balance between the hydrostatic and interfacial tensions gives:

$$1/2\rho_o g w h^2 - 2\sigma_{o/w}(1 - \cos\theta)h - \sigma_{o/w}(1 - \cos\theta)w = 0. \tag{21}$$

Solving this quadratic equation in h gives:

$$h = \frac{2\sigma_{o/w}(1 - \cos\theta) \pm \sqrt{4\sigma_{o/w}^2(1 - \cos\theta)^2 + 2\rho_o g w^2 \sigma_{o/w}(1 - \cos\theta)}}{\rho_o g w}. \tag{23}$$

Note that there were several inconsistencies in the original manuscript for the derivation of Equation (23). These have been corrected and are presented here in a simpler form than

---

* While the authors wrote this expression with ($\cos\theta - 1$), many other authors (for example, Bannerjee, 1980) use the reversed form, as shown above. Note that Equation (23) is numerically tractable only for ($1 - \cos\theta$).

originally used by the authors. However, a comparison of the results generated by the corrected Equation (23), above, and the graphical results given by the authors reveals that the errors in the original manuscript were probably typographical.

An estimate of the average gap size in an ice field was reported by Free *et al.*, 1981 as:

$$b = d\left(\frac{1}{\sqrt{c}} - 1\right), \qquad (9)$$

where b is the average gap width ($\bar{w}$), d is the (average cubic root) linear dimension of the ice blocks, and c is the ice concentration, which the authors estimated as:

$$c = \frac{nd^2}{W\,L}, \qquad (10)$$

where n is the number of ice blocks in an ice field of rectangular dimensions, W by L (note that this expression has been corrected from the original manuscript).

The authors also report the expression Free *et al.*, 1981, derived for the rate of seepage, q, of a diesel fuel slick (of thickness h) through an ice field as:

$$q = 2.74\times10^{-5}\frac{h^{4.37}}{b^{2.87}}. \qquad (10)$$

Note, however, that the BOSS analysis of the same results (see BOSS Review of Free *et al.*, 1981) indicated that:

$$q = 1.66\times10^{-6}\frac{h^{3.51}}{b^{2.01}}$$

better represented the experimental data reported in Free *et al.*, 1981.

Methods

The experimental apparatus used in this study is shown in Figure 3. The water and ice tanks

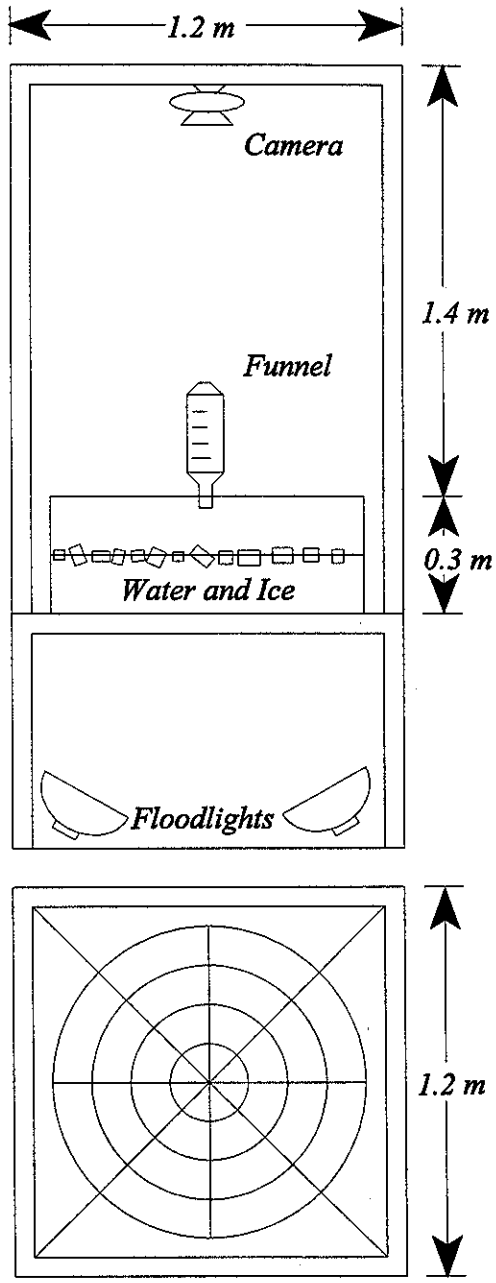

Figure 3 Test Tank for R&D Center Oil Spreading

were 120 cm square and 29.5 cm deep. The tank was lit from underneath by floodlights, which were diffused to provide even lighting. A concentric grid was marked on the plexiglass tank cover. A 35-mm camera was mounted above the tank and used for time-lapse photos. Oil could be introduced to the tank either as a continuous discharge through a separatory funnel or instantaneously, by dropping a metal cylinder into the tank.

The oils used in the experiments were No. 4 and No. 2 fuel oils, and a Prudhoe Bay crude oil. The relevant physical properties for each oil are given in Table 4. These three oils were chosen for their wide range of physical properties and because they were similar to the oils used by Free *et al.*, 1981. Most of the oil properties were taken from the oil weathering study of Mackay *et al.*, 1982. However, the viscosities were measured on a Brookfield LVF viscometer. The authors' results for the No. 4 fuel oil and Prudhoe Bay crude at several temperatures are shown in Figure 4.

In the open-water spreading experiments, known volumes of oil (50 and 25 mL) were discharged into the tank using both continuous flow and instantaneous release methods. Multiple time-lapse photographs were taken during spreading until the slick reached an equilibrium area.

Similar procedures were followed for some of the broken ice experiments. A constant volume of oil, 250 mL, was discharged in a continuous stream into an ice field composed of 10-cm^3 ice blocks in fresh water. Ice concentration was controlled by adding a known number of ice blocks (40, 80, 120, 160, or 200). No repetitions were performed; a single run was carried out for each oil/ice concentration configuration.

A second group of experiments was conducted to examine the ice gap spreading Equations (8) and (23). The oil was released into the ice field instantaneously by dropping an open metal container into the centre of the ice field. Only the No. 4 and Prudhoe Bay crude oils were used in these experiments. The discharge volumes of oil were 125 mL, 250 mL, and 500 mL. Ice concentrations were controlled by the number of ice blocks (120 and 165) as before. Again, only one run was performed for each oil/volume/ice concentration. Time-lapse photography was used to monitor spread, but an effort was also made to determine the average gap spacing, the spacing at which the flow of oil stopped.

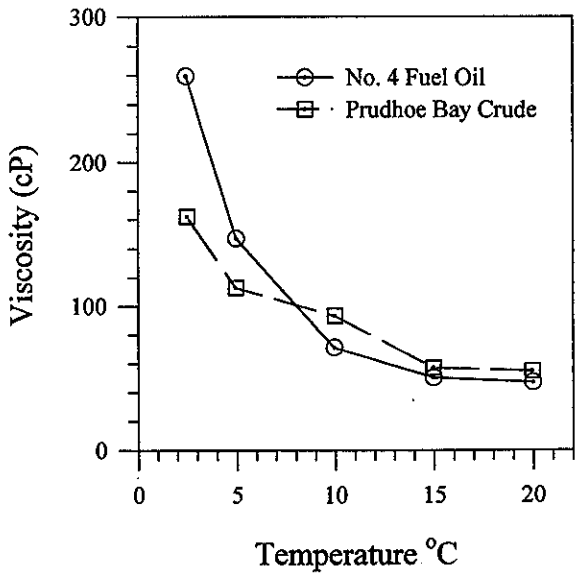

Figure 4 **Plot of Oil Viscosity and Oil Temp. for Prudhoe Bay Crude and No. 4 Fuel Oil**

The authors note that, in order to scale their results for use in field conditions, the Froude number ($U/\sqrt{gL}$) must be comparable when considering the gravitational and inertial forces, and the the Reynolds numbers (UL/ν) must also match for models that include friction. In

addition, interfacial forces require a constant Weber number ($\rho_o U^2 L/\sigma_{ow}$) between model and prototype. In Equations (8) and (23), U is the speed of the front of the oil slick, L is the ice gap width, and ν is the kinematic viscosity. The Froude number indicates that speed (U) must scale as $\sqrt{L}$. Similarly, the Reynolds number dictates that the viscosity must scale as $L^{2.5}$ and the Weber number shows that the interfacial tension must vary as L^2. The authors could not obtain any model fluids that satisfied these scaling conditions for a typical water/oil system. Therefore, they state that their results must be used only at a one-to-one scale. The authors' primary intent, therefore, was to examine the qualitative behaviour of the ice/oil system.

Table 4 Oil Physical Properties

Oil Type	No. 2 Heating Oil	Prudhoe Crude	No. 4 Fuel Oil
Density (g/mL)			
0°C	0.849	0.909	0.938
20°C	0.840	0.901	0.925
Pour Point (°C)	-27	-2	-3
Viscosity (cP)			
0°C	7.74	1500	
10°C		96	47.2
20°C	4.04	35	22.7
Interfacial Tension			
oil-water	25.6	27.0	30.23
oil-air	26.2	30.1	32.10

Results

The authors remark that, during the tests on open water, the oil slicks displayed three distinct spreading behaviours. The first consists of a thin final slick only a few molecules thick. In the second case, oil spreads out in a well defined lens and terminates at a measurable thickness. The third type of behaviour occurs when the oil temperature is close to its pour point and the oil forms a semi-solid mass on the surface of the water.

The authors found that No. 2 oil always behaved as the first case, while the Prudhoe Bay crude and the No. 4 fuel oil exhibited both the second and third types of behaviour. They observed that the No. 2 oil quickly spread to the tank dimensions and thus final areas could not be determined. The No. 4 and Prudhoe Bay oils both spread as thick lenses while at temperatures well above their respective pour points (20°C and 10°C for the Prudhoe Bay crude only), but became increasingly solid and resistant to flow in colder conditions. At 0°C, the No. 4 oil "congealed" into thick lumps with a thinner slick spreading concentrically from the lumps. The central congealed areas were solid, and cracking was visible in the later spreading stages.

The authors conclude that solidification of the oil reduced the final area considerably, compared to the final areas at warmer temperatures. This phenomenon of congealed oil at the centre of the slick surrounded by a thin spreading layer was observed for both the Prudhoe Bay and No. 4 oils under cold conditions. It was determined by gas chromatography that the solid and liquid areas were chemically identical. The final areas and thicknesses are shown in Table 5. The authors note that their results were "inconclusive" and "often inconsistent with existing theory".

Table 5 Final Area and Equilibrium Thickness Data for Open-Water Spreading Tests

Oil Type	Volume (mL)	Temperature (°C)	Final Area (cm^2)[a]	Thickness (cm)[b]
Constant Release Rate Data				
No. 2 Heating Oil	50	0	Entire tank	
	50	10	Entire tank	
	50	20	Entire tank	
Prudhoe Crude	50	0	2827	0.0177
	50	10	5867	0.0085
	50	20	3988	0.0125
No. 4 Fuel Oil	50	0	2827	0.0177
	50	10	4369	0.0114
	50	20	2631	0.0190
Instantaneous Release Data				
Prudhoe Crude	50	0	2178	0.0230
	25	10	5557	0.0045
	25	20	2631	0.0095
No. 4 Fuel Oil	50	0	3091	0.0166
	25	10	3790	0.0061
	25	20	4106	0.0061

[a]Appears to be calculated as: π(Measured Radius)^2

[b]Appears to be calculated from: (Initial Volume)/(Calculated Area). The method for determining final thickness is not discussed in the manuscript.

It was found that the spreading coefficients, $S_{o/w}$, for the three oils were positive. Equation (6) predicts that all three oils used by the authors would spread to monolayer thicknesses, as was observed for the No. 2 heating oil. However, as described earlier, this was not the case for the Prudhoe Bay crude and No. 4 fuel oils. The authors speculate that this inconsistency may be due to oversimplifications in Equation (6), poor interfacial tension values (taken from Mackay *et al.*, 1982), or edge effects in the spreading tank. The No. 4 and Prudhoe Bay oils spread as a thin slick surrounding a thick centre which probably thinned out at the edges to an invisible monolayer. This invisible leading edge of the slick could "feel" the sides of the tank and act to restrict further spreading. The authors conclude that oil spreading data from experiments in enclosed tanks, particularly where interfacial tension is a controlling parameter, may not accurately reflect the spreading behaviour that would be encountered in the open ocean. The

authors also note that Equation (7) predicts a slight increase in equilibrium slick thickness, based on the temperature dependencies of σ and ρ, which was not observed in the experimental data.

The final spill areas and slick thicknesses for the continuous discharge tests into a broken ice field are shown in Table 7. The results of the instantaneous discharge tests are shown in Table 8.

Table 7 Ice Concentration, Final Area, and Equilibrium Thickness Data for Broken Ice Tests (Constant Volume, Constant Flow Release)

Oil Type[a]	Number of Ice Blocks	Ice Concentration	Final Area (cm^2)	Thickness (cm)
No. 2 Heating Oil	120	0.69	1388	0.1801
	160	0.80	1296	0.1929
	200	0.81	1335	0.1873
Prudhoe Crude	40	0.27	3191	0.0784
	80	0.48	848	0.2948
	120	0.71	740	0.3378
	160	0.85	240	1.0417
	200	0.83	214	1.1682
No. 4 Fuel Oil	40	0.44	3118	0.0802
	80	0.57	636	0.3931
	120	0.73	251	0.9960
	160	0.76	84	2.9762
	200	0.86	101	2.4752

[a]Discharge volume 250 mL

Table 8 Ice Concentration, Final Area, and Equilibrium Thickness Data for Broken Ice Tests (Variable Volume, Instantaneous Release)

Oil Type	Volume (mL)	Number of Ice Blocks	Ice Concentration	Final Area (cm^2)	Thickness (cm)
Prudhoe Crude	125	120	0.84	811	0.1541
	125	165	0.50	306	0.4085
	250	120	0.80	905	0.2762
	250	165	0.48	311	0.8039
	500	120	0.74	1530	0.3268
	500	165	0.56	377	1.3263
No. 4 Fuel Oil	125	120	0.65	660	0.1894
	125	165	0.77	136	0.2867
	250	120	0.59	640	0.3906
	250	165	0.65	357	0.7003
	500	120	0.74	1476	0.3388
	500	165	0.73	334	1.4970

The authors conclude that the No. 2 heating oil exhibited the non-contained spreading behaviour as defined by Free *et al.*, 1981, while the heavy oils, the Prudhoe Bay crude and No. 4 fuel oil, were totally or virtually contained by the ice field. The Prudhoe Bay crude oil was virtually contained at 0.71 ice concentration and totally contained at higher concentrations, while the No. 4 fuel oil was totally contained at a concentration of 0.74.

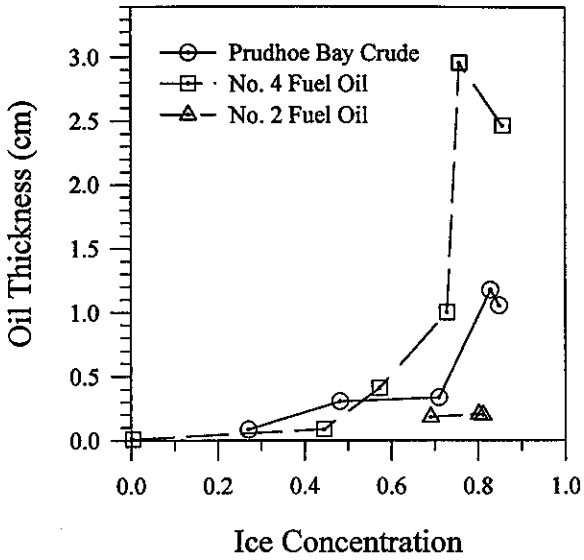

Figure 12 **Plot of Equilibrium Oil Thickness *vs* Ice Concentration for No. 2 Heating Oil, Prudhoe Bay Crude and No. 4 Fuel Oil**

The authors remark that for heavier oils and higher ice concentrations, ice concentration becomes more important in controlling spill behaviour, while the properties of the oil become less important. The results of the experiments are summarized in Figure 12 which shows equilibrium thickness as a function of ice concentration for all three oils. The authors remark that, while the No. 2 oil is insensitive to ice concentration, Figure 12 suggests that the equilibrium thickness of the No. 4 fuel oil and the Prudhoe Bay crude is highly dependent on ice concentration, especially for coverages greater than 50%. They further speculate that the specific ice concentration ranges probably depend on the physical properties of the oil. At very high ice concentrations, the equilibrium thickness is reduced because of oil seepage over the tops of the ice blocks, which increases the final spill area.

The authors conclude from the area *versus* time graphs of spreading that the final spill area is a function of volume only above a certain "threshold volume." This observation supports the model of a minimum slick thickness required to initiate spreading through an ice gap predicted by Equations (8) and (23). In addition, the authors found that in the runs with higher ice concentrations (the 165-block tests), more oil was trapped in the ice in a thicker layer than was observed for the 120-block trials. They conclude that, with ice concentration above a certain value, the ice field has a greater oil storage potential.

The authors note that the ice concentration numbers in Tables 7 and 8 were experimental and were obtained by estimating the actual oil spill area in the contaminated sectors of the grid. They assumed that the oil spill area in the contaminated sectors consisted only of the open areas between the ice blocks. This would not account for oil trapped underneath or covering the ice blocks. Their results are summarized in Table 10.The values were calculated using Equation (10) from Free *et al.*, 1981. The differences between the calculated and measured values were attributed to the submergence of ice blocks and rafting effects.

Table 10 Summary of Average Measured and Calculated Ice Concentration Values

Number of Test Runs	Number of Ice Blocks	Average Measured Concentration	Calculated Concentration
2	40	0.36	0.28
2	80	0.53	0.56
9	120	0.73	0.83
3	160	0.80	1.00
3	200	0.83	1.00

The average gap width, *w*, used in Equations (8) and (23), was determined by measuring the gap widths from the photographs for some of the 120-block runs. Of the six photographs measured, an average of 30 gaps per run had an average width of 1.6 cm with a standard deviation of 2 cm.

The average gap width was also calculated to be 1.0 cm using Equation (9) of Free *et al.*, 1981. The authors comment that the broken ice experiments conducted in the laboratory are probably the least severe test of the model equations. They expect that greater inaccuracies would be encountered when estimating the typical gap width in a real ice field.

The oil thickness required for spreading to begin in a broken ice field was also evaluated for both the flow discharge and the instantaneous release tests. The results of the instantaneous discharge experiments are shown in Figure 18 together with the maximum equilibrium oil thicknesses predicted by Equation (8). Note that the "gap widths" used by the authors in Figure 18 and in calculating the oil thicknesses were determined photographically, not using Equation (10). The authors found that, for both series of experiments, Equation (8) was not a very good predictor of oil thickness and consistently overestimated the maximum oil thickness, as can be seen in Figure 18.

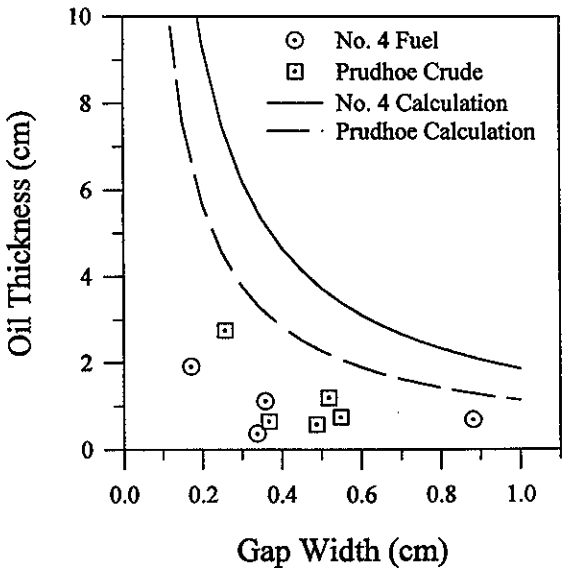

Figure 18 Experimental and Theoretical Oil Spill Thickness *vs* Gap Width for Capillary Flow, Equation (8)

The authors remark that Equation (8) models the oil seepage as Poiseuille flow through two parallel walls of ice which is appropriate for narrow gap widths and high oil thicknesses where the area of contact between ice and oil is large. The authors contend, however, that for larger gap widths and thinner oil slicks, the situation is more like oil flow in a water-filled channel with ice on either side. In fact, Free *et*

al., 1981, considered the seepage of oil through narrow ice cracks to be resisted by capillary-like surface tension forces, while the authors' model, Equation (23), represents a laminar Poiseuille flow through an open channel with a Gaussian distribution of flow velocities across the channel mouth. The authors' results for the instantaneous release tests are shown in Figure 21. The authors observe that there appears to be good agreement between the results of the channel flow model of Equation (23) and their experimental results, particularly for the larger gap widths, i.e., when channel flow dominates the spreading process. The contact angle used, 180°, implies complete wetting of the ice by the oil.

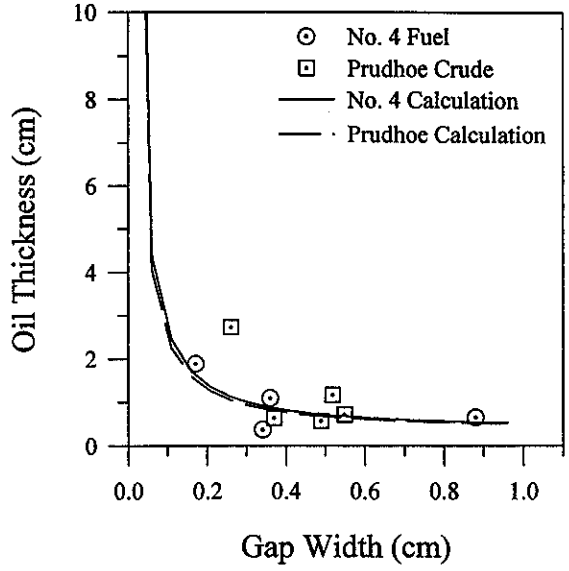

Figure 21 **Experimental and Theoretical Oil Spill Thicknesses *vs* Gap Width for Wide Channel Flow, Equation (23)**

The authors also attempted to evaluate the seepage rate model of Free *et al.*, 1981 for the No. 2 heating oil as a function of ice field concentration. The seepage model, consisting of Equations (9) and (13), predicts that as the ice concentration increases, the average gap width should decrease and the seepage rate per unit width of the ice field, q, should increase, as shown in Table R1. However, the authors remark that all three ice concentrations, shown in Table 7, had spreading kinetics that were very similar to those plotted in Figure 8, with the 120-block experiment exhibiting the fastest spreading. Similar results were found for the Prudhoe Bay crude and No. 4 oils, with comparable spreading rates observed for the 160- and 200-block trials and much shorter spreading times observed for the 120-block experiments. However, Table R.1 shows that Equation (13) predicts an increase in seepage per width of ice field, q, with increasing ice concentration. The authors remark that this experiment suggests the exponent b in Equation (13) should be negative. They remark that Free *et al.*, 1981 developed Equation (13) by varying the block sizes, d, in Equations (9) and

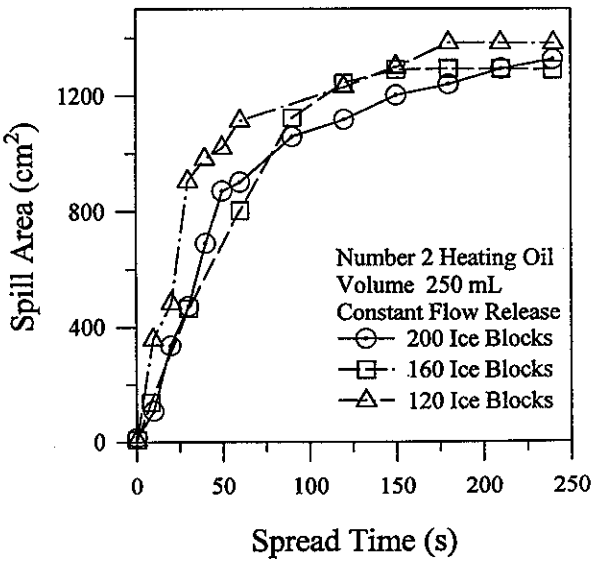

Figure 8 **Plot of Spill Area *vs* Spread Time for No. 2 Heating Oil at Three Ice Concentrations (Constant Flow Rlease)**

(10), to change the gap widths between the ice blocks. Larger blocks pack less well and therefore have larger gaps, *b*, but Free *et al.*, 1981 found that the seepage rate per width of ice field, *q*, was smaller, which is reflected in their Equation (13). This is a reasonable conclusion when one realizes that larger ice blocks will have fewer gaps than smaller blocks and thus there will be less seepage through the ice field. The authors therefore conclude that Equation (13) does not apply to all broken ice conditions, only those with differing block sizes.

Table R1 Calculated Gap Width and Oil Seepage for No. 2 Heating Oil

Ice Concentration	*b* [Equation (9)] cm	*q* [Equation (13)] mL/s
0.80	1.18 cm	0.018
0.90	0.54 cm	0.171
0.99	0.05 cm	158.3

Application of Results to Real Spill Situations

The authors state that, based on their open water spreading tests, the final spill area would not be expected to vary with temperature except when the oil is close to its pour point and begins to solidify. They base this conclusion on the assumption that the slick area is determined by the oil-water interfacial tension, which is "relatively insensitive" to temperature. They also note, however, that their results indicate that oil slicks are strongly affected by edge effects and may terminate spreading early if close to shore or ice.

The authors note that the laboratory conditions are not dynamically similar to real-world ice conditions. Thus the results of their experiments are likely to be quantitatively valid only for ice conditions similar to the experimental ones. Stationary brash ice, where the ice pieces are small and the ice concentration is fairly uniform, is expected by the authors to behave as the experiments shown in Figure 21. Therefore, they expect that equilibrium oil thicknesses could be predicted using Equations (8) and (23) and seepage rates using Equation (13).

Normal ice pack conditions include a wide range of ice sizes and concentrations, however, and can change rapidly. Gap widths can also range up to several metres and the small-scale phenomena examined by the authors are not likely to strongly influence oil spreading. The authors remark that the oil dynamics will likely be governed primarily by the gravity-viscous spreading phase until the equilibrium thickness is reached or a blockage is encountered. They thus conclude that it will be "very difficult" to extrapolate from their experiments to real-world spill behaviour.

BOSS Critique

The authors develop an equation for the seepage of oil through broken ice and test it in small-scale conditions. As their own analysis shows, however, a lack of dynamic similarity limits their results quantitatively to conditions similar to those in their laboratory: high, stable ice concentrations and small, uniform ice sizes. As the authors note, this includes only brash ice,

probably compressed in an ice field, under calm conditions. More typical ice fields that would have a wide range of ice sizes and large gaps between the ice, may behave quite differently than even the qualitative behaviours described by the authors.

However, the authors do provide a good discussion of the effects of ice block size on the oil containment and seepage rate, particularly for the conditions where it is appropriate to use the channel flow equation or the capillary flow model of Free *et al.*, 1981, for oil seepage. This had previously been largely unexamined and adds an important factor to the seepage models. It indicates that ice block concentration is not enough to predict seepage rates. The concentration of the gaps in the ice is more important.

Except in a few cases, the authors did not explicitly evaluate errors in their work or perform duplicate runs under the same conditions. It is therefore difficult to estimate the precision of their work. However, given the variations observed in their spreading data, a relative error of 10 to 25% is probably a reasonable estimate of the uncertainty in the results presented by the authors.

M.S. Uzuner, F.B. Weiskopf, J.C. Cox, and L.A. Schultz, *Transport of Oil Under Smooth Ice*, EPA-600/3-79-041, Environmental Protection Agency, Corvallis, Oregon, 62 p., 1978.

Summary

Laboratory studies on the movement of oil under ice cover were performed with an emphasis on the effects of water currents on slick movement.

1. It was found (experimentally) that the slick velocity (U_s) for an oil slick under an ice sheet is a function of the water current (U_w), as shown in the following table.

Oil Type	Viscosity (cP)	Threshold Velocity (cm/s)	Slick Velocity as a Function of Water Current (cm/s)	Applicable Current Velocity Range (cm/s)
Number 2 Fuel	7	4	$U_s = 0.38U_w - 1.26$	0 to 36
Crude	24 500	8	$U_s = 8.6 \times 10^{-6}\, U_w$	8 to 28
			$U_s = 1.10U_w - 16.60$	28 to 36

2. For water currents significantly greater than the ranges in the above table, the slick will disperse into a suspension in the water column. Further investigation was beyond the scope of the authors' work.

3. For oils other than the Number 2 fuel oil or the crude oil examined in this study, a first approximation of the relationship between slick velocity and water velocity for slicks under an ice surface is given as:

$$(1\text{-}U_s)^2 = \frac{0.146}{N_F^2} + 0.450$$ for slicks oriented parallel to the flow direction,

and,

$$(1\text{-}U_s)^2 = 0.346 \left(\frac{1}{N_F^2}\right)^{1.15} \dagger$$ for slicks oriented transverse to the flow direction.

4. To apply the relationships given above, the properties of the spilled oil must be known or estimated. The behaviour of crude oil spills will necessarily be uncertain.

5. Significant differences were observed between the Number 2 fuel and the crude oil. The crude oil slicks typically became shorter and wider as they moved downstream, thickening in the upstream edge at higher current velocities. These slicks appeared to "slide along" the underside of the ice sheet. The Number 2 fuel oil slicks became longer and narrower and appeared to "roll" on the ice undersurface.

---

† The authors report a value of 2.15 for the multiplicative constant, not 0.346. See the Results section for further details.

6. It was found that slicks under plexiglass behaved very differently than those under ice. The crude oil formed a 0.25 to 0.5 cm film on the plexiglass sheet. In no case did any oil adhere to either fresh or salt water ice in the course of other tests.

7. Discontinuities in the ice sheet (an open water edge or a slot) caused retention of the moving oil slick. In addition, the authors caution that their results apply only for "unbounded under ice oil slicks". Contact with a boundary, such as a river shore, would also be expected to retard slick movement.

Objective

This study developed a model for predicting the behaviour of an oil slick in a straight stream or river of uniform depth, covered with a consolidated ice cover of uniform thickness. It is assumed that the water is flowing in one direction and at a uniform rate.

Theory

In developing their oil spill model, the authors review the work of Glaeser and Vance, 1971; McMinn, 1973; Hoult, 1974; Chen *et al.*, 1974; and Mackay *et al.*, 1976 for information on spreading of oil on ice, oil on water, and oil under ice, all in calm conditions. The authors then develop their own model using a method similar to the force balance technique basic to the Fay-Hoult models described in the reviewed references. It should be noted, however, that the authors do not develop a spreading model, but rather an oil slick drift theory, without reference to the kinetics of the oil slick shape.

The Oil Slick Drift Model

"Consider that a known amount of oil is injected into a stream beneath a continuous ice sheet as [shown] in Figure 5." The authors note that after the initial release behaviour, *i.e.*, the formation of a vertical "plume", the oil will collect in a layer on the undersurface of the ice.

The forces promoting layer spreading include form drag (the pressure difference between the upstream and downstream parts of the slick) and the shear force due to the water current. The retarding force is "the sliding or rolling friction between the ice surface and the oil, treating the oil as a solid".

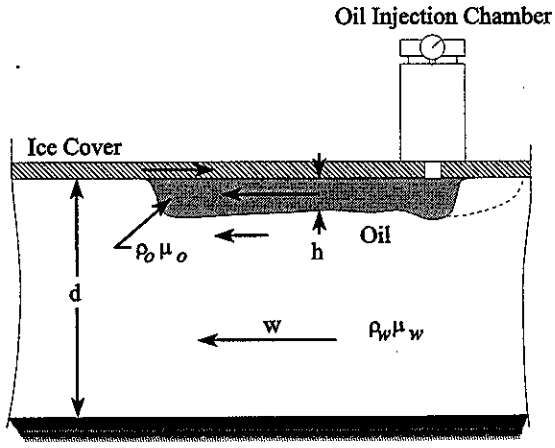

Figure 5 Schematic Representation of Oil Slick Transport Under an Ice Cover

Because this model is not axially symmetric, the authors' define the slick volume as:

$$V = h\ l\ w, \tag{70}$$

where l is the longitudinal dimension parallel to the current flow and w is the perpendicular slick dimension.

The form drag is given as:

$$F_d = \frac{1}{2}\ C_d\ \rho_w (U_w - U_s)^2\ wh, \tag{70}$$

where C_d is a drag coefficient, ρ_w is the water density, U_w is the water velocity, and U_s is the mean slick velocity. The authors note that: "this force becomes more important as the slick formed beneath the ice cover thickens".

The shear force is given as:

$$F_s = \frac{1}{2}\ C_s\ \rho_w (U_w - U_s)^2\ wh. \tag{71}$$

"The shear stress coefficient, C_s, is not the same as a drag coefficient over a flat plate." Two references (Jeffereys, 1925 and Jirka *et al.*, 1975) are cited to show that C_s is estimated to be in the range of 0.6 to 0.01. "The most significant point is that values of C_s for this case are at least one to two orders of magnitude larger than those for a rigid flat plate."

The authors estimate the "interfacial friction force" as the product of the force normal to the surface (the buoyancy) and a coefficient of friction, C_f:

$$F_f = C_f\ (\rho_w - \rho_o)\ gV. \tag{72}$$

The balance between driving and retarding forces is:

$$F_f = F_d + F_s. \tag{73}$$

Substituting Equations (71) and (72) into (73):

$$C_f\ (\rho_w - \rho_o)\ ghwl = \frac{1}{2} C_d \rho_w (U_w - U_s)^2\ wh + \frac{1}{2} C_s \rho_w (U_w - U_s)^2\ wh. \tag{74}$$

Introducing the densimetric Froude number:

$$N_F = \frac{U_w}{\sqrt{\Delta g h}}, \tag{75}$$

reduces Equation (74) to:

$$(1-U_s)^2 = \left[\frac{2C_f}{C_d\frac{h}{l}+C_s}\right]\frac{1}{N_F^2}. \tag{76}$$

Thus, the slick motion could be expected to follow the form:

$$(1-U_s)^2 = \frac{B}{N_F^2}. \tag{77}$$

The authors take special note of the *h/l* term in Equation (76), commenting that this term makes form drag the dominant driving force if the slick elongates perpendicularly to the current flow, while if the slick becomes narrow in the current, shear stress becomes dominant.

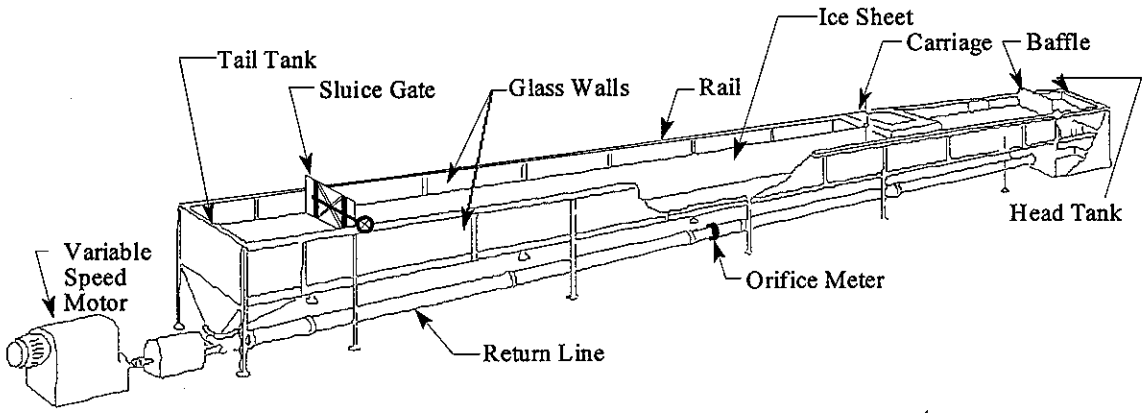

Figure 6 Schematic Depiction of ARCTEC's Ice Flume

Experimental

The experiments were conducted in ARCTEC's ice flume, shown in Figure 6. The test section of the flume was 13.7 m long, 0.94 m wide, and 0.61 m deep. Flow rates in the flume could be varied up to 170 L/s. The maximum water depth used was 46 cm, leaving 18 cm of freeboard. The flume discharge was measured by a precalibrated orifice-meter in the return line.

Oil was injected through a 2-cm hole in the ice in the middle of the flume using a pressurized box. The injection box had a capacity of 26.5 L of oil and injection was controlled pneumatically. The oil volume was monitored by a float in the reservoir attached to a swing arm on a potentiometer. Calibration data (Figure 7, not reproduced here) indicate that the injected volume

was a complicated function of the potentiometer resistance. The difficulties associated with repeatably injecting oil volumes were probably a major source of the authors' experimental error.

A new ice sheet was used for each test. While the sheet was being frozen, the specific gravity, viscosity, and oil-water surface tension of the sample oil were measured in cold-room conditions. Specific gravity was measured on a hydrometer following the ASTM E 100-66 procedure. Viscosity was measured on a Brookfield LVT viscometer, following ASTM specification D 2983-72. The viscosity as a function of oil temperature is shown in Figure 9. The oil-water surface tension was measured on a Fisher Surface Tensiometer, Model 20, a torsion balance, as specified by ASTM methods D-971 and D-1331. The authors note that the crude oil was too viscous at 0°C to measure the surface tension. It appears that the readings were taken at room temperature; the procedure is not completely described by the authors. In addition to the series of tests before the experiments, the oil was tested by the same methods afterwards. Parameters for all the runs performed are shown in Table 2.

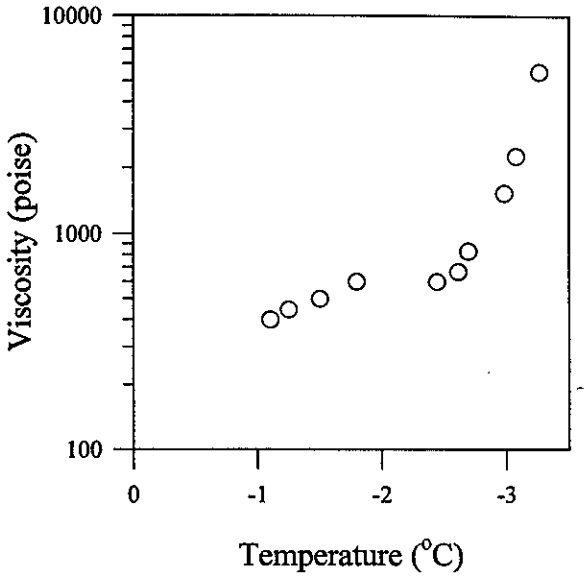

Figure 9 Viscosity *versus* Temperature for Crude Oil

During injection, the oil flow rate through the 2-cm hole in the ice was estimated to be 0.12 L/s. A total of 18.9 L of oil was injected for each test. Starting with the injection and for the duration of oil flow in the ice flume, still photographs and video were taken. The experiment was terminated when the oil reached the tail tank of the ice flume.

Results

Differences in behaviour between the Number 2 fuel and crude oil were noticed as soon as the oil was discharged. The Number 2 fuel oil broke up into large drops, while the crude formed a continuous plume rising to the ice sheet. Also, because the Number 2 fuel oil had a much lower density than the crude oil, after the injection, it rose to the ice sheet much faster and reached the ice undersurface noticeably closer to the discharge point than the crude oil, at higher water currents.

At low current velocities, the crude oil rose to the undersurface of the ice at the injection point and spread laterally and downstream. In addition, the slick stuck to the injection hole for a period of time before being swept downstream as a solid body. At higher water velocities, the high viscosity oil formed a rope-like streamer which came into contact with the ice sheet downstream from the injection hole. The oil rope would break, forming small oblong blobs of oil which were

wider perpendicular to the water current than parallel to it. These would then collect to form a larger slick. "As the slick formed and moved downstream, its upstream edge thickened as a result of water accelerating around the edge of the slick as shown in Figure 13." Small patches of crude oil would move faster than the larger slick, but were also oriented transverse to the current flow.

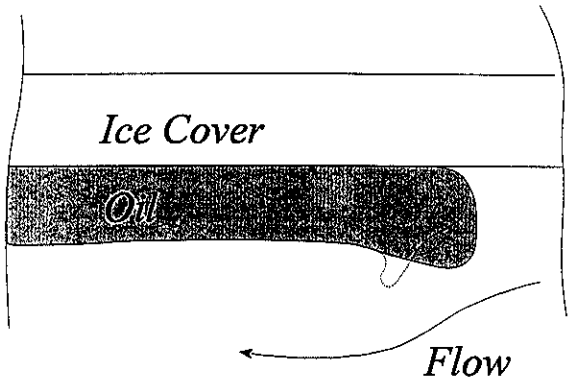

Figure 13 Schematic Representation of the Folding Phenomena at the Upstream End of a Crude Oil Slick

The Number 2 fuel oil quickly developed into a layer of uniform thickness (approximately 0.5 cm) under the ice sheet with a smooth oil/water interface. Waves were observed at the oil water interface at higher water current velocities. Also, "the fuel slick 'rolled' along the underside of the ice sheet". In higher currents, the large slick would lose small blobs of oil from its edges, which then "blew" downstream, faster than the main oil mass.

In all experiments, the Number 2 fuel oil rapidly spread into a slick with a limiting thickness which was the same for all trials. The crude oil also showed this behaviour, but only when left overnight in calm water with oil temperatures close to 0°C. In the one crude oil trial using hot oil (50°C), the slick spread rapidly to a limiting thickness. No spreading of the cold crude oil slicks (~0°C) was observed in any of the other trials.

Both oils exhibited similar behaviour in salt and fresh water. However, the authors note that fine oil droplets became entrained in the ice sheet in salt water, giving the ice sheet a dirty appearance. Plexiglass was investigated as an alternative to using ice in the tests, but with no success. The authors found that a coating of oil adhered to the sheet with both oils. They conclude: "The oil beneath a plexiglass sheet therefore showed a totally different behaviour than oil under an actual ice cover."

In the test conducted with hot crude oil (50°C), the authors remark that the hot oil behaved similarly to the cold Number 2 fuel oil. The high water current used in the trial broke up the oil slick and little ice/oil interaction was observed.

The parameters for each trial are shown in Table 2. Figures 14 and 15 are plots of the mean slick velocity *versus* the water current for the Number 2 fuel oil and the crude oil respectively. The authors note that the results for tests 20 and 21 (see Table 2) are not shown in Figure 14. These two trials were suspect because the slicks broke up as "smaller slicks seem to move at much higher velocities than larger slicks for the same current speed".

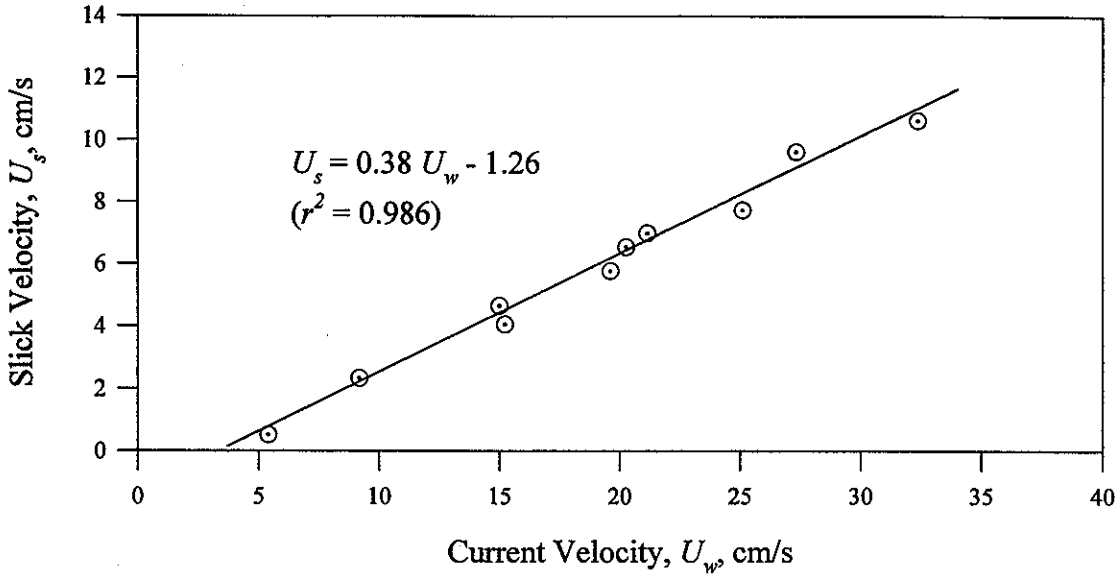

Figure 14 Plot of Slick Velocity *versus* Current Velocity for Number 2 Fuel Oil

The authors conclude that the slick velocity for Number 2 fuel oil is linearly proportional to the water current:

$$U_s = 0.38\,U_w - 1.26, \quad \text{for } 0 \le U_w \le 36 \text{ cm/s} \tag{78}$$

They note that the oil slick would not move at currents below 4 cm/s.

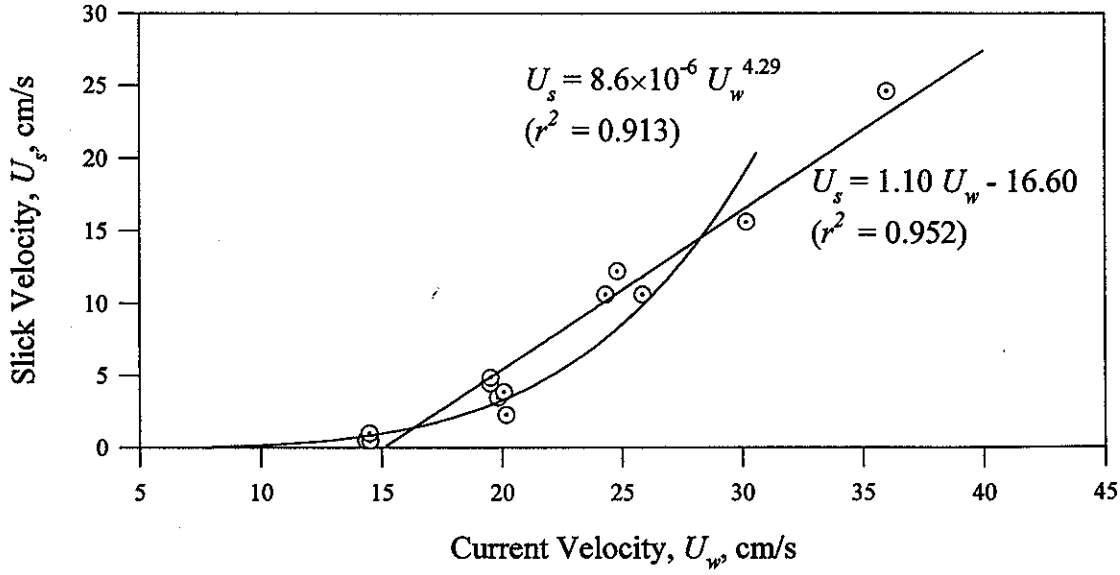

Figure 15 Plot of Slick Velocity *versus* Current Velocity for Crude Oil

Table 2 Summary of Test Data

Test No.	Water Velocity, U_w (cm/s)	Oil Type	Slick Velocity,[a] U_s (cm/s)	Oil Viscosity, μ_o (cP)	Slick Thickness, h (cm)	Oil Density, ρ_o (g/mL)	Water Depth, d (cm)	Oil Temp.,[b] T_o (°C)	Interfacial Surface Tension, σ (dyne/cm)	Froude Number, N_F	Non-dimensional Velocity, U
1	5.0	No. 2 Fuel	0.4	7	0.5	0.86	27.8	–	–	0.60	0.08
2	14.0	No. 2 Fuel	3.5	7	0.5	0.86	27.4	1.5	–	1.69	0.25
3	5.4	No. 2 Fuel	0.6	7	0.5	0.86	25.6	-2.6	16.6	0.65	0.11
4	9.9	No. 2 Fuel	2.0	7	0.5	0.86	23.5	1.0	12.8	1.20	0.21
5	15.1	No. 2 Fuel	4.1	8	0.5	0.86	23.6	-1.4	14.8	1.82	0.27
6	20.1	No. 2 Fuel	6.6	7	0.5	0.86	22.7	-0.4	19.3	2.43	0.33
7	20.1	Crude	2.3	25 500	1.3	0.91	23.0	-0.8	69.0	1.88	0.12
8	9.8	Crude	0.0	15 000	1.3	0.91	21.7	-0.8	38.0	0.92	0.00
9	20.0	Crude	3.7	15 000	1.3	0.91	21.7	-0.8	38.0	1.87	0.18
10	20.0	Crude	4.4	15 000	1.3	0.91	21.7	–	38.0	1.39	0.22
11	14.9	Crude	0.5	25 500	1.3	0.91	23.4	1.8	15.8	1.33	0.03
12	14.3	Crude	0.5	25 500	1.3	0.91	23.4	1.8	15.8	1.84	0.04
13	19.7	Crude	3.4	36 500	1.3	0.91	16.1	-0.3	17.0	2.26	0.17
14	24.2	Crude	10.6	36 500	1.3	0.91	16.1	–	17.0	1.48	0.44
15	15.8	Crude	1.9	36 500	1.3	0.91	16.1	–	17.0	2.19	0.12
16	24.8	Crude	12.3	25 500	1.3	0.90	13.4	2.0	15.8	2.67	0.50
17	30.1	Crude	15.7	25 500	1.3	0.90	13.4	2.9	15.8	2.67	0.52
18	36.1	Crude	24.6	25 500	1.3	0.91	13.4	5.5	15.8	3.37	0.68
19	19.4	Crude	4.4	25 500	1.3	0.91	13.4	1.5	15.8	1.81	0.23
20	21.3	No. 2 Fuel	9.8	7	0.5	0.86	10.5	2.4	13.4	2.57	0.46
21	24.5	No. 2 Fuel	16.7	7	0.5	0.86	10.5	2.2	13.4	2.95	0.68
22	19.5	No. 2 Fuel	5.8	7	0.5	0.86	13.9	-0.1	10.1	2.35	0.30
23	27.2	No. 2 Fuel	9.7	7	0.5	0.86	13.9	0.0	10.1	3.28	0.36
24	32.3	No. 2 Fuel	10.7	7	0.5	0.86	13.9	0.0	10.1	3.90	0.33
25	25.0	No. 2 Fuel	7.8	7	0.5	0.86	13.9	0.1	10.1	3.02	0.31
26	9.1	No. 2 Fuel	2.4	7	0.5	0.86	14.9	-0.4	9.3	1.10	0.27
27	14.9	No. 2 Fuel	4.7	7	0.5	0.86	14.9	-1.0	9.3	1.80	0.32
28	21.0	No. 2 Fuel	7.0	7	0.5	0.86	14.9	-1.0	9.3	2.54	0.33
29	14.5	Crude	1.0	25 500	1.3	0.91	15.2	-1.5	16.4	1.35	0.07
30	19.4	Crude	4.8	25 500	1.3	0.91	15.2	0.7	16.4	1.81	0.25
31	25.8	Crude	10.6	25 500	1.3	0.91	15.2	-2.3	16.4	2.41	0.41

[a]Computed as the change in downstream position of the slick edge divided by the change in time and average overall readings.

[b]Temperature of oil before being injected into the stream.

A similar analysis for the crude oil gave good results for water velocities above 20 cm/s, but predicted a threshold current for slick movement (~15 cm/s) that the authors felt was too high. Therefore, a power function was also fit to the data, which gave a threshold velocity of 8 cm/s. The expressions the authors derived were:

$$U_s = 8.6\times10^{-6} U_w^{4.29}, \text{ for } 8 \le U_w \le 28 \text{ cm/s, and} \tag{79}$$

$$U_s = 1.10\,U_w - 16.60, \text{ for } 28 \le U_w \le 36 \text{ cm/s.} \tag{80}$$

The authors note that the crude and Number 2 fuel oil slicks behaved very differently in the water current. The Number 2 oil slick was always long and narrow. By assuming that only shear forces were important, the authors reduced Equation (76) to:

$$(1-U_s)^2 = \frac{B_1}{N_f^2}, \tag{83}$$

with,

$$B_1 = \frac{2C_f}{C_s} \tag{84}$$

for Number 2 fuel oil. This relationship is examined in Figure 16.

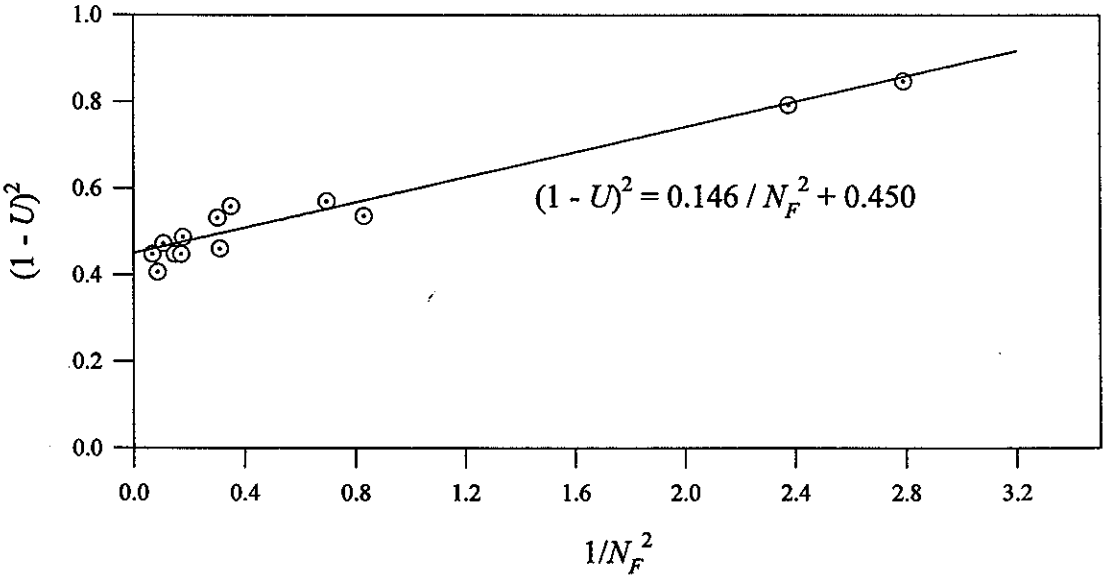

Figure 16 Generalized Slick Transport Relationship Based on Number 2 Fuel Oil Tests Where the Slick is Oriented Parallel to the Flow

The fit to the data shown on Figure 16 is:

$$(1-U_s)^2 = \frac{0.146}{N_f^2} + 0.450. \tag{85}$$

The constant term, while not predicted by the force balance model of motion, Equation (73), "could be momentum losses due to wave formation at the oil water interface". The authors theorize that this would depend on the square or the water velocity:

$$F_f = F_s + C\rho_w U_w^2 \tag{86}$$

and that for "large enough" Froude numbers, this interfacial flow resistance term would dominate and cause the slick to break up.

Conversely, the crude oil slicks were always "short and wide", oriented transverse to the current flow. Assuming that form drag is the dominant driving force gives:

$$(1-U_s)^2 = \frac{B_2}{N_f^2}, \tag{87}$$

where

$$B_2 = \frac{2C_f l}{C_d h}. \tag{88}$$

This is plotted for the crude oil results in Figure 17. The best fit to the data is reported to be:

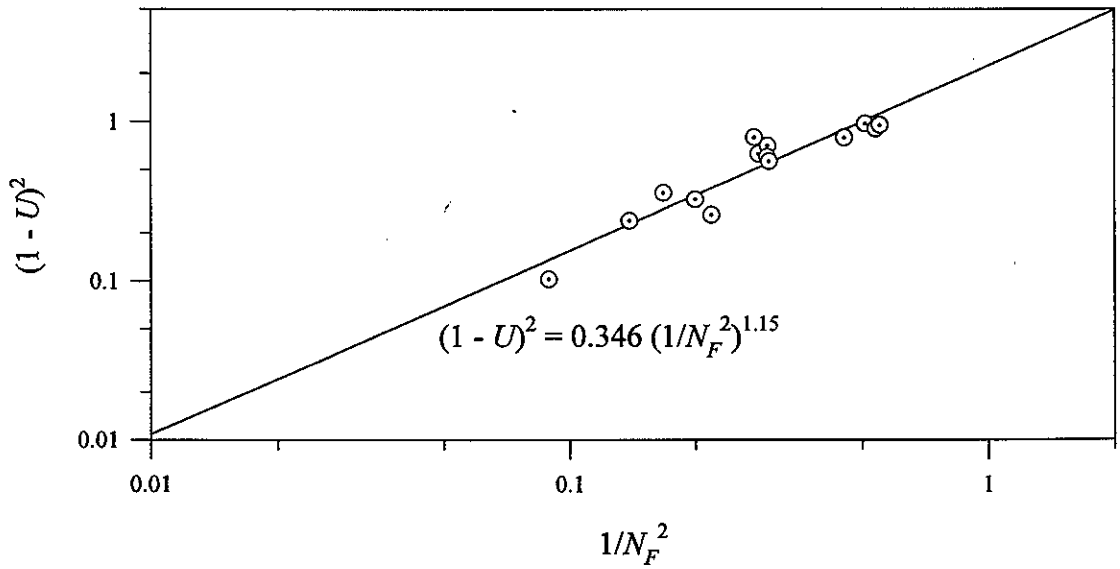

Figure 17 Generalized Slick Transport Relationship Based on Crude Oil Tests Where the Slick is Oriented Transverse to the Flow

$$(1-U_s)^2 = 2.15\left(\frac{1}{N_f^2}\right)^{1.15} \tag{89}$$

although, a re-examination of the data suggests that the multiplicative constant should be 0.346 (with a correlation of: $r^2 = 0.880$). The authors note that the exponent in Equation (89) is close to unity, "indicating the approximate validity of the force balance". The authors remark that the quality of fit of Equation (89) "compares favourably" with that of Equation (80), although the threshold velocity is still not accurate [however, the linear correlation of Equation (80) is better]. Also in Equation (87) and (88), B_2 is not truly a constant, but depends on l/h.

Application of Results

The authors state that their expressions can be applied directly to field spills under ice sheets, without scaling the results, and that Equations (78) to (80) may be used without modification. To use the more general Equations (85) and (89), the properties of an oil must be known, and also the orientation adopted by the oil slick, whether perpendicular or parallel to current flow.

BOSS Critique

The authors report a model for oil slick drift in a water current under ice by comparison with oil-spreading theories. When considering this study, it is important to note that, even though the authors present their model development in the context of spreading theory, the end result is applicable only to the motion of a bulk slick without reference to slick formation or dimensions. For example, their model does not predict spreading kinematics or a terminal layer thickness. The model divides oil slick motion under ice into two cases: a viscous oil, moving in a slick transverse to the water current and a relatively fluid oil slick oriented parallel to the water flow. It is anticipated that the non-dimensional expressions [Equations (85) and (89)] would be most applicable to field behaviour, although certain oil properties, specifically viscosity, must be known and the slick dimensions, particularly length (parallel to the water current) and height, must be known or calculated using a spreading model.

The authors performed many tests for each of the two cases, which gives their results significant statistical validity. It must be noted, however, that the variability of the oil volumes injected under the ice was an important source of error in the authors' results. Also, while the authors have described the motion of the "main" oil slick under ice, the velocities of smaller blobs or drops of oil are not included in the models presented here. For both the viscous and non-viscous oil, the authors remarked that smaller blobs of oil would split off from the main slick and travel downstream at a higher velocity than the main blob.

As a final note, the author's rationale for deriving two expressions for crude oil motion [Equations (79) and (80)] seems inappropriate. Referring to Figure 15, the data seems to correlate very well to the straight line given by Equation (80). The power curve, Equation (79), seems to fit the data less well, as can be seen by comparing the correlation parameters given on Figure 15. The authors' argument that the power expression is necessary to correctly describe the threshold of slick motion also does not appear to be borne out by an examination of their results. From

Figure 15, it can be seen that there are three points with very low slick velocities near the threshold of motion predicted by the linear model, Equation (80), while there are no data points near that of the power series expression, Equation (79). It is therefore recommended that only Equation (80) be referred to for future work.

L.W. Rosenegger, *The Movement of Oil Under Sea Ice*, Technical Report No. 28, Beaufort Sea Project, Environment Canada, Victoria, B.C., 81 p., 1975.

Summary

"An evaluation of some of the parameters affecting the flow and areal distribution of crude oil under a sea ice canopy has been presented. It was found that the interfacial tensions between oil and brine (12 $^{o}/_{oo}$) for Swan Hills and Norman Wells crude oils were 24.5 and 23.8 dynes/cm respectively. Interfacial tensions at salinities other than 12 $^{o}/_{oo}$ have also been presented. Effects of aging on the interfacial tension could not be determined... The equilibrium thickness of these two crude oils under ice was found to be 0.80 and 0.88 cm for the Swan Hills and Norman Wells samples respectively."

The author also presents equations for the minimum force required to initiate motion in an oil bubble attached to the underside of an ice sheet as a function of the oil mass. The "residual" forces were calculated to be (in dynes, for grams of oil) $R' = 58.3 M_o^{0.461}$ for Swan Hills crude and $R' = 23.8 M_o^{0.785}$ for the Norman Wells oil.

Using the measured surface tensions for the two oils, the "surface-tension limited" thickness of both crudes was calculated to be 0.25 cm, which the author considers to be a conservative, i.e., low, estimate of the ultimate spreading thickness of slicks of Swan Hills or Norman Wells crude oils on water.

The author also concludes that the maximum possible salt content of oil, if any, is insufficient to contribute to under-ice surface rot. As well, based on reported porosity measurements, the author concludes that little incorporation of oil into an ice sheet would be expected. If the oil is close to an oversized drainage channel (1.4 mm in diameter or larger), however, some penetration would occur. In the spring, as melting proceeds and the brine drainage channels open, a significant amount of oil penetration should be expected.

Objective

The major objectives of the study were: to measure the interfacial tension of oil on ice in brine for Norman Wells and Swan Hills crude oils; to observe the motion and/or surface absorption of oil drops at the interface of ice and salt water as a function of ice sheet tilt; to determine the ultimate size of an oil slick; and to determine the extent of oil penetration into a growing ice sheet from underneath.

Theory

Surface Tension Measurements by the Sessile Drop Method

The interfacial tension of a liquid on, or hanging from, a liquid surface was related to a constant, β, by Bashford and Adams, 1883 in the form:

$$\beta = \frac{g\rho b^2}{\sigma}, \quad \dagger \tag{1}$$

where g is the gravitational acceleration, ρ is the density difference between the fluids, b is the radius of curvature at the origin of the coordinate system, and σ is the interfacial tension. The author notes that β must be positive for hanging drops.

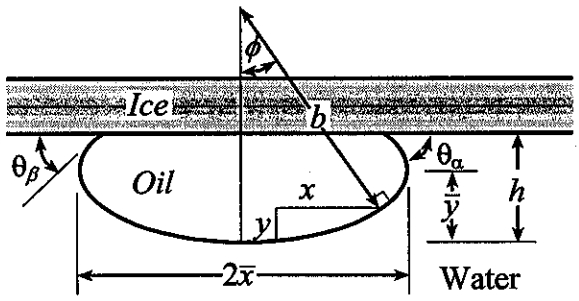

Figure 1 (Modified) Schematic of Measurement Parameters in the Sessile Drop Method

Bashford and Adams, 1883 proposed a method of calculating β from a second order differential equation in x and y (see Figure 1), and presented calculation tables for various values of ϕ. Later authors (Staicopolus, 1962, 1963, and 1967 and Parvatikar, 1966 and 1967) recast the original differential equation in x and y and solved for the interfacial tension. From Staicopolus, 1962:

$$\sigma = \frac{g\rho}{B_\phi F_\phi^2}(\bar{x})_\phi^2 \tag{3}$$

$$\sigma = \frac{g\rho}{B_\phi G_\phi^2}(\bar{y})_\phi^2 \tag{4}$$

where $\bar{x}$ and $\bar{y}$ are the drop dimensions (see Figure 1), and the terms $B_\phi = \beta$, $F_\phi = \left(\frac{\bar{x}}{b}\right)_\phi$, and $G_\phi = \left(\frac{\bar{y}}{b}\right)_\phi$ are derived from fourth order polynomials in $\bar{x}/\bar{y}$. The author gives tables of these quantities, taken from Staicopolus, 1962.

Surface Tension Measurements by the du Noüy Ring Detachment Method

To calculate oil-brine interfacial tensions from the air-oil and air-brine surface tensions measured by the du Noüy technique, the empirical relationship of Good *et al.*, 1958 was used:

$$\sigma_{ab} = \sigma_a + \sigma_b - 2\Phi\sqrt{\sigma_a\sigma_b}, \tag{9}$$

---

*Rosenegger used γ as a symbol for the surface tension, which is often found in chemical literature. For consistency with the rest of the BOSS reviews, σ is used here.

where $$\Phi = \frac{4V_A^{1/3} V_b^{1/3}}{\left[V_a^{1/3} + V_b^{1/3}\right]^2}, \quad (10)$$

and V_x is the molar volume of phase x.

Movement of Oil Drops

The residual force on an oil droplet buoyed up against a tilted ice sheet (the force which initiates motion parallel to the ice sheet), R', is given as:

$$R' = \left(\frac{\rho_w - \rho_o}{\rho_o}\right) M_o g \sin\alpha \quad (11)$$

where ρ_w and ρ_o are the water and oil densities respectively, M_o is the mass of the oil droplet, g is the acceleration due to gravity, and α is the angle of the ice sheet from the horizontal.

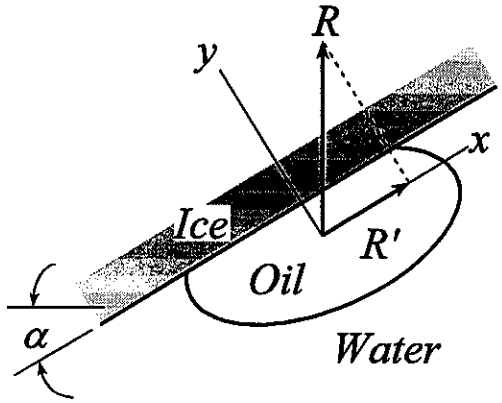

Figure 31 Schematic of the Force R' Causing Motion in the x Direction

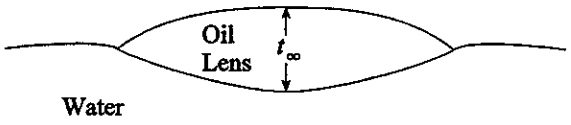

Figure 38 Profile of an Oil Lens on Water

Surface Tension Limits of Slick Thickness

The author calculates the thickness of oil floating on water at equilibrium, t_∞, using the formula given by Langmuir, 1933:

$$t_\infty^2 = -2S \frac{\rho_{water}}{g\rho_{oil}} \cdot \frac{\rho_{water} - \rho_{oil}}{\rho_{water}}, \quad (15)$$

where S is the spreading coefficient, which must be negative for Equation (15) to be valid. It was defined by Adamson, 1960 as:

$$S_{oil/water} = \sigma_{water} - \sigma_{oil} - \sigma_{water/oil} \quad (16)$$

for pure liquids. However, at equilibrium, the two liquids will become mutually saturated which alters the surface tensions: $\sigma_{water} \rightarrow \sigma'_{water}$, $\sigma_{oil} \rightarrow \sigma'_{oil}$. The spreading coefficient becomes:

$$S' = \sigma'_{water} - \sigma'_{oil} - \sigma_{water/oil} \quad (17)$$

Methods

Surface Tension Measurements by the Sessile Drop Method

A 12 part-per-thousand (by weight) brine solution was frozen in a clear plexiglass tank until a 5-cm ice layer had formed. A heating tape in the bottom of the tank ensured a temperature gradient in the brine solution during freezing. After freezing, a hole was drilled in the ice and oil was injected into the brine using a stainless steel syringe. The author notes that it was very difficult to control the size of the bubbles formed by this procedure. Two hundred individual droplets attached to the ice were photographed with a 200-mm lens. The resulting slides were projected on an optical comparator and the dimensions of the oil droplets were measured directly from the slides. The maximum diameter of the droplets ($2\bar{x}$), the distance from the drop apex to the ice sheet (h), and the distance from the line of maximum diameter ($\bar{y}$) and the contact angles, θ_α and θ_β, were all recorded, as shown in Figure 1. The pair of contact angles were averaged for further calculation. The interfacial tension was then calculated using Equations (3) and (4).

A string of thermistors was frozen into one of the sample tanks and readings were taken before and after the test to determine temperature drift during the readings. The ice-air surface warmed considerably, but the temperature at the brine-ice interface differed by slightly more than 0.5°C before and after the measurements. It was reported that the 12 $^{o}/_{oo}$ brine solution froze at between -1.6 and -1.3°C.

Errors in measuring drop dimensions were reported to be less than 0.001 in. (0.025 mm) in both x and y using the optical comparator. It was found that the precision of the measurements depended heavily on the picture quality and image focus. The 0.025 mm estimated error was further multiplied by the inverse of the image reproduction size ratio (typically 1× or 2×) for the true estimated error. Variations in the ice sheet also caused measurement difficulties. Oil bubbles usually settled into a hollow in the ice surface which made it difficult to measure the dimensions of the bubbles.

Surface Tension Measurements by the du Noüy Ring Detachment Method

Surface tensions were measured by ring detachment with a Fisher Tensiomat, model 21, at 25.8 to 28.2°C. Four or five trials were performed on each fluid and the apparatus was cleaned using the "ASTM 1970" procedure. The apparatus was calibrated before and after the tests. Specific densities were determined, by an unspecified technique, for each fluid except the 6 $^{o}/_{oo}$ brine solution. This solution was interpolated between the values for the other solutions and that of air, a technique taken from Kreith, 1968.

Movement of Oil Drops

The limit-of-motion tests were performed with the same apparatus as the sessile drop measurements, using a hinged table to tilt the tanks. The tanks were modified so that there was an air space between the tank and insulating walls, which helped to prevent the brine from freezing down the walls of the tanks. The author also notes that, while growing flat ice sheets was difficult, a method was found for growing parallel plates of ice, then levelling the tanks prior to the experiments.

Oil was injected under the ice sheet, using a method similar to that for the sessile drop experiments. The bubbles were photographed and the test apparatus tilted until the oil bubbles began to move, which was determined visually. As the author found it difficult to obtain useful pictures of the bubbles, the oil volume was often estimated from the amount of oil injected and the relative size of other bubbles. Measuring bubble velocity was complicated by the frequent "necking" into multiple droplets. Velocities were recorded for the first of the multiple droplets to reach the final marker and therefore were not representative of the whole oil bubble.

Tests were performed on both Norman Wells and Swan Hills crude oils. The oil bubble masses were estimated from the sessile drop measurements using a formula described by Staicopolus, 1962. The author found that Staicopolus' formulae were limited to values of $\bar{x} \approx 1$.

Results

Surface Tension Measurements by the Sessile Drop Method

The author reports that, of the 200 oil droplets photographed (111 of Swan Hills crude and 89 of Norman Wells crude), 26 were discarded due to poor image quality (19 of Swan Hills and 7 of the Norman Wells crude oils). The experimental results are summarized in Table 4. Measurement histograms are shown in Figure 13 for the Swan Hills oil and in Figure 14 for the Norman Wells oils.

Table 4 Interfacial Tensions Between Oil and 12 $^{o}/_{oo}$ Brine Calculated From Experimental Data

Oil Type	Number of Observations	Mean	Standard Deviation	Maximum	Minimum	Range	Mean Deviation
Swan Hills	92	25.456	7.009	47.693	6.925	40.768	4.960
Norman Wells	82	23.982	7.904	49.151	5.686	43.465	6.103

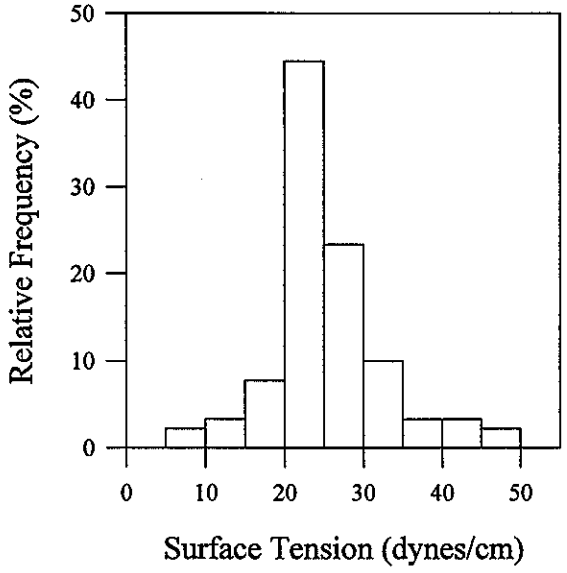

Figure 13 Surface Tension Frequency Distribution, Swan Hills Crude

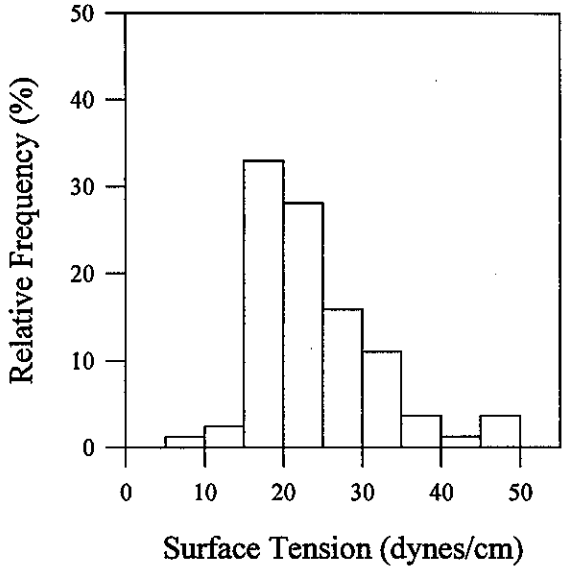

Figure 14 Surface Tension Frequency Distribution, Norman Wells Crude

As the standard and mean deviations are quite high, the author questioned the usefulness of the sessile drop technique. The measurements were analyzed by computing the interfacial tensions using both x and y [Equations (3) and (4)]. There was essentially no difference between the results in all cases. However, the author notes that there was large scatter in both σ_x and σ_y for low values of x. A further examination showed that for drop sizes up to $x = 2$ mm, the ratio $x/y \approx 1$, i.e., the oil droplets were very close to spherical. It was found that at $x/y = 1$, the polynomial B_ϕ approaches 0, while the terms F_ϕ and G_ϕ are both equal to 1. It was therefore clear from Equations (3) and (4) that small measurement errors in either x or y for nearly spherical drops resulted in large calculated errors in σ.

The author concludes that the sessile drop method is not reliable for measuring interfacial tension of oil droplets with radii, x, smaller than 2 mm. Furthermore, because the term B_ϕ grows rapidly as x/y increases, especially with respect to the relatively constant behaviour of the polynomials F_ϕ and G_ϕ, small variations in droplet height, y, when $x \gg y$ will also cause significant errors in σ. The author reports that a measurement range of $2 \text{ mm} < x < 3$ mm gave the best results for the calculated surface tension.

The interfacial tension was seemingly unaffected by aging. The author notes that weathering effects would be well within the limits of accuracy of the sessile drop method. The length of the observation period is not reported, but it was probably not more than a few hours.

In addition, the author was able to predict a minimum slick spreading thickness from the asymptotic limit of y which was then correlated to the total droplet height experimentally. For the

Swan Hills crude, 0.80 cm maximum thickness was predicted, while 0.88 cm was predicted for the Norman Wells Crude.

Surface Tension Measurements by the du Noüy Ring Detachment Method

The measured air-liquid surface tensions are shown in Figure 30 as a function of the brine concentration. The best fit results are shown in Table R.1 (as calculated for this review). The low correlations of these lines reflect considerable scatter in the data. For 12 $^{o}/_{oo}$, -1.0°C brine-ice solutions, the author reports temperature-corrected oil-water interfacial tensions of 26.65 dynes/cm for the Swan Hills crude and 27.06 dynes/cm for the Normal Wells crude. Based on variations in the reading, the author estimates that experimental error in the ring detachment values is at most 10%, including errors in the temperature corrections.

Table R.1 Fit Results for Air-Liquid Surface Tension Measurements

System (liquid-air)	Fitted Curve	Correlation
Brine	$\sigma = 0.116$ (Brine ‰) + 65.3	0.23
Brine saturated with Swan Hills oil	$\sigma = -2.71 \times 10^{-2}$ (Brine ‰) + 53.5	0.034
Brine saturated with Norman Wells oil	$\sigma = 0.223$ (Brine ‰) + 38.3	0.22
Swan Hills oil saturated with brine	$\sigma = 1.06$ (Brine ‰) + 24.8	0.012
Norman Wells oil saturated with brine	$\sigma = 3.56 \times 10^{-2}$ [(Brine ‰) -5.90]$^{1.28}$ + 21.6	

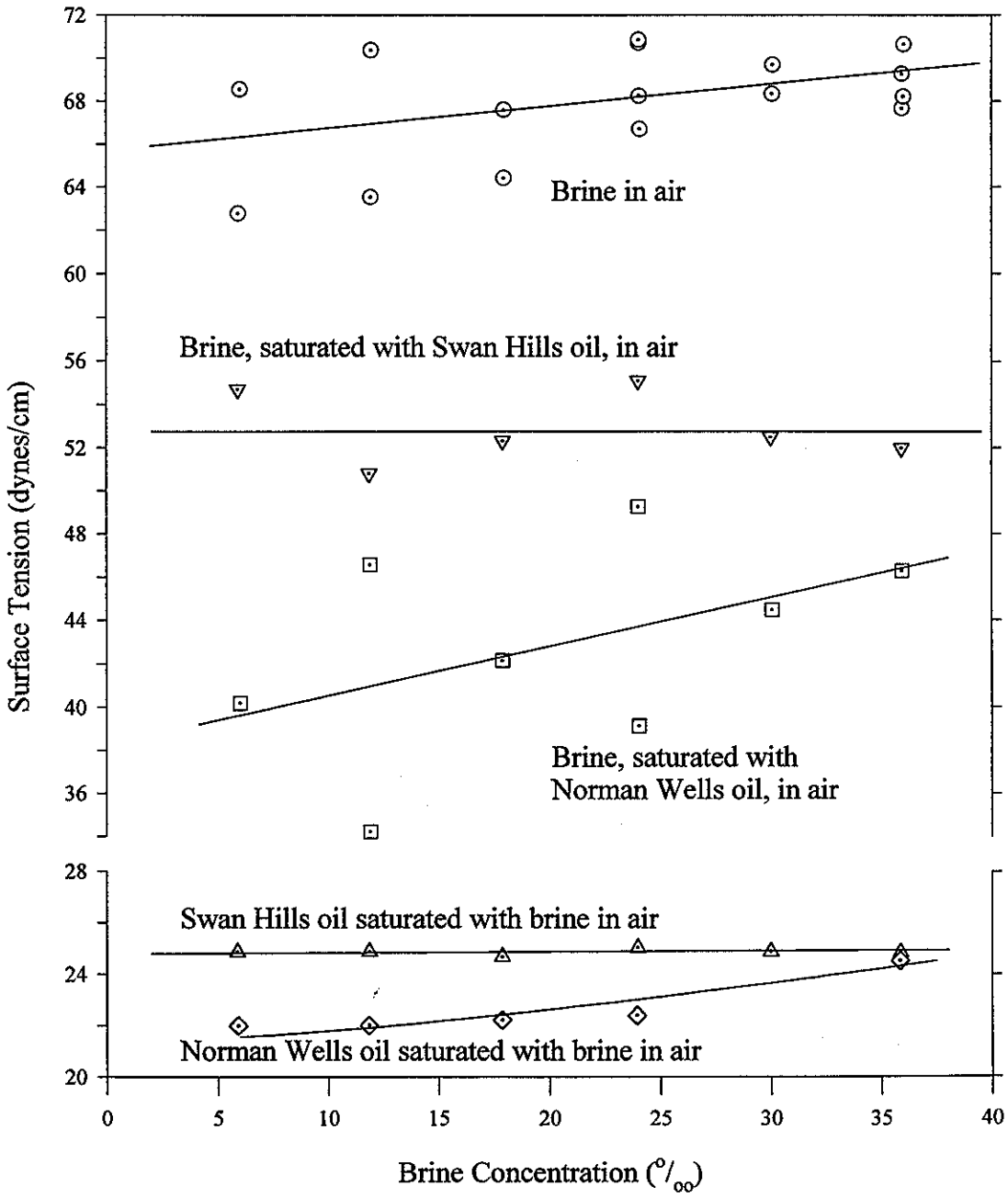

Figure 30 **Surface Tension *vs* Brine Concentration from Ring Detachment Method**

Movement of Oil Drops

The results showed that the angle that initiated motion correlated to the oil bubble mass. Using Equation (11), the results for Swan Hills and Norman Wells oils are shown in Figures 36 and 37 respectively. The author reports the best fit lines as:

For Swan Hills crude: $R' = 48.5 M_o^{0.486}$ (13)

For Norman Wells crude: $R' = 23.4 M_o^{0.659}$ (14)

A regression of the data suggests that the best fit values are:

For Swan Hills crude: $R' = 58.3 M_o^{0.461}$ ($r^2 \approx 0.828$)

For Norman Wells crude: $R' = 23.8 M_o^{0.785}$ ($r^2 \approx 0.785$)

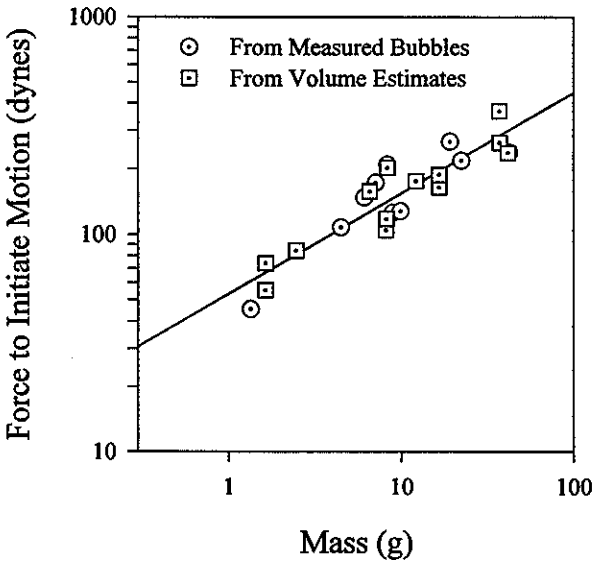

Figure 36 **Force to Initiate Motion *vs* Mass for Swan Hills Crude**

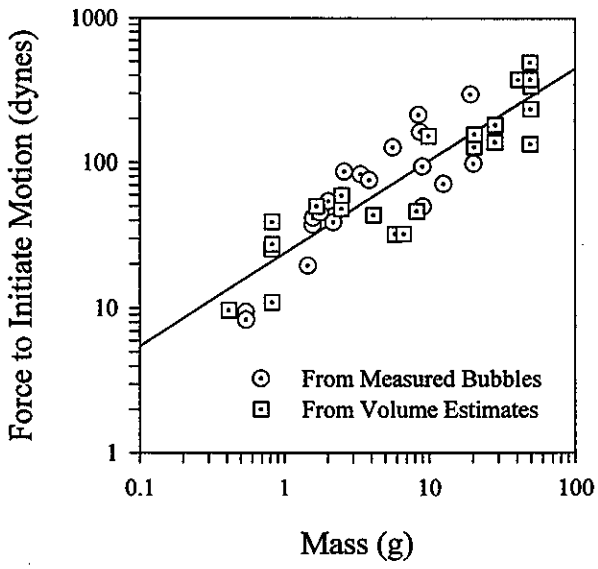

Figure 37 **Force to Initiate Motion *vs* Mass for Norman Wells Crude**

Surface Tension Limits of Slick Thicknesses

The results of the author's calculations are shown in Tables C-1 and C-2 for the Swan Hills and Norman Wells crude oils respectively. Rosenegger notes that the saturated surface tensions measured using the ring detachment technique are taken from the best-fit lines on Figure 30. The saturated solutions were prepared by allowing brine-oil mixtures to sit for 24 hours in a sealed container to prevent oil weathering. As the measurements were performed at room temperature, a temperature correction was applied to both the brine and the oil surface tensions, as shown in the

tables. No reference was given for the temperature corrections. The author also notes that his measured surface tension differed from that reported by Adamson, 1960. The values shown on the tables have been modified "to account for the 5% error" between the author's and Adamson's values. The source of this discrepancy is unclear.

Extracted from **Table C-1 Data Used for Calculating the Spreading Coefficients for Swan Hills Crude**

Salinity	σ'_{water}	σ'_{oil}	σ'_{water} (TC)[a]	σ'_{oil} (TC)[b]	$\sigma_{water/oil}$[c]	S'	σ''_{water} (TC)[d]	S''[e]
‰	dynes/cm	dynes/cm	dynes/cm	dynes/cm	dynes/cm	dynes/cm	dynes/cm	dynes/cm
6	55.6	26.2	60.0	29.0	26.0	5.0	58.7	3.7
12	55.6	26.2	60.0	29.0	26.3	4.7	58.7	3.4
18	55.6	26.2	60.0	29.0	26.6	4.4	58.7	3.1
24	55.6	26.2	60.0	29.0	26.9	4.1	58.7	2.8
30	55.6	26.2	60.0	29.0	27.2	3.8	58.7	2.5
36	55.6	26.2	60.0	29.0	27.5	3.5	58.7	2.2

[a]Temperature corrected (to 0°C) using $\sigma'_{water} = \sigma_{water} - 0.16\,\Delta T$
[b]Temperature corrected (to 0°C) using $\sigma'_{oil} = \sigma_{oil} - 0.1\,\Delta T$
[c]Calculated using Equation (9) with $\Phi = 0.832$
[d]Sample aged one week
[e]Aged sample, calculated as: $S'' = \sigma''_{water}\,(TC) - \sigma'_{oil}\,(TC) - \sigma_{water/oil}$

Extracted from **Table C-2 Data Used for Calculating the Spreading Coefficients for Norman Wells Crude**

Salinity	σ'_{water}	σ'_{oil}	σ'_{water} (TC)[a]	σ'_{oil} (TC)[b]	$\sigma_{water/oil}$[c]	S'	t_e
‰	dynes/cm	dynes/cm	dynes/cm	dynes/cm	dynes/cm	dynes/cm	cm
6	41.9	23.2	46.1	25.9	26.4	-6.2	0.29
12	43.2	23.2	47.4	25.9	26.7	-5.2	0.27
18	44.4	23.4	48.6	26.1	27.0	-4.5	0.25
24	45.7	23.6	49.9	26.3	27.3	-3.7	0.22
30	46.9	24.7	51.1	27.4	27.5	-3.8	0.22
36	48.2	26.9	52.4	29.6	27.8	-5.0	0.25

[a]Temperature corrected (to 0°C) using $\sigma'_{water} = \sigma_{water} - 0.16\,\Delta T$
[b]Temperature corrected (to 0°C) using $\sigma'_{oil} = \sigma_{oil} - 0.1\,\Delta T$
[c]Calculated using Equation (9) with $\Phi = 0.831$

Note that the spreading coefficient for the Swan Hills crude is positive. The author remarks that aging would lower the spreading coefficient as do the surfactants naturally present in the oil. Finally, he states that even if a negative spreading coefficient had been measured at 0°C for the Swan Hills samples, the terminal spreading thickness predicted by Equations (15) through (17) would not be useful due to the high pour point (-9.5°C) of the oil.

The author regards the thickness calculated for the Norman Wells crude as a minimum, and expects that, as the oil weathers or as temperatures decrease, the equilibrium spreading thickness would increase.

Solute Distribution

The author reports the salt content of 22 crude oils, shown as a frequency histogram in Figure 39. This work was not performed by the author and is of unknown origin, and the salt analysis technique is referred to only as the "Blair Method". From the average of these salt contents and some sample calculations based on an underwater well blowout of 1500 bbl, the author concludes that an "average" blowout would result in an under-ice oil slick of 3.0×10^4 m^2, 8 mm thick with a bulk salt concentration of 0.08 $^{o}/_{oo}$. He further concludes that this salt concentration is not sufficient to rot the under-ice surface. Also, since the salt is more likely to be dissolved in dispersed water droplets than in the oil, he suggests that most of the salt would be released to the water column during the oil's ascent.

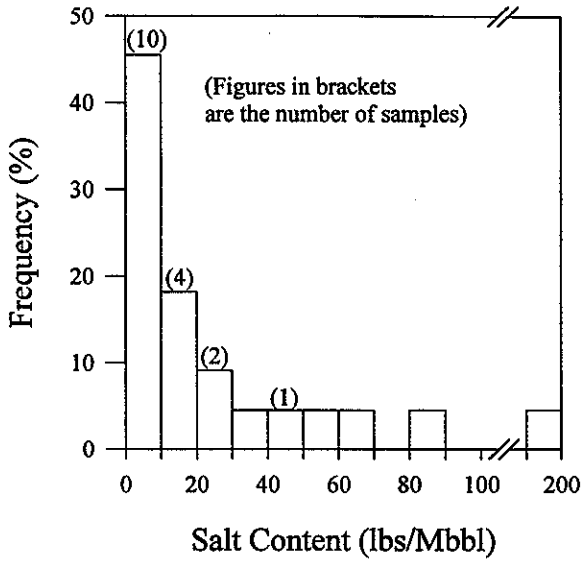

Figure 39 **Histogram of Salt Content from 22 Locations**

Oil Penetration

The author performed some sample calculations to evaluate the migration of small oil drops into brine channels based on reported channel sizes (Assur, 1958 and Eide and Martin, 1975). From Anderson, 1960, the author reports that the pressure drop across a circular brine channel opening, that is the pressure required to penetrate the meniscus, is given by:

$$\Delta P = \left(\frac{2\sigma}{r}\right)\cos\theta,$$

where r is the radius of the capillary, σ is the oil-ice interfacial tension, and θ is the contact angle. Assuming σ to be 25 dynes/cm and θ as 150°, then ΔP is a function of the diameter, r, of the capillary opening:

r (mm)	0.1	0.2	0.5	0.7
ΔP (dyne/cm^2)	4330	2167	866	617

Note that the pressure drops, ΔP, are negative, which is interpreted as a resistance to flow up the capillary.

The author includes a sample calculation of the pressure differential across an oil bubble at a capillary mouth. He presumes that the bubble is 8 mm thick and that the specific gravity of the

oil is 0.81. The author states that this gives a pressure drop of 636 dynes/cm^2 at the interface between oil and ice. He concludes that, when the radius of a capillary orifice expands to approximately 0.7 mm, which would perhaps happen during a thaw, an 8-mm thick layer of oil beneath the ice would begin to penetrate into such an opening. However, the source of the author's buoyancy calculations is unclear. By comparison, Equation (11) with $\alpha = 90°$ gives the buoyant force of approximately 165 dynes/cm^2 on a 1 cm^2 area of oil 8 mm thick. Using Equation (11), the oil layer would have to be slightly less than four times the author's reported value, 30 mm, before oil would be able to travel into a brine channel with a radius of 0.7 mm.

From these calculations, the author concludes that significant penetration of oil into ice would not occur except when brine drainage channels are oversized or during the spring melt as the brine channels open.

BOSS Critique

The author presents a catalogue of original surface tension measurements and also reports a number of other studies from unknown sources pertaining to oil behaviour in cold water. The author notes that the measurements of the interfacial tensions by the sessile drop technique are highly variable, with errors of at least 30%. By contrast, the values measured by the ring detachment method are much more reliable, with an estimated error of 10%.

The force required for motion of oil droplets on the underside of an ice sheet should be calculated from the regression values evaluated for this review, not the values reported by the author. In addition, the regressions had only a moderate level of correlation; the errors in the work should be considered to be approximately 25%. As the force is expressed as an exponential function, these errors become very large for larger masses of oil, and should thus be used with caution.

The spreading limits calculated by Equations (15) to (17) are reported with little comment. As no spreading experiments were presented to validate the calculated values, it is impossible to evaluate their applicability.

The author argues that little salt will be present as a solute in oil and will not contribute to under-ice rot. As neither the source of the author's data nor the locations from which the samples were taken are given, however, the applicability of these conclusions cannot be determined from this study.

Finally, the minimum thickness that oil must be in order to penetrate into a brine channel is calculated. While it appears that the quantitative thickness reported by the author is incorrect, it seems that his conclusions that oil will migrate only through wide brine channels, such as those during spring melt, are borne out by the work of other authors.

T.J. McMinn, *Crude Oil Behaviour on Arctic Winter Ice,* Project 734108, United States Coast Guard, Washington, D.C., 75 p., 1972.

Summary

The spreading of small spills of oil on snow and ice was investigated in Arctic mid-winter conditions. The aging of oil and the effects of snow were also examined.

"Oil spreading over ice and snow is dominated by gravity and inertia forces. Spreading rate is independent of the properties of the oil and is not affected by temperature. Terminal pool size of a known volume of oil is, however, indirectly related to temperature [in that the final area is a function of the 'effective surface roughness' which, in turn, is a function of temperature.]"

"Snow tends to combine with pooled oil until the oil is effectively saturated with snow crystals. The resulting mixture may be as high as 80% snow. After saturation (which can happen in a few hours) additional snow covers the oil making visual detection of areal extent impossible.... Absorbtion of [warm] oil into the snow or ice surface is minimal." [Note: the author used 16°C oil in all experiments].

"The winter aging rate [of oil] is significant and should not be discounted.... [T]he density of crude oil will increase with time, eventually becoming more dense than sea ice (0.901 g/mL) and sea water (1.04 g/mL)."

Objective

This study developed and evaluated a model for oil spreading on snow-covered and windswept ice. Oil aging in snow and on bare ice was also examined experimentally. Cleanup techniques (burning and the use of sorbents and dispersants) were also discussed, but are not covered in this review.

Theory

The author presents a theory based on the three-phase spreading model of Fay, 1969 (hereafter, the Fay-Hoult equations), with modifications for continually increasing spill volume (to simulate a pipeline break or tanker seepage) and spreading in snow.

The gravitational force, F_g, is related to the hydrostatic pressure, P, by:

$$F_g = \int_o^h P\,dA,$$

where $P = \rho g h$. The slick area is defined as $A = 2\pi r h$, with $dA = 2\pi r dh$.

Therefore:

$$F_g = r\pi g h^2[\rho]. \qquad (1)$$

[Note that the author omits the density term (ρ) in Equation (1). This appears to be a simple typographical error; the derived expressions are correct.] Surface tension, σ, acts as a second spreading force, given as:

$$F_s = \sigma_r(2\pi r),$$

where σ_r is "the resultant surface tension vector when oil interfaces an ice surface" which acts over the slick circumference. The thickness at which these two driving forces is equal, when surface tension forces begin to dominate the spreading, is:

$$h_c = \sqrt{\frac{2\sigma_r}{\rho g}}. \tag{2}$$

The author gives a similar analysis for the retarding forces of inertia and viscosity. The inertial force is:

$$F_i = m\frac{dv}{dt},$$

where the oil mass, $m = V\rho = \pi r^2 h\rho$ and the slick edge spreading velocity, $v = r/t$.

Substituting,

$$F_i = \frac{\pi\rho r^3 h}{t^2}. \tag{3}$$

The viscous force is derived from the definition of (dynamic) viscosity, μ:

$$\mu = \frac{\tau}{\left(\frac{dv}{dh}\right)},$$

where $\tau = F_\mu/\pi r^2$ and $dv/dh = v/h$. Velocity, v, is assumed to be r/t. The viscosisty term can therefore be written as:

$$\mu = \frac{F_\mu\, ht}{\pi r^3}.$$

Note that the author had this as r^{-2}, which again was probably a typographical error. The corrected form is shown above. Solving for the viscous force, F_μ, gives:

$$F_\mu = \frac{\pi\mu r^3}{ht}. \tag{4}$$

The ratio of inertial and viscous forces, Equation (3), divided by Equation (4), $\rho h^2/\mu t$, depends on the slick thickness and inversely on the time since the spill. At the small times, the ratio is large and the inertial term dominates the resistive forces. At later times, the viscous force comes to be more important than the inertial force.

The author wished to model spills from a broken pipeline or a slowly leaking surface vessel. The conventional Fay-Hoult equations are therefore modified to account for an increasing spill volume. For an average flowrate, $\overline{Q}$, the total volume spilled after time, t, is:

$$V_t = \bar{Q}t. \tag{5}$$

However, the total volume is also:

$$V_t = \pi r^2 h. \tag{6}$$

Thus:

$$r = \sqrt{\frac{\bar{Q}t}{\pi h}}. \tag{7}$$

To quantify the roughness of the snow/ice surface, the author introduces z_0, the effective roughness height. The author defines this quantity as a function of surface roughness, ice permeability, and oil viscosity. Citing a private communication with D.P. Hoult, the author indicates that the effective roughness heights have been found to vary widely, but in practice are seldom less than 0.1 ft. or 3 cm.

The author concludes that spreading will stop when the slick thickness is approximately equal to z_0. Substituting this into Equation (7), the maximum predicted radius of the slick is:

$$r_m \approx \sqrt{\frac{\bar{Q}t}{\pi z_0}}. \tag{8}$$

In Figure 6, Equation (8) is plotted for a range of roughness heights. Although typical roughness heights were unknown at the time of this work, the estimated lower limit for z_0 of 3 cm was used by the author to determine final spill areas.

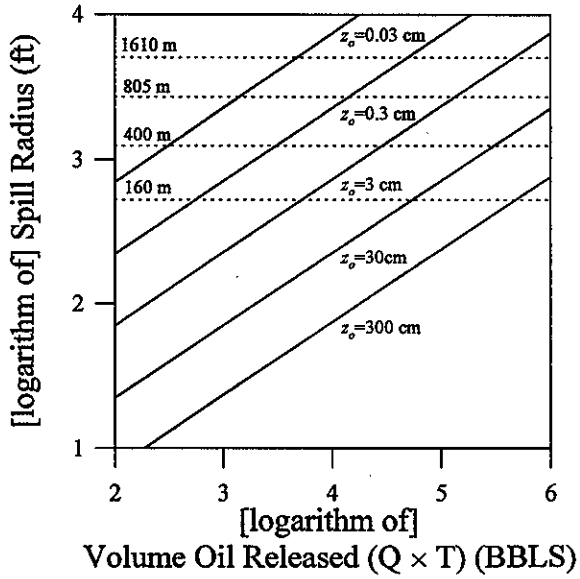

Figure 6 Maximal Area Coverage - Ice Spill

The author reports a value for h_c from Equation (2) for Prudhoe Bay crude (described in the Method section of this review). To estimate the value for the resultant surface tension, σ_r, the surface tension vector tangent to the liquid surface at the liquid-solid interface, the author uses the formula:

$$\sigma_r = \sigma(1+\cos\theta). \tag{8}$$

For σ, a value of 30 dynes/cm is used (no reference is given but this is the value listed in Whiticar *et al.*, 1992). The author arbitrarily assigns a value of 45° to θ as a "conservative" estimate. This gives a value of 0.342 cm for h_c. Note that the contact angles of similar oils, such as North Sea Brent, range from 20 to 25° (Liukkonen *et al.*, 1995), which results in a critical height of 0.365 cm. A contact angle of 0° gives a maximum critical height of 0.371 cm.

However, since the author has assumed that the slick will stop spreading when the oil thickness reaches the surface roughness height, z_0, assumed to be at least 3 cm, the author predicts that the transition to spreading caused by surface tension is never reached and that gravity is the only significant driving force. In addition, "since the final thickness of an oil spill on ice is quite large

compared to an oil spill on water, and as previously discussed the ratio of inertia to viscous retarding forces vary as h^2, we can also make the assumption that viscous retarding forces are negligible contributors to the resulting retarding force".

Therefore, the author concludes that the gravity-inertial phase is the only important spreading mechanism for oil on ice. Equating the two forces [Equations (1) and (3)] gives:

$$\pi r \rho g h^2 = \frac{\pi \rho r^3 h}{t^2}. \tag{10}$$

Solving Equations (5) and (6), for the oil slick height, h, gives:

$$h = \frac{\overline{Q} t}{\pi r^2}. \tag{11}$$

Substituting this expression for variable volume into Equation (10) and solving for the slick radius gives:

$$r = \left(\frac{g \overline{Q}}{\pi} \right)^{1/4} t^{3/4}. \tag{12}$$

The author's spreading model is thus: spreading progresses as Equation (12) until the slick thickness reaches the effective roughness height, at which point the spreading stops.

Non-dimensionalization of Data [From Appendix B]

The experimental data was non-dimensionalized in length (L) and time (T) by apportioning the constants in Q and g into distance and time fractions.

Dimensionally $\quad Q = L^3 T^{-1}$
and $\quad g = L T^{-2}$.

To non-dimensionalize time and length:

$$T_{nd} = T_{data} / Q^x g^y, \quad \text{where } Q^x g^y = T, \text{ and} \tag{C1}$$

$$L_{nd} = L_{data} / Q^a g^b, \quad \text{where } Q^a g^b = L. \tag{C2}$$

Solving this system of equations gives: $x = 1/5$, $y = -3/5$, $a = 2/5$, and $b = -1/5$.

Thus:

$$T_{nd} = T_{data} / (Q/g^3)^{0.2}, \tag{C3}$$

and

$$L_{nd} = L_{data} / (Q^2/g)^{0.2}. \tag{C4}$$

Substituting $Q = 0.172$ ft.^{3}/s (see Method section) and $g = 32.2$ ft./s^2, (C3) and (C4) become:

$$T_{nd} = T_{data} / 0.08758, \tag{C3}$$

and

$$L_{nd} = L_{data} / 0.24707. \tag{C4}$$

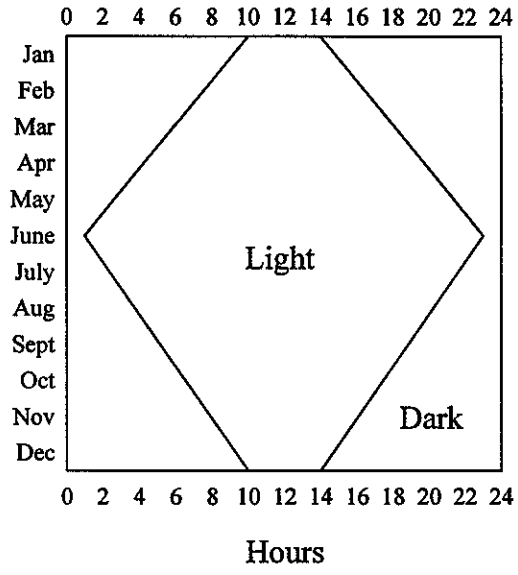

Figure 1 Port Clarence Daylight Chart

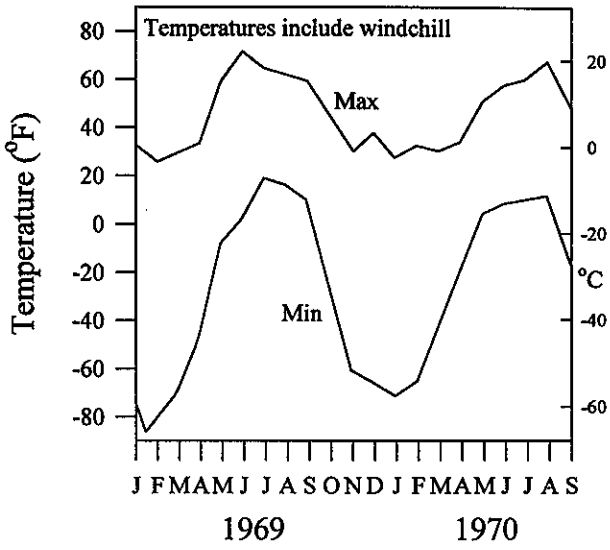

Figure 2 Port Clarence Temperature Profile

Method

To duplicate the environmental areas where crude oil would most likely be spilled, a test site was selected that was close to 1) bay ice, 2) pack ice, and 3) tundra. The tests were conducted in Port Clarence Bay, 65° 15`N, 160° 55`W, a salt water bay on the Bering Sea.
Year-round site conditions are shown in Figures 1 and 2. The experimental work was conducted in January,1972.

The spreading experiments were conducted on both windswept and snow-covered ice. Surface 1 was stationary ice (0.6 to 1 m thick) and covered with 200 mm of snow. Surface 2 was the windswept surface of a fresh water lake, located just inland (~300 m) from the Bering Sea. The fresh-water site was chosen because it was the only ice surface completely bare of a snow cover. At the sites chosen, the ice was as level as possible.

Oil was contained at the site in an insulated 100-gal (378.5-L) oil storage tank mounted on a sled. The rate of oil discharge from the tank was controlled by blowing compressed air into the storage tank. Oil was discharged through a line attached to a 3.7-m boom.

Aluminum stakes were driven into the ice surfaces at 30-cm intervals radially from the point of discharge. The crude oil was poured into the centre of the stakes at a known rate of flow. Spreading was recorded with an 8-mm camera. The spreading rate was determined by analyzing the film. The average discharge rate was 0.172 ft^3/s (4.9 L/s).

Four slicks were created - three on the snow surface and one on bare ice. The oil was kept in the storage tank at 58°F (14°C) before pouring. The oil used was a North Slope (Prudhoe Bay) crude

oil, with properties shown in Table R.1 (from Appendix C, reprinted from the *Oil and Gas Journal*).

For the oil-weathering experiments, two oil pools of 50 gal (189.3 L), 10 ft. (3.1 m) in diameter, were used for collecting samples. One spill was discharged on smooth ice, the other on a snow-covered ice surface. Samples were collected once a day in two 8-oz. (237-mL) aliquots, and stored in Teflon-gasket Nalgene bottles. The first aliquot was measured for viscosity using a Brookfield LVF rotational viscometer. The second sample was sent to the Exxon Research and Engineering Company in Bayton, Texas, for analysis of density, boiling point distribution, ratio of water to oil, and ratio of saturates to aromatics. North Slope (Prudhoe Bay) crude was used in the aging pools, the same as for the spreading experiments.

Table R.1 Routine Analysis of Prudhoe Bay Crude Oil

Colour		brownish black	
Gravity	Specific	0.893	
	°API	27.0	
Pour Point		15°F	(-9.4°C)
Viscosity	77°F (25°C)	111 s (Saybolt Universal)	(22.7 cSt)
	100°F (38°C)	84 s (Saybolt Universal)	(16.6 cSt)
Sulphur %		0.82	
Nitrogen %		0.230	

[Note: fractionation data omitted]

Results

The raw spill data measured from the films is shown in Table 1, with the non-dimensionalized values shown in italics (constructed as previously described in the Theory section of this review). A log-log plot of the non-dimensionalized slick radius against time, as well as the predictions of Equation (12) are shown in Figure 7..

Table 1 Spreading Data [and non-dimensionalized data in italics from Appendix B]

Spill Radius			Time (seconds)							
(ft)	(m)	*(ND)*	Spill 1[a]		Spill 2[a]		Spill 3[a]		Spill 4[b]	
1	0.305	*4.1*	0.7	*8.0*	0.7	*8.0*	0.9	*10.3*	0.7	*8.0*
2	0.61	*8.1*	2.3	*26.3*	4.2	*50.0*	4.2	*50.0*	4.3	*49.1*
2.5	0.762	*10.1*	–	–	–	–	5.8	*66.2*	–	–
3	0.914	*12.1*	6.5	*74.2*	8.6	*98.2*	–	–	11.3	*129.0*
4	1.219	*16.2*	10.6	*121.0*	14	*159.9*	–	–	21.4	*244.4*
4.5	1.372	*18.2*	–	–	–	–	–	–	29.9	*341.4*
5	1.524	*20.2*	15.6	*178.1*	19.5	*222.7*	–	–	–	–
6	1.829	*24.3*	–	–	28.1	*380.9*	–	–	–	–

[a]Spilled on snow-covered ice (Surface 1).
[b]Spilled on bare ice (Surface 2).

The author observes that the linear correlation of slick radius and time supports the hypothesis of a single spreading phase. (A second phase would presumably cause a discontinuity or curvature in the relationship.) However, the rate of spreading predicted by the author's model does not agree well with the experimental results. The author's best-fit line (solid line through the data on Figure 7) is:

$$r = 1.3(Q^3 g)^{0.1} T^{1/2}.$$

[The linear regression line, shown as a dashed line through the data on Figure 7, gives the (very similar) result:

$$r = 1.2 Q^{0.31} g^{0.07} T^{0.45}.$$

The regression coefficient for the dashed line is: $r^2 = 0.943$.] Recall that Equation (12) gives exponents of *1/4* for Qg and *3/4* for t. The author claims that the mismatch between experimental results and Equation (12) is largely attributable to experimental error. However, a re-examination of Figure 7 indicates a significant discrepancy between theory and experiment which is clearly not simply statistical.

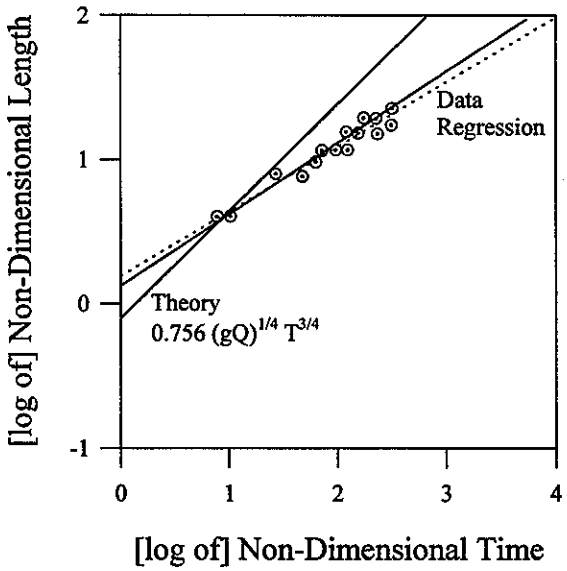

Figure 7 Spreading Rate - Winter Ice
(Q=0.172 ft^3/sec, g = 32.2 ft/sec^2)

Oil-Ice Interaction

When the warm oil [60°F (16°C)] was poured on snow, no migration of the oil into the ice was observed. The snow onto which the oil was poured was described as approximately 60% porous.

The author therefore assumed that some of the oil would migrate into the snow. However, little or no penetration of the oil into the snow was observed.

The snow/ice surface was between 5 and -15°F (-15 and -26°C) during all the tests. This was generally warmer than ambient temperatures and the author speculates that the snow/ice was warmed by the 29°F (-1.7°C) salt water underneath and by solar absorption.

Thus, when the oil was poured on the snow, an average temperature difference of 70°F (40°C) was created between the slick and the underlying surface. The author conjectures that the warmer oil layer immediately melted the top layer of snow or ice. This melt water was then absorbed into the colder snow to a distance of approximately 2 mm and refroze, blocking the channels in the surface, and forming an impermeable ice layer beneath the oil.

Effect of Blowing Snow

Snow blowing across the surface of the oil slicks tended to stick to the oil and sink. The oil and snow mixtures were "largely crystalline", up to 80% snow (by volume), and formed a dry, mechanically stable "mulch" at temperatures below the pour point of the oil [15°F (-9.5°C)].At warmer temperatures, however, the oil would flow or drip out of the oil-snow mixture.

Effects of Heavy Falling Snow

While the lightly blowing snow formed a "mulch" with the oil, much heavier snowfalls formed a compacted layer on top of the slick, which remained separated from the oil. The author theorizes that the heavy snowfall rapidly built-up a layer of snow upon the surface of the oil which compacted at the oil-snow interface. This compressed layer of snow formed a barrier to further incorporation of snow into the oil. The snow-mixing effects for two sample pools are shown in Figure 11.

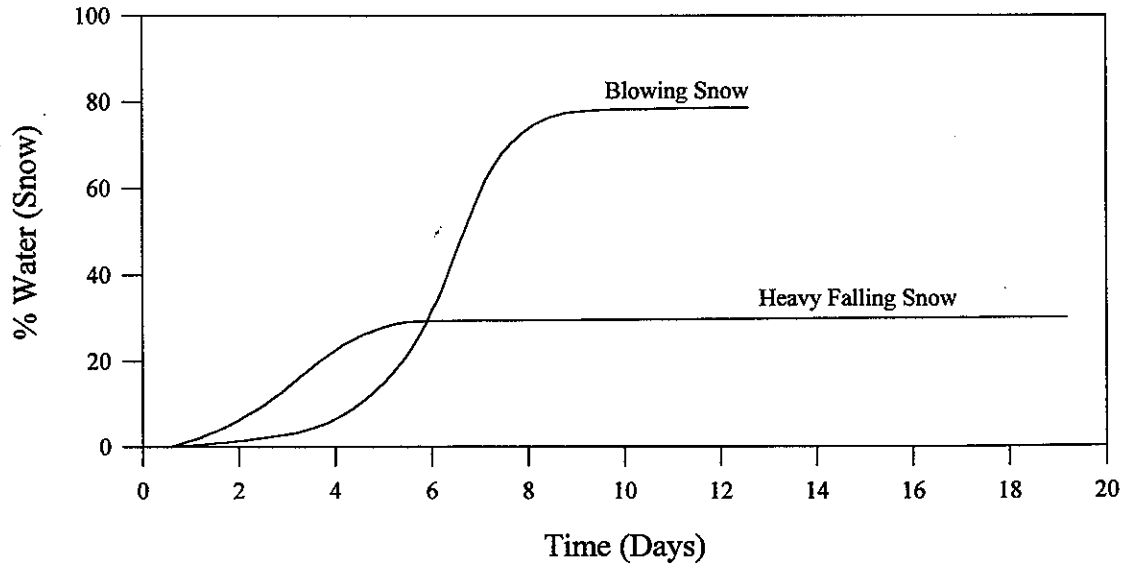

Figure 11 Water (Snow) Content of Oil-Snow Mixture

The author notes that the two curves in Figure 11 represent data from two different pools aged over different time periods and in different weather conditions. There was little initial mixing for the "blowing snow" results because a minimum amount of wind and blowing snow were present for the first four days of the spill. By day six, however, conditions had shifted to high winds and blowing snow. On day eight, a heavy snowfall occurred, resulting in a "leveling-off" of snow and oil mixing. The other oil slick ("Heavy Falling Snow" in Figure 11) was subjected to an extremely heavy snowfall the day after the spill and took approximately four days to reach equilibrium with the snow cover. The author speculates that the compressed, heavy snow layer prevented further mixing with the lighter, blowing snow.

The author points out the serious implications of these results for spill detection. These experiments indicated that a major spill, occurring during or before a winter storm, could become completely hidden under a snow layer in a matter of hours.

Oil Aging

Density, viscosity, and distillation fractions were measured over a period of days to observe the effects of weathering on the oil slicks. The effects of winter aging for the two oil pools, oil on ice and oil on snow, are shown in Figures 14 to 18.

The author notes that a) winter aging does occur, but at a much lower rate than in summer and, b) North Slope crudes will age to the density of sea ice (0.9010 g/mL) and further to that of sea water (1.030 g/mL) over a long period of time.

As shown in Figure 14, there was a substantial increase in the density of the oil aged on ice after the sixth day. A severe storm occurred on the seventh day with winds of more than 30 knots. The author concludes that high winds during the storm greatly increased the weathering rate of the oil.

The oil slick on snow was unaffected because the oil was protected by an 8 to 10 in. (20 to 25 cm) layer of snow. The oil pool on bare ice was not covered before the storm.

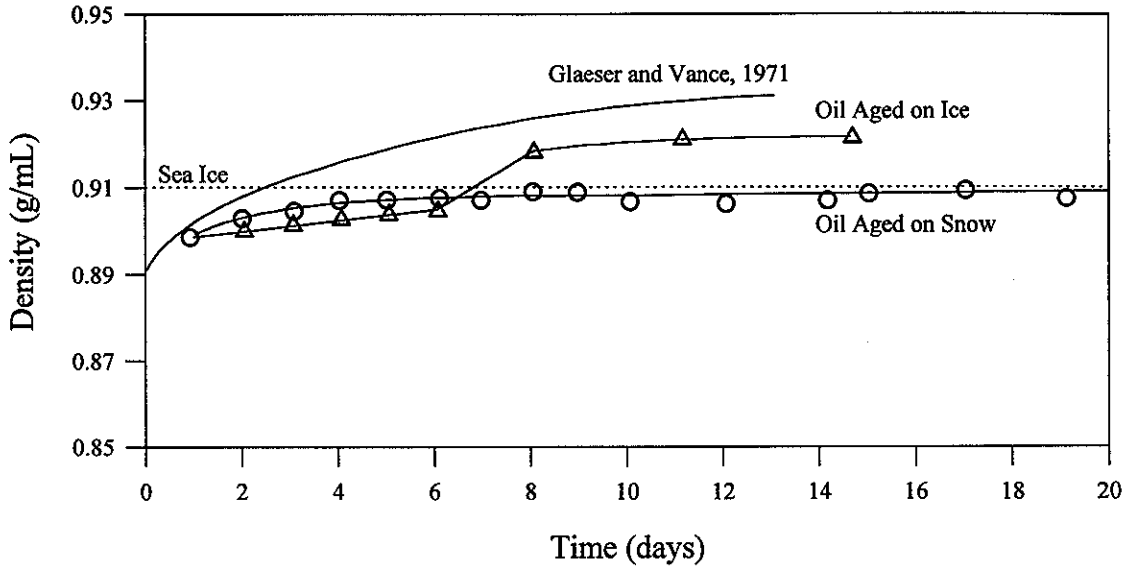

Figure 14 **Oil Density *versus* Time**

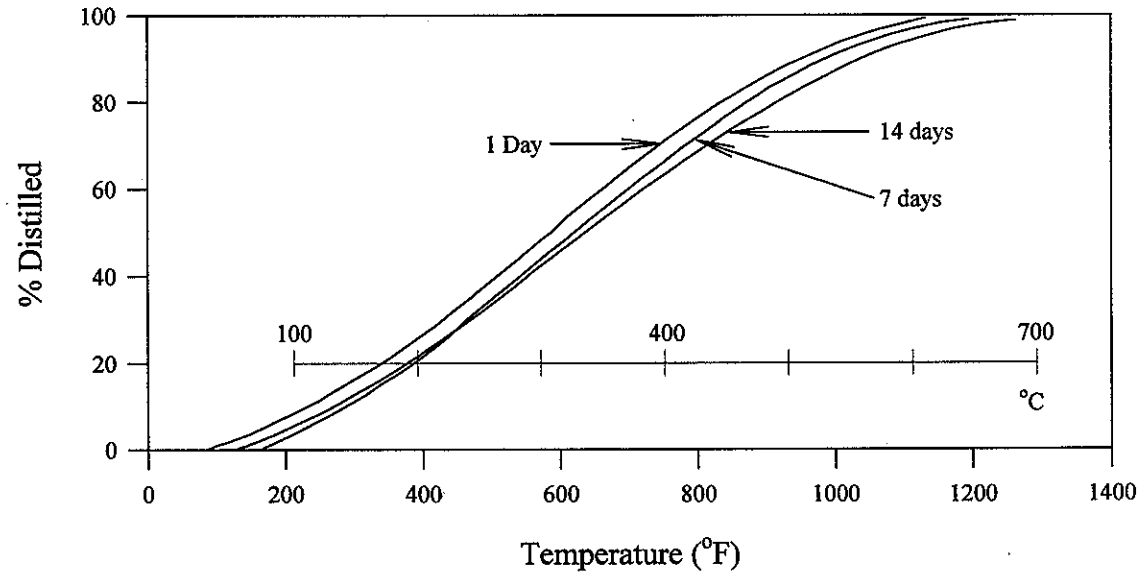

Figure 15 **Distillation Curve - Oil with Heavy Snow** [Oil Aged on Snow, Under Snow Cover]

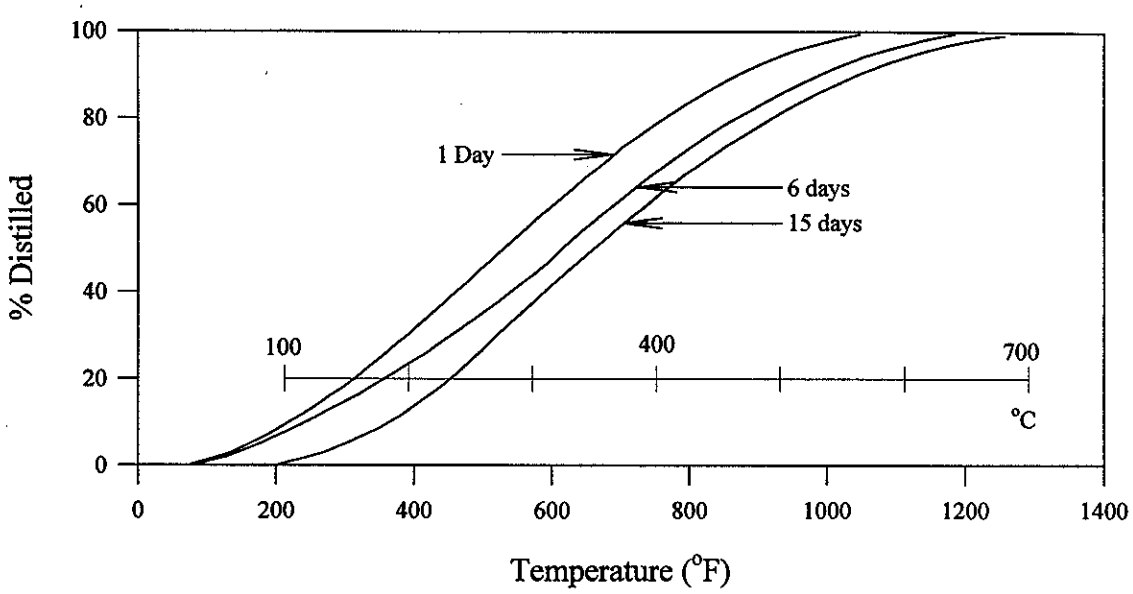

Figure 16 **Distillation Curve - Oil with Blowing Snow** [Oil Aged on Ice, Exposed]

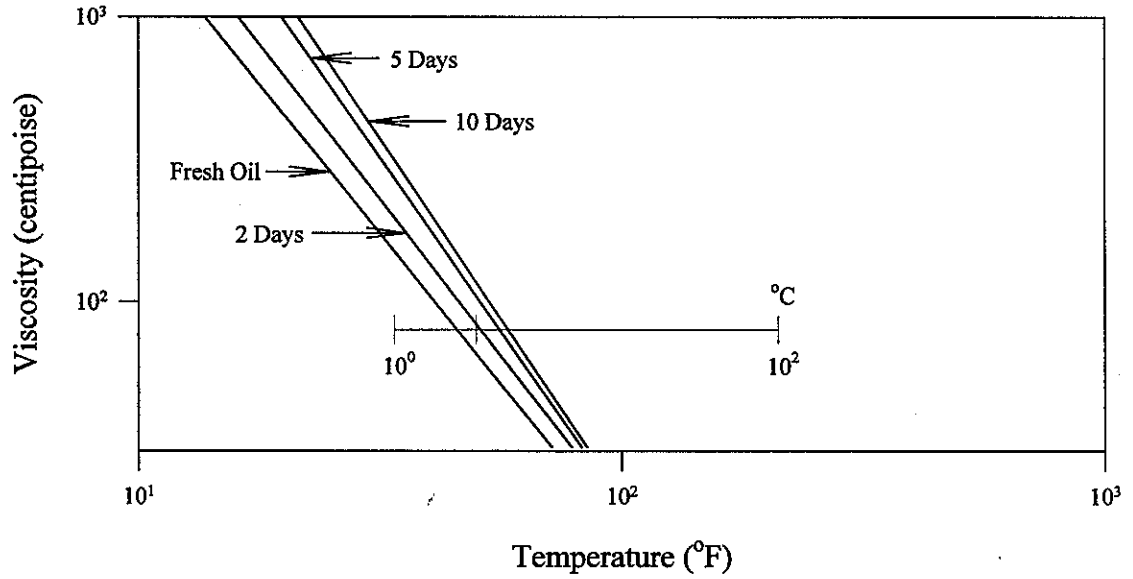

Figure 17 Oil Aged on Snow [Oil Aged on Snow, Under Snow Cover]
Absolute Viscosity *versus* Temperature

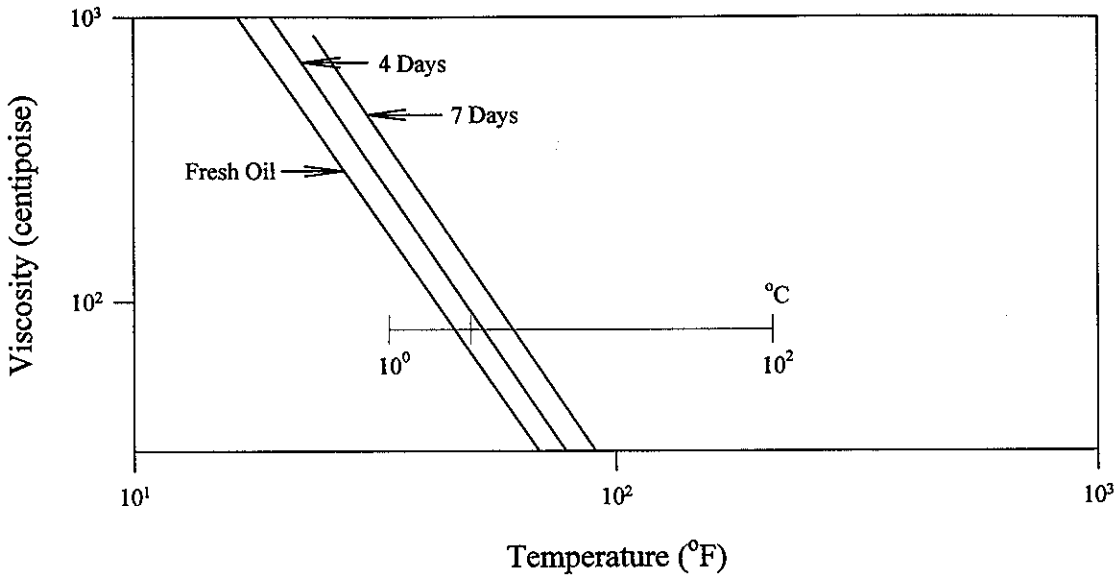

Figure 18 **Oil on Ice** [Oil Aged on Ice, Exposed] Absolute Viscosity *versus* Temperature

The increased rate of aging after the sixth day for the oil on ice is also apparent in Figures 15 and 16. The 15-day distillation curve is further to the right for the oil which weathered on bare ice, Figure 16, than for the oil which aged under snow, Figure 15, indicating a higher fraction of boiling point components, and thus a greater degree of weathering. The author also concludes that moderate wind velocities influence oil aging to a greater degree than moderate variations in temperature. The oil under the snow cover was significantly warmer (by 20 to 30°F or 11 to 17°C) than the exposed oil slick on ice (see Figure 19), but aged more slowly. As the author points out, the aging of this oil was also slowed by the trapping effect of the snow cap. He concludes that the oil continues to age even when covered by a thick layer of snow, but is significant only over long periods of time.

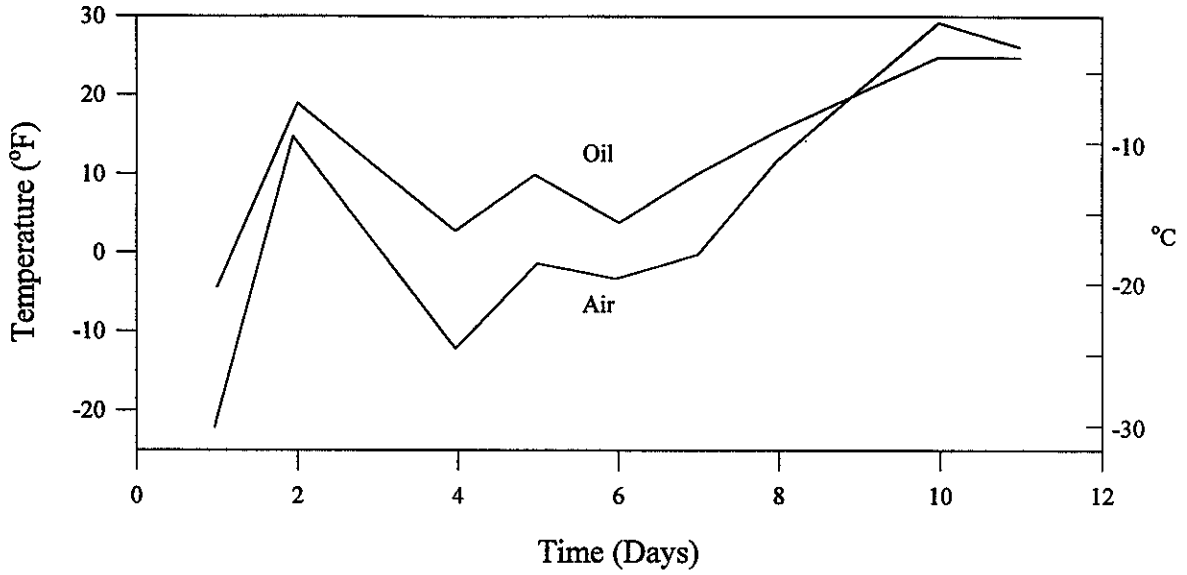

Figure 19 Oil Temperature *versus* Air Temperature
(Note: Oil covered by 7 in. [18 cm] snow)

BOSS Critique

As one of the first published studies of the spreading of oil on snow and ice, this paper (McMinn, 1972) is significant in several ways. Although the study was limited in scope, it presents considerable useful data with regard to oil spreading. Also, it is clear (from Figure 7) that the modified Fay-Hoult theory presented by the author does not appear to adequately describe the experimental results. Furthermore, the author makes a compelling case for the existence of only a single driving-retarding force regime for oil spreading on snow and ice. A scheme for predicting spill extent on snow and ice is presented, but not examined or experimentally validated.

Also important, although less quantified, are the author's findings for the mixture of snow with oil for both blowing and falling snow. The oil aging results are less useful (because of few statistics and uncontrolled environmental variables), although they provided the experimental design used by other authors in later work.

Dome Petroleum Ltd., *Oil and Gas Under Sea Ice*, Report CV-1, Canadian Offshore Oil Spill Research Association (COOSRA), Volumes 1 and 2, 286 p. and appendices, Calgary, Alberta, 1981.

Primary authors: I.A. Buist and D.F. Dickins

These results were also reported in:

D.F. Dickens, I.A. Buist, W.M. Pistruzak, "Dome Petroleum's Study of Oil and Gas Under Sea Ice", in *Proceedings of the 1981 International Oil Spill Conference*, American Petroleum Institute, Washington, D.C., pp 183-189, 1981.

I.A. Buist, W.M. Pistruzak, D.F. Dickins, "Dome Petroleum's Oil and Gas Undersea Ice Study", in *Proceedings of the Fourth Arctic Marine Oilspill Program Technical Seminar*, Environment Canada, Ottawa, Ontario, pp 647-686, 1981.

I.A. Buist, "Measured Behaviour of an Oil/Gas Plume Under Ice", in *Proceedings of a Workshop on In-Water-Large-Drops Sub-Sea Containment of Oil*, EE-18, University of Toronto, Institute for Environmental Studies, Toronto, Ontario, pp 55-62, 1981. This reports the plume measurements only. Figure 9.25 of this review presents the relevant data.

Summary

Three gas and oil blowouts under continuous ice cover were simulated in the field (McKinley Bay, Alaska) and the fate of the oil followed through to break-up of the ice sheet. Care was taken to ensure the discharges were "typical" and simulated a well-head blowout. Three trials were conducted: December, April and May.

"There were three basic configurations of oil and gas under the ice [after the blowout]: oil droplets; gas bubbles with a coating of oil; and large pools of oil underneath gas pockets. The oil droplet and gas bubble configurations predominated for the discharge under new flat ice and the oil pool configurations predominated for the discharge under older ice with under-ice undulations.

"Oil discharged under newly-formed 'flat' ice in December was found to exist mainly as discrete droplets, whereas oil [discharged in] April and May . . . tended to be concentrated in pools in under-ice undulations created by refrozen cracks and the insulating effect of surface snow drifts.

"The oil, shortly after it was discharged, was observed to have formed a water-in-oil emulsion. This emulsion was unstable.

"The oil was encapsulated by the growing ice sheet within 24 to 48 hours, even in May. The incorporation was not adversely affected by the presence of gas.

"The gas rose to the under-ice surface, and during the discharge in December, formed into a large bubble that domed and cracked the ice. This doming was not observed during the discharge under thicker ice in the spring.

"In spring, ...the oil appeared on the ice surface by two competing mechanisms: ablation and brine channel migration. Ablation was the main mechanism for the exposure of the oil discharged under newly formed flat ice in December. Brine channel migration....was responsible

for the appearance of most of the oil at the latter two [spring] discharge sites where significant oil pooling had occurred.

"By the time the ice sheet had rotted through and broken up, approximately 81% of the oil had appeared on the ice surface....The majority of the oil appeared in the period two weeks prior to breakup." Further, "the timing of the oil's appearance was related to the time of discharge. Oil spilled early in the winter appeared first.

"Oil pools on the surface melt water ranged in size up to 135 m^2 with the average oil pool being 1 - 5 m^2 in diameter at the December site and 10 - 20 m^2 at the spring discharge sites. The average slick thickness was estimated to be 1 cm... Oil on the ice surface lost most of its light ends through evaporation... The presence of oil on ice and in melt pools did not appreciably accelerate breakup of the ice sheet."

Objectives

This study simulated sub-sea blowouts in shallow water under first-year ice. Of particular interest was the behaviour of oil and gas mixtures when discharged under ice, the oil's behaviour in the ice sheet, its weathering behaviour, and the formation of water-in-oil emulsions.

Also discussed are oil and gas dispersion in the blowout plume, the efficacy of various cleanup techniques (particularly burning), and the capability of 1980 technology to clean up oil spilled from a sub-sea blowout under ice. These topics are not included in this review.

Method

In December, 1979 and April and May, 1980, three separate oil spills of approximately 6 m^3 each were discharged 8 km offshore into McKinley Bay in the Beaufort Sea. The oil used was Prudhoe Bay Crude (Atlantic Richfield Company, Alaska). The oil was released with compressed air to simulate a sub-sea blowout of natural gas in 20 m of water. In addition, just before the December oil spill, a "dry" run of compressed air alone was conducted.

The flowrates were 400 m^3/day of oil (2500 BOPD) at a gas-to-oil ratio of 200:1 m^3/m^3 (900 ft^3/bbl). Logan *et al.*, 1975 suggest that a typical flowrate for a Beaufort Sea well blowout is 398 m^3 of oil per day with a gas-to-oil ratio of 140:1. While the flowrates for the two spring runs are close to this "typical" Beaufort Sea blowout rate, the December run was approximately 500 m^3/day. The gas-to-oil ratio for the December and May blowouts was 50% higher than that specified by Logan *et al.*, 1975, but for the April discharge, it was much lower. In addition, air was used to purge the equipment after the oil/air blowout, which introduced considerable variability in the total amount of air released.

As well as the main air/oil releases, four small control volumes of pure oil and water-in-oil emulsions were pumped under the ice. These are described in Table 9.1 under columns labeled "Control".

The oil-release mechanism is described in detail in Volume 2, Appendix B of the Dome Report. This appears to have been the first use of this apparatus.

Before, during, and after each discharge, air, ice, and water conditions were measured with anemometers, current meters, thermistor chains, ice thickness profilers, salinometers, ice cores, and fluorometers. For the air-only release, ice deflection was recorded with an array of ice strainguages, a centrally located accelerometer, time-lapse photography, and a tiltmeter. For all the simulated blowouts and the air discharge, levels were checked with a survey rod before, during, and half an hour after the blowouts.

Extracted from **Table 9.1** **Dome Petroleum, 1981, Oil and Gas Discharges**

	Air Only	Simulated Blowout	Control	Simulated Blowout	Control	Control	Simulated Blowout
	12/17/79	12/18/79	12/19/79	4/10/80	4/11/80	4/12/80	5/2/80
Total Oil Discharged (m^3)	0	5.85	0.14[a]	6.56	0.08	0.16[a]	6.8
Total Air Discharged (m^3)	950	1711	0	435	0	0	1219
Duration of Oil Flow (min)	-	17	-	24	-	-	25.5
Duration of Air Flow (min)	-	36	-	32.5	-	-	30
Mean Oil Flow Rate (m^3/min.)	0	0.34	-	0.270	-	-	0.267
Mean Air Flow Rate (m^3/min.)	48	48	-	7.1	-	-	48
Gas to Oil Ratio	-	210 (292[b])	-	25 (60[b])	-	-	180 (224[b])
Oil T (°C) in Tank	-	+39 °C	-	+36 °C	-	-	+34 °C
Oil/Air T (°C) at exit	0	+25 °C	-	+25 °C	-	-	+20 °C

[a] Control Discharges were 60% water.

[b] With "air blowback taken into account". Air was used to flush the oil lines for 3 to 4 minutes following the simultaneous air and oil release. The "Total Air Discharged" entries do not include this extra purge gas.

For the December events (the air only and first oil/air discharges), broken ice conditions were simulated by drilling a 20-m square grid of 12-cm auger holes on 2-m centres. Several 4 m^2 holes were also cut within 10 m of the centre and the ice blocks removed.

Before and after each survey, divers with a TV system conducted under-ice surveys to map the ice and record the distribution of oil and gas. Divers also provided qualitative descriptions of the oil and gas under the ice. Samples of the under-ice oil were collected. Ice cores were taken in January, February, June, and July.

Ice ablation was measured by coring and depth gauges. Melt, drainage, and pool formation were recorded photographically. A 100-L pool of oil was monitored for two weeks in June to provide oil-weathering data.

Results

Oil Analysis

The Prudhoe Bay crude was analyzed for density$_{20}$°$_C$, viscosity, pour point, flash and burn points, and chemical composition. (Mackay, 1980 describes the test methods in detail.) Tests were also carried out for lab-weathered samples (volume reductions of 10.4 and 16%).

Extracted from **Tables 9.2** and **9.3**

Volume % Weathered	Density (g/mL @ 20°C)	Viscosity (mPas) 0°C	15°C	25°C	Pour Point (°C)	IBP (°C)	Flash Point (°C)	Fire Point (°C)
For December and April discharges								
0	0.884	50	26	17	-27	67	30	35
10.4	[a]	110	62	38	[a]	[a]	[a]	[a]
16	0.910	204	105	61	-3	192	84	91
For May discharge								
0	0.885	75.5	48.5	29.5				

[a]There appears to have been a typographical error in Table 9.2 of the Dome Report. The values given for the 10.4% oil are identical to those for the unweathered oil. The viscosity numbers were taken from Figure 9.28 (reproduced below).

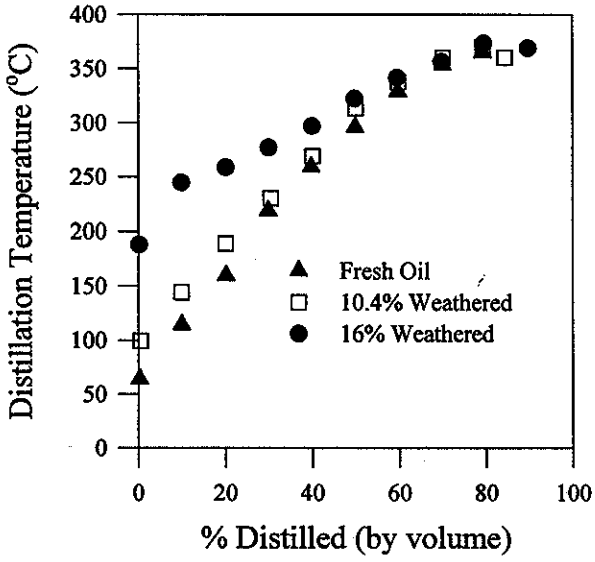

Figure 9.27 Distillation Curves for Prudhoe Bay Crude Oil

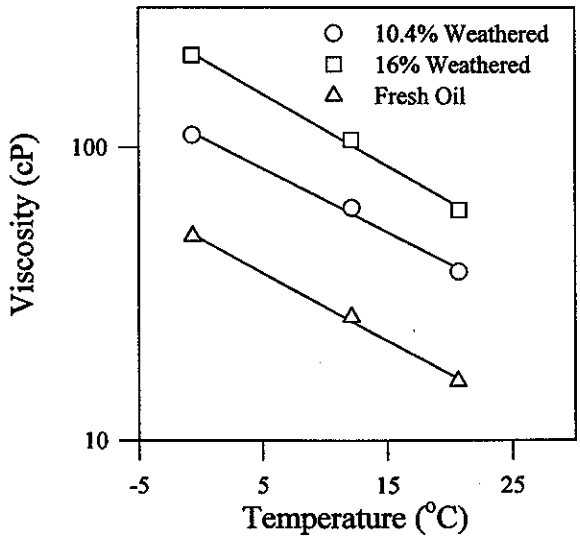

Figure 9.28 Viscosity of Prudhoe Bay Crude Oil as a Function of Temperature

On the basis of the density and a comparison of GC traces (although the spectrum for the oil used in May is not shown), the authors remark that they found no difference between the two batches of Prudhoe Bay crude, other than for viscosity. They note that the differences in the viscosities were possibly due to measurement error, implying an uncertainty of at least 75%.

They conclude that, as Prudhoe Bay crude oil weathers, the viscosity, density, pour point, and flash and fire points all increase, while the aqueous solubility decreases.

Air/Ice Interaction

During the air-only discharge (12/17/79), over a 45-minute period, an air bubble formed 65 m from the discharge site, which heaved the ice sheet 75 cm up at the centre of the bubble. The ice thickness around the bubble is reported as 58.5 cm with a surrounding mean ice thickness of 62.4 cm. The bubble was circular, 40 m in diameter, and ended abruptly, from which the authors concluded that there was a circumferential crack pattern around the bubble perimeter. A radial pattern of 1- to 2-cm wide cracks appeared at the centre of the bubble. Venting air was observed but no water spray was visible.

One hour after the discharge and 15 minutes after the bubble had formed, a 12-cm hole was drilled through the ice at the centre of the bubble. A 3-m "geyser" of air and water lasted for 5 to 6 minutes, during which time the bubble collapsed. The following day, it was observed that the ice surface had collapsed and was within 5 cm of its original level. The authors note that the ice fractures were not visible.

One day after the air-only event and in the same location, similar results were observed during the air/oil discharge with a maximum ice rise of 21 cm. The much-reduced bubble size was presumably due to venting through the cracks and holes caused by the discharge the day before.

The April and May discharges under 164 to 185 cm of ice resulted in much smaller vertical heaves, approximately 1 to 2 cm over the discharge point. No ice 'bubble,' or fractures were observed.

The authors compare the experimental results with the thin plate calculations of Topham, 1977, and conclude that the fracture radius is so sensitive to bubble depth that any uncertainty in ice properties makes prediction of failure difficult. Nevertheless, they state that ice less than 1 m thick would be likely to form gas bubble fractures. They point out that later in the winter, when ice is thicker, larger bubbles are required to fracture the ice sheet. Later in winter, however, the under-ice surface is much less regular, precluding the formation of large bubbles. The authors conclude that failure of ice sheets thicker than one meter is improbable, even if a much higher gas flow rate occurred.

The authors assume that the under-ice gas pressure is equal to the hydrostatic head pressure of 1 psig. From this and simple assumptions about the bubble shape, they estimate that roughly 50% of the gas from the air-only discharge and 10% from the oil/air simulation was trapped in the large bubble. They argue that most of the remaining gas vented through the ice and escaped, leaving less than 20% in small bubbles under the ice.

Air/Oil Interaction Under Ice

In the December discharge, with a smooth under-ice surface, a fairly uniform distribution of oil-coated air bubbles is reported. The oil coated the air bubbles in thin amber-coloured films less than 1 mm thick. Small "flecks" of oil were observed which the authors concluded had a distinctly weathered appearance. The largest concentration observed under the ice sheet after the December discharge was an 8-cm bubble of air coated with a very thin film of oil at the air-water interface. The ice undersurface was covered with many oil droplets a few millimetres in diameter. The authors report that these small droplets had migrated into the ice surface.

At the April spill, which was discharged with much less air than the December or May spill, the under-ice surface was noticeably cleaner than at the December spill, with oil concentrated in globules 3 to 4 cm in diameter, much larger than the tiny oil bubbles observed in the other two spills. The under-ice surface was also characterized by troughs up to 30 cm deep. One particularly large trough contained a very large air bubble and approximately one quarter of the total oil discharged.

The under-ice surface after the May discharge appeared much as it did after the December experiment, with thousands of small air bubbles coated with oil films and weathered oil flecks. The oil was rusty red in colour, which the authors remark probably indicates the presence of an emulsion. Oil layers up to 1 cm thick were overlain by air bubbles in troughs in the ice surface.

Emulsions were observed under the ice after all three discharges, particularly after the May discharge.

Incorporation of Oil and Air

In all cases, 24 hours after the discharges, small oil and air globules were being incorporated into the ice sheet. In December, 20 hours after the release, most of the gas and oil pockets were covered by a thin layer of new ice. The encapulated oil is described as having been very viscous. In April, 48 hours after the discharge, the largest of the oil- and air-filled troughs had begun to ice over and most of the smaller bubbles were encapsulated by the ice. Twenty-four hours after the May release, some of the smaller oil bubbles had frozen into the ice sheet. Cores taken two weeks later were found to have up to 10 cm of new ice below the oil pockets.

Note that, while the fate of the oil was tracked until breakup, the disposition of the gas was unknown beyond this point.

Oil and Gas Distribution

The size and distribution of oil drops was determined by a coring program at each release site. In all cases, more than 80% of the oil was found within 30 m of the release site. For the April site, which had a smaller air discharge, most of the oil was deposited within a 20 to 25 m radius.

It was found that drop size was smaller farther from the discharge site. This was modeled by assuming a Stokes behaviour of the oil droplets entrained in a laminar flow. The terminal rise velocity of the particles could then be calculated as a function of drop size. Given the velocity of the current under the ice and the distance from the blowout site up to the ice sheet, particle size as a function of drift distance could be expressed as (reworked from Appendix G of the Dome report):

$$D = \sqrt{\frac{18\mu V_c Z}{gx(\rho_w - \rho_p)}},$$

where: D is the droplet size, μ is the sea water viscosity (1.84×10^{-3} kg m^{-1} s^{-1}), V_c is the lateral drift current under the ice sheet (0.040 m/s), Z is the vertical distance from discharge site to ice sheet (5 m), g is the gravitational constant 9.8 m/s^2, x is the lateral drift distance, and ρ_w and ρ_p are the seawater and oil densities respectively (1,025 and 930 kg/m^3). Note that the Stokes regime applies only to particles 100 μm or smaller. Results from cores from the December release are given with the model prediction in Figure 9.25.

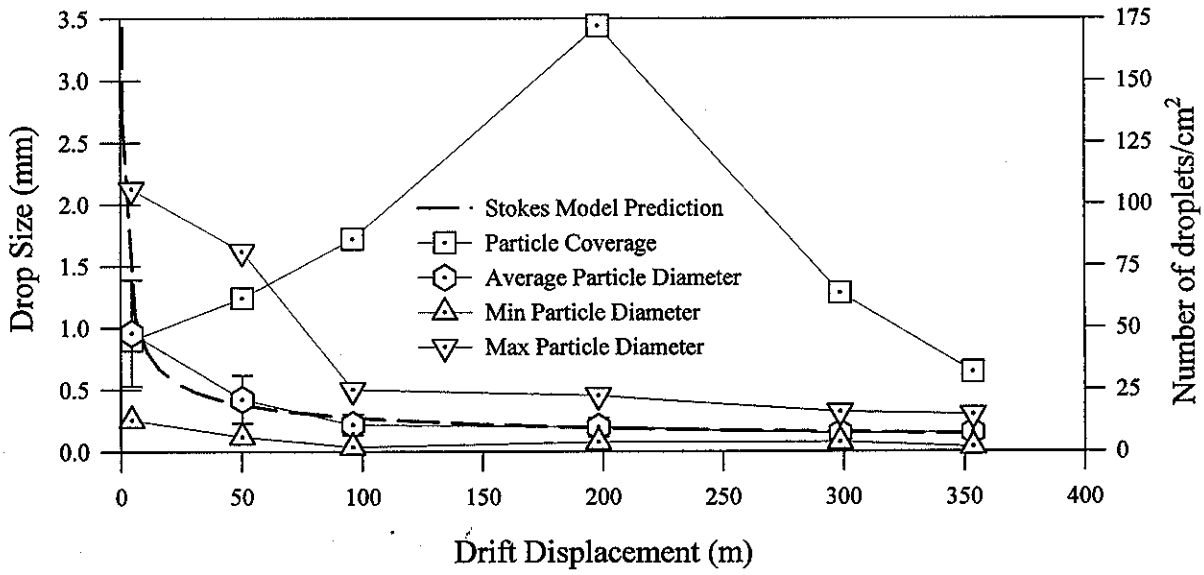

Figure 9.25 Oil Droplet Distribution

The authors note that the model does not predict the wide range of particle sizes seen on the under-ice surface. They attribute this to: i) turbulent, as opposed to laminar flow in the discharge plume; ii) the use of a constant drift current rather than the observed variation with depth; and iii) transient water-in-oil emulsification (presumably because this would change particle size). It would also seem reasonable to include behaviour that does not follow the Stokes regime (for oil drops larger than 200 to 300 μm), droplet breakup/recombination, and the effects of non-spherical droplet shapes. In addition, a cursory look at the data used to generate Figure 9.25 indicates that the particle size distributions for all drift distances were strongly non-Gaussian and

thus probably not well reflected by an arithmetic mean. The use of a median particle size would give an experimental curve at least 50% lower than the model points. Although the apparent agreement in Figure 9.25 may be largely fortuitous, this model seems to serve as a good first approximation of the distribution of oil particle sizes.

Oil Exposure

The authors state that oil is released from the ice sheet by brine channel migration and ice ablation. The extract of Figure 10.1 shows the competition between the two processes. The heavy solid line on the lower graph in Figure 10.1 gives the total percentage of oil spilled as a function of date. The lighter lines represent the oil exposure expected from ablation alone. This appears to have been derived by ablative exposure of oil lenses at known depths in the ice sheet as determined by coring. The oil that has arrived at the ice surface by migration is represented by the difference between these two curves.

The top graph in Figure 10.1 shows ablation of the ice sheet for clean sites and an average of the oiled sites, as well as the depth of large oil lenses in the ice.

The first sighting of oil on the ice surface at the April 10 discharge site occurred on June 8, about 20 m NW of the blowout point. The initial patches of oil grew rapidly, forming a large pool by the next day. Migration from the May site was first observed on the surface on June 11 and took 8 days to form a large pool. The authors state that the lesser quantity of air in the April discharge led to larger concentrations of oil beneath the ice and thus enhanced brine channel migration. The coring program revealed that oil migrated faster from larger conglomerations in the ice. The effects of porosity of the ice cores are discussed anecdotally, but no statistical data are presented. From their coring program, the authors conclude that oil migration depends on the presence of oil pools or lenses within the ice, as opposed to smaller drops, and that there be channels between the oil pools, the air above, and the sea below.

Cores taken at both the April and May sites showed that the oil migrated in concentrated pockets, leaving behind large cavities in the ice sheet. The authors postulate that discrete pockets of oil could surface by buoyancy alone if the ice sheet was thin enough and had begun to melt.

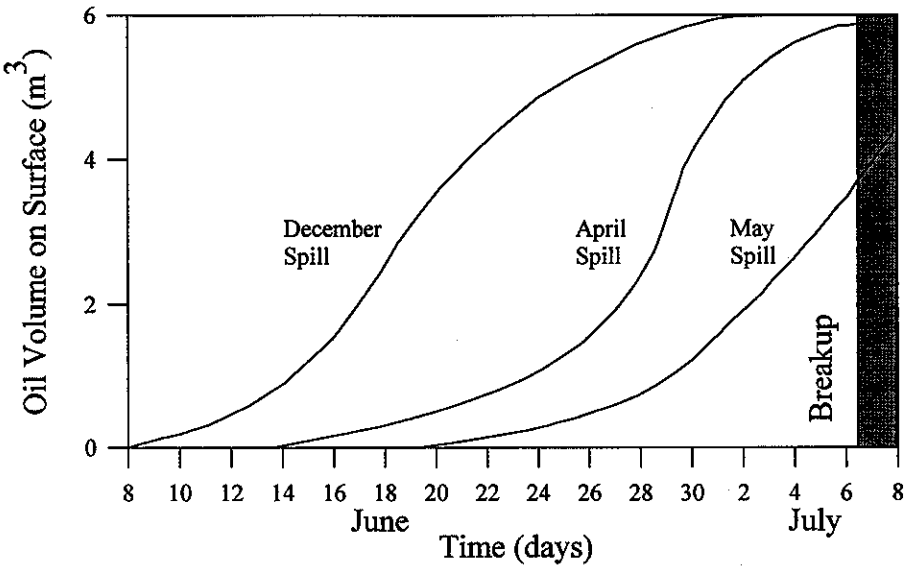

Figure 10.5 Timing of Oil Exposure in Spring

The fine oil droplets and the "flecks" observed on the under-ice surface after the May blowout did not appear on the surface until four days before ice breakup when the ice was very rotten. However, no significant migration was observed in the December area. At the December site, oil was completely exposed by ablation.

Timing of the appearance of oil on the ice surface at each discharge site is shown in Figure 10.5. It is apparent that the oil began to surface slowly and then most of it was exposed in a matter of days. Secondly, the timing of the oil's surfacing depended on the time of year it was spilled, or

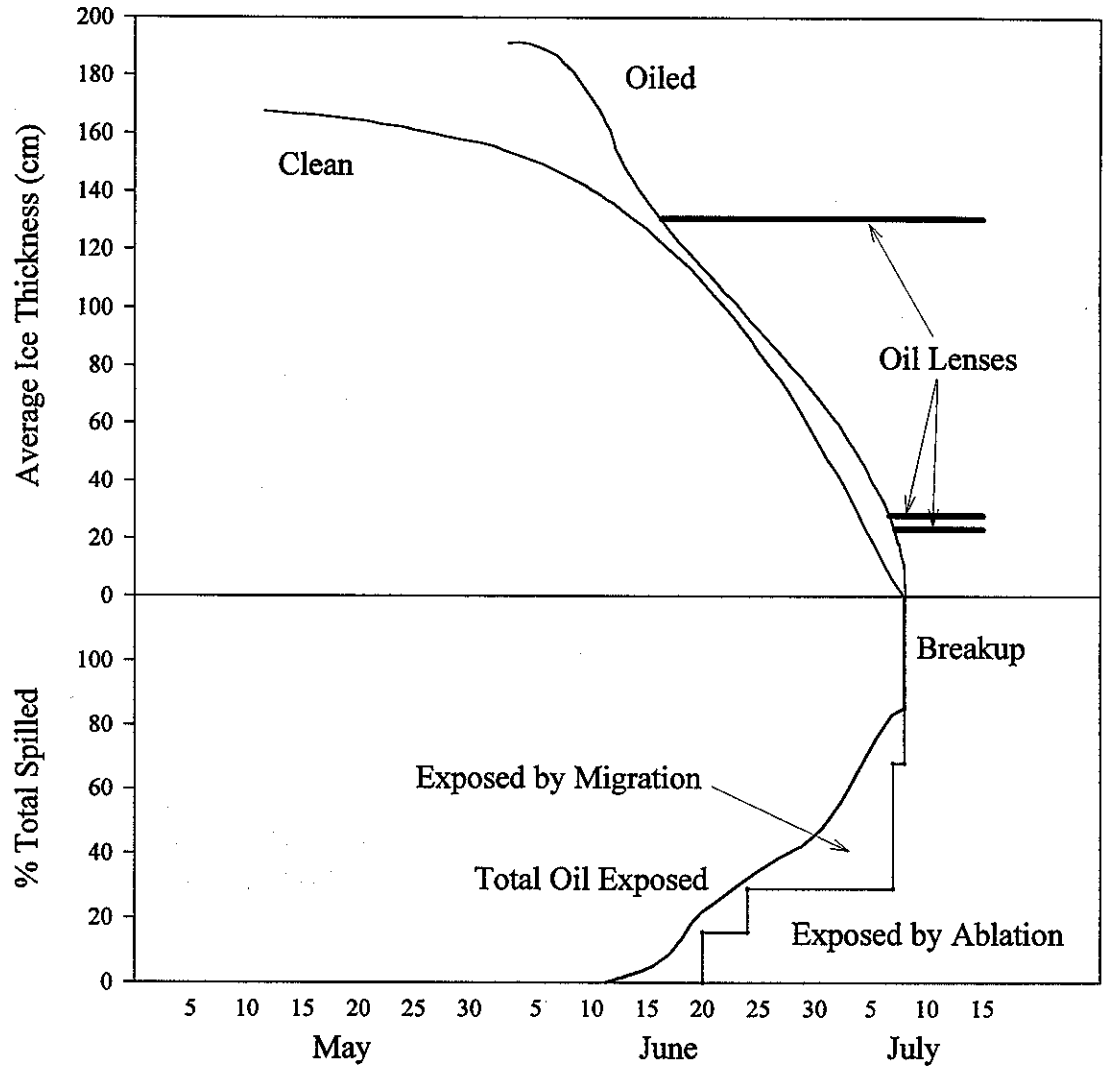

Taken from Figure 10.1 Ice Ablation and Oil Exposure

the thickness of the ice. The earlier it was spilled, the earlier it appeared.

The authors state that approximately 80% of the oil had surfaced at all three sites before breakup. None of the oil rising from the ice sheet was in an obvious emulsified (water-in-oil) form.

The size and volume of oil pools at each of the three sites are shown in Figure 10.6. Most of the pools were less than 20 m^2 in area, with the majority from 1 to 5 m^2 in area. The authors note, however, that most of the oil, particularly at the spring discharge sites, was contained in the larger pools. The pools were generally 1 cm thick and subject to wind herding.

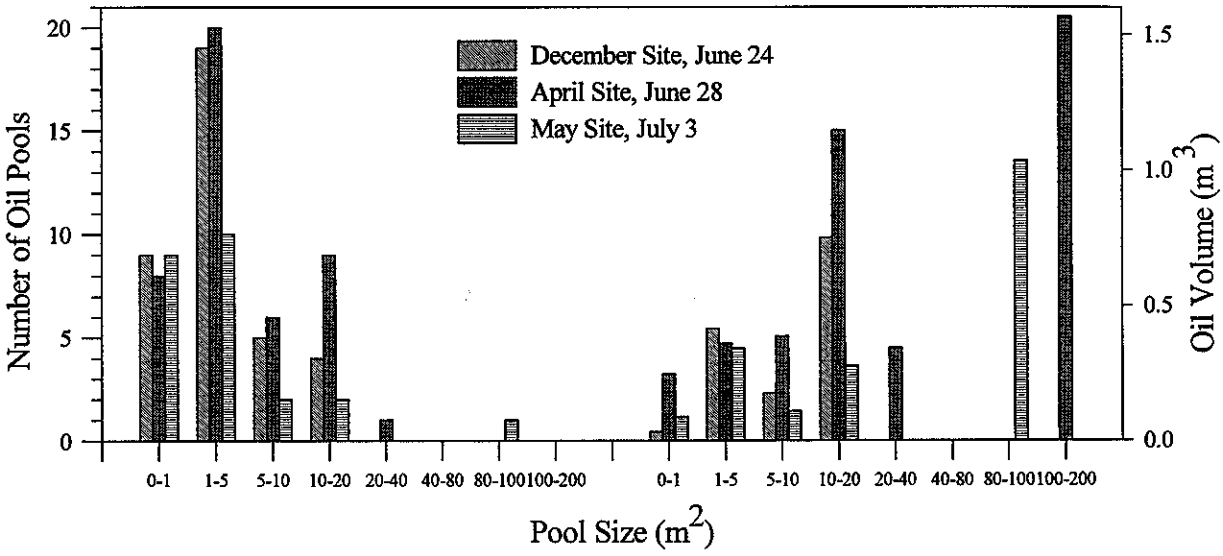

Figure 10.6 Oil Pool Size and Volume

Oil Weathering

During the discharges, heated oil (30 to 40°C) mixed with compressed air to cause a loss in oil volume, as the lighter fractions evaporated into air bubbles. This ranged from a 3% loss by volume at the April spill to a 10% loss at the December spill. The authors note that in a real incident, the oil and gas discharge would be in equilibrium and such a volume loss would not occur.

While most of the oil was not significantly weathered in the water, the appearance of the small "flecks" observed in the December and May spills suggested heavy weathering. It is not clear that this weathering was caused by exposure to the seawater or by mixing with compressed air in the plume. The ice cores indicated that there was little weathering of the oil lenses in the ice sheet over the winter months. As the oil began to surface, however, the authors suggest that migration rates may differ for the oil factions, "migration weathering" the lenses. The authors remark that chromatograms of the ice immediately above oil lenses indicated that some of the light ends may have been lost as the oil began to surface. Some spring core samples also showed evidence of biodegradation.

Two tests of oil on the ice surface were performed during the winter months. Oil slicks resulting from the venting of the December blowout showed almost a complete loss of components under C_{14} and a volume loss of 40% after 33 days. Oil spilled on the surface in April had a volume loss of 25%, with very few components lighter than C_{12} after 72 hours. Note that both the winter

pools were covered with snow within 24 hours of exposure. The authors conclude that the oil spilled on ice during winter weathered considerably, even when covered with snow.

Limited analyses were carried out on the oil that migrated to the surface beginning in June. The authors observe that significant losses of the light ends occurred once the oil appeared on the ice surface in spring. The authors estimate that in the exposed pools, the average volume loss was 20 to 25%. They note that these losses were lower than expected, and speculate that this was due to the thickness of the slicks and the relatively high viscosities of the weathered oil (100 to 400 mPa-s). It is also interesting to note that the oil pools are reported as being thin (1 cm) and 5 to 10°C warmer than the surrounding air and water during the day.

Some emulsification was observed in the oil pools, forming a thin skin on the oil slicks. As the day progressed, this emulsified skin would break as the temperature of the slick increased. The small amounts of oil exposed in lightly contaminated areas, usually highly weathered, formed stable water-in-oil emulsions.

Because of the varied composition of the surface pools, with oil from the ice sheet mixing with the heavily weathered surface oil, the oil pools were not extensively analyzed. The physical properties of a 100-L control pool were followed for a period of two weeks, however, and the results of this analysis are shown in Figures 10.11 to 10.14, reproduced here.

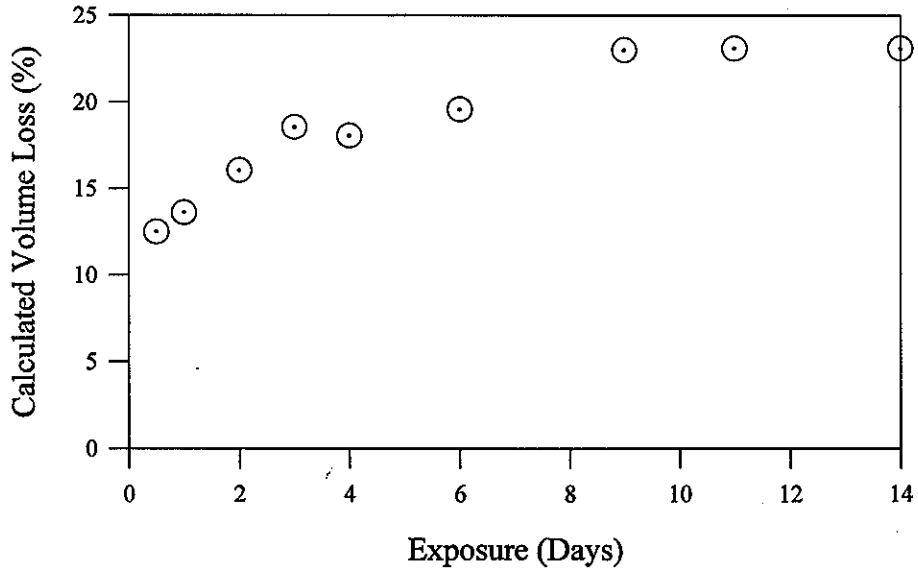

Figure 10.11 Control Pool Evaporative Loss

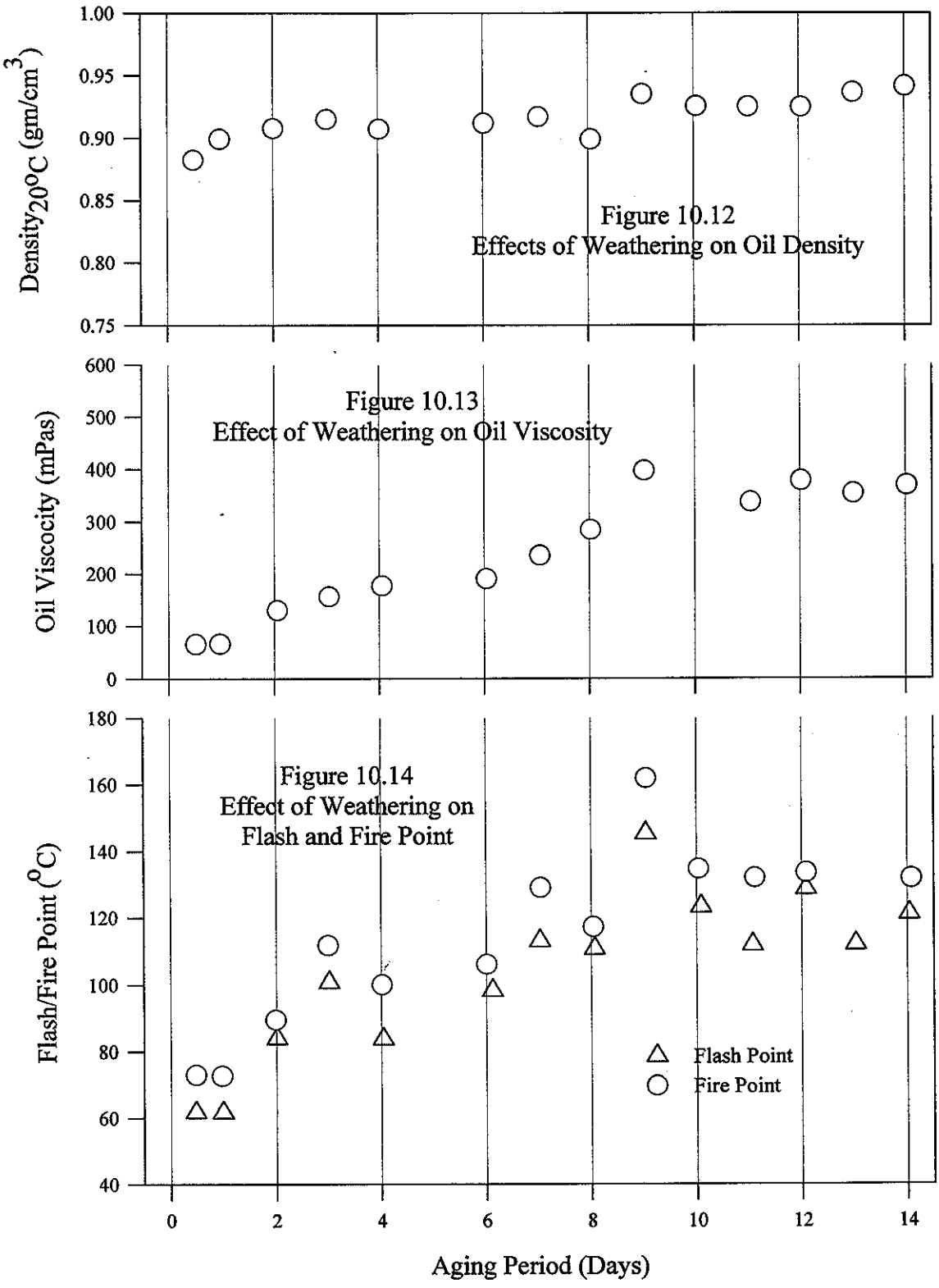

Figures 10.12 to 10.14

BOSS Critique

While the objectives of this study were realized, its applicability to other work is limited due to the sampling methodology and experimental design used. Much of the evidence presented is photographic and descriptive rather than quantitative, particularly concerning oil and gas entrapment in the ice sheet, brine channel formation, and density and oil migration to the surface. While this provides a good qualitative understanding of the oil/ice behaviour, the use of these results to quantitatively predict the evolution of future spills is very limited. For example, the encapsulation of oil into the ice sheet was described, but the rate of uptake was not well determined. Similarly, brine channels in the ice sheet were photographed, but the ice porosity at the McKinley Bay site was not measured even though the authors note that very little data for brine channel spacing in sea ice existed at the time of the report. Without knowing ice porosity or brine channel density, it is difficult to quantitatively predict oil migration.

In addition, the use of compressed air as a blowout gas caused problems in determining the weathering characteristics of the oil. As mentioned in the Results section of this review, mixing of the oil and air in the discharger and the plume resulted in a 3 to 10% volume loss before the material reached the ice sheet. This increased the errors in the weathering data, but should not greatly affect the conclusions drawn about oil weathering.

Finally, the work is limited due to variations of the rate of release of oil and gas, the gas-to-oil ratio, and the air "blowback". Few comparisons can be made between the discharges due to the variety of the initial conditions. While this does serve to explore a wider range of blowout behaviour, it reduces the study's quantitative usefulness.

In summary, this work's descriptive reports provide a qualitative understanding of shallow blowouts under ice and are of primary interest. Also, the weathering data with regard to the oil in the control pool provide considerable data about the fate of oil in an Arctic environment.

C-CORE (Centre for Cold Ocean Resources Engineering), *An Oilspill in Pack Ice*, EE-15, Environment Canada, Ottawa, Ontario, 231 p., 1980

This work is also reported in:

Reimer, E.M., "Aspects of Oil-Ice Interaction Subsequent to the Kurdistan Spill", in *Proceedings of a Workshop on Oil, Ice and Gas,* Institute for Environmental Studies, University of Toronto, Toronto, Ontario, pp 75-86, 1979.
This is a very short summary. [Note: This has been previously reviewed for the BOSS project.]

Reimer, E.M., "Oil in Pack Ice: The Kurdistan Spill", in *Proceedings of the Third Arctic Marine Oilspill Program Technical Seminar*, Environment Canada, Ottawa, Ontario, pp 529-544, 1980.
This paper discusses only the pack-ice behaviour of the oil.

Reimer, E.M., "The Visual Identification of Bunker-C Oil in Dynamic Pack Ice", in *Scientific Studies during the "Kurdistan" Tanker Incident: Proceedings of a Workshop*, BI-R-80-3, Bedford Institute of Oceanography, Dartmouth, Nova Scotia, pp 74-85, 1980.
This paper deals only with aspects of remote sensing and identifying oil in ice.

Summary

"About 1100 tonnes of [Bunker C] oil... was entrained in pack ice off the Cape Breton coast. The oil, which was below its pour point at the prevailing seasonal temperatures, was distributed in streaks and patches as a fine particulate dispersion in the ice. Oil concentrations were as high as 200 ppm in heavily contaminated areas.

Only a small fraction of the oil-contaminated ice was deposited along shorelines. Most of the shoreline contamination in the area studied occurred after the ice pack had dispersed or melted."

Objectives

This report documents oil migration and weathering in pack ice during the KURDISTAN spill in the St. Lawrence Basin in the spring of 1979. Interactions of the oil with sea floor sediment and the shore are also analyzed. Remote sensing and spill cleanup are also discussed in the report, but are not included in this review.

Method

This was a "spill of opportunity" and a completely uncontrolled event. Initial observations began eight days after the breakup of the KURDISTAN and took two days to complete. Aerial over-flights were made 12 and 17 days after the spill, in conjunction with additional ground-based monitoring teams. Ground monitoring continued until 23 days after the breakup. Several one-day return visits were made over the following two months to observe ice that had come ashore. Approximately two months after the spill, samples of bottom sediment were taken "to ascertain the sinking rate for oil from the ice cover which had persisted in the area for several weeks". Ice movement was tracked using Orion buoys which were found to be very effective for determining ice drift.

Oil Characterization

The physical properties of Bunker C for both the original crude (as reported by Gulf Oil) and weathered samples are given in Tables 3.1 and 3.2, combined below. Figure 3-2 shows the UV-visible absorption spectrum of fresh Bunker C oil. The hydrocarbon component distribution of unweathered Bunker C oil is shown in Figure 3-3.

Extracted from **Table 3.1, Reported Properties of Bunker C** and **Table 3.2, Measured Properties of Bunker C Samples**

Sample	Sample Location	Viscosity (cP) 40°C	Pour Point (°C)	Density (g/mL) -2°C	Water Content
Bunker 6C-3 (Gulf Oil)	Measured on ice	3500	22 to 28	0.987	5 to 20%
March 25	Taken from the side of ice floe 10 km off-shore Fourchu Head	2800	28		4%[a]
April 25	Gabarus Beach, taken from a blob on a grounded ice floe	4700	22	0.987	18%
April 25	Fourchu Head, taken from 10-day-old deposit overlying rocks at high tide line	3400	27		13%

[a]May have been as high as 20%; sample originally contained ice crystals which had thawed and separated from the oil by the time of analysis.

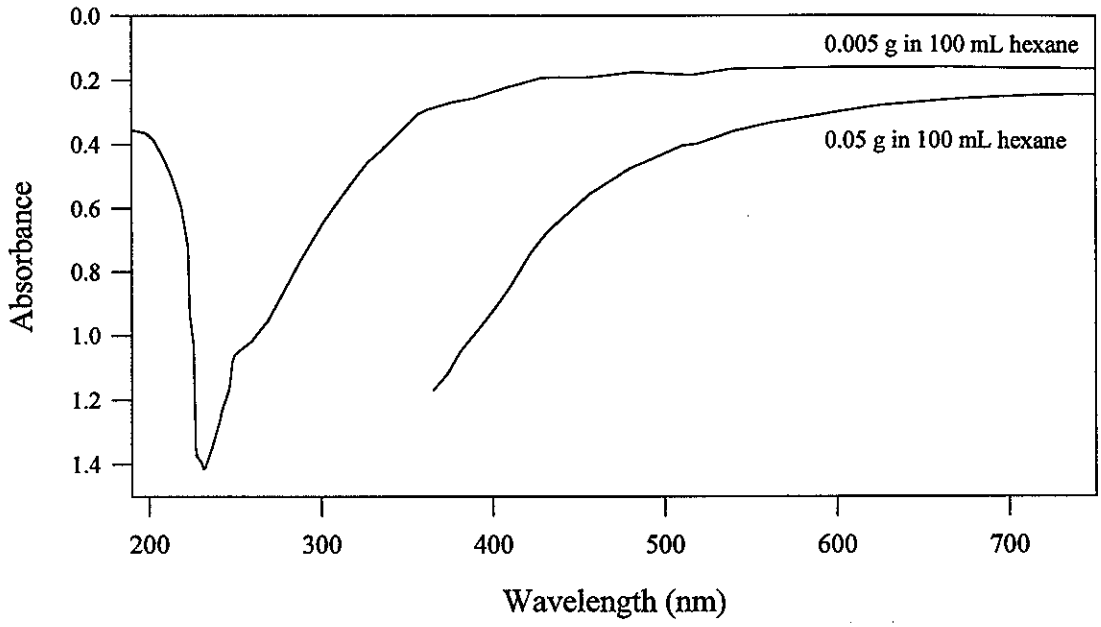

Figure 3-2 The Absorption Spectrum of Bunker C Diluted in Hexane

Results

The authors note that the samples contained many contaminants including water, mineral sediment and organic debris. The contaminants were not removed during analysis.

The analysis showed that:

- the density of the oil was only 0.04 g/mL less than that of the sea water;
- no emulsions were observed either on the ice or the shore; and
- ice from most samples had normal (C_{14} - C_{15} to C_{24} - C_{28} ratios, as determined by GC). Only one sample, exposed for 70 days and described as "emulsified balls", was determined to be abnormal, and identified as not being Bunker C.

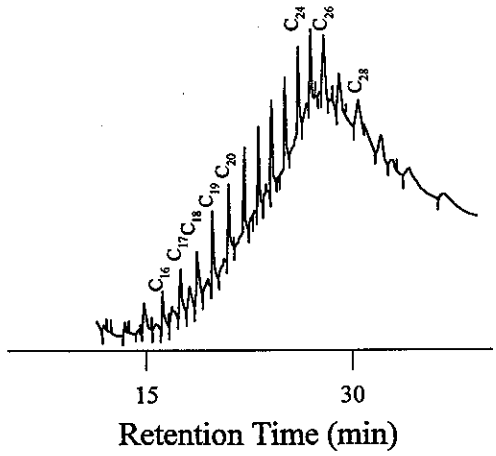

Figure 3-3 Gas Chromatogram of Bunker C

Distribution of Oil in Pack Ice

The authors observed that the oil slick was initially present as concentrated bands or streaks on the ice, but dispersed or diluted in the pack over time. The authors were unable to describe what drove the dispersive processeses. They note however, that maximum mixing occurred when the pack was loose and drift between floes was possible.

Oil was observed on, in and under the ice floes. Occasionally, floes totally covered with a film of oil were seen. Upon close examination, the film was found to be only a few millimetres thick and the underlying ice surface to be relatively smooth. The authors suggest that the complete oiling of a floe must happen during the original breakup. Cold oil is too viscous to spread evenly and solar-heated oil would tend to melt into the surface of the floe rather than forming a film.

The oil on most floe surfaces is described as being concentrated in "small blobs and spatters", with most oil found within a few metres of the edge of the floe. Oil was also found to have melted into pockets. The main mechanism for floe contamination was assumed to be wave action.

Circumferential dykes and/or oil-contaminated brash were frequently observed on floes in heavily contaminated areas. Some of these appeared to have a very high oil content - possibly due to the concentration of surface oil by melting of the brash."

Large blobs of oil were seen on the floes, particularly later in the season. The authors speculated that these may have been present from the initial oiling of the ice, but were subsequently covered by snow and ice.

Brash Ice - The authors found an "innumerable" number of small oil particles distributed in the ice brash, ranging from 1 mm to 10 microns in size. Oil was also found as a coating on "football-sized" ice chunks. They note however that the bulk of the oil was normally contained in a few large blobs. The brash ice had a mean oil concentration of 200 ppm, however, a very large range of concentrations (0 to 700 ppm) was observed. The authors were not able to determine the distribution of particle size as a function of depth because of mixing problems during transport.

Water Column - Water column samples were taken 22 days after breakup at which time the oil had become very finely dispersed. While most of the oil was located near the surface, particles were found distributed throughout the water column. In general, the water column contamination was between 1 ppm and 0.1 ppm, considerably higher than the normal levels in the area of the spill (1 - 2 ppb measured by Levy, 1971; 1972).

Large-Scale Mixing - While differential movement between brash and floes was observed, the authors remark that motion of the ice field did not appear to disperse the contaminated areas to any great extent. Pack ice, even when heavily contaminated, held the oil offshore.

Small-Scale Mixing - The authors found that, in general, as the semi-solid oil was entrined in pack ice the oil was dispersed into progressively smaller particles.

One of the primary dispersion processes was found to be the grinding of oil in brash ice as a result of floe impact and differential movement.... The grinding process was leisurely and resulted in particles from a few centimetres in diameter down to micron sizes." Breaking waves in the ice field, especially during heavy weather, had a similar "grinding" effect. "A concomitant of the grinding process appeared to be a considerable incorporation of organic or mineral material into the oil...."

Melting also served to reduce particle size. It was observed that solar heating of the oil on ice surfaces caused stretching of oil puddles "until surface tension effects intervened to produce

micron sized oil particles". Fast melting was found to have an opposite effect, however, causing pockets of concentrated oil blobs in the ice.

The authors observed the presence of large blobs of oil on the floe surfaces, sometimes covered by a layer of snow or ice, particularly late in the season. They speculated that these large concentrations of oil may have formed by splash up onto the flow which was later covered by blowing snow or ice rafting.

Hydrocarbon Fractionation in Sea Ice - Gas chromatographs of samples of a brash ice/water mixture and water alone revealed "an order of magnitude enrichment of low molecular weight hydrocarbons..." for brash ice samples. These results are shown in Figure 4-17. "A similar enrichment of even numbered hydrocarbons was seen in analyses of ice cores from floes and from ice rubble drifts." The authors offer no explanation for this phenomenon.

Oil Sediment Interaction Offshore

"A survey of bottom sediments was undertaken in Gabarus Bay in late May (1979) in order to assess the rate of oil sedimentation from the oil-contaminated ice which had occupied the bay from approximately March 23 to April 21..." The sediments were analyzed for total hydrocarbons and fingerprinted by GC. The authors conclude: "Sedimentation... occurred in Gabarus Bay only in shallow low-energy areas of less than 12 metres. Oil contamination was, therefore, a direct near-shore sedimentation process. Shallow areas of high turbulence presumably received little contamination."

Shoreline Deposition Phenomena

"The pack ice tended to hold oil offshore. It was not until the disappearance of most of the pack ice that significant quantities of oil came ashore... Even in the case where the ice itself was heavily contaminated... the shorelines were not fouled until meltout. Fouling from ice-entrained oil tended to take the form of a highly dispersed deposit of small blobs and blotches."

The authors mention that oil/water emulsions were not a significant feature at any time during the spill. Self-cleaning of the shores did not occur except on vertical rock surfaces in the intertidal zone.

Oil Spill Motion Modelling

The authors attempted to model the drift of oil from the KURDISTAN to the Cape Breton coast. Inputs to the model were real wind data measured at Port aux Basques, Eddy Point, and Sable Island. Historical data, which were scant at the time of the study, were used to generate two water current vector fields, designated "standard" and "gyre".

"The standard grid illustrates predominant southwestward flow along the southeast Cape Breton coast while the gyre pattern includes a stream which swings into an anticyclonic gyre when rounding Scatarie Island, and returns in a northeastward flow along the southeast coast."

Oil sighting data was used to verify the simulations. "Model scenarios which predicted oil impact at times and in locations consistent with [the real-world data] were considered successful." Two such trajectories are shown in the combined Figures 5-1, 5-2, and 5-3.

"...The basic conclusions of the real-data modelling work are: a) Standard currents have been more generally successful than gyre currents in generating realistic model predictions; and b) Wind source is not the prime determining factor in model success as reasonable trajectories were projected for each of the three wind sources employed." The authors conclude that water current was the most important factor in their drift models and the unknown current residuals were the main source of error in the models.

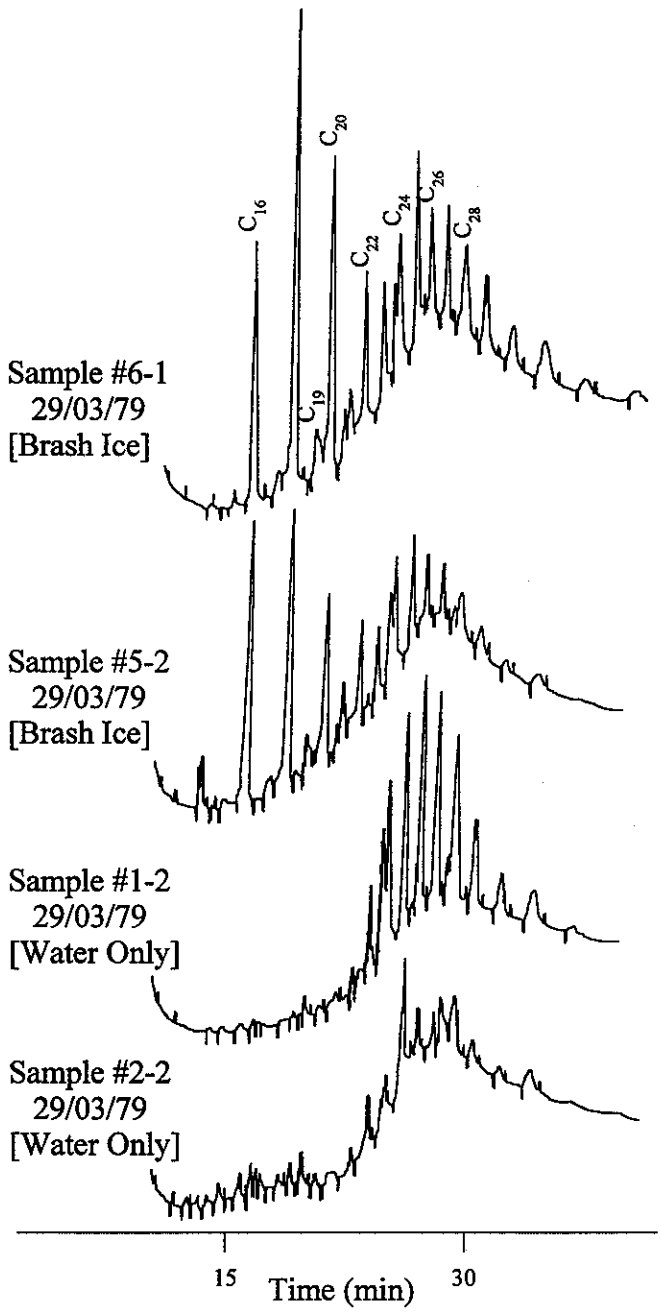

Figure 4-17 These four gas chromatograms show the respective depletion and enrichment of light hydrocarbons in samples of water only (bottom) and samples of water and brash (top)

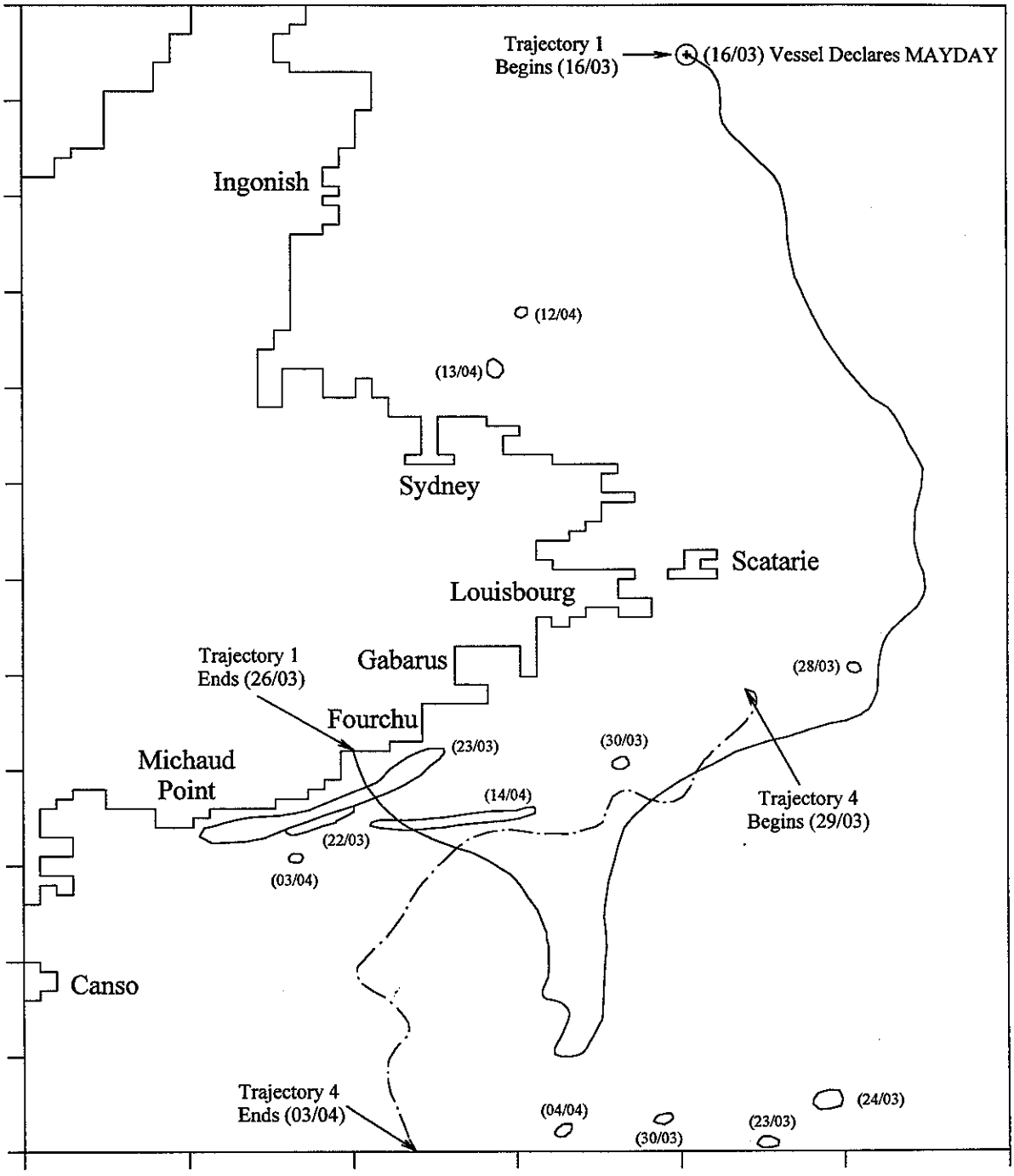

Extracted From Figures 5-1, 5-2 and 5-3. Real oil sightings are marked as irregular closed shapes together with the date spotted. Selected model trajectories are shown as lines. See text for details.

BOSS Critique

While this report was based on a limited observation schedule of the evolution of an oil spill in heavy pack ice, it does illustrate many key features of a spill at temperatures below the pour point of the oil. The study focuses on the behaviour in and on ice with less emphasis on the grounding of the ice on the shore and mixing with the ocean floor.

It is worth noting, however, that there were several details the authors were unable to completely examine. The fate of oil in the ice of the floes is largely undetermined by this work. For example, phenomena such as the appearance of large blobs on the ice later in the season were not completely explained by the authors. Also, the authors were unable to examine the behaviour and disposition of the oil in brash ice as the samples were agitated by helicopter transport before analysis. In addition, the drift models were preliminary as this was one of the first times these models were used. Further work in this area has yielded more reliable results.

D.G. Wilson and D. Mackay, *The Behaviour of Oil in Freezing Situations*, EE-92, Environment Canada, Ottawa, Ontario, 65 p., 1987.

This work has also been reported in:
D.G. Wilson and D. Mackay, "The Behaviour of Oil in Freezing Situations", in *Proceedings of the Ninth Arctic Marine Oilspill Program Technical Seminar*, Environment Canada, Ottawa, Ontario, pp 51-63, 1986. Only the oil incorporation studies (laboratory and field) were covered in this report.

Summary

"An experimental study of the behaviour of an oil spill in a developing (grease) ice field is described. It was found that significant quantities of oil may be entrained within and beneath a grease ice field."

Factors that were found to increase the amount of oil entrained include a high oil density or viscosity which can be natural or induced by weathering, sufficient turbulence to disperse the surface oil at an appreciable rate and induce mixing within the forming ice field; the formation of small oil droplets and emulsions of sea water and/or ice in the oil; and the formation or coalescence of ice particles of approximately 5 mm in diameter.

Other results of the study include the observation that, in calm water, an oil layer will retard ice development, but under turbulent conditions, oil will have a negligible effect on ice formation. In addition, it was observed that solar radiation has little effect on the development of ice in the presence of oil, except in calm conditions when formation of ice may be significantly retarded. Solar radiation will hasten melt, however, as oil collects on the surface. And finally, it was observed that it takes longer for the least buoyant oils to be released from a melting ice pancake.

Objective

This study investigated the effects of oil on developing ice fields. Of particular interest were the effect of oil on ice formation, the amount of oil incorporated into the growing ice sheet under turbulent conditions, and the effect of oil in the ice on the kinetics of ice thawing.

Theory

No formal theory was discussed by the authors, although they present an extensive review of the experimental literature for oil spills in ice.

Methods

Apparatus

The principal experimental apparatus is illustrated in Figure 3.1. It consisted of a clear Lucite tank (a 35-cm cube) in which oil, ice, and water were mixed and agitated by an oscillating hoop, driven by a 12-volt DC motor. The 33-cm diameter hoop could be oscillated at 120 cpm in a

vertical direction. The mixtures were arranged so that the hoop was just beneath the water surface and created a "low energy ripple/wave" in the tank when it moved.
The experiments were conducted in a cold room to control the temperature in the apparatus. Still photographs were taken during each run. Oil samples taken during these runs were analyzed with a Hewlett-Packard 5700A gas chromatograph with a Shimadzu C-R1A integrator and a 30-m by 0.75-mm glass capillary column.

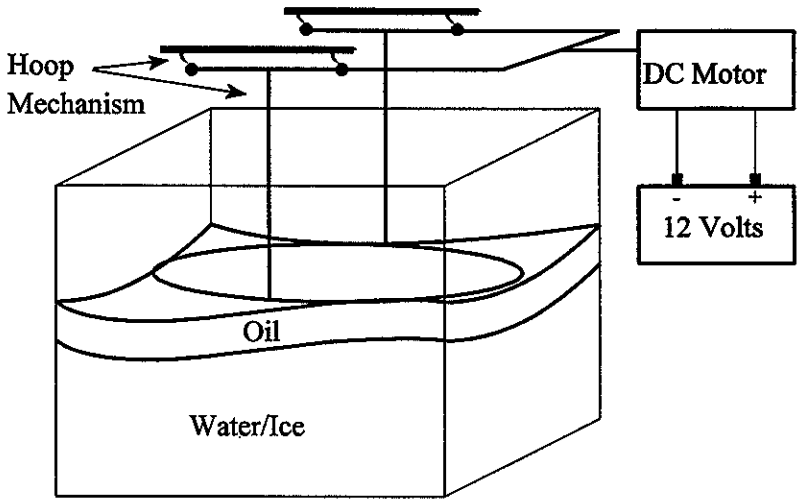

Figure 3.1 Oscillating Hoop and Tank Apparatus

Oil Weathering

Two sample mixtures of 70% No. 2 and 30% No. 6 fuel oils were weathered for several days at -5°C. One sample mixture was contained in a grease ice field and the other, a control, was weathered in the absence of ice. Samples were taken periodically and analyzed by gas chromatography and pycnometer.

Oil Incorporation in Grease Ice Fields

The authors wished to examine a series of oils of varying density, but with constant viscosity. They used a mixture of a light hydrocarbon oil, Bayol 35 (s.g. = 0.790) and a dense organo-chlorine solvent, tetrachloroethylene (s.g. = 1.615). Mixtures of various densities and layer thicknesses were introduced to fields of grease ice consisting of varying ice particle diameters and field depths. The ice fields were not compressed and were allowed to reach equilibrium thickness and ice-to-water ratio.

These experiments were carried out in 2.5- to 3.5-L glass beakers. The oil was dyed with Sudan Red so that the clear, colourless mixture could be seen in ice. The ice was allowed to freeze, and the volumes of oil incorporated into the ice were then measured. Ice-to-water ratios were measured by water displacement when the ice was put into the water.

These tests were conducted with fresh water, which the authors note, greatly simplified the experimental procedure. They contend that this is reasonable as layers of fresh water are often found in salt water in Arctic conditions especially in areas close to rivers, icebergs, or floes.

Effect of Oil on the Thawing Process

These experiments were conducted on the frozen oil-in-ice samples described in the previous section. Beakers of the solid ice/oil mixtures were held at room temperature (21 °C) and allowed to thaw. The volume of oil released was monitored as a function of time, density of the oil, and extent of incorporation. Clean ice samples were used as a control.

Cold Emulsions

Several emulsions were formed under freezing conditions using a rotating shaker maintained at -5 °C. Emulsions were formed from a 70/30% mixture of No. 2 and No. 6 fuel oils as well as Arabian heavy crude. Samples were prepared with ice crystals of varying size to simulate formation in a grease ice field. The shaker was rotated at 48 rpm for 3 to 4 hours to form the emulsions. Once formed, the emulsions were put into grease ice fields and observed. Emulsion density and water content were also monitored.

Effect of Solar Radiation on Ice Formation

The apparatus used for these experiments is shown in Figure 3.2. A 2-mm layer of the 70/30% mixture of No. 2 and No. 6 fuel oils was poured over a freshwater bath and allowed to freeze, undisturbed at -5 °C. Samples were illuminated by a 60-W incandescent light bulb 1 m above the oil surface. An identical control sample was kept in the dark. The time to initial ice formation and thicknesses of ice as a function of time were recorded for both samples.

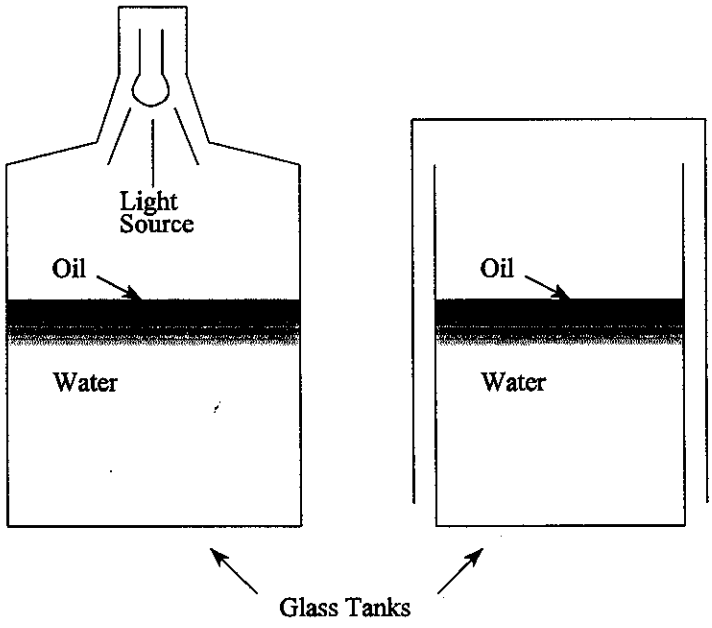

Figure 3.2 Solar Radiation Apparatus

Effect of Oil on Growth of Turbulent Ice Field

The effects of layers of varying thicknesses of 70/30% mixtures of No. 2 and No. 6 fuel oils on a turbulent ice field were investigated. The experiments were conducted in the apparatus shown in Figure 3.1. The hoop was oscillated at maximum speed and the cold room maintained at -5°C. Qualitative observations were made and the time to initial ice formation was compared with that of ice formation in the absence of oil.

Field Study of Oil In Ice

A spill of No. 6 fuel oil was observed in the St. Lawrence River, Quebec, in a developing salt water ice field in December, 1985. Oil and ice mixtures were sampled. Oil was analyzed for density increase using a densitometer at the Environmental Technology Centre, River Road, Ottawa, Ontario.

Results

Weathering of Oil in the Presence of Ice

The authors' results for the oil-in-ice samples are shown in Table 4.1.4 and for ice-free controls, in Table 4.1.2. The authors note that, since the oil was refined, it already had many of the light ends removed and was, in a sense, pre-weathered. The oils showed no evidence of weathering either in ice or without ice. The oil entrained in the ice was not tested. After 144 hours, the specific gravity of the oil had risen from 0.9056 to 0.9061. The authors state that there was little air movement in the cold room, other than the occasional operation of a refrigeration fan.

Table 4.1.1 Oil [Weathering] in the Presence of Ice

Time (h)	C_{12}/C_{14}	C_{14}/C_{16}	C_{18}/C_{16}	C_{20}/C_{16}	C_{24}/C_{16}
0	0.3280	1.0172	0.9593	0.6468	0.0618
10	0.3250	1.1393	0.9351	0.6320	0.0663
20	0.3357	1.1612	0.9391	0.5452	0.0641
50	0.3681	1.1198	0.9101	0.5455	0.0654
150	0.3067	0.9829	0.9212	0.5417	0.0752

Table 4.1.2 Oil [Weathering] in the Absence of Ice

Time (h)	C_{12}/C_{14}	C_{14}/C_{16}	C_{18}/C_{16}	C_{20}/C_{16}	C_{24}/C_{16}
0	0.3280	1.0172	0.9593	0.5863	0.0618
10	0.3527	1.1189	0.9461	0.5983	0.0728
20	0.3462	1.0105	0.9446	0.6314	0.0781
50	0.3393	1.1369	0.8726	0.519	0.0362

150	0.3674	1.1796	0.9279	0.7514	0.0757

The authors compare their results with weathering experiments "performed in parallel with this study" (no further details are given) on Alberta sweet crude, a very light oil. The specific gravity of the crude oil increased from 0.865 to 0.894 after 50 hours at ambient temperature in a wind tunnel. The authors conclude that the presence or absence of ice does not seem to be significant to oil weathering, oil weathering occurred at a much slower rate than in "more temperate" conditions, and any significant weathering for an oil may require a longer time than the expected life of the spill.

The results shown in Tables 4.1.1 and 4.1.2 reveal that the authors' error in abundance ratios must have been at least 0.05. This can be seen by comparing the "0" time values for the C_{20}/C_{16} on the two tables and also in the unlikely variation reported for the C_{14}/C_{16} ratio in Table 4.1.1 which increases to 20 hours then decreases at 50 and again at 150 hours. It is likely that the results shown on Tables 4.1.1 and 4.1.2 are significant to only two decimal places.

Oil Incorporation in Grease Ice Fields

The fraction of oil volume incorporated into the ice as a function of the size of ice crystals is shown in Figure 4.1. Grease ice fields were composed of ice particles of different sizes to simulate the natural processes that transform grease ice into pancake ice.

The densest oil had the highest fraction incorporated into ice, and the least dense mixture was the least entrained in the ice. The extent of incorporation for all oils and layer thicknesses reached a maximum for ice particles from 5 to 8 mm in size. The authors speculated that, with larger ice particles, the interstices are too large to capture oil droplets. It appeared that the smaller droplets

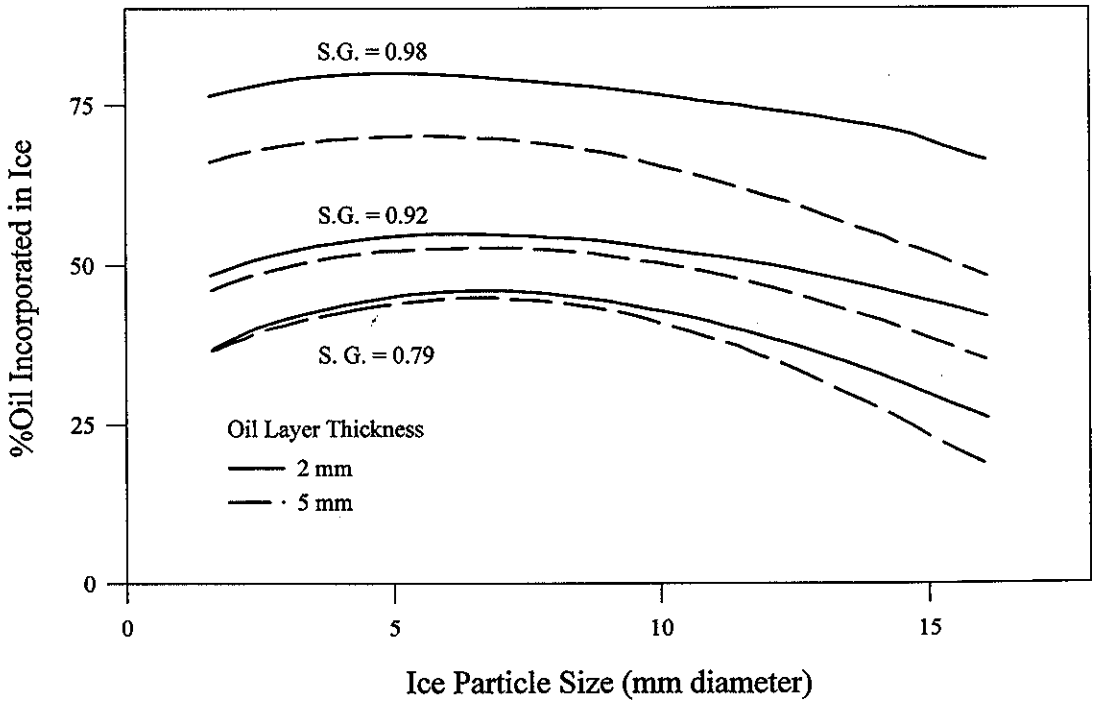

Figure 4.1 Plot of % Oil Incorporated *vs* Ice Particle Size

(less than 3 mm in diameter) were too small to trap oil droplets below the ice crystals with the result that the oil droplets pushed aside the ice particles as they surfaced.

The authors concluded that there is an optimum size of ice particle, at which the crystals are small enough to accommodate the oil, while large enough to trap individual oil droplets beneath them. The authors remark that mixtures of different sizes of ice particles would probably trap oil more efficiently and have higher fractions of incorporated oil.The thickness of the oil layer appeared to have little effect on oil incorporation for the low density oils. For the densest oil, however, significantly more oil was incorporated into the ice for the thin oil layer. The authors remark that this was probably a result of the size of the oil bubbles formed by the breakup of the oil layer. They contend that, for thicker layers of oil, the oil droplets tended to be much larger than those created with a thin oil layer. The larger drops (4 to 6 mm) produced by the thicker layer (5 mm) had a higher buoyancy than the smaller drops (1 to 3 mm) created from a thin layer (2 mm). This allowed the larger drops to float to the water surface and avoid being trapped in new ice.

Effect of Oil on Thawing Process

Figure 4.1 shows the fraction of oil remaining in the ice as a function of time for ice blocks at 21 °C. Ice melts primarily from the top down. As the melt water runs off, the ice surface is continuously re-exposed for further melting. Given a constant external temperature, the authors surmise that the thickness of an ice sheet would decrease proportionately with time. The authors

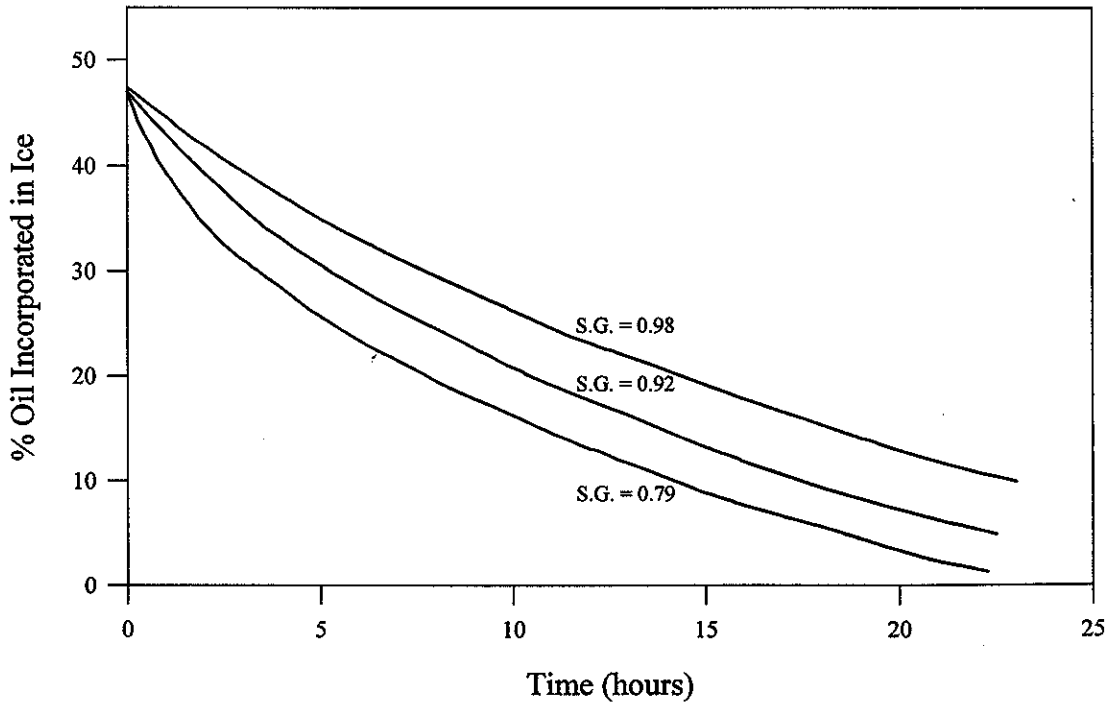

Figure 4.4 Percentage Oil Incorporated in Ice *vs* Time During Thawing of Oil/Ice Mixture.

remark that there would be a nearly linear decrease in the fraction of oil incorporated in the ice sheet provided that the oil is evenly dispersed in the ice. It was observed that oil was quite evenly dispersed throughout the top 9 cm of the ice and appeared to be released proportionately to the decreasing ice thickness. However, as the oil layer was never completely incorporated within the ice during the freezing process, there was always a slick of oil on the melting ice block.

The authors state that the deviations from linearity after five hours, shown in Figure 4.4, were probably due to oil pooling on the ice. They hypothesize that the oil covered the melting ice and insulated it from the room temperature air. In contrast, the melt water does not from melt pools as it is more dense than ice, and provides no insulation during the thaw.

As can be seen in Figure 4.4, significantly longer times were required for the denser oils to be released from the ice. The authors speculate that, since the denser oils are less buoyant, the agitation in the tank during ice formation dispersed the oil droplets to a greater depth in the final ice mass. The photographs of the ice samples (not reproduced for this review) are inconclusive in this regard. Also, the authors had previously remarked that dispersal in the ice was generally uniform. The authors note that, as sea ice forms, salt is expelled from the ice sheet, forming brine channels which are an important pathway for oil migrating to the surface. They conclude that a denser oil will migrate more slowly through the brine channels than a lighter oil due to a smaller buoyant force. They also state that, since a denser oil is entrained at a greater depth, it has farther to travel and therefore a longer time is required to form brine channels to the surface. The authors also note that the denser oils have a slower Stoke's Law rising velocity. By contrast, other authors (Nelson and Allen, 1981) have concluded that brine channel migration rates are dominated by oil viscosity, which does not always correlate with density. Viscosity effects are not discussed by the authors.

Cold Emulsions

Emulsions of Arabian heavy crude oil and salt water were formed, composed of approximately 40% water and 60% oil, and with a specific gravity of 0.946 . The emulsion remained stable in the absence of ice for about 50 hours. This emulsion was stirred into a grease ice field in a large beaker. The authors observed that there appeared to be much greater incorporation into the ice field than in the oil-in-ice experiments described earlier. They conclude that oil viscosity strongly influences the fraction of oil incorporated during ice formation. In the crude oil experiments, oil mixtures were prepared that were dense but with low viscosity. These mixtures remained fluid at low temperatures.

The authors remark, however, that in general, crude oils and crude oil emulsions become very viscous with decreasing temperature. The authors observed that the bubbles of emulsion incorporated into the ice field were much larger (10 to 20 mm) than those in the crude oil experiments. Continued agitation reduced the size significantly (to 5 mm), but the relatively large size of the drops prevented upward movement in the ice field.

The authors estimated the amount of oil incorporated into the grease ice by pouring off the unincorporated surface oil and measuring its volume. The amount of oil incorporated in the grease ice, emulsified or otherwise, was 80 to 90%.

The ice concentration of the grease ice field was varied. In the denser ice field, the average oil drop size was 5 to 10 mm; in the thinly packed ice, the drop size was 10 to 20 mm. The authors state that stirring the mixture seemed to cause a "greater grinding motion between ice particles" in the densely packed ice than in the loosely packed field, which caused the formation of smaller droplets.

An emulsion of a 70/30% mixture of No. 2 and No. 6 fuel oils, salt water, and 2-mm ice crystals was mixed in a ratio of 1:9:1 (oil:water:ice). The authors were unable to obtain a water/oil ratio or density for these emulsions as they were very unstable. The presence of the ice crystals seemed to hinder the emulsion formation. Once incorporated into the ice field, however, the emulsions remained stable over an observation period of 48 hours with no sign of oil/water separation.

Effect of Solar Radiation on Ice Formation

The authors remark that limited information was obtained from the solar radiation experiments due to uncontrolled temperature fluctuations. However, for a 2-mm thick layer of a 70/30% mixture of No. 2 and No. 6 fuel oils, a 60-W light bulb positioned 1 m above the oil surface prevented ice formation for the 24-hour observation period. For an identical sample in darkness, ice crystals began to form after 1 hour (see Figure 3.2). A complete ice layer formed underneath the oil in 4 hours and was 10 cm thick after 12 hours.

Effect of Oil on Growth of a Turbulent Ice Field

These experiments were performed in the test apparatus shown in Figure 3.1 with a 2-mm layer of a 70/30% mixture of No. 2 and No. 6 fuel oils. The authors expected, but did not observe, a frazil/grease/pancake formation process. Instead, a "slushy, crystal-like porous frozen mixture" formed which incorporated "significant quantities" of oil. Columnar ice was formed underneath this layer which trapped round oil droplets (0.5 to 10 mm diameter) in the first few centimetres below the surface. The porous upper layer was solid, but contained many oil droplets in the interstices.

During the agitation cycles of the oscillating hoop, the oil was initially momentarily driven under water, then resurfaced. As freezing progressed, ice chunks forming the increasingly solid porous layer inhibited the oil's ascent to the surface. The oil was close to neutrally buoyant (specific gravity 0.919) and was trapped in large quantities in the first 10 cm of the developing ice. Shortly after columnar ice began to develop, the ice was able to trap larger drops of oil, and columnar ice began to from around and beneath the oil. The ice was of such a porosity that, when the ice was pushed down in the vessel, oil would flow upwards, out of the channels in the ice. The authors explain that as the forming ice was oscillated by the hoop, the fragile "vertical fingers" of the columnar ice would collapse to form horizontal plates of ice. Oil driven downwards by the hoop would become trapped in the collapsing ice fingers, forming a porous mixture. Once this layer had formed, oil droplets were driven beneath the forming ice and became directly entrained in the forming ice fingers.

A similar experiment was performed with a much less dense mineral oil (Bayol 35, specific gravity of 0.790). Due to its greater buoyancy, the mineral oil surfaced much more quickly than the crude oil mixture and thus far less was entrained in the ice. The porous ice/oil layer was not

observed. In general, far less mineral oil was entrained, at a shallower depth and in much smaller droplets than was the case for the crude oils.

The hoop did not oscillate with enough energy to break up the oil layer except around its perimeter. The authors were thus unable to quantify the "insulating, ice growth retarding" and "wave dampening, ice growth promoting" behaviour. The authors speculate that solar radiation, which was not included in their experiments, would "add to the insulating effect of the oil and further retard ice development." They also suggest that the experiments predict that in a real spill situation, the oil layer would be broken up by wave action and not be thick enough to dampen wave action and insulate the water below. The authors also note that there was "no significant difference" in time for ice formation with or without a thin layer of oil under turbulent conditions.

Field Study of Oil in Ice

The authors report field observations of a spill of No. 6 fuel oil in the Gulf of St. Lawrence, three days after it had occurred. The ice consisted of a 5-m wide strip of grease and pancake ice along the river bank, then a 20-m strip of frazil/grease ice, and then open water. The oil was originally spilled in the open water beyond the ice edge and had been forced by waves and wind into the ice along the shore. No oil was visible on the surface. Oil was washed ashore in grease ice that had been compressed by the pressure of the ice on the shore. The result was a porous ice mixture that contained up to 50% oil.

The densities of several samples are shown in Table 4.7.1. The density of the slightly salt water at the spill site was approximately 1.02 g/mL. The authors comment that, given the density of the oil at 0°C, (see Table 4.7.1), large amounts of oil could have been present below or within the ice, even though none was visible on the surface. They further note that there was a high level of turbulence and water/oil emulsions may have formed.

Table 4.7.1 [Oil Sample Densities of Mantane Oil Spill]

	Density (g/mL)	
Temperature (°C)	**Sample 1**	**Sample 2**
25	0.9996	1.0020
20	1.0033	1.0061
15	1.0073	1.0098
0	1.0178	1.0204

Discussion

The authors categorize oil/ice interactions as either oil spills on open water with ice development under the slick or spillage into an existing, or developing, ice field. For spills of oil on open water, the authors remark that Cross *et al.*, 1986, showed that an oil slick may act as an insulating

layer equivalent to a 15-times thicker ice sheet. The authors note, however, that static ocean environments are not common. Turbulent seas would likely break up the slick and the water would freeze at the normal rate. The authors also contend that a very thick layer of very viscous oil would be required to significantly dampen wave action. Furthermore, if such a thick layer of oil were present, ice formation would be enhanced by the calming effect of a heavy layer on the water, effectively negating the thermal insulating effect of the oil layer. The authors state that, in calm seas, the ice structure is not altered by the presence of oil with columnar ice growing beneath the oil. In turbulent water, the frazil-grease-pancake growth chain still occurs, except that the resulting ice sheet contains oil-filled inclusions.

For oil spilled into an ice field, the authors looked only at spills into frazil or grease ice. Their stated concern was to determine the quantity of oil entrained, and hidden from view, by the ice field. The authors felt that oil density is the main factor that determines the extent of oil incorporation. Oil is easily submersed in grease or frazil ice because ice is much less dense than water (a specific gravity of 0.917 is given by the authors). The authors also remark that, because of the interfacial tension between oil and water particles as well as high oil viscosities, an oil that is less dense than the grease ice/water mixture may remain submerged within the grease ice layer. They argue that this was demonstrated by their observation of approximately 50% entrainment of the 0.790 g/mL oil in the oil incorporation experiments.

Effective oil density, and thus incorporation in ice, can be increased through weathering and emulsion formation. In cold conditions, evaporation occurs slowly. It was not clear from this work whether an oil slick lasts long enough to allow significant weathering for oil entrainment into ice. The authors note that No. 6 fuel oil showed a noticeable increase in density in their observations of the St. Lawrence spill. The emulsion formation studies reported by the authors indicate that emulsions can form in a reasonably short period and that emulsions may possibly form with a density greater than ice.

The size of ice particles is also significant for determining oil incorporation. It appears that maximum incorporation occurs for ice particles in the 2 to 5 mm range. The authors remark that there is a trade-off between particle size and porosity of the ice field. Very large particles form wide channels through which oil can move easily, while small particles have low porosity and individual oil drops are buoyant enough to push aside the tiny particles of ice. In the optimal size range, the ice crystals are large enough to resist displacement by the oil, while the interstitial spaces are too small to allow the oil to pass easily. The authors remark that this is potentially very important because, in turbulent seas, grease ice fields, susceptible to constant compaction from waves, floes, etc., may reach this optimal particle size and thus entrain large amounts of oil. The authors conclude that dynamic action of a grease ice field may be a key factor in the incorporation of oil into ice.

The authors also state that turbulence is an important mechanism for oil encapsulation in a growing ice field. They note that, while a grease ice field would dampen waves, only a small amount of turbulence was necessary to submerge the oil particles. Once under the ice, the oil droplets would be entrained in the ice as previously described. The authors remark that this is reinforced by their observations of the spill of No. 6 fuel oil in the Gulf of St. Lawrence. In that

case, the grease ice field did not suppress breaking waves and thus did not prevent the submergence of the oil.

The authors describe their solar radiation results as inconclusive. They state that, while a layer of oil heated by sunlight may prevent or delay ice formation, particularly when temperatures are close to freezing, under turbulent conditions, the oil layer would be too broken up to have any effect. The authors remark that solar heating would likely be important only when oil is hastening the thawing of ice.

The ice thaw studies showed that lighter oils were released faster from melting ice than denser oils. The authors attribute this to differential submergence dependent on oil density during ice formation. The authors also speculate that solar radiation would heat the surface oil, further speeding the melting of ice.

BOSS Critique

The authors present an extensive catalogue of experiments on the effects of oil on the formation and thawing of ice. Their main experimental parameters were oil density/buoyancy and water turbulence. They elucidate several mechanisms of oil entrainment in ice and its release from the ice upon thawing.

Of primary interest in this work are:

- the observation that oil weathering is not affected by the presence or absence of ice and happens very slowly at Arctic temperatures;
- the observations about the effects of particle size on oil entrainment, in particular, the determination of the optimal crystal size for maximum entrainment;
- the description of ice formation in an energetic wave field in the presence of both oil and oil-in-ice emulsions;
- the development of a mechanism for oil entrapment in forming ice; and,
- the observations concerning the effects of oil on melting ice as a function of the oil density.

While providing excellent qualitative insight into the processes involved in ice formation and melting in the presence of oil, few quantitative results are presented that would be applicable to future spills. It should also be noted that ice thawing observations in particular were not made in typical salt water conditions. The experiments were performed in fresh water in which no brine channels will form in the resultant ice. It is known that brine channel migration is a major mechanism for oil release from ocean ice packs. In addition, the effects of viscosity and surface tension are not examined in this work, although they are probably as important to the oil slick behaviour as oil density.

S. Liukkonen, R. Koskivaara, J. Rytkonen, and K. Lampela, "Adhesion of Oil to Plastic, Stainless Steel and Ice", in *Proceedings of the Eighteenth Arctic Marine Oilspill Program Technical Seminar*, Environment Canada, Ottawa, Ontario, pp 69-90, 1995.

Summary

"The apparent adhesion strength test yielded low values for the adhesion of oil on ice", a result expected from empirical evidence. However, "the contact angle measurements yielded small contact angles for oil drops on ice indicating rather strong adhesion between oil and ice." The authors remark that this was unexpected and conflicts with much empirical evidence.

Objective

The authors report adhesion parameters of oil on a range of surfaces. Only their results for sea ice are included in this review.

Theory

Contact angles are defined by a formulation in Zisman (1962, p. 180) for the reversible work per unit area, W_A, needed to pull a liquid drop off a surface:

$$W_A = \gamma_L(1+\cos\theta), \quad (1)$$

where γ_L is the surface energy of the liquid interface and θ is the contact angle. The larger the contact angle, the weaker the adhesion of the liquid to the solid substrate. The contact angle is governed by the Young-Duprè equation (Moore, 1975, p. 148):

$$\gamma_S = \gamma_{SL}+\gamma_L\cos\theta, \quad (2)$$

where γ_S, γ_{SL}, and γ_L are the surface energies of the solid, solid-liquid, and liquid interfaces respectively. The authors note that the interfacial energies are very difficult to determine individually and contact angles are therefore best determined experimentally.

Apparent adhesion values are not rigorously discussed. The authors note that the apparent adhesion values may include contributions from viscosity as well as surface effects.

Method

Two oils were used for contact angle measurements: a light fuel oil and North Sea Brent crude oil. A heavy fuel oil was used for the surface adhesions test. The authors give physical properties for each oil in Table 2.

Table 2 Properties of the Pre-altered Oils

Property		Test Method	North Sea Crude	Light Fuel Oil	Heavy Fuel Oil
Density	+15°C	ASTM D 4052	0.8495	0.8433	0.9820
[kg/L]	+10°C	[a]	0.8529	0.8467	0.9853
	0°C	[a]	0.8598	0.8536	-
	-10°C	[a]	-	0.8608	-
Viscosity	+10°C	ASTM D 445	20.56×10^{-6}	4.37×10^{-6}	[b]
[m^2/s]	0°C	ASTM D 445	[b]	5.79×10^{-6}	[b]
	-10°C	ASTM D 445	[b]	8.18×10^{-6}	[b]
Pour Point [°C]		ASTM D 97	8	-	3
Water Content [% by weight]		ASTM D 1744	0.05	0.01	1.55

[a] Conversion from +15°C, ASTM D 1250.
[b] Oil solidified in viscosimeter pipes.

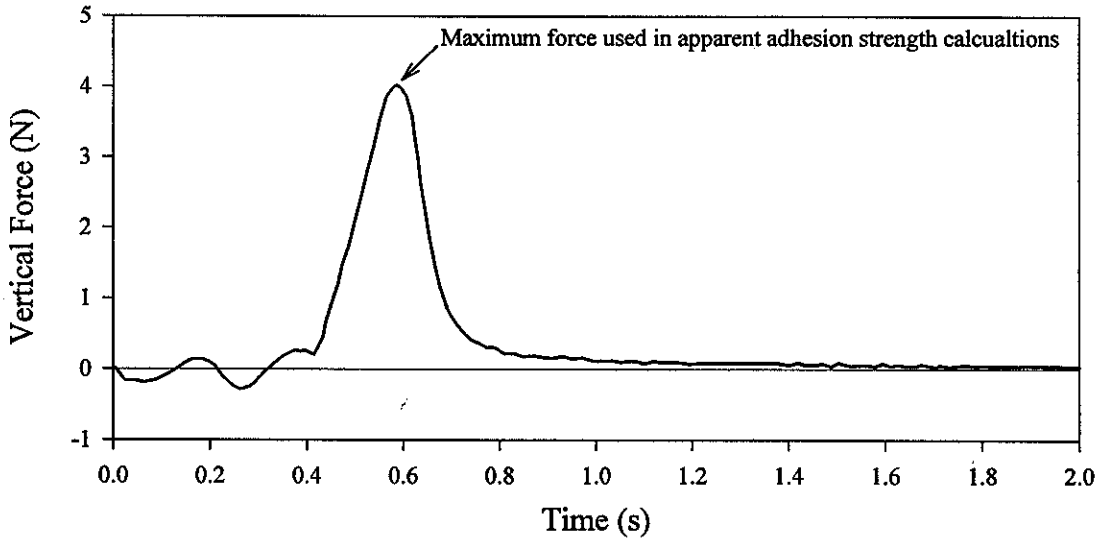

Figure 9 Sample of Force Time History Recorded for a Vertical Apparent Adhesion Strength Test

The ice was frozen sea water from the Gulf of Finland offshore from the city of Helsinki. The roughness of the ice surface was measured with a portable Taylor and Hopson roughness meter. The mean roughness height (5 measurements) was reported as 1.88 ± 1.05 μm.
The experimental apparatuses are described in detail. Contact angles were measured from tangent lines drawn on photographs of the oil droplets on the ice. Several drops were used for each

reading. The sample surface was cleaned with hexane and ethanol before each measurement. The authors note that, they were unable to determin contact angles for the heavy fuel oil as it did not form a defined drop at any of the experimental temperatures.
The apparent adhesion was measured by both vertical pull and horizontal shear. The maximum separation force was divided by the post-test oil blot diameter to derive the interfacial tension. Figure 9 shows a sample force vs. time plot for a vertical separation test.

Results

The contact angles for ice are reported in the following table.

Extracted from **Table 4** **Results of Contact Angle Measurements** (degrees)

Liquid on Ice	**0°C**	**-10°C**
Crude Oil	20 ± 2	27 ± 7
Light Fuel Oil	[a]	[a]
Water	[b]	

[a] Angle was too small to measure (the smallest angle reported was 4°)
[b] The authors remark that the contact angle of water on ice at 0°C is known to be almost zero (Hobbs, 1974, pp 437-438). They did not report a water-on-ice value themselves.

The apparent adhesion values for the heavy fuel oil are shown in the following table.

Extracted from **Table 5** **Results of Apparent Adhesion Strength Tests** (Pa)

	0°C	-10°C
Vertical	1.04 ± 0.68	3.24 ± 2.38
Horizontal	0.29	0.91

By comparison with the other results in Table 5, it is likely that errors in the horizontal apparent adhesions would be as large as the values themselves. The authors do not report an estimated error.

Boss Critique

The measured angles and apparent adhesion values give an indication of the relative surface binding strengths for various oils. A further improvement to the otherwise solid experimental work would have been a measurement of the apparent adhesions of all the oils (and thus the work per unit area). This would allow an estimate of the surface interface energies, γ_L, using the contact angles for the light fuel oil and crude oil. By this means, the results for all three oils on ice would have been comparable.

Kawamura, P., D. Mackay and M. Goral, *Spreading of Chemicals on Ice and Snow,* EE-79, Environment Canada, Ottawa, Ontario, 106 p, 1986.

Technical Summary:

"A relatively simple, liquid spill behaviour model has been developed which includes terms for the extent and rate of spreading, as well as absorption, evaporation and snow and ice dissolution. Experiments were performed on snow and ice surfaces to determine the spreading behaviour and characteristics.... The chemicals studied were: m-xylene, bayol (white mineral oil), and light and heavy mineral oils."

"The final spill area and spreading rate results were correlated with the spill volume, chemical viscosity, [and, for snow-covered surfaces,] snow depth and properties, in dimensional and dimensionless form. These correlations... are believed to enable predictions to be made of the spreading behaviour for most chemicals under actual spill conditions."

Objective:

The study is concerned with the development of a kinematic model for the spreading of chemicals on snow and ice and the evaluation of the model by a series of experiments. The final spill area is experimentally correlated to physical and chemical properties. Both oil- and water-soluble chemicals are discussed, however only oil products are included in the present review.

Theory:

Existing Spreading Models

The authors review the existing spill modelling literature starting with Fay, (1969). They also discuss the work of Raisbeck and Mohtadi (1974), McMinn (1972) and Hoult *et al.* (1975). The authors point out the dependency of all of the above theories on surface parameters (such as contact angle and roughness) which are often difficult to obtain.

The work of Chen *et al.* (1974) and Chen and Charles (1976) "correlated the [spill] data in dimensionless form," but "combining these results into a general spreading model proved to be difficult..."

Theory of Spreading

The spreading theory developed by Fay (1969) and Chen's studies (as above) is presented in detail. The model considers spreading to occur in three phases, in which a spreading force is balanced by a retarding force. These three regimes are gravity-inertia, gravity-viscous, and surface tension-viscous. The first two stages were described by the work of Chen and co-workers, but the third stage, involving all of the air-liquid, liquid-solid and air-solid interfacial tensions had not been well described prior to the authors' work. The authors note that "there are at present [1986], no simple models or equations which can be used to predict the degree of spreading for any liquid...."

The force balance of the three interfacial tensions and the viscous force. F_v are illustrated in Figure 3.1. During the final phase of spreading the net force is given by:

$$\Delta\sigma = \sigma_i - (\sigma_{ic} + \sigma\cos\theta) \qquad (3.1)$$

where $\Delta\sigma$ is the net spreading force; σ_i is the air-solid interfacial tension, or the solid surface tension; σ_{ic} is the liquid solid interfacial tension; σ is the liquid-air interfacial tension, or the liquid surface tension; and θ is the contact angle. When the spill has stopped spreading, then the following equality applies ($\Delta\sigma=0$):

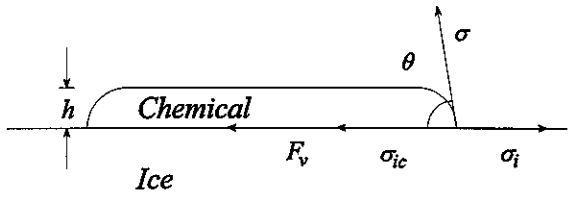

Figure 3.1 Interfacial Tensions Which Influence Spreading (After Chen and Charles, 1976)

$$\sigma_i = \sigma_{ic} + \sigma\cos\theta_e \qquad (3.1a)$$

where θ_e is the equilibrium contact angle.

Contact angles have been described as a wetting or "spreadability" parameter (Banerji, 1981):

$$\text{Degree of spreading} = (1+\cos\theta_e)/2 \qquad (3.2)$$

A chemical with an equilibrium contact angle of zero will completely wet a surface; a substance with a contact angle of 180° will not wet the surface at all, forming beads. "It is possible, if the solid-liquid adhesion energy exceeds the energy of cohesion [of the liquid], to have a case where there is 'no contact angle.'" In this case, the kinetics are driven by the intermolecular cohesive forces of the liquid and the chemisorption attachment forces to the surface and not the interfacial tensions.

Behaviour of Chemical on Snow and Ice

"It is expect that most chemicals will have a fairly high degree of spreading on ice." The authors argue that ice has a high energy surface (ice-air interfacial tension of 80.2 dynes/cm, Spelt *et al.* (1982)) and that spreading minimizes energy since the ice-chemical interfacial energy is less than that of ice and air.

Spills on snow are more complex. Models require accounting for absorption into the snow and diffusion once absorbed. This depends on the nature of the snow including porosity and crystal size. The "infiltration of liquids into snow may be determined by Darcy's Law" (Collins, 1961). The authors consider snow over ice to be a typical for most spill situations.

The authors propose a basic spill model (for ice only surfaces) of the form:

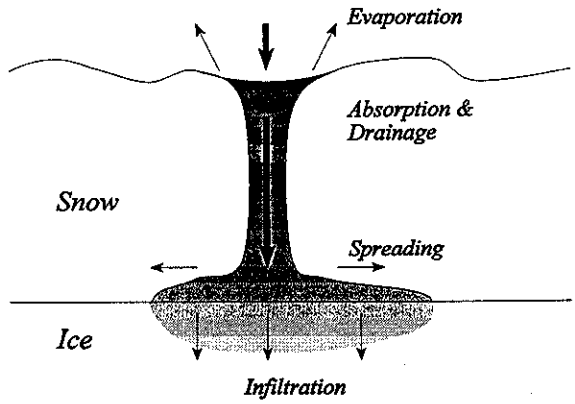

Figure 3.2 Transport of Chemicals in Snow Media

$$A = A_F(1-e^{-(t/\gamma)^x}) \tag{3.3}$$

where A is the spill area, A_F is the final area at infinite time, t is time and γ and x are constants. Note that when $\gamma = t$, $A/A_F \approx 63\%$ regardless of the value of x.

The final spill area can be estimated from the initial spill volume, V, the volume change (due to evaporation, absorption, etc..., ΔV, and the final spill depth, h_f, as:

$$V-\Delta V = A_F\ h_f \tag{3.4}$$

The authors estimate ΔV as the sum of three terms:

$$\text{Loss due to evaporation} = h_e\ A_F \tag{3.5a}$$
$$\text{Loss due to absorption in soil} = h_a\ A_F \tag{3.5b}$$
$$\text{Gain due to dissolution of snow} = h_s\ A_F \tag{3.5c}$$

therefore:

$$\Delta V = A_F\ (h_e+h_a-h_s) \tag{3.6}$$

For evaporation, the authors hypothesize that:

$$h_e = C_e K_e (Pv/RT)\gamma \tag{3.7}$$

where C_e is a dimensionless constant, K_e is a mass transfer coefficient, (Pv/RT) is the dimensionless ratio of chemical concentration in air to concentration in the chemical phase (P is vapour pressure, v is molar volume, R is the gas constant, T is the absolute temperature). The time term is γ and C_e thus "corrects" for the change in area with time.
Similarly, for absorption,

$$h_a = C_a K_a \gamma \tag{3.8}$$

where K_a is an absorption velocity controlled by the ice/snow porosity.
For snow dissolution,

$$h_s = \phi H_s \tag{3.9}$$

where ϕ is the volume fraction of water in the snow and H_s is the mean snow depth dissolved. For oil products, dissolution is effectively zero.
Thus:

$$A_f = V/(h_f+h_e+h_a-h_s) \tag{3.10}$$

Combining Equations (3.3) to (3.10):

$$A_f = \frac{V(1-e^{-(t/\gamma)^x})}{h_f+[C_e K_e (Pv/RT)+C_a K_a]\gamma-\phi H_s} \tag{3.11}$$

The parameters that must be determined experimentally in Equation (3.11) are:

- γ, the spreading time constant, which the authors suppose to be a function of viscosity, μ,
- x, the slope term,
- C_a, the absorption constant,
- C_e, the evaporation constant, and,
- h_f, the final spill thickness which is expected to depend on the interfacial tensions (Figure 3.1).

The other parameters, K_a, P, V, T, K_e, ϕ and H_s "can be estimated directly from spill conditions and chemical properties."

The authors estimate the total spreading time as that when A is 99% of A_F:

$$t_f = (4.605)^x \gamma \tag{3.12}$$

Although they proposed a detailed model, the authors tested a much more restricted version, specifically ignoring evaporation and absorption. Oil and petroleum products do not appreciably dissolve ice or snow and thus, those aspects of the authors' work are not discussed in the present review. The equation evaluated by the authors for spreading on ice was:

$$A_f = \frac{V}{h_f}(1-e^{-(t/\gamma)^x})$$

for snow, terms for snow depth and type were included (see the Results: section).

In addition, the authors also correlated spill volume and chemical viscosity to the final area/spill depth ($A_F h_f = V$) for spreading on both ice and snow. The hypothesis outlined above in Equations (3.3) to (3.12) does not give absolute equilibrium values for final spill area or height, except in the broadest sense (q.v. the "degree of spreading," Equation (3.2)).

Experimental:

Contact angles were measured on glass and ice from photographs of beads on glass and on ice. Two photographs were used for each reading. Precision of the measurements is not reported.

"Small-scale spreading experiments were performed on artificially prepared smooth and rough ice surfaces." The ice area was 61×61 cm square and held to -5 °C. The smooth ice was "free from cracks or apparent roughness." Rough ice surfaces were prepared by sifting ice crystals of the desired size over a smooth ice surface. Two size ranges were used: 0.5–1.0 mm and 1–2 mm. the

crystals were prepared by forcing crushed ice through a sieve. The crystals were allowed to partially melt and refreeze into the surface before the experiments.

The chemicals used were m-xylene, n-pentanol, heavy USP mineral oil and a white mineral oil called Bayol 35 (abbreviated to Bayol in the present review). These chemicals were chosen for their wide range of viscosities (see table R.1 below), low solubility in ice and snow, small evaporation rate and non-hazardous nature. Volumes of 25 and 50 mL were used on the smooth ice surfaces; only 50 mL was used for rough ice spills. The liquid was spilled effectively instantaneously at the start of the experiment. Spreading was recorded photographically. New surfaces were used for each experiment.

Table R.1 Viscosities of Spilled Chemicals
in cp at -5 °C

m-Xylene	0.9
Bayol	8
n-Pentanol	11
Light Mineral Oil	450
Heavy Mineral Oil	1500

The outdoor experiments were carried out on a 2.4×2.4 square metre platform, marked in 10 cm intervals. Five "oil" spills were conducted: m-xylene, 450 mL and 1 L; n-pentanol, 1 L; Bayol 700 mL; and light mineral oil, 2 L. The discharge time was less than 5 seconds. Spreading was recorded photographically. After each experiment, the surface was cleaned and water poured over the ice sheet to form a clean layer of ice. The surface are reported as "relatively smooth for most experiments, although several 'rough' (<1 mm) areas were observed for some experiments, which may have been due to wind effects during freezing. A few cracks in the ice were also present."

The spill spreading experiments were carried out over glass and over ice, outdoors. The glass apparatus consisted of a sheet 91×91 cm with a 1 cm grid. the snow was placed on the glass and the spreading of the chemical (dyed red) was observed from underneath. Unlike the ice spreading experiments, the spreading on snow was slow enough to be recorded by stopwatch. Penetration time (the time needed to penetrate the snow cover), air and snow temperatures were also recorded. After each experiment, the cross section of the snow was examined and drainage and the amount of "slush" was recorded. The experimental conditions are given in table 4.1.

In addition, a spreading experiment was carried out on the outdoor ice surface. The spread of the spill (Bayol) was measured using dipsticks through the snow. Spreading was assumed to have stopped after a 3 hour period in which less than 5 cm of spreading had taken place. The final spill area was determined by removing the snow.

Table 4.1 Experimental Conditions for Snow Spreading Experiments...

Experiment	Vol. (L)	Ave. Temp. (°C)	Snow Density (g/mL)	Snow Depth (cm)	Snow Type*	Age (days)	
Volume	0.5	-6	0.25	3	a, b	1	Dry
	1	-8	0.25	3	a, b	1	Dry
	2	-8	0.25	3	a, b	1	Dry
	3	-3	0.25	3	a, b	1	Dry
Snow Depth	2	-6	0.27	4	b	2	Dry
	2	-6	0.27	9	b	2	Dry
	2	-9	0.26	15	b	2	Dry
	2	-4	0.25	30	a, b	1	Dry
Snow Density	1	-4	0.12	10	a, b	1	Dry
	1	-1	0.25	10	b	3	Wet
	1	-1	0.42	10	b	3	Wet
Viscosity	1	-2	0.25	10	b	2	Dry
	1	-3	0.25	10	b	2	Dry
	1	-5	0.25	10	b	2	Dry
	1	-6	0.24	10	b	2	Dry
	1	-3	0.25	10	b	3	Dry
Snow Type†	3	-2	0.41	3	c, e	>10	Dry
	3	-3	0.34	9	c	7	Dry

*Snow types from NRC Canada, 1954: Type a is fresh snow with grain < 0.5 mm (crystals can be as large as 5 mm). Type b is settled snow that has lost most of its structure and is fairly soft; grain 0.5–1 mm. Type c is composed of irregular or rounded crystals as a result of freeze-thaw. Very hard when frozen; grain size 1–2 mm. Types d and e refer to successively more weathered and compacted snow.
†This experiment conducted outdoors.

Results:

Contact Angle Measurements

The equilibrium contact angles measured for water-insoluble compounds are given in the extract from table 5.3. The authors remark that there does not seem to be any overall correlations in the data, which is in agreement with the general results found in the literature. The surface tensions in table 5.3 were calculated from the equation of state given by Gerson, 1982. The authors note that the calculated ice surface tension values are very different from the literature value of 80.2 dynes/cm (Spelt *et al.*, 1982). They speculate that the calculated values "are not the true surface tensions but

are rather measures of an apparent of effective surface tension. The true value of 80.2 dynes/cm is applicable only for pure ice without the presence of chemicals or other substances." The true value reflects a clean surface, while the apparent values will reflect the ice surface in the presence of another chemical. In other words, a bare ice surface differs chemically from a covered one. The authors remark that the small chemical-ice interfacial energy is also a property of high surface energy materials, such as ice.

Extracted from Table 5.3 Experimental Contact Angles and Interfacial Energies (dynes/cm) for Various Chemicals on Ice

Chemical	Equilibrium Contact angle (degrees)	Chemical Surface Tension	Ice Surface Tension	Chemical-Ice Interfacial Tension
m-xylene	14	32	31	-0.04
bayol	10	27	26	-0.23
mineral oil	27	32	29	+0.21
toluene	15	33	32	+0.05
n-pentane	10	19	19	-0.01
n-hexane	11	21	21	+0.06
n-octane	12	24	24	-0.02
n-nonane	12	25	27	+0.06
n-decane	14	28	27	+0.06

Spreading on Ice Surfaces, Correlations with the Final Spill Area/Depth.

For the four chemicals (m-xylene, bayol, n-pentanol and heavy mineral oil) viscosity and total spill volume were plotted against final spill depth on log-log plots, Figures 5.4.1 and 5.4.2 respectively. The authors note that (for the viscosity experiment) spills on the rougher ice surface generally had smaller final heights. "The effect of roughness on spreading is believed to be dependent on the roughness height, relative to the height of the final chemical pool, and on the wettability of the chemical to the ice surface. A decrease in final spill depth... may occur when the final spill height is approximately equal to or less than the height of roughness.... This action is a result of interfacial forces..." the authors argue that since rough surfaces have a higher surface area, the net surface-liquid force term, σ_{ic} in Equation (3.1), is higher on a rough surface than on a smooth one, thus increasing the final spill area .

However, the authors point out that roughness has a relatively small effect on the final spill height and thus can be ignored to a first approximation. Regression fits to the four data sets on Figure 5.4.1 gave an average slope of 0.24 (correlations and errors are discussed in the BOSS Critique).

Similarly, from Figure 5.4.2, an average slope of 0.11 was determined for the correlation of volume to spill height. The authors remark that the low value for the 1 L m-xylene spill was caused by wind-thinning of the slick (this experiment was conducted outdoors).

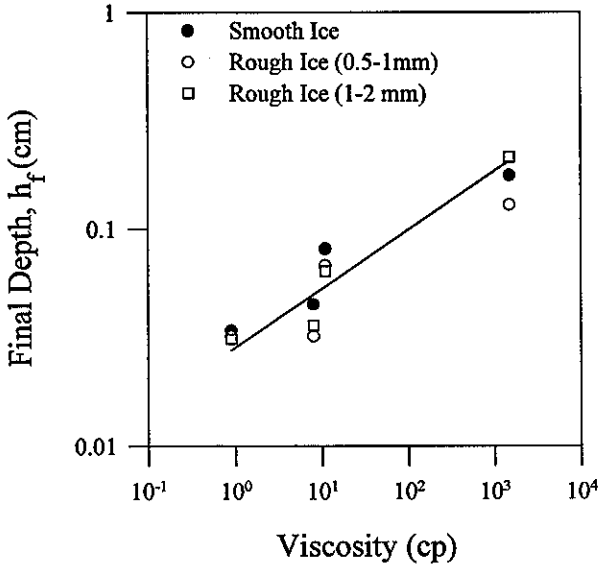

Figure 5.4.1 Effect of Viscosity on Final Spill Depth on Ice

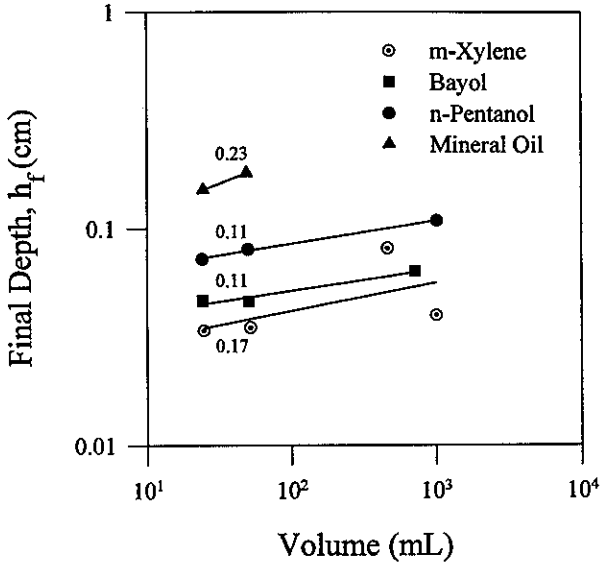

Figure 5.4.2 Effect of Volume on Final Spill Depth

From the two figures, the correlations for final height and area ($A_F = V/h_f$) are $h_f \propto V^{0.15}\mu^{0.24}$ and $A_f \propto V^{0.85}\mu^{-0.24}$, where μ is the chemical viscosity and V is the total spill volume.

The expression for volume was non-dimensionalized by introducing multiplicative terms in the chemical density, ρ_c, the liquid surface tension, σ, and the gravitational constant, g. There is no explanation of why these particular factors were chosen, however, it is likely that the authors used them in consideration of the various forces acting on the spill. Note that Chen *et al.*, 1974 performed a similar analysis for oil under ice spills. The non-dimensionalized form:

$$\frac{A_f}{V^{2/3}} = 6.0\ \frac{V^{0.18}\rho_c^{0.33}g^{0.21}}{\mu^{0.24}\sigma^{0.09}} \qquad (5.2)$$

The slope value of 6.0 was determined by a log-log plot of the right-hand side of Equation (5.2) *vs* the left-hand side, shown in Figure 5.4.3. Note that the exponents of ρ_c, σ, and g were determined by the

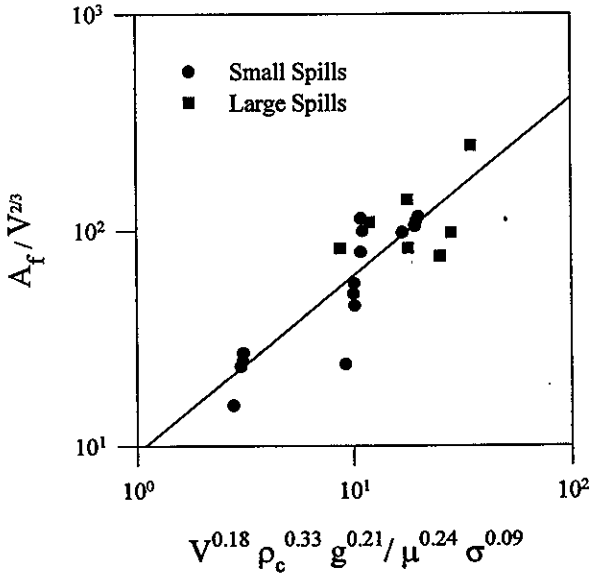

Figure 5.4.3 Correlation of Final Spill Area on Ice

non-dimensionalization procedure only, not experimentally. For the spill height, in metres:

$$h_f = 0.008\, V^{0.15} \mu^{0.24} \qquad (5.2a)$$

The authors note "since ρ_c and σ do not vary greatly for most chemicals, similar results will be obtained using either Equation (5.2) or (5.2a)."

While the authors make no further correlations with the experimental data, it seems natural to plot the "degree of spreading" parameter (Equation (3.3)) against the spill depth. This is shown for the 50 mL spills on Figure R.1. While there may be a linear relationship between the cosine of the contact angle and the spill depth, the data presented in the authors' work are insufficient to form any conclusions.

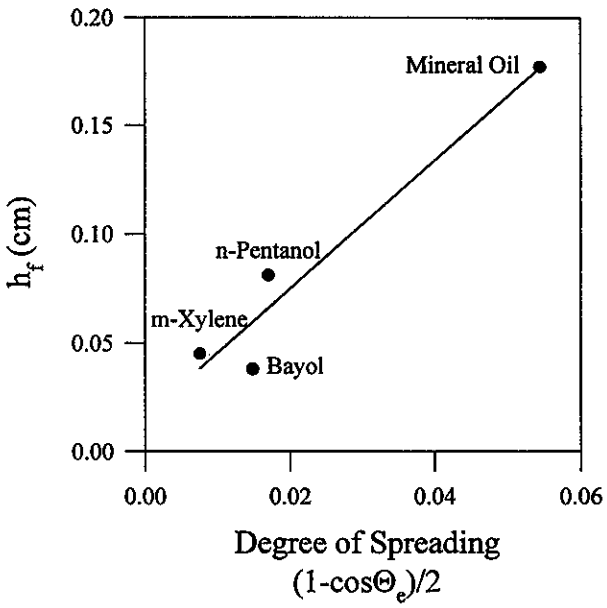

Figure R.1 Correlation of Final Spill Depth and "Degree of Spreading" Parameter

Kinetics of Spreading on Ice

The spreading time constant, γ, of Equation (3.3) was estimated from the time necessary to reach 63% of the final spill area, that is, when $t=\gamma$, regardless of x. The time constant was plotted as a function of viscosity for constant spill volume experiments (Figure 5.4.4 for smooth ice, Figure 5.4.5 for rough ice) and as a function of spill volume (Figure 5.4.7 for all four compounds). Errors on the plots were estimated from the uncertainty of reading the time at 63% from the time series plots (see Figures 5.4.9 and 5.4.11). From the best-fit slopes of these plots, the authors determined the average relationship: $\gamma \propto \mu^{0.5} V$. In non-dimensional form this becomes:

$$\frac{\gamma V^{1/6}}{g^{0.5}} = 2.5\times10^{-5}\ \frac{V^{7/6}\mu^{0.5}\rho_c^{1.625}g^{1.875}}{\sigma^{2.125}} \qquad (5.3)$$

where the constant was determined from the slope of Figure 5.4.8. In SI units, Equation (5.3) is:

$$\gamma = 5\times10^{5}\mu^{0.5}V \qquad (5.3a)$$

The authors remark, "from Figure 5.4.8 it can be seen that the spreading time constants predicted

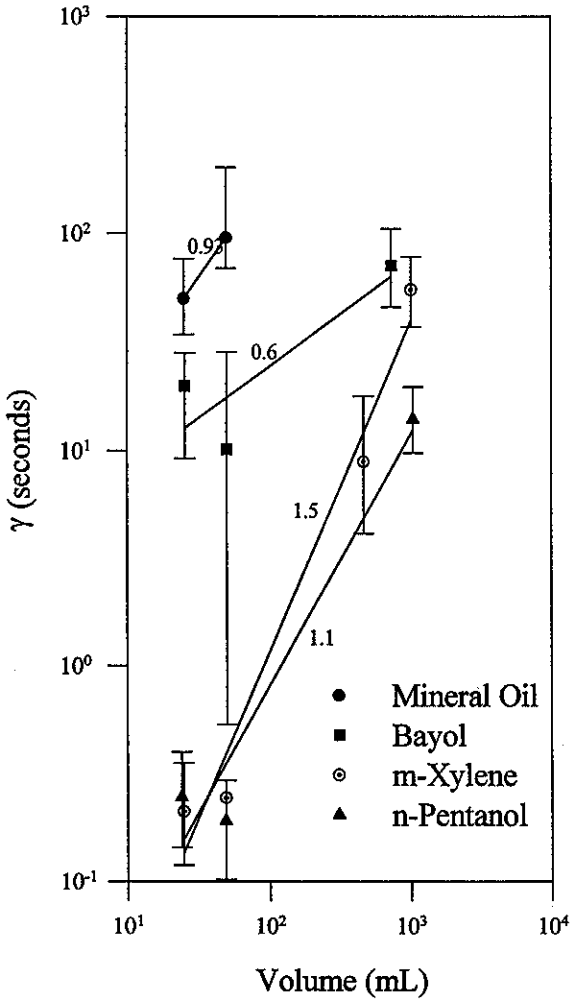

Figure 5.4.7 Effect of Spill Volume on Spreading Time Constant (Slopes Indicated Above Lines)

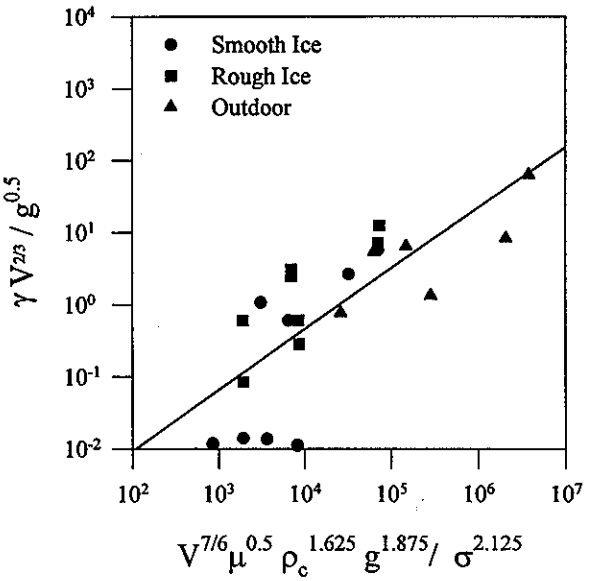

Figure 5.4.8 Correlation of Ice Time Spreading Constant

by Equations (5.3) and (5.3a) can... overpredict or underpredict the actual time constant by an order of magnitude. Thus caution should be exercised when applying these equations to determine the spreading rates for actual spills." The authors mention that real spills are usually not discharged instantaneously as in their experiments, but leak onto ice over time. This would be expected to have a large effect on the spreading kinetics. "It appears that a more accurate correlation cannot be developed without including effects of chemical-ice interaction, surface roughness and the spill discharge rate."

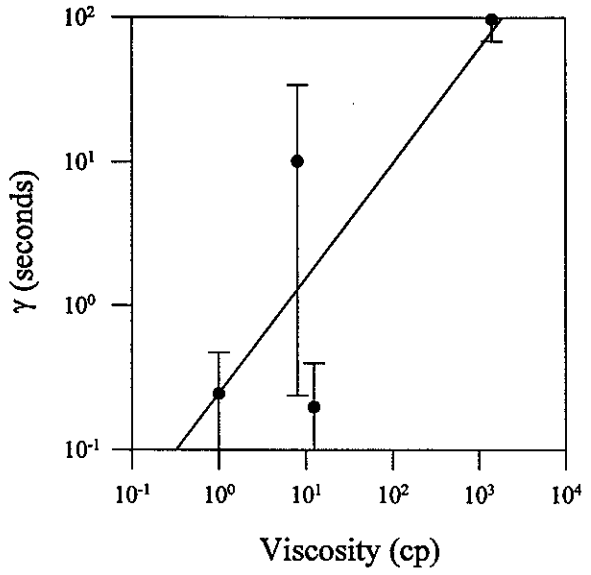

Figure 5.4.4 Effect of Viscosity on the Spreading Time Constant (Smooth Ice)

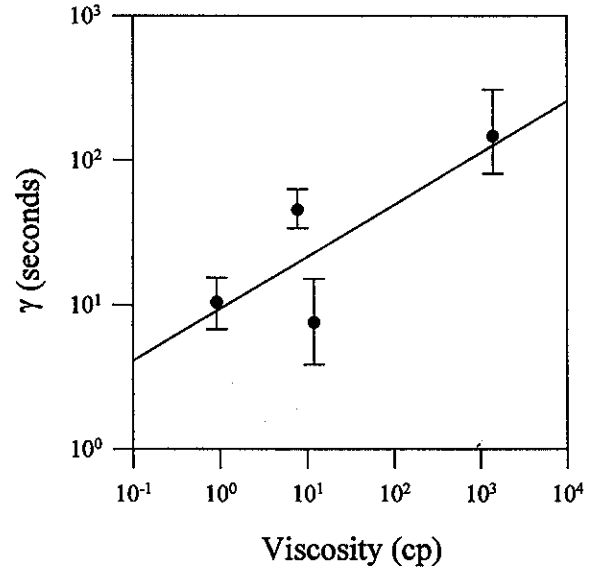

Figure 5.4.5 Effect of Viscosity on Spreading Time Constant (Average of Two Rough Surfaces)

To determine a value for x, the "slope term" of Equation (3.3), various spill-area profiles were matched with the experimental data for all ice experiments. See Figures 5.4.9 and 5.4.11. The small inset panels on both figures show the "linearized" relationship between the data and the model. "It was determined that the best value of x ranged between 0.3 and 0.7 for all but one experiment, with 0.5 being the best or next-to-best value for 14 out of 21 experiments." The "one experiment" mentioned as not fitting Equation (3.3) was an outdoor m-xylene (low viscosity) spill that was highly wind-herded during the experiment.

Thus a value of 0.5 was chosen for x. Estimating the total spreading time to be when the area is 99% of the final area gives:

$$t_f = 20\gamma \tag{5.4}$$

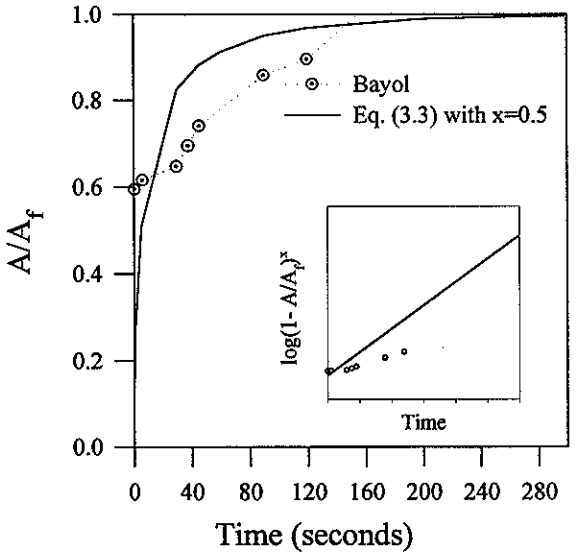

Figure 5.4.9 Spreading Kinetics of Bayol on Smooth Ice [Inset: Linear form of Eqn. (3.3)]

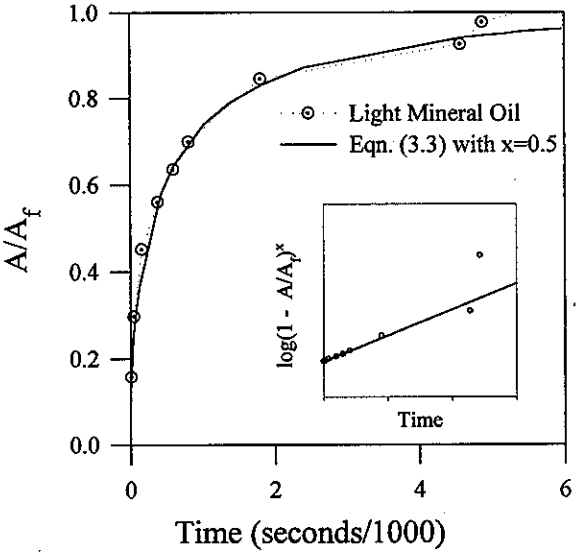

Figure 5.4.11 Spreading Kinetics of Light Mineral Oil (Outdoor Ice Experiment) [Inset: Linear form of Eqn (3.3)]

Spreading on Snow

"Results from experiments... on snow confirmed the expectation that the chemical is readily absorbed by snow and will spread radially along the bottom of the snowcover.... The extent of the surface spreading was found to be minimal in most experiments, and its magnitude was found to depend mostly on the compaction of the snow and the chemical viscosity. [An] increase in either of these variables resulted in an increase of surface spill area."

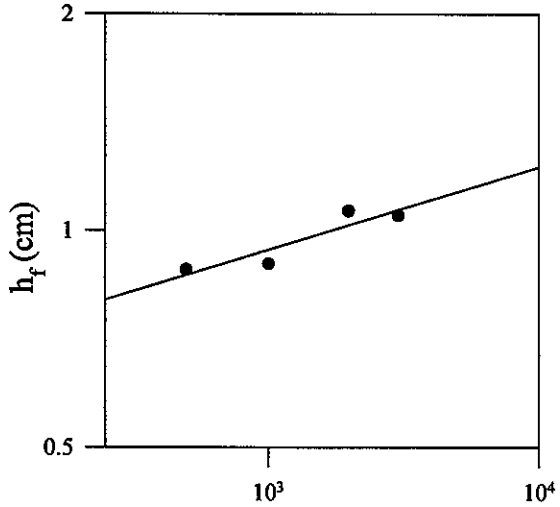

Figure 5.5.3 Effect of Spill Volume on Snow Final Spill Depth

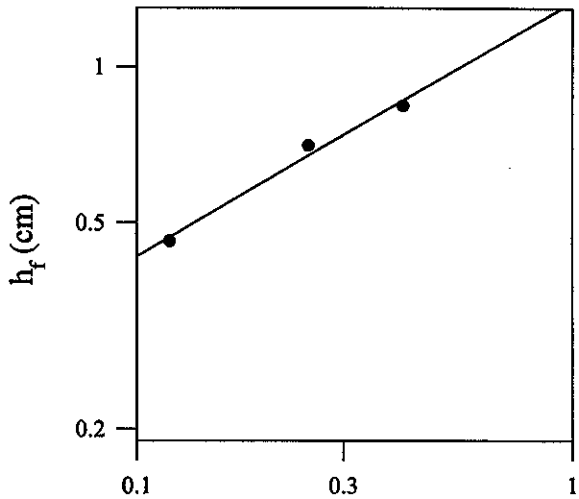

Figure 5.5.4 Effect of Snow Bulk Density on Final Spill Depth

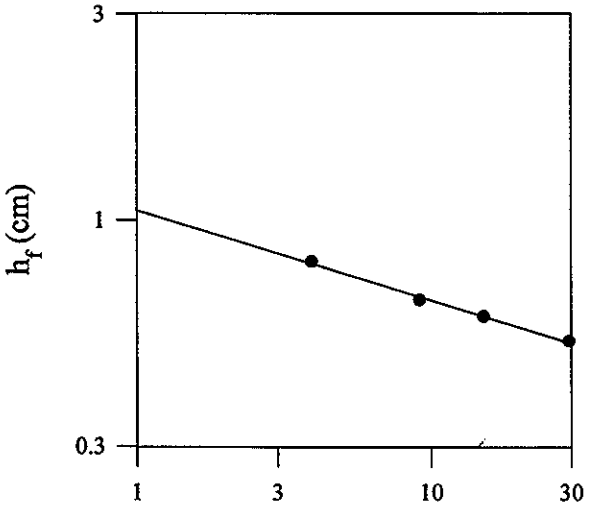

Figure 5.5.5 Effect of Snow Depth on Final Spill Depth

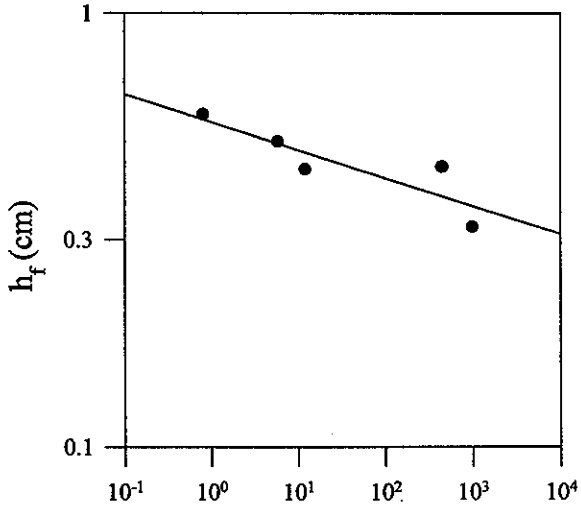

Figure 5.5.8 Effect of Viscosity on Final Spill Depth in Snow

The bottom spill areas (see Figure 3.2) were correlated with spill volume, snow density, snow depth and viscosity. Results are shown in Figures 5.5.3, 5.5.4, 5.5.5 and 5.5.8. The authors note that the "snow density study indicates that as the snow density increases (snow porosity decreases), the final spill areas decreases (final spill height increases). This is due to the increase in resistance to the radial flow of the chemical, as a result of greater packing of snow crystals. The snow depth result

revealed that an increase in [bottom] spill area occurred with increase in snow depth." In contrast to the results for bare ice, the authors found that spill depth decreased with increasing viscosity. They argue that observed reductions in capillary movement up through the snow (not shown in the study) and longer spreading durations resulted in greater final bottom spill areas for more viscous liquids. For spill height, the observed correlations were: $h_f \propto V^{0.13} d^{-0.2} \rho_s^{0.48} \mu^{-0.05}$ and for the final bottom area: $A_f \propto V^{0.87} d^{0.2} \rho_s^{-0.48} \mu^{0.05}$, where d is the depth of the snowcover and ρ_s is the snow density. These expressions were non-dimensionalized using the same procedure as for the ice equations. For fresh snow, the authors found a linear correlation for these four parameters, however when older (c and e type) snow was used, this was not the case. As a first approximation, the snow density was scaled by a "snow density parameter," ζ *, which was determined by snow crystal type, table 5.8.

Table 5.8 Snow Density Parameter

Snow Description	Crystal Type	ζ
Fresh snow, wet or dry, crystalline structure still present.	a,b	1.0
Crusty, firn (rounded) snow, approx. 1 mm in dia.	c	0.5
Advanced firn snow, 2–4 mm dia.	c,e	0.1

"Specifically, the snow density parameter reflects the degree of resistance to the radial, subsurface spreading of the chemical. The maximum value of 1.0 applies for snow crystals which still possess some crystalline structure, and this offers the greatest resistance to flow. As metamorphic processes or freeze-thaw cycles convert these crystals to a more or less round shape the resistance decreases, and is indicated by smaller ζ values."

With this addition, all the measurements could be correlated. In non-dimensional form the relationship is:

$$\frac{A_f}{V^{2/3}} = 0.45 \frac{V^{0.2} d^{0.2} \rho_c^{0.8675} g^{0.4125} \mu^{0.05}}{(\zeta \rho_s)^{0.48} \sigma^{0.4375}} \quad (5.6)$$

where the constant reflects the slope of the best-fit line of Figure 5.5.12. Correlation is quite

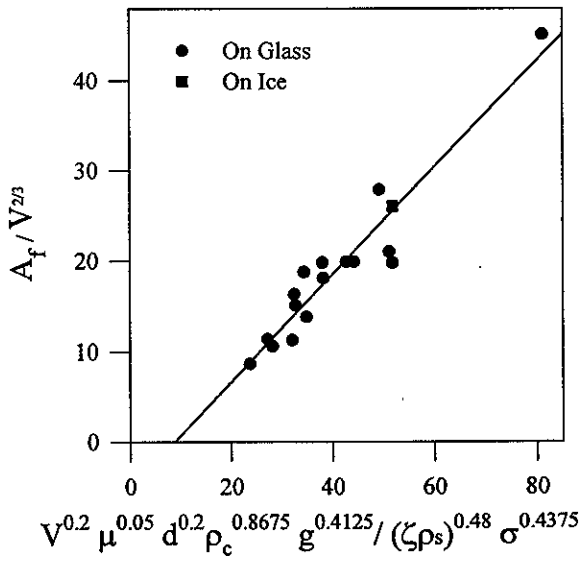

Figure 5.5.12 Correlation of Snow Final Spill Area

*In the original text φ was used to represent the snow density parameter. This has been altered in this review to ζ to distinguish it from the volume fraction of water in snow, ϕ.

good in this case, with predicted areas being different by no more than 30% with an average difference of 12%. In SI units, the spill depth is:

$$h_f = 5.3\times10^{-4}\ V^{0.13} d^{-0.2} \mu^{-0.05} (\zeta \rho_s)^{0.48} \qquad (5.6a)$$

"One problem of using Equation (5.6) or (5.6a) in actual spill conditions is that snow type and density are usually unknown.... Nevertheless, is the age of the snow and the area's overall climate are known, one can make an intelligent estimate...." The authors also note that this theory applies only for the simplest of snow covers with a uniform density and consistency and for a non-porous undersurface.

Kinetics of Spreading on Snow

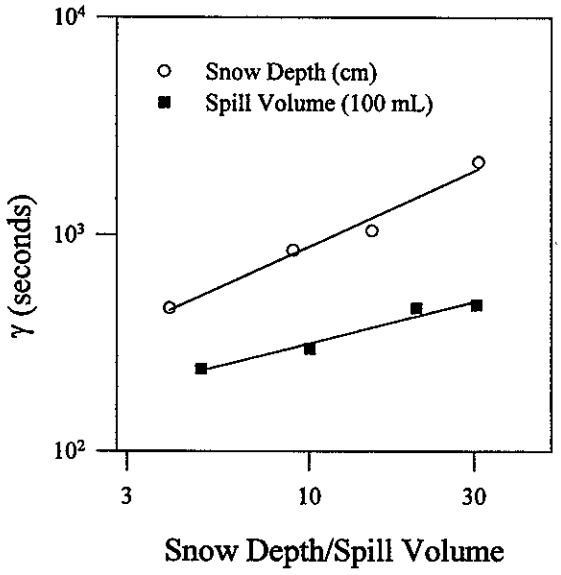

Figure 5.5.13 Effect of Snow Depth and Spill Volume on Spreading Time Constant

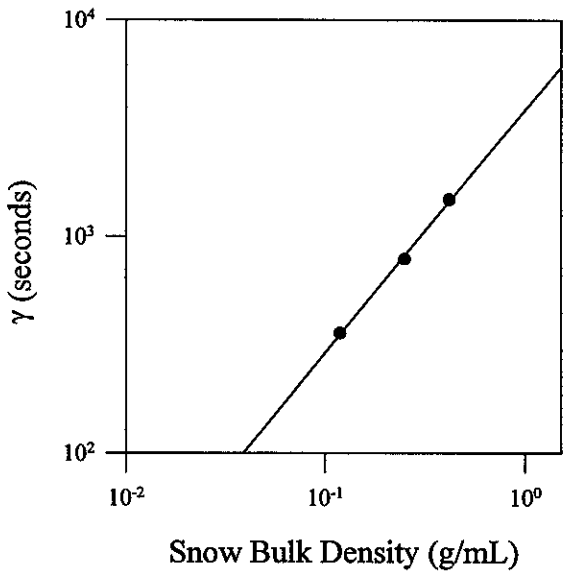

Figure 5.5.14 Effect of Snow Bulk Density on Time Constant

The spreading time constants were determined from the area *vs* time profiles, as for the bare ice experiments. These were plotted (on log-log scale) against the four variables used in the final area studies, Figures 5.5.13 to 5.5.15. The correlation obtained from the slopes of these graphs was: $\gamma \propto V^{0.45} d^{0.6} \rho_s^{1.1} \mu^{0.78}$. In non-dimensional form this was plotted (Figure 5.5.16) giving:

$$\frac{\gamma V^{1/6}}{g^{0.5}} = 0.18 \frac{V^{0.62} d^{0.6} \rho_s^{1.1} \mu^{0.78} g^{1.425}}{\rho_c^{0.065} \sigma^{1.815}} \qquad (5.7)$$

where the proportionality constant ranged from 0.13 to 0.27 for the 18 snow experiments. The final spill height, in SI units is:

$$\gamma = 5700 V^{0.45} d^{0.6} \rho_s^{1.1} \mu^{0.78} \qquad (5.7a)$$

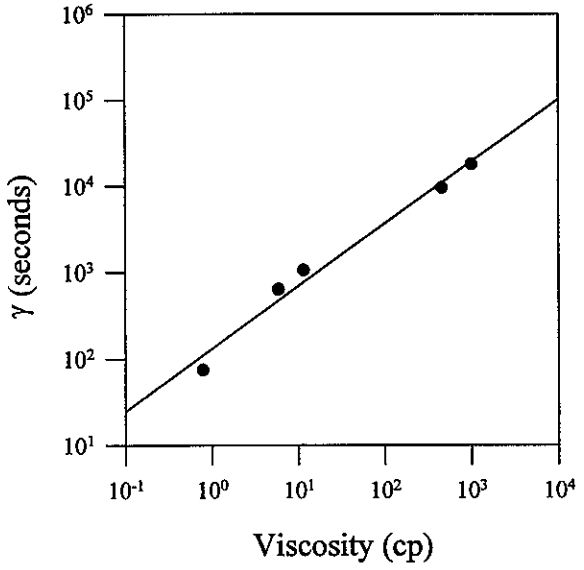

Figure 5.5.15 Effect of Chemical Viscosity on Snow Time Constant

Note that the correlation given in Equation (5.7) is better than that for bare ice (Equation (5.3)). This suggests that additional factors (such as chemical-snow interactions) may not be very important for spreading rates in snow. The authors also mention that they did not use the snow density parameter, ζ, to scale the snow density when plotting Figure 5.5.16. With the older snows, a larger final area was attained, apparently cancelling out the effect of faster spreading. It is important to remember that γ reflects relative areas and is not an absolute spreading rate. Thus, snow type does not seem to greatly affect the spreading time constant.

The value of the slope constant, x, was determined as before, by plotting best-fits of Equation (3.3) to the area-time series. The values ranged from 0.5 to 1.0, with an average of 0.75. Using this value, the final spreading time is:

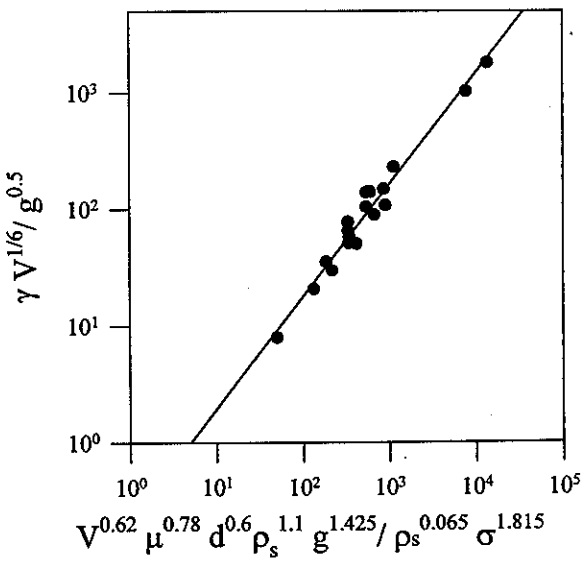

Figure 5.5.16 Correlation of Snow Spreading Time Constant

$$t_f = 8\gamma \qquad (5.8)$$

Application to an Actual Spill Situation

On an ice surface, the final spill area can be predicted by Equations (5.2) and (5.3), knowing the chemical viscosity and spill volume. Small scale surface roughness has minimal effects. Spreading rate can be predicted from Equation (3.3) using a value of 0.5 for x. The total spreading time can be estimated as twenty times the spreading constant. The authors note that these correlations break-down for low viscosity chemicals in high winds.

On snow, "the chemical will be absorbed into the snow and will spread radially along the ground-snow surface. The spreading on the surface of the snow will be relatively small under most conditions." Exceptional cases would be for a very viscous chemical and/or highly dense snow. Spreading under snow is very much slower than on bare ice. The final spill area can be predicted from Equations (5.6) and (5.7). The total spreading time is approximately eight times the spreading constant. Important variables are: chemical viscosity, spill volume, snow depth, snow density and snow type. The last two snow parameters can be estimated from historical or typical values. The authors note that these should provide "reasonable estimates of spreading behaviour," but caution that significant ground slope or highly stratified snow layers will cause problems.

Boss Critique:

This study presents a comprehensive model for chemical (not just oil) spills on ice and snow-covered ice. Its predictive value lies in the correlation relationships developed for final spill area and kinematic constants. While these would require significantly more testing before they could be considered trustworthy (in most cases three or four points were used to derive the relationships), they provide a usable model of spills on solid surfaces. Correlation parameters for the various relationships (r^2) are provided in table R.2. In most cases correlations appear to be reasonable (>90%), however there is very little data in most cases. Also, note the low correlation values for the expressions of A_F and γ for bare ice spills (5.4.3 and 5.4.8). This may indicate that additional factors are needed in the expressions of final area and spreading time constant (Equations (5.2) and (5.3) respectively) such as surface roughness or other chemical properties. In this respect, it is odd that the relationships for spills on snow are so much better than those on bare ice.

One difficulty that arises with the non-dimensionalized forms (Equations (5.2), (5.3), (5.6) and (5.7)) is the introduction of the terms in σ, the liquid-solid surface tension, and ρ_c, the chemical density. The meaning of these terms are unclear, undefined theoretically, and as such, are of questionable value. In addition, it is not clear how Equations (5.2) and (5.2a) (for example) relate for different chemicals, except in a loose fashion.

The simple model of the kinematic theory is tested thoroughly, however, none of the proposed volume change effects (Equations (3.5a) to (3.5c)) are discussed in detail, almost certainly due to project constraints. Also, while the kinematic theory is well developed, the model of the final extent of the spill is left undefined, except experimentally. In particular, the relationship between contact angle and final area/height is not discussed.

Table R.2 Linear Fit Statistics for Correlations

Spills on Ice				Spills on Snow			
Fig.	r^2	# Pts		Fig.	r^2	# Pts	
5.4.1	0.936177	12	h_f *vs* Viscosity	5.5.3	0.841402	4	h_f *vs* Spill Volume
5.4.2	0.31358 [a]	4	h_f *vs* Spill Volume	5.5.4	0.98522	3	h_f *vs* Snow Density
	0.947654 [b]	3		5.5.5	0.995327	4	h_f *vs* Snow Depth
	0.995645 [c]	3		5.5.8	0.765481	5	h_f *vs* Viscosity
	1 [d]	2		5.5.12	0.907705	18	Correlation of A_F
5.4.3	0.748176	22	Correlation of A_F	5.5.13	0.961138	4	γ *vs* Spill Volume
5.4.4	0.661617	4	γ *vs* Viscosity (smooth ice)		0.979131	4	γ *vs* Snow Depth
5.4.5	0.650789	4	γ *vs* Viscosity (rough ice)	5.5.14	0.998082	3	γ *vs* Snow Density
5.4.7	0.973283 [a]	4	γ *vs* Spill Volume	5.5.15	0.981443	5	γ *vs* Viscosity
	0.735285 [b]	3		5.5.16	0.968367	18	Correlation of γ
	0.947906 [c]	3					
	1 [d]	2					
5.4.8	0.582724	22	Correlation of γ				
R.1	0.940059	4	h_f *vs* $(1+\cos\theta_c)/2$				

[a]m-Xylene [b]Bayol [c]n-Pentanol [d]Mineral Oil

Review of a manuscript by Fay, J.A., and D.P. Hoult, entitled *Physical Processes in the Spread of Oil on a Water Surface*, report AD-726 281 for US Coast Guard, 1971.

Although this paper does not concern itself directly with oil-in-ice it is one of the main papers that are referenced for the movement of oil whether the case is for oil on water, oil in ice, or oil on ice.

Technical Summary

"Formulae are recommended for calculating the extent of the spread of oil slicks on water as a function of time. They are based on empirical measurements of spreading rates and analytical and theoretical studies of the physical processes which accelerate or retard the spread of a film. Both one-dimensional and two-dimensional (axisymmetric) slicks are treated. Comparisons of the recommended formulae are made with the limited number of field observations, both for the rate of spread and the maximum slick size."

Theory

The authors have laid out a compelling argument for the formulae first presented in Fay's paper, as order of magnitude approximations, and now presented here in Table I with constants to allow for scaling effects. The arguments are presented here intact.

" Spreading and Retarding Forces

Although the force of gravity acts downward, it causes a side-wise spreading motion of a floating oil film by creating an unbalanced pressure distribution in the pool of oil and the surrounding water. This force on an element of oil film acts in the direction of decreasing film thickness and is proportional to the thickness, its gradient, and the difference in density between oil and water. (See Fig. 1.) As the oil film spreads and becomes thinner, the gravity force diminishes.

At the front edge of the expanding slick an unbalance exists between the surface tension at the water-air interface and the sum of surface tensions at the oil-air and oil-water interfaces. The net difference, called the spreading coefficient, is a force which acts at the edge of the film, pulling it outwards. This spreading force does not depend upon the film thickness as does the gravity force, and will not decrease as the oil film thins out (unless the chemical properties change through aging). Eventually the surface tension force will predominate as the spreading force.

These spreading forces are counterbalanced by the inertia of the oil film and of the thin boundary layer of water below it which is dragged along by friction (see Fig. 1). The inertia of an element of the oil layer decreased with its thickness as time progresses and the film spreads, but the inertia of the viscous layer of water below the oil increases with time as its thickness grows. Consequently, the viscous retardation will eventually outweigh the inertial resistance of the oil layer itself.

It is also informative to consider these effects from the point of view of an energy balance. A pool of oil floating on water possesses a greater potential energy than the water it displaces, in proportion to its thickness. As it spreads and its thickness decreases, there is a loss of potential energy. Also, as air/water surface is replaced by an oil film, the surface energy per unit area (which

has the same physical value as the interfacial tension) is reduced by an amount equal to the

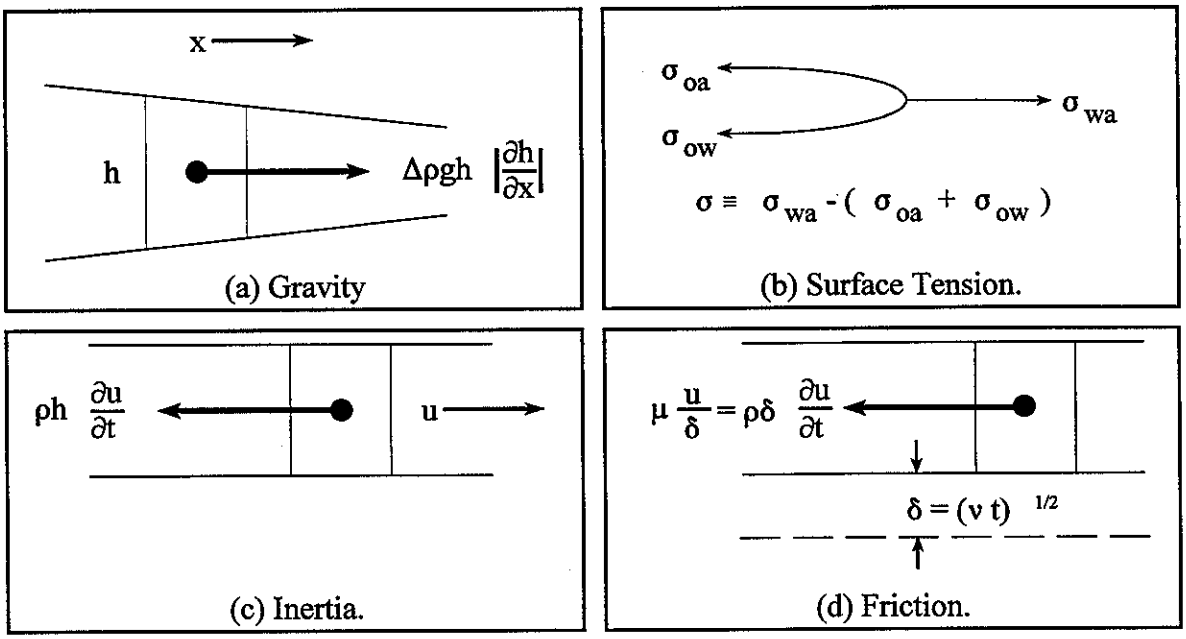

Figure 1. The four forces which act on an oil film (see list of symbols).

spreading coefficient. Thus both surface energy and potential energy are decreased as the slick spreads. This energy is converted either into heat by viscous dissipation in the water beneath the slick or into the energy of gravity surface waves which propagate away from the expanding oil pool. In other words, each spreading force is associated with an energy-producing process and each retarding force with an energy dissipating process.

It is thus clear that the spread of an oil film will pass through several stages as time progresses, in each of which one spreading force will be balanced by one retarding force "(reference to Fay's paper 1969). "Although there are four such possible combinations, for large scale slicks only three regimes are important: (i) the gravity-inertia regime (called "inertial spread"), (ii) the gravity-viscous regime (called "viscous spread") and the surface tension-viscous regime (called "surface tension spread"). As time progresses, a large spill will pass through these three regimes in succession. A very small spill (a few liters, say) will almost from the start behave as a surface tension spread.

The spreading laws for each regime have been determined, to within an unknown constant, for each regime and for the cases of a one-dimensional and two-dimensional (axisymmetric) slick. These laws give the linear extent of the slick (length ℓ or radius r) as a function of the time t since the oil was released at the origin of the spread, the volume of the oil spill and the physical properties of the oil and water. These spreading laws are given in Table I, and the undetermined proportionality coefficients are denoted by the symbol k." In this manuscript *k* was used and the coefficients are listed in Table II.

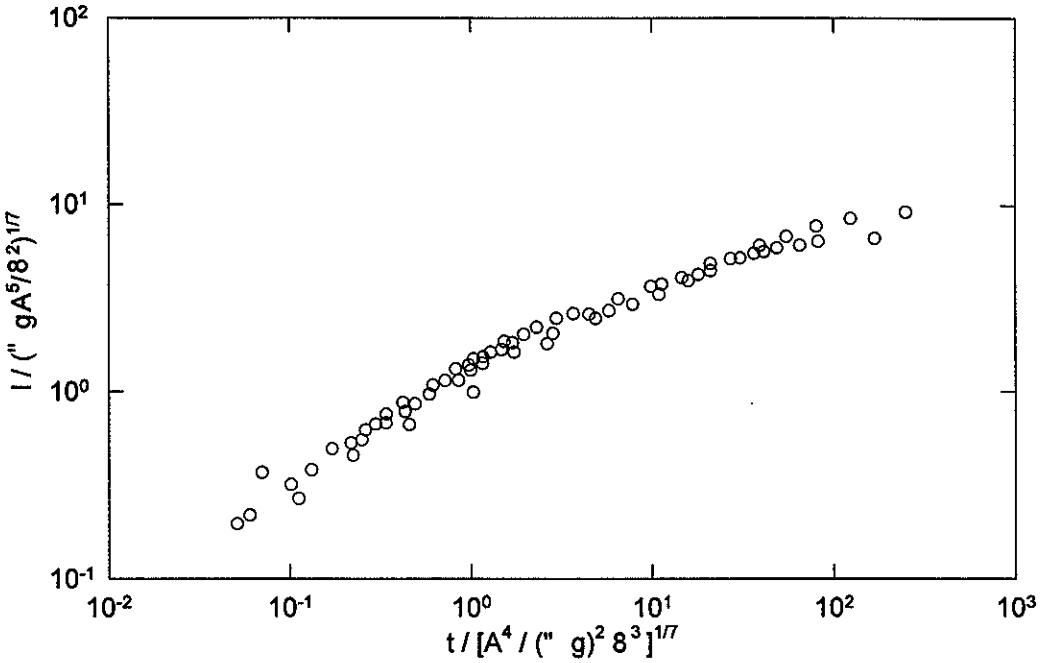

Figure 2. Experiments showing the transition from inertial to viscous spread for a one-dimensional flow. The y-axis should have *l* instead of l (See below). The authors two lines, inertia and viscous spreading equations from Table I, have not been included since they have the dimension of cm and can not be plotted on this figure.

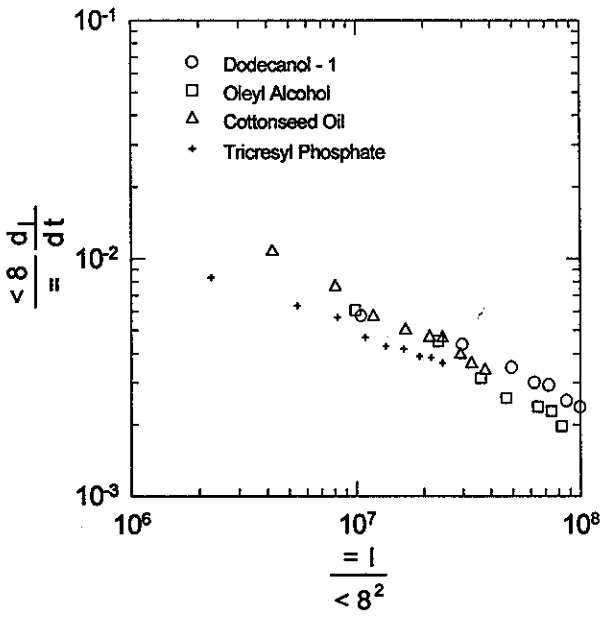

Figure 3. Measurements of spreading velocity versus slick length for one-dimensional surface tension spreading experiments.

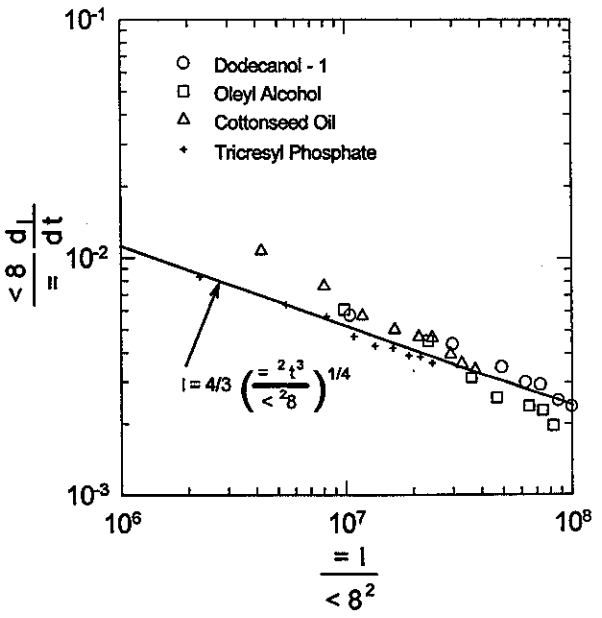

Figure 3 Reproduced. The line from the original plot is here and it is discussed later.

that the flow at the edge is the same for one-dimensional viscous spreading and two-dimensional viscous spreading. Therefore the boundary values for the two-dimensional viscous spreading case would be the same as the boundary values for the one-dimensional case and thus instead of solving the complicated flow at the edge a simple analysis was used. Two-dimensional surface tension spreading is represented by Fay and Hoult as being the same as one-dimensional surface tension spreading with simple change in the spreading coefficient. This outcome results from following the same procedure for the viscous spreading case above. The data for one-dimensional surface tension spreading and theoretical surface tension spreading is compared in Figure 5 and this is discussed further in the BOSS Critique section.

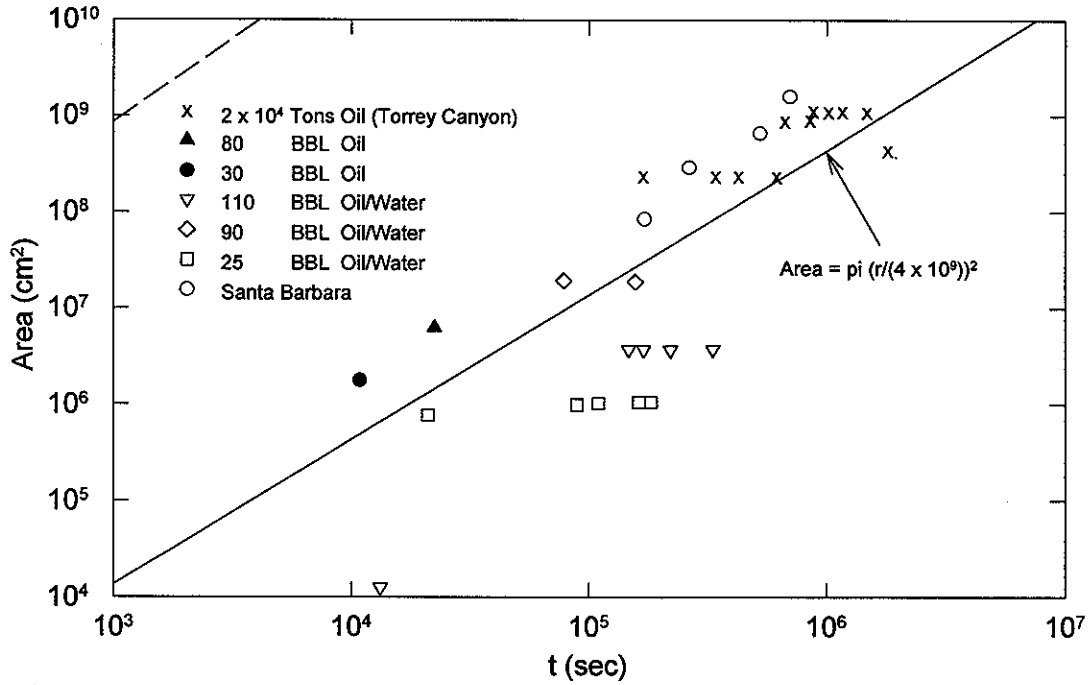

Figure 5. A comparison of the theoretical axisymmetric slick area (for surface tension spread) with observed values. Note the solid line is approximately the same as in Fay-Hoult Figure 5. This will be discussed in the BOSS Critique section.

BOSS Critique

The reviewer calculated a dimensional analysis of the equations presented in Table I and found all of the equations had the units of cm which is expected for a radius or length.

Figure 2 data was from Hoult, D.P. and W. Suchon, *The Spread of Oil in a Channel*, Fluid Mechanics Laboratory, Department of Mechanical Engineering, Massachusetts Institute of Technology, Cambridge, Massachusetts, 1970. Using the equations form Table I for inertial and viscous spreading for a one-dimensional case with the constants set to 1.5,

$$(\Delta g A t^2)^{1/3} = \left(\frac{\Delta g A^2 t^{3/2}}{\nu^{1/2}} \right)^{1/4}$$

and solving for time, $t = [A^4/(\Delta g)^2 \nu^3]^{1/7}$ with the units of seconds. This can then be substituted for time in the viscous one-dimensional equation and if k_v is assumed to be 1, the equation can be solved for length, $\ell = [\Delta g A^5/\nu^2]^{1/7}$ with the units of cm. If time were divided by the first equation and

length divided by the second equation the results are the labels for the x and y axes, respectively, of Figure 2. No explanation is given by the authors for calculating these terms nor for plotting the data in this manner. The reviewer did not reproduce the lines on Figure 2 to preserve dimensionality.

Although Figure 3 is reproduced here Figure 4 is not and this is because the same information is present in both figures. Starting with the equation used, which is the equation for surface tension regime (third equation in Table I, with the coefficient set to 4/3). To restate that:

$$\ell = 4/3\left(\frac{\sigma^2 t^3}{\rho^2 \nu}\right)^{1/4}$$

which has the correct dimensions of $(cm^4)^{1/4}$. The derivative of ℓ with respect to time is

$$\frac{d\ell}{dt} = 4/3\,\frac{\sigma^{2/4} t^{(3/4-4/4)}}{\rho^{2/4}\nu^{1/4}} = 4/3\left(\frac{\sigma^2}{\rho^2\nu}\frac{1}{t}\right)^{1/4} = 4/3\left(\frac{\sigma^2 t^3}{\rho^2\nu}\right)^{1/4}\frac{1}{t} = \ell\frac{1}{t}$$

which also has the correct units of cm/sec. To get the y axis values (Figure 3) we multiply the left side and right side of the above equation by $\rho\nu/\sigma$ (units of s/cm) resulting in

$$\frac{\rho\nu}{\sigma}\frac{d\ell}{dt} = \frac{\rho\nu}{\sigma}\ell\frac{1}{t}.$$

Then multiply and divide the right hand side of the equation by $\sigma/\rho\nu^2$ (with units of 1/cm)

$$\frac{\rho\nu}{\sigma}\frac{d\ell}{dt} = \left(\frac{\sigma}{\rho\nu^2}\frac{\rho\nu^2}{\sigma}\right)\frac{\rho\nu}{\sigma}\ell\frac{1}{t} = \frac{\sigma}{\rho\nu^2}\ell\left[\frac{\rho^2\nu^3}{\sigma^2}\right]\frac{1}{t}$$

which has the correct unitless form. Now a plot can be made of the left hand-side of the equation, $\left(\frac{\rho\nu}{\sigma}\frac{d\ell}{dt}\right)$, and a part of the right hand-side of the equation, $\left(\frac{\sigma}{\rho\nu^2}\ell\right)$. The portion that is left over is the slope of the line, $\left(\frac{\rho^2\nu^3}{\sigma^2}\frac{1}{t}\right)$ since there is no intercept calculated. Therefore the reviewer does not understand the authors reference in Figure 3 to a line that is plotted from the equation of $\ell = 4/3\left(\frac{\sigma^2 t^3}{\rho^2\nu}\right)^{1/4}$ which has the incorrect dimensions to be plotted on the graph in Figure 3. Note that the reviewer determined the above relationship it was not presented by the authors in the paper.

In the reproduced Figure 5 (above) there are two lines drawn in. The solid line was calculated (as mentioned in the plot) by squaring the radius divided by 4×10^9 (a rather large number). If this was not done the result was the dashed line up in the left-hand corner. The authors do not explain how The data for the line in their Figure 5 is calculated and the reader is expected to know what equation is used (assumed to be axisymmetric since that is what is suppose to be indicated in Figure 5) and what values are used in the equation. The values used here are the same as the values used in Figure 2 of Fay's 1969 paper which has the same experimental data however the plot was for the length of spill vs time not area of spill vs time. See the BOSS Critique for a discussion of errors (which were not discussed for Fay's original paper either).

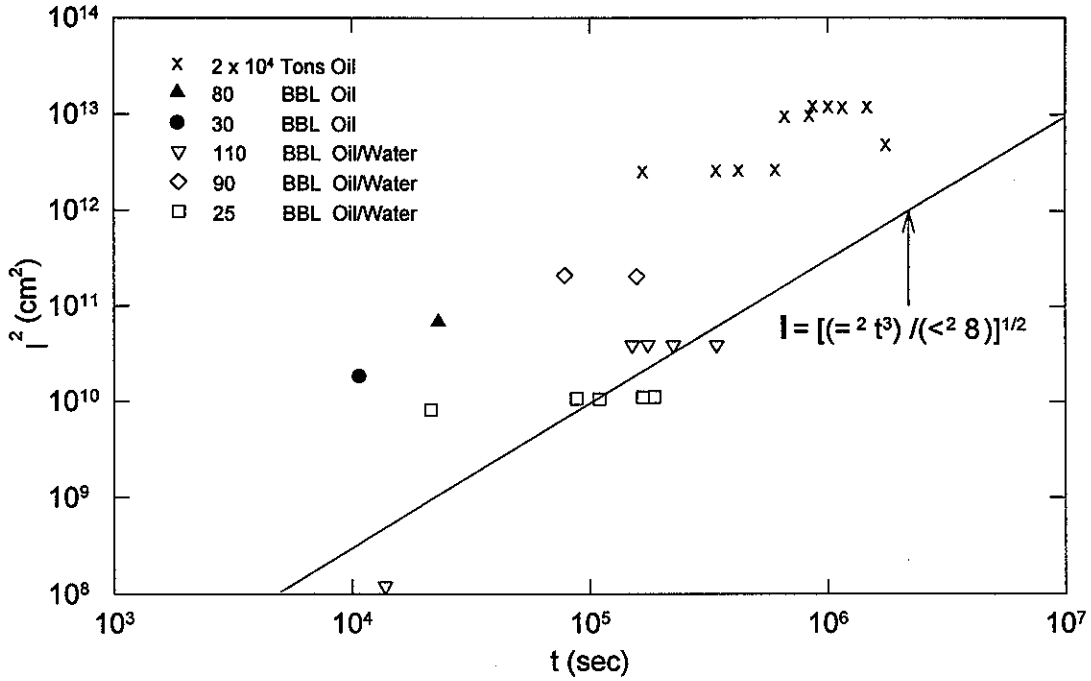

This is an approximation to Figure 5 plotted using the square of the y values given in Fay's paper since Fay had stated that area was approximated with length squared.

The data plotted above has the same change (10^6) in the y-axis as presented in Figure 5 but the areas in Figure 5 are shifted by four orders of magnitude. The line in the plot is calculated using the equation stated in the plot but the line does not fit any sets of data well. Fay and Hoult do not explain how their data for Figure 5 was calculated and there is no discussion of the error of the data so a best fit line can not be determined. As can be seen from comparison of the one-dimensional and axisymmetric spreading laws listed in Table 1 the only difference that Fay and Hoult believe to exist is the coefficient value otherwise the equations are the same.

The plots below (Figure 6) are variations on Fay's theme final slick area being related to volume of the spill. The use of volume to a fractional power, leaves the dimensions of the equations used to relate area to volume, to be incorrect. The slope of plot of area *versus* volume is $1/h$ (m^{-1}) the thickness of the slick. Fay and Hoult have stated that real oil slicks have a final thickness ranging from 10 to 100 μm (10^{-6} m). Inverting 10^{-5} results in 10^{+5} which is the value of the constant used in Fay and Hoult's equation (2), however, no explanation is given for their choice of constant. In Figure 6(a) the solid line represents $A = 10^5[V]^{3/4}$. The reviewer used several different constants, and different equations, to see what relationship evolved for the comparison of log of area *versus* log of volume. In Figure 6(b) a comparison is made between equation (2) with volume to the power 3/4 and volume taken to the power of 2/3, $(m^3)^{2/3} = m^2$. The two constants (5×10^5 and 1×10^5) used result in two parallel lines that cover the range of experimental data and represent a thickness range range from 2 to 10 μm (10^{-6} m). The equation was then changed to use volume to a power of unity and a range of constants from 1×10^4 to 1×10^5 resulting in lines shown in Figure 6(c), dashed lines, and 6(d), solid line. Note that as the thickness is increased (constant is decreased) the line migrates toward the bottom right of the plot and as the thickness is decreased (constant is increased) the

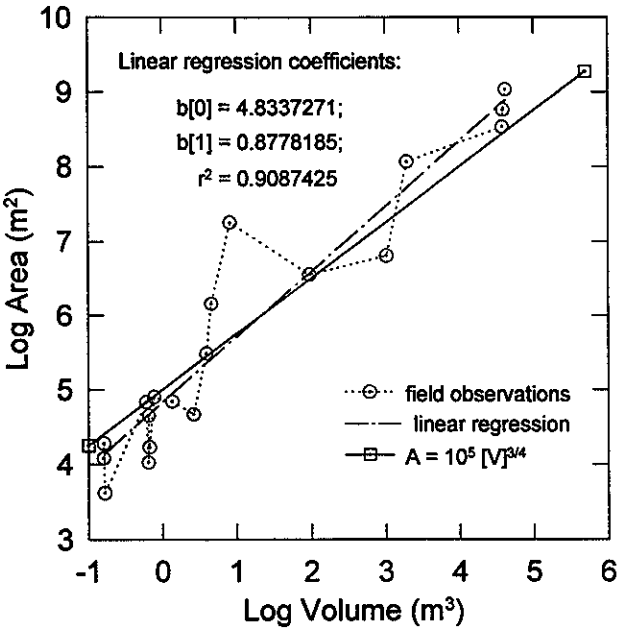

Figure 6(a). Log of area vs log of volume.

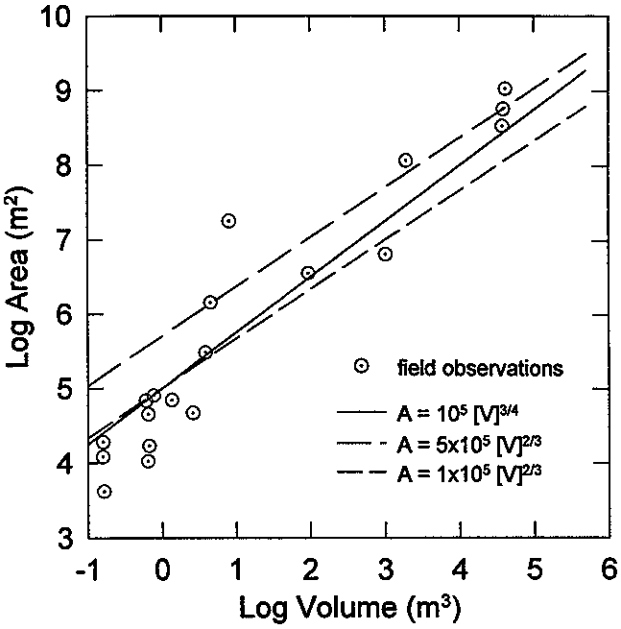

Figure 6(b). Log of area vs log of volume.

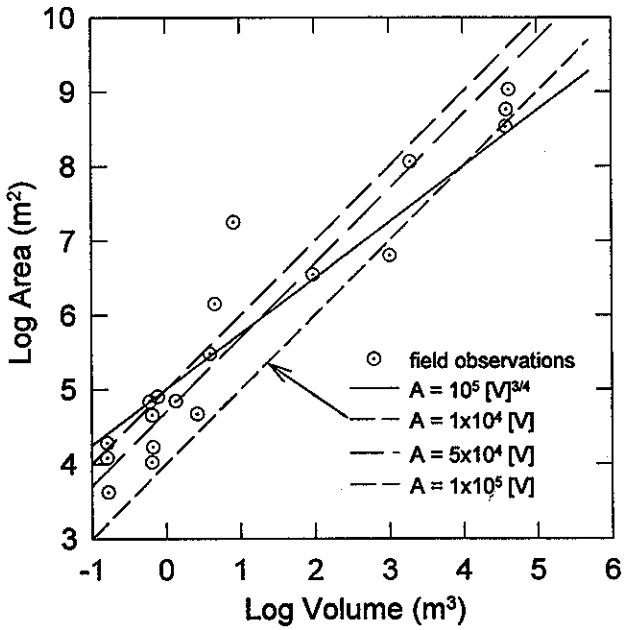

Figure 6(c). Log of area vs log of volume.

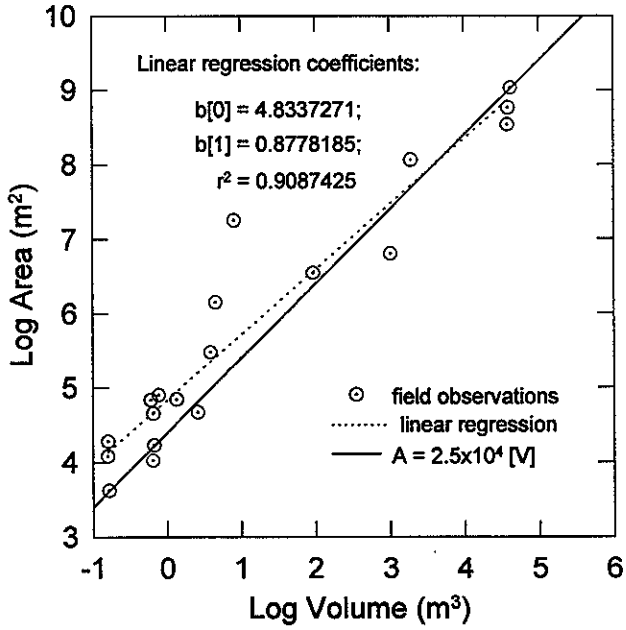

Figure 6(d). Log of area vs log of volume.

line migrates toward the top left of the plot. The solid line in Figure 6(d) is for a thickness of 40 μm ($h^{-1} = 2.5 \times 10^4$) and this line fits the data as well as the proposed line of Fay and Hoult which is the solid line in Figure 6(a). Only the lines in Figure 6(b) have the correct dimension of m^{-1}.

Review of a manuscript by Fay, J.A., entitled *The Spread of Oil Slicks on a Calm Sea*, Fluid Mechanics Laboratory, Department of Mechanical Engineering, Massachusetts Institute of Technology, Boston, Massachusetts, 1969. Also available as "The Spread of Oil Slicks on a Calm Sea", pp 53-64, in *Oil on the Sea*, Hoult, D. (ed.), Plenum, New York, 1969.

Although this paper does not concern itself directly with oil-in-ice it is the main paper that is referenced (as by Glaeser, 1971) for the movement of oil whether the case is for oil on water, oil in ice, or oil on ice.

Technical Summary

A set of approximations are proposed to be used to model the spread of an oil slick in calm seas. The equations were first order approximations and were made keeping in mind the conservation of energy available to the oil slick. The potential energy is due gravitational forces and oil-water surface-tension while the losses are to heat (viscous forces) and the kinetic energy of oil movement.

Theory

The author assumes that all of the oil to be spilled (V) is available at once and the spill volume is approximated by:

$$V = l^2 h \qquad (1)$$

where the area is approximated by l^2 and l is the length of the spill, while h is the thickness (or height) of the spill. The author states that "The thickness δ of the uppermost layer of water so set into motion by viscous forces has the magnitude:

$$\delta = \{\nu t\}^{1/2} \qquad (2)$$

in which ν is the kinematic viscosity of the water. This is the thickness of the boundary layer at the edge of a fluid in which the viscous force can accelerate the fluid up to the speed of a moving boundary."

The surface tension force per unit volume of oil is determined "by dividing the net surface tension σ by the cross-sectional area of the slick, lh and then using Eq. (1) to find

$$\text{Surface tension:} \qquad \frac{\sigma}{lh} = \frac{\sigma l}{V} \qquad (3)$$

The other spreading force, gravity, produces a horizontal force per unit volume (pressure gradient) of $\Delta\rho V g / l^3$, or using equation (1),

$$\text{Gravity:} \qquad \frac{\Delta\rho V g}{l^3} \qquad (4)$$

in which $\Delta\rho$ is the difference in mass density between water and oil, and g is the gravitational acceleration. The inertia force, which retards the flow, is the product of mass density ρ and

acceleration l/t^2:

$$\text{Inertia:} \qquad \frac{\rho l}{t^2} \tag{5}$$

The viscous force per unit volume is the viscous stress $\rho\nu(l / t)/\delta$, or product of absolute viscosity $\rho\nu$ and velocity gradient $(l / t)/ \delta$ in the water, divided by the film thickness h:

$$\text{Viscous:} \quad \frac{\rho\nu(l/t)}{\delta h} = \frac{\rho\nu^{1/2} l^3}{Vt^{3/2}} \tag{6}$$

in which Eqs. (1) and (2) were used to derive the expression on the right."

The author states that early in the spreading process inertia forces dominate since the ratio of viscous to inertia forces ($l^2 t^{1/2}$) which is small at time ≈ 0. This implies that the early spreading force is inertial and the early retarding force is due to viscous forces. As the oil spill spreads these forces will become equal when the film thickness h is equal to the viscous layer δ.

As the slick spreads gravity is the dominant force initially and surface tension is the final force.

When these two forces, that are causing the oil slick to spread, become equal a critical thickness is defined h_c:

$$h_c = \left(\frac{\sigma}{\rho \Delta g} \right)^{1/2} \tag{7}$$

and for typical values($\Delta\rho = 0.05$ g/cm^3, and $\sigma = 30$ dynes/cm) $h_c = 0.8$ cm. Thus gravity dominates the spreading process for $h > h_c$ and surface-tension dominates for $h < h_c$.

The author states that the spreading of an oil slick has three phases:

" (i) the beginning phase in which only gravity and inertia forces are important,

(ii) an intermediate phase in which gravity and viscous forces dominate and

(ii) a final phase in which surface tension is balance by viscous forces.

The spreading laws for each of these phases may be found by equating, respectively, the pairs of forces as given in Eqs. (3) through(6):

$$\text{Gravity-inertia:} \quad l = (\Delta g V t^2)^{1/4} \tag{8}$$

$$\text{Gravity-viscous:} \quad l = \left(\frac{\Delta g V^2 t^{3/2}}{\nu^{1/2}} \right)^{1/6} \tag{9}$$

$$\text{Surface tension-viscous:} \quad l = \left(\frac{\sigma^2 t^3}{\rho \nu} \right) \tag{10}$$

To illustrate the respective regimes of the different phases of spreading, we have plotted Eqs. (8) - (10) in Fig. 1 for the special case of 10, 000 ton spill of oil (about the size of the Torrey Canyon initial spill)."

The author then expands the above situation to include the spreading of a slick in a moving stream by first replacing equation (1) with :

$$\dot{V} = hlu \tag{11}$$

There are also changes to the equations relating to surface tension, gravity, inertia, and viscous phase.

Surface tension: $$\frac{\sigma u}{\dot{V}} \tag{12}$$

Gravity: $$\frac{\Delta\rho\dot{V}g}{l^2u} \tag{13}$$

Inertia: $$\frac{\rho l u^2}{x^2} \tag{14}$$

Viscous: $$\frac{\rho\nu^{1/2}l^2u^{5/2}}{\dot{V}x^{3/2}} \tag{15}$$

The resulting spreading equations are:

Gravity-inertia: $$l = \frac{(\Delta g\dot{V}x^2)^{1/3}}{u} \tag{16}$$

Gravity-viscous: $$l = \left(\frac{\Delta g\dot{V}^2x^{3/2}}{\nu^{1/2}u^{7/2}}\right)^{1/4} \tag{17}$$

Surface tension-viscous: $$l = \left(\frac{\sigma^2x^3}{\rho^2\nu u^3}\right)^{1/4} \tag{18}$$

Fay stated in his paper that their had only been limited reports of oil spill observations and so he had limited data with which to check his equations.

The theoretical relationship of final slick length (ℓ_∞) and molecular diffusivity (D, expected to be about 10^{-5} cm^2/sec for the conditions of Fay's work) were related by Fay to surface tension and absolute viscosity by:

$$\ell_\infty = \left(\frac{\sigma^2V^6}{\rho^2\nu D^3}\right)^{1/16} \tag{21}$$

Results

Fay plotted the three regimes of spreading in his Figure 1, reproduced below. There are several differences between the reproduced Figure 1 (below) and Fays' which are discussed in the BOSS Critique section.

In reproduced Figure 2 the slick size (length in cm) *versus* time after initial spill, is plotted and the line drawn in the plot is for the case of surface tension-viscous spreading.

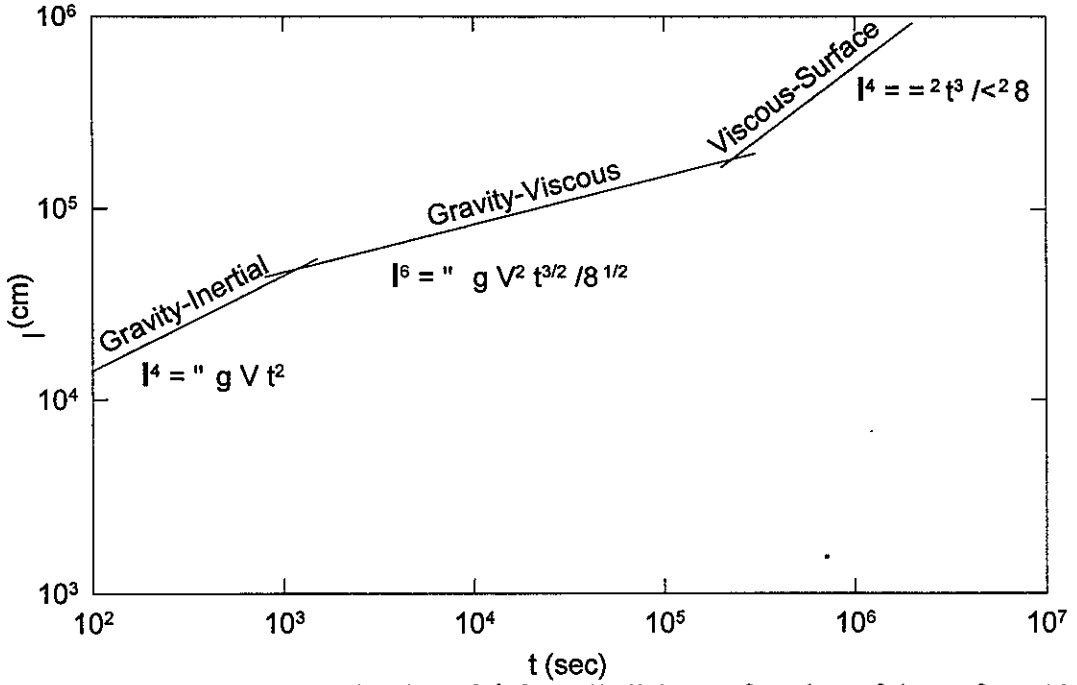

Figure 1 for Fay's paper. The size of *l* of an oil slick as a function of time t for a 10 000 ton spill. Note that there are 3600 seconds in 1 hour, 8.64 x 10^4 seconds in a day, and 6.048 x 10^5 seconds in a week.

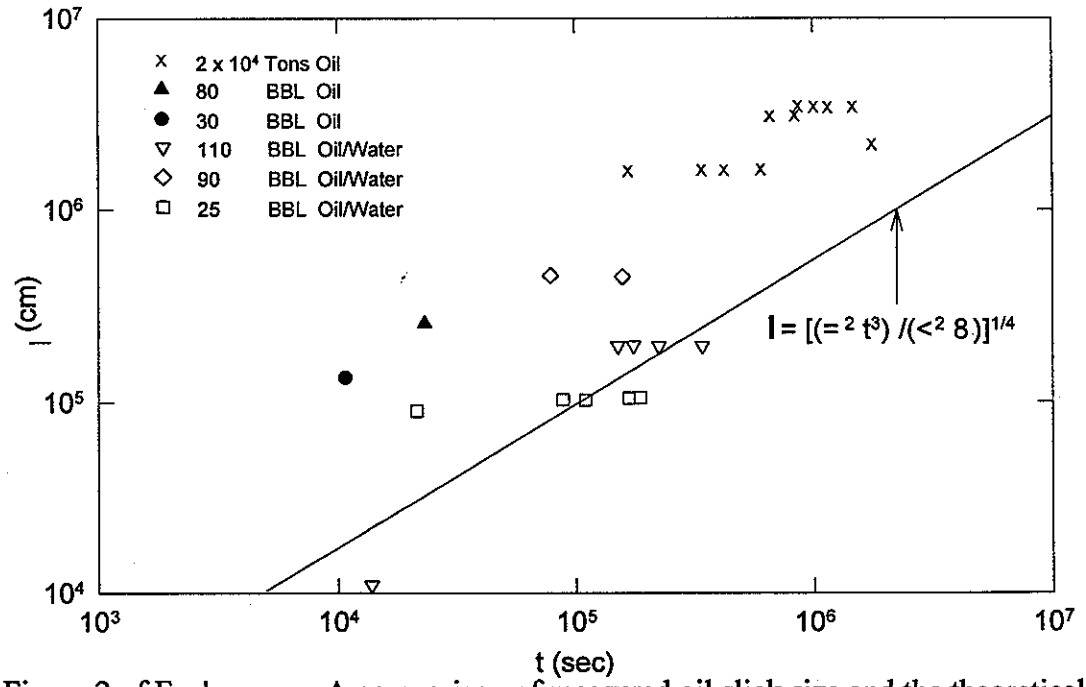

Figure 2 of Fay's paper. A comparison of measured oil slick size and the theoretical estimate for surface tension-viscous spreading.

In reproduced Figure 3, the final slick length (ℓ_∞) is plotted *versus* the volume of the spill. Fay states that although the final slick length line plotted in Figure 3 does not fit the experimental data it does, however, show the slow rate of increase of ℓ_∞ with slick volume.

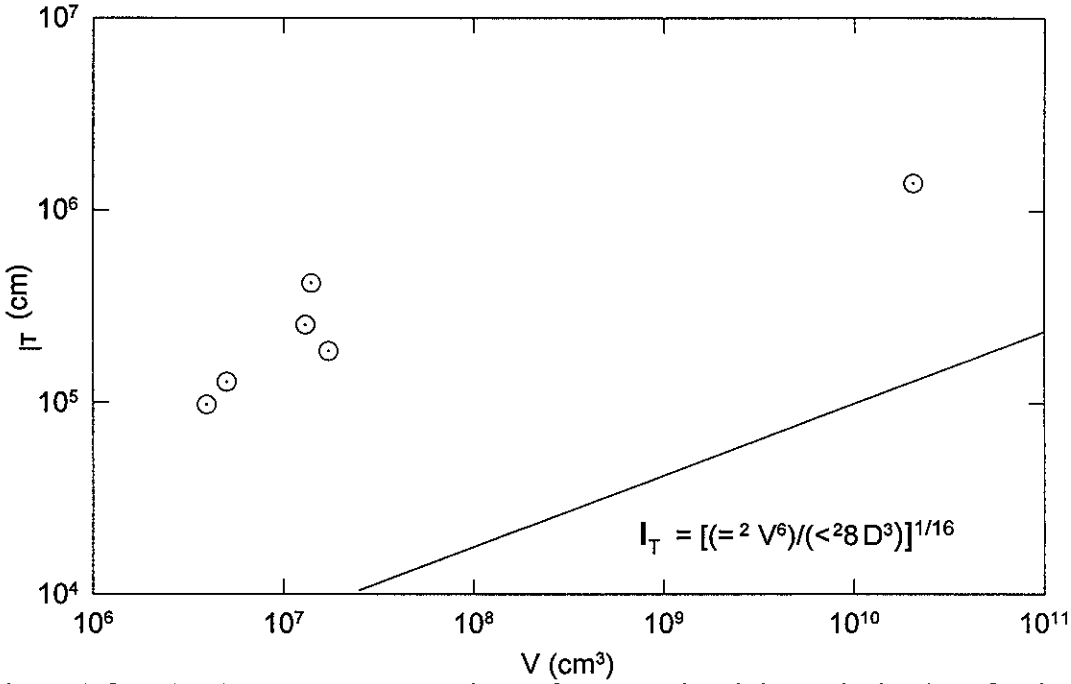

Figure 3 from Fay's paper. A comparison of measured and theoretical values for the final size ℓ_T of a slick as a function of the spill volume V. The only new variable here is D = 10^{-5} cm^2/s.

BOSS Critique

Fay's original Figure 1 differs from the reproduced Figure 1, above, for the transition points. In Fay's original Figure 1 the gravity-inertial phase starts at $\ell = 10^4$ for t = 100 with a change to gravity-viscous at approximately one hour (3600 seconds). The reproduced Figure 1 was done using the equations stated by Fay and presented on the reproduced Figure 1. However, the start is at 1.4 x 10^4 for t = 100 seconds not 10^4 and the change to gravity-viscous takes place at about 1400 seconds not 3600 as in Fay's plot. The second transition was at ≈2.5 x 10^5 not 6.048 x 10^5 (one week) as in Fay's plot. Note that both of these changes are approximately a factor of 2.4 different. The slopes of the lines plotted in the reproduced Figure 1 are the same as the slopes of the lines in Fay's original Figure 1, only the intersection points differ. Fay did not directly state what values he used for the variables in the equations of the Figure 1. However, throughout his manuscript he stated typical values for the variables and those were used here to reproduce his plots. Fay had originally defined the difference in density of the oil and water as 0.05 and assigned a combination of variables ∀<. However when he used these variable in his derivation he cancelled < out and left a unitless ∀. The acceleration of gravity was 9800 cm/s^2, the volume of 10 000 tons of oil was calculated to be V = 8.08 x 10^9 cm^3, with 8 = 0.01 cm^2/s, < = 1.0 g/mL, and = = 30 dynes/cm. The attitude that it is up to the reader to figure out what values have been assigned to the variables is typical of the literature reviewed here.

Reproduced Figure 2 plots the slick size (length in cm) *versus* time after initial spill and the line drawn in the plot is for the case of surface tension-viscous spreading. There does not seem to be a very good fit to the data especially considering that the formula relating length to surface tension and time is to the fourth root. This means that in order to see a one order of magnitude change in the length the other terms must change by four orders of magnitude. With such a wide range of possibilities for the terms (right hand side of the equation) there should be a much better fit of the data to the line drawn.

The same problem exists with Figure 3 as does with Figure 2 and any plot of any equation taken to a large power. Whichever side of the equation that is taken to a large power must change by a large number of orders of magnitude before the left hand-side of the equation changes by one order of magnitude. This allows for large errors (or guesses) in the variables on the right-hand side of the equation to be used (or errors hidden) but does not give specific information about which variables are the most important to model the spill correctly. In Figure 3 the right-hand side of the equation is taken to the sixteenth root which allows for the variables on the right hand side to change by sixteen orders of magnitude to produce a one order of magnitude change in the maximum slick size ℓ_∞.

Fay states that the experimental data was from Smith, J.E. (ed.) *Torrey Canyon Pollution and Marine Life*, Cambridge University Press (Cambridge, 1968) and Stroop, D.V., "Report on Oil Pollution Experiments - Behavior of Fuel Oil in the Surface of the Sea", pp 41-49, *Pollution of Navigable Water*, Bureau of Standards, Washington (1927). However, Fay does not state the error of the measurements nor whether the data was taken directly from these reports or had to be converted to get ℓ_∞ *versus* V or ℓ *versus* t (time).

Review of a manuscript, written by Yapa, P.D., S.A. Weerasuriya, D.P. Belaskas, and T. Chowdhury entitled *Oil Spreading in Surface Water with an Ice Cover*. Report 93-3 from Civil and Environmental Engineering, Clarkson University, Potsdam, NY.

Department of Clarkson University, Potsdam, NY, report 93-3 is a compilation of several Departmental reports and other publications. This starts with report 89-10, *Spreading of Oil Spilled Under Ice*, (which is itself completely contained in T. Chowdhury's M. Sc. thesis, *Spreading of Oil Spilled Under Ice*, from the Department of Civil and Environmental Engineering, Clarkson University, Potsdam, NY). Next is a paper by Yapa, P.D. and T. Chowdhury, *Spreading of Oil Spilled Under Ice*, in the Journal of Hydraulic Engineering, Vol 116, 1990, pp 1468-1483. Also included is report 91-6 (Belaskas, D.P. and P.D. Yapa, *Oil Spreading in Broken Ice*) of the Department of Civil and Environmental Engineering, Clarkson University, Potsdam, NY. Finally is the paper by Weerasuriya, S.A. and P.D. Yapa, *Unidirectional Spreading of Oil Under Solid Ice*, in the Canadian Journal of Civil Engineering, Vol 20, 1993, pp 50-56. The original data for report 93-3 is in T. Chowdhury's M. Sc. thesis, and report 91-6.

Technical Summary

The authors have presented a detailed theoretical description of the processes involved in oil spreading under a continuous ice sheet and then this was modified to explain the spreading of oil in broken ice conditions. The authors performed experiments to support the derived theory. The measured results support the theory for the continuous ice sheet but do not support the theory outlined to explain oil spreading in broken ice situations.

Objective

To test several models and determine the best model to explain the behaviour of oil in ice. Several mathematical equations are derived and experiments are performed to justify these models. There are different models proposed for continuous ice and broken ice. The solid ice cover is simulated with a continuous piece of plastic and ice that has been grown on a piece of rigid insulation. The broken ice cover was simulated using four different types of material and or shapes which are listed in the methods section.

Literature Review

The literature review lists equations that have been used by various people to explain oil spreading under various ice conditions. None of the literature reviewed nor the present paper takes into account wave action. The reviewed papers are, Glaeser and Vance (1971), McMinn (1973), Ramseier (1973), Hoult *et al* (1975), Keevil and Ramseier (1975), Chen *et al* (1976), Ross and Dickins (1987), Comfort and Purves (1979), C-CORE (1980), Cox and Schultz (1980), Allen (1983), Stringer and Weller (1985), and Venkatesh *et al* (1990).

Method

The experiments were done using a video camera, with built in timing ability (0.1 seconds) and a mirror assembly, to record the oil spill movement in a laboratory plexiglas tank that was kept

in a thermostated "cold" room. The ice covers were grown and a grid was incorporated into the ice to be used to monitor the movement of the oil. The grid was used to reduce the visual error caused by the camera. Several ice covers, as listed below, were used and the data was recorded using the video camera system. Type I is polyethylene blocks (20.6 x 19.1 x 6.4 mm) with a density of 0.92 g/cm^3 and a porosity of 0.37. Type II is small plastic cylinders (diameter 3.33 mm, length 3.25 mm) with a density of 0.87 g/cm^3 and a porosity of 0.36. Type III is crushed ice from an ice machine with a density of 0.92 g/cm^3 and a porosity of 0.55. Type IV is made up of very small ice blocks (12.7 x 12.7 x 9.5 mm) with a density of 0.91 g/cm^3 and a porosity of 0.39.

There is a short description of the apparatus that was used to measure surface tension between the surfaces (used in the experiments) and water and oil. There is no mention about the size (area) of surfaces used to measure the surface tension. The usual apparatus that is used to do these types of measurements have extremely small surface areas to reduce errors. No mention is made of the area used in these measurements and no mention is made of the weight of water/oil that is used on the 0.01 g accuracy scale. The weight of water (oil) used determines how many significant figures should be used in the reported value. The authors values are in Table 6.2.

The viscosity of each oil was measured using a Zeitfuchs cross arm viscometer. The viscosities ranged from 0.700 to 5.312 cm^2/s for solid ice cover (Tables 6.1 and 6.4) , and from 2.41 to 769.0 for broken ice cover (Tables 6.6 and 6.11).

The oil discharge was done using a diffuser to "provide a place for the oil to be discharged, to reduce the momentum of the oil as it was discharged, and to provide a means for having the oil-water or oil-air interface as close to the point of discharge as possible." Two different types of diffusers were used but no comparison of results is done.

Theory

The sections used in the report will be used here as reference points.

3.1 Oil Under Solid Ice- Axi-Symmetrical Spreading

3.1.1 Gravity (Buoyancy)-Inertia Phase

$$R = 0.751\left[\left(\frac{\rho_w}{\rho_o}-1\right)gQ\right]^{1/4} t^{3/4} \qquad (3.3)$$

where R is radius of the oil slick, ρ_w is density of water, ρ_o is the density of the oil, g is acceleration due to gravity, Q is rate of discharge of oil, and t is time in seconds.

Equation (3.3) was rederived and shown to be correct.

3.1.2 Gravity (Buoyancy)-Viscous Phase

There are two equations for this case:

$$R = k_{1a}\left[\frac{(\rho_w-\rho_o)gQ^3}{\mu_o}\right]^{\frac{1}{8}} t^{\frac{1}{2}} \quad (Q=constant) \quad (3.19)$$

and

$$R = k_{2a}\left[\frac{(\rho_w-\rho_o)gV^3}{\mu_o}\right]^{\frac{1}{8}} t^{1/8} \quad (V=constant) \quad (3.20)$$

where k_{1a} and k_{2a} are dimensionless constants, μ_0 is the oil viscosity, and V is volume of oil in slick. Q is constant at the beginning of an experiment (constant discharge) and then the discharge is shut off and the experiment is then in a constant volume state.

Rederivation of these equations, from the equations given in the report, indicate that $k_{1a} = \pi^{-3/8}$ and $k_{2a} = 2^{1/4}*\pi^{-3/8}$ which means that these 'constants' have a similar value but they are not identical.

The authors also derived a time equation:

$$t = \left(\frac{k_{1a}}{0.751}\right)^4 \left[\frac{Q}{g\nu_o(\frac{\rho_w-\rho_o}{\rho_o})}\right]^{\frac{1}{2}} \qquad (3.21)$$

where ν_o is the kinematic viscosity of the oil.

Equation (3.21) was also rederived and shown to be valid, at least as valid as the equations from the report upon which the derivation is based. Actual derivation showed that the coefficient in front of the square bracket should be $\pi^{-5/2}$.

3.1.2 Buoyancy-Interfacial Tension Phase (Termination of Spreading)

$$R_f = k_3\left[\frac{g(\rho_w-\rho_o)}{\sigma_n}\right]^{\frac{1}{4}} V^{1/2} \qquad (3.23)$$

where σ_n is the surface tension of the oil.

Rederivation of this equation, from equations supplied in the report, yielded $k_3 = 2^{-1/4}*\pi^{-1}$.

3.2 Oil Under Solid Ice- Uni-Directional Spreading

3.2.1 Buoyancy-Viscous Phase

There are two equations for this case:

$$x = k_{1u}\left[\frac{(\rho_w-\rho_o)gq^3}{\mu_o}\right]^{\frac{1}{5}} t^{4/5} \quad (q=constant) \qquad (3.36)$$

and

$$x = k_{2u}\left[\frac{(\rho_w-\rho_o)}{\mu_o} g \forall^3\right]^{\frac{1}{5}} t^{1/5} \quad (\forall = constant) \qquad (3.37)$$

where q is the rate of discharge of oil, and [is the volume of oil spilled.

These equations were rederived using the equations present in the report and $k_{1u} = (5/16)^{1/5}$, while $k_{2u} = (5/4)^{1/5}$.

3.2.2 Buoyancy-Interfacial Tension Phase
(Termination of Spreading)

$$x_f = \forall \sqrt{\frac{g(\rho_w-\rho_o)}{2\sigma_n}} \qquad (3.39)$$

This equation for the final slick length was rederived and shown to be correct.

4.1 Oil Under Broken Ice- Axi-Symmetrical Spreading

4.1.1 Bottom slick radius

Basically the authors believe that equations (3.19) and (3.20) can be used with a factor to account for seepage.

4.1.3 Top slick radius

(b) Spreading of oil on the water surface near the top of ice cover

$$R = K_{1t}\left[\frac{Q\sigma_n}{\mu_o}\right]^{\frac{1}{4}} t^{1/2} \quad (Q = constant) \quad (4.12)$$

and

$$R = K_{2t}\left[\frac{\forall\sigma_n}{\mu_o}\right]^{\frac{1}{4}} t^{1/4} \quad (\forall = constant) \quad (4.13)$$

The authors assume that K_{1t} and K_{2t} are the same as the coefficients for oil under solid ice multiplied by a constant. There is no scientific explanation given for this assumption and the experiments prove that it is not valid.

4.2 Oil Spilled Under Broken Ice- Uni-Directional Spreading

4.2.1 Bottom slick length

The authors use equations (3.36) and (3.37) with some modifications of q and V but they do not specifically state what the modifications are.

4.2.3 Top slick length

(b) Spreading of oil on the water near the top of ice cover

$$X = K_{1t}\left[\frac{q\sigma_n}{\mu_o}\right]^{\frac{1}{3}} t^{2/3} \quad (q = constant) \quad (4.25)$$

and

$$X = K_{2t}\left[\frac{\forall\sigma_n}{\mu_o}\right]^{\frac{1}{3}} t^{1/3} \quad (\forall = constant) \quad (4.26)$$

The rederivation of the above equations allowed calculation of $K_{1t} = (3/4)^{1/3} = 0.90856$ and $K_{2t} = (3/2)^{1/3} = 1.1447$.

The equations presented above are summarized below in Table 1.

Table 1: Listing of equations.

equation #	power of t	constant	derived	reported
3.3	0.750 (3/4)			
3.19	0.500 (1/2)	q	k_{1a} 0.65098	0.495
3.2	0.125 (1/8)	V	k_{2a} 0.77415	0.508
3.36	0.800 (4/5)	q	k_{1u} 0.7924	0.7??
3.37	0.200 (1/5)	[	k_{1u} 1.0456	0.621
4.12	0.500 (1/2)	Q	K_{1t} 0.89324	?
4.13	0.250 (1/4)	[	K_{1t} 1.06225	?
4.25	0.667 (2/3)	q	K_{1t} 0.90856	?
4.26	0.333 (1/3)	[	K_{1t} 1.1447	?

Results and Discussion

The tables presented in section 6 (Results and Discussion) of report 93-3 are reproduced here.

Table 6.1: Parametric Values in Axi-symmetrical Experiments for Solid Ice

Run #	Roughness 0(cm)	Q (cm^3/sec)	V (cm^3)	v_o (cm^3/sec)	ρ_o (g/cm^3)
SD1	0.084	18.42	1050	1.863	0.868
SD2	0.084	26.22	1075	1.885	0.868
SD3	0.084	48.611	875	2.133	0.867
SD4	0.084	58.67	880	2.067	0.867
SD5	0.084	28.67	1075	2.292	0.865
SD6	0.084	55.55	1250	0.7	0.853
SD7	0.084	9.52	800	1.501	0.852
ST1	0.53	29.31	850	2.276	0.865
ST2	0.53	17.66	1360	2.21	0.867
ST3	0.53	28.57	850	1.929	0.867
ST4	0.53	8.621	1000	0.776	0.855
ST5	0.53	57.47	1034.5	0.802	0.853
SS1	0.236	51.75	1087	0.788	0.853
SS2	0.236	36.8	1225.5	1.453	0.866
SM1	0.00015	8.104	778	6.94	0.872
SM2	0.00015	8.104	1013	6.94	0.872
SM3	0.00015	8.104	1244	6.94	0.872
SM4	0.00015	8.104	1479	6.94	0.872
SM5	0.00015	8.104	1126.5	6.94	0.872
SM6	0.00015	816.13	911.35	3.8735	0.87
CR1	1.64	8.69	500	1.96	0.866
CR2	1.64	4.545	682	1.41	0.886
PL1	0.00015	15.385	992.3	1.433	0.866

Table 6.2: Table of Interfacial Tension for Different Surfaces

Type of surfaces	Surface tension in water* *dyne/cm*	Surface tension in oil* *dyne/cm*
Plexiglas	70.256	40.59
Sand	98.145	55.92
Small Stone	132.58	75.145
Stone	150.389	82.313
Crushed Ice **	159.46	86.486

* In computing these the tortuous path of fluid/solid interface is not considered.
** The value obtained by extrapolation.

Table 6.3: Error Analysis for Evaluating Radius

Type of experiment	St. error (%) Q = constant	St. error (%) V = constant
Real ice cover experiments	4.75	5.22
Art. ice cover experiments	6.43	7.8
constant k experiments	5.77	5.01
variable k experiments	6.01	9.88
All experiments	5.87	7.12

Table 6.4: Parametric Values in Uni-directional Experiments for Solid Ice

Run #	q ($cm^3/s/cm$)	Roughness 0(cm)	[(cm^3/cm)	ν_o (cm^2/sec)	ρ_o (g/cm^3)
SS1-U	0.58	0.00015*	35	3.79	0.884
SS2-U	2.06	0.00015*	123.6	2.88	0.878
SS3-U	0.63	0.00015*	44.4	5.312	0.881
SS4-U	2.25	0.00015*	45	2.112	0.883
SD1-U	0.55	0.2	55.1	3.18	0.878
SD3-U	2.2	0.2	59.4	3.442	0.877
SD4-U	3.13.	0.2	62.6	1.524	0.859
ST1-U	0.84	0.47	63.7	3.429	0.882
ST2-U	0.44	0.47	48.1	1.507	0.878
BS1-U	0.46	0.94	48.6	2.129	0.88

* Assumed value for smooth surface (White, 1986).

Table 6.5: Results from Uni-directional Experiments for Solid Ice

Exp #	Exp. of t in q cons.	error %	Exp. of t in [cons.	error %
SS1-U	0.8	0	0.193	3.5
SS2-U	0.769	3.9	+	--
SS3-U	0.807	0.9	0.25	25
SS4-U	0.665	16.9	0.149	25.5
SD1-U	0.823	2.9	0.215	7.5
SD3-U	0.702	12.25	0.204	2
SD4-U	0.826	3.25	0.196	2
ST1-U	0.783	2.1	0.24	20
ST2-U	0.828	3.5	0.23	15
BS1-U	0.829	3.6	0.209	4.5

+ Slick extended beyond the edge of the ice cover - no data.

The error analysis was done by the reviewer but the data in the table is the authors. The authors have stated that the errors were only 4-5%.

Table 6.6: Parametric Values in Axi-symmetrical Experiments for Broken Ice.

Exp #	Q (cm^3/s)	V (cm^3)	ν_o (cm^2/s)	ρ_o (g/cm^3)	Ice Cover Type	ζ_i (cm)	ϕ %	ρ_i (g/cm^3)
1AB1	22.61	2097.8	214.8	0.85	I	5.08	0.4	0.92
2AB1	54.69	3281.4	212	0.84	I	4.57	0.37	0.92
3AB1	31.53	1891.8	209.2	0.85	I	4.83	0.4	0.92
4AB1	44.7	2682	219	0.85	I	4.57	0.35	0.92
5AB1	53.93	3235.8	215	0.85	I	4.72	0.37	0.92
6AB2	53.3	3198	179.3	0.88	I	7.7	0.36	0.92
7AB2	22.7	1362	161.2	0.88	I	7.42	0.33	0.92
8AB2	43.7	2622	209	0.89	I	7.57	0.35	0.92
9AR1	44.38	2664	192.1	0.85	II	4.83	0.36	0.87
10AR1	22.2	1332	219.2	0.85	II	4.83	0.32	0.87
11AR1	51.37	3082.2	279.2	0.85	II	5.59	0.39	0.87
12AR7	53.48	3208.8	193	0.88	II	1.95	0.32	0.87
13AR6	53.82	3229.2	209	0.89	II	1.55	0.43	0.87
14RF1	18.31	1281.7	769	0.88	III	4.37	0.55	0.92

Exp #	Q (cm^3/s)	V (cm^3)	ν_o (cm^2/s)	ρ_o (g/cm^3)	Ice Cover Type	ζ_i (cm)	ϕ %	ρ_i (g/cm^3)
15RB	17.99	1259.3	378.1	0.87	IV	4.22	0.37	0.91
16RB	47.74	3341.8	387.8	0.87	IV	3.81	0.31	0.91
17RB	77.22	4247.1	170	0.87	IV	4.7	0.44	0.91
18RB	18.34	1283.8	648.5	0.88	IV	4.52	0.42	0.91

ζ_i is the ice cover thickness.
ϕ is not defined by the authors.

Table 6.7: Slopes and Intercepts ($R\Sigma$) of log R *vs* log t - Type I Ice Cover.

Run	Bottom View		Top View		
#	Q = Constant		Q = Constant		V = Constant
	slope	$R\Sigma$	slope	$R\Sigma$	slope
1AB1	0.41	0.23	0.66	-0.02	0.25
2AB1	0.33	0.55	0.71	0.07	0.2
3AB1	0.49	0.23	0.75	-0.12	0.19
4AB1	0.35	0.47	0.69	0.07	0.2
5AB1	0.37	0.54	0.69	0.1	0.22
6AB2	0.37	0.57	0.72	0.01	0.23
7AB2	0.36	0.4	0.67	-0.03	0.28
8AB2	0.38	0.51	0.71	-0.04	0.23

Table 6.8: Slopes of log R *vs* log t - Type II Ice Cover.

Run #	Bottom View	
	Q = Constant	V = Constant
9AR1	0.47	0.08
10AR1	0.52	0.05
11AR1	0.48	0.19
12AR7	0.48	0.12
13AR6	0.48	0.09

note intercept $R\Sigma = 0$.

Table 6.9: Slopes and Intercepts ($R\Sigma$) of log R *vs* log t - Type III Ice Cover.

Run	Bottom View		Top View		
#	Q = Constant		Q = Constant		V = Constant
	slope	$R\Sigma$	slope	$R\Sigma$	slope
14RF1	0.51	0.26	*	-	-
15RB	0.48	0.24	0.68	-0.114	0.27
16RB	0.48	0.45	0.52	0.375	0.35
17RB	0.42	0.62	0.57	0.4	0.34
18RB	0.46	0.28	0.57	0.085	0.26

* experimental problems.

Table 6.10: Input Parameters for Axi-symmetrical Numerical Simulations.

Experiment #	K_{z0} (cm/s)	K_{x0} (cm/s)	MFB*	MFT+	h_c (cm)	σ_n (dyne/cm)
AB 1	0.7	0.7	0.95	1.35	0.05	40
AB 2	0.7	0.7	0.95	1.35	0.05	40
AB 3	0.7	0.7	0.95	1.35	0.05	40
AB 4	0.7	0.7	0.95	1.35	0.05	40
AB 5	0.7	0.7	0.95	1.35	0.05	40
AB 6	0.7	0.7	0.95	1.35	0.05	40
AB 7	0.7	0.7	0.95	1.35	0.05	40
AB 8	0.7	0.7	0.95	1.35	0.05	40
RB 15	0.7	0.7	0.95	1.6	0.05	35
RB 16	0.7	0.7	0.95	1.6	0.05	35
RB 17	0.7	0.7	0.95	1.6	0.06	35
RB 18	0.7	0.7	0.95	1.6	0.05	35

* Modification factor for bottom slick.
+ Modification factor for top slick.

Table 6.11: Parametric Values in Uni-directional Experiments for Broken Ice.

Exp #	q (cm^3/s)	[(cm^3)	ν_o (cm^2/s)	ρ_o (g/cm^3)	ζ_i (cm)	ϕ %	ρ_i (g/cm^3)
LW 1	1.45	88	4.01	0.883	5.4	0.672	0.92
LW 3	0.8	70.7	2.89	0.878	4.5	0.62	0.92
LW 4	1.19	81.2	3.02	0.88	3.5	0.697	0.92

Exp #	q (cm^3/s)	[(cm^3)	ν_o (cm^2/s)	ρ_o (g/cm^3)	ζ_i (cm)	ϕ %	ρ_i (g/cm^3)
SB 1	2.35	55.1	2.67	0.883	4.2	0.58	0.87
SB 2	3.93	50.8	2.41	0.875	2	0.608	0.87
SB 3	3.27	60.2	2.76	0.878	1.8	0.574	0.87

Table 6.12: Input Parameters for Uni-directional numerical simulations.

Experiment #	K_{z0} (cm/s)	K_{x0} (cm/s)	MFB*	MFT+	h_c (cm)	σ_n (dyne/cm)
LW 1	0.7	0.3	0.95	1.7	0.09	40
LW 3	0.7	0.3	0.95	1.7	0.09	40
LW 4	0.65	0.3	0.98	1.9	0.09	40
SB1	0.025	0.025	1	1.5	0.22	50
SB 2	0.025	0.025	1	1.3	0.22	50
SB 3	0.009	0.009	1	1.5	0.22	50

* Modification factor for bottom slick.
+ Modification factor for top slick.

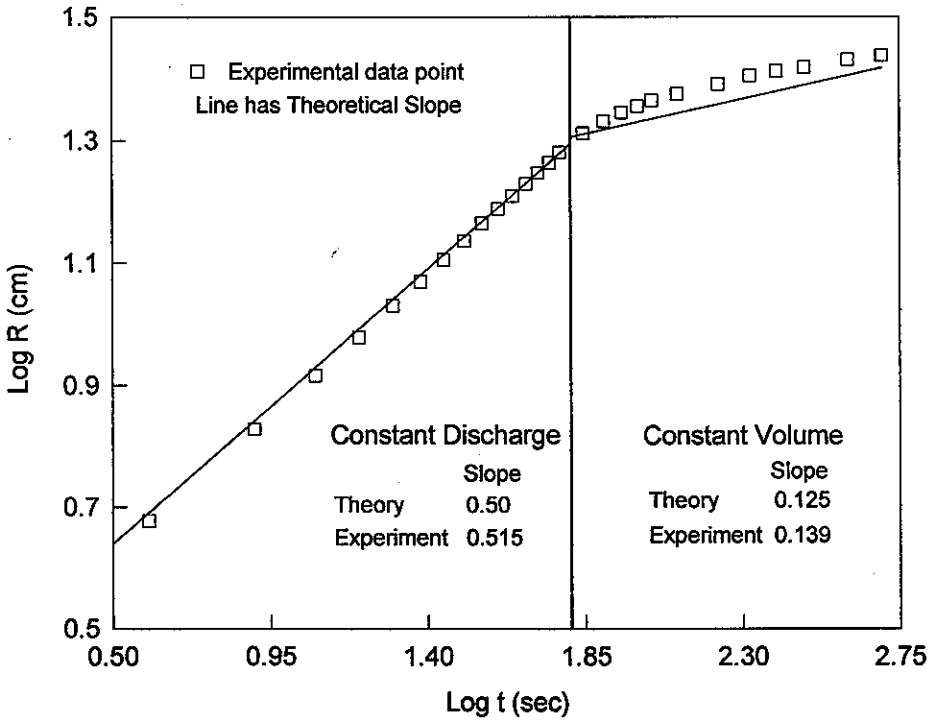

Figure 6.1: Log of R *vs* Log t for Run #PL1

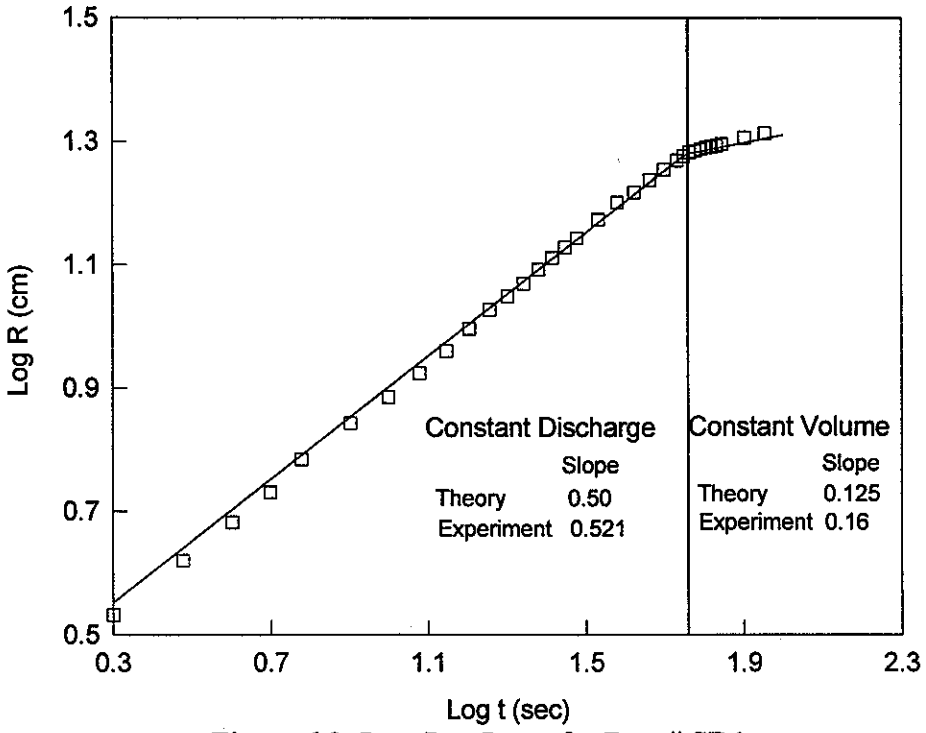

Figure 6.2: Log *R vs* Log t for Run # SD1

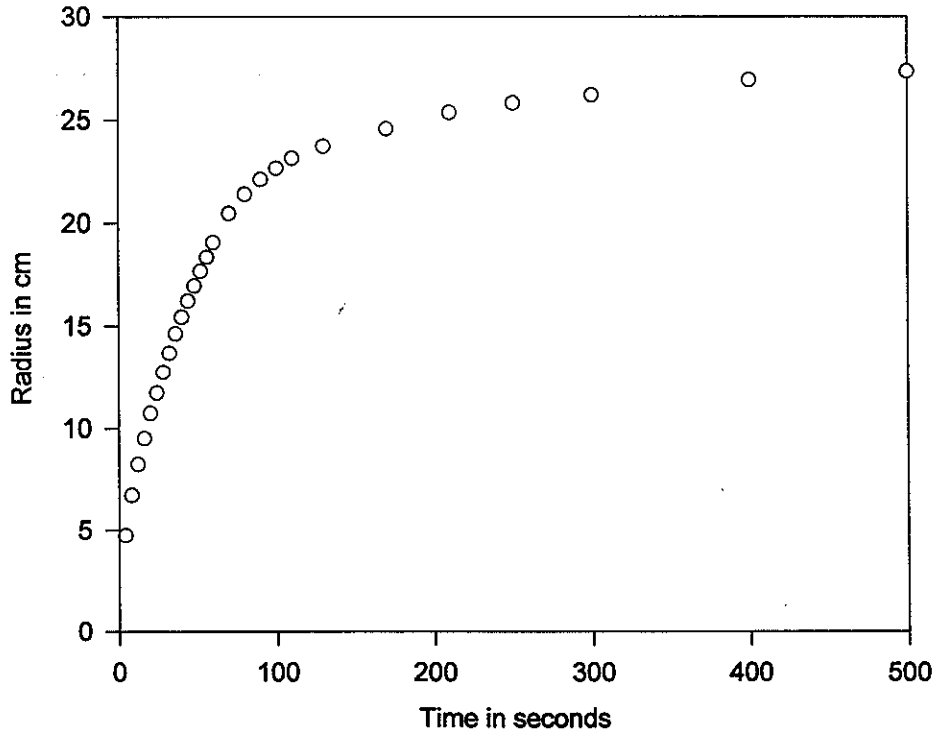

Figure 6.1 Supplementary: Plot of *R* (cm) *vs* t (seconds) Run #PL1

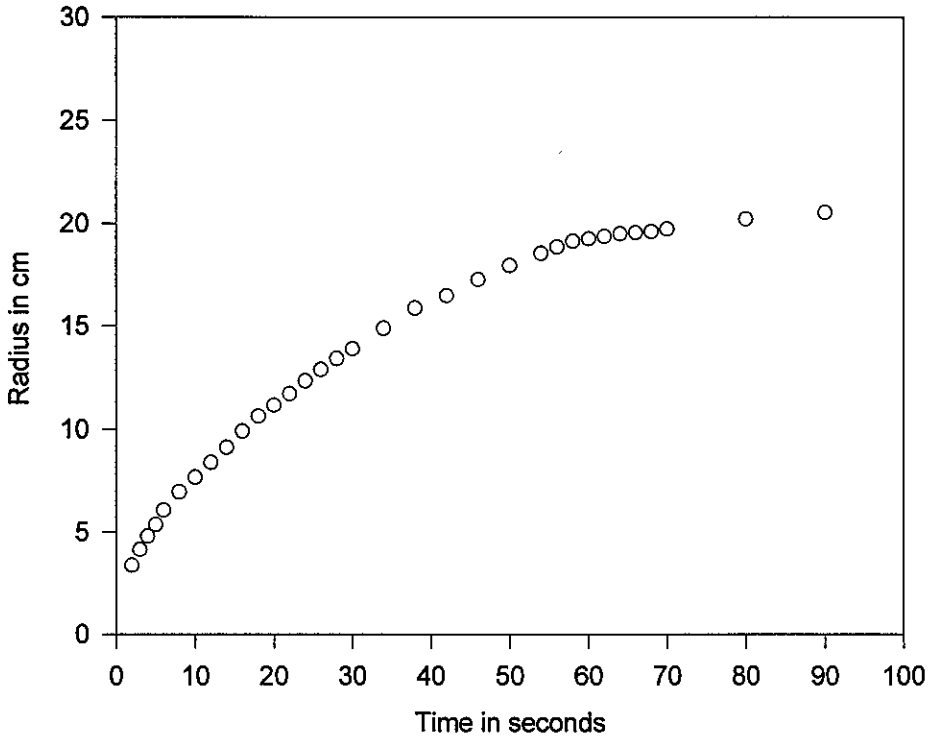

Figure 6.2 Supplementary: Plot of R (cm) *vs* t (seconds) Run #SD1

Figures 6.1 Supplementary and 6.2 Supplementary are included to allow a comparison of data that is plotted on log, log scale (Figures 6.1 and 6.2) and the same data plotted on a linear x and y axes.

BOSS Critique

There is a very detailed explanation of the experimental apparatus. The explanation of how ice covers are made is good but the method of determining the depth of the ice roughness is not as well explained or is too simple of a process to provide useful data.

Plotting log Y *vs* log X is not an acceptable method for this type of work. Log, log plots allow for huge errors to be hidden. This is confirmed when the R *vs* "whichever" is plotted (*i.e.* Figures 6.3, 6.4 or 6.8) and there is a large scatter in the results. This is also a problem with the k_{1a} and k_{2a} plots (Figures 6.5, 6.6, and 6.7) and there is no complete proof given to plot k_{1a} *vs* $Q^{0.4}/(g^{0.2}0)$. The physical reasons for raising either g or Q to the power presented in report 93-3 are not given.

A more direct comparison is needed of both Axi-symmetric and Uni-directional equations for continuous and broken ice conditions. Even though some of the simulations resemble (slope wise) the measured data, the experimental data do not, generally, support the theory. The errors calculated and tabulated in Table 6.5, are much larger than the 4-5% error expected by the authors (Table 6.3). There is no description of the values expected and realized for K_{1t} nor K_{2t} for the axi-symmetric case. There is very little discussion of equations 4.12, 4.13, 4.25, and 4.26 all of which are for the broken ice section of report. The assumption for spreading under broken ice for both axi-symmetric and uni-symmetric is that surface tension has a large effect. It is more likely that the ice is going to break through any surface tension since the ice is denser than the oil and thus specific gravity of the oil (weathered or not) is of more importance.

Review of a manuscript by Glaeser, LTJG J.L., and LCDR G.P. Vance, *A Study of the Behaviour of Oil Spills in the Arctic,* U.S. Coast Guard, Washington, D.C., 1971.

Technical Summary

"...It was found that an upper layer of recrystallized ice in the test area absorbed 25 per cent of its volume in oil which had been released on the surface. The oil travelled through the upper layer seeking the lowest possible level, eventually migrating to the melt ponds present. Data from the spreading experiments on ice show power law relationships between certain of the parameters investigated.···

Crude oil which was released under ice cover rose to the surface, where it remained without dispersing to any great extent.···

An investigation into the effect of an oil spill on the Arctic heat budget showed general agreement with past work done on the subject.

Samples were collected of oil aged in the environment up to 13 days. Physical and chemical analysis showed measurable changes in certain characteristics of the crude oil. Loss of the volatiles occurred in less than 5 days.···"

Information was also presented, in the manuscript, for oil spreading on water, crude oil burning on ice (after a five day aging period), and use of absorbants to remove oil, but this review will not discuss any of these sections.

SECTION I: Spreading of Oil on Ice

Objective

To obtain quantitative data on oil spill ice interaction that could be scaled up to large size spills as well as qualitative data on the oil spreading process.

The parameters that were to be controlled in the study were:

a) Oil volume,
b) Oil viscosity,
c) Oil density,
d) Oil temperature,
e) Oil release rate.

Method

Oil was released onto the snow/ice from 55 gallon tanks through either a 3 inch orifice or a 12 inch orifice in a pipe which ended four feet above the ice/snow surface. Two types of oil, diesel oil or North Slope crude, were used and were also heated for some experiments. This was done to provide a change in viscosity.

Theory

The first assumption is that area is similar to the length of the slick squared, ($A = l^2$) instead of the accepted $A = \pi r^2 = \pi (D/2)^2$. This introduces an error into the calculation.

The authors then derive two equations for the length of the oil slick. One for the gravity-

inertia phase (initial spreading) and the other for gravity-viscous phase.

For gravity-inertia spreading,

$$l \sim (gV)^{\frac{1}{4}} t^{\frac{1}{2}},$$

and for gravity-viscous spreading,

$$l \sim (gV^2t^2)^{\frac{1}{7}}.$$

No publications or other material is referenced to provide a scientific bases for these assumptions although it is believed that the authors are paraphrasing equations from J.A. Fay's, "The Spread of Oil Slicks on a Calm Sea", in *Oil on the Sea*, edited by D.P. Hoult and published by Plenum Press, 1969, pp 55-63..

Results

Figures 3 and 4 are reproduced here, complete with theoretical lines indicating the slope expected for the two cases, gravity-viscous phase and gravity-inertia spreading. The data that is used to plot the two figures is presented in (five) tables, on the next few pages.

The tables are from the manuscript with no additions nor deletions except that instead of blanks spaces, as in the original table, a series of three dashes (---) have been used here to represent a situation of no data point. The authors do not explain the (a) and (b) designation for the time data. Nor do they explain the value used for *s* (specific gravity) for the types of oil used.

List of Symbols

g	gravitational constant
h	average slick thickness
l	slick length
L	characteristic length
s	specific gravity
t	time
V	oil volume
w	channel width
δ	boundary layer thickness
Δ	percentage density difference
μ	absolute viscosity of water
ν	kinematic viscosity of water
σ	surface tension

Tables from Appendix 1: Data for oil spills on ice

55 gal of cold (8 °C)diesel, 12" orifice, 3.3 second release.

l (ft)	t (sec) (a)	(b)	$\frac{l}{V^{1/3}}$	$t/\sqrt{\frac{V^{1/3}}{gs}}$ (a)	(b)
3	0.45	0.80	1.55	1.67	2.98
5	0.80	0.90	2.58	2.98	3.35
7	---	1.2	3.60	---	4.46

55 gal of cold (10 °C)diesel, 3" orifice, 26.3 second release.

l (ft)	t (sec) (a)	(b)	$\frac{l}{V^{1/3}}$	$t/\sqrt{\frac{V^{1/3}}{gs}}$ (a)	(b)
2	1.5	1.0	1.03	5.59	3.72
3	1.7	4.1	1.55	6.33	15.3
4	6.5	6.0	2.06	24.2	22.3
5	---	7.75	2.58	---	28.8
6	---	10.1	3.09	---	37.6

45 gal of warm (29 °C) crude, 12" orifice, 3.0 second release.

l (ft)	t (sec) (a)	(b)	$\frac{l}{V^{1/3}}$	$t/\sqrt{\frac{V^{1/3}}{gs}}$ (a)	(b)
2	0.5	0.3	1.10	1.98	1.19
3	0.6	0.7	1.65	2.38	2.77
4	0.9	1.0	2.20	3.56	3.96
5	1.4	1.1	2.75	5.55	4.35
6	1.8	1.2	3.30	7.13	4.75
7	2.1	---	3.85	8.31	---
8	2.4	---	4.40	9.50	---

97 gal of warm (48 °C) crude, 12" orifice, 3.0 second release.

l (ft)	t (sec)		$\frac{l}{V^{1/3}}$	$t\Big/\sqrt{\frac{V^{1/3}}{gs}}$	
	(a)	(b)		(a)	(b)
3	---	0.39	1.28	---	1.35
5	0.6	0.75	2.13	2.07	2.59
7	1.7	1.09	2.99	5.86	3.76
9	1.75	1.3	3.84	6.05	4.49
11	---	3.0	4.69	---	10.4
13	---	3.4	5.54	---	11.7

55 gal of crude (6 °C) on saturated ice, 428 second release.

l (ft)	t (sec)		$\frac{l}{V^{1/3}}$	$t\Big/\sqrt{\frac{V^{1/3}}{gs}}$	
	(a)	(b)		(a)	(b)
1	---	1	0.521	---	3.88
2	---	3.4	1.04	---	13.2
3	---	15.5	1.56	---	60.1
4	---	26.3	2.08	---	102
5	---	32.4	2.60	---	126
6	---	48.3	3.12	---	188
7	---	74.7	3.64	---	290
8	---	88.2	4.16	---	342
9	---	106	4.69	---	409
10	---	119	5.21	---	464
11	---	136	5.72	---	527
12	---	192	6.25	---	745
13	---	275	6.77	---	1067
14	---	310	7.29	---	1203

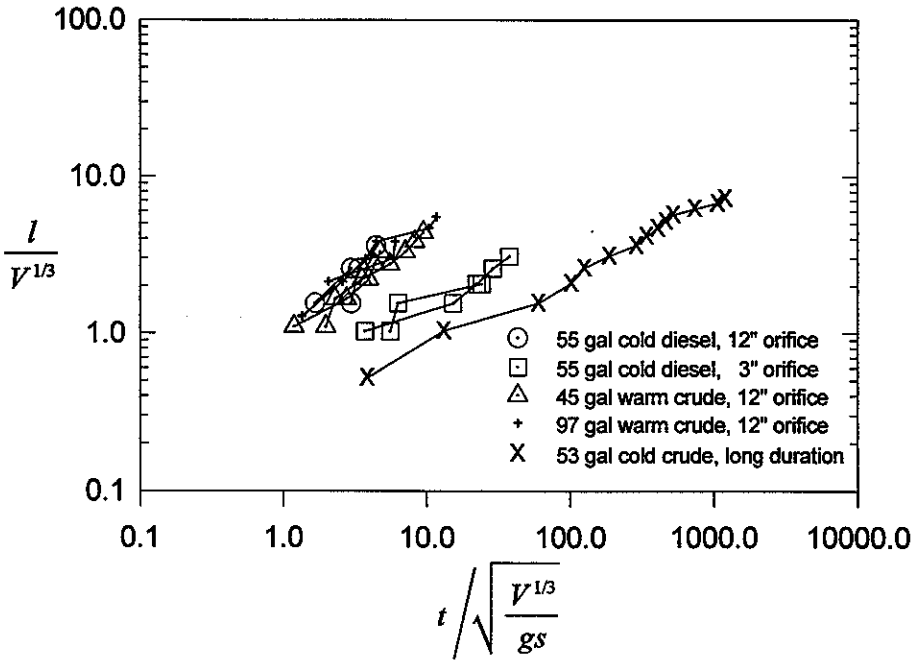

Figure 3.- Data for spreading of oil on ice. Nondimensional relationship between slick length and time.

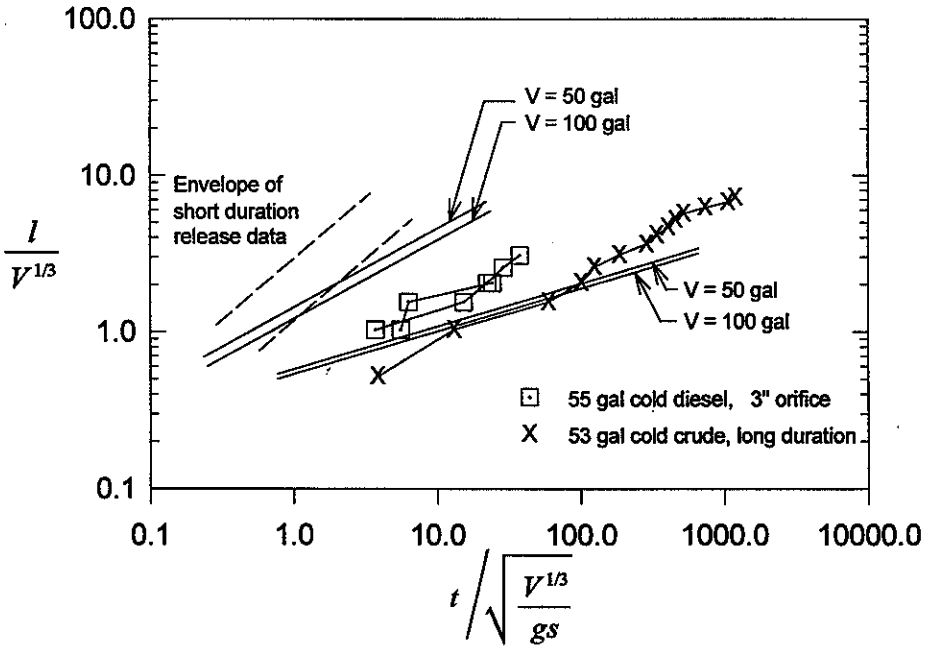

Figure 4.- Comparison of oil-on-ice spreading data with theory.

SECTION III: Spreading of Oil Under Ice

Objective

The purpose of the oil under ice visual experiments were to provide some understanding of the process of oil spreading under ice.

Method

Divers visually inspected the experimental site before, during, and after the oil had been pumped through a hole drilled in an ice cover of approximately 3.66 meters (12 feet).

Results

Several dives were made over a 24 hour period and the oil did not appear to move very far once it had occupied the various pockets and pores of the ice. The underside of the ice was not flat but curved downward and ice caverns were present several meters from the site of the spill. There was not a major current in the area and the oil stayed where it had been spilled, so the authors believe.

SECTION VI: A Comparison of the Heat Budget Over Oil-Covered and Clean Ice in the Arctic Environment

Written by LTJG T.C. Johnson, Applied Science Division

Objective

To measure the change in heat budget caused by oil spilled on ice. This difference is expected to cause the ice to melt at a faster rate where oil covers the ice.

Theory

The heat budget for an ice surface was expressed (by the author) as follows:

$$F_r + F_s + F_l + F_c + F_m = 0$$

Where

- F_r = radiation balance at the ice surface. This takes into account the incoming solar radiation, reflected solar radiation, emitted long wave radiation from the ice, and atmosphere, and reflected long wave radiation from ice and atmosphere;
- F_s = sensible heat to ice surface by turbulent exchange with the atmosphere;
- F_l = flux of latent heat by evaporation or condensation;
- F_c = flux of heat from below to ice surface;
- F_m = flux of heat utilized in melting (negative) or freezing (positive) of ice.

The author mentions that Badgley had done a heat budget using various Russian and American data from the Arctic and concluded that only F_r, F_c, and F_m were of any consequence (90% of the heat budget). No references were given for these statements.

F_c can be determined by $F_c = -kA \frac{dT}{dz}$;

where k = thermal conductivity of ice = 5×10^{-3} g cal/sec °C cm,
A = surface area = 1 cm^2,

$\frac{dT}{dz}$ = vertical temperature gradient.

F_r can be measure directly with a radiometer.

Method

The test was conducted by spilling two barrels of Prudhoe Bay crude oil on ice that was 5 meters thick.

The vertical temperature gradient was measured by inserting thermistor probes, at 12 cm intervals, directly into an ice core and thereby determining the temperature differential of the ice. Two sets of thermistors were imbedded into oiled ice and a single set was imbedded in clean ice, each with 5 thermistors at 40 cm intervals.

F_r was measured every hour over clean ice and oiled ice, with a ventilated net radiometer.

Results

The author determined that the measurements from the oiled ice surface and clean ice surface were in question and therefore he disregarded them. However, he believed that the ice core temperature gradient was correct. It was quite small, 3.7×10^{-3} °C/cm, resulting in a F_c value = -0.5 kg cal/cm^2/month and so was not included in the heat budget equation. Leaving only two terms, F_r and F_m.

Table two is of the values of F_r for clean and oiled ice (7 ± 1 kg cal/cm^2/month) and the author states that this is similar to Badgley's July number of 3.11 kg-cal/cm^2/month. He questions the results since only 10 hours of reading were taken (the apparatus was damaged) instead of the 3 days of data and secondly the data was only to one significant figure. The authors states that if readings had been taken for 3 days there would have been an averaging effect and the overall reading would have been reduced by a factor of two to 3-5 kg-cal/cm^2/month.

Table 2: Values of F_r over oil covered ice and clean ice.

Time	F_r (g cal/cm^2/hour)	
	clean ice	oil covered
1100	10	18
1300	8	20
1400	8	10
1500	8	10
1600	10	20
1700	10	4
1800	10	8
1900	10	8
2000	10	10
Average	9	12

The author also stated that the oiled ice melted at a rate of 2 cm/day faster than the surrounding clean ice. He calculated the heat requirement to be 280-400 g cal/cm^2/day which he says agrees with F_m = 278 g cal/cm^2/day reported by Langleben (no reference) on the melting of sea ice in early summer of 1965.

Basically the author suggests that ΔF_r be measured and ΔF_m determined from the change in ice depth of the oil covered ice and see if these are indeed similar as $F_r + F_m = 0$ would suggest. He also admits that because of the problems incurred in the measurements the results are only a ball park figure which could be improved with better instruments and data collected over a longer time interval. Finally, he suggests that the other terms may be more important during a winter test of oil spilled on ice.

SECTION VII: Aging of Crude Oil

Objective

To determine the physical and chemical changes of oil aged in the summer Arctic environment.

Method

Prudhoe Bay crude oil was spilled onto melt ponds, ice, and under the ice and then aged for up to 13 days. Samples were taken and placed in sealed jars. Most of the physical analysis was done on board the ship and included density, viscosity, and oil-water surface tension. The chemical analysis was done by independent laboratories.

Specific gravity measurements were done using hydrometers, no manufacture or type is mentioned. The scatter in the measurements is attributed to sampling problems not measurement problems.

Viscosity was measured using a Brookfield viscometer. The sample was preheated to its cloud point (approximately 150 °F) and then cooled down to near 32 °F.

Air-oil surface tension was calculated by measuring the oil rise in a capillary tube. No dimensions nor test standards (ASTM) are mentioned.

Results

Figures 13, 15, and 16 are reproduced from the figures in the manuscript, since no tables of data were in the manuscript for these figures. Figure 13 is a plot of specific gravity (at 20 °C) for Prudhoe Bay crude oil that has been aged in summer Arctic conditions on water and ice. Figure 15 is a plot of viscosity *versus* temperature for fresh Prudhoe Bay crude oil and Prudhoe Bay crude oil that has been aged on ice for up to seven days. Figure 16 is a plot of air-oil surface tension for Prudhoe Bay crude oil during the various stages of aging.

Generally the aged oil had higher viscosity, higher specific gravity, and higher surface tension due to the loss of low end hydrocarbons as shown by the chemical analysis. The distillation plots are not reproduced here but the table of saturates to aromatics is presented in the authors Table 3.

Table 3. - Effect of Arctic aging on crude oil composition.

Type of Sample	Aging Time in days	Boiling Range* (deg. F)	Sat./Arm.	Sat./Arm.	Gasoline (C_4-C_7)%
Aged on Water	0	130-852	3.2	1.3	5.6
	1			1.2	4.4
	5	376-920	4.79	1.2	0.38
	8				0.27
	11	201-827	4.37		0.65
Aged on Ice	0	157-870	3.11		
	5	175-877	4.60		
	13	254-863	3.20		
Aged Under Ice	1	140-933	4.62		

*Range of maximum distillable liquid fraction by glass spiral still at pressures from 1 atm. down to 1 mm Hg.

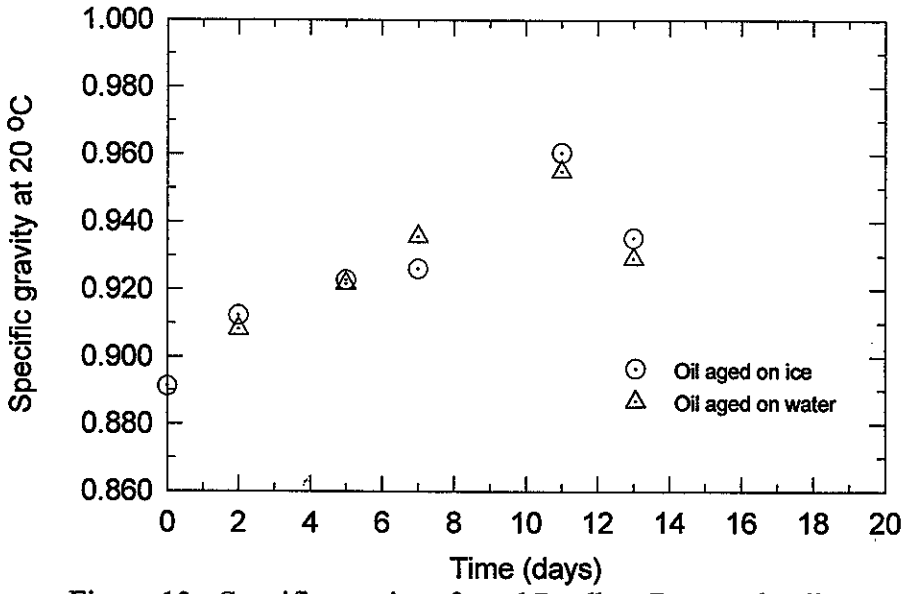

Figure 13.- Specific gravity of aged Prudhoe Bay crude oil.

Information was also presented, in the manuscript, for oil spreading on water, crude oil burning on ice (after a five day aging period), and use of absorbants to remove oil, but this review will not discuss any of these sections.

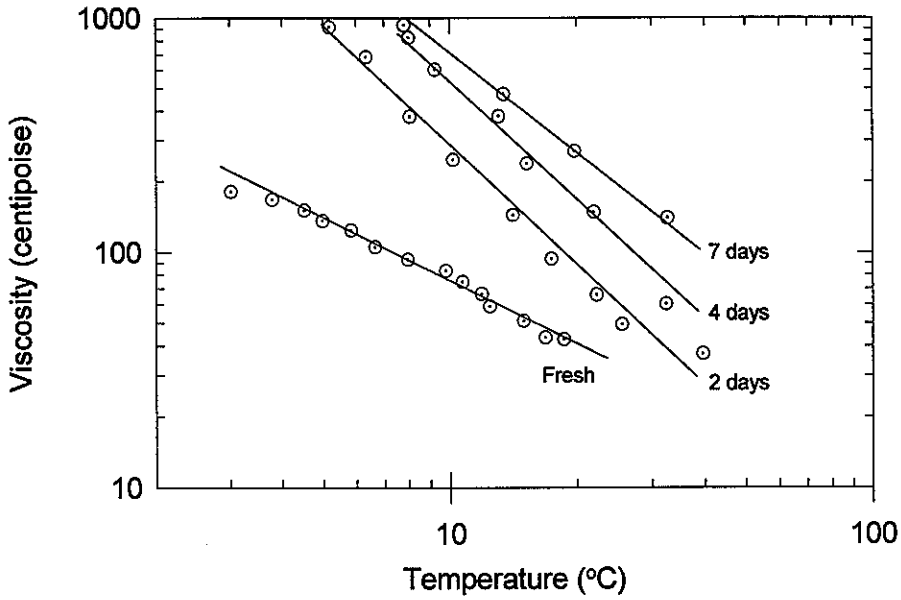

Figure 15.- Viscosity of Prudhoe Bay crude oil aged on ice.

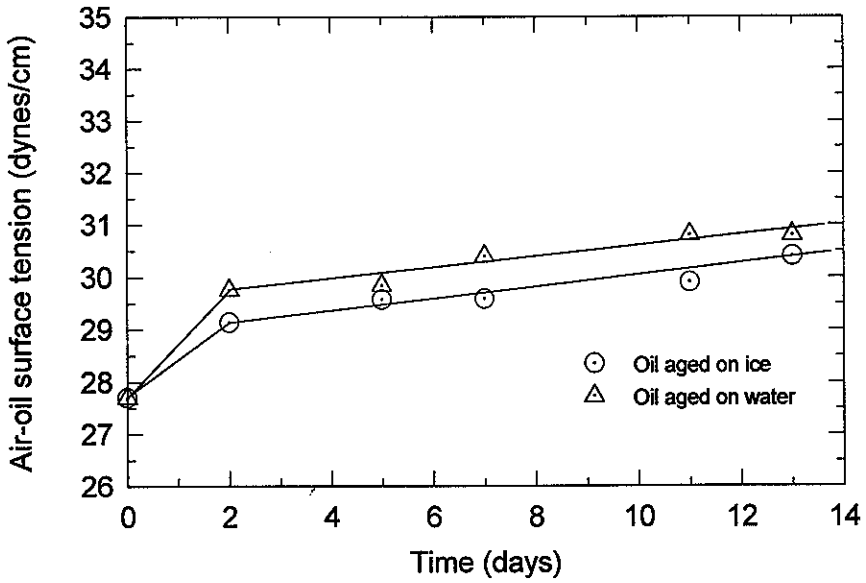

Figure 16.- Air-oil surface tension for aged Prudhoe bay crude oil.

BOSS Critique

There is no clear discussion of how the parameters (a) Oil volume, b) Oil viscosity, c) Oil density, d) Oil temperature, and e) Oil release rate) that were to be controlled in the study were controlled. The oil volume of the spill was used in the calculations and the plots but no mention is made in the manuscript of how this value was determined. It is not clear from the report whether

the oil spill volume was measured from the flow rate or whether it was measured from the tank level decrease. The specific gravity of the oil was also used in calculations and plots of the data but again no value for this is stated in the section on oil spreading on ice. The oil viscosity was controlled by using two different oils and by heating those oils so two parameters were combined. In fact the oil temperature would also affect the oil release rate, and the oil density since density, and viscosity are interrelated with the temperature and these parameters would all effect the release rate even if the orifice is kept the same.

The assumption that area is similar to the length of the slick squared, ($A = l^2$) instead of the accepted $A = \pi r^2 = \pi (D/2)^2$, introduces an error into the calculation.

No references are listed, and in some cases not even quoted, for the statements that are made about equations nor outcome of the derivations of the equations.

The heat budget section as the author states only produced ball park figures but it does describe the short comings of the experiment and how to improve on this in a future experiment.

The specific gravity data, Figure 13, indicates that oil aged on ice had a higher specific gravity for the first five days then at seven days of aging the oil aged on water had a higher specific gravity and then for the two remaining data points oil aged on ice had a higher specific gravity. It would have been helpful if more data points could have been collected to see exactly when the change over occurred.

It would also have been beneficial for the air--oil surface tension measurements to have been made more often over the 13 day period of the aging process. There seems to be a large scatter in the data and the authors have stated that they believe this to be due to poor sampling procedure.

It would also have be beneficial if the American Society for Testing and Materials (ASTM) standard methods have been used and referred to when the data was plotted and analyzed. The ASTM standards are for products manufactured from crude oil and tested in a laboratory environment not the crude oils themselves in the environment. Also of interest is that to the date of this review there are no ASTM standards for measuring viscosity, density, and surface tension of aged crude oil.

Review of a manuscript by Comfort, G. and F. Purves, entitled "An Investigation of the Behaviour of Crude Oil Spilled Under Multi-Year Ice at Griper Bay", in *Proceedings of the Third Arctic Marine Oilspill Program Technical Seminar*, Environment Canada, Ottawa, pp 62-86, 1980.

Other manuscripts covering this data are:

Comfort, G. and W. Purves, *The Behaviour of Crude Oil Spilled Under Multi-Year Ice.* Prepared by ARCTEC Canada Limited for the Environmental Protection Service, Environment Canada, Report No. EPS 4-EC-82-4, Ottawa, 1982.

Site Visit of Oil Spill Under Multi-Year Ice at Gripper Bay, N.W.T., report EE-42 for Environment Canada, by ARCTEC Canada Limited, 1983.

Comfort, G., T. Roots, L. Chabot, and F. Abbott, "Oil Behaviour Under Multi-Year Ice at Griper Bay, N.W.T.", in *Proceedings of the Sixth Arctic and Marine Oilspill Program Technical Seminar*, Environment Canada, Ottawa, pp 14-19, 1983.

Technical Summary(from the third manuscript)

"The results of the investigation indicates no oil remained trapped in the ice or on the surface. Three data points for the interaction of crude oil spilled under multi-year ice have been obtained. These are 100% of oil volume at 0 years, 10% remaining after two years and no apparent oil remaining after five years. The actual time required for the oil to disappear is not known; this could have taken place after only three years. The data can be bounded by an equation of the form: $A = me^{-bt^c}$."

Where A is % oil remaining, m is 100%, b and c are undefined parameters and t is time in years.

Objective

To do a field study, over several years, on the behaviour of oil spilled under multi-year ice at Griper Bay, N.W.T.

Theory

The authors stated that the disappearance of oil under ice can be evaluated with an equation for determining the percent left, $A = me^{-bt^c}$, where A = % of oil remaining, m = 100%, t = time in years, b and c are undefined parameters.

Method

1.8 m^3 of Norman Wells crude oil was discharged under ice, that was at least two years old, at three sites in 1978. The sites were visually inspected , from the air, three times in 1978 and site visits were done in October, 1978, March, 1979, September 1979, and final site visit and clean up in September, 1982.

The oil spill sites were cored in an attempt to measure the amount of oil left in the ice. It was expected that some oil would be reincorporated into the ice during fall freeze up after flowing up through brine channels during the short summer thaw.

The degree of weathering of the samples was done by comparing the gas chromatographs of unweathered and weathered samples. "The percentage of evaporation (by weight) of each oil sample, with respect to fresh Norman Wells crude oil, has been estimated by comparing the gas chromatograms of each sample to standard gas chromatograms for various degrees of evaporation (by weight) of Norman Wells crude." For example gas chromatographs were performed on Norman Wells crude that had been weathered to 0%, 6%, 12%, 20.4%, 29%, 36.7%, and 43.2% (by weight).

The second manuscript has an appendix (Appendix II) written by Mackay, D., W.Y. Shiu, and M. Tsang that describes the process of sample preparation preceding the injection of said sample (0.5 µl of oil or oil in benzene) into a gas chromatograph (Hewlett-Packard model 700 or 5750 equipped with a dual flame ionization detector). The electronic integrator was a Hewlett-Packard model 3380A. The peaks of the chromatograms were marked with hydrocarbon numbers. The

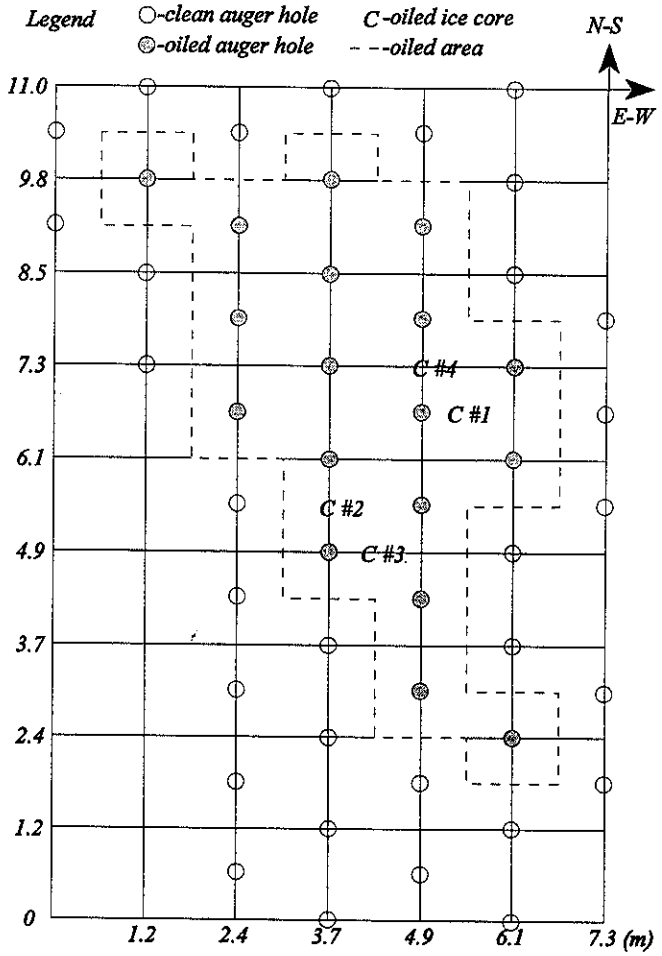

Figure 2. Coring program site 1, area of soiled ice is 26.3 m^2. The plot, including the axes values, was reproduced from the 1st manuscript.

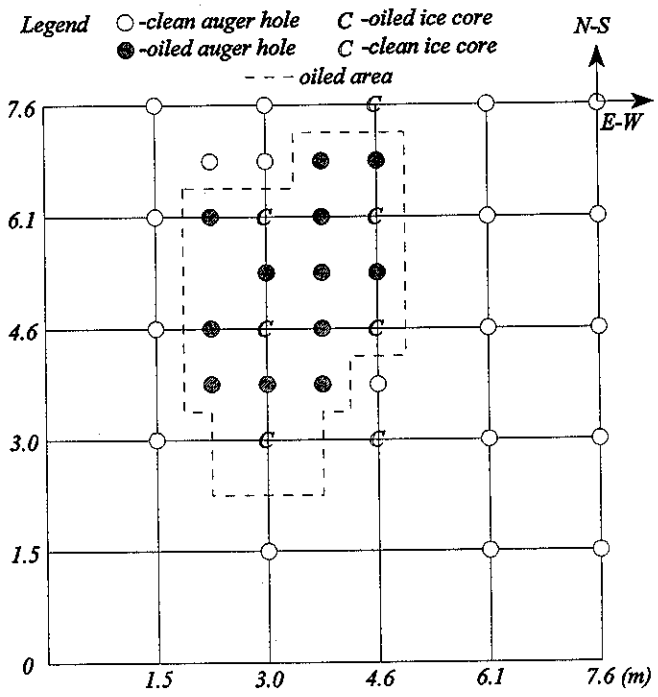

Figure 3. Coring program site 2. Area of oiled ice is 11.6 m^2. Plot, including axes values, reproduced from 1st manuscript.

authors also state in this section that the final error of this mass determination method is ±10%. Part of this error was the extraction process of the samples. The samples were extracted from the water using benzene, the benzene was removed and the recovered oil was added to the oil phase of the original sample. These authors do state that problems occur when the sample submitted was less than one gram, due to weathering of the sample (evaporative loss of lighter components to the air space in the sample container) during transport. Also some of the samples had become mousse during transport and were estimated to be 75% water and 25% oil.

The gas chromatograph "conditions were as follows:

- the columns were 3.05 m long, 0.32 cm O.D. stainless steel tubing packed with 10% SE30 Ultra Phase Chromosorb P, acid washed, DMCS treated and 60/80 mesh,
- the temperature of the injection port was 300 °C and the detector was at 320 °C,
- the oven temperature was held initially at 50 °C for one minute after sample injection, then programmed at 15 °/min until it reached 280 °C for 30 minutes."

Results

The sites were overflown three times in 1978, June 13 no oil visible on surface, July 1 no oil visible at sites 1 and 2, however oil was visible at site three due to a crack penetrating the ice and oil was visible at adjacent melt ponds. The sites were overflown again on August 20th, and oil was on the surface at sites 1 and 2 but had not spread, while at site 3 considerable oil was present on the surface. In October (13) the sites were revisited and while no oil was visible on the surface, site 3 was cored with oil present in only the top 2-4 cm. Site 1 was cored within the vicinity and no oil was found. Site 2 was not cored.

The spill site was revisited March 1979 and no oil was visible on the surface. Site 3 was cored and no oil found. No oil was found in the vicinity of site 1 either and site 2 was not drilled.

"In September, 1979 the sites were revisited. The location of each test site was determined from an air photo taken on August 20th, 1978, showing oil on the surface. This was confirmed by drill holes, suggesting the test site location measured at the time of discharge were incorrect."

The oil spill sites were next overflown in August 1982, and all sites were covered by refrozen melt pools. All sites were drilled and no trace of oil was found.

The authors, of the third manuscript, state that initially there was 100% oil trapped, after two years 10% remained and after five years 0% remained giving them three data points. The authors, of the third manuscript, presented an equation, stated in the theory section, and derived a set of values for the parameters that matched the three data points. The authors, of the third manuscript, determined that for the lower bound case $b = 1.00$, and $c = 1.2$, which results in $A = 100e^{-t^{1.2}}$ while for the upper bound case $b = 3.07$, and $c = 0.6$, giving $A = 100e^{-3.07t^{0.6}}$.

The authors, of the third manuscript, have stated that since no data was taken during the first season no accuracy was assigned to the values for upper and lower bounds. The lower bound was calculated from 1% oil remaining after 2 years, while the 0.1% was expected to be remaining after 4 years. No explanation is given for the upper bound parameters that were chosen.

The following tables are from the first manuscript and are data for the September, 1979 site visit.

Table 1. Oil in Ice Volume -- Site No. 1.

Core No.	Sample No.	Sample Depth (m)	Total Core Length (m)	Oiled Core Length (m)	Mass of Oil in Sample (g)	Sample Volume of Oil (cc)	Volume of Oil in Core (cc)	Average % Oil in Core by Volume
1	-	-	1.95	-	-	-	0	0
2	-	-	1.9	-	-	-	0	0
3	25	1.0-1.1	1.9	0.1	0.46	0.40	0.40	0.0046
4	26-1	0-0.1	2.0	1.1	0.13	0.11	2.28	0.025
	26-2	0.5-0.6			0.12	0.11		
	26-3	1.0-1.1			0.38	0.33		
	27	1.1-1.2			0.32	0.28		

Core No.	Sample No.	Sample Depth (m)	Total Core Length (m)	Oiled Core Length (m)	Mass of Oil in Sample (g)	Sample Volume of Oil (cc)	Volume of Oil in Core (cc)	Average % Oil in Core by Volume
	26-4	1.5-1.6			0	0		
	26-5	1.9-2.0			0	0		
								mean 0.0074

Tables 1 and 3 list the various conditions of the oil found in the ice cores taken from site 1 and the coring program is displayed in reproduced Figure 2. It is expected that some of the oil present in the ice core is from oil that was refrozen into the ice after the summer melt season allowed the oil to move up through the brine channels. Each of the heavily oiled cores had 1-2 cm of clean ice on top of them which was expected to be from formation of new ice, on top of the oil pool, during the fall season.

Table 2. Oil Densities

Sample	Type and Location of Sample	Temp (C)	Density (g/cc)
6	Core No. 5 -- Site No. 2 at 0.6 m depth	25	0.86
6	Core No. 5 -- Site No. 2 at 0.6 m depth	5	0.88
21	surface sample of "mousse" in sea ice at Site No. 3	25	0.88
21	surface sample of "mousse" in sea ice at Site No. 3	5	0.90

The oil densities, as listed in Table 2, are only for two sites (2, and 3) and are of the same samples at different temperatures.

Table 3. Overall Volume of Oil in Ice.

Site No.	Area of Contamination (m^2)	Mean Ice Thickness (m)	Total Volume of Oiled Ice (m^3)	Volume of Oil in Ice (m^3)	% of Volume Oil Spilled in Ice
1	26.3	1.95	51.3	0.0038	≈ 1
2	11.6	2.24	26.0	0.065	10
3	-	-	-	-	-

Table 3 is a listing of the volumes of oil left at the various sites. There is no exact description of how the volume of oil in ice (m^3) is determined from ice core measurements.

Table 4. Oil in Ice Volume -- Site No. 2.

Core No.	Sample No.	Sample Depth (m)	Total Core Length (m)	Oiled Core Length (m)	Mass of Oil in Sample (g)	Sample Volume of Oil (cc)	Volume of Oil in Core (cc)	Average % Oil in Core by Volume
2	3	1.0-1.1	2.4	0.15	0.78	0.69	1.04	0.0095
3	4	0-0.1	1.8	0.4	2.67	2.35	9.4	0.11
5	6	0.6-0.7	1.8	0.2	4.23	3.72	7.4	0.09
6	8	0.5-0.6	2.5	1.8	6.96	6.12	68.8	0.60
	9	1.0-1.1			4.71	4.14		
	10	1.5-1.6			5.6	4.93		
	11	2.0-2.1			0.11	0.10		
7	12	0.5-0.6	2.4	1.9	0.25	0.22	67.0	0.61
	13	1.0-1.1			2.43	2.14		
	14	1.5-1.6			12.45	10.96		
	15	2.0-2.1			0.90	0.79		
1-11	28-1	0-0.1	2.55	1.7	0.0086	0.0076	8.4	0.072
	28-2	0.5-0.6			0.49	0.43		
	28-3	1.0-1.1			0.59	0.52		
	28-4	1.5-1.6			0.015	0.013		
	28-5	2.0-2.1			0.0075	0.0066		
	28-6	2.5-2.6			0.0043	0.0038		
	29	0.7-0.8			2.24	1.97		
								mean 0.25

Table 4 lists the various conditions of the oil found in the ice cores taken from site 2 and the coring program is displayed in reproduced Figure 3. Site 2 had the most varying results for the two sites that had cores with appreciable amount of oil in them and core No. 6 had a heavy amount of oil throughout its length except for the top which is expected to be new ice growth. It is also expected that core No. 6 of site 2 was from the deepest pool of oil from the initial discharge.

Table 5. Oil in Ice Volume -- Site No. 3.

Core No.	Sample No.	Sample Depth (m)	Total Core Length (m)	Oiled Core Length (m)	Mass of Oil in Sample (g)	Sample Volume of Oil (cc)	Volume of Oil in Core (cc)	Average % Oil in Core by Volume
1	20	0.95-1.05	1.1	0.1	1.63	1.43	1.43	0.029
2	23	1.4-1.5	2.4	0.1	0.061	0.054	0.054	0.00049
								mean: 0.0147

Table 5 list the conditions of the oil found in ice cores taken from site 3. This is really a case of a null result. Very little if any oil can be said to have been found at site 3 and it was believed that this was because of the crack in the ice during the first summer and the large oil pool seen on the surface at that time.

Table 6. Degree of weathering of the oil.

Sample No.	Discharge No.	Type and Location of Sample	Estimated Mass % Evaporated
1	2	Oiled snow	>43
5	2	Surface "mousse" mixed with fresh snow	43
8	2	Core No. 6 at 0.5 m depth	20
9	2	Core No. 6 at 1.0 m depth	12-15
10	2	Core No. 6 at 1.5 m depth	20
17	-	Surface sample at Position 2 (110' from radar reflector, 140' parcol)	43
18	3	Surface sample from open hole	37
22	3	Surface sample of "mousse" from open hole	37
25	1	Core No. 3 at 1.0-1.1 m depth[2]	43
26-2	1	Core No. 4 at 0-0.1 m depth[1]	43
26-3	1	Core No. 4 at 1.0-1.1 m depth[2]	40
28-2	2	Core No. 1 at 0-0.1 m depth[1]	43
28-3	2	Core No. 1 at 1.0-1.1 m depth[2]	40

Notes 1 These samples were considered as surface samples since they represent new growth on the melt pools that has encapsulated oil that surfaced during the 1979b summer.

2 These samples contained less than 1 gram of oil and have not been included in the analysis.

Table 6 lists the cores taken and the percent of oil evaporated which had been determined by a gas chromatograph technique performed at Prof. Mackay's laboratory at the University of Toronto.

Table 7. Overall estimated mass percent evaporated.

Sample Type	Min.	Max.	Mean
Surface	37	>43	>42
Oil in Ice	12	20	17

Table 7 lists the evaporative loss estimates (no errors mentioned) of surface samples and ice embedded samples.

The authors state that the most important information to come from the report is that ""*At the end of two melt seasons, a maximum of 10% of the original volume of spilled oil is still in the ice.*""

The authors also noted that site 2 seemed to be the heaviest oiled site and did not have a reason for this. It should be noted that site 3 had the crack in the ice and site 1 was cored and drilled several times before the ARCTEC crew showed up to do their analysis in September, 1979. Site 2 was the only site left untampered with for two melt seasons.

Table 2 (from the fourth manuscript) Oil-in-Ice Concentration

Time	Area of Oiled Ice (m^2)	Mean Ice Thickness (m)	Volume of Oil in Ice (m^3)	Mean Oil-in-Ice Concentration (%)
Spill Site 1				
June 1978 (*i.e.* Discharge)	6.1[a]	2.7[b]	0.,61	3.7
Sept. 1979	26.3	1.0	0.0038	0.007
Sept. 1982	0[c]	.0[c]	0[c]	0c
Spill Site 2				
June, 1978 (*i.e.* Discharge)	3.1[a]	2.7[b]	0.61	7.3
Sept.,1979	11,6	2.2	0.065	0.25
Sept.,1982	0[c]	0[c]	0[c]	0c

[a] Area of oil pool underneath ice immediately after discharge.
[b] Mean ice thickness at time of discharge.
[c] Below measurable limits.

Table 2 from manuscript four is a list of oil-in-ice concentration data and otherwise is a complete restatement of the previous manuscripts with no new interpretations or analysis.

BOSS Critique

The volume of oil used in this test was small and no mention is made of how the drilling of

holes into the ice nor the coring of the ice would or could effect the distribution of the oil under the ice, after each investigation was made. However, the authors have stated that varying ice conditions could cause some problems in using the data from this work to predict the behaviour of oil spilled under multi-year ice and that the three sites did give a variety of results that could be considered a range of values that might be representative of the conditions available to a large scale oil spill. The evidence presented in these reports indicates that the drilling of site 1 effected the results since only site 2 had oil present in the ice (10%) and site 3 had the crack in the ice which allowed a path to the surface for the spilled oil.

Given the steep decline, indicated by the equation presented by the authors, more than two data points per season would be needed for the first two years. In fact, for the first summer daily data points should be gathered. The problem is to find a nonintrusive manner in which to determine the depth the oil is in the ice. There are current methods for determining the presence of oil under ice but they may not determine whether the oil is at some depth within the ice.

The authors, of the third manuscript, state that some confusion existed about the site locations during the second site visit, March, 1979.

In Appendix I, of manuscript two, there are illustrations of each ice core and the various sections are termed clean ice, oil globule, lightly oiled, heavily oiled, oil brine channels, new ice or water (unfrozen melt pool). The reports seem to indicate that this was a visual determination not a spectroscopic determination. These terms are subjective and there is no discussion of how clean the "clean" ice cores were. There is no discussion of any analysis being done on the "clean" cores to determine if there was any trace amounts of oil present and therefore there is no definition (in parts per million of oil contamination) for which the ice core goes from being "clean" to lightly oiled or any other term used above.

Table 2, of manuscript four, there is no discussion of what information was used to determine the 3.7% mean oil-in-ice concentration. No previous information is presented for this number.

The accuracy of using gas chromatographs in determining the weathering of crude oil (by weight) is not detailed. Since the standard is really ±10% there is no reason to state that the sample was weathered 43.2% but instead the weathering of the sample should be stated as 43±10%. The standard chromatograms presented in Appendix II, manuscript two, do not seem to match the site samples as decided by the authors. The reviewer believes that several samples could be less or more than those chosen by the authors.

A final note, Appendix III of manuscript two (EPS 4-EC-82-4) is not a listing of samples from site visits on October, 1978 and March, 1979 (as stated in the title page of Appendix II) since all of the samples are numbered the same as the samples listed in the text of the report for the site visit on September, 1979. Also note that Table 1 of Appendix III listed site 2 being cored and the text specifically states that site 2 was never cored until the September, 1979 visit.

Review of a final report by Buist, I., S. Joyce, and D.F. Dickins, entitled *Oil Spills in Leads: Tank Tests and Modelling*, report EE-95, for Environment Canada, 1987.

This review also covers the manuscript by Buist, I.A., S.P. Joyce, and S.L. Ross entitled "Modelling Oil Spills in Leads: Wind/Wave Tank Testing and Preliminary Results", in the *Proceedings of the Tenth Arctic and Marine Oilspill Program Technical Seminar,* June 1987, Edmonton, Alberta.

Technical Summary

"A computer model has been developed that predicts the amount of an oil spill in a pack ice lead that remains exposed to the atmosphere, and is thus available for countermeasures, as a function of time. The results of indoor wind/wave tank experiments and outdoor test tank experiments show that the fraction of a slick that is incorporated into new, growing ice in a lead is generally very small; most of the oil remains on the surface of the new ice.

The major factors that increase the fraction of oil incorporated into growing ice in a lead are:

* increasing oil density
* decreasing oil viscosity
* the presence of waves
* the presence of grease ice at the time of the spill

The factors that result in encapsulation of the oil, or that render it unavailable for countermeasures are:

* lead closure resulting in ridge formation
* snowfall resulting in water content in the oil greater than about 75%.

It must be emphasized that the model is intended as a preliminary formulation."

Objective

The objective of this work was to develop a computer model to predict the amount of oil left in the environment (and thus available to countermeasures) as a function of parameters such as time, initial oil properties, and environmental conditions after a significant oil spill in ice leads. The authors believed, after a review of previous work, that more experimental data was needed to improve on past models. In particular they wanted information "on 1) the spreading rate and wind herding of oil on frazil and grease ice over a range of development stages; 2) weathering rates of oil in freezing situations; and 3) data on the fraction of oil remaining as a surface slick as a function of freezing."

Theory

The theory section is mainly to due with the formation of the equations used in the computer model and will follow the sections used in report EE-95.

4.2 PROCESS EQUATIONS

4.2.1 Ice Growth

4.2.1.1 Open Water

"The ice growth routine for oiled areas in a lead was developed using equations for grease formation reported by Dickins *et al.* (1986).

$$P = 1.2 + 0.0312\,U(T_w - T_a) \quad (1)$$

and

$$P = 3.0 + 0.0204\,U(T_w - T_a) \quad (2)$$

where
P = production rate (kg/m^2/h)
U = wind speed (m/s)
T_w = water temperature (°C)
T_a = air temperature (°C)
$U(T_w - T_a)$ = wind chill factor (°C m/s)

Equation (1) is used for mild conditions (wind chill less than 200 °C m/s), and equation (2) for severe conditions (wind chill greater than 200 °C m/s). The final coverage thickness is estimated by H (m) = $0.06\,U$ where U is the wind speed in m/s. The rate of ice cover can be calculated using the density of the grease ice (ρ_i) and the final thickness of the cover (H) as:

$$dA_I = \frac{P}{\rho_i H} \quad (3)$$

where A_I is the ice coverage in m^2 of ice per m^2 of open water remaining per hour. If the width of the lead (W) is known, the differential linear grease ice cover for one 100 second program pass is calculated by:

$$dL = \frac{PA_w}{\rho_i HW}\left(\frac{100}{3600}\right) \quad (4)$$

in linear metres of grease ice, where A_W is open water area. This length is combined with that generated beneath the slick and subtracted from the length of open water for each iteration.

4.2.1.2 Beneath Oil

On of the problems that this study addressed was that of predicting the initial freezing rate of water beneath an oil slick spilled in a lead under calm conditions. Once a solid sheet of ice has formed beneath the oil the countermeasures approach for exposed oil becomes one of oil on ice as opposed to oil on water.

The predictive equation developed in this section is concerned primarily with calculating the time required to form a "solid" ice cover in the presence of oil and the

absence of snow (see section 4.2.6 for the treatment of snow in the model). The approach taken is to calculate the amount of ice formed beneath the slick based on heat transfer considerations and convert this to a length of new ice thickness H (see Section 4.2.1.1 above) that is wind herded against the downwind ice edge. Although the equations are only truly valid for calm, low turbulence conditions the presence of an oil film is assumed to dampout any waves that would normally be present under higher wind conditions.

The equation used is an adaptation of the formulation of Ashton (1986) which treats snowcover and ice as resistances in series. Oil is introduced in the classic heat transfer equation as an additional resistance to yield:

$$\frac{\Delta h}{\Delta t} = (T_m - T_m)/(\rho_i \lambda)((h_i/k_i) + (h_o/k_o) + (1/H_a)) \qquad (5)$$

where
- h_i = ice thickness (m)
- h_o = oil thickness (m)
- t = time (s)
- T_a = air temperature (°K)
- T_m = water temperature (°K)
- $k's$ = thermal conductivities of ice (i) and oil (o) (W/m °C)
- H_a = surface heat transfer coefficient (W/m^2 °C)
- λ = latent heat of fusion of water (J/kg)
- ρ_i = density of ice (kg/m^3)

Once the ice has formed an additional resistance due to the presence of snow on ice could be added; this was not considered to be warranted for this study since snowfall obscures any surface oil which then becomes unavailable for countermeasures (see Section 4.2.6 below).

The only term in equation 5 that cannot be readily obtained from the literature is H_a. As a first approximation, its value was determined using the results of the outdoor tank tests to provide estimates of the initial ice growth rate $\Delta h/\Delta t$. Table 2 summarizes the data used in solving for H_a in equation 5. Table 3 shows the results; the very small change in H_a with oil thickness and the seeming dependence only on the presence of oil indicate that the correct form of equation was chosen. The values shown in Table 3 were used in the computation of ice growth beneath oil in the model."

Table 2 Initial Ice Growth Rates and Ice Property Data

SURFACE CONDITION	TEMPERATURE DIFFERENCE (°C)	ICE GROWTH RATE (m/s x 10^7)
Clean ice	18	6.36
Oiled ice 1 mm oil	18	4.10
2 mm oil	18	3.64

Table 2 Initial Ice Growth Rates and Ice Property Data		
SURFACE CONDITION	TEMPERATURE DIFFERENCE (°C)	ICE GROWTH RATE (m/s x 10^7)
5 mm oil	18	3.18
10 mm oil	18	<2.55

Oil/Ice Properties

Thermal conductivity:	oil	0.149 W/m °C
	ice	2.200 W/m °C
Ice density:	primary	916.6 kg/m ^{3}
	snow ice	803-900 kg/m ^{3}
Latent heat of fusion:	pure water	333.4 x 10^3 J/kg
	sea water to sea ice	200 x 10^3 J/kg

Table 3 Calculated Heat Transfer Coefficients

Surface Condition	Experimental Heat Transfer Coefficient (W/m^2 °C)
Clean Ice	10.8
1 mm oil	7.3
2 mm oil	6.7
5 mm oil	6.6
10 mm oil	6.1
Clean snow slush	10.1
oiled snow slush	6.4

4.2.2 Slick Advection

The oil slick on the open water is estimated to drift at 3% of the wind speed (only wind parallel to the length of the lead is included) across the water surface. This continues until the leading edge of the thick slick reaches the downward ice edge.

4.2.3 Oil Spreading

During the time that the oil is in open water, and the calculated area of thick oil does not exceed the area of open water, the thick/thin spreading routine is utilized. If the thin slick area exceeds the open water area it is reset to the difference between the lead area (length x width) and the thick slick area and thin spreading ceases. If the thick click area equals the open water area the thin slick area is set to 1 m^2 and

the thick slick spreading ceases. Otherwise the slick is allowed to spread until the leading edge of the thick slick reaches the downward grease ice edge. If the slick diameter is less than the lead width at this point the slick continues to spread, but only laterally until it fills the width of the lead. When the thick slick fills the width of the lead and is touching the downwind ice edge all spreading stops and wind herding commences.

4.2.4 Wind Herding

Eventually the leading edge of the slick will encounter the downwind edge of the lead where drift and spreading will stop., Wind herding will determine the final slick area and thickness at this point. Energetex Engineering (1981) performed a series of experiments on wind herding of fresh and aged Prudhoe Bay crude oil. They found that the wind herded oil thickness is primarily a function of the initial oil thickness and the wind speed. The empirical equation used in this model is:

$$T_H = 1.01\,T_I + 0.72\,U \qquad (5)$$

where
T_H = herded thickness (mm)
h_o = initial thickness (mm)
U = wind speed (m/s)

This equation shows a good correlation for initial thickness between 1 and 6 mm and wind speeds between 2.78 and 8.3 m/s.

A final thick slick area is calculated based on the wind herded thickness; no further spreading takes place.

4.2.5 Fraction of Oil Frozen into Ice

The wind/wave tank tests showed that a small percentage of the oil slick may become trapped in the developing grease ice. During each program iteration a volume of oil becomes trapped in the differential area of new ice growing beneath the slick. The fraction encapsulated is based on the oil properties, and is increased by a density factor:

$$K_1 + K_2\rho_o \qquad (6)$$

and decreased by a viscosity factor: $K_3 + K_4\,\mu_o$ (7)

The fraction (F) of the oil in that is underlain by new ice growth for that iteration that becomes encapsulated is then given by:

$$F = (K_1 + K_2\rho_o) - (K_3 + K_4\mu_o) \qquad (8)$$

or

$$F = (K + K_2\rho_o) - K_4\mu_o) \qquad (9)$$

where
ρ_o = density of oil,
μ_o = viscosity

Substituting from the experimental results and solving for the constants yields values of:

$K = -0.19966$
$K_2 = 0.31053$
$K_4 = 0.0000709$

The differential volume encapsulated is then given by:

$$dV = (-0.19966 + 0.31053\rho_o - 0.0000709\mu_o)\, dA_I . T_H \quad (10)$$

where dA_I is the differential ice area for that program pass and T_H is the wind herded slick thickness.

Effect of Waves. In order to include the effect of waves on oil incorporation it was first necessary to calculate the significant wave height that would exist in a lead. The following equation is used to calculate fetch-limited wave conditions (Department of the Army 1984):

$$H = 5.112 \times 10^{-7} U F^{1/2} \quad (11)$$

where H = significant wave height (m)
U = wind speed (m/s)
F = fetch (m)

The effect of wave properties on increasing the fraction of oil incorporated in the grease ice was not fully investigated in the experimental portion of this study, thus a very simple algorithm was used to estimate their effect. If the calculated wave height in the unfrozen length of the lead exceeds a certain value (that is input by the operator) the fraction of oil incorporated is arbitrarily increased by 0.2, consistent with the results of the wind/wave tank tests.

4.2.6 Snowfall

Based on the results of the outdoor test tank experiments the effect of snowfall is twofold: initially snow is absorbed by the oil until such time as the water content of the oil (or emulsion) reaches a maximum (presumed to be in the range of 75% for the model), after this the snow covers the oil rendering it unavailable for countermeasures.

The water content increase of the oil due to snowfall is calculated by dividing a snowfall rate per iteration by ten (to account for the lower density of snow) and adding the equivalent fraction of water (based on the existing slick thickness) to the oil.

4.2.7 Lead Closure

The model includes the ability to close the lead at a specified rate. This has the effect of decreasing the width of the lead thus reducing the slick width and increasing its thickness if its diameter equals that of the lead. If the thick slick fills the lead, closure thickens the oil. Once the lead edges touch, all of the oil is unavailable for countermeasures being either under the ice edges or incorporated into the resulting ridge.

4.2.8 Natural Dispersion

The equation used to calculate losses to natural dispersion on the open sea was modified to account for the fact that the wind over a lead will generate smaller, less energetic waves (see Section 4.2.5 above).

"

Method

Indoor experimental work was carried out at the wind/wave tank at the R.L. Ross Laboratory.

Table 1 Test Oil Properties

Oil Type	Test Temp.	Density (g/cm^3)	Dynamic Viscosity (mPas)	Kinematic Viscosity (mm^2/s)
Bunker C[1]	1 °C	1.025	2,310,000	2,253,658
Diesel[2]	0 °C	0.838	3.9	4.65
MSW[2]	0 °C	0.847	47.3	55.9
Bunker C/19% Diesel[1]	7.5 °C	0.981	1480	1509
Bunker C/55% Diesel[3]	2 °C	0.917	71.8	78.3

Source
1. S.L. Ross 1987;
2. Bobra and Chung 1986;
3. Measured.

" The tank is 11 m long by 1.2 m wide by 1.2 m deep. A large fan and ductwork allow the passage of outside air over the water surface at varying wind speeds. A wave paddle is used to mechanically generate waves of varying amplitude and period. The tank was fitted with a 40 cm wooden barrier 7.2 m from the upwind edge. This section of the tank simulates a small 1.2 m wide section of a pack ice lead at the downwind edge.

Ice formation in the freshwater tank was found to be very similar to ice formation in actual pack ice leads as described by Dickins et al. (1986). Ice crystals formed in the open water area and drifted down the length of the tank to pile up against the fixed barrier to formed grease ice. Without mechanically generated waves the grease ice eventually forms a dense dead zone where it behaved as a solid. Allowed to continue, the entire tank became covered with slush ice which formed a hard impermeable layer on the surface."

The authors used four variables to set up the tests, wind speed, oil type and volume, wave height, and initial ice maturity. The properties of the three types of oil used, are listed in Table 1. The ice conditions were varied from no ice, to grease ice 15 cm thick, and finally semi-solid dense grease ice, no thickness given. The process was done without waves, and with waves with a wind speed of either 3.5 m/s or 7 m/s measured with a hot-filament anemometer at 30 cm above ice surface.

Test Matrix

		S_1			S_2		
		I_1	I_2	I_3	I_1	I_2	I_3
W_1	O_1		Run 9		Run 1, Run 2	Run 3	Run 4
	O_2					Run 13	
	O_3					Run 8	Run 12
W_2	O_1				Run 7	Run 6	Run 5
	O_2				Run 14		
	O_3					Run 10	Run 11

Initial Ice Maturity, I_1 - no ice present, I_2 - covering of grease ice about 15 cm thick, I_3 - slush grease ice to semi-solid but malleable dense grease ice.
Oil Type, O_1 - Mixed Sweet Western, O_2 - Bunker C/19% Diesel, O_3 - Bunker C/55% Diesel.
Wind Speed, S_1 - 3.5 m/s, S_2 - 7 m/s.
Wave Conditions, W_1 - no waves, W_2 - mechanically generated waves (different for each run).

Outdoor experimental work was done at the manoeuvring basin of the National Research Council, Ottawa and the basin is 120 m long by 60 m wide and has 3 m of fresh water in it. During the experiments the ice was 29 cm thick and there was 50 cm of snow on the ice which was removed in the areas where ice was removed. There were 2 leads 10 m by 1 m cut into the ice perpendicular to each other, which were used to determine the behaviour of oil in freezing conditions under two different wind conditions. The four 1 m by 1 m test plots were used to determine the effect that different slick thicknesses (1 mm, 2 mm, 5 mm, and 10 mm) would have on fate and behaviour of oil in freezing conditions. The authors state that the thickness was initial set by pouring 1, 2, 5, and 10 litres of oil onto the surface of the 1 m^2 open surfaces of the test squares. Pre-weighed absorbent pads were used to gather oil samples, reweighed and corrected for density and then the thickness was determined. Density was measured using a Parr densitometer which was used to determine evaporative loss. This involved using field and laboratory data (S.L. Ross and D.F. Dickins 1987).

Wind speed, wind direction and air temperature were monitored by a computerized weather station 10 m above the ice surface. Surface temperature (water, oil and air 1 cm above surface) were measured using a thermistor and a hand held anemometer was used to measure surface wind.

Results

The authors state that fifteen experimental runs were done in the wind/wave tank of S.L. Ross. All runs used 1 litre of oil which are listed in Table 1 except for run 15 which used Hibernia B-27.

		S_1			S_2		
		I_1	I_2	I_3	I_1	I_2	I_3
W_1	O_1		0(+3)		-7(2)	-2(0)	-7(-3)
	O_2					-2(+2)	
	O_3					-8(-3)	-2(1.5)
W_2	O_1				-16(-9)	-6(-2)	-5(-1.5)
	O_2				-1(1)		
	O_3					-4.5(-1)	-3.5(0)

Final Surface Area of slick (cm^2)

		S_1			S_2		
		I_1	I_2	I_3	I_1	I_2	I_3
W_1	O_1		8592		3120	3960	3456
	O_2					7200	
	O_3					960	255
W_2	O_1				3600	5100	14400
	O_2				5400		
	O_3					1700	4800

Percentage (%)of original volume frozen into ice

		S_1			S_2		
		I_1	I_2	I_3	I_1	I_2	I_3
W_1	O_1		0		0	6	1
	O_2					8	
	O_3					0	0
W_2	O_1				20	10	2
	O_2				30		
	O_3					5	1

The effect of wind speed, for the indoor wind/wave tank experiments, indicated that with high wind speed the oil was driven across the open water or dense grease ice until it comes in contact with compact ice or another barrier to movement. The authors state that the 3.5 m/s experiment resulted in a large slick with little or no oil incorporated into the ice and that there was difficulty in

getting the water to freeze with the low wind speed setting (which in the reviewer's opinion was most likely caused by the high air inlet temperatures).

The authors believe that since the density determines the buoyancy of the oil it also determines the amount of oil that will be encapsulated into the new forming ice. The experiments with oil O_1 and O_2 indicate this is likely since these oils have similar viscosity but in the case of the denser oil more of the oil was encapsulated into the ice. The viscosity determines wether the oil will be able to form droplets or not and thus wave action would break up the oil and allow it to be encapsulated into the ice as it forms. This happens with lower viscosity oils. The high viscosity oils will not be encapsulated not even with wave action since it will remain as large slick and not break into small droplets.

The authors state that the increase of wave action increased the amount of oil encapsulated into the forming ice. The initial maturity of the ice also effect the oil present in the ice by effecting the dispersion of the oil into the water and the formation of droplets of oil in the water. With no wave action present significant oil was found in the ice only when initially there was a large amount of grease ice present.

Table A1 (from Appendix 2 of EE-95) is a listing of the data collected in the manoeuvring basin of the National Research Centre. The experiments at the outdoor basin were done with wind conditions from calm to 10 m/s and temperatures from -10 °C at the time of the spills to -2 °C ten hours after the spills to -3 °C after 3 days.

Table A1. Ice Thickness Measurements and Associated Surface Conditions

Date	Time	Site	Ice Thick-ness (mm)	Water Depth (mm)	Slush Depth (mm)	Snow Depth (mm)	Temp. Air (°C)	Temp. Oil (°C)
27	1213	L1,C					-5.9	-1.8
	1244	L1,C	1				-5.0	1.6
	1330	L1,C					-4.8	2.0
	1400	L1,C	3					
	1630	L1,C	8					
28	1000	L1,C	45				-8.0	-3.0
	1017	L1,O	30					
	1020	TA1	30					-1.0
	1021	TA2	30					-1.0
	1022	TA3	30					0.0
	1023	TA4	25					1.0
	1045						-6.5	
	1500	L1,C	50				-5.0	

Table A1. Ice Thickness Measurements and Associated Surface Conditions

Date	Time	Site	Ice Thick-ness (mm)	Water Depth (mm)	Slush Depth (mm)	Snow Depth (mm)	Temp. Air (°C)	Temp. Oil (°C)
	1501	L1,O	18	3				
	1530	TA1	23	3				0.5
	1531	TA2	20	5				0.0
	1532	TA3	20	4				0.0
	1533	TA4	20	3				0.5
29	1015	L1,O	33	4			-6.0	-3.2
	1130	TA1	31	4				-3.4
	1131	TA2	30	5				-2.9
	1400	TA3	29	3			-2.0	1.0
	1401	TA4	25	4				1.5
30	1030	L1,C	77					
		L1,O	46					
		TA1	39					
		TA2	39	2				
		TA3	33	3				
		TA4	32	4				
	1120	L2			15			
01	1000	L1,C	90		30	60		
	1015	L1,O	40		25	45		
	1030	L2,O			35			
		L2,C			55			
		TA1	45	20	10	95		
		TA2	40	20	10	70		
		TA3	35	20	30	80		
		TA4	28	20	25	90		

L1, L2 = Lead 1&2; O = oiled; C = clean; TA = Test squares (1 m^2)

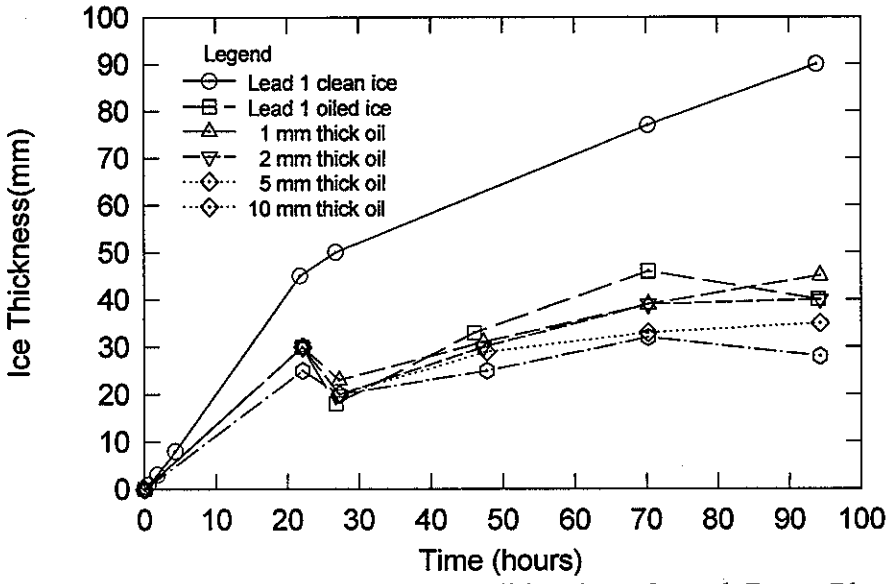

Reproduced Figure 15 (EE-95): Consolidated Ice Growth Data. Plot of ice thickness versus time (in hours) from release of oil on to open water. Information is presented in Table A1.

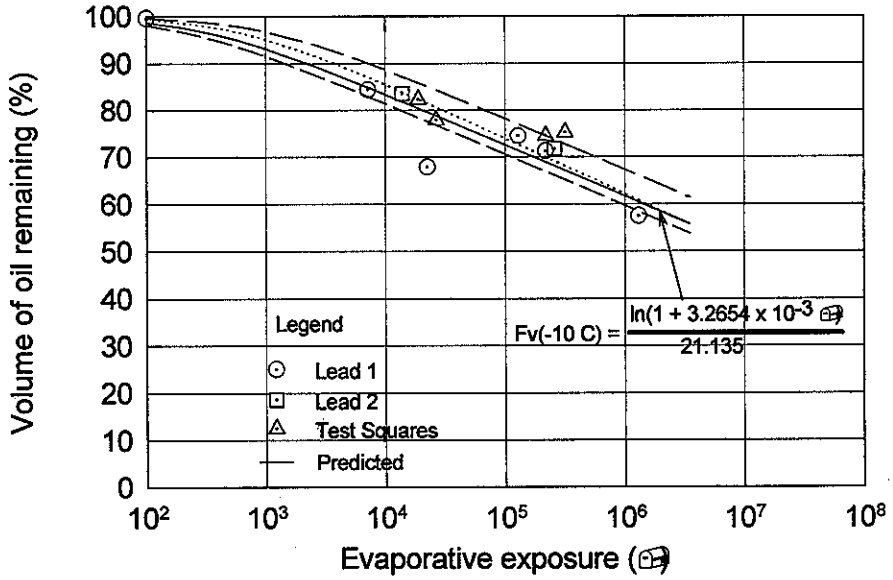

Reproduced Figure 19 of report EE-95, entitled Evaporative Loss. All nonsolid lines were added by the reviewer. The top dashed line used $\ln(1 + 1.0 \times 10^{-3}\ \theta)/21.135$, the dotted line used $\ln(1 + 1.6 \times 10^{-3}\ \theta)/19.5$, and the bottom dashed line used $\ln(1 + 5.0 \times 10^{-3}\ \theta)/21.135$, but the authors state that $\ln(1 + 3.2654 \times 10^{-3}\ \theta)/21.135$ is the correct choice (solid line in graph above). The dotted line data was the closest fit to the line drawn on the original Figure 19 of report EE-95. This is discussed further in the BOSS Critique section.

The information presented in Table A1 is plotted in reproduced Figure 15 above. In the original Figure 15 the authors had drawn in oscillating curves instead of the straight lines presented here (see BOSS Critique for reasons). When data points were collected several times in a single day, the ice thickness showed a decreased which is expected and is due to absorption of solar energy and subsequent heating of the oil which then heats and melts the underlying ice.

Evaporative loss is plotted in reproduced Figure 19 (EE-95) and was determined using a modified ASTM distillation procedure and equation given by Stiver and Mackay (1983). The authors note that snowfall had little affect on evaporative loss.

The authors do present the result of a single run of the computer program which is not reproduced here (see BOSS Critique, below, for reasons).

Boss Critique

The authors discussion of experimental runs in the wind/wave tank are confusing. The test matrix (see above) outlines runs 8, 10, 11, and 12 used oil type O_3 which the reader is left to assume is in Table 1 as the Bunker C/19% Diesel oil mixture. In report EE-95 the section in which the runs of the wind/wave tank are discussed, run 12 is stated to be a mixture of 86% Bunker C and 14% Diesel with a density of 0.995 g/cm^3 and a viscosity of 2570 mPas at 10 °C which is markedly different from the assumed O_3 from Table 1 which had a density of 0.981 g/cm^3 and a dynamic viscosity of 1470 mPas at 7.5 °C. There is no discussion about the specific rate of movement of the oil in the ice and the movement is only discussed in qualitative terms not quantitative terms. The objectives stated that spreading rates were needed and weathering rates were needed and rates are quantitative (m/s or w%/hour) not qualitative (fast, quickly).

In the discussion of the wind/wave experimental runs 1-15 no discussion or explanation is made of how the % of oil encapsulated in the ice is actually calculated. Nor is there any discussion of the magnitude of error for the measurements of oil encapsulated in ice or the slick area or the average temperature of the inlet and surface air.

In section 4.2.1.1 there is an obvious mistake in equation (5) where (T_m - T_m) and one of T_ms should be a T_a but which is not clear. However the assumption by the authors that since there is a very small change in H_a with a change in oil thickness the correct form of the equation has been chosen does not follow. The authors state in section 4.2.2 that the oil slick on open water drifts at 3% of the wind speed but there is no reference to a publication that proved this was a correct assumption.

In the presentation of Section 4.2.5 the Effect of Waves paragraph does not explain the use of 5.112×10^{-7} in equation (11). Although the authors do state the reference for this, there is still a need to give the reader a few statements concerning the reasons for the coefficients used in these equations. Earlier in this same section there is a statement that experimental values (which ones are not stated and should be) are used to determine the values for K, K_2, and K_3. These constants are then used to determine a differential value of volume of encapsulated oil and no procedure is given for this derivation it just appears.

The effect of oil, on top of ice, on the ice growth is observed by the authors and the plots in reproduced Figure 15 would have been much clearer on this change had the thickness been measured four or five times a day instead of only once per day.

In Figure 19, the plot of a function $100*(1-F_v)$ is the correct value for what is plotted on the y axis and this is not mentioned in either manuscript. The use of numbers with several decimal

places, as in Figure 19, are shown to be incorrect. Secondly as has been shown by the reviewer, the choice of values to use to plot the line has a wide range and in fact 100*(1-ln(1+2.2 x 10^{-3} θ)/21.135) produces very similar data to the data that was used to produce the dotted line in reproduced Figure 19, above. There is a very large range of values that can be used to fit a line, based on 100%*(1-F_v) with F_v = ln(1 + number 1 x 10^{-3} θ)/number 2, to the scattered data that is presented in the manuscripts.

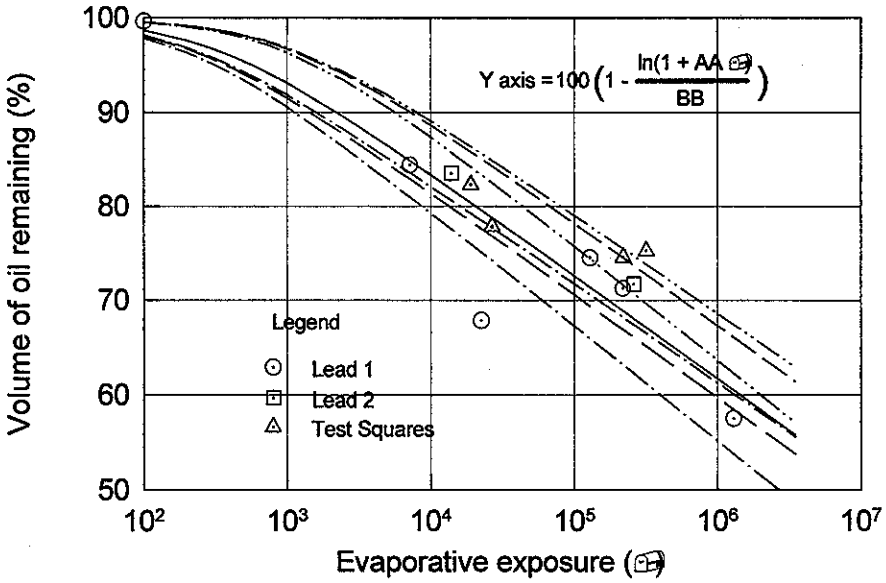

An expansion of reproduced Figure 19. Taking the vertical line at θ = 10^5, the top line is for AA = 1.0 x 10^{-3}, and BB = 22, while for the next line AA = 1.0 x 10^{-3}, and BB = 21.135, the next AA = 1.0 x 10^{-3}, and BB = 19, the next AA = 3.2654 x 10^{-3}, and BB = 21.135, the next AA = 5.0 x 10^{-3}, and BB = 22, the next AA = 5.0 x 10^{-3}, and BB = 21.135 and finally for the bottom line AA = 5.0 x 10^{-3}, and BB = 19.

The above figure was drawn to present the range of values that y can take on for the sets of conditions stated in the figure caption. The choice of AA and BB used in the equation (stated in the above figure) depends upon the error assigned to the data points (which are the same as the data points in the reproduced Figure 19). The authors do not explain their choice of AA value of 3.2654 x 10^{-3} and a BB value of 21.135 when as shown in the reproduced Figure 19, AA could be 1.6 x 10^{-3} with BB = 19.5, the dotted line. If the y value error was 10% (as in ±5%) then the top line and the bottom line are the limits of that error and any line that falls inside those two would be scientifically acceptable but not to three or four significant figures.

In report EE-95 a single run of the computer program is displayed in Figure 20 which is not reproduced here since there was no comparison made of the results from the computer program and an oil spill.

Review of a manuscript, by Chen, E.C., C.K. Overall, and C.R. Phillips entitled, "Spreading of Crude Oil on an Ice Surface", in the *Canadian Journal of Chemical Engineering*, Vol. 52, pp 71-74, 1974.

Technical Summary

"The gravity-viscous spreading of crude oil on artificially prepared ice surfaces was investigated. Five different types of crudes were studied with three surface roughness at -14 °C. Crude oil No. 1 was also studied at -8 and -3 °C. All spreading experiments were made with an oil volume of 45 and 20 ml. Regardless of temperature, surface roughness, oil type and oil volume, all data may be correlated by:

$$(R/V^{1/3}) = 0.24(t\rho g V^{1/3}/\mu)^{1/5} + C$$

where ρ, V, and μ are the density, volume and viscosity of the oil, respectively, R is the radius of the oil slick, t is time, *C* is a constant and *g* is the acceleration of gravity."

Objective

To quantify information on the spreading of oil on ice surfaces.

Theory

The authors state that a volume, V, of oil is release instantaneously on the ice and then the oil spreads outwardly with a radius, R, over time, t, and a thickness, *h*. These authors reiterate Fay's idea that oil spreading (even on ice) will go through three regimes, (1) gravity-inertia, (2) gravity-viscous, and (3) surface tension-viscous.

$$F_g = \rho g h \, A/V \tag{1}$$

and for a circular slick, $A = \pi R^2$. As noted in Figure 1, F_p is an outward (spreading) force caused by gravity and presented as:

$$F_p = kF_g = k\rho g A/V \tag{2}$$

where *k* is a proportional constant. Since $V = Ah$, assumed to be constant ,

$$F_p = k\rho g. \tag{3}$$

The authors state that the viscous force per unit volume, F_v, is

$$F_v = \tau A/V \tag{4}$$

where

$$\tau = \mu(du/dh) \tag{5}$$

and μ is viscosity of the oil and *u* is the velocity of spreading, (R/t), assuming linear profile in the vertical direction the derivative, *du/dh,* is replaced with *u/h* and the force is determined to be,

$$F_v = \frac{\pi^2 \mu R^5}{tV^2}. \tag{6}$$

The authors state that these two forces are at equilibrium, $F_p = F_v$. Therefore, setting equation (4)

equal to equation (6) and solving for the radius gives,

$$R = \left(\frac{k}{\pi^2}\right)^{1/5} (\rho g V^2)^{1/5} \left(\frac{t}{\mu}\right)^{1/5} \tag{7}$$

The authors rearrange this to give a unitless form,

$$\frac{R}{V^{1/3}} = \left(\frac{k}{\pi^2}\right)^{1/5} \left(\frac{t}{\mu}\right)^{1/5} (\rho g V^{1/3})^{1/5} \tag{8}$$

and plotting $(R/V^{1/3})$ *versus* $(t/\mu)^{1/5}(\rho g V^{1/3})^{1/5}$ should yield a straight line with slope $(k/\pi^2)^{1/5}$ and intercept *C*. This is the equation, with a slope of 0.24, that was presented in the technical summary.

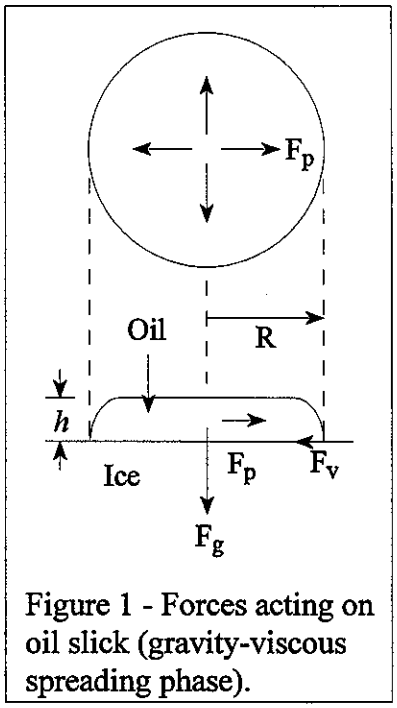

Figure 1 - Forces acting on oil slick (gravity-viscous spreading phase).

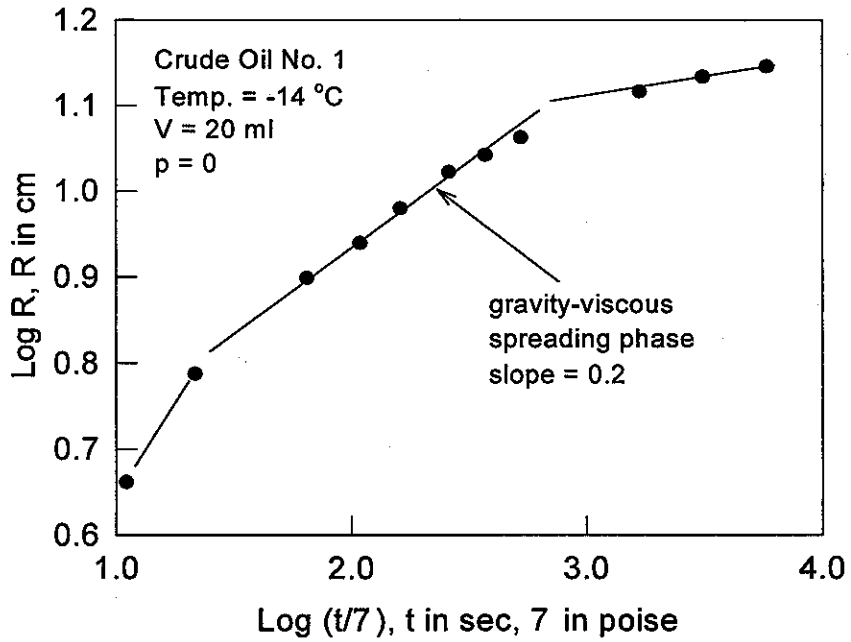

Figure 2-Sample of log R vs log (t/μ) plots.

Method

The spreading experiments used artificially prepared ice sheets prepared in a room thermostated to ±1 °C. This was done to create and keep ice of different roughnesses. A monolayer of glass beads (6-8 mesh) was placed on a glass plate to create a circular area with a 30 inch diameter. Deionized, distilled water was poured onto this surface and then frozen. The amount of water determined the depth of coverage and the roughness, p, of the surface created.

$$p = \frac{\text{Volume of void - Volume of water added} \times \text{(factor for ice expansion)}}{\text{Volume of beads + Volume of void}}$$

The ice of roughness p = 0 was prepared by freezing ice sheets 12 inches by 12 inches. Once the ice surface was prepared it was then levelled and a Plexiglass sheet with 0.1 cm scale was placed above the ice surface. The oil was released at the center of the scale and a Bolex 16 mm camera with electronic time frame reference was used to photograph the spill spread. The rates of spreading were determined using a Ruscom Logics Digitizer.

Results

Five different crude oils, listed in Table 1, were used in these studies. Crude oil No. 1 was used at three temperatures, -3 °C, -8 °C, and -14 °C while the other crudes were only used at -14 °C. Two different spill volumes, 45 ml and 20 ml were used and three different roughnesses, p = 0, 0.15, and 0.34. The oil viscosity was measured from samples spilled on a glass plate and taken over time specified in Table 2 and measured with a Haake Rotovisko (Model RV1).

Table 1. Origin and Properties of the Crude Oils

	Crude Oil No. 1	Crude Oil No. 2	Crude Oil No. 3	Crude Oil No. 4	Crude Oil No. 5
Origin	Norman Wells N.W.T.	Essex County Ontario	Lambton County (Brooke Tp.) Ontario	Lambton County (Dawn Tp.) Ontario	Lambton County (Dawn Tp.) Ontario
Colour	Dark green	Brown	Brownish black	Brownish black	Brownish black
Pour Point °F	-60	0	0	-50	-50
Specific gravity at 60 °F	0.833	0.828	0.885	0.821	0.812
Degrees A.P.I. at 60 °F	38.4	39.4	28.4	40.8	42.8
Viscosity at 100 °F Saybolt Universal sec.	35	41.3	84.1	36.4	35.8
Sulfur . wt%	0.3	0.15	1.06	0.66	0.72

Table 2. Viscosity Data*

Elapsed Time, Minutes	Viscosity, cP						
	Crude No. 1			Crude No. 2	Crude No. 3	Crude No. 4	Crude No. 5
	at -3 °C	at -8 °C	at -14 °C	at -14 °C	at -14 °C	at -14 °C	at -14 °C
0	9.6	13.0	18.1	63.2	465.0	13.6	20.1
10	11.4	14.2	19.8	72.7	536.6	17.2	25.0
20	13.8	15.8	20.9	81.2	620.7	22.4	28.1

Table 2. Viscosity Data*							
Elapsed Time, Minutes	Viscosity, cP						
	Crude No. 1			Crude No. 2	Crude No. 3	Crude No. 4	Crude No. 5
	at -3 °C	at -8 °C	at -14 °C	at -14 °C	at -14 °C	at -14 °C	at -14 °C
30	15.0	17.9	22.0	87.8	654.1	24.1	35.0
40	16.8	18.9	23.7	95.8	706.7	29.7	41.6
50	18.7	20.0	24.5	102.9	865.7	33.3	53.3

*Based on spilling 20 ml of oil on a glass plate. (The use of glass plate instead of ice is due to the difficulty of collecting enough oil samples from a thin slick on the ice).

Table 3. Deviation of Data from Equation (8) with a C value of 0.35		
Crude Oil	Temp °C	Average* Absolute % Deviation
No. 1	- 3	3.45
No. 1	- 8	2.84
No. 1	-14	1.92
No. 2	-14	4.67
No. 3	-14	3.44
No. 4	-14	16.28
No. 5	-14	3.48

*Absolute % Deviation = $|y_{calc.} - y_{expt.}| \times 100/y_{calc.}$
where $y_{calc.}$ = calculated value of $(R/V^{1/3})$,
$y_{expt.}$ = experimental value of $(R/V^{1/3})$

Nomenclature			
A	= area covered by the oil slick, cm^2	p	= roughness parameter, dimensionless
C	= constant, dimensionless.	**R**	= radius of oil slick, cm
d	= differential operator	t	= time, sec
$\mathbf{F_g}$	= gravity forces, $dynes/cm^3$	u	= velocity of spreading, cm/sec
$\mathbf{F_p}$	= outward pressure forces, $dynes/cm^3$	**V**	= oil volume, cm^3
$\mathbf{F_v}$	= viscous forces, $dynes/cm^3$	π	= 3.1416

Nomenclature			
g	= acceleration of gravity 980 cm/sec^2	μ	= viscosity of oil, poise
h	= thickness of oil slick, cm	ρ	= density of oil, g/cm^3
k, K	= constant, dimensionless	τ	= shear stress, dynes/cm^2

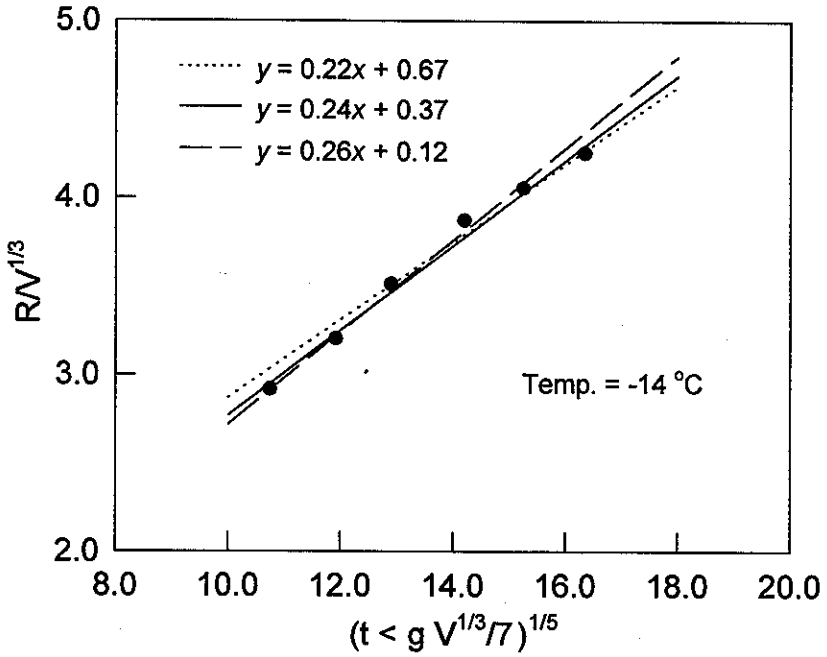

Figure 3 replacement. Plot of $(R/V^{1/3})$ *vs* $(t\rho gV^{1/3}/\mu)^{1/5}$ for crude oil No. 1, the same data as used in Figure 2 with $\rho = 0.833$ g/cm^3 (see text), g = 980 cm/s^2, and V = 20 cm^3.

Figure 2, recreated here, was used as an example of how the spreading occurred. The authors then plotted the data for only the gravity-viscous spreading phase in the form of $R/V^{1/3}$ *vs* $(t\ \rho\ g\ V^{1/3}/\mu)^{1/5}$ with lines fit to an equation of the form $y = Kx + C$ where K was chosen by the authors to be 0.24. There were six sets of data, described above, one of which was reproduced in Figure 3 replacement, above, and which will be discussed in the BOSS Critique section. Table 1 gives the specific gravity of the oil at 60 °F as being 0.833 and this is the value that is used in the calculations here.

Figures 3 and 4 were for two different volumes of oil spills, at different temperatures, on three different types of ice surfaces, and using three different crude oils as described earlier. The data from these figures is similar to data presented in Figure 3 replacement and Figure 5, below.

Figure 5 is a plot of crude oil No. 1 for three temperatures and two volumes but for only one roughness, p = 0.15. There does not seem to be a large change in the plot for different volumes nor different temperatures and the authors fit a single line, give in the plot to all of the data. The one

difference of the plots in Figures 3 and 4 was that different roughnesses were used but the scatter of the data was similar to the scatter shown in Figure 5.

The authors evaluated the data fit to a line of slope 0.24, *K*, and an intercept value of 0.35, *C*. The deviation of the data from the equation is presented in Table 3 and the authors state that the equation reproduces the experimental results, except for crude oil No. 4, within acceptable limits with no serious errors.

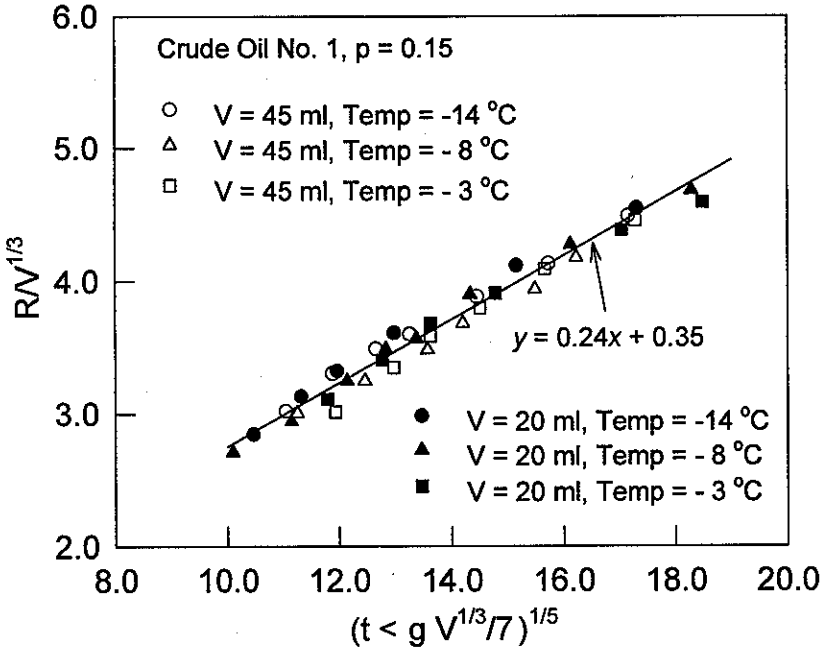

Figure 5 - Effect of temperature on the spreading.

BOSS Critique

The authors state several times in this manuscript that the data fit a line of slope 0.24 and intercept 0.35 quite well. The reviewer has shown in the lines plotted in Figure 3 replacement, that several lines with similar slopes but quite different intercepts can be drawn through the data from one experiment. The scatter of the data sets in Figure 5 indicates that the lines in Figure 3 replacement are well within the range provided by the experimental data sets. However, using simple regression fit to the data present in Figure 3, produces a line of slope 0.24 but with an intercept value of 0.32 and $r^2 = 0.989$. A simple regression fit to all of the data present in Figure 5 results in a line of slope 0.24 and an intercept value of 0.4, $r^2 = 0.975$ which is not as good a fit as the previous line. The point is that although for the data presented in this review the slope is consistent to two decimal places, the intercept varies. It would be more beneficial to the reader to have a range of slopes and a range of intercepts that are representative of the experimental error. The data may fit a line $y = Kx + C$ where $K = 0.24(\pm 0.01)$, and $C = 0.35(\pm 0.05)$, however the authors have not made such a determination only that the absolute deviation can be from 2 to 5 % as presented in Table 3.

Review of a manuscript, by Chen, E.C., B.E. Keevil, and R.O. Ramseier entitled, *Behaviour of Oil Spilled in Ice-Covered Rivers*, Inland Waters Directorate, Water Resources Branch, Environment Canada, Scientific Series No. 61, Ottawa, 1976.

Another manuscript covering similar information is Chen, E.C., B.E. Keevil, and R.O. Ramseier, "Behaviour of Crude Oil Under Fresh-water Ice", in the *Journal of Canadian Petroleum Technology*, April-June, 1976.

Technical Summary

"The oil, when released in water under the ice, separates into droplets; the drops rise to the ice-water interface where they coalesce and form a slick.

In calm waters, the oil drops rise vertically and spread at the ice-water interface. The spreading process is complex. The radius of the oil slick is proportional to ~0.25 power of the elapsed time.

In turbulent waters, the oil drops also rise to the ice-water interface. They travel some distance following the flow direction of water, however, before reaching the interface. Some of the small drops are suspended and dispersed in the water column. The slick formed at the ice-water interface does not adhere to the ice and contains some water-in-oil emulsions.

The oil, when spilled under the ice, acts as an insulating layer and thus increases the temperature drop across the ice; the surface temperature of ice with an oil lens underneath is a few degrees lower than that of the clean ice.

If the oil is spilled as a lens under the ice and the ice continues to grow, the oil will be sandwiched between the ice layers.

The behaviour of oil spilled in ice-covered rivers is difficult to predict. Observations of accidental oil spills show that the oil, when spilled in a river, will quickly be dispersed downstream."

Objective

To relate experimental work to theoretical equations for useful prediction of the behaviour of oil spilled under fresh water ice.

List of Symbols			
A	area of oil slick, cm	Q_{io}	amount of heat transferred through the ice with an oil lens, cal/cm^2-hr
c	constant, dimensionless	R	radius of oil slick, cm
d	droplet diameter, cm	t	elapsed time, s
D	diffusion coefficient, cm^2/s	T_{ia}	temperature at the ice-air interface, °C
D_n	nozzle diameter, cm	T_{iao}	temperature at the ice-air interface above the oil lens, °C
F_b	buoyancy force, dynes/cm^3	T_l	temperature at the top of the oil lens, °C

List of Symbols			
F_p	outward pressure force, dynes/cm^3	T_2	temperature at the bottom of the oil lens, °C
F_v	viscous force, dynes/cm^3	u	velocity of spreading, cm/s
g	acceleration due to gravity, 980 cm/s^2	v_n	nozzle velocity, cm/s
h	thickness of oil slick or lens, cm	v_t	drop terminal velocity, cm/s
k	mass-transfer coefficient, g/(s)-(cm^2)-(g/cm^3)	V	oil volume, cm^3
K_i	thermal conductivity of ice, cal/s-cm-°C	δ	thickness of water film under the oil so set into motion by the viscous force, cm
K_o	thermal conductivity of oil, cal/s-cm-°C	μ	viscosity of oil, poise
L_1	thickness of ice layer above the oil lens, cm	μ_w	viscosity of water, poise
L_2	thickness of ice layer below the oil lens, cm	π	3.1416
N_{Re}	Reynolds number, $(d\ v_t\ \rho_w)/\mu_w$, dimensionless	ρ_d	density of dispersed phase, *i.e.*, density of crude oil, g/cm^3
N_{Sc}	Schmidt number, $\mu_w/(\rho_w D)$, dimensionless	ρ_w	density of water, g/cm^3
N_{Sh}	Sherwood number, k/(dD), dimensionless	σ	interfacial tension, dynes/cm
Q	oil spill rate, cm^3/s	τ	shear stress, dynes/cm^2
Q_i	amount of heat transferred through the clean ice, cal/cm^2-hr		

Theory

The authors explain droplet formation, emulsification, dissolution, spreading, and thermal effect of oil under the ice.

The authors state that since oil is an immiscible fluid in water, the injection of oil into water under ice results in the formation of droplets of oil in the water. The droplet size is "increased by increased interfacial tension, decreased by difference in density between two liquids, increased viscosity of the aqueous phase, and by increased opening of the injection nozzle; it is practically unaffected by viscosity of the dispersed phase." The authors describe a method (attributed to Hayworth, C.B. and R.E. Treybal, "Drop Formation in Two-Liquid Phase Systems", *J. Ind. Eng. Chem.*, Vol. 42, p. 1174, 1950) of determining the droplet size and state that for Norman Wells crude, properties listed in Table 1, the theoretical droplet size is 1.2 cm.

The authors state that velocity of droplets rising to the ice-water interface is determined by internal circulation, droplet deformation and oscillation. The authors refer to an equation (Klee, A.J. and R.E. Treybal, "Rate of Rise or Fall of Liquid Drops," *A. I. Ch. E. Journal*, Vol 4, p 273, 1958) that they used to determine the terminal velocities of oil drops of diameter 0.1 cm, 1.0 cm, and 2.0 cm, to be respectively, 4 cm/s, 21 cm/s and 35 cm/s. Also if there is sufficient turbulence the oil may become incorporated into the water and form an emulsion which would be stabilized by hydrophilic components such as $-COO^-$, $-OH^-$, -CHO, OSO_3^{2-}, and $-SO_3H$. The properties of an emulsion are

different than that of the oil, *i.e.* the viscosity can increase by 3 orders of magnitude.

Some components of oil, low boiling, are water soluble and therefore when oil comes in contact with water the low boiling aromatic components will dissolve into the water. The dissolution rate, and mass transfer coefficient k are related to physical and flow properties, $N_{Sh} = f(N_{Re}, N_{Sc})$, where N_{Sh}, N_{Re}, and N_{Sc}, are the Sherwood number, Reynolds number, and Schmidt number. Also note that the Sherwood number is related to the mass transfer coefficient by $N_{Sh} = k\,d/D$ so for a diameter of 0.1 cm, a rising velocity of 4 cm/s and a diffusion coefficient, $D = 0.5 \times 10^{-5}$ cm^2/s for water at 0 °C, $k = 2.18 \times 10^{-3}$ g/(s)-(cm^2)-(g/cm^3). The authors assume that the crude oil has 1% water-soluble components and therefore the dissolution rate is 1.8×10^{-5} g/s-cm^2 and the time required to remove half of the soluble components is 7.6 s. No measurements are reported.

The authors state that spreading of oil under ice has the same three regimes that Fay outline for oil on water except that gravity is replaced with buoyancy.

$$F_p = F_b = c\rho_w g h A/V = c\rho_w g \tag{1}$$

and the viscous force, F_v, per unit volume is

$$\begin{aligned} F_v &= \tau A/V = \mu(du/dh)(A/V) = \mu R/(th^2) \\ &= \pi\mu R^5/(tV^2) \end{aligned} \tag{2}$$

where

F_b = buoyancy force per unit volume
c = constant
ρ_w = density of water
g = acceleration due to gravity
A = area of oil slick = πR^2
R = radius of oil slick
V = oil volume = hA
h = thickness of oil slick
τ = shear stress
μ = oil viscosity
u = spreading velocity
t = elapsed time.

For buoyancy-viscous spreading at equilibrium, the two forces are equal, that is

$$c\rho_w g = \pi\mu R^5/(tV^2) \tag{3}$$

The volume can be stated as Qt, where Q is the rate of spilling and t is time then equation (3) can be restated as,

$$t(Qt)^2 c\rho_w g = \pi\mu R^5 \tag{4}$$

The authors then express the radius as

$$R = \left(\frac{c\rho_w g Q^2}{\pi\mu}\right)^{0.2} t^{0.6} \tag{5}$$

The authors refer to Fay's work (reviewed elsewhere) to discuss the layer of water and the viscous forces of a water film, that would be in between the oil and ice layers,

$$\delta = (\mu_w t/\rho_w)^{0.5} \tag{6}$$

where μ_w is the viscosity of water.
Therefore replacing one h with δ the revised viscous force per unit volume would be,

$$\begin{aligned} F_v &= \mu_w(R/t)/h(\mu_w t/\rho_w)^{0.5} \\ &= (\mu_w\rho_w)^{0.5}R/(t^{1.5}h) \\ &= \pi(\mu_w\rho_w)^{0.5}R^3/(Qt^{2.5}). \end{aligned} \tag{7}$$

Setting equation (1) = (7) results in

$$c\rho_w g = \pi(\mu_w\rho_w)^{0.5}\ R^3/(Qt^{2.5}) \tag{8}$$

which can be solved for the radius,

$$R = \left(\frac{c\rho_w^{0.5}gQ}{\pi\mu_w^{0.5}}\right)^{0.3} t^{0.8} \tag{9}$$

Thus the authors have two different time dependencies for the radius of the slick and as they note neither of these time dependencies fit the data give in Table C-1 and plotted in Figure 5.

The authors have determined the different heat transfer rates, temperature gradient, of ice with and without an embedded oil lens and the theoretical calculations indicated that there should be different ice growth under the oil lens. Experimental data proved this to be untrue. The heat transferred per unit area is Q_i, for clean ice, Q_{io}, for the oil lens, yielding equations

$$Q_i = K_i \frac{(T_{ia}-T_{iw})}{(L_1+h+L_2)} \tag{10}$$

$$Q_{io} = K_i \frac{(T_2-T_{iw})}{L_2} = K_o \frac{(T_1-T_2)}{h} = K_i \frac{(T_{iao}-T_1)}{L_1} \tag{11}$$

where K is thermal conductivity, the subscript i is for ice, and o for oil. The temperatures are T with subscript iw for ice-water interface, ia for ice-air interface and iao for ice-air interface above oil lens. These results are illustrated in Figures 12, and the experimental data is presented in Tables C-2 and C-3 and plotted in Figure 13 (see the results section). The authors state that thermal conductivity for oil ranges from 0.0003 - 0.0004 cal/s-cm-°C, at 0 °C, while for ice it is 0.005 cal/s-cm-C, at 0 °C.

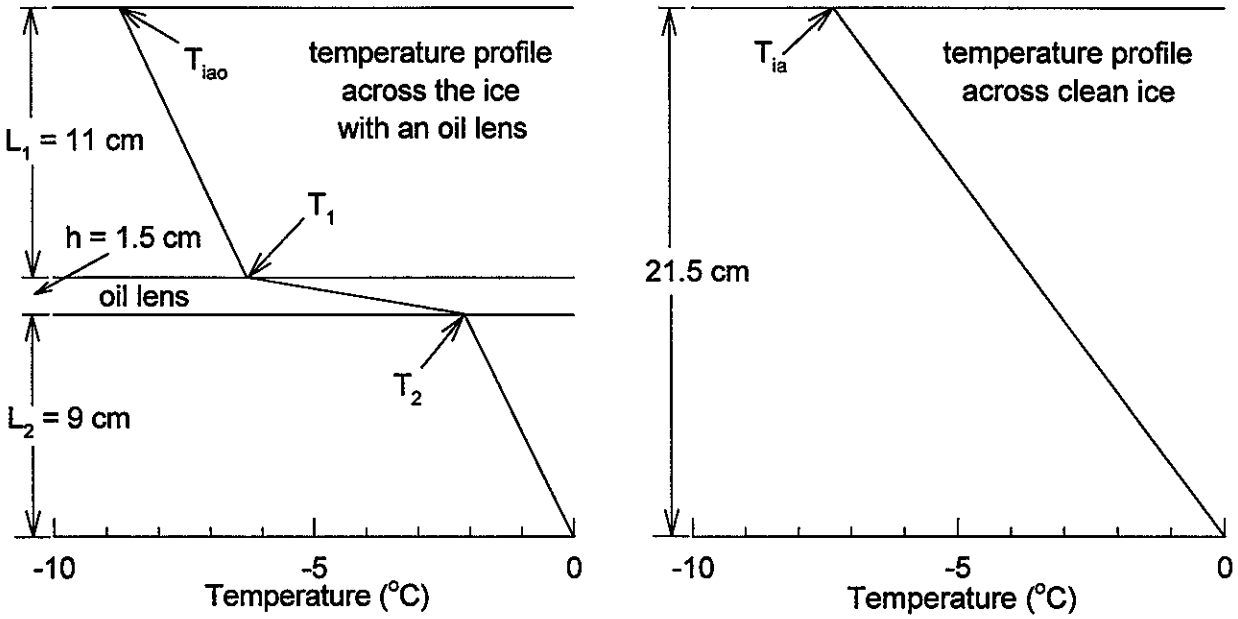

Figure 12. Temperature profiles - a sample calculation.

Method

The water content of the oil was measured using the Karl Fisher method and a Metrohm automatic titrator.

"A circular aluminum basin, inner diameter 150 cm and 70 cm deep, was installed in a cold room where the air temperature was maintained at -15° ± 2°C (Fig. 1). The cold room was equipped with a fan to ensure uniform air flow and heat transfer in the basin. Heating tapes were glued to the outside wall of the tank and covered with polystyrene insulation 10 cm thick. The heating tapes were connected to Variacs set at very low power to cancel out the bottom and side heat losses. This combination of heating tapes and insulation allowed one-dimensional freezing in the basin and effectively simulated the growth of natural ice similar to the type found in lakes, reservoirs and rivers with low flow velocities.

The ice thickness was measured with ice thickness gauges (6). The gauge was a small steel cylinder suspended by a wire under the ice. To measure the thickness the cylinder was raised to the ice-water interface, and the distance from the ice-air interface was measured and subtracted from the total wire length.

An air-ice-water thermistor probe obtained a temperature profile with relative accuracy of ± 0.2 °C. The probe contained 19 precision thermistors, manufactured by Yellow Springs Instruments (YSI No. 44033), mounted in a PVC rod at a separation of 1 cm in the ice and 5 cm in the air and water. Each thermistor solder joint and wire was waterproofed with epoxy resin. A multiconductor plug was installed at the top of the probe for connection of the bridge circuit. A rotary switch enabled each thermistor to be switched into the bridge, to be balanced, and record resistance.

Most oil spilled under the ice is initially hot because the transit temperatures of the well head, tanker and pipeline are about 60 °C. The crude, however, was injected at a room temperature of

about 20 °C, as heating of oil in the laboratory is dangerous. The oil injection system was a 25-litre plastic tank and gravity-fed electric pump (Fig. 2). The system is portable and can easily be carried into the cold room and connected to the oil injection pipe.

The typical test procedure was as follows. The basin was filled with water to a height of 60 cm at a room temperature of -15 °C. Two days later, a primary ice layer began to form. Its growth was predominantly in the horizontal plane, forming a very thin ice layer. The secondary ice grew parallel to the heat flow, perpendicular to the water surface and reached the desired thickness three days later. The crude oil (5 l at 20°C) was pumped for about 70 s through a 1.27-cm pipe and released 30 cm below the ice-water interface in the centre of the basin.

For some experiments carried out under a circular current, an electric outboard motor was mounted on the side of the basin, and a circular oil boom was installed to prevent the oil from rising up the tank walls and spreading over the ice surface. The outboard motor was turned on when the basin was filled with water and left running for the duration of the test. A detailed velocity profile across the basin was not obtained. A small current meter, however, indicated an average velocity of about 10 cm/s.

A few tests were made in a simulated ice-covered flume with water flowing in one direction. The recirculating flume was 250 cm long, 15 cm wide and 30 cm deep (Fig. 3). A screw-type valve controlled the flow from the circulation system into the flume, and the depth of flow was established by adjusting the tailgate setting. The average current in the flume was around 15 cm/s. The flume was filled with water of 6 °C and the centrifugal pump maintained a continuous flow of water. Two litres of crude oil at 20 °C was injected under the Plexiglass cover from a pipe 1.27 cm in diameter.

Norman Wells crude oil was used in this investigation; its properties are given in Table 1."

Table 1a. Properties of Norman Wells Crude Oil	
Pour point	-50 °C
Colour	dark green
Degree API at 15 °C	38.4
Specific Gravity at 15 °C	0.833
Surface tension at 24 °C	27.8 dynes/cm
Interfacial tension (with water) at 24 °C	21.0 dynes/cm

Table 1b. Components of Norman Wells Crude Oil	
Component	Percent by Volume (approx.)
Light gasoline	10.5
Total gasoline and naphtha	35.6
Kerosene distillate	5.7
Gas oil	19.5
Nonviscous distillate	8.1
Medium distillate	5.7
Viscous distillate	2.9
Residuum	21.5
Distillation loss	1.0

Results

The experimental droplet size was determined, from photographs of oil droplets at the ice-water interface, to be 0.1 cm to 2.0 cm which averages to the predicted value of 1.2 cm.

An emulsion was formed during the circular current experiment and the water content was determined to be 23% for a sample taken one day after the spill. A sample taken one day after a spill with no current had 700 ppm water. The authors state that this is a clear indication that emulsions

will not form in calm waters.

Table C-1. Oil Spreading Data

	Elapsed time t (s)	Log t	Radius of oil slick R (cm)	Log R
Test 1	5	0.70	24	1.38
	10	1.00	28	1.45
	13	1.11	30	1.48
	18	1.26	32	1.51
	24	1.38	34	1.53
Test 2	1	0.00	10	1.00
	4	0.60	20	1.30
	6	0.78	22	1.34
	11	1.04	26	1.41
	16	1.20	32	1.51
	20	1.30	34	1.53
	24	1.38	36	1.56
Test 3	1	0.00	10	1.00
	7	0.85	24	1.38
	10	1.00	28	1.45
	13	1.11	30	1.48
	18	1.26	32	1.51
	23	1.36	34	1.53
	28	1.45	36	1.56
	38	1.58	38	1.58
	43	1.63	40	1.60
Test 4	1	0.00	10	1.00
	2	0.30	16	1.20
	3	0.48	20	1.30
	4	0.60	22	1.34
	5	0.70	24	1.38
	7	0.85	28	1.45
	10	1.00	30	1.48
	11	1.04	32	1.51
	14	1.15	34	1.53
	17	1.23	36	1.56
	19	1.28	38	1.58
	23	1.36	40	1.60
Test 5	1	0.00	4	0.60
	4	0.60	20	1.30
	8	0.90	26	1.41
	10	1.00	28	1.45
	13	1.11	30	1.48
	18	1.26	32	1.51

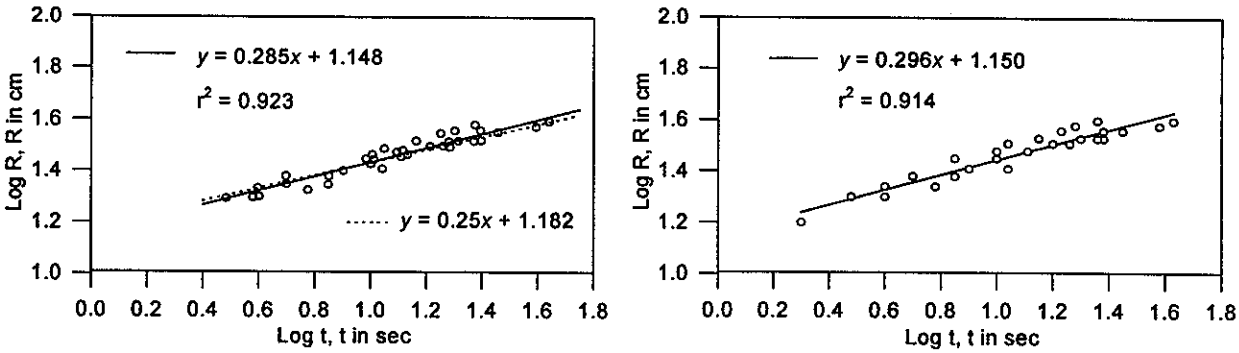

Figure 5 . Log R *vs* Log t - experimental results. Left plot is (a) and right plot is (b). The right figure is a plot of the data presented in Table C-1, see BOSS Critique for details.

Table C-2. Temperature Profiles across the Ice (0-6 days)

Height from tank bottom (cm)	Day 0		Day 1		Day 2		Day 3		Day 4	
	control	oil lens	control	oil lens	control	oil lens	control	oil lens	control	oil lens
70	-11.8	-12.2	-11.8	-13.2	-13.4	-14.8	-13.8	-14.8	-10.6	-11.6
65	-11.2	-11.6	-11.4	-12.8	-12.8	-14.4	-13.2	-14.4	-10.2	-11.4
60	- 5.4	- 5.8	- 5.6	- 9.2	- 6.2	- 9.6	- 6.8	- 11.2	- 5.8	- 7.8
55	- 3.0	- 3.2	- 3.4	- 7.8	- 4.0	- 8.2	- 4.8	- 8.6	- 4.4	- 6.8
50	- 0.6	- 0.6	- 1.2	- 6.4	- 1.8	- 6.8	- 2.8	- 6.0	- 3.0	- 5.8
45	0.0	0.0	+ 1.6	+ 0.0	+ 0.0	- 0.4	- 0.8	- 0.8	- 1.8	- 1.4
40	0.0	0.0	+ 1.8	+ 1.2	+ 0.6	+ 0.4	+ 0.0	+ 0.0	- 0.2	- 0.4
30	+ 0.2	+ 0.2	+ 2.0	+ 1.8	+ 1.0	+ 1.0	+ 0.4	+ 0.4	+ 0.2	+ 0.2
20	+ 0.4	+ 0.4	+ 2.0	+ 2.0	+ 1.4	+ 1.4	+ 0.4	+ 0.4	+ 0.4	+ 0.4
10	+ 0.8	+ 0.8	+ 2.2	+ 2.2	+ 1.8	+ 1.8	+ 0.8	+ 0.8	+ 0.8	+ 0.8
Ice thickness (cm)										
	11.0	-	12.5	-	14.0	-	16.0	16.0	20.0	20.0

Table C-3. Temperature Profiles across the Ice (0-6 days)										
Height from tank bottom (cm)	Day 7		Day 8		Day 9		Day 12		Day 13	
	control	oil lens	control	oil lens	control	oil lens	control	oil lens	control	oil lens
70	-12.4	-12.4	-11.4	-12.2	-12.6	-12.4	-13.0	-13.8	-13.4	-13.2
65	-12.0	-12.4	-11.0	-12.0	-12.2	-12.4	-12.6	-13.4	-13.2	-13.0
60	- 7.2	- 9.0	- 6.6	- 8.6	- 7.4	- 9.8	- 8.6	- 10.6	- 8.8	- 13.0
50	- 3.8	- 7.0	- 3.8	- 6.6	- 4.6	- 7.6	- 5.8	- 8.6	- 6.0	- 8.6
55	- 5.4	- 8.0	- 5.2	- 7.6	- 6.2	- 8.8	- 7.2	- 9.6	- 7.4	- 9.8
45	- 2.2	- 1.8	- 2.4	- 1.8	- 3.0	- 2.6	- 4.4	- 3.8	- 4.6	- 4.0
40	- 0.8	- 0.8	- 1.0	- 1.0	- 1.6	- 1.4	- 2.8	- 2.6	- 3.2	- 2.8
30	+ 0.2	+ 0.2	+ 0.2	+ 0.0	+ 0.0	+ 0.0	- 0.2	+ 0.0	- 0.6	- 0.4
20	+ 0.2	+ 0.2	+ 0.2	+ 0.2	+ 0.0	+ 0.0	+ 0.0	+ 0.0	+ 0.0	+ 0.0
10	+ 0.4	+ 0.4	+ 0.2	+ 0.2	+ 0.2	+ 0.2	+ 0.2	+ 0.2	+ 0.2	+ 0.2
Ice thickness (cm)										
	22.0	21.5	23.0	23.0	25.0	25.0	30.0	30.0	32.0	32.0

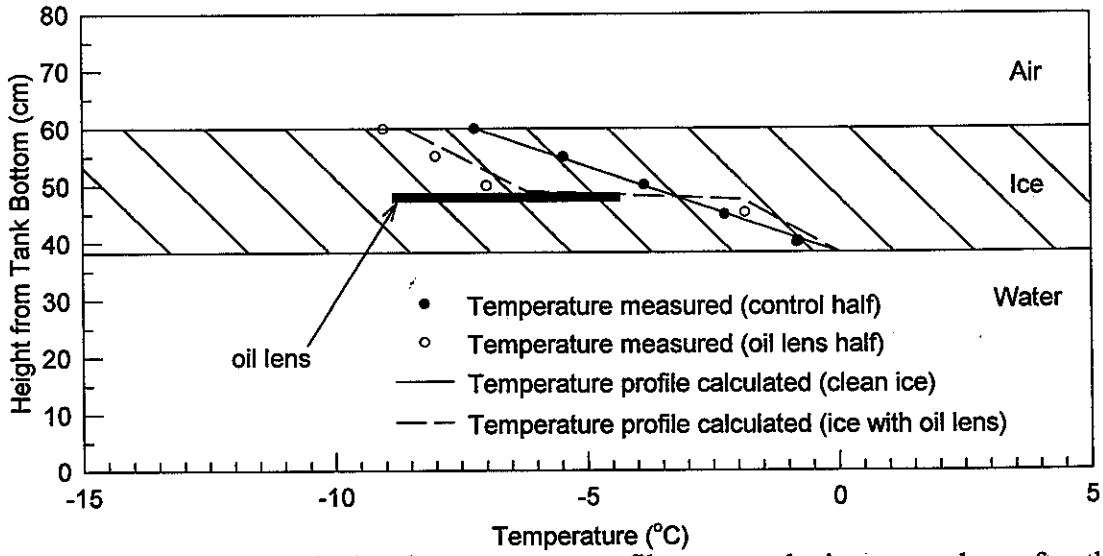

Figure 13. Measure *vs* calculated temperature profiles across the ice seven days after the oil spill.

"Figure 13 shows the measured temperature profiles and the calculated temperature profiles across each half of the ice seven days after the oil spill. ··· It is seen that the measured temperature

profiles are in good agreement with those calculated. The ice growing rate was about 2 cm/day, which agrees with the theoretical value (1.90 cm/day) for the clean ice. The total ice thicknesses between halves, i.e., between the clean ice and the ice with and oil lens, however, showed no significant difference; this is contrary to the prediction by calculations."

The authors discusses several spills of oil in Canadian rivers and state,

"Two conclusions may be drawn from this survey of reported oil spills in Canadian rivers: 1) oil spilled in ice-free rivers is quickly dispersed downstream and 2) the behaviour of oil spilled in ice-covered rivers depends mainly on the ice conditions and the currents at the time of the spill."

BOSS Critique

The authors stated that the rate of oil droplet formation and rising to the water-ice interface could be a determining factor in emulsion formation, however, no experimental evidence was found to validate this statement. The authors had calculated a expected value of droplet size but the experimental evidence indicated a range of sizes. Thus reality (experimental time lapsed photographs) shows that even droplet formation is a complicated process governed by more than the simple process outlined by the authors. The simple experimental introduction of a current does not explain the formation of an emulsion. Only one type of crude oil was used in this set of experiments and a different type of crude may form an emulsion under different conditions.

A distillation curve would be more helpful to the reader instead of Table 1b. Since the component description, that is used in Table 1b is not standardized, a temperature range should be provided with the percent by volume distillation data.

Figure 5(a) was reproduced from Figure 5 of the Chen, Keevil, Ramseier manuscript by "reading" the data points from the plot. There are several groupings of data points with three or four data points to a group, which are in the original and in the reproduced Figure 5,(a) but not in the data of Table C-1, Figure 5(b), the plot in the right column. The authors state that the line in the plot had a slope of 0.25 which has been reproduced in Figure 5 (a) as a dashed line. The solid lines in Figure 5 (a) and (b) are from regression fits to the data using a straight line of the form y = (slope)x + intercept. The slopes are different than that stated by the authors, however, there is no error range stated for the data and thus a suitable error for the slope (*i.e.* ± value) can not be determined.

Review of a manuscript, written by Cox, J.C., and L. A. Schultz entitled, "The Transport and Behaviour of Oil Spilled Under Ice", in *Proceedings of the Third Arctic Marine Oilspill Program Technical Seminar*, Environment Canada, Ottawa, pp 45-61, 1980.

Other manuscripts covering this data are:

Cox, J.C., and L. A. Schultz, "The Containment of Oil Spilled Under Rough Ice" in *The Proceedings of the 1981 Oil Spill Conference*, pp 203-208, 1981.

Cox, J.C. and L.A. Schultz, "The Mechanics of Oil Containment Beneath Rough Ice", in *Proceedings of the Fourth Arctic Marine Oilspill Program*, Environment Canada, Ottawa, pp 3-44, 1981.

Schultz, L.A. and J.C. Cox, "The Transport and Behaviour of Oil Spilled In and Under Sea Ice: Phase II of Physical Processes", in *Environmental Assessment of the Alaskan Continental Shelf: Annual Reports of Principal Investigators For the Year Ending March 1980, Vol. VII: Transport Data Management*, Outer Continental Shelf Environmental Assessment Program, National Oceanic and Atmospheric Administration, Ocean Assessment Division, Alaska, pp 349-360, 1980.

Additional reports with the same information.

Cox, C., L.A. Schultz, R.P. Johnson, and R.A. Shelsby, *The Transport and Behavior of Oil Spilled in and under Sea Ice*, ARCTEC Incorporated for NOAA/OCSEAP, Research Unit 568, Final Report, 170 p, 1980.

Cox, J.C., *The Transport and Behaviour of Oil Spilled in and Under Sea Ice*, ARCTEC Incorporated Report, No. 460, 1980.

Technical Summary (quoted directly from the first manuscript)

"The categories of small roughness and large roughness result in the division of theories according to containment and noncontainment. The two theories are differentiated by the relationship of the slick thickness to the ice roughness amplitude. The results of the two theories do not necessarily merge when the ice roughness is exactly equal to the equilibrium oil thickness. In fact, a current of roughly 10 cm/s is needed before the large roughness theory can be applied. This is a transition point where both containment phenomena and transport phenomena are occurring simultaneously. This anomaly does not, however, limit the usefulness of the two theories.

It is also very important to stress that as current speeds approach critical, containment by large roughness becomes relatively independent of roughness amplitude provided the amplitude of roughness is at least as large as the slick thickness dictated by flow conditions. This strongly suggests that it is not always true that oil can continue to pile-up in front of a blockage of ice until it has reached the bottom tip of the ice. The actual volume of oil that can be contained by any ice roughness is controlled by the density of the oil and the ambient current.

The examination of the transport of spilled oil beneath sea ice has thus revealed these fundamental conclusions.

1. The thickness of an unaccelerating moving oil slick is equal to the static thickness of the slick, and for the oils tested ranged between 0.5 and 1.2 cm. Further, the slick thickness was found to be a linear function of the difference

between water and oil density.

2. The threshold velocity of an oil slick beneath smooth ice cover varied from about 3 to 4 cm/s for No. 2, No. 4, and No. 5 light oil to 7 cm/s for No. 5 heavy oil.

3. The presence of the slightest roughness on the under-ice surface, even roughness having an amplitude of 1 mm, significantly increases the threshold velocity of the oil and decreases its transport rate.

4. Oil trapped upstream of a large roughness element can be flushed out at current velocities in the 15 to 25 cm/s range for typical oils regardless of the depth of the roughness element.

5. In general terms, some of the oil which cannot be trapped by a large roughness element on its up-stream side may be captured within the wake region downstream of the roughness element.

6. Large roughness features such as pressure ridges are not likely to be major factors in the trapping of oil released beneath ice cover since a release of even the largest conceivable volume of oil will be confined to a relatively limited area by the normal under-ice surface roughness."

Objective (quoted directly from the first manuscript)

"1. Determine the kinds of roughness and the range of ocean current velocities for which oil can be driven under sea ice having different underside roughness characteristics.
2. Determine the kinds of roughness and the range of ocean current velocities for which oil can be constrained beneath ice so that the oil may become frozen into place or migrate into the ice and ultimately become incorporated therein."

Theory

The authors determined several empirical relationships (listed in Table 1) for slick thickness and oil density as well as threshold velocity and viscosity. The authors also present sketches, such as Figure 2 (from the third manuscript) on how the oil interacts with a change in ice roughness. These are theoretical in nature since no actual photographs or other direct evidence was presented, in the first manuscript, to prove the sketches to be a proper representation of oil interaction with ice. However, in manuscripts two and three plots, labelled Figures 6 to 13, of oil entrapment between ice barriers, such as in Figure 4 (of second manuscript), were presented for different flow rates, barrier depths and barrier spacings. The parameters for Figures 6 -13 (third manuscript) are listed in Table 3 of this review.

Table 1 (from manuscript two and three). Summary of Equations for Calculating the

Transport or Containment of Oil Beneath Ice in the Presence of a Current.

Equation	Manuscript Numbering	
	2	3
$\delta_{eq} = 1.67 - 8.50(\rho_w - \rho_o)$	14	18
$\left(1 + \frac{U_s}{U_w}\right) = \frac{K}{0.115F_\delta^2 + 1.105}$	15	19
$\epsilon = \frac{U_w^2}{3.46\Delta g}$	16	20
$U_{fail} = 1.5\left\{2\left(\frac{\rho_w + \rho_o}{\rho_w \rho_o}\right)\left[\sigma_{o/w}\ g(\rho_w - \rho_o)\right]^{1/2}\right\}^{1/2}$	17	21
$\ell = 4U_w$	18	22
$X_{shear} = \frac{4\Delta g}{f_s U_w^2}\left[\eta^2 - \left(\eta - \frac{\epsilon}{2}\right)^2\right]$	19	23
$V' = \ell(\eta - \epsilon) + \left[\frac{\delta_{tail} + \left(\eta - \frac{\epsilon}{2}\right)}{2}\right](\lambda - \ell)$	20	24
where $\delta_{tail} = \left[\frac{(\lambda - \ell)f_s U_w^2}{4\Delta g} + \left(\eta - \frac{\epsilon}{2}\right)^2\right]^{1/2}$	(20a)*	(24a)*
$\delta_{stagnation} = \left[\eta^2 - \frac{(\lambda - \ell)f_s U_w^2}{4\Delta g}\right]^{1/2}$	21	25
$V' = \frac{\left(\eta + \frac{U_w^2}{4\Delta g}\right)}{2}\left(\frac{4\Delta g}{f_s U_w^2}\right)\left[\eta^2 - \left(\frac{U_w^2}{4\Delta g}\right)^2\right]$	22	26
$V' = 6C_D\,\eta\delta eq$	23	27
$V' = \frac{1}{2}\left[\eta + \left(\eta^2 - \frac{\lambda f_s U_w^2}{4\Delta g}\right)^{1/2}\right]\lambda$	24	28

Note that Equations 14, 16, and 18 are dimension equations written in cgs units. *reviewer's note.

Table 2 (from manuscript two and three). Definition of Terms for Equations for Calculating the Transport or Containment of Oil Beneath Ice in the Presence of a Current

C_D	roughness form drag coefficient; 1.98 for flat plate, 1.55 for triangular shape.	-
F_δ	densimetric Froude number. $F_\delta = U_w / \sqrt{\Delta g \delta}$; for this case , $\delta = \delta_{eq}$.	-
f_s	oil-water interfacial friction factor empirically assumed in this report as 0.016.	-
g	gravitational acceleration	cm/sec^2
K	ice friction amplification factor, 1.0 for smooth ice, and approximated from Figure 1 (of manuscript three but Figure 4 of this review) for small roughness ice.	-
U_{fail}	current speed for containment failure	cm/sec
U_s	oil slick speed	cm/sec
U_w	water current speed	cm/sec
V'	approximate volume of trapped oil per unit width	cc/cm
X_{shear}	length of the shear dominated portion of the slick in a cavity	cm
Δ	relative density ratio = $(\rho_w - \rho_o)/\rho_w$	-
δ	local slick thickness	cm
$\delta_{stagnation}$	thickness of slick in a cavity at the end of the vortex zone	cm
δ_{eq}	equilibrium oil slick thickness beneath smooth ice	cm
δ_{tail}	thickness of contained slick at the downstream wall	cm
ϵ	vortex zone offset into a cavity	cm
η	ice roughness height or cavity depth	cm
ℓ, l	length of vortex cell	cm
λ	cavity length	cm
ρ_o	density of oil	g/cm^3
ρ_w	density of water	g/cm^3
$\sigma_{o/w}$	interfacial tension between oil and water, typically 30 to 35 dynes/cm for crude oils.	dynes/cm

As shown in Figure 2 (from the third manuscript), the authors state that there are three distinct regions formed for the oil in front of an obstruction. These are the head region, the neck region and the tail region all of which will have different dimensions for a respective current speed. The oil may move by an obstruction in two ways. The obstruction may become "filled" and the residual oil flows over and the second situation happens if the current is fast enough to flush the oil

out of the obstruction. This second case happens when there is "a Kelvin-Helmholtz instability in the slick which occurs at higher current velocities"

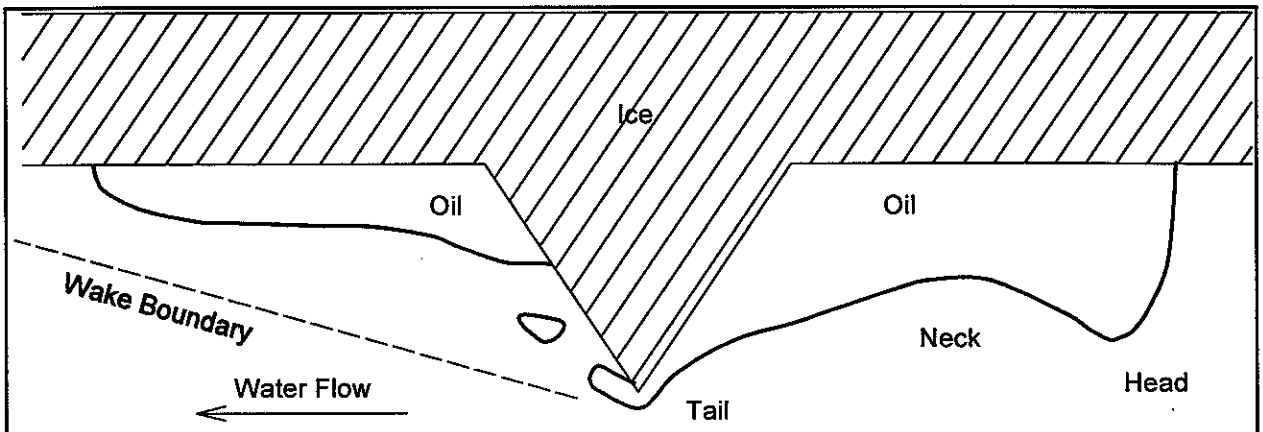

Figure 2 (from manuscript three). Sketch showing shape taken by a slick trapped upstream of a large roughness element and oil leakage from upstream to the wake region.

The slick thickness is measured from the bottom of the ice surface to the bottom of the slick and this distance is called δ. As outlined in Table 1, there are slick thickness for the neck and the tail (for non over-flow conditions) and the depth of the water is D. The authors have based the model on a wake trapping model of Lin and Landweber ("Laventiev Wake Model and Its Cascade", *Journal of Fluid Mechanics*, **79**, Part 4, 1977) . The authors also refer to Grove, Shair, Peterson, and Acrivos("An Experimental Investigation of Steady Separated Flow Past a Circular Cylinder", *Journal of Fluid Mechanics*, **19**, Part 1, pp. 60-80, 1914). The authors use the wake theory in combination with a barrier, as described by Schichting (*Boundary Layer Theory*, New York, McGraw-Hill, 1968), to predict the wake length for any roughness shape in deep water. The authors then interrelate these works to present the idea that "the length of a slick contained by the wake could not exceed this length since reattachment of free stream current would result in tearing any excess oil away. The thickness of the oil slick trapped in the wake should be equal to the static equilibrium thickness."

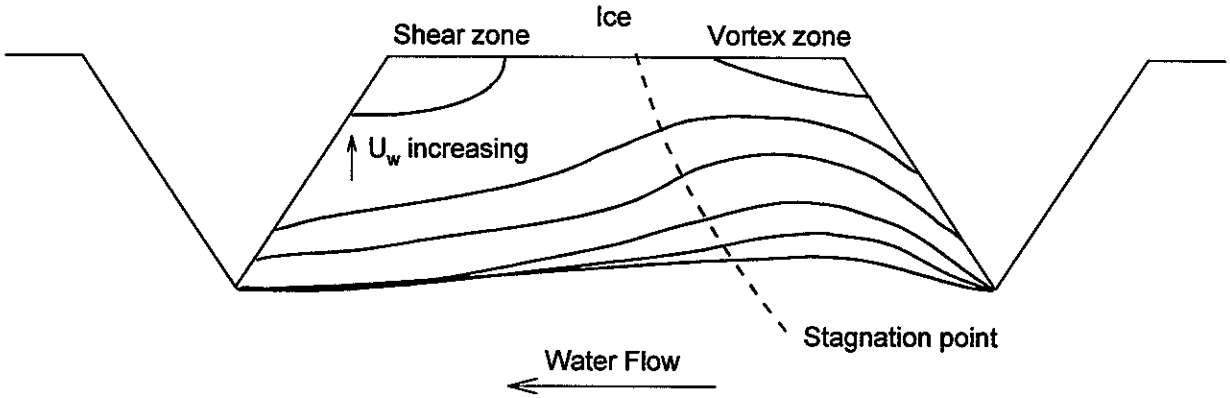

Figure 4 (from the second manuscript). Schematic representation of the shift in oil-water interface position within cavity as a function of increasing current.

The authors also relate the thickness of the oil to the Froude Number, F, see Figure 6, via:

$$\Psi(2-\Psi)\frac{(1-\Psi)}{(1+\Psi)} = F^2 \qquad (1)$$

where, as stated in Figure 6, $\Psi = \delta/D$ (where δ and D are as defined above). Ψ is the slick thickness ratio and according to the authors F has a maximum value of 0.527 after which the containment will always fail. The line drawn in Figure 6 is produced using equation (1) above.

These ideas are then used to prove a theory for cavity trapping which has a vortex zone and a shear zone which are separated by a stagnation "point" which is really a line as shown in Figure 4 (from the second manuscript). The vortex zone has depth ϵ into the cavity and is l in length with the stagnation slick thickness being $\delta_{stagnation}$ and the tail of the slick being δ_{tail} thick. These are calculated using equations 20a and 21 listed in Table 1, respectively. The authors state that "The thickness at the tail can never exceed the roughness height of the tail. If the vortex zone has penetrated the cavity so deep that the interfacial shape can no longer remain parabolic, and if the slick stays attached to the tip of the roughness, draining of oil from the cavity will occur until the oil-water interface has retreated to a parabolic shape higher up in the cavity."

Table 3. Listing of the Figure numbers from manuscript three, and the associated water velocity, cavity depth and cavity length.

Figure #	Velocity (cm/s)	Oil Type	Cavity		Figure #	Velocity (cm/s)	Oil Type	Cavity	
			length (m)	depth (cm)				length (m)	depth (cm)
6	24 32 40 48	# 4 oil	0.5	14	10	7 12 19 27	#4 oil	1 recessed	9

Table 3. Listing of the Figure numbers from manuscript three, and the associated water velocity, cavity depth and cavity length.

Figure #	Velocity (cm/s)	Oil Type	Cavity		Figure #	Velocity (cm/s)	Oil Type	Cavity	
			length (m)	depth (cm)				length (m)	depth (cm)
7	8 15 19 24 32 38 45	# 4 oil	0.5	19	11	24 32 40 48	#5 Heavy oil	0.5	15
8	0 7 12 16 19 26 32	# 4 oil	1	9	12	8 16 19 24	# 5 Heavy oil	1	9
9	0 7 12 16 19 23 26 32	# 4 oil	2	9	13	7 12 16	# 5 Heavy oil	2	11

Method (initial section quoted directly from the first manuscript)

"Tests on the horizontal transport of oil beneath ice were performed in ARCTEC's 12 metre long glass-walled ice flume. Freshwater ice was grown over 40 cm of water in the flume. With the pump running at its full capacity, oil behaviour for currents up to 35 cm/s could be observed through the glass walls of the flume. By performing the experiments in the laboratory, measurements of the under-ice spreading and containment could be made in a controlled environment. This eliminated the danger of creating a hazardous spill while in the process of studying one. Laboratory analyses also allowed for the detailed observations and measurements required for a fundamental study; not practical in the field.

Normally, tests involving only one fluid being driven by gravity forces are modeled according to Froude number considerations; however, in two fluid flow this is not often convenient. In particular, when trying to experimentally test with two prototype liquids in the laboratory, the effects of fluid properties such as surface tension or viscosity make it virtually impossible to scale the results. For example, the hydrostatic balance between the buoyancy of the oil and water, and the surface tension of the oil dictate that a static oil slick will have some constant equilibrium thickness. It therefore is impossible using that same oil to create scale models which require a model

equilibrium thickness to be less than or greater than the prototype thickness. Testing with prototype fluids requires a full-scale experiment, which means that any ice roughness forms used must also be considered full-scale. Therefore, it is not practical to investigate large features such as major ice ridges in a laboratory flume experiment. Consequently, all results presented are full-scale results.

To relate the laboratory results to field conditions, a different argument must be used. Conceptually, it is the shear stress applied to the oil slick by the current which causes the slick to move. By matching shear stress generated under an ice cover in the field to the shear stress generated in the flume, the laboratory results can be applied to field situations."

In manuscript three, the authors added "Ice roughness forms were grown separately and inserted into slots cut into the ice cover. The ice was then refrozen to create a homogeneous ice cover of specified under ice roughness."

Four types of oil were reported in the first manuscript. The static slick thickness of these oils was, 0.52 cm for No. 2 oil, 0.94 cm for No. 4 oil, 1.03 cm for No. 5 light, and 1.16 cm for No. 5 heavy. In manuscript three only two oils were used. No. 4 fuel oil, with a specific gravity range of 0.90 to 0.94 and a viscosity of 100 to 300 centipoise, and a No. 5 heavy oil with a specific gravity range of 0.94 to 0.97 and a viscosity range of 500 to 2000 centipoise.

Results

The authors treated the surface tension, of the oils investigated, as constant and using the data determined from the static slick measurements they related the slick thickness, δ, to the density difference between the oil and the water with several constants included, resulting in: $\delta_{eq} = 1.67 - 8.50(\rho_w - \rho_o)$ listed in Table 1 as equation 14. The authors then plot threshold velocity, U_{th}, *versus* oil viscosity (poise) and this is plotted in Figure 1, where the x-axis is a log axis. The equation that is stated in Figure 1 was proposed by the authors to relate the threshold velocity of the oil slick to the viscosity of the oil in question. The solid line in Figure 1 is a plot of the equation stated in Figure 1.

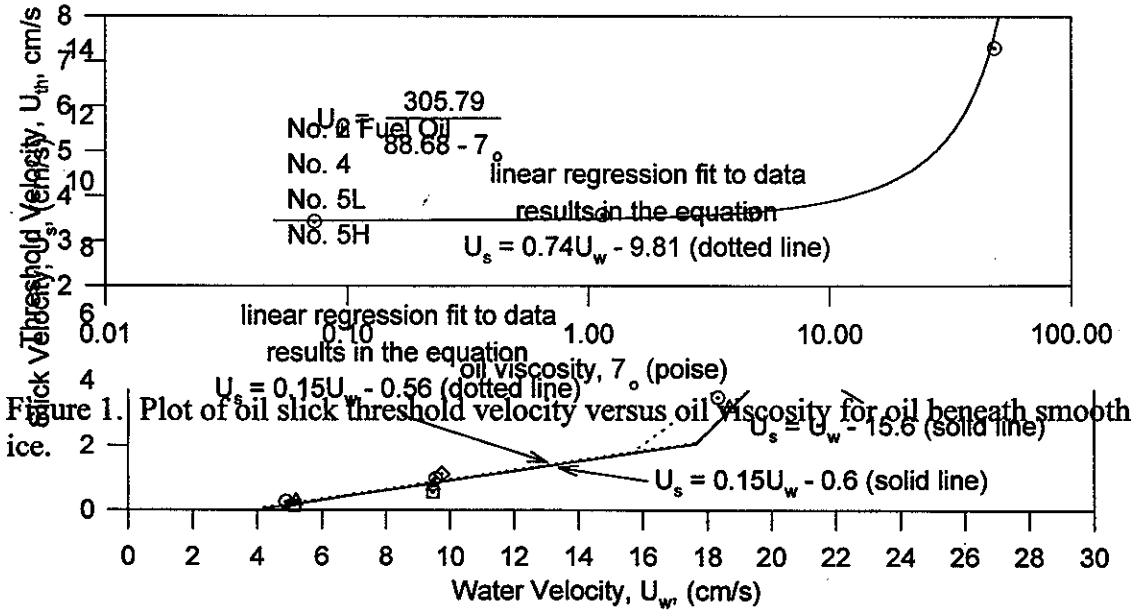

Figure 1. Plot of oil slick threshold velocity versus oil viscosity for oil beneath smooth ice.

Figure 2. Plot of oil slick velocity versus current velocity for the horizontal transport of oil beneath smooth ice cover.

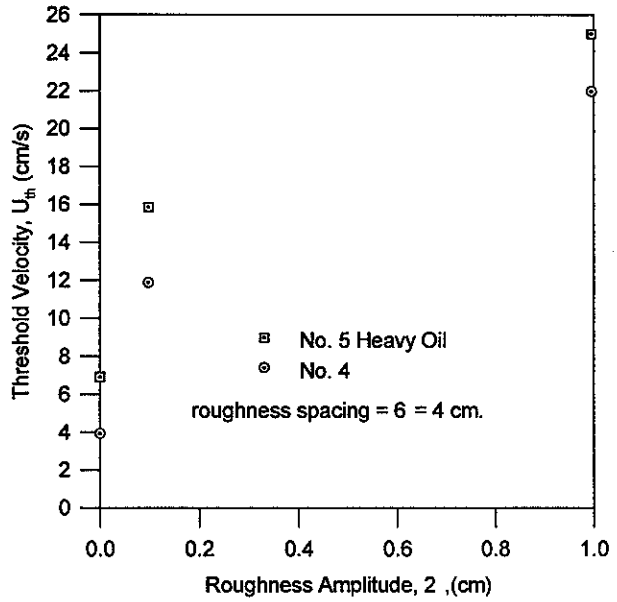

Figure 3. Variation of under ice slick threshold velocity with ice surface roughness.

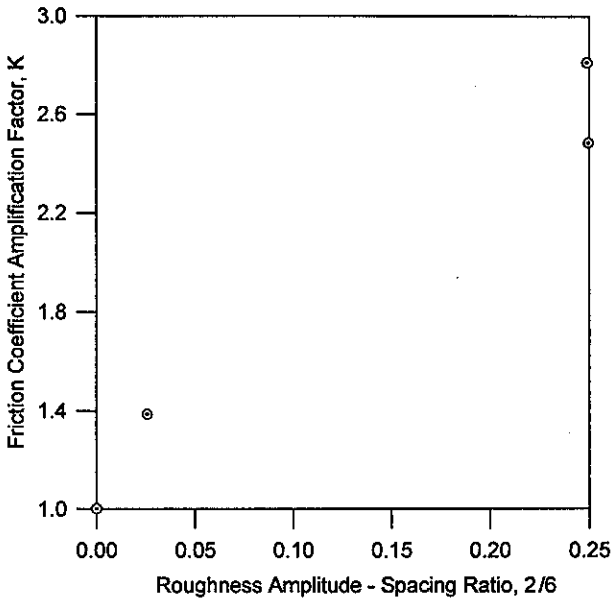

Figure 4. Projection of friction coefficient amplification factor as a function of the roughness amplitude to spacing ratio.

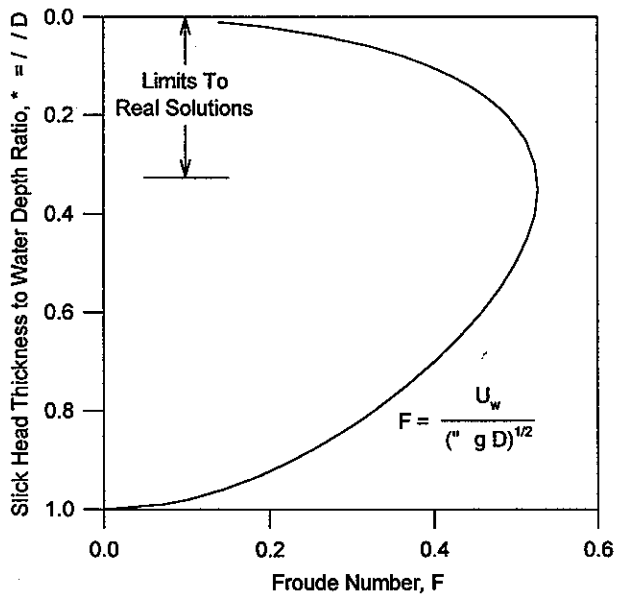

Figure 6. Slick thickness ratio versus free stream densimetric Froude number for large roughness.

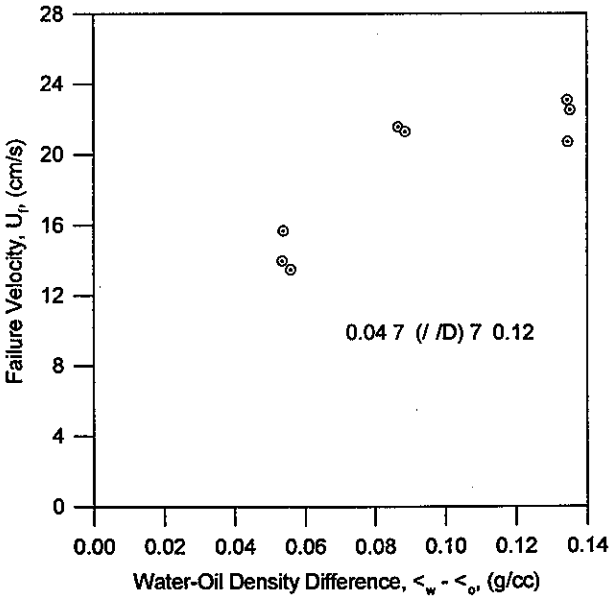

Figure 7. Relationship between failure velocity and water-oil density difference for containment of oil upstream of an obstruction.

In Figure 2 the authors have plotted slick velocity *versus* water velocity and have stated that there are two regimes that the behaviour falls into and these are indicated on the plot with solid lines. The dotted lines are a result of line regression fits to the data and are discussed in the BOSS Critique section.

Figure 3 is a plot of threshold velocity, U_{th}, *versus* roughness amplitude, η, for only a single roughness spacing, λ, of 4 cm and only two oils, No. 5 heavy and No. 4.

Figure 4 is a plot of friction amplification factor, K, versus roughness amplitude - spacing ration, η/λ with no description of how K is measured experimentally.

In Figure 7, the relationship between containment failure velocity and water-oil density difference is plotted for a range of slick thickness to depth ratio (δ/D) of 0.04 to 0.12.

"TEST RESULTS (quoted directly from the third manuscript)

The results of under ice containment of oil by single barrier roughness forms were presented in an earlier paper by Cox and Schultz (1980)."(first manuscript listed in this review) "The present phase of work extended this analysis to examine the containment potential of wakes and cavities created by the flow around rough under-ice features.

Wake Trapping of Oil

The trapping of oil in a wake of a roughness peak was largely studied for relatively high current speeds, generally 20 cm/s or greater. These speeds coincide with typical speeds when barrier trapped oil can fail, feeding oil into the wake. These tests revealed that in this current range the highly erratic flow patterns in the wake prevented a stable slick from forming. During short time periods, on the order of tens of minutes, the downstream end of the captured slick never exceeded 70% of the wake length. In all cases the slick thickness equalled its natural under ice equilibrium thickness except immediately behind the ice roughness where reverse circulation locally thickened the oil layer.

One set of wake trapping tests was run for a current speed below 15 cm/s. In this case containment was more stable with little decrease in the size of the slick with time. Based on this it appears that stability of wake containment may also be controlled by Kelvin Helmholtz instabilities since it can be shown that, for most oils, the failure velocity falls in the 15-20 cm/s range

It, therefore, appears reasonable to expect the length of a slick trapped in a wake to be approximately predicted by:

$$X = 6C_D\eta \qquad (10)$$

The thickness of the trapped slick should be roughly the equilibrium thickness. When local currents are below the failure velocities measured for barrier trapping, long term containment can be expected. When local currents exceed this value, only a quasi-short-term stability of the wake is expected, and in the long-term total flushing of the oil will occur.

Cavity Trapping of Oil

Under ice cavities were created in various lengths and depths to cover a large range in possible flow interactions. Sketches of the transformation of the oil-water interface as a function of current speed and cavity geometry are presented in Figures 6 to 13. A marked depression in the interface is always apparent in the first 50 to 100 cm of the cavity for all current speeds. The half

metre long cavities totally absorb the depression in the interface. The 1 and 2 metre cavities are long enough to allow the shape of the interface to reform further downstream. This depression, or offset, which develops in the position of the interface is caused by vortex sheading from the tip of the upstream ice roughness elements. The non-linear increase in the magnitude of the offset is most apparent in Figure 10, which shows the No. 4 oil in the 20 cm deep cavity. The magnitude of the offset increases as the square of the current speed until the thickness of the oil in the cavity approaches some apparent minimum thickness. This thickness is more stable and harder to remove with further increase in the free stream velocity. The results also show that the less the density of the oil , the smaller is the offset for a given current speed. This implies that a greater volume of lighter density oil can be contained in cavities for much higher velocities than more dense oils .

In order to generalize the predictive relation for the magnitude of the offset as a function of oil properties and current speed, the test results were nondimensionalized into a densimetric Froude Number relationship based on offset size "ϵ_1". Plotted in Figure 14 is the local current speed versus this densimetric Froude Number, $U_w/\sqrt{\Delta g \epsilon_1}$. Allowing for variations in the measured magnitude

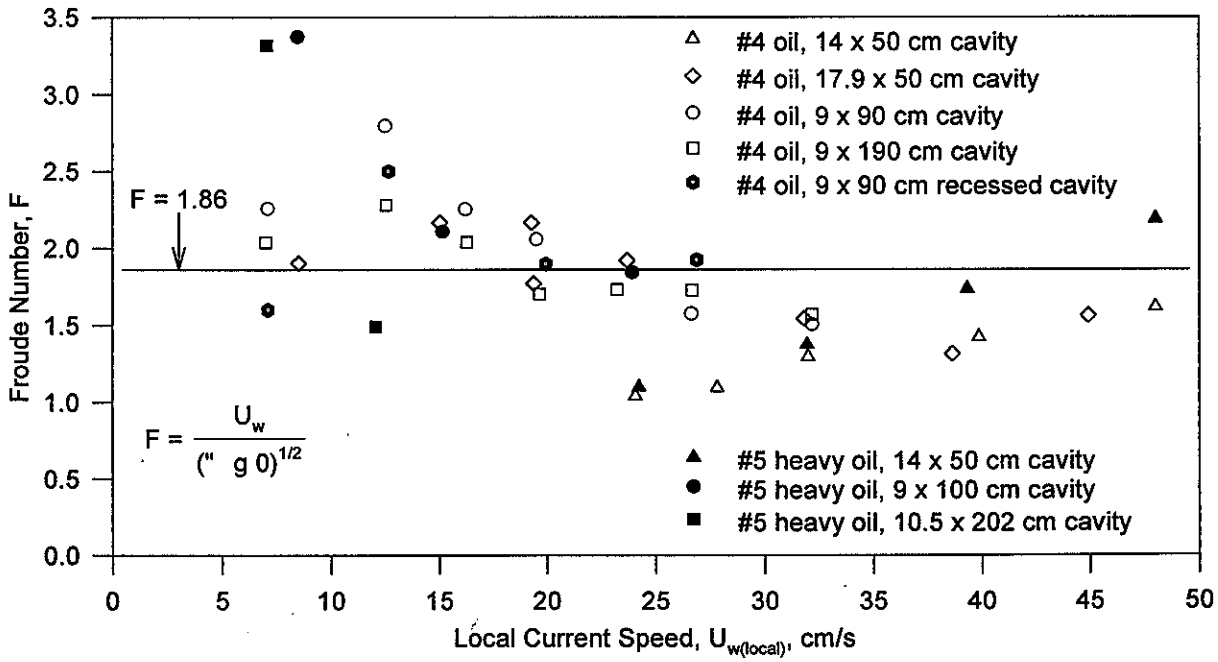

Figure 14 (third manuscript). Densimetric Froude number, based on offset size, vs local current speed for oil trapped in a cavity. Since there were no symbols assigned to the legend captions of the original Figure 14 they were determined from the legend used in Figure 15 and from data listing cavity size and conditions for Figures 6 to 13 which are listed in Table 3.

of the offset due to errors in visually estimating the actual thickness of the slick, Figure 14 suggests that particularly as the current speed increases, the Froude Number is nearly constant, empirically taken to be 1.86. Lower current speeds seem to exhibit somewhat higher values for Froude Number, however, since the Froude Number is based upon the size of the offset, when the offset is small the magnitude of the error in estimating its size has a greater impact on the value of the Froude Number. Fortunately, at low currents the absolute value of the offset is so small that the adverse impact of

small errors in estimating its size is insignificant.

An empirical estimate of offset magnitude is then given as:

$$\epsilon_1 = 0.29 \frac{U_w^2}{\Delta g} \tag{11}$$

The length of the offset vortex zone is plotted in Figure 15 versus local current speed.

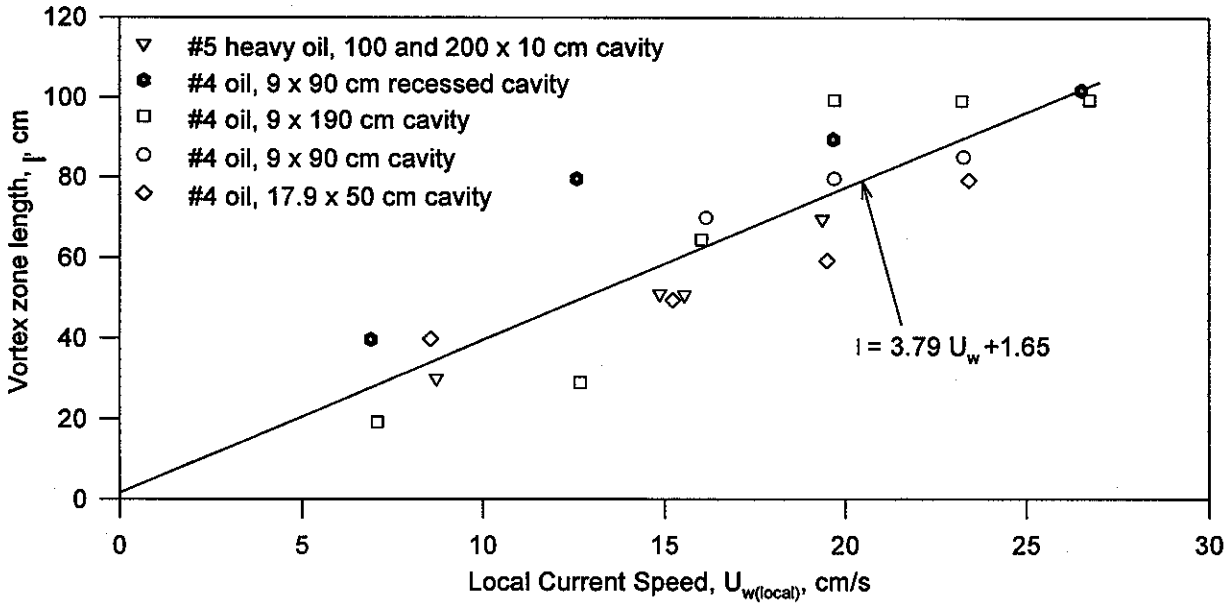

Figure 15 (third manuscript). Vortex zone length versus local current speed for oil trapped in a cavity.

Initially, it was expected that the length of this vortex zone would approach some constant proportional to the offset magnitude. This would be consistent with the general observations of a relationship between wake length and roughness height. However, Figure 15 demonstrates a strong linear relationship between the cell length and current velocity, rather than the squared Froude Number relationship observed in the size of the offset versus velocity. This suggests that, within the range of accuracy of our estimates, the cell length grows linearly with current speed. A least squares analysis of the data gives a relation between cell length and current speed as:

$$l = 3.79 U_w + 1.65 \tag{12}$$

Intuitively the relationship for cell length should go to zero as the current speed goes to zero. A visual curve fit of cell length versus current speed suggests that the cell length could be approximated by:

$$l = 4 U_w \tag{13}$$

The largest cell observed was of the order of 100 cm in length. This value may be a natural limiting length of the cell, or it may be due to the cavity depth limiting the size of the offset that can

develop. The scale of roughness used in these tests would then limit the cell to be not greater than 100 cm in length.

When cavities are short in comparison to the length of the vortex zone, a relatively stable vortex region develops at the mouth of the cavity. Some oil seems to be trapped within the cavity even when current speeds reach 40 cm/s. However, the layer of oil that remains can no longer be predicted by the simple densimetric Froude Number relation proposed for offset magnitude. Once the oil layer becomes comparatively thin, the freestream current is able to "feel" the presence of the ice cover through the oil slick resulting in substantial adjustment in the flow profile. The remaining oil becomes more stable and harder to remove. This is in contrast to the behaviour of a wake at the same current speed. The thickness of this minimum layer cannot be determined with presently available information.

The size of the offset seems to be insensitive to the overall length of the cavity. An offset of the same magnitude will develop for the same current speed in a cavity which just encompasses the vortex zone as in a cavity which includes a vortex zone and a shear zone. This suggests that the two zones act independently, and allows for computation of the captured oil volume for any size cavity. Downstream of the vortex zone in a cavity, a shear region develops analogous to the barrier shear zone. With the No. 4 oil in both the 1 and 2 metre cavities, a very distinct shift in the position of the interface occurs when the freestream reattaches behind the vortex zone. Recognizing that the slope of the interface of the shear zone is relatively flat over long distances, the magnitude of the offset, "ϵ_2", which initiates this region can be estimated. Measurements of the initial shear zone offset "ϵ_2" ranged from 59% to 86% of the vortex zone offset. A conservative estimate for the shear zone offset would be 50% of the vortex offset.

The location of the shear interface is determined by the offset formed in the vortex zone; when the vortex offset grows, the initial shear offset also grows. As the current speed increases, the oil will initially remain attached at the downstream wall, while the interface tilts to accommodate the growth of the offset zone. If the offset grows too large, it becomes no longer possible to maintain the stable parabolic interfacial shape, and substantial amounts of oil drain until the interface can reestablish itself higher in the cavity. For increasing velocity, this procedure will continue until the offset finally penetrates the oil layer and divides the slick at the cavity roof, forming a separate frontal slick and a wake contained slick.

The location of an oil-water interface in a cavity based upon presently available data can, therefore, be defined in terms of two regions. In the vortex zone, the depth of the offset follows the empirical relation

$$\epsilon_1 = \frac{0.29 U_w^2}{\Delta g} \tag{14}$$

and the length of the offset follows an empirical relation:

$$l = 4 U_w \tag{15}$$

The shear zone will develop with an initial offset of:

$$\epsilon_2 = 0.15 \frac{U_w^2}{\Delta g} \tag{16}$$

and continue to grow parabolically to the back wall of the cavity according to:

$$X = 250\frac{\Delta g}{U_w^2}\left(\delta_{tail}^2 - \delta_{stagnation}^2\right) \tag{17}$$

where "$\delta_{stagnation}$" is the oil thickness at "ϵ_2". The tail thickness is controlled by either the depth of the cavity or the magnitude of the offset.

Figure 10 shows the behaviour of the oil-water interface in a pure recess in the ice cover. The offset depth and the shear zone shape appear to be consistent with the test results observed for the protruding type of cavity. However, the vortex zone appears to extend somewhat farther down stream."

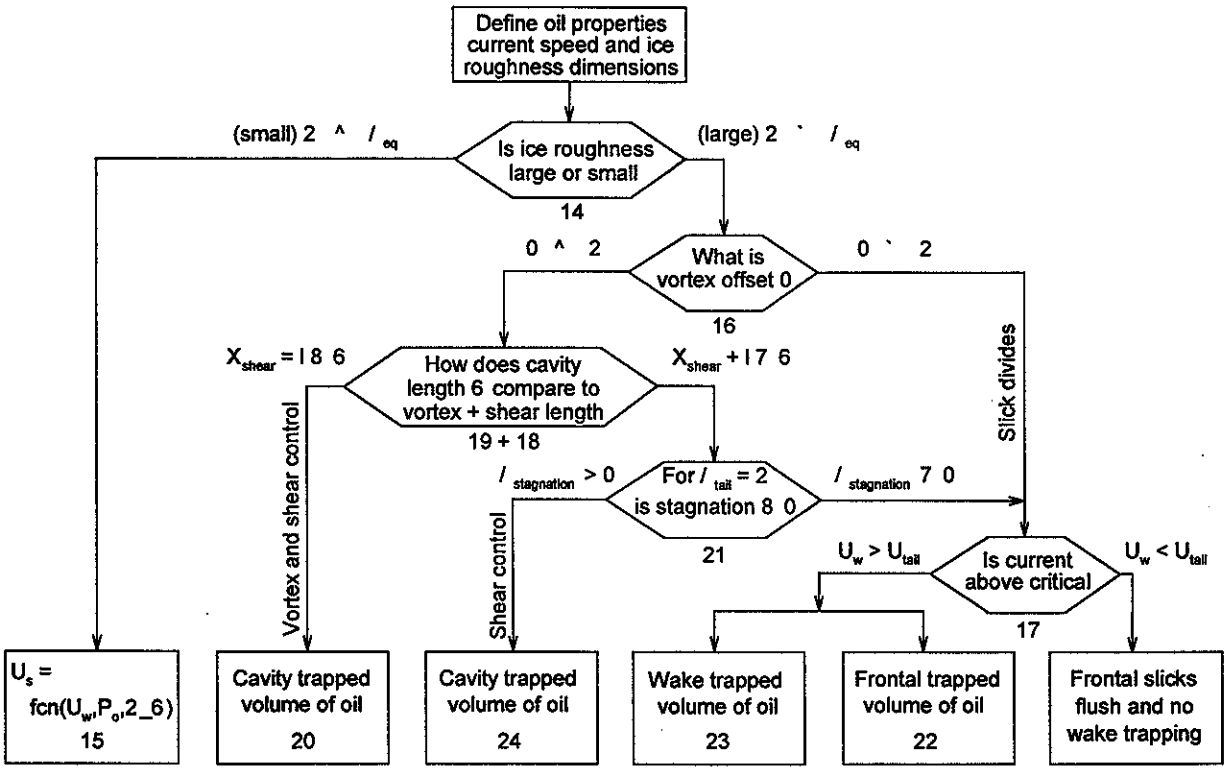

Figure 5 (from the second manuscript). Flow chart of the procedure for calculating the transport or containment of oil beneath ice in the presence of a current. The numbering refers to equations in Table 1 (from the second manuscript) and listed in the theory section of this review.

"Application of Results (quoted directly from the second manuscript)

In order to make the results of this study immediately useful for projecting oil spill behaviour in ice-infested waters, a methodology has been developed for addressing any under-ice spill situation. The confidence level varies for the different oil-ice interaction situations, but an effort was made to assemble the most complete and best available statement of the containment and transport of oil beneath ice in the presence of a current, making reasonable approximations and estimates where more concrete information was not available.

Figure 5 presents in flowchart form the procedure for quantitatively determining the transport or containment of oil beneath ice in deep water. Table 1 summarizes the equations referred to in the

flowchart and Table 2 summarizes the nomenclature and units for the parameters used in the equations. For a given spill, the properties of the oil, the current speed, and the under-ice roughness characteristics are required as input data. The class of ice roughness is then established relative to the smooth ice equilibrium slick thickness given by Equation 14. If the roughness is classed as small roughness, the slick will advance at a speed given by Equation 15. If the roughness is classed as large roughness, the slick has the potential of being trapped or contained by the under-ice roughness. Equation 16 tests to determine whether the roughness elements can form a cavity, or simply act as individual barriers or obstructions. If the offset of the oil-water interface as calculated by Equation 16 is greater than or equal to the local roughness height, the slick will divide and the roughness elements act as individual barriers. The containment of oil by a barrier will be possible if the local current is below the critical value which causes an instability to develop at the oil-water interface. This criteria is given by Equation 17. If the current is below the critical value, the volume of oil trapped in front of, and behind, the barrier can be computed using Equations 22 and 23. If the current is above the critical value, complete flushing of the oil will occur beneath the barrier and no oil will be contained. In this case, envisioned as a small roughness ice field with occasional large roughness elements present, the advance of the slick will largely be controlled by its transport beneath the surrounding small roughness ice, and the speed of advance can be approximated by using Equation 15.

If the offset as determined by Equation 16 is less than the local roughness height, the volume of oil trapped in the cavity is dependent on the cavity length. If the cavity length is less than the combined length of the calculated slick shear length and vortex length as defined by Equations 18 and 19, the volume of contained oil can be calculated from Equation 20.

If the cavity length exceeds the sum of the calculated shear and vortex lengths, the slick may completely divide, or it may equilibrate to some intermediate position. If the curvature of the interface causes the shear zone to neck down to zero somewhere in the cavity, as determined by Equation 21, the slick will divide and the cavity transforms to simple individual barriers with the corresponding containment potential determined as previously described through the use of Equations 17, 22, and 23. If the shear zone thickness as determined by Equation 21 does not dissipate to zero, the entire cavity will fall under the influence of the shear zone and the trapped volume can be estimated by projecting the shear zone interface back through the vortex zone to the front wall of the cavity as given by Equation 24."

BOSS Critique

The authors have stated that the experimental work was carried out using a flume with glass walls. Thus the authors could observe the oil-water interaction and several different cases were presented in the manuscript with the ice-oil-water profiles drawn in schematic representative form. However, the authors do not explain how this interaction was quantified. The authors do not mention how these profiles were measured or digitised in order that the information could be drawn graphically in the report. If the glass wall of the flume had a scale marked out on it and the experiments were photographed or video equipment had been used to capture the oil and water movement then an analysis could have been performed on the still images. The authors have not given detailed information on the errors involved in the experiments and the errors involved in the analysis. The errors will not necessarily scale in the same manner as the data.

The manuscripts reviewed here did not discuss how the velocity of the water or oil was measured in the glass walled tank. There is also no mention of the error of this measurement. These may have been discussed in another publication but no reference was given. There is not a complete discussion of what exactly is meant by the term threshold velocity. The implication is that U_{th}, the term used for threshold velocity, is the velocity of the water at which the oil just starts to move. However, there is no explanation of how the threshold velocity is determined. The authors do not explain to the reader what the physical significance is for the selection of the number 305.79 and the number 88.68 in the equation stated in Figure 1. The selection of these numbers provides a line that is an extremely good fit to the few data points that are plotted. However, an equation with out a physical explanation for the terms chosen does not allow the experimenter to fully utilize the strengths of the scientific method.

The authors have presented measured data in Figure 2 to relate the slick velocity, U_s, to the water velocity, U_w, for two regimes of behaviour. The authors do not explain why they believe that a water velocity of 18 cm/s is the transition point between the two regimes of behaviour. As can be seen in the recreated Figure 2, the regression curve for the data obtained at relatively slow velocities is similar to the curve presented by the authors. However, the regression curve for the data at higher velocities is dissimilar to the line drawn by the authors. The authors do not explain their choice of slope for the second curve except to say that is was the best fit to the data. The extension of the two lines in the authors Figure 2 results in their intersection at approximately 18 cm/s (actually happened at 17.6 cm/s). This same reasoning could be used to extend the new (dotted) lines and then the change over (intersection) would occur at 15.6 cm/s and this would be rounded up to 16 cm/s.

The authors had two smooth curves not straight lines, drawn between the data points presented in Figure 3. They did not give an equation for the smooth curve nor did they explain the motivation for drawing the smooth curves to relate threshold velocity to roughness amplitude, η.

This lack of explanation is also extended to the data presented in Figure 4, where the authors related friction coefficient, K, to roughness amplitude ratio, η/λ. The smooth curve in Figure 4 is placed half way between the two final data points with no reference to the physical significance of the smooth curve and no equation for the smooth curve. The authors do not explain or otherwise inform the reader how K was determined from the experiments that are discussed in the manuscripts reviewed in this work.

Equation (1) is not explained in detail and the implication from the manuscripts is that this is an expected results from the containment reference. The equation has four roots that result in real values for F^2, which are $\Psi = 0, +1$, and $+2$ and the root $\Psi = -1$, results in $F^2 = \infty$. Notice that in

Figure 6, the authors only plot F values for Ψ between 0 and 1. This is expected since these are the only roots that result in real values of F, while any $\Psi > 1$ results in F = imaginary number as will any $\Psi < 0$. While this does explain why data for only Ψ values between 0 and 1 were plotted in Figure 6, it does not explain their choice of equation (1) .

In the second and third manuscripts the authors have taken the results of the ice obstruction experiments and developed a set of equations to be used to determine the out come of oil spilled under ice. This is shown in the flowchart in Figure 5 (from the second manuscript). The equations are based upon oil parameters and current speed, however no results are shown comparing flowchart results and an actual oil spill or even a comparison to their laboratory results.

Table 3 is a listing of the parameters as they were presented in Figures 6 to 13, of manuscript three, however there are differences in the text of the third manuscript and the description in the Figures. In the manuscript a cavity may be described as being only 190 cm in length but the annotation in the figure would state that the cavity was 200 cm. This is confusing and makes it difficult to relate the data for the different manuscripts. It is, however, quite evident that the data was the same for the different manuscripts just not discussed in a clear manner.

The authors have stated that an empirical estimate allowed them to determine an offset magnitude (equations (11) or (14)), as well as cell length of l (equations 13 and 15). However, the shear zone was determined by the authors to have an initial offset approximately one-half of the vortex zone offset. The authors do not explain the physical reason for this difference.

In Figure 14 the authors have drawn a straight line (F = 1.86) for a constant Froude Number. The data has a large scatter about this straight line with the Froude Number for the lower velocity cases having the largest scatter. The data assigned with solid circles seems to have an exponential decay while the data labelled with solid triangles would appear to follow a linear relationship with a slope other than 1 and a slightly positive intercept. The straight line drawn by the authors implies that there is no dependence of the Froude number on velocity of the local current. None of the data sets, taken individually, follow this rule. If the authors had provided the reader with errors associated with the measurements of local current speed and offset parameter ϵ, these could perhaps be used to explain the scatter in the data.

A linear regression analysis of the data in Figure 15 resulted in an equation with an intercept of 2.74 instead of 1.65 and a slope of 3.73 instead of 3.79. This results in a line very similar to the line shown in Figure 15. There is a rather large scatter in the data, however, several of the data sets do exhibit a some what linear behaviour.

Review of a manuscript by Cammaert, A.B., entitled *Oil and Gas Under Ice Laboratory Study*. Acres Consulting Services for Canadian Marine Drilling Limited and Canada Environmental Protection Service (sponsors), Beaufort E.I.S. reference work, No. RWC17, 1980.

Technical Summary

"From the short series of tests performed it can be concluded that the spreading of oil under an ice cover, when released in the presence of gas, depends on the effective configuration of the underside of the ice cover. The volume of gas and undulation geometry combine to determine the behavior of the oil slick on the gas/water interface.

For the meter-long undulations tested, if the gas volume is small or the undulation depth is large enough that the gas/water interface is more than about 5 cm above the bottom of the undulation or lower ice surface, the oil slick seems to be protected from the flow. The only effect on the oil slick at velocities as high as 44 cm/s was herding or migration of the oil slick to the downstream limit of the gas/water interface below the gas pocket.

However, when the ice extended only 1.5 cm below the gas/water interface, the oil slick was forced out of the undulation at a flow velocity of 44 cm/s and migrated under the ice cover. When the ice cover extended 0.5 cm below the gas/water interface, a flow velocity of 25 cm/s was required to force the oil out of the undulation. (It should be noted that the size of the ice lip was difficult to observe under a fluctuating water level.)

A relationship between flow velocity and depth of ice below the gas/water interface can not be determined for the limited amount of data available and it is suspected that the slope and wave length of the undulation is equally important. Further investigation should be directed toward the configuration of the contact point between the gas pocket, water level and ice cover to determine the effect of the depth and angle of the depression that the oil must descend to be forced from the undulation at a given flow velocity.

Similarity to previous studies of oil containment at fixed barriers or in slots cut in an ice cover are evident. Movement of oil slicks and droplets under the ice cover suggest comparison to various sediment transport theories, with further observations, theories to predict oil movement under undulating ice covers could be formulated.

It appears that it is very difficult to dislodge oil from under a broken ice cover, unless sufficient air volumes are present or the flow is turbulent enough."

Objective

"- To determine the influence of currents on oil herding within depressions and under broken sea ice.
- To determine the influence of currents on oil migration between depressions and

under broken sea ice."

The tests done in this work were also done to include gas with the oil and air was used in place of natural gas for safety sake.

Method

"Testing was carried out in the Acres' ice flume facility. The flume is a self-contained recirculating system measuring 12 m long, 1.2 m high and 1.2 m wide. The flume and recirculating line are fully insulated with 10 cm of styrofoam. One wall incorporates a 5.5 m length of acrylic windows behind hinged insulation panels, allowing visual inspection of test events. Bottom windows were installed to permit viewing and photographic lighting. A vinyl liner was installed to prevent leakage and fouling of flume walls with oil. (see Plate 1, not included in this review).

A variable-speed pump provides continuous flow from 0 to 0.3 m^3/s. Velocities under the ice cover were measured with a miniature flow meter. The ice cover was formed by circulation of air at a minimum temperature of -20°C at a velocity of 7.4 m/s over the water or ice surface. Air was cooled by a conventional 21 kW refrigeration system.

Air and water temperatures were monitored throughout the ice cover formation and testing period using sensing probes (thermistors) containing high purity nickel foil sensors with resistance proportional to temperature.

TEST PROCEDURE

The flume was filled with water to a depth of 0.6 m and a sufficient quantity of salt was added to the fresh water to bring the salinity to 32 pro mille. The water was cooled to the freezing point (approximately -2°C) over a period of two days. The miniature flowmeter was frozen in place in preparation for the test runs. Thickness measurement scales were frozen in the cover at half-meter intervals along the length of the flume to measure ice thicknesses at undulation crests and troughs. At the same time insulated 20 cm diameter gas/oil injection ports were frozen in the cover at the trough locations.

Undulations were formed by placing 2.5 cm thick sheets of rigid polyurethane insulation on the crest areas of the undulations, halting the growth of the ice cover at the desired thickness. The uninsulated trough areas of the cover were allowed to continue growing until the desired undulation shape had been attained. Undulation wave lengths were 1 m long for the 15 cm deep undulations and 1.5 m long for the 7.5 cm and 2 cm deep undulations.

Plexiglas panels were placed in the ice cover parallel to the flume sides, and separated from the flow walls to contain gas/oil volumes in the undulations. A poor freezing bond between the salt ice cover and the vinyl liner allowing gas and oil to escape made this measure necessary.

An air piston and curved delivery tube was used to release air through the injection ports directly below the center of the depressions in the ice cover. After the desired volume of gas (air was substituted for natural gas for safety purposes) was placed in the depression under the cover, the required volume of oil was added (proportional to the volume of gas) by gravity feed through the

curved delivery tube. The spreading and interaction of the oil and gas were observed under static conditions, and the oil was allowed to cool.

The flow was gradually increased in steps. The flow was allowed to stabilize at each step and the behavior of the oil and gas was observed. Tests were performed for gas/oil ratios of 150:1 and 15:1. Undulation amplitudes tested were 15 cm, 7.5 cm and 2 cm. Some difficulty was experienced in creating the exact undulation depths specified in the contract. The undulations tested were close enough to the specifications that no adverse effects on test results were anticipated. Spatial variation in the cover growth made 2 cm undulations over a 1 m wave length very difficult to achieve, so that only one 2 cm undulation was tested. Only one 6 cm depression was formed and used for several tests.

Similar tests were performed for a broken cover with varying degrees of reconsolidation. The cover was cut into blocks of varying sizes and partially refrozen. For those tests, the gas and oil were injected under the broken area of the ice cover and the rise of the gas and oil between the blocks of ice was observed. The flow was increased in steps to produce a final velocity greater than 30 cm/s (see Table 1). At each step, movement of the gas and oil was observed.

Table 1. Conversion Table for Water Velocities

cm/s	ft/s	mi/h	knots
5	0.16	0.11	0.1
10	0.33	0.22	0.19
15	0.49	0.33	0.29
20	0.65	0.45	0.39
25	0.82	0.56	0.49
30	0.98	0.67	0.58
35	1.15	0.78	0.68
40	1.31	0.89	0.78
45	1.48	1.01	0.88

The tests were completed in a slightly different a sequence from that originally planned. Two different ice covers were used, and the first series of tests on the smaller undulations did not meet with success because of the problems of gas leakage. Hence, these tests were repeated on the second ice cover, after the broken cover tests. The following is a summary of the tests completed. The remaining sections of the report deal with detailed test observations and conclusions.

Test 1

Gas and oil were injected into the 15 cm undulation at a gas/oil ratio of 150:1. Following the

injection of 9 L of air, 60 ml of oil was injected. The undulation was approximately one-third full.

Test 2
Gas and oil were injected at a gas/oil ratio of 150:1 into a second 15 cm undulation located upstream of the undulation used in Test 1. A considerably larger volume of gas was injected in the depression (12 L of air with 80 ml of oil). Initially the air/water interface was at approximately two-thirds of the undulation depth.

Test 3
Additional oil (540 ml) was added to the 15 cm undulation used in Test 1 to bring the gas/oil ratio to 15:1 with the undulation half full. The oil slick covered the bottom of the gas pocket, but the slick thickness was less than 0.5 cm. Tests 2 and 3 were then run simultaneously.

Test 4
A section of ice cover measuring 1.25 m long (in the downstream direction) and 0.75 m wide was cut into blocks varying in size from 10 cm to 20 cm square on the surface. The ice cover thickness was approximately 15 cm. The blocks were replaced and orientated to create a rough under-surface with deep projections and crevices between blocks. Accumulated slush from the cutting operation resulted in a blanket of slush several centimeters thick between the blocks of ice. The cover was allowed to refreeze for 45 minutes prior to the test. The slush between blocks had begun to set and a thin layer of ice had formed. The cover had no strength and could easily be deflected with a gentle push.

Using the air piston and curved delivery tube, approximately 9 L of air were released under the ice cover. The air rose to the underside of the cover into the spaces between the blocks. Directly above the injection point, an irregular hole was broken in the cover between ice blocks. The majority of the air released was assumed to have escaped through the hole in the ice. The oil injected under the ice (60 ml for a gas/oil ratio of 150.-l) surfaced in the hole in the cover as well. An additional 100 ml of oil were injected and rose into the depressions between blocks or into the hole in the cover. Some of the oil was unintentionally injected under the smooth areas of the ice cover outside of the test area.

Test 5
A section of ice cover measuring 1.25 m long and 0.75 m wide was cut into blocks as in Test 4 and allowed to refreeze for 5 hours. The cover was very hard and strong. A total volume of 20 L of air was injected under the ice cover, and a corresponding volume of oil(135 ml) was injected for a gas/oil ratio of 150:1.

Test 6
A 7.5 cm undulation was formed by cutting out strips of ice across the flume and refreezing thinner strips of ice in place. After the undulation had refrozen smoothly, 10 L of air and 65 ml of oil were injected under the cover so that the cover was initially half full of air and oil with no flow.

Test 7

Air was vented and the test was repeated with holes in the cover upstream to prevent entrainment of air in the headbox from ruining the test. The slot was filled two-thirds full with 30 L of air and 200 ml of additional oil.

Test 8
A 2 cm undulation was filled with 15 L of air and 100 ml of oil to make it half-full."

Results
"TEST 1
When the oil was being injected it rose from the tip of the injection system at the bottom of the flume near a series of pinched off jets (pinched off in the form of pendent drops). The pendent drops were characteristically approximately 1 cm or 2 cm in diameter at the most, and they rose to the undersurface of the ice as a series of drops under the action of buoyant forces. The drops would impact on the ice surface and bounce and deform slightly, gradually roll up the underside of the curved ice surface to meet the air/water interface at the bottom of the air pocket. The amount of oil injected was not large (60 ml) and the oil pool collected at the upstream end of the air/water interface in the undulation. After the oil was injected the pump was turned on and the velocity increased gradually.

As the flow increased to 14 cm/s, the oil began to migrate across the undulation. At 18 cm/s, most of the oil had been herded against the downstream edge of the gas pocket under the ice. At 30 cm/s, it was observed that at a significantly high velocity of water flow under the pocket, the oil slick gradually circulated within the air/water interface, but the oil motion was not particularly rapid; no oil drops were broken off from the oil slick and swept downstream in the high currents flows and, in fact, no motion of the air within the pocket or waves on the air/water interface were observed whatsoever.

TEST 2
At a flow velocity of 14 cm/s, the oil slick started to migrate to the downstream edge of the gas pocket in the undulation. As the flow was increased in steps beyond 24 cm/s, the oil was definitely herded against the downstream edge of the undulation. At 27 cm/s, the slick began to thicken. At 28 cm/s, fine air bubbles were visible in the flow indicating entrainment of air in the flume headbox. At a flow of 30 cm/s, the slick thickened against the downstream edge of the gas pocket against the ice. Air entrained in the flow began filling the undulation. With approximately 2 cm of ice below the gas/water interface, the slick was forced out of the undulation. When the slick had been forced out of the undulation, rippling of the oil/water interface and shedding of oil droplets from the slick were observed. The slick elongated and droplets of oil were broken off. The oil moved slowly and erratically under the rough ice cover. The oil seemed to alternately stick to the rough ice surface and break free.

TEST 3
As the flow was increased to 30 cm/s, no reaction to the flow was observed beyond migration of oil downstream and slight thickening of the oil slick. Undoubtedly, the oil slick was protected from the

high flows by the depth of the undulation below the gas/water interface.

TEST 4

Most of the oil and gas rose into the spaces between ice blocks, and could not be seen. Some oil droplets that adhered to the underside of the projecting ice blocks could be observed.

After the static behavior of the gas and oil injection was observed, the flow under the cover was started. When the velocity reached 6 cm/s, the oil droplets adhering to the underside of the ice cover began to vibrate or oscillate with the flow. At 12 cm/s, one "blob" of oil was displaced and rose up between the blocks into the hole in the cover. Movement of gas and oil bubbles continued up to 16 cm/s. At that point, most of the gas and oil had been moved from the underside of the cover into the spaces between ice blocks. Air entrained into the flow in the headbox was observed moving under the ice. No significant changes were observed until the velocity reached 28 cm/s. An oil 'blob" under the ice near the hole in the cover slowly migrated toward the hole, eventually joining the slick of oil on the water surface. Pockets of oil visible under the ice surface were growing noticeably larger and oil was slowly seeping upward to the surface through the soft slush ice cover. Air entrainment into the flow in the headbox was more pronounced and the pockets in the underside of the cover began to fill with air. A minor quantity of entrainment of gas and oil from under the broken up area back into the flow was suspected. Bubbles of air surfaced at the hole in the ice cover. Under the smooth cover outside of the broken up test area, gas and oil were observed moving under the ice. As the flow was increased to 34 cm/s, more air was entrained into the flow at the headbox. This air moved downstream into the test area enlarging the hole in the ice cover as it escaped. Large quantities of air were observer surfacing in the oil recovery slot which had been cut in the cover downstream from the test area.

After the test was completed, the cover was found to be very weakly consolidated.

Most of the oil was trapped in the slushy ice between blocks and was not carried away with the flow. When the thin film of ice on the surface was broken, the oil contained in the slush ice seeped to the surface. Blocks of ice which were overturned were coated with oil. It can be concluded that no significant amount of oil was carried away by the flow.

Examination of the cover on the following day after 15 hours of freezing showed that the cover was frozen through completely (approximately 15 cm thick). Oil pockets were frozen into the cover but oil at the surface remained unfrozen.

TEST 5

Most of the gas and oil rose up into crevaces or depressions between blocks and could not be observed.

At a velocity of 6 cm/s, some oil on the underside of the ice cover outside of the test section moved in a series of short steps. At 9 cm/s, several small droplets and one large droplet which were clinging to the lower projections of the ice cover, broke free and rose up into the depressions under the cover. At 14 cm/s, small air pockets (approximately 5 cm diameter) were observed moving under the

smooth ice cover outside the test area. At 15 cm/s the gas and oil clinging to the projections under the ice cover began to vibrate. A significant increase in the number of droplets detaching from the ice and drifting up into depressions occurred at 18 cm/s. As the flow increased above 25 cm/s, increasing numbers of oil droplets were swept from the ice projections up into the holes in the cover. Larger air pockets (5 cm by 10 cm) from air entrained into the flow in the headbox were observed migrating downstream under smooth sections of the cover. At 27 cm/s the oil droplets were moving under the cover, alternately coalescing and shedding droplets from the downstream end of larger slicks. At 30 cm/s small oil drops (2 mm diameter) and gas bubbles were entrained in the flow from under the broken up area, rising and falling out of the depressions. At the final flow of 38 cm/s, great quantities of air entrained in the flow through the headbox moved under the cover, filling the depressions and floating the oil downstream out of the broken up area. Air and oil were carried into the containment slot cut in the cover downstream from the test area. The oil was contained in the cut slot.

Under static conditions following the test, the cover was examined to characterize the undersurface. As a section of the cover was cut out, air vented from the depressions. A large volume of oil remained under the cover in spite of the amount of air from the flow which filled the depressions and swept oil downstream. The cover was found to be frozen half to two-thirds through (7 - 8 cm). The blocks were 13 - 14 cm deep with crevaces 5 - 6 cm deep. Outside of the broken section the ice thickness was 18 cm which would have held the air in the broken area until the depressions were full. In conclusion, although the depressions were full of air not all the oil was removed.

TEST 6

The oil formed a thin, patchy slick and did not spread to cover the entire air/water interface. Some oil was observed on the meniscus at the air/water/ice contact point.

At a flow of 9 cm/s, some disturbance of the air/oil/water interface was observed. At 15 cm/s some herding of oil downstream in the depression was observed but no thickening of the oil was evident. At 21 cm/s more herding of oil without thickening of the slick was observed. The test was abandoned due to air from the flow entering the undulation and creating large interfacial waves which carried fine bubbles of oil down into the flow. Oil coated the underside of the depression.

TEST 7

The flow was increased in steps to 18 cm/s, at which point, significant herding of smaller slicks to form one large slick at the downstream edge of the depression occurred. The slick thickened to form a 7.5 mm thick lens. At 25 cm/s, a steady supply of air from upstream entered the undulation and was vented to maintain an air pocket thickness of 6 cm, leaving a 1.5 cm depth of ice (to the trough of the undulation) below the lower level of the air. The slick rotated to align itself against the downstream edge of the air/water/ice contact. At 30 cm/s no significant change had occurred. At 44 cm/s, 1 mm diameter oil droplets were entrained in the flow. Turbulence and entrained air made observation difficult but it was felt that most of the oil had been removed. A considerable amount still remained, coating ice and Plexiglas surfaces.

TEST 8

The slick configuration was as observed before; randomly distributed thin patches of oil.

At a flow of 12 cm/s some herding of oil was observed at the downstream end of the shallow depression. Herding was more evident at 18 cm/s, but the oil was still contained in the depression. At 21 cm/s, a droplet of oil was sheared away from the downstream edge of the main slick of oil which was starting to flow slowly under the ice out of the air filled part of the undulation. At 23 cm/s, the shedding of droplets from the main slick was more pronounced. At 25 cm/s the major portion of the patch had moved out of the air filled undulation under the ice at a velocity of 0.5 cm/s and was elongating and breaking up under the shearing action of the flow. At 30 cm/s, interfacial waves on the oil slick were observed and shedding of 2 cm diameter droplets (larger than the previously observed droplets) was observed. The slick was 0.5 - 1 cm thick. More air had collected in the undulation leaving a 0.5 cm depth of ice below the air in the undulation."

BOSS Critique

The report, when originally released, was released with a video tape (Beta format) which is not available for general release and was not included in this review. This tape may provide much needed depth to the report. There is no discussion of errors for the measurements that were done with the flow meter nor for the measurements done with the thermistors. The authors do not explain the error for determining the size of oil droplets in the moving water nor the error of slick thickness determination. An analysis of the video tape may have provided the author with a rate of mixing of the oil in the water under the extreme circumstances when the velocity of the current caused the circulation of the air/water interface as in Test 1 and Test 7 for example.

Review of a manuscript by Malcolm, J.D. and A.B. Cammaert, "Transport and Deposition of Oil and Gas Under Sea Ice", in *Proceedings of the Fourth Arctic Marine Oilspill Program*, Environment Canada, Ottawa, pp 45-73, 1981.

Another manuscript with the same information is:

Malcolm, J.D., and A.B. Cammaert., entitled "Movement of Oil and Gas Spills Under Sea Ice", in *Proceedings, POAC 81: Sixth International Conference on Port and Ocean Engineering under Arctic Conditions*, Quebec, pp 923-936, 1981.

Technical Summary

"Laboratory and analytical investigations have increased our knowledge of some of the physical processes involved in the event of an oil well blowout under ice. In particular, mechanisms controlling spill thickness and mobility have been studied. The presence of gas in the well blowout products is shown to greatly change the nature of the spill and the mechanisms controlling its spread beneath ice.

In the event of a well blowout under Arctic ice, there is evidence that the blowout produces will have spread out under the ice rather that fracture it. Laboratory studies re ported in this paper indicate that gas will fill the under-ice undulations near the blowout zone, probably creating a continuous gas/water interface for the oil to spread on in the form of thin lenses. At a greater distance from the blowout, the gas bubble will be fragmented and oil and gas will become trapped in the ice cover undulations. In this region the oil lenses will be partially protected from currents by the ice keels below the gas/water line in each undulation.

Future studies directed toward understanding the blowout generated currents, and the action of a continuously discharged oil and gas mixture under rough ice are recommended. Only when detailed topographic mapping of the local under-ice surface, together with detailed knowledge of local currents, becomes available for a particular well site, then forecasting of the areal extent and ultimate deposition of well blowout products may become viable."

Objective

The authors objective was to report laboratory studies done on the relative motion of oil well blowout products.

Theory

"In general, if the flattened spherical shape of most drops is truncated at some angle of contact with the solid which supports the drop, and the contact angle could be in the range of 0 to 180 degrees, depending on the surface. In the case of crude oil under ice, water which separates the oil drop from the ice, ensuring an effective contact angle of 180 degrees as reported by Malcom and Dutton ("Interfacial Tension and Contact Angle of Crude Oil Under Ice", *Proceedings, 5th International Conf. Port and Ocean Engineering Under Arctic Conditions*, Vol.1, p 771, 1979).

Solution by computer of the nonlinear ordinary differential equation which governs the shape of all axisymmetric interfaces illustrates that as oil is added to the drop, the drop thickness increases

to a maximum value, 'H_{max}', and that additional volume causes a subsequent decrease in thickness toward a limiting thickness, 'H_L', for drops of infinite volume. Relation for drop thickness when contact angle is 180° are:

$$H_{max} = 2.12953\,(\sigma/\rho g)^{1/2} \quad (1)$$

$$H_L = 2.0 \quad (\sigma/\rho g)^{1/2} \quad (2)$$

where σ = interfacial tension

ρ = density difference between oil and water; and

g = gravitational acceleration.

Density measurements of oil and water are quite routine compared to measurements of interfacial tension, which is known to vary with temperature, chemical impurities and even electric charge. A tenfold variation in 'σ' for crude oil in water has been reported (Rosenegger, "The Movement of Oil Under Sea Ice", *Beaufort Sea Tech. Rep. No. 28*, Dept. of the Environment, 1975), and criticized (Malcom and Dutton, as above, 1979). Our own work suggests a more modest range for crude oils in seawater from 10 to 30 dynes/cm. Substituting seawater for freshwater can change interfacial tension of the oil/water system as well as change the density difference.

Table 1 shows the results of oil pool thickness calculations using equations (1) and (2) for two crude oils in seawater. The heavy oil is assumed to be API gravity 25 and the light API gravity 45. In these terms, oil from Hibernia is light, and Prudhoe Bay crude is heavy.

The importance of the interfacial tension on pool thickness is apparent from Table 1. The variability of 'σ' for a particular crude oil/water system can be quite large, so in situ measurement techniques have been developed, which are based on measurements of drop height and diameter (Malcolm and Elliot, "Interfacial Tension from Height and Diameter of a Single Sessile Drop or Captive Bubble", *Can. Journal of Chem. Eng.*, **58**, 151, 1980; Malcolm and Paynter, "Simultaneous Determination of Contact Angle and Interfacial Tension from Sessile Drop Measurements", *Journal of Colloid and Interface Science*, 1981).

Table 1. Pool Thickness of Crude Oils in Seawater (SG 1.025)

	H_{max}, (mm)		H_L, (mm)	
σ dynes/cm	Heavy	Light	Heavy	Light
10	6.14	4.51	5.81	4.27
15	7.52	5.53	7.12	5.24
20	8.68	6.38	8.22	6.04
25	9.70	7.14	9.19	6.76
30	10.63	7.82	10.06	7.40

The assumption made by Cox and Schultz (1980) that the surface tension of all crude oils is constant, is a needless oversimplification. Their empirically derived linear relationship between fluid densities and pool thickness has no physical validity.

INTERACTION OF THE ICE SHEET FEATURES WITH AN OIL POOL

Equations (1) and (2) give the upper and lower bounds on large oil pool thickness beneath a smooth horizontal ice sheet in water. The interaction of an ice sheet depression or keel with an oil pool is illustrated in Figure 2.

Figure 2 (a) shows the cross section of a pool of oil, volume 'V_O' under smooth ice in water. Small depressions in the horizontal ice sheet (Figure 2 (b)), will contain oil which displaces the denser water from the depression. If the depression volume 'V_D' is less than the available oil volume 'V_O', the oil pool thickness of the overflow remains unchanged, but of course, the pool diameter is smaller. When the ice depression volume exceeds the available oil volume, the oil becomes lodged in the upper portion of the depression (Figure 2(c)). Small protrusions of ice beneath the horizontal plane do not affect the pool thickness either (Figure 2 (d, e)). Ice projections with thickness exceeding 'H_L' will form ice islands which push the pool aside, but do not affect the pool thickness (Figure 2 (e)).

Narrow depressions in the ice surface such as brine drainage channels may not become filled with oil for a considerable time, due to oil viscosity and capillarity effects which may partially block the drainage of brine past the buoyant oil plug.

THE SHAPE OF A LARGE OIL POOL UNDER ICE

We commonly classify drops as being axisymmetric; that is, they appear circular when viewed along a vertical line, whereas a pool is large and almost never circular in appearance. The transition from drop to pool occurs where the thickness is near the maximum value, for at 'H_{max}', the radius of curvature 'b', at the drop apex is :

$$b = 37.86(\sigma/\rho g)^{1/2} \qquad (3)$$

and 'b' increases to infinity as pool thickness approaches 'H_L', signifying a perfectly flat apex region. The bending strength of the interface in the region of the drop apex diminishes to a minimum as the interface flattens. The tension of the interface remains constant as the interface area increases. Thus a large pool is free to assume any shape convenient to the local solid surface topography which supports it. In the case of an oil pool under ice, the shape of the pool will depend on the location and size of ice undulations, whose amplitude and wave length only need to be of the order of the pool thickness to produce large distortions from the circular shape, for example, the formation of rivulets, as reported in the study by NORCOR ("The Interaction of Crude Oil with Arctic Sea Ice", *Beaufort Sea Tech. Rep. No. 27*, Dept. of the Environment, Victoria, B.C., 1975).

OIL MOBILITY UNDER ICE

The mobility of spilled oil beneath ice is an important consideration for those attempting to monitor, control or clean up the oil. Topham ("Hydrodynamics of an Oil Well Blowout", *Beaufort Sea Tech. Rep. No. 33*, Dept. of the Environment, Victoria, B.C., , 1975) estimates that a blowout in 60 m depth could create a plume of oil and gas with vertical velocities of 70 cm/s. Ocean currents of 45 cm/s have been observed and velocities of 15 to 30 cm/s are common. The hydrophilic nature of ice which ensures a thin film of water between the oil and the ice could create a film bearing for the oil, allowing it to slide along the bottom surface of the ice leaving no tracks behind. Large pools as well as individual drops would be swept along under the ice until blocked by ice topographic features which were large enough to contain the oil.

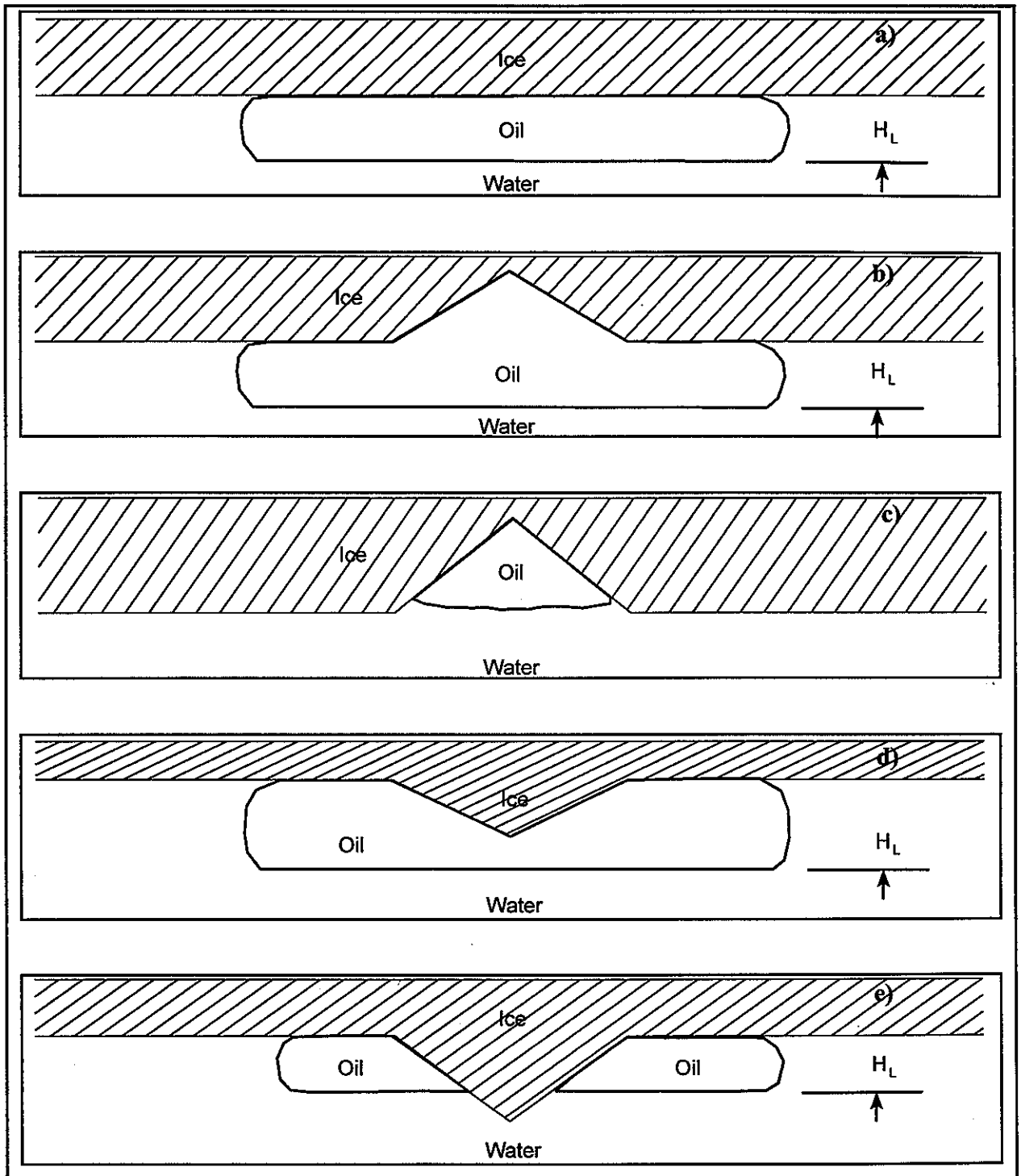

Figure 2. a) Large oil pool, volume V_O under smooth horizontal ice, pool thickness H_L given by equation (2) in text. b) Large oil pool fills depression, volume V_D when $V_D < V_O$. c) Large depression contains oil when $V_D > V_O$. d) Small ice keel covered by oil when keel height less than H_L. e) Large ice keel forms island in the oil pool.

THE POTENTIAL FOR ICE FRACTURE BY A WELL BLOWOUT

An Arctic oil well blowout in ice-covered water would release a mixture of gas and oil which would rise to the bottom of the ice cover and spread out beneath it. The volume of gas released is expected to exceed the volume of oil by a factor of about 150. As the gas moves out under the ice, driven by either existing currents in the area or the horizontal currents generated as the blow out plume impacts the ice cover, the gas will displace the water from beneath the ice cover. At some distance from the plume impact zone, the plume currents may be reduced to the point where the gas comes to rest, relative to the ice cover.

The forces exerted by a trapped gas bubble under thin ice, which tend to lift and fracture the ice sheet, have been analyzed by Topham ("The Deflection of an Ice Sheet by a Submerged Gas Source", *Trans. ASME Journal of Applied Mechanics*, 279, 1977). Assumptions in the model include isotropic elastic properties for the ice sheet, which in reality is nonisotropic, exhibiting both plastic and elastic properties dependent on the past history and climatic conditions. The analysis considered the ice to be thin, and deflections small, and fracture was shown to occur either at the bubble centre or just beyond the bubble edge--depending on bubble depth, ice thickness, and material properties assumed for the ice.

The thickness of a gas bubble beneath a horizontal ice sheet can be calculated with accuracy by equations (1) and (2). Under flat horizontal ice sheets, gas bubble thickness is calculated to be no more than 6 mm. Topham's analysis shows that a bubble thickness of the order 40 to 50 mm is required to fracture 0.5-m thick ice, and the bubble radius required is of the order 60 to 100 m. Ice 2 m thick could fracture at the bubble centre when the bubble is 150 mm thick and 200 m diameter.

We may thus conclude from this that only gas bubbles trapped in very large undulations are capable of fracturing the ice.

SEA ICE ROUGHNESS

Undersurface roughness and topographical features of sea ice are essential factors governing the long-term spread of oil and gas under ice. In earlier sections of this paper it has been shown that ice features of the order of 5 mm in height can create discontinuities of oil and gas spills. We now review some literature on Arctic sea ice roughness.

In the inner fast ice zone the ice cover is found to be smooth, i.e. the roughness scale is of the order of 2 to 3 mm (NORCOR, 1975). Data from several sources is summarized by Stringer and Weller (1980) who report undulating ice topography with an amplitude of 0.10 m and wave length typically 10 m.

The shear zone or seasonal ice zone features the greatest degree of roughness since it is characterized by hummocks and ridges. Wadhams ("Sea Ice Morphology in the Beaufort Sea", *Beaufort Sea Tech. Rep. No. 36*, Dept of the Environment, Victoria, B.C., 1975) reports on the topography of the Beaufort Sea ice cover giving mean ridge height and spacing from airborne laser profiles can act to contain the area of spill, and occur with a mean spacing of 1.5/km to 2.1 /km in the Beaufort Sea with heavy ridging up to 8/km. Keel depths can average 21.2 m for light ridging and slow drift, 26.8 m for heavier ridging and fast drift with a 10-year maximum depth of 32.8 m. Wadhams estimates a vertical roughness scale of approximately 5 cm for ice floes between ridges.

The roughness of the bottom of sea ice provides for potential oil and gas spill containment and protection from currents. The containment potential can be expressed in terms of void volume per unit area (Stringer and Weller, "Studies of the Physical Behaviour of Oil in Ice", *Proceedings*

3rd Arctic Marine Oil Spill Program Tech. Seminar, Environment Canada, pp. 31-44, 1980). Shore fast ice near Prudhoe Bay contains subice voids of 0.02 to 0.047 m^3/m^2 for annual ice, and 0.293 m^3/m^2 for multiyear ice. This represents a theoretical containment potential of 0.17 million bbl/km^2 and 1.8 million bbl/km^2 for annual and multiyear ice respectively (Stringer and Weller, 1980). Based on these figures we might be encouraged to conclude that the standard Beaufort Sea blowout of 4 x 10^5 bbl/yr would be contained under 2.35 km^2 of first-year ice or under 0.22 km^2 of multiyear ice. Unfortunately, these figures are quite unrealistic because they are based on simplifying assumptions which all tend to underestimate the area of ice affected.

Firstly, the figures above assume that no gas is present which implies that the blowout gas is vented through a hole in the ice above the wellhead. This is unlikely, as discussed already. Secondly, the figures imply a uniform coating of oil under the ice cover, which is impossible unless the ice is perfectly flat, horizontal and no currents are present.

The experimental spill of crude oil under ice in Amundsen Gulf (NORCOR, 1975) demonstrates how optimistic the theoretical treatment is. An oil spill of 0.68 m^3 was found to occupy an area of about 237 m^2 in a very patchy fashion. The effective containment potential of this ice is thus 0.0029 m^3/m^2, fully ten times less than the theoretical value suggested by Stringer and Weller (1980).

The experimental spill at Amundsen Gulf did not reproduce the high energy dispersive forces believed to be present during a blowout. Topham (1975) demonstrated that blowout plumes in 23 m and 60 m depths spread out to impact circular areas of diameter 40 and 72 m respectively at the water surface. Wadhams (1975) likened this to a paint brush which does not carry enough paint to fully cover the swath area behind the brush.

Wadhams (1975) also examined the effect of ice drift on distributing a low concentration of oil over a very wide geographical area. The long-term westward drift of about 2.4 km/day is multiplied by a meander coefficient of between 2 and 4 to obtain the actual distance travelled by ice and, hence, the swath velocity. For a nice drift of 9.6 km/day the 2 500-bbl/day blowout results in a "very sinuous swath track which may spread 1 000 km to the westward in a year and yet be 2 000 to 4 000 km long".

The importance of local topographic features and surface roughness on the underside of the sea ice is to provide oil and gas spill pathways which will result in stable disconnected spill patches and pools. Ice drift, blowout swath width and the presence of gas in the spill all play important roles in distributing oil over a large area under ice in very low concentrations. By ignoring these effects, the simplified analysis based on void volumes under the ice seriously underestimates the potential spill areal extent and the ensuing cleanup problems."

The section entitled "EFFECT OF CURRENTS ON OIL AND GAS SPILLS UNDER SEA ICE" is essentially identical to the report by Cammaert, 1980 reviewed previously and therefore not included here.

Method

"Laboratory studies consisting largely of photographic observations have been conducted on the deposition of finite quantities of oil and air under smooth horizontal ice, or rather, its physical analog, plate glass. Air bubbles, like oil drops, lack sufficient pressure to squeeze out the thin water film separating the bubble from the glass. The gas bubbles are thus guaranteed to possess a contact

angle of 180 degrees and the bubble thickness under horizontal glass or ice is given by equations (1) or (2).

An air bubble 40 to 50 mL was first formed under a glass plate submerged 10 to 15 mm below the free surface in a tank of water. Crude oil drops with volume 0.5 mL were released at 10- to 15-s intervals 25 cm beneath the gas bubble."

Results

" Tests at Memorial University demonstrate the mobility of oil due entirely to buoyancy. Oil drops were released from the bottom of a specially constructed tank, 1.2 m deep. Plate glass provided a smooth hydrophilic surface substitute for an ice cover. The rising oil drop flattened out on impact with the glass, then oscillated about the equilibrium shape on the rebound. However, the splashing drop did not rebound completely free of the glass, nor did it fission into smaller droplets. After the drop oscillations had damped out, the stable equilibrium drop shape, Figure 1, was achieved. Subsequent drop motion depended on whether the glass surface supporting the drop was tilted to the horizontal or whether currents were present along the surface which could move the drop.

The test rig was designed to study individual drops rising under buoyant forces only, and surface currents were negligible. However, glass-plate tilt angles as low as 2 degrees to the horizon were found to be sufficient to cause oil drops to slide along the glass surface after impact. The sliding velocity appeared to become constant after four or five drop diameters distant from the splash zone. The buoyancy driven sliding velocity depended on the plate tilt angle and could be 30 percent of the drop impact velocity when the plate tilt angle is 10 degrees. Table 2 shows some results when the crude oil size was 1.2-cm diameter.

Table 2. Sliding Velocity along Glass Plate Tilted to Horizon (Oil-drop diameter 1.2 cm, rising velocity before impact 11.3 cm/s).

Tilt angle	2.67 degrees	2.80	4.36	9.37
Average speed along plate	0.84 cm/s	0.95	1.88	3.15

The drop impact and sliding tests indicate the water film separating the oil from the glass is not removed or penetrated during the impact process. The oil drop is highly susceptible to buoyancy-induced motion along the solid surface if tilt angles exceed 2 degrees. Currents beneath the ice will readily move the oil as well, if the ice surface is smooth.

... ...

THE DEPOSITION OF CRUDE OIL AND GAS BUBBLES UNDER ICE

The arrival of the first drop of oil at the gas/water interface creates a miniature spill of gas and oil with volume ratio about 150:1. The oil drop was found to remain intact for several seconds, presumably waiting for the thin film of water surrounding it to drain away. The oil drop then coalesces with the gas/water interface and spreads over it to form either a very thin film extending to the edge of the bubble, or a thick lens of oil confined to the bottom of the gas bubble. In the case

of spreading crudes, the film covering the bubble can be extremely thin, exhibiting some colours of the spectrum, but a thicker lens of crude near the original oil drop location remains.

The arrival of a successive train of oil drops at the gas bubble interface produces a growing oil lens in the gas bubble after each drop coalesces with the lens. Drops that land near the edge of the gas bubble slide upward along the bubble contour since the bubble surface is not horizontal, but curved As the drop slides along the bubble contour, the film of water preventing immediate coalescence is gradually draining away. Some drops slide off the gas bubble and onto the ice (or glass in our experiments) before coalescence takes place. In general, coalescence time is short for the first oil drop then increases when a thick lens is present in the gas/water interface. Coalescence time can range from 1 to 2 s to 15 to 20 s and longer. As the oil lens thickens to about 2 mm, the gas bubble thickness is correspondingly decreased. When a thick oil lens covers the bottom of the gas bubble, oil drops tend to slide off the bubble more readily, and in the process, drag oil from the lens up the side of the gas bubble. Oil drops shed from the gas bubble accumulate on the glass surface and can coalesce to form a puddle, which is connected to the lens on the bottom of the gas bubble. This occurs when the addition of oil, drop by drop has reduced the ratio of gas to oil close to 1:1.

Figure 3 illustrates the appearance of a gas bubble with a small amount of oil forming a lens in the bubble interface, and a thin oil film surrounding the lens. After a large number of oil drops have coalesced with the oil lens, the increased lens size and a number of oil drops which have slid from the gas bubble contour to take up positions beside it (see Figure 4).

The experiments just described generally confirm the two-dimensional analytical study of Topham ("The Disposition of Gas-Oil Mixtures Trapped Under Ice", *Canadian Journal of Physics*, **58**, pp. 1183-1190, 1980), which suggests several stable configurations of oil and gas beneath a planar ice sheet. Our experiments provide additional insight into the physical mechanisms controlling the various stable configurations observed."

BOSS Critique

The authors have not discuss the errors involved in interpreting the photographic experimental evidence nor how errors could effect the outcome of the conclusions stated in the report. There was no discussion of the errors for the interfacial tension measurements and how these will effect the results obtained from equations (1) and (2). The authors have not discussed whether the substitution of glass for ice causes a small or large error in the results.

Review of a manuscript, written by Deslauriers, P.C., S. Martin, B. Morson, and B. Baxter entitled, *The Physical and Chemical Behavior of the Bouchard #65 Oil Spill in the Ice Covered Waters of Buzzards Bay*, 1977.

This information is also contained in the manuscripts Deslauriers, P.C. and S. Martin."Behaviour of the Bouchard No. 65 Oil Spill in the Ice Covered Waters of Buzzards Bay", in *Proceedings, 10th Annual Offshore Technology Conference*, pp 267-276, 1978; and Deslauriers, P.C., "Oil Spill Behaviour in Ice During the 1977 Buzzards Bay Oil Spill", *Proceedings of the Conference on Assessment of Ecological Impacts of Oil Spills*, American Institute of Biological Sciences, Washington, D.C. pp 197-215, 1978.

Technical Summary (taken from the conclusions section of the manuscript)

"The major conclusions which can be drawn from the 1977 Buzzards Bay oil spill on the behavior of oil spilled in ice infested waters are as follows:

A. Rafted ice led to the formation and containment of oil pools with depths of up to 0.15 m on the ice surface. These pools held approximately 30% of the spilled oil. The presence of these pools made possible the recovery of 15% of the spill by direct suction into vacuum trucks. Further, the formation of these pools occurred within a day of the spill and was unexpected on the basis of previous work on oil spills in ice.

B. A comparison of the 1977 spill in ice covered waters with previous open water spills in Buzzards Bay showed that the ice served as a containment mechanism against the spread of oil into the near-shore areas which were covered with shore fast ice. The presence of ice also prevented wave action from distributing large amounts of oil into the water column and sediments.

C. After ice breakup, oiled ice floes were exported throughout the bays and coves of Cape Cod where they subsequently distributed the slightly weathered oil as they melted. These oily ice floes could not have been contained by conventional containment. This, therefore, appears to be a mechanism for the long-range transport of oil, one which will likely be important in Arctic oil spills.

D. Weathering of the oil occurred despite the ice, snow, and cold temperatures. Sample analyses showed that the more exposed the oil was to the air, the greater it weathered. The two extremes found were oil underneath the ice having a 6.2% volume loss and oil incorporated in rotated ice blocks having a 47.4% volume loss.

E. Oil was not contained by the ice edge, rather, it was transported underneath the ice by the strong tidal currents of approximately 0.5 ms^{-1}. Oil sheen was detected moving underneath the ice even in a shore fast ice zone.

F. Nearly all the oil being transported underneath the ice settled within two days into hummocks, ridges, and rafted ice where it was sheltered from the strong tidal currents. The oil remained fairly stable in these formations until the ice began to breakup.

G. Approximately 0.1 m of snow covered the oil seven days after the spill occurred. The snow cover greatly hampered aerial surveillance, research activities, and cleanup efforts. The snow combined with the pooled oil to form a slush-like mixture of 30% oil by volume..

H. Oil spread from concentrated pools by the wind and was distributed as a thin layer across the relatively smooth surface of the ice floes. This lowered the solar albedo of the ice, increased the amount of oiled ice, and provided a mechanism for increased weathering of the oil.

I. Typically, the oil penetrated 50 mm into solid ice, varying in volumetric concentration up to 5%. These variations appeared to be dependent upon the amount of oil in contact with the ice, the extent of the period of contact, the ice surface roughness, and the porosity of the ice.

J. After the oil was released from the ice, it spread in a thin sheen onto the surrounding water, greatly, increasing the aerial coverage of the spill. When locked into the ice, the oil covered a 0.1 km^2 area. Upon ice breakup, the oil spread to a 19.4 km^2 area.

K. Because of the formation of the oil pools, the best cleanup technique was the direct suction of oil using vacuum hoses. Burning of the oil appeared to dispose of approximately 50% of the oil at Cleveland East Ledge, according to Coast Guard estimates, but burning also generated a long soot trail. The brute force recovery of oil by hauling oiled ice upon the beach and loading it into trucks was extremely ineffective, both because the amount of oil recovered was only about 1% of the volume of oiled ice hauled away, and also because some of the oil soaked into the beach. The use of mechanical oil skimming devices proved to be ineffective in recovering the spilled oil under these icy conditions."

Objective

The authors objective was to report on the No. 2 oil spilled by BOUCHARD #65 in Buzzards Bay, Massachusetts on January, 1977.

Theory

There are no clear theoretical definitions in this work. The empirical relationships as stated by the authors are used in place of theory.

Method

"1.3 TECHNICAL APPROACH

Data were gathered in the form of photographic documentation, in situ measurements, observations, and samples for subsequent analysis.

Throughout the period for which the No. 2 oil was visible in the Bay, observers gathered data in the form of photographs, in situ measurements, observations, and water, oil, ice, and sediment samples. Constant and careful attention was paid to the modification of the sampling program and the research objectives to stay within the limits of the logistics of the program and to obtain the best research results possible under changing and often unsafe ice conditions. Debriefings of all observers were held every evening to summarize the day's work, discuss problems, and schedule the next day's activities.

To determine the location and possible movement of the spilled oil, aerial surveillance began on the morning after the spill, using hand-held 35 mm cameras with 35, 55, and 135 mm lenses. Also, two high altitude over-flights (2,400 m) were made using vertically mounted Hasselblad cameras. Over-flights were made of the affected areas to map and photograph the spilled oil in order to obtain a fairly continuous record of its movement (see Appendix IV). After a 120 mm snowfall on February 5, oil tracking, field observations, sampling effort, and cleanup activities were all seriously hindered (Figures 1.6 and 1.7).

Surface and water column samples were taken at several locations throughout the affected area to determine hydrocarbon content. A more detailed description of the sampling stations is provided in Appendix V-A. The surface water samples were collected in hexane-rinsed glass jars placed just below the water surface for filling. Where ice was present, holes were either cored or sawed through the ice to gain access to the water. Water column samples were taken using either a Nisken, Sterile Bag (Butterfly) or 885 Vacuum Tube Sampler. Few samples were taken with the Nisken sampler due to the risk of sample contamination while lowering it through the air/water interface and the water column to the desired sampling depth. The most favored sampler for ease of handling and obtaining uncontaminated samples was the Vacuum Tube Sampler. The analytical procedure consisted of the extraction of 250 ml of the sample into 10 ml of nanograde hexane. Using a Perkin-Elmer 204 Fluorescence Spectrophotometer, with an excitation wavelength of 295 nm and an emission wavelength range of 315 to 350 nm, the concentration of oil was recorded in parts per billion. The analyses and results for oil weathering are described in Section 2.3.3.

Sediment samples were collected with either a Peterson, Boston, or Eckman grab (Figure 1.8) throughout the affected areas to determine the biological impact of the spill and the presence of hydrocarbons. All grabs were easily contaminated since they had to be lowered through the water column before the sample was taken. The removal of the samples from the center of the grab reduced this contamination problem. Also, the University of Rhode Island sent a diver under water to collect samples in a sterile bag, thereby avoiding possible contamination from the water column. Two types of analyses were performed on these sediment samples. The first type, performed by ENDECO, emphasized the absolute volume of oil in the sediments by a wet sample of a specific volume. The second type, performed by Woods Hole Marine Biological Laboratories, emphasized the effect on the benthic organisms by a dried particle size analysis. Results are presented in Appendix V-B.

Ice samples were collected using a 7.6 cm diameter SIPRE corer and a Russian Corer which produced a 12.7 cm diameter core (Figure 1.9). Measurements of oil penetration, brine channels,

salinity, and temperature were made. Chemical analyses were performed to determine the quantity of oil present using a Fluorescence Spectrophotometer. These results are tabulated in Appendix V-B. The weathering of the oil in the ice will be discussed later."

Results

"2.2 LARGE SCALE BEHAVIOR

2.2.1 Oil Transport Under Ice

Large amounts of oil were initially transported by currents underneath the ice and deposited in crack systems where they remained relatively stable until ice breakup.

Under-ice oil transport primarily occurred at Wings Neck, and possibly at Cleveland Ledge. Observers on the leaking barge at Wings Neck stated that after the oil was released from the barge, it built up along the edge of the ice surrounding the barge and was forced under the ice by the strong tidal currents. Once under the ice, the currents transported the oil laterally to ridges, leads, hummocks, and rafted ice. Because of the oil's density it rose into the openings in the ice where it was trapped and restrained from further spreading under the ice.

Experimental studies on the spreading of oil beneath ice have shown that the size of the affected area is governed by the ambient temperature, oil properties, ice characteristics, rate and volume of oil released, and current velocity. If the ice is smooth, the oil will spread to an equilibrium thickness determined by temperature and oil properties [4,5]. For No. 2 oil release in quiescent waters, experiments [6] have shown that the equilibrium thickness ranges between 2.5 and 5 mm. This implies that if the oil at Buzzards Bay had evenly spread to its equilibrium thickness, the areal coverage would have been between 61,00 m^2 and 122,900 m^2. However, due to the currents and crack systems, the oil encompassed an area of 94,700 m^2 and was not evenly distributed.

The ice properties which affect oil spreading include its porosity, slope, and roughness, with under-ice roughness being the most important. When oil is spilled under ice which is rough, the oil will radiate outward, filling interconnecting pockets until the volume released is contained. This pocket-filling process has been observed in a number of experiments [7,8]. At Buzzards Bay, the pocket-filling process was not evident due to the smoothness of the under-ice surface (Figure 2.1).

The current velocity in the spill area was found to be the most important factor in the spreading of the No. 2 oil. When currents under the ice exceed a certain threshold velocity, the oil can be sept along the under-ice surface. Experiments [6] have shown that the threshold current velocity for moving No. 2 oil under smooth ice is 0.035 ms^{-1}. Above the threshold velocity, the oil velocity V_o in ms^{-1} depends on the current velocity V_c in ms^{-1} according to the following linear relation:

$$V_o = 0.38V_c - 0.0133$$

up to a current velocity of 0.3 ms^{-1}. The water velocities in Buzzards Bay off Wings Neck were of the order of one knot or 0.5 ms^{-1}, which is over ten times the threshold velocity. Because of the strong currents and the lack of change in the appearance of the spill one to two days following the spill, it appears that most of the initial under-ice transport probably took place within this initial one to two day period. Ice cores taken from a number of ice floes several days after the spill consistently showed that the underside of these floes were free of oil (Figure 2.2). During this one to two day period, the No. 2 oil spread from its source off Wings Neck to as far as Mashnee Island, a distance of 4.3 km. Part of this spreading took place under the ice, and part through a lead going out into Hog

Island Channel (Appendix IV).

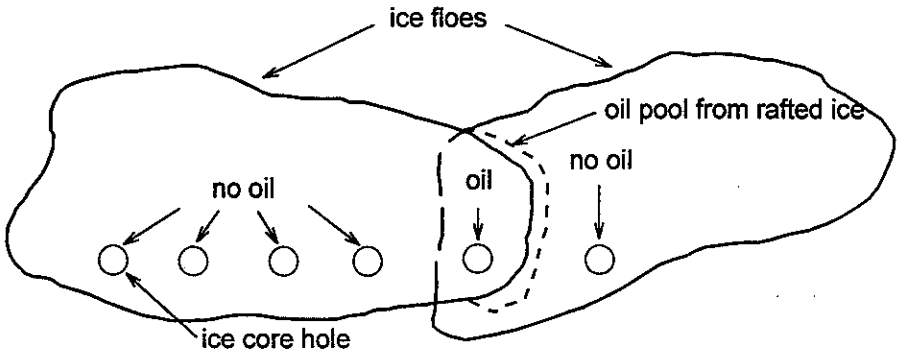

Figure 2.2. Ice cores taken along ice floes consistently revealed no concentration of oil under the ice except along the ice edge.

Following the snow storm on February 5 and the subsequent break-up of the ice, oil was released from the ice in the form of a thin sheen. As this sheen moved over the open water, some of it was also forced under the remaining shore fast ice. The small amount of sheen detected under the ice was observed by field personnel taking samples throughout the area. Surface and water column samples were taken at many stations (Appendix V-A) and the analyses of the presence of hydrocarbons are presented in Appendix V-B. The amount of oil transported under the ice in this manner cannot be estimated; however, as time progressed, the amount detected at the various stations throughout the shore fast zone areas increased. The only oil detected underneath the ice was at the edge of the ice floes where it was trapped between layers of rafted ice.

Besides these observed thin sheens, in many of the ice cores taken, loose floating brash ice was found underneath the ice in both the active and shore fast ice zones. This brash ice, consisting of small fragments of ice less than 30 mm across and having a thickness of 13 cm, did not appear to affect the under-ice oil transport. The presence of brash which formed in open water was forced under the ice is further evidence of material on the surface being forced under the ice.

Finally previous investigations have revealed that if the ice growing process continues, oil which is underneath the ice will be sandwiched in by the new ice growth [8, 9, 10]. At Buzzards Bay, the ice growth process essentially halted after the spill occurred because temperatures did not remain cold enough for the ice to grow a significant amount. Furthermore, since oil was not pocketed underneath the ice, the ice-oil-ice lens typically found in other cold regions spills did not form.

2.2 LARGE SCALE BEHAVIOR

2.2.2 Oil Pools in Rafted Ice

The rafted ice formed pockets where the oil concentrated in pools and was sheltered from further spreading by currents.

Approximately 30% of the spilled oil was contained in "deep pools" on the surface with depths of about 0.12 m which were formed by rafted ice. Their formation resulted in the natural

containment of pure oil product in quantity soon after the spill. This section discusses the formation of the rafted ice due to the ice movement and proposes a scenario for the filling of the rafted ice pockets with oil.

Parmerter and Coon [11] and Parmerter [12] describe the formation of the rated ice as follows. When a flat sheet is subject to a compressive stress, which would be generated by a combination of current and wind forces, the ice breaks by buckling rather than by crushing which frequently results in segments of ice sheets sliding over the other. Parmerter points out that for thick ice, or ice which is brittle, the stresses generated by the bending will cause additional fractures and result in the formation of a hummock or pressure ridge. If the ice has a thickness which is much less than 1 m and is elastic, one sheet will slide over the other to form a raft. The shape of the rafted ice is further determined by the fact that sea ice must everywhere be in near hydrostatic equilibrium with the underlying sea water. The weight of the upper ice depresses the lower sheet to a point where, as observed in the Arctic, sea water will flow up over the lower sheet to form a wedge-shaped fluid layer (Figure 2.3a).

For Buzzards Bay, the stresses which distorted and rafted the sea ice were generated by wind, currents, and ship traffic. In days preceding the BOUCHARD spill, the wind was primarily from the west and southwest at 5 to 10 ms^{-1}. This provided a long fetch for the wind forces to act on the ice, causing many of the ice floes in the active ice zone to raft on top of each other throughout Buzzards Bay.

Oil which flowed from the barge under the ice, encountered several rafted floes. The sequence of sketches in Figure 2.3 shows a possible oil capture scenario. As the current carried the oil under the ice, the oil encountered the bottom of the rafted formations, and would collect and be sheltered from the current in the lee of the submerged part of the raft. The buoyant oil would then rise through an opening between the two ice sheets to replace the heavier sea water in the pond. Once on the surface, the oil was protected from the currents. As tidal current oscillated back and forth, the fuel which was not protected from the currents would then be swept away.

Figure 2.2 is a schematic diagram of where spilled oil was discovered along a rafted ice flow. This core survey showed that the oil was underneath the upper rafted blocks. In addition, interviews with the clean-up crews revealed that the oil would be more heavily concentrated on the down current side of the rafted pool. When the tide changed, the pool would concentrate near the opposite side of the rafted section.

Estimated made at the spill site suggested that a typical pool measured 0.1 m deep by 2 m wide by 4 m in length with an oil volume of 0.8 m^3 (200 gallons). In one area, there were five such pools over 50 m distance which yielded approximately 1,000 gallons of visible oil. There also were some very large pools which contained as much as 1,000 to 2,000 gallons (see Figure 2.4). The oil concentrated in this type of deformed ice was pure product. This natural containment of the oil in these pools made direct suction by hoses into vacuum trucks an encouraging recovery possibility.

2.2 LARGE SCALE BEHAVIOR

2.2.3 Incorporation of Oil in Pressure Ridges and Hummocks

Pressure ridges and hummocks throughout the active ice zone provided a means for containing the oil in a thin layer within the voids between the broken ice pieces.

Pressure ridges and hummocks in the active ice zone at Buzzards Bay served as effective containment mechanisms for the spilled oil. Oil entrapment in ridges and hummocks occurred along the ship track between Cleveland Ledge and Wings Neck, and off Wings Neck.

Pressure ridges and hummocks form in a manner resembling the formation of rafted ice. The ice deformation generated by wind, water, or stress from a moving ship, forces ice pieces on top of one another. Unlike rafting, the ice sheet either has been previously broken or breaks up causing the broken ice to form a ridge extending above and below the waterline. Figure 2.5 is an idealized sketch of a cross section of a pressure ridge following Weeks and Kovacs [13], in which the ice above the waterline is called the sail and the ice below is called the keel. Weeks [14] states that the ratio of sail height to keel depth is about 1 to 5 and that the mass of ice above and below the

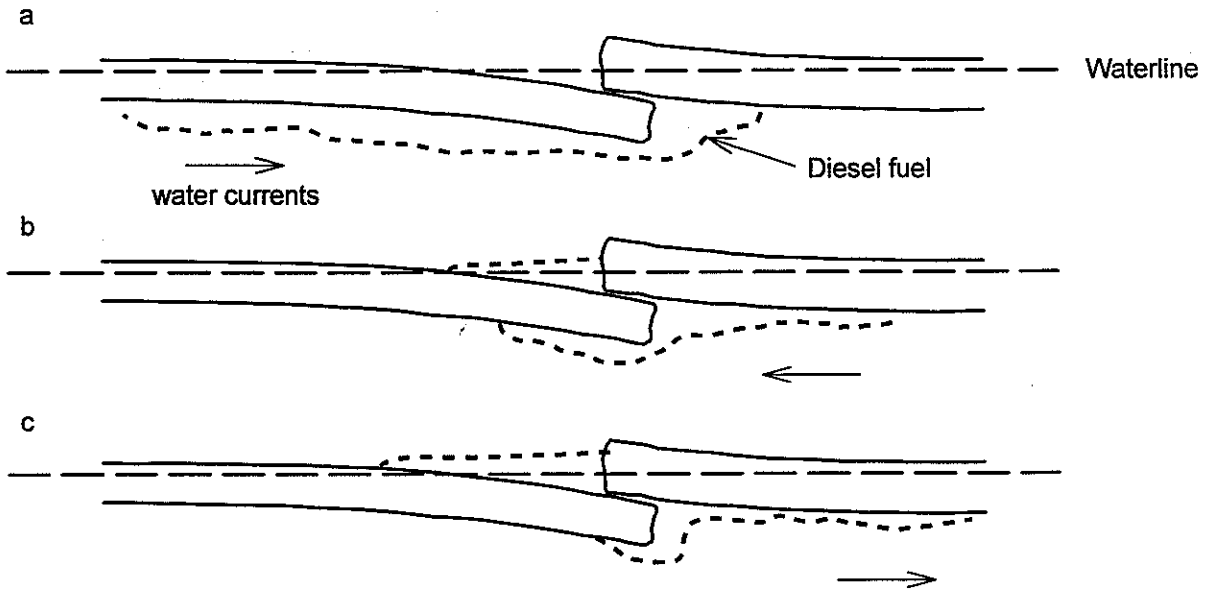

Figure 2.3. Flow of oil rafted in ice, a) oil flowing underneath the ice comes in contact with rafted ice, b) current reversal encourages oil filling into rafted ice pocket, c) reversal of current sweeps unsheltered oil away.

waterline is in approximate hydrostatic equilibrium. When ridges first form, the blocks making up the ridge are separated from one another by air and water-filled spaces, called voids. Weeks states from field observations that approximately 30% of a young pressure ridge is void space, making it highly permeable to oil.

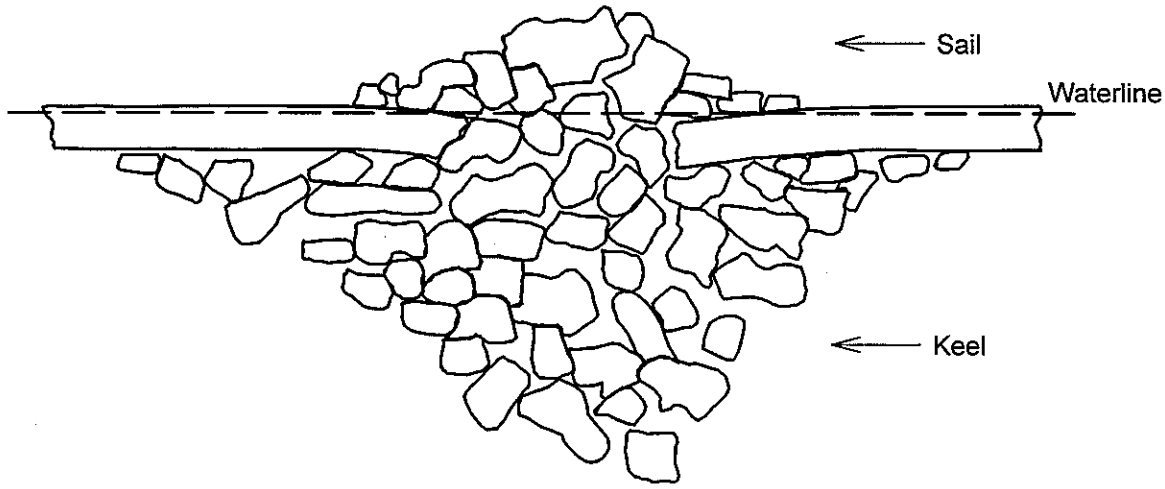

Figure 2.5. Idealized sketch of the cross section of a pressure ridge.

Unlike the ridges with its clear-defined crest, the ice from a hummock is pile haphazardly one piece over another to form an uneven surface. Parmerter and Coon [11] have shown that a hummock should also have a sail height to keel depth ration of 1:5. Hummocks presumably will also have a high void content making them permeable to oil.

In general, oil interacts with pressure ridges and hummocks in two ways. The first occurs when oil is incorporated during the formation of the pressure ridge or hummock. This happens when small contaminated ice pieces are compressed together into a pressure ridge or hummock creating a pile of oiled ice pieces or when oil in a lead along the ice edge is squeezed and coats the ridge walls during the formation of the pressure ridge or hummock. Numerous observations [11] point out that flat ice bending down at the ridge base could yield another possibility for oil entrapment.

Secondly, oil can flow into previously formed pressure ridges and hummocks (see Figure 2.6). The porous pressure ridges and hummocks create numerous small crack systems for the oil to fill in hydrostatically, thus allowing oil to coat the ice and settle within the crack systems. It is hypothesized that a ridge or hummock may or may not contain oil in volume depending upon the currents, oil properties, ice properties, and porosity of the ridge or hummocks. The keel can also provide a means for containment of oil [15].

Throughout the active ice zone in Buzzards Bay, ridges and hummocks comprised approximately 15% of the surface area. These ridges and hummocks extended up to 1 km in length, with widths ranging from 1 to 10 m and a maximum sail height of 1 m. The oil contained in this deformed ice was much less concentrated that the pooled oil in the rafted ice. A core taken through a pressure ridge revealed no flow of oil into the core hole. No pooling was observed, rather the ridge

consisted primarily of oily ice (Figure 2.7). Also, there was no concentrated oil underneath the ice along the ice keel for the ridges investigated. In many cases, the hummocks, being more porous, allowed heavier concentrations of oil to form (see Figure 2.8), making oil cleanup by direct suction feasible in some instances. However, oil pooling in hummocks was not as extensive as that observed in rafted ice.

2.3 SMALL SCALE BEHAVIOR

2.3.1 Oil Migration Into Ice

The oil spilled at Buzzards Bay typically penetrated approximately 50 mm into the ice surface.

The report thus far has discussed large scale transport, entrainment, and release of the oil. Although less dramatic, small scale processes can provide information of equal importance. The small scale migration of oil into ice is primarily a function of ice surface roughness, ice porosity, oil viscosity, volume of oil in contact with the ice, and the duration of oil exposure to the ice. For the Buzzards Bay spill, the ice porosity and oil viscosity are of particular importance. Sea ice is often porous due to its crystal structure and the brine channels formed by drainage of brine. These numerous small openings allow oil to seep into the ice. Field experiments [10 and 23] conducted in the Arctic, involving both heavy and light crude oils, showed that oil flowed through brine channels into the interior of the ice resulting in oil concentrations ranging from one to five percent by volume. If the oil has a low viscosity, it would be able to flow into the ice rather freely, while a more viscous oil would not penetrate the pores as easily.

The Buzzards Bay ice, with an average thickness of about 0.3 m, appeared to be considerably different from Arctic sea ice in terms of its salinity, harness, and permeability. A salinity profile, taken from an ice core and measured with an A_0 refractometer reading to an accuracy of about 1 part per thousand, showed that the ice had a low overall salinity. Figure 2.13 shows that the surface salinity was nearly fresh, with the interior salinity constant at about 4 parts per thousand. For comparison, the surface salinity of winter Arctic sea ice is 20 to 40 parts per thousand and the interior salinity is about 8 parts per thousand. The Buzzards Bay ice, therefore, was a hybrid of lake and sea ice. It grew from water slightly less saline that sea water, and due to the thermal diurnal temperature cycle and rain which tended to wash the salt out of the ice, the resulting ice had the harness and impermeability of lake ice.

Samples taken throughout Buzzards Bay revealed varying degrees of oil absorption into the ice. These variations were due primarily to the volume and duration of the oil's exposure to the ice. A brief description of what was observed and noted by field investigators follows:

1. The highest concentration of No. 2 oil in the ice was recorded along the edges of the oil pools. Oil mixed with slush ice resulted in a 30% volume concentration of No. 2 oil. Solid ice pieces along these areas typically contained 5% oil by volume.
2. Heavily stained ice appeared dark yellow and was typically found amidst brash ice and small ice pieces. Oil penetrated approximately 25 to 60 mm into the ice, resulting in a 3% concentration by volume.
3. Lightly yellowed ice showed an oil penetration of between 25 to 60 mm into the ice surface. This surface layer was approximately 0.05% oil by volume.
4. Windblown No. 2 oil found on top of the ice had, on average, penetrate 3 mm into the ice; 50% of this penetrated layer was oil. The number of pores available on the surface of the ice floes for the oil to penetrate deeper into the ice was small,

consisting primarily of occasional brine channels. In Arctic ice, brine channels provide a route for oil beneath the ice to flow up to the surface [10]. At Buzzards Bay, the few brine channels observed played the opposite role in that they permitted the flow of No. 2 oil down into the ice.

5. Ice in the affected shore fast and active ice zones had the smell of No. 2 oil on the bottom of the ice. When holding a piece of the ice up to the light, a sheen could be detected on the underside surface. There was no visibly detectable migration of oil into this ice. Chemical analysis revealed oil concentrations averaging 310 ppb for the bottom 80 mm.

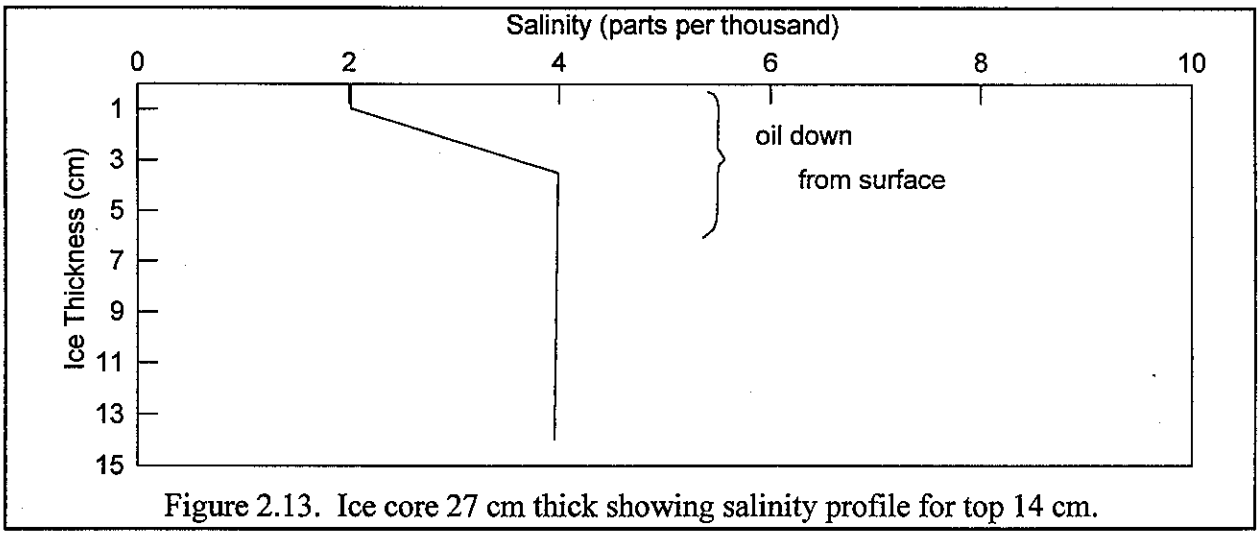

Figure 2.13. Ice core 27 cm thick showing salinity profile for top 14 cm.

"

"2.3.3 Weathering of Oil Under Varying Field Conditions

Spilled oil samples taken under varying field conditions showed different weathering rates.

When oil is exposed to the atmosphere, the oil properties change due to weathering. The weathering of the oil in the environment is governed by three types of processes; physical, such as evaporation, dissolution, emulsification, and adsorption; chemical, such as direct oxidation and reduction reactions in the water column; and biological, such as aerobic and anaerobic microbial degradation. Of the physical processes, evaporation is of particular interest. Evaporation, the process by which low molecular weight compounds are volatilized into the atmosphere, is affected by the partial vapor pressure of the individual component of the oil, the surface area of the pool, the average wind velocity, and the ambient temperature. For No. 2 oil, components with boiling points below 200 °C normally comprise 5% of the oil, while those having boiling points between 200 and 270 °C comprise 45% of the oil, and the boiling point of the remainder is above 270 °C. It was found that the loss of these oil components by evaporation from a solution in a bubbler apparatus which was run for 40 hours at 25 °C was 13.1% of the total volume [28].

There are two extreme conditions which may occur in the evaporation process. First, if there is a perfect liquid mixing of the oil, the vapor formed will be in equilibrium with the bulk of the oil. As evaporation proceeds, the oil becomes depleted in the more volatile components, its total vapor

pressure drops, and the rate of evaporation falls. Second, if no mixing takes place, evaporation can be visualized as layers of hydrocarbons being peeled off the surface. For this case, the liquid composition will remain unchanged with time and the evaporation rate will tend to be lower but constant [29]. With No. 2 fuel oil in concentrated pools, the first case applies because the liquid is able to mix due to its low viscosity.

Experience gained through tests and spill incidents in cold regions shows that oil will weather at different rates for different field situations. Results of field tests [27] showed that the aging of crude oil in the Arctic winter is considerably slower than in the summer, although the oil does age during these lower temperature periods. Also, variations were found between the aging rates of oil spilled in snow and on ice. In an oil spill at Riviere St. Paul, P.Q. [21], the losses due to weathering of the oil underneath the ice cover were in the range of 1/9 th loss for an exposed sample over the same period. It was concluded that the ice tended to shield the oil from evaporation and dissolution. In a spill at Deception Bay, the oil was quickly absorbed by the porous ice surface with an evaporation rate of only 25% of the rate from the free surface [19]. It can be concluded, therefore, that prohibiting the wind from making contact with the volatiles and the lower temperature reduce evaporative losses.

In Buzzards Bay, the No. 2 home heating oil was distributed in various snow and ice formations. The variation in filed conditions resulted in the oil being exposed to different temperatures and amounts of air. Samples from these formations were taken on the twelfth day after the spill incident. Chemical analyses on the original cargo and the weathered samples were conducted by the NOAA/National Marine Fisheries Service (NMFS). It was concluded from the weathered oil samples that the saturated hydrocarbons consisting of alkanes represented over 80% of the oil, and the aromatic hydrocarbons consisting of arenes represented under 20% of the cargo. The analyses on the weathered oil samples are provided in Table 2.1, a description of the sample location, field conditions, percentage loss of alkanes, percentage loss of arenes, and approximated total losses are provided. Losses of selected arenes are estimates because they are both highly volatile wand water soluble. It was found that evaporation was confined to the more volatile $C_{16}H_{32}$. The relative loss expressed in percentage volume loss was the greatest for oiled ice that was rotated up into the air and was the least for oil underneath the ice along rafts. It was also observed, even in the case of heavy weathering, that the oil did not sink in the water column (Figure 2.18), therefore, even the most heavily weathered oil did not sink to the bottom of the bay by mere hydrostatic forces. If oil did get entrained in the sediments, forces other than gravity had to come into play.

It is also interesting to note that four days after the spill, considerable amounts of vapor from the No. 2 oil could be detected in the air. The smell of oil was evident miles downwind of the spill. An air sample collected at Buzzards Bay offered interesting results. In a sample taken during the last week of January, it was found that the hydrocarbons entering the atmosphere were predominantly the at or below C_{14} [30]. In conclusion, from various degrees of weathering found at Buzzards Bay, it becomes evident that the media upon which oil is spilled is very important, particularly in cold regions. All samples showed varying degrees of weathering, and the more weathered the sample, the more air exposure the oil had.

Table 2.1 Weathered oil samples taken from different field conditions on February 10.

Location	Field Condition	Percent Loss Alkanes (%)	Approximate Percent Loss Arenes (%)	Approximate Total Percent Loss (%)
Wings Neck Tower	Oil underneath ice near edge of rafted ice. Oil was approx. 13 mm thick (see Figure 2.4)	4	14	6
Wings Neck Tower	Oil in ice sheltered by overlying ice sheet	4	16	6
Wings Neck Cove	Oil in ice near edge of ice floe. Sample taken from top 38 mm of ice core. Medium stained ice (Section 2.4 defines light, medium, and heavily stained oiled ice)	5	20	8
Wings Neck Cove	Slush oil/snow mixture from shallow oil pool in hummock (see Figure 2.8)	7	31	12
Wings Neck Cove	Oil taken from deep oil pool in rafted ice (see Figure 2.4)	7	38	13
Wings Neck Cove	Heavily oil stained ice from ice floe near edge of small oil pool	10	33	15
Wings Neck Tower	Ice piece 0.3 mm thick taken from small pressure ridge. Ice appeared to be medium stained	9	38	15
Wings Neck Tower	Wind blown oil on top of ice (see Figure 2.9)	21	54	28
Wings Neck Tower	Wind blown oil on top of ice	25	64	33
Wings Neck Cove	Ice piece rotated in the air similar to Figure 2.1. Scraped off of top of medium stained oily ice	29	58	35
Wings Neck Cove	Ice piece rotated in air. Scraped off top of lightly stained oily ice	37	89	47

2.3.4 Distribution of Oil in Water Column and Sediments

Hydrocarbon levels detected in the water column and sediments throughout the spill site area were much less that those which would be expected under comparable open water conditions.

Samples were taken throughout the Buzzards Bay area to determine if No. 2 oil was entrained in the sediments or present in the water. Only one station, Phinney's Harbor, was sampled repeatedly during the initial study period to determine if oil was spreading into the shellfish beds in that region. The primary effort was directed toward monitoring a large number of stations over a greater area with few multiple readings.

Oil was found at all of the stations sampled, with most stations yielding concentrations of 10 to 200 parts per billion in the water column (Appendix V). Only in one instance could the hydrocarbon level in the water column be related to the oil on the surface. From February 2 to February 14, station 10 at the entrance to Phinney's Harbor was monitored during the daylight hours. Samples were taken hourly using the Nisken sampler at the surface, at mid-depth of 4 m, and on the bottom of 8 m, and then analyzed for hydrocarbon content. This data is presented both as daily averages (see Figure 2.19) and hourly plots for each day (Appendix V-C). The daily average shows very little or no trend over the eleven day observation period, however, the hourly plots of oil

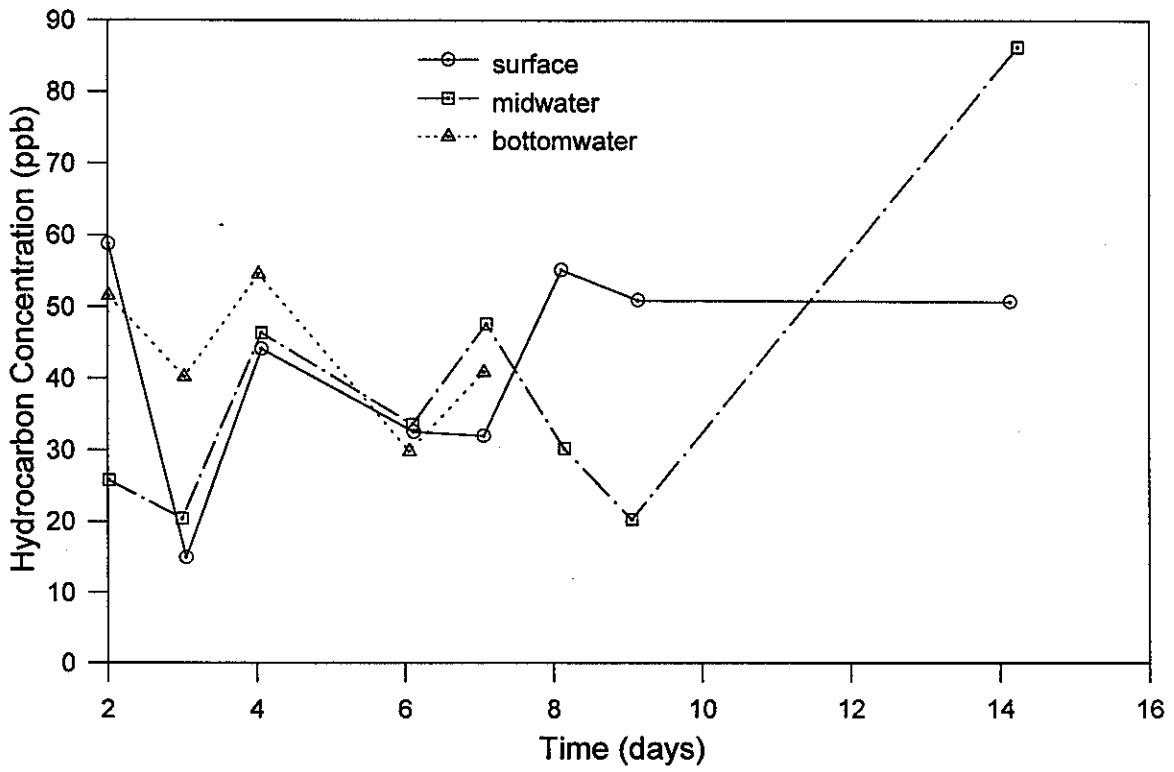

Figure 2.19. Daily average of hydrocarbon concentrations at surface, mid and bottom water for master station 10, Phinney's Harbor, 2-14 February, 1977.

concentration at each depth and at high and low tides suggest that hydrocarbon levels decreased on the outgoing or southward moving tide and increased on the incoming tide. The lack of repeatability and progression of data at the one established station is caused by the station location which is on a point adjacent to a strong tidal flow and by the fact that the sample period was fixed while the tidal cycles changed.

For the most part, oil concentrations in the sediments ranged from 0.7 to 23 parts per million, with one isolated station in Wings Cove yielding 770 parts per million. No recognizable patterns in occurrence or concentration were obtained. Further analysis of these data will not proceed until gas chromatographic oil identification work can be completed to determine the source of the oil. The results of these additional studies will be presented in a future NOAA report.

2.4 OIL MASS BALANCE

Mass balance estimates were made for the No. 2 oil incorporated in the active ice zone.

A more complete understanding of the mechanisms surrounding the transport of oil in ice covered waters requires an analysis of the mass balance of the spilled oil. This leads to a quantitative overview of the types of oil/ice involvement and provides information on the effectiveness of the various cleanup methods employed during the spill incident.

The oil mass balance for Buzzards Bay was constructed from aerial photo mosaics (see Figure 2.20) from January 31 to February 5, prior to the snowfall. During this time period, the oil remained stable within the active ice zone.

These aerial mosaics were combined with lower altitude and ground level photographs to compile the best possible description of the oil's involvement with the ice. These photographic records were cross-referenced with field samples to determine the percent and depth of oil saturation into the ice and the depth of the oil pools.

From the observations described in Sections 2.3 and 2.4, the following six categories of oil concentrations were developed for use with the aerial photographs:

1. Deep Oil Pools - These were pools of oil ranging in depth from 0.1-0.11 m, which were associated with rafted ice and were the primary sites for cleanup operations (see Figure 2.4).
2. Shallow Oil Pools - These pools ranged in depth from 0.01-0.04 m and were often incorporated in hummocks (see Figure 2.8).
3. Heavily Stained Ice - This ice appeared dark yellow and was found amidst brash ice and small ice floes. Oil penetration typically reached a depth of 0.12 m, with a concentration of 5% oil by volume.
4. Medium Stained Ice - These ice surfaces were clearly stained with oil, but were lighter in color than the heavily stained ice. Oil penetration was typically 0.12 m and reached a concentration of 1% oil by volume.
5. Lightly Stained Ice - The oil staining of the ice surface was not uniform and was barely visible from the air. Oil penetration was measured to be 0.12 m at a concentration of 0.5% oil by volume.
6. Windblown Oil - Oil blown or transported onto the surface of the ice floes from concentrated areas was typically 0.001-0.003 m thick (see Figure 2.9).

The quantification of these classifications included the variables of the depth of oil penetration into the ice and the percent oil concentration volume for the penetration depth. Actual percent composition by volume was determined by melting selected samples from areas representing each major type of oiling. Irregularities in the shape of the ice within rubble fields required that the initial surface area estimates as derived from aerial photographs be doubled. Weathered losses from each type of oil/ice involvement were estimated on the basis of samples taken from representative areas which were analyzed for percent loss of their volatile portions. The percent loss for each of the six categories of oil concentrations was then averaged and factored into the volumes present. A more detailed discussion of weathered losses is presented in Section 2.3.3. It should be noted that the analysis is based on the best available field information and that the results are an approximation. There are certain limitations to these estimates, including an inability to account for the initial losses in the water column prior to the stabilization of oil within the ice, an inability to quantify the amount

of oil hidden beneath the rafted floes, the arbitrary classification of the oil concentrations, and the approximation of the amount of oil loss due to weathering.

The results of the oil mass balance analysis are presented in Table 2.2. The first column lists the six oil/ice categories and the burn site. The following three columns provide the areal coverages. The fifth column provides the mean percent of oil saturation, and the sixth column gives the depth of oil saturation. Columns seven and eight show the approximate volumes of oil associated with each category. The last column lists the volumes of weathered oil based on percent loss of volatiles.

It is interesting to note that less than 30% of the total oil spilled was detectable in the form of large concentrated pools. Also, 15% of the oil was available in shallow pools, making approximately 45% of the oil available in a form capable of being pumped. However, the logistical problems of getting to these widely scattered patches of oil before the snow fell prevented the cleanup crews from taking full advantage of this natural containment. The majority of the 81,150 gallons spilled was spread over an area of approximately 95,000 m^2, with an average concentration of one gallon per 1.2 m^2. This oil was primarily in the form of contaminated ice which could not be practically recovered.

Table 2.2 Oil Budget for Bouchard #65 Oil Spill, January 1977.

Type of Oil/Ice Config-uration	Area Encom-passed by Spill from Mashnee Island to Wings Neck Tower (m^2)	Area Encom-passed by Spill from Wings Neck Tower to Cleveland Ledge (m^2)	Total Area (m^2)	% Oil Saturation	Depth of Saturation (m)	Volume (liters)	Volume (gallons)	Weather-ed Losses (gallons)
Deep Oil Pools	400	300	700	100	0.13	91,000	24,000	3,100
Shallow Oil Pools	1,500	300	1,800	100	0.025	45,000	12,000	1,400
Heavily Stained Ice	7,400	2,400	9,800	5	0.05	49,000	13,000	2,000
Medium Stained Ice	26,500	3,200	29,700	1	0.05	30,000	8,000	1,500
Lightly Stained Ice	28,700	3,800	32,500	0.5	0.05	16,000	4,000	1,900
Wind-blown Oil	2,100	12,600	14,700	50	0.003	22,000	6,000	1,800

Type of Oil/Ice Configuration	Area Encompassed by Spill from Mashnee Island to Wings Neck Tower (m^2)	Area Encompassed by Spill from Wings Neck Tower to Cleveland Ledge (m^2)	Total Area (m^2)	% Oil Saturation	Depth of Saturation (m)	Volume (liters)	Volume (gallons)	Weathered Losses (gallons)
Burn Site (heavily stained ice and shallow oil pools)	---	---	5,600	5	0.05	14,000	4,000	500
Weathered Evaporation Losses	---	---	---	-	---	46,000	12 000	---
Totals	≈66,000	≈22,600	≈94,800			≈313,000	≈83,000	≈12,000

"

In section 2.5 of the report the authors compare the 1977 oil spill in ice to 1969 and 1974 oil spills in open water. There was little data for the 1974 spill since only 4,200 barrels of No.2 oil was released and the spill was not followed to any great extent. However, there is more data about the 1969 spill, 172,000 to 185,000 of No. 2 was spilled during a southwest gale. This gale was believed to have caused extreme mixing of the oil and water and there was a drastic number of dead fish, worms, crustaceans, and mollusks. The area had hydrocarbon content in the sediment 12 m below the water surface and destruction of fisheries continued for a long time.

Section 2.6 is a discussion by the authors comparing the BOUCHARD 65 oil spill coastal conditions with the coastal conditions of Alaska and the conclusion was that the two systems are completely different but that the behaviour of oil under ice could be the same.

The following data is from the appendices of the report.

Two figures are included here that are plots of the mean values (temperature or wind speed) that were calculated from six measurements made during a 24 hour period. The "error bars" are used to denote the maximum and minimum values for the twenty four hour period for which the mean value was calculated.

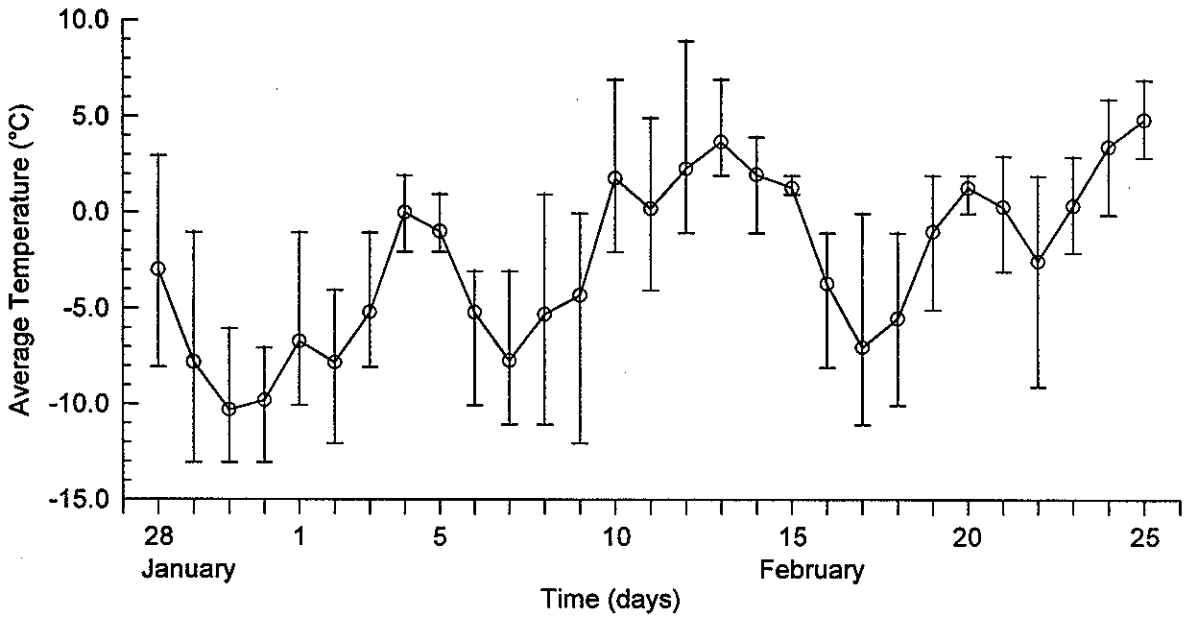

Figure from appendix III. Daily mean and range of air temperature at Wings Neck Station, 28 January - 25 February, 1977 (Army Corps of Engineers).

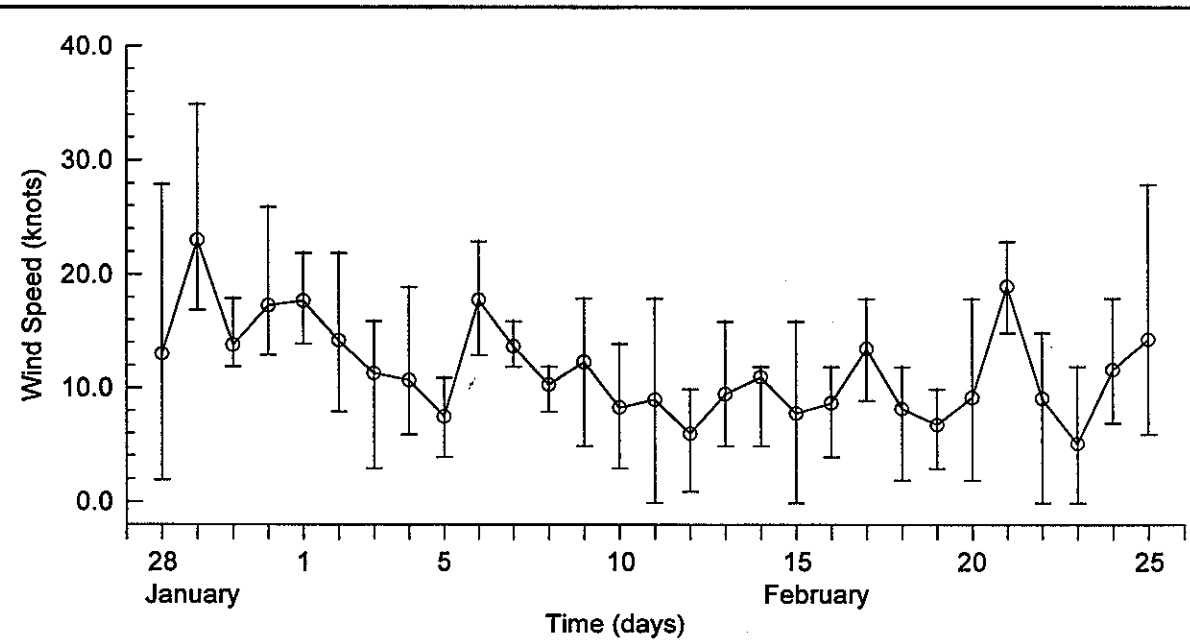

Figure from appendix III. Daily mean and range of wind speeds at Wings Neck Station, 28 January - 25 February, 1977 (Army Corps of Engineers).

The organizations and institutions that participated in the investigation and documentation of the oil spill are as follows:

ARCTEC, Incorporated
Department of Natural Resource, Town of Bourne
Energy Resources Company
Environmental Devices Corporation
Environmental Protection Agency
Massachusetts Division of Marine Fisheries
Massachusetts Division of Water Pollution Control
National Oceanic and Atmospheric Administration(NOAA)
MESA, OSCEAP, SOR, and EDS
Pacific Marine Environmental Laboratories
Science Applications, Incorporated
University of Rhode Island
University of South Carolina
University of Washington
U.S. Coast Guard Operations
U.S. Coast Guard R & D Center
U.S. Fish and Wildlife Service
U.S. Navy Atlantic Audiovisual
Woods Hole Marine Biological Laboratories
Woods Hole Oceanographic Institute

V-A Master List for Sampling Chronology
"BOUCHARD 65" Oil Spill
January 30-March 2, 1977

Master Chart No. (Map Reference)	Organization (Org. Reference No.)	Date (Time) of Sample	Type of Sample	Analysis of Sample
1 (H-1)	EPA, MMF (1)	1/30 (1000) 2/7 (1500) 2/24 (0930)	sediment (2), surface water, shellfish	
2 (I-3)	EPA, MMF (2)	1/30 (1110) 2/2 (1310) 2/7 (1530) 2/14 2/24 (0830)	sediment(2), surface water, shellfish	
3 (H-4)	EPA, MMF (3)	1/30 (1215) 2/2 (1200)	sediment(2), surface water, shellfish	
4 (H-5)	EPA, MMF (4)	1/30 (0945) 2/7 (1500) 2/24 (0830)	sediment(2), surface water, shellfish	
5 (H-5)	EPA, MMF (5)	1/30 (1115)	sediment(2), surface water, shellfish	
6 (G-6)	EPA, MMF (6)	1/30 (1200) 2/7 (1500)	sediment(2), surface water, shellfish	
7 (G-8)	EPA, MMF (7)	1/30 (1055)	sediment(2), surface water, shellfish	

Master Chart No. (Map Reference)	Organization (Org. Reference No.)	Date (Time) of Sample	Type of Sample	Analysis of Sample
8 INSET	EPA, MMF (8)	1/30 (1025)	sediment(2), surface water, shellfish	
9A (G-3)	MMF (9A)	2/2 (1030)	sediment(2), surface water, shellfish	
9B (H-3)	MMF (9B)	2/2 (1400)	sediment(2), surface water, shellfish	
10 (H-4)	ENDECO (3)	2/2 (1000-1700) 2/3 (1000-1500) 2/4 (1100-1500) 2/6 (1300-1600) 2/7 (1345-1500) 2/8 (1600) 2/9 (1030) 2/14 (1245) 2/17 (1115)	current meter lowering and multicast water samples	Fluorescence +
11 (H-3)	WHOI (4)	2/3 (1015)	sediment, surface water, benthos	Fluorescence +
12 (E-6)	ENDECO (10)	2/9 (1530) 2/14 (1410) 2/17 (1330)	water surface, mid-depth	Fluorescence +
13 (F-6)	EPA (13)	2/2 (1515)	sediments(3), benthos(3)	
14 (G-5)	EPA (14)	2/3 (1015)	sediments(3), benthos(3), surface water, water column (3 m)	
15 (H-4)	EPA (15)	2/3 (1245)	sediments(3), benthos(3), surface water, water column (3 m)	
16 (G-6)	EPA (16)	2/4 (1000)	sediment(3), benthos(3)	
17 (G-6)	EPA (17)	2/4 (1045)	sediment(3), benthos(3)	
18 (F-6)	EPA (18)	2/4 (1155)	sediment(3), benthos(3)	
19 (F-6)	EPA (19)	2/4 (1230)	sediment(3), benthos(3)	
20 (G-5)	NOAA, MBL (12)	2/4 (1220)	surface water, sediments(7)	Fluorescence *+
21 (G-5)	NOAA, MBL (11)	2/4 (1145)	surface water, sediments(7)	Fluorescence *+
22 (G-5)	NOAA, MBL (10)	2/4 (1115)	surface water, sediments(7)	Fluorescence *+
23 (G-5)	NOAA, MBL (9)	2/4 (1040)	surface water, sediments(7)	Fluorescence *+
24 (F-6)	NOAA (1)	2/6	surface ice sample	
25 (H-3)	NOAA (2)	2/6	water column (1.5 m)	
26 (H-3)	MBL (13, 42)	2/7 ,18	sediments(7)	Fluorescence 13(*), 42(*+)

Master Chart No. (Map Reference)	Organization (Org. Reference No.)	Date (Time) of Sample	Type of Sample	Analysis of Sample
27 (H-3)	MBL (14, 43)	2/7, 18	sediments(7)	Fluorescence 14(*), 43(*+)
28 (H-3)	MBL (15)	2/7	sediments(7)	Fluorescence *
29 (H-3)	MBL (16)	2/7	sediments(7)	Fluorescence *
30 Canal	NOAA (3)	2/6 (1445) 2/9 (1305)	surface water, water column (6 m)	Fluorescence +
31 Canal	NOAA (4)	2/6 (1505) 2/9 (1245)	surface water	Fluorescence +
32 Canal	NOAA (5)	2/6 (1545)	surface water	Fluorescence +
33 Canal	NOAA (6)	2/6 (1610) 2/9 (1315)	surface water	Fluorescence +
34 (F-6)	URI, NOAA (7)	2/8	surface water, ice scraping, water column (6 m)	
35 Sandwich	MMF (35)	2/8 (0830) 2/14 2/24 (1100)	surface water, sediment, shellfish	
36 (H-3)	MBL, WHOI (17, 41)	2/8 (1130) 2/18	benthos, sediments(7)	Fluorescence 17(*), 41(*+)
37 (H-3)	MBL (18)	2/8	benthos, sediments(7)	Fluorescence +
38 (H-4)	MBL (19)	2/8	benthos, sediments(7)	Fluorescence
39 (F-5)	NOAA (8)	2/8 (1030)	surface water, water column (2 and 3 m)	Fluorescence +
40 (F-5)	NOAA (9)	2/8 (1350)	surface water, water column (2, 3 and 5 m)	Fluorescence +
41 (G-7)	ENDECO (12)	2/8 (1530)	surface water, mid-depth (2 m), bottom 4" of ice core	Fluorescence
42 (A-6)	ENDECO (13)	2/8 (1510)	surface water, mid-depth (2 m), bottom 4" of ice core	Fluorescence
43 (D-7)	ENDECO (14)	2/8 (1450) 2/14 (1600) 2/17 (1545)	surface water, mid-depth (2 m), bottom 4" of ice core	Fluorescence
44 (H-3)	MBL, WHOI (5)	2/3 (1115)	surface water, sediments, benthos(2)	
45 Canal	NOAA (10)	2/9 (1330)	surface water, water column (2 and 5 m)	Fluorescence
46 Canal	NOAA (11)	2/9 (1345)	surface water, water column (2 and 5 m)	Fluorescence
47 (F-5)	MBL (31)	2/11	sediments(7)	Fluorescence *
48 (F-5)	MBL (22, 39)	2/10 2/18	sediments(7)	Fluorescence 22(*), 39(*+)
49 (G-5)	MBL, WHOI (23)	2/10	sediments(7)	Fluorescence *
50 (H-4)	MBL, WHOI (6)	2/3 (1445)	sediments(7), benthos(2)	

Master Chart No. (Map Reference)	Organization (Org. Reference No.)	Date (Time) of Sample	Type of Sample	Analysis of Sample
51 (H-4)	MBL, WHOI (7)	2/3 (1500)	sediments(7), benthos(2)	Fluorescence +
52 (F-5)	MBL (20)	2/9	sediments(7)	Fluorescence *
53 (G-5)	MBL (21)	2/9	sediments(7)	
54 (F-5)	ENDECO (9)	2/8 (0900) 2/14 (1400) 2/17 (1315)	surface water, water column (2 m)	Fluorescence +
55 (F-5)	ENDECO (8)	2/8 (0850) 2/14 2/17 (1300)	surface water, water column (2 m)	Fluorescence +
56 (F-5)	ENDECO (7)	2/9 (1400) 2/14 (1345) 2/17 (1245)	surface water, water column (2 m)	Fluorescence +
57 (G-5)	ENDECO (6)	2/9 (1430) 2/14 (1330) 2/17 (1200)	surface water, water column (2 m)	Fluorescence +
58 (G-5)	ENDECO (5)	2/9 (1500) 2/14 (1315) 2/17 (1145)	surface water, water column (2 m)	Fluorescence +
59 (H-4)	ENDECO (4)	2/9 (1120) 2/14 (1300) 2/17 (1130)	surface water, water column (2 m)	Fluorescence +
60 (H-4)	ENDECO (2)	2/9 (1100) 2/14 (1645) 2/17 (1000)	surface water, water column	Fluorescence +
61 (H-3)	NOAA (12)	2/7	ice core	Fluorescence +
62 (H-4)	NOAA (13)	2/7	surface water	Fluorescence +
63 (G-4)	NOAA (14)	2/7	surface water, bottom 4" of ice core	Fluorescence +
64 (F-5)	NOAA (15)	2/7	surface water	Fluorescence +
65 (H-2)	ENDECO (17)	2/14 (1630) 2/17 (1500)	surface water, water column (2 m)	Fluorescence +
66 (H-4)	WHOI, MBL (8)	2/3 (1520)	sediments(7), benthos(2)	Fluorescence +
67 (H-6)	MBL (34)	2/14	sediments(7)	Fluorescence +
68 (H-6)	MBL (33)	2/14	sediments(7)	Fluorescence *
69 (G-6)	MBL (28)	2/11	sediments(7)	Fluorescence *
70 (G-6)	MBL (27)	2/11	sediments(7)	Fluorescence
71 (H-6)	MBL (32)	2/14	sediments(7)	Fluorescence +
72 (G-5)	MBL (25)	2/11	sediments(7)	Fluorescence *

Master Chart No. (Map Reference)	Organization (Org. Reference No.)	Date (Time) of Sample	Type of Sample	Analysis of Sample
73 (H-4)	MBL (26)	2/11	sediments(7)	Fluorescence *
74 (G-3)	MBL (29)	2/11	sediments(7)	Fluorescence *
75 (G-3)	MBL (30)	2/11	sediments(7)	Fluorescence *
76 (F-5)	WHOI, MBL (24)	2/10 (1340)	sediments(7), benthos(2)	Fluorescence *
77 (H-7)	MBL (35)	2/16	sediments(7)	Fluorescence *
78 (H-7)	MBL (36)	2/16	sediments(7)	Fluorescence *
79 (G-7)	MBL (37)	2/16	sediments(7)	Fluorescence *
80 (G-7)	MBL (38)	2/16	sediments(7)	Fluorescence *
81 (H-1)	ENDECO (16)	2/8	ice core, surface water, column (2 m)	Fluorescence *
82 Sandwich	MMF (100)	2/14 (1200)	surface water, sediments, shellfish	
83 Sandwich	MMF (101)	2/14 (1100)	sediments, ice	
84 Barnstable	MMF (102)	2/14 (1130)	sediments	
85 Canal	MMF (103)	2/14 2/24	shellfish	
86 (J-2)	MMF (105)	2/14 2/24	surface water, sediments, shellfish	
87 (H-1)	MMF (106)	2/14	water	
88 (H-1)	MMF (107)	2/14	sediment	
89 (H-2)	MMF (108)	2/14 2/24 (0930)	sediment	
90 (G-2)	ENDECO (18)	2/14 (1615) 2/17 (1515)	surface water, water column (2 m)	Fluorescence +
91 (C-6)	ENDECO (13B)	2/14 (1445) 2/17 (1600)	surface water	Fluorescence +
92 (G-3)	MMF (109)	2/15	water	
93 (E-5)	MMF (110)	2/15	water	
94 (C-4)	MMF (111)	2/15	water	
95 (F-5)	MBL (40)	2/18	sediments(7)	Fluorescence +
96 (H-3)	MBL (44)	2/22	sediments(7)	Fluorescence *
97 (H-4)	MBL (45)	2/22	sediments(7)	Fluorescence *
98 (G-6)	MBL (46)	2/22	sediments(7)	Fluorescence *
99 (G-2)	MBL (51)	3/2	sediments(7)	Fluorescence *
100 (H-2)	MBL (52)	3/2	sediments(7)	Fluorescence *

Master Chart No. (Map Reference)	Organization (Org. Reference No.)	Date (Time) of Sample	Type of Sample	Analysis of Sample
101 (H-1)	MBL (53)	3/2	sediments(7)	Fluorescence *
102 (H-1)	MBL (54)	3/2	sediments(7)	Fluorescence *
103 (H-1)	MBL (55)	3/2	sediments(7)	Fluorescence *
104 (H-1)	MBL (56)	3/2	sediments(7)	Fluorescence *

V-B Results of hydrocarbon analysis of water column, ice and sediment samples taken in Buzzards Bay, Massachusetts, January 30 - February 24, 1977 (analysis by Environmental Devices Corporation).

Collector	Master List No.	Collector Station Code	Location	1977 Date/Time	Type Sample	ppb
ENDECO	10	3	Phiney's Harbor Entrance	2-8/1600	WS	55
				2-8/1600	WM5(2)	30
				2-8/1600	ICE	340
				2-8/1600	WSK	
	55	8	500 yd (457 m) SW Wing's Cove	2-8/0940	WSK	>1000
				2-8/0945	WS	110
				2-8/0945	WM5(2)	95
				2-8/0850	ICE	280
	54	9	Wings Neck Lighthouse	2-8/0900	WS	20
				2-8/0900	WM5(2)	70
				2-8/0900	WM5 B.F.*	180
				2-8/0900	ICE	
				2-8/0900	WSK	
	41	12	Megansett Harbor	2-8/1530	WS	40
				2-8/1530	WM5(2)	40
				2-8/1530	WSK	135
				2-8/1530	ICE	170
	42	13	Sippican Harbor, W. of Bird Is.	2-8/1510	WS	60
				2-8/1510	WM5(2)	30
				2-8/1510	WSK	280
				2-8/1510	ICE	330
	43	14	Little Bird Island	2-8/1450	WS	40
				2-8/1450	WM5(2)	
				2-8/1450	ICE	310
				2-8/1450	WSK	
	81	16	Buttermilk Bay	2-8/1350	WS	30
				2-8/1350	WM5(2)	30
				2-8/1350	ICE	310
				2-8/1350	WSK	>1000

Collector	Master List No.	Collector Station Code	Location	1977 Date/Time	Type Sample	ppb
	60	2	Phinney's Harbor Middle	2-9/1100 2-9/1100 2-9/1100 2-9/1100	WS WM5(2) ICE WSK	80 90 190
	10	3	Phinney's Harbor Entrance	2-9/1030 2-9/1030 2-9/1030 2-9/1030	WS WM5(2) WSK ICE	50 20 85
	59	4	S. Phinney's Harbor Entrance	2-9/1120 2-9/1120 2-9/1120 2-9/1120	WS WM5(2) ICE WSK	40 30 165
	58	5	500 yds. (457 m) SW of 4	2-9/1500 2-9/1500 2-9/1500 2-9/1500	WS WM5(2) ICE WSK	160 50 85
	57	6	500 yds (457 m) SW of 5, near buoy	2-9/1430 2-9/1430 2-9/1430 2-9/1430	WS WM5(2) ICE WSK	130 180 505
	56	7	Wings Cove	2-9/1400 2-9/1400 2-9/1400 2-9/1400	WS WM5(2) ICE WSK	445 >1000
	12	10	1000 yd. (914 m) SW Wings Neck Light	2-9/1530	WS	280
	60	2	Phinney's Harbor Inside	2-14/1645	WM5	70
	10	3	Phinney's Harbor Entrance	2-14/1245 2-14/1245	WSK WM5(2)	50 85
	59	4	S. of Phinney's Harbor Entrance	2-14/1300 2-14/1300	WS WM5(2)	110 95
	58	5	500 yd. (457 m) SW of 4	2-14/1315 2-14/1315	WSK WM5(2)	85 70
	57	6	500 yd (457 m) SW of 5, near buoy	2-14/1330 2-14/1330	WSK WM5(2)	>1000 350
	56	7	Wings Cove	2-14/1345 2-14/1345	WSK WM5(2)	250 200
	55	8	500 yd. (457 m) S. of Wings Cove	2-14/1400 2-14/1400	WSK WM5(2)	>1000 85

Collector	Master List No.	Collector Station Code	Location	1977 Date/Time	Type Sample	ppb
	54	9	Wings Neck Lighthouse	2-14/1415 2-14/1415	WSK WM5(2)	>1000 50
	12	10	S. of Wings Neck Light	2-14/1410 2-14/1410	WSK WM5(2)	440 100
	42	13	E. of Bird Island	2-14/1445	WSK	20
	43	14	W. of Bird Island	2-14/1600 2-14/1600	WSK WM5(2)	20 40
	65	17	Canal West Entrance	2-14/1630 2-14/1630	WSK WM5(2)	170 160
	90	18	Onset Island	2-14/1615 2-14/1615	WSK WM5(2)	>1000 190
	60	2	Phinney's Harbor Inside	2-17/1100	WM5(2)	240
	10	3	Phinney's Harbor Entrance	2-17/1115 2-17/1115	WSK WM5(2)	
	59	4	S. Phinney's Harbor Entrance	2-17/1130 2-17/1130	WSK WM5(2)	>1000 100
	58	5	500 yd. (457 m) SW of 4	2-17/1145 2-17/1145	WSK WM5(2)	30 100
	57	6	500 yd (457 m) SW of 5, near buoy	2-17/1200 2-17/1200	WSK WM5(2)	90 85
	56	7	Wings Cove	2-17/1245 2-17/1245	WSK WM5(2)	475 95
	55	8	500 yd. (457 m) S. of Wings Cove	2-17/1300 2-17/1300	WSK WM5(2)	105 85
	54	9	Wings Neck Lighthouse	2-17/1315 2-17/1315	WSK WM5(2)	180
	12	10	S. of Wings Neck Light	2-17/1330 2-17/1330	WSK WM5(2)	85 50
	42	13	E. of Bird Island	2-17/1600 2-17/1600	WSK WM5(2)	95 60
	43	14	Little Bird Island	2-17/1545 2-17/1545	WSK WM5(2)	65 85
	65	17	Canal West Entrance	2-17/1500 2-17/1500	WSK WM5(2)	60 45

Collector	Master List No.	Collector Station Code	Location	1977 Date/Time	Type Sample	ppb
	90	18	Onset Island	2-17/1515 2-17/1515	WSK WM5(2)	40 35
NOAA, Kate Baker	30	3	Mid Canal in front of Coast Guard	2-6/1442	WM20(6)	40
	31	4	Mid Canal Sagamore Bridge	2-6/1505	WS	30
	32	5	50 yd. (46 m) off dock master Cape Cod Coast Guard	2-6/1545	WS	>1000
	33	6	Buoy 3 E. Ent. Canal	2-6/1610	WS	50
NOAA, Barbara Morson	39	8	41° 41' 05" N Tug 1, 70° 39' 25" W	 2-8/1055 2-8/1030 2-8/1055	 WS WM5(2) WM10(3)	340 320 35
	40	9	41° 41' 31" N Tug 1, 70° 39' 00" W	 2-8/1350 2-8/1410 2-8/1415 2-8/1435 2-6/1515	 WM5(2) WM10 WS WM15(4) ?	 >1000 >1000 70 20
	30	3	Canal Sagamore Bridge	2-9/1245 2-9/1245 2-9/1245	WS WM5(2) WM15(4)	50 90 50
	37	4	Coast Guard Station	2-9/1305 2-9/1305 2-9/1305	WS WM5(2) WM15(4)	50 45 50
	32	5	Channel Marker 3	2-9/1315 2-9/1315 2-9/1315	WS WM5(2) WM15(4)	70 30 40
	45	10	Canal North Shore E. End	2-9/1328 2-9/1328 2-9/1328	WS WM5(2) WM15(4)	40 385 265
	46	11	Canal South Shore E. End	2-9/1345 2-9/1345	WS WM15(4)	60 40
NOAA, PCD	64	15	Transect 8	2-7/ *	WS	635
	64	15	Transect 8	2-7/ *	WS	280
	62	13	Transect 2	2-7/ *	ICE	---
	63	14	Transect 4	2-7/ *	ICE	545
	63	14	Transect 4	2-7/ *	WM5(2)	35

Collector	Master List No.	Collector Station Code	Location	1977 Date/Time	Type Sample	ppb
	61	12	Transect 1	2-7/ *	ICE	400
EPA, Peter Nolan	16	16	Scraggy Neck N.	2-4/1000	WS	225
	17	17	Scraggy Neck N.	2-4/1045	WS	75
	18	18	Scraggy Neck N.	2-4/1155 2-4/1200	WS ICE	40 380
	19	19	Scraggy Neck N.	2-4/1230	WS	45
	13	13	Wings Cove	2-2/1415	WM9	50
	15	15	Phinney's Harbor	2-3/1415	WS	30
	14	14	Wings Cove	2-3/1015	WS	50
	15	15	Phinney's Harbor	2-3/1245	WB	
WHOI, Hampson	11	4	Mouth of Black River	2-3/1015 2-3/1015	Sed.** W	4.7 15
	44	5	Head of Old Cape Cod Canal	2-3/1130 2-3/1130	WS Sed.**	20 5.6
	51	7	Monks Cove Little Bay	2-3/1500	Sed.**	10.0
	66	8	In Channel of Little Bay	2-3/1520	Sed.**	1.8
MBL, Gifford	23	9	----------	2-4/1040 2-4/1040	WS Sed.**	150 2.3
	22	10	Wing's Cove	2-4/1115 2-4/1115	WS Sed.**	70 770
	21	11	Wing's Cove	2-4/1145 2-4/1145	WS Sed.**	40 11.5
	20	12	Wing's Cove	2-3/1220 2-3/1220	WS Sed.**	 8.6
	70	27	Bassetts Island	2-11/1130	Sed.**	2.0
	69	28	Bassetts Island	2-11/1200	Sed.**	2.1
	71	32	Bassetts Island	2-11/1200	Sed.**	14.8
	67	34	Bassetts Island	2-11/1200	Sed.**	5.6
	68	33	Bassetts Island	2-11/1200	Sed.**	8.6
	48	39	Off Wing's Cove	2-18/1005	Sed.**	2.0
	78	36	Squeleque Harbor	2-16/1050	Sed.**	5.8

Collector	Master List No.	Collector Station Code	Location	1977 Date/Time	Type Sample	ppb
	79	37	Cove Ly Scragy Neck Meganset Harbor	2-16/1155	Sed.**	0.7
	95	40	Wings Cove	2-18/1034	Sed.**	1.6
	80	38	Meganset Harbor	2-16/1234	Sed.**	1.6
	27	43	Phinney's Hrbr. Mid Channel	2-18/1220	Sed.**	23.2
	77	35	Squeakage Harbor	2-16/1020	Sed.**	8.1
	26	42	Mashnee Island	2-18/1150	Sed.**	8.1
	36	41	Mouth of Back R.	2-18/1115	Sed.**	17.1

* These samples were received with insufficient information on the identification tag.
** Sediments in ppm (µg/ml of wet sediment)

V-B Results of Hydrocarbon analysis of sediment samples taken in Buzzards Bay, Massachusetts, February 3 - March 2, 1977 (Woods Hole Marine Biological Laboratories)

Master List #	MBL Station #	Sample Date	µg Oil/g wet sediment wgt.
44	5	2/3	3.5
23	9	2/4	1.8
22	10	2/4	2.2
21	11	2/4	5.3
20	12	2/4	2.0
26	13	2/7	2.0
27	14	2/7	1.8
28	15	2/7	5.6
29	16	2/7	2.8
52	20	2/9	274.0
48	22	2/10	1.4
49	23	2/10	0.4
76	24	2/10	3.0
72	25	2/11	0.4
73	26	2/11	2.9

Master List #	MBL Station #	Sample Date	µg Oil/g wet sediment wgt.
70	27	2/11	0.7
69	28	2/11	0.4
74	29	2/11	2.1
75	30	2/11	130
47	31	2/11	1.1
68	33	2/14	0.8
67	34	2/14	2.3
77	35	2/16	2.7
78	36	2/16	0.5
79	37	2/16	0.4
80	38	2/16	2.5
48	39	2/18	0.4
36	41	2/18	3.1
26	42	2/18	2.3
27	43	2/18	4.7
96	44	2/22	5.0
97	45	2/22	0.7
98	46	2/22	5.1
Control	47	2/28	N.D.
Control	48	2/28	N.D.
Control	49	2/28	N.D.
Control	50	2/28	N.D.
99	51	3/2	4.4
100	52	3/2	5.1
101	53	3/2	3.4
102	54	3/2	2.1
103	55	3/2	1.9
104	56	3/2	19.0

V-B Results of hydrocarbon analysis of water column, sediment and shellfish samples taken in

Buzzards Bay, Massachusetts, January 30 - February 24, 1977 (Massachusetts Division of Marine Fisheries)

Master List #	Org. Ref #	Sample Date	Sample Type	Hydrocarbon content
1	1	1/30 2/7 2/24	water water quahogs	negative negative negative
2	2	1/30 2/2 2/7 2/14 2/24	water water sediment quahogs	negative negative positive negative
3	3	1/30 2/2	water	negative
4	4	1/30 2/7 2/24	water water oysters	negative negative negative
5	5	1/30	water	negative
6	6	1/30 2/7	water water	negative negative
7	7	1/30	water	negative
8	8	1/30	water	negative
9A	9A	2/2	water	negative
9B	9B	2/2	water	negative
35	35	2/8 2/14 2/24	water sediment water	negative negative negative
82	100	2/14	sediment water	positive (old #2 oil) positive
83	101	2/14	water sediment	positive positive
84	102	2/14	sediment	positive
85	103	2/14 2/24	mussels mussels	positive (old #2 oil) positive (old #2 oil)
86	105	2/14 2/24	sediment mussels	negative positive
87	106	2/14	sediment	negative
88	108	2/14 2/24	sediments quahogs	positive (old #2 oil) negative

V-B Hydrocarbon content of water at Phinney's Harbor entrance, Buzzards Bay, Massachusetts, February 2-7, 1977 (Environmental Devices Corporation)

Date	Time	Surface Water	Mid-water (4 m)	Bottom (8 m)
2/2	1000	141	23	ins
	1130	ins	<10	<10
	1330	39	41	45
	1500	8	27	120
	1600	ins	10	ins
	1700	45	45	53
2/3	1000	<10	<10	40
	1100	<10	<10	84
	1200	33	36	47
	1400	<10	40	<10
	1500	<10	43	22
2/4	1100	61	24	50
	1200	46	58	72
	1300	ins	45	49
	1400	36	58	33
	1500	33	44	40
2/5	1300	17	43	48
	1400	65	60	<10
	1500	<10	19	44
	1600	38	<10	18
2/7	1345	45	55	55
	1445	35	40	40
	1530	15	45	30

V-B Results of hydrocarbon analysis of sediment samples taken in Buzzards Bay, Massachusetts, January 30 - February 4, 1977 (Environmental Protection Agency).

Station #	Master List #	Sampling Sate	Conc. #2 Fuel Oil in Sediments - ppm dry wgt.
1	1	1/30/77	<2
2	2	1/30/77	<2
3	3	1/30/77	<5
4	4	1/30/77	<3
5	5	1/30/77	<5
6	6	1/30/77	<2
7	7	1/30/77	<2
8	8	1/30/77	<6
2	2	2/2/77	<8
3	3	2/2/77	<4

Station #	Master List #	Sampling Sate	Conc. #2 Fuel Oil in Sediments - ppm dry wgt.
13	13	2/2/77	<1
14	14	2/3/77	<2
17	17	2/4/77	<2
18	18	2/4/77	<1
19	19	2/4/77	<1

Three diagrams are included here that were presented in the appendix and labelled V-C and are for three days in February, however, there is no source quoted for this data.

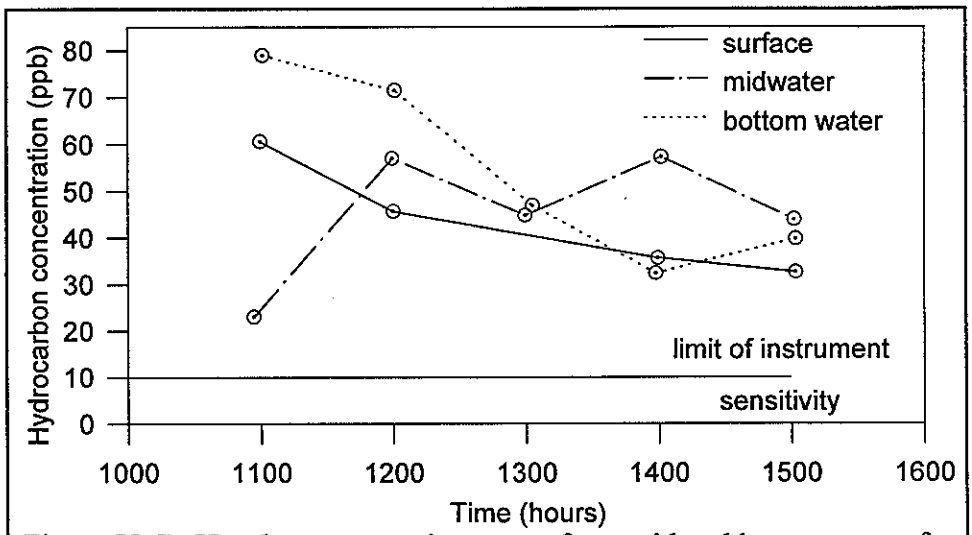

Figure V-C. Hourly concentrations at surface, mid and bottom water for master station 10, Phinney's Harbor, 4 February, 1977.

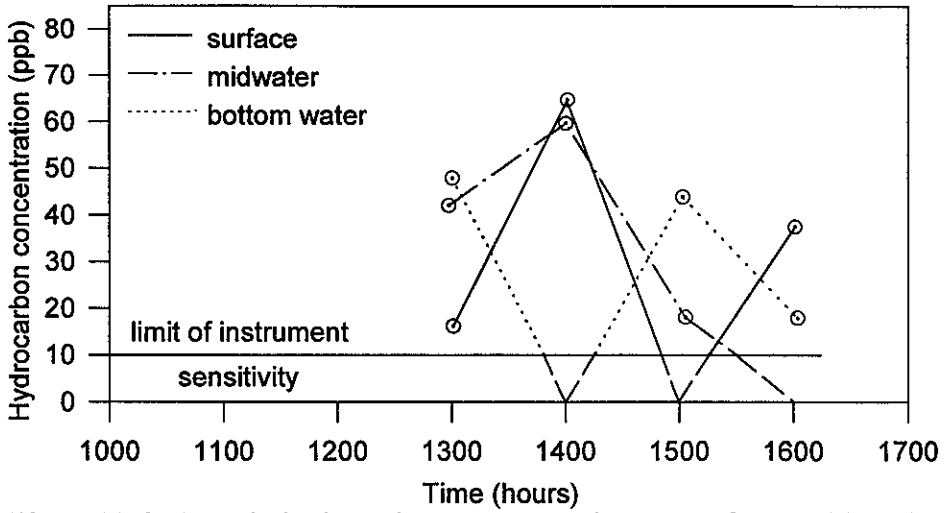

Figure V-C. Hourly hydrocarbon concentrations at surface, mid and bottom water for master station 10, Phinney's Harbor, 6 February, 1977.

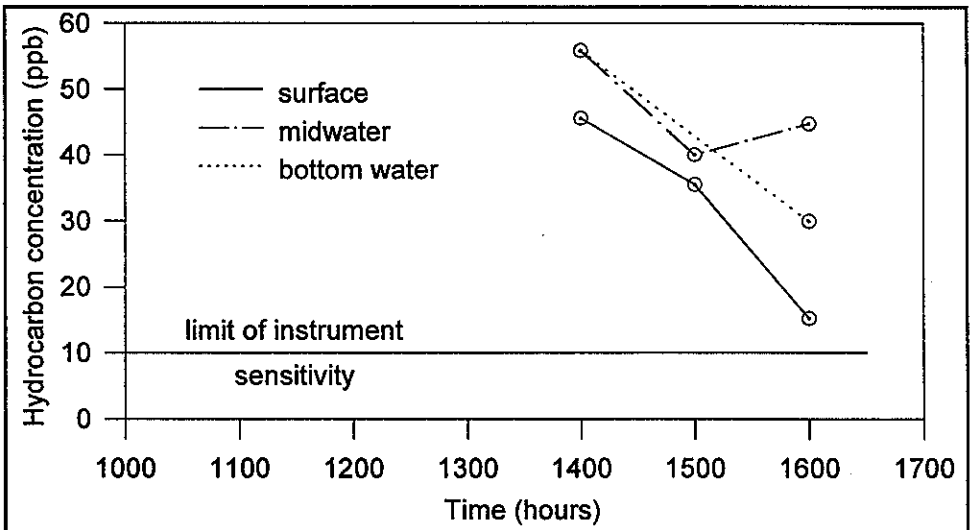

Figure V-C. Hourly hydrocarbon concentrations at surface, mid and bottom water for master station 10, Phinney's Harbor, 7 February, 1977.

Since the text was included, in most cases completely intact, the reference section is also reproduced intact.

"Section 6 References

1. World Meteorological Organization, *WMO Sea-Ice Nomenclature, Terminology, Codes, and Illustrated Glossary.* Secretariat of the WMO, Geneva, Switzerland, 1970.

2. Anraku, Masateru, *Influence of the Cape Cod Canal on the Hydrography and on the Copepods in Buzzards Bay and Cape Cod Bay, Massachusetts. I. Hydrography and*

Contribution of Copepods, Woods Hole Oceanographic Institute, Woods-Hole, Massachusetts.

3. Wilcox, B. W., "Tidal Movement in the Cape Cod Canal, Massachusetts," *Journal of the Hydraulics Division, Proceedings* of the American Society of Civil Engineers, April 1958.

4. Rosenegger, L. W., *Movement of Oil Under Sea Ice,* Imperial Oil Limited, Production Research and Technical Service Laboratory, Calgary, Alberta, September 1975.

5. Keevil, Benjamin E., and Rene 0. Ramseier, "Behavior of Oil Spilled Under Floating Ice," *Proceedings,* Joint Conference on the Prevention and Control of Oil Spills, American Petroleum Institute, 1975, pp. 497-501.

6. Uzuner, Mehmet Secil and Francis B. Weiskopf, *Transport of Oil Slick Under a Uniform Smooth Ice Cover,* Draft Report prepared for Office of Research and Development, U.S. Environmental Protection Agency, Washington, D.C., December 1975.

7. Glaeser, John L., and George P. Vance, *A Study of the Behavior of Oil Spills in the Arctic,* United States Coast Guard, Office of Research and Development, Washington, D.C., February 1971.

8. Hoult, David P., *Oil in the Arctic,* U.S. Coast Guard, Office of Research and Development, Washington, D.C., March 1975.

9. Task Force, Operation Oil, *Report of the Task Force - Operation Oil (Cleanup of the Arrow Oil Spill in Chedabucto Bay) to the Ministry of Transport,* Vol. II, pp. 15-21.

10. NORCOR Engineering and Research Limited, *The Interaction of Crude Oil with Arctic Sea Ice,* Beaufort Sea Technical Report #27, Beaufort Sea Project, Victoria, B.C., December 1975.

11. Parmerter, R. R., and M. D. Coon, "Model of Pressure Ridge Formation in Sea Ice," *Journal of Geophysical Research,* No. 77, 1972, pp. 6565-6575.

12. Parmerter, R.R., "A Mechanical Model of Rafting," *AIDJEX Bulletin*, No. 23, 1974, pp. 97-115.

13. Weeks, W F., and A. Kovacs, *On Pressure Ridges,* U.S. Amy Cold Regions Research and Engineering Laboratory, Draft Report, Hanover, New Hampshire, 1972.

14. Weeks, W. F., "Sea Ice Properties and Geometry," *AIDJEX Bulletin*, No. 34, 1976, pp. 137-172.

15. Moir, J. R., and Y. L. Lau, *Some Observations of Oil Slick Containment by Simulated Ice*

Ridge Keels, March 1975.

16. Getman, J. H., *Arctic Oil Cleanup System-Subsystem Requirements,* U.S. Coast Guard, Office of Research and Development, Washington, D.C., 1975.

17. Glaeser, J. L., "A Discussion of the Future Oil Spill Problem in the Arctic," *Proceedings,* Joint Conference on the Prevention and Control of Oil Spills, 1971, pp. 479-484.

18. Deslauriers, Paul C., and Lawrence A. Schultz, *Oil Spill Equipment and Oil Behavior in Cold Regions,* ARCTEC, Incorporated Report No. 261C, Prepared for the University of Alaska, September 1976.

19. Ramseier, R. O., G. S. Gantcheff, and L. Colby, *Oil Spill at Deception Bay, Hudson Strait,* Inland Waters Directorate, Water Resources Branch, 1973.

20. Schultz, L. A., *Tests of Oil Recovery Devices in Broken Ice Fields, Phase II,* Final Report, U.S. Coast Guard, U.S. Department of Transportation, Washington, D.C., January 1976.

21. NORCOR Engineering and Research Limited, *Investigations of the Oil Spill at Riviere St. Paul, P.Q., March 1974,* Report on Gulf Oil Canada Limited, Confidential, n.d.

22. Lamp'l, Howard J., "Lake Champlain: A Case History on the Cleanup of #6 Fuel Through Five Feet of Solid Ice at Near Zero Temperatures," *Proceedings,* Joint Conference on the Prevention and Control of Oil Spills, American Petroleum Institute, 1973, pp. 579-582.

23. Martin, Seelye, *The Seasonal Variation of Oil Entrainment in First Year Arctic Sea Ice: A Comparison of NORCOR/OCS Observations,* Department of Oceanography Special Report No. 71, University of Washington, March 1977.

24. Adams, W. A., *Light Intensity and Primary Productivity Under Sea Ice Containing Oil,* Beaufort Sea Technical Report #29, Beaufort Sea Project, Victoria, B.C., December 1975.

25. Mackay, Donald, "The Behavior of Crude Oil Spilled on Snow," *Arctic*, Vol. 28, No. 1, March 1975, pp. 19-20.

26. Mackay, D., M. E. Charles, and C. R. Phillips, *The Physical Aspects of Crude Oil Spills on Northern Terrain,* Report 73-43, University of Toronto, Department of Chemical Engineering and Applied Chemistry, January 1974.

27. McMinn, T. J,., "Oil Spill Behavior in a Winter Arctic Environment," *Proceedings,* Offshore Technology Conference, Vol. I, 1973, pp. 233-248.

28. Smith, Craig L., and William G. MacIntyre, *Initial Aging of Fuel Oil Films of Sea Water,* Virginia Institute of Marine Science.

29. Mackay, D., M. E. Charles, and C. R. Phillips, *The Physical Aspects of Crude Oil Spills on Northern Terrain,* Report No. 73-42, University of Toronto, Department of Chemical Engineering and Applied Chemistry, January 1974, pp. 58-71.

30. Wilson, Mason P., Jr., Environmental *Assessment of Treated Versus Untreated Oil Spills,* Report No. 4047, University of Rhode Island, College of Engineering.

31. Blumer, M., and J. Sass, *The West Falmouth Oil Spill,* Woods Hole Oceanographic Institute, Woods Hole, Massachusetts, April 1972.

32. Blumer, Max, Howard L. Sanders, J. Fred Grassle, and George R. Hampson, "A Small Oil Spill," *Environment*, Vol. 13, No. 2, March 1971.

33. Blumer, M., G. Souza, and J. Sass, *Hydrocarbon Pollution of Edible Shellfish by an Oil Spill*, Woods Hole Oceanographic Institute, Woods Hole, Massachusetts, and Shellfish Warden, Town of Falmouth, Massachusetts.

34. Blumer, Max, and Jeremy Sass, "Oil Pollution: Persistence and Degradation of Spilled Fuel Oil," *Science*, Reprinted from 9 June 1972, Vol. 176, pp. 1120-1122.

35. Eidam, Carl L. Personal communication, November 19, 1974.

36. Burns, J. J., L. H. Shapiro, and F. H. Fay, *The Relationships of Marine Mammal Distributions, Densities and Activities to Sea Ice Conditions,* Annual Report to OCSEAP, March 1976, RN # 248-249.

37. Kondratyev, K. Ya. (ed.), "Procedures of the Final Symposium on the Result of the Joint USSR/U.S. Bering Sea Experiment," Available from NASA, Greenbelt, Maryland.

38. Weeks, W. F., "Sea Ice Conditions in the Arctic," *AIDJEX* Bulletin, No. 34, pp. 173-205."

BOSS Critique

The authors have used areal photography to capture the evolution of the BOUCHARD 65 No. 2 oil spill in Buzzards Bay, Massachusetts. The report is written in a style that is difficult to break up into pieces such as objective, theory, method, and results. Thus a lot of the manuscript was quoted directly. The appendices had very detailed maps of the area of the spill and the testing locations were designated on these maps, none of which was duplicated here.

There is no discussion of the errors involved in any of the measurements not even the volume calculations made by the authors and observers.

The fluorescence measurements are not described in detail and specifically there is no reference made to the calibration of the emission spectra. There is no statement made about which compounds are the fluorescing components of No. 2 oil and if pure No. 2 oil or a weathered No. 2 oil was used for calibration. There is no description in the report for the designations * and + associated with the fluorescence measurements in Table V-A.

There are no definitions in the manuscript for WS, WSK or other abbreviations used in tables V-B.

Review of a manuscript by Nelson, W. G., and A. Allen entitled "Oil Migration and Modification Processes in Solid Sea Ice", in *Proceedings of the 1981 Oil Spill Conference*, pp 191-196, 1981.

Technical Summary

"The migration of Prudhoe Bay crude oil and diesel fuel through first year ice and the effect of entrained oil on sea ice growth rates were examined. Physical and chemical changes within the oils were examined during and after the entrainment process. Several crude oil and diesel fuel injections beneath solid sea ice were conducted off Prudhoe Bay during the winter of 1979/1980. Oil layers of 2.5 15 and 30 centimeters (cm) were formed under 15, 30, and approximately 60 cm of sea ice. The sea ice growth under the injected oils was monitored. At the end of the ice growing season the individual oil injection sites were excavated from the ice. Each site was studied to determine the extent of vertical oil migration. The field results are compared to laboratory salt water ice growth experiments with entrained oil layers. The laboratory test results include oil migration as a function of ice temperature and the effect of various oil layer thicknesses upon the ice growth rates. Direct heat flux measurements are included from which the thermal conductivity of oil layers is obtained as a function of the oil layer thickness. These data illustrate the relationships among oil layer thickness, temperature gradient across the oil layer, oil viscosity, and convective motion occurring within the oil layer."

Objective

"Specific areas of research included the migration of Prudhoe Bay crude oil and diesel fuel within sea ice, and the effect of oil inclusions on ice growth rates. Tests were also conducted to determine the feasibility of recovery of crude oil from within the ice by pumping, and to measure the weathering of crude oil encapsulated within sea ice."

Theory

The brine volume as a function of sea salt content in parts per thousand by weight % and temperature in °C is calculated using equations (1)-(3) of Frankenstein and Garner 1967("Short note: equations for determining the brine volume of sea ice from -0.5 to 22.9 °C", *Journal of Glaciology*, **6**(48), pp, 943-944).

$$\nu = s\left(\frac{52.56}{\Theta} - 2.28\right) \qquad -0.5\ ^\circ C \le \Theta \ge -2.06^\circ C \quad (1)$$

$$\nu = s\left(\frac{45.917}{\Theta} - 0.930\right) \qquad -2.06^\circ C \le \Theta \ge -8.2^\circ C \quad (2)$$

$$\nu = s\left(\frac{43.795}{\Theta} - 1.189\right) \qquad -8.2\ ^\circ C \le \Theta \ge -22.9^\circ C \quad (3)$$

where, ν = relative brine volume in parts brine per thousand parts ice and brine,

s = ice salinity in parts per thousand,

Θ= absolute value of ice temperature in °C.

The authors state that heat conduction is governed by an equation such as (4);

$$q = \frac{T_{iw} - T_{sa}}{R} \qquad (4)$$

where, q = the rate of heat conduction,
T_{iw} = the temperature of the ice-water interface,
T_{sa} = the temperature of the snow-air interface,
R = the thermal resistance of the material between the ice-water interface and the snow-air interface.

Method

"The 1979 to 1980 ABSORB field study of the interaction of oil and sea ice was conducted at Prudhoe Bay, Alaska, at a site located approximately 200 m west of the West Dock. Supplemental experiments were conducted at the University of Alaska, Anchorage, using the UAA cold chamber. The water depth at the experiment site was 2.1 m with a bottom consisting of fine silty material containing small rocks. The overall philosophy of the experiments was to maximize data obtained from oil injected beneath ice under field conditions, while ensuring that oil loss to the environment was avoided.

The Prudhoe Bay oil injection site was surrounded by a 61 cm fence-type boom (Harbor Dike) manufactured by Enviro-Pro Industries and furnished to the project by Arctic Oilfield Environmental Services, Anchorage, Alaska. The boom defined a circular 20 m diameter area, within which eighteen 55-gallon (gal) plastic drums were positioned to act as oil containment vessels for the various experiments. The top and bottom of each drum was removed. Each drum was fitted with an oil injection tube and a weighted hot wire ice depth measurement device as shown in Figure 1. Some of the drums were positioned from a boat during the frazil ice formation freeze-up period, while others were subsequently positioned by cutting holes in 15-cm-thick new ice.

Each drum was positioned vertically so that it would prohibit lateral migration of crude oil and diesel fuel which was to be injected as ice depths reached approximately 15, 30, and 60 cm. The installed drums are shown in Figure 2.

One plastic drum with an ice depth measurement device was placed outside of the boom to act as a control and to facilitate the measurement of surface ice ablation during the melt period after the end of the experiment.

Injection of hot crude oil (60 °C) and ambient temperature diesel fuel was accomplished using a sliding vane hand pump connected to the injection tube. Premeasured volumes of crude and diesel fuel were pumped from insulated 20-gal drums. Table 1 documents the injection dates, ice thickness, and volumes of crude oil injected.

Table 1. Hydrocarbon Injection Schedule

Date	Site Number	Ice Depth, cm	Hydrocarbon		
			Type	Quantity[a], gal	Temperature, °C
10-19-79	8	15	Diesel	18.	-1
10-19-79	10	15	Diesel	1.5	-1
10-19-79	11	15	Crude	1.5	60
10-19-79	13	15	Crude	9	60
10-19-79	17	15	Crude	13	60
11-16-79	2	28	Crude	18	48
11-16-79	3	25	Crude	1.5	48
11-16-79	4	21	Crude	9	48
11-16-79	5	24	Emulsion[b]	12.3	2
11-16-79	6	32	Diesel	1.5	-1
11-16-79	7	32	Diesel	18	-1
12-06-79	1	42	Crude	9	48
12-06-79	14	47	Diesel	9	-1
12-06-79	16	48	Crude	1.5	48
12-21-79	15	57	Emulsion[c]	4.8	2

[a] For volume in liters multiply by 3.785.
[b] 40% crude oil 60% water.
[c] 20% crude 80% water.

Samples of crude oil and diesel fuel were obtained at the injection site during each injection. These samples were stored in sealed containers fro comparison with recovered samples, at the termination of the experiment.

Data recorded during the test included snow depth and density, ice depth below each injection site and at control sites, and daily maximum and minimum temperatures. Ice depth measurements were obtained by means of an 0.8 mm (0.032 in.) diameter aircraft safety wire (corrosion-resisting wire) from which was suspended a 2-lb lead weight. The wire was heated by a 24-V battery to free the weighted segment and to allow the weight to be raised to the bottom of the ice sheet for measurement. The weight was then lowered to prevent ice encapsulation (see Figure 1).

Snow and ice thermal conductivity measurements were recorded is situ with two Thermonetics Model H 11-18-1-SHF heat flux plates and a series of Yellow Springs Instrument thermistors. The thermal conductivity of the ice and snow at the site was determined from the heat flux measurements and the interface temperatures.

An oil recovery test using a Jabsco Model 11810-003 Rubber Impeller 1/'3-hp electric pump was conducted March 7, 1979. A 2.5-cm diameter hole was drilled through the ice into the

encapsulated oil contained in Site 2. Fifteen liters (4 gal) of oil were then pumped at a rate of 1 gal/min from the oil zone. A photograph of the pumping test is shown in Figure 3. It was noted that the oil did not flow to the surface after the top of the encapsulated oil zone was pierced with the 2.5 cm ice drill.

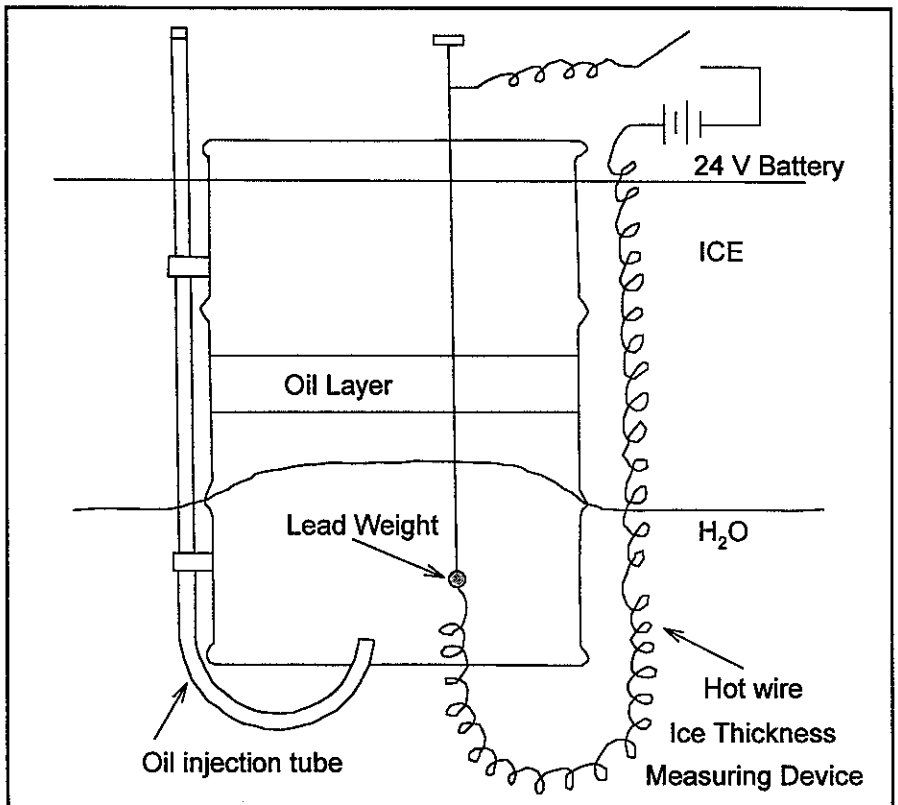

Figure 1. Oil containment and ice thickness measurement device.

The Prudhoe Bay ABSORB test was terminated March 25, 1980, with the recovery of the barrels containing previously injected crude oil and diesel fuel. The barrels and surrounding ice were removed by means of a Ditch Witch to cut the ice sections as shown in Figure 4. The ice sections were then lifted with a rubber tired Type 988 front end loader (figure 5), and removed to a suitable onshore solid waste facility where the barrels were removed from the ice and samples taken for analysis. A longitudinal wedge-shaped section was cut from each barrel to recover an oil sample and to observe oil migration and ice formation adjacent to the oiled zones. Each barrel was also labelled and photographed.

Laboratory analyses performed on the samples obtained during injection and the samples recovered from the ice included (1) an analysis of the mole fraction of methane through hexane, hydrogen sulfide, carbon dioxide, and nitrogen; (2) a simulated ASTM D86 distillation using a gas chromatograph; (3) density measurements; and (4) viscosity measurements.

Supplemental oil-in-ice work was performed at the University of Alaska, Anchorage. A 0.2-m^3 water bath with one side of tempered glass was constructed to allow the production of an ice sheet and the injection of oil below the ice sheet. The water bath was insulated on the bottom and

sides and contained regulated heat tape between the insulation and the aluminum structure to permit control of ice growth rate and geometry. A sampling and pressure relief port was also insulated and heated.

The bath was contained within a Type S-32 Thermotron temperature control chamber permitting adjustment of ambient temperature from 150 to -100 °C. The physical apparatus is shown in Figure 6. Measurements conducted included oil migration in salt ice and thermal resistance of crude oil layers at various temperatures and thicknesses."

Results

"**Oil migration**. The ABSORB oil-in-ice study differed from the NORCOR oil-in-ice study (Beaufort Sea Project 1975) in that the ABSORB experiment was removed from the ice before the spring melt season. The ABSORB observations with respect to oil migration within the ice sheet, however, agreed with those of the NORCOR study."..."During these periods of high insulation, it can be shown that the ice sheet temperatures approached that of the ice sheet during spring months. The 1979/1980 ABSORB study thus established that oil migration in first-year ice can be induced by adding surface insulation to the ice sheet.

It was also found that diesel fuel migrated much more readily than Prudhoe Bay crude oil." The authors attributes the fuel migration difference solely to the difference in viscosity of diesel fuel and Prudhoe Bay oil. The authors also stated that the emulsions did not migrate due to stabilization of emulsified water because it was ice.

The authors computed the thermal resistance of oil layers by comparing growth rates of ice for the oiled and unoiled sites. "These resistances were converted to the thermal conductivity of the oil within the layer by dividing the computer resistance into the observed oil layer thickness. The thermal conductivity of the oil layer at each site was thus normalized to values having the same dimensions." The authors report that the thermal resistance of the typical "hard-packed" snow near the area was from 0.18 to 0.53 m °C/W and that the expected values of thermal resistance for sea ice were a range from 0.13 m °C/W for ice 0.3 m thick to 0.52 m °C/W for ice 1.8 m thick. "It is thus apparent that the thermal resistance of encapsulated oil layers whose thermal resistance could reach 20 times that of ice ... or 1.3 m °C/W for a 12.5 cm-thick-layer could greatly alter the ice growth rate under the oil layer." The authors listed (Table 2) the preliminary work done in the laboratory to verify the field results.

Table 2. Laboratory Measurement of the Thermal Conductivity of Prudhoe Bay Crude Oil Layers

Crude Oil Layer Thickness, cm	Temperature of Layer Bottom, °C	Temperature of Upper Surface, °C	Thermal Conductivity, W/m °C
12.5	-0.1	-3	0.78
12.5	0.1	-28	0.29

The oil weathering was determined and the results are listed in Tables 3, 4, and 5 for the molecular content and physical properties of the crude oil.

Table 3. Molecular Content and Physical Properties for Sites 11 and 17

Component and Physical constants	Mol percent		
	Injection Sample	Weathered Sample	
		Site 11	Site 17
Hydrogen Sulfide	0.00	0.00	0.00
Carbon Dioxide	0.03	0.01	0.00
Nitrogen	0.19	0.12	0.16
Methane	0.00	0.01	0.00
Ethane	0.09	0.01	0.09
Propane	0.84	0.32	0.88
iso-butane	0.45	0.30	0.50
n-butane	2.02	1.41	2.12
iso-pentane	1.33	1.00	1.43
n-pentane	2.35	2.13	2.33
Hexanes	2.43	7.98	5.86
Heptanes plus	90.27	86.71	86.63
totals	100.00	100.00	100.00
Density at 15.5 °C, g/cm^3	0.884	0.883	0.833
Molecular Weight	254	254	262
Viscosity at 100 °F, centistokes	8.88	10.6	10.6

Table 4. Molecular Content and Physical Properties for Sites 2, 3, 4, and 5

Component and Physical constants	Mol percent					
	Injection Sample	Weathered Sample				
		(Site 2)[a]	Site 2	Site 3	Site 4	Site 5 (Emulsion)
Hydrogen Sulfide	0.00	0.00	0.00	0.00	0.00	0.00
Carbon Dioxide	0.04	0.01	0.02	0.00	0.00	0.00
Nitrogen	0.33	0.08	0.16	0.10	0.13	0.12
Methane	0.00	0.00	0.02	0.01	0.01	0.00
Ethane	0.17	0.05	0.19	0.10	0.17	0.17
Propane	1.18	0.62	0.88	0.85	1.06	1.42
iso-butane	0.55	0.41	0.30	0.45	0.44	0.69
n-butane	2.33	1.88	1.11	1.81	2.03	2.78

Component and Physical constants	Mol percent					
	Injection Sample	Weathered Sample				
		(Site 2)[a]	Site 2	Site 3	Site 4	Site 5 (Emulsion)
iso-pentane	1.40	1.34	1.59	1.34	0.99	1.67
n-pentane	2.47	2.32	2.86	1.77	2.03	2.80
Hexanes	3.20	4.08	4.41	8.01	7.13	3.18
Heptanes plus	88.33	89.21	88.46	85.56	86.01	87.17
totals	100	100	100	100	100	100
Density at 15.5 °C, g/cm^3	0.890	0.888	0.891	0.883	0.891	0.891
Molecular Weight	255	261	256	259	256	258
Viscosity at 100 °F, centistokes	8.6	10.5	9.52	13.3	10.4	9.88

[a] (Site 2) Sample pumped from ice into open container and weathered at -9 °C.

Table 5. Molecular Content and Physical Properties for Sites 15 and 16

Component and Physical constants	Mol percent		
	Injection Sample	Weathered Sample	
		Site 15 (emulsion)	Site 16
Hydrogen Sulfide	0.00	0.00	0.00
Carbon Dioxide	0.17	0.00	0.02
Nitrogen	0.28	0.18	0.15
Methane	0.17	0.00	0.01
Ethane	0.27	0.05	0.19
Propane	1.21	0.57	1.07
iso-butane	0.56	0.30	0.42
n-butane	2.26	1.28	1.72
iso-pentane	1.44	0.75	0.80
n-pentane	2.46	1.62	1.23
Hexanes	3.97	4.77	2.67
Heptanes plus	87.21	90.48	91.72
totals	100.00	100.00	100.00
Density at 15.5 °C, g/cm^3	0.890	0.897	0.885
Molecular Weight	255	262	259

Component and Physical constants	Mol percent		
	Injection Sample	Weathered Sample	
		Site 15 (emulsion)	Site 16
Viscosity at 100 °F, centistokes	8.58	14.7	8.56

The authors state that the increase in viscosity, in above tables, is unexplained but may be due to thermal cycling of the oil.

The simulated distillation data presented in Tables 6, 7, and 8 also confirm that oil injected under the ice does not tend to show signs of weathering.

Table 6. Simulated Distillation Data for Injection Sample and Samples from Sites 11 and 17

Percent Evaporated	Temperature °C		
	Injection Sample	Site 11	Site 17
1	39	43	41
2	88	97	93
3	106	110	111
4	119	126	127
5	130	131	133
10	161	162	167
15	189	189	197
20	217	217	235
25	256	255	263

Table 7. Simulated Distillation Data for Injection Sample and Samples from Sites 2, 3, 4, and 5.

Percent Evaporated	Temperature °C					
	Injection Sample	(Site 2)[a]	Site 2	Site 3	Site 4	Site 5
1	39	39	39	39	39	39
2	88	88	61	99	92	98
3	108	107	109	114	108	112
4	121	126	122	129	124	128
5	131	133	132	134	133	133
10	163	167	164	167	164	166
15	190	199	191	196	191	196

Percent Evaporated	Temperature °C					
	Injection Sample	(Site 2)[a]	Site 2	Site 3	Site 4	Site 5
20	219	239	222	229	220	231
25	256	264	257	260	256	261

[a] (Site 2) Sample recovered by pumping crude oil from ice.

Table 8. Simulated Distillation Data for Injection Sample and Samples from Sites 15 and 16

Percent Evaporated	Temperature °C		
	Injection Sample	Site 15	Site 16
1	39	43	39
2	93	109	46
3	114	128	98
4	129	136	111
5	137	146	127
10	168	182	158
15	196	213	186
20	228	254	214
25	259	269	254

The barrel that was left outside the experimental boom showed an ablation of 76 cm to July 1, 1980. For a single week, from June 24, 1980 to July 1, 1980 the rate was 3.3 cm/ day.

The authors computed that the ambient temperature of the encapsulated oil was 15 °F and could be pumped with a positive suction pump.

BOSS Critique

The authors used the incorrect units when they discussed thermal resistance and the units were corrected by the reviewer for this report. The authors discuss thermal resistance of ice when they mean thermal capacity which is dependent upon the thickness of the ice times the thermal resistance of the ice or divided by the thermal conductivity of the ice. Thermal resistance (m°C/W) is the inverse of thermal conductivity (W/m°C) and therefore has the inverse units. The authors stated in the abstract, for this manuscript, that the heat flux measurements were included in this report but these measurements were not in this report.

The authors have included a discussion of the instruments used but not the errors associated with the measurements made with these instruments.

Review of a manuscript by MacNeil, M.R., and R.H. Goodman entitled *Oil Motion during Lead Closure*, Environmental Studies Revolving Funds Report No. 053, 1987.

The same data is present in a manuscript by MacNeil, M.E., and R.H. Goodman, entitled "Motion of Oil in Leads", in *Proceedings of the Eighth Annual Arctic Marine Oilspill Program Technical Seminar*, pp 42-52, 1985.

Technical Summary

"In the unlikely event of an oil spill occurring in Arctic waters during the spring break-up season, oil may appear in the leads between ice floes. To develop suitable mitigation tools for this situation, it is essential to know where the oil will move, that is, its fate. This paper reports data on the motion and fate of oil as leads close. The oil used was typical Arctic oil, Adgo, a relatively heavy crude.

This paper describes the experimental apparatus and the data collected during four tests. The closure rate of the leads was varied over a range of 0 to 12 cm/s and the amount of oil that remained on the surface within the closed lead and under the water was measured as a function of closure rate. Results of these tests give a clearer understanding of how oil will react when natural leads close and improve our capability of handling oil in such situations."

Objective

"Progress in the development of clean up methods for Arctic oil spills has improved over the past few years, in support of the advancements in exploration and production technology. Although exploratory drilling from artificial islands and drillships continues in the Canadian Beaufort, coping with a major oil spill would pose a difficult problem. One of the most challenging aspects of an oil spill in the Arctic would be dealing with oil in leads or in broken ice where conventional mechanical methods for clean up are not successful. Although dispersants may eventually prove valuable in treating oil spills in cold waters, their use is still controversial. Dispersants are expected to be less efficient in the Arctic not only because of the cold, but also because the presence of ice reduces turbulence and hence chemical dispersion. However, brash ice actually increases chemical dispersion. Research into clean-up techniques could be facilitated if more were known about the behaviour and fate of oil spilled in leads between large ice floes. An understanding of the behaviour of oil spilled in leads is important in estimating the threat posed by oil to the environment because birds, fish, marine mammals and plankton frequent leads, especially in the spring.

To focus on the "fate of oil", we decided to study the motion of oil in leads on a near field-sized scale. Assuming little natural dispersion because of low turbulence levels, eventually the oil will interact with the ice as the lead either refreezes or closes up. (There is less likelihood of refreezing in the spring than in fall or winter because of warmer weather.) In this experiment, we set out to observe oil motion only during lead closure, and have not looked at refreezing."

Theory

None stated.

Method

"EXPERIMENTAL FACILITY

The experiment was carried out in an outdoor test basin especially designed for this project and located on the site of the Esso Resources Canada Limited laboratory in Calgary, Alberta (Figure 1), close to a much larger ice test basin. The dimensions of the basin are 15 m x 19 m, with a maximum depth of 2 m. An 0.8-m deep excavation is surrounded by 1.2-m walls, using steel barriers for end walls (see Figure 1B) and steel trusts retainers lined with 18.5-mm plywood for side walls (see Figure 1C). From the side walls, the sand excavation slopes at 30° down toward a flat, sand bottom. The whole basin is lined with a sealed, 0.5-mm PVC liner, which is insulated from the steel and plywood walls by a 25-mm thick styrofoam to prevent icing on the plastic. Plywood (60 cm wide), attached to the upper sides of the basin, secures the liner and protects it from being ripped by ice. Ordinary salt was added to the water to bring the salinity up to about 28 0/00, corresponding to the surface salinity that would typically be measured in the southern Beaufort Sea in winter.

For the purpose of recording the tests photographically, a light steel beam was erected between two steel A-frames at 3.6 m above the basin (Figure 1D). Four, Hulcher 35-mm, motor-driven cameras (5 to 10 frames per second) were suspended from the beam using a pulley system, so that the position of the cameras over the basin could be adjusted easily. The cameras were activated remotely just prior to each test. Because the A-frames were mounted on wheels that ran in tracks on either side of the basin, the entire structure could be moved to any cross-section of the basin.

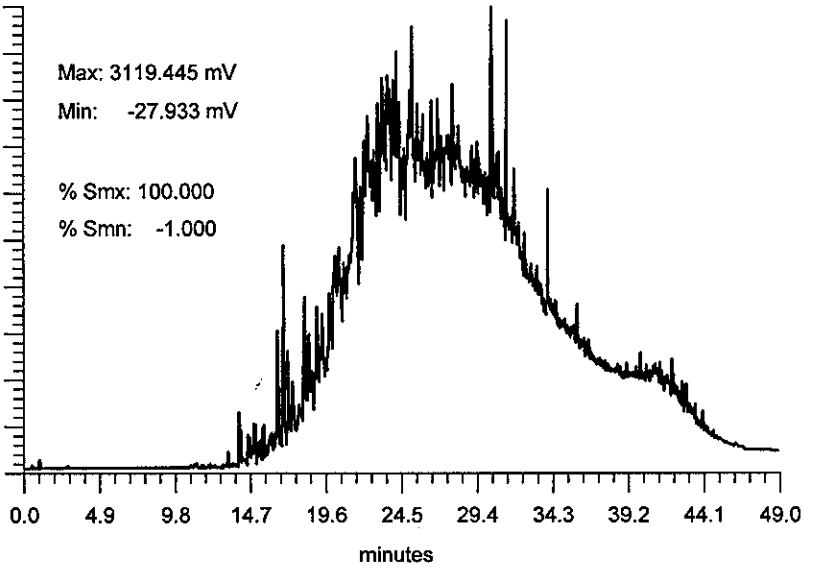

Reconstructed Figure 2. Gas Chromatograph of ADGO P25.

DEVELOPMENT OF TESTING PROCEDURES

In December 1983, an extended period of cold weather established a 30-cm thick ice sheet in the basin. A single pre-test was performed to test equipment, to establish experimental procedures, and to confirm the suitability of chosen parameters. The experimental procedure was:

a) Chain saws were used to cut a straight lead in the ice sheet 1 m wide across the width of the basin. The ice sheet on one side of the lead was stationary and on the other side was moveable.
b) Thirty litres (L) of oil was applied to the surface of the lead over a pour plate and the oil was allowed to spread to an equilibrium thickness.
c) The lead was closed by pulling the "free" ice sheet straight into the stationary one using two hand winches (one at either end of the moving sheet).
d) Video and overhead 35-mm photography were used to record the lead closure.
e) After the lead was closed, underwater photographs were taken of the underside of the lead.
f) A rough estimate was made of the fate of the oil.

The oil used in this and all subsequent tests was unweathered Adgo, a heavy Arctic crude, chosen for its availability and low pour point. Figure 2 shows the gas chromatograph of Adgo oil, and Table 1 presents the properties of this oil.

Table 1. Properties of Unweathered Adgo Oil.

Viscosities (mm^2/s)			Flash Point °C	Fire Point °C	Pour Point °C	Density @ 20 °C	Emulsion
-10 °C	0 °C	15 °C					
661.3	233.9	73.01	95	116	-26	0.9520	Fairly Quick Separation

During the initial experiments, 30 L of Adgo oil was applied in an air temperature of -15 °C on water with a temperature of -2 °C. Based on this run, the following changes were made to the method:

a) The amount of oil used for each test was reduced to 5-10 L.
b) Wire was used in the hand winches, instead of 6 mm polypropylene rope.
c) The lead would be created using a single cut across the basin, then pulling the two ice sheets apart, so that the sides of the lead match.
d) Although slush is found floating naturally on some leads in the field which will affect results, it was decided to eliminate slush for the initial tests to avoid a further complication to interpreting the experiment.
e) Estimating the amount of oil reaching the surface of the ice was accomplished by multiplying the area of the oil by the thickness. The thickness of the oil was measured directly in numerous locations. Overhead 35-mm photographs, taken immediately after lead closure, were used to measure the areal extent of patches of oil of varying thickness. The resulting volumes were estimates.
f) Using manual lead closure meant that the rate of the closure could

not be controlled with precision, and high rates (greater than 15 cm/s) could not be attained easily. Two rough classifications of lead closure rates were achieved. These rates were about 5-10 cm/s and about 15 cm/s.

g) The underwater photographs showed that some oil may have reached the underside of the ice, hence, more sophisticated underwater photography was warranted. During the subsequent tests in January, underwater photography consisted of real-time underwater video, along with 35-mm motor-drive photography (18-mm and 35-mm lenses) during lead closure and post-test 35-mm shots.

Following the December test, the oiled ice was cut out and manually removed. A crane was then used to break up and remove the remaining ice sheet. A new ice sheet was grown for the next tests.

TEST PARAMETERS

By late January 1984, a new 30-cm ice sheet had grown over the basin. Using the method described, four tests were carried out on four different leads over a two-day period. Table 2 presents the parameters of each test.

Table 2. Test Parameters.

Test No.	Volume of Oil (L)	Air Temp. (°C)	Water Temp. (°C)	Ice Thickness (cm)	Freeboard (cm)	Oil Temp. (°C)	Salinity (0/00)	Rate of Closure (cm/s)
1	10	-3	-0.5	30	0-3	4	24	<5
2	5	-2	-0.5	30	f3	7	24	6
3	5	+9	-0.5	30	f3	7	24	6
4	5	+2	-0.5	30	f3	7	24	12

... The main parameter to be varied was the rate of closure. As mentioned previously, the rate could not be changed with precision but could be measured accurately using the change of the lead width in the pictures from the motor-driven cameras. Three rates were attained: less than 5 cm/s, 6 cm/s, and 12 cm/s. Although freeboard may also change the fate of the oil, except for Test 1, it was kept constant in this set of experiments. In Test 3, dispersant (Corexit 9550) was sprayed on the oil to investigate any effect on its behaviour."

Results

"TEST 1

Ten litres of oil were applied to a lead with some slush in it. The oil spread very little on the surface of the lead, creating a slick 0.5 to 1 cm thick. The freeboard on the west (moving) side of the lead was about 2.5 to 3 cm but the other ice sheet was still frozen to the basin walls, and freeboard along the eastern edge of the lead was negative in places, with water flowing over the ice. When the lead closed, there was no observable flow of oil along the lead, but an estimated 3 L of oil

flowed over the ice sheet on the east side of the lead (in regions of negative freeboard) as the sides of the lead pressed together. No oil was squeezed out onto the west side of the lead, or under the ice. Figure 3A shows an aerial view of the oil on the ice."

TEST 2

The amount of oil poured onto the lead was reduced to 5 L. Probably as a result of less slush in the lead, the oil spread more evenly and thinly that in Test 1, to about 0.2 cm thick. On both sides of the lead, the freeboard was 2-3 cm. As the lead closed at about 6 cm/s, oil was squeezed over the ice on both sides of the lead (Figure 3B), to a maximum of 20 cm from the edge of the lead. An estimated 0.5 to 1 L of oil covered the ice. Underwater video and photography showed that some oil was squeezed downward between the ice sheets upon impact. Four to 4.5 L remained between the ice sheets. Again, the oil did not move along the lead.

TEST 3

Extensive slush in the lead prevented complete lead closure.

Test 4

The oil spread over the lead to s similar thickness as in Test 2. However, the lead closed at twice the rate (12 cm/s), causing the oil to splash over both sides of the ice to a distance of 30-40 cm from the ice edges all along the lead. An estimated 4 L was spread on top of the ice (see Figure 3C). Underwater photography showed that the impact of the ice sheets coming together forced some oil onto the underside of the ice, although the actual amount was negligible, probably less than 0.1 L. This oil appeared as globules scattered as far as 75 cm from the closed lead."

The authors then state that the rate of lead closure has the most affect on the fate of the oil, the oil getting placed on the ice. They also state that the negative freeboard caused oil to be deposited on the ice.

<u>BOSS Critique</u>

There is no statement of theory. The authors do not state the errors of the measurements made. There is no discussion of the error in the rate closure determined from the motorised camera photographs. There is no discussion of errors for the volumes of the oil spills calculated using the photographs taken during the experiments and thickness of oil, which was manually measured to some unmentioned accuracy. The authors state that there were no know rates of closure of leads for the Beaufort Sea area to compare these results to.

Review of a manuscript by Martin, S., entitled "A Field Study of Brine Drainage and Oil Entrainment in First-Year Sea Ice", *Journal of Glaciology*, Vol. 22, pp 473-502, 1979.

Technical Summary (Abstract)

"From field observations this paper describes the growth and development of first-year sea ice and its interaction with petroleum. In particular, when sea ice initially forms, there is an upward salt transport so that the ice surface has a highly saline layer, regardless of whether the initial ice is frazil, columnar, or slush ice. When the ice warms in the spring, because of the eutectic condition, the surface salt liquifies and drains through the ice, leading to a formation of top-to-bottom brine channels and void spaces in the upper part of the ice. If oil is released beneath winter ice, then the oil becomes entrained in thin lenses within the ice. In the spring, this oil flows up to the surface through the newly-opened brine channels and distributes itself within the brine-channel feeder systems, on the ice surface, and in horizontal layers in the upper part of the ice. The paper shows that these layers probably form from the interaction of the brine drainage with the percolation of melt water from surface snow down into the ice and the rise of the oil from below. Finally in the summer, the oil on the surface leads to melt-pond formation. The solar energy absorbed by the oil on the surface of these melt ponds eventually causes the melt pond to melt through the ice, and the oil is again released into the ocean."

Objective

The author's objective is to bring observations from three sources together into one publication, (1) NORCOR oil-in-in experiment 1974-75, (2) unoiled first-year ice growth done in the Beaufort Sea for the United States Outer Continental Shelf Environmental Assessment Program (OSCEAP) during 1975-78, and (3) laboratory studies on the growth of oiled and unoiled sea ice.

Theory

The basic theory here is that during the freezing of sea-ice salt is concentrated on the surface. Thus the surface snow-ice or ice has a high salinity and thus a depressed melting point and will melt before the regular ice does. This brine then falls through the defects in the crystal structure of the sea-ice forming brine channels. These brine channels are known to allow oil spilled under the surface of the ice to come to the surface.

Method

The basic method through all of the reported experiments was to take ice cores from the experimental sites and photograph these cores, some of which were oiled and some not. Temperature profiles and salinity of the cores were also determined. A more detailed explanation is presented in the author's own words.

"In the following, much of our data consists of photographs of 76 mm diameter ice cores taken with a SIPRE corer. Depending on whether the resultant core was oiled or unoiled , we used several different photographic techniques. In the NORCOR field observations, we generally placed the oiled core on a sheet of oil absorbent, a white felt-like material, then photographed the core either with a front flash or by natural light. Figure 16a shows a typical oiled ice core. For unoiled sea ice,

we treated the cores to enhance their photographic contrast in the following way: First we cut the core longitudinally in half. Then we rubbed the flat surface of the half core with an alcohol-water solution which dissolved the saw cuts and melted away some of the surface so that the crystal structure stood out. Finally, we rubbed the ice surface with an oil-soluble dye which settled in the cracks between the individual crystals, thus greatly increasing the contrast.

To photograph the unoiled cores, we used either a front or back flash. In the fall 1975 OSCEAP traverse we used a front flash; Figure 3a shows an example. After that time we used a back flash, which consisted of a box containing a half-cylinder "Plexiglas" (polymethylmethacrylate) insert with flash tubes beneath it. To photograph the core, we placed the dyed half-core in the box, then took flash a photograph. Figure 9a, a typical photograph, shows that this technique not only shows the crystal structure, but also brings out the presence of air bubbles within the ice.

The temperature profile within the ice was also determined in two different ways. In the NORCOR experiments several thermistor chains were frozen into the ice and the temperature sampled throughout the season. In our OSCEAP observations, we determined the temperature profile from the ice core. Immediately after pulling the core, we placed it inside an insulated box with a cylindrical cut-out so that the box fitted snugly around the ice. Because ice has a thermal diffusivity of about 10^{-6} m^2 s^{-1} and the ice core has a radius of about 38 mm, the time in which the ice will equilibrate to a uniform outside temperature even without insulation is about 1500 s or 25 minutes. We sampled the ice-core temperature by drilling holes into the core at 50 mm intervals through holes pre-placed in the insulation. We placed thermistors into the drilled-out holes and measured their resistance with an ohmmeter. The resistances were then converted to temperatures using a programmable hand calculator; the accuracy of these measurements was about 0.1 deg.

Finally, we determined the salinity profile of the core by cutting into transverse sections with thicknesses of 50-100 mm, melting these sections down, and measuring their salinities with an optical salinometer which was accurate to 0.2 ‰. For each core, we also sampled the salinity of the surface snow, the salinity of the salt flowers if they occurred, and the surface salinity. To determine surface salinity we would clean the snow off the ice, scrape up a sample 1-3 mm thick from the ice surface with a chisel, then melt the sample and measure its salinity."

The author states that the NORCOR field experiments were carried out with two types of oil, (1) Norman Wells crude oil with a pour point of -50 °C, and a specific gravity of 0.845 at 0°C and (2) Swan Hills crude oil with a pour point of -5 °C and a specific gravity of 0.835 at 0 °C. The author states that Balaena Bay, where the NORCOR work was done, had conditions which formed a slush -ice layer that was from 70 180 mm thick. The author has reported three types of oil-ice interaction, (1) immediately following the release of oil, (2) after the brine channels had been opened and oil rose to the surface, and (3) while oiled melt ponds were formed and drained.

On May 15, 1975 the author discharged 0.42 m^3 of Norman Wells crude, under 1.95 m of ice from which the snow had been removed, in a three minute period.

On April 8, 1975, 0.82 m^3 of Norman Wells crude oil was spilled in an offshore site under ice adjacent to a weathered pressure ridge.

Results

The author states that the report will present data for three types of ice, columnar, frazil and slush (snow mixed with water). In all cases there is a higher salinity content for the surface portion of the core than for the ice lower down.

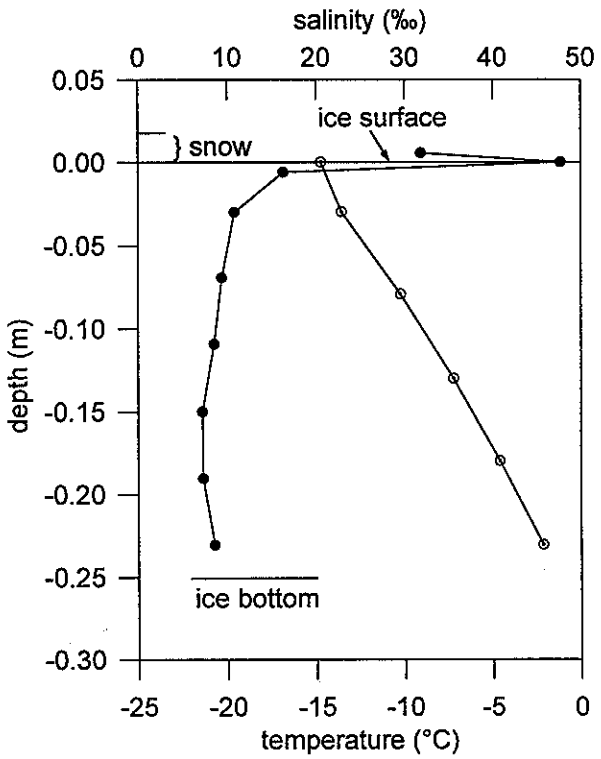

Figure 3. Columnar ice. (b) Salinity and temperature profile of the core shown in (a); salinity 2, temperature /.

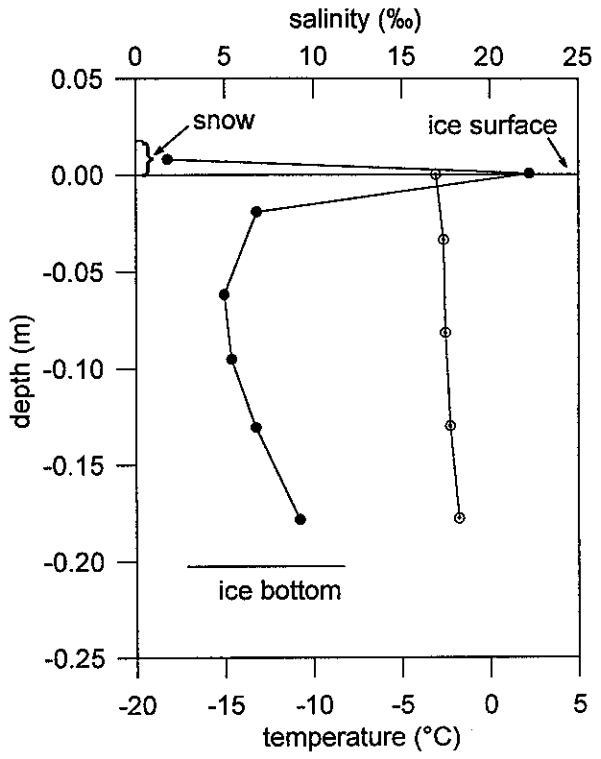

Figure 5. Frazil Ice. (b) Salinity and temperature profile of the core shown in (a); salinity 2, temperature /.

A typical core that would be called columnar ice has a top layer (10-20 mm) with small randomly oriented ice crystals, a mid section of long columnar crystals, and a bottom lay (10-40 mm) of skeletal ice that is porous and fragile. The core temperature and salinity profiles of such a core are presented in the author's Figure 3(b). Notice that both the surface snow close to the ice surface and the ice surface have a high (>15‰) salinity content while the ice itself has a fairly constant salinity of 10‰. As would be expected the temperature increases as the data point approaches the bottom of the ice.

Frazil ice is formed from water that is constantly stirred as opposed to columnar which is from quiescent sea conditions. The constant stirring results in no formation of long columnar ice crystals and the ice crystals form platelets that are typically 1-10 μm thick and diameters of 1-2 mm. The frazil core salinity profile presented in Figure 5(b) shows a much smaller range of surface salinity and salinity change with respect to depth. The temperature profile has a very small range of change and this ice is formed under warmer conditions.

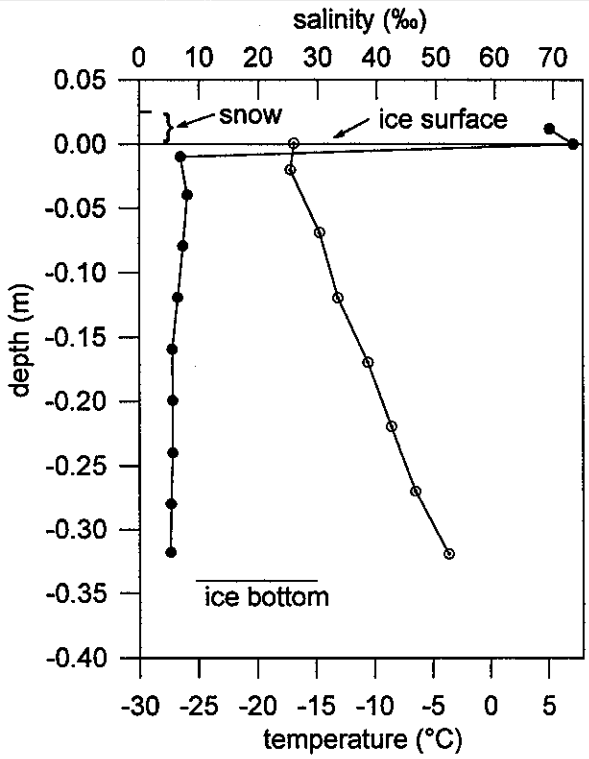

Figure 6. Ice grown from snow mixed with sea-water. (b) Salinity and temperature profile for core in (a); salinity 2, temperature /.

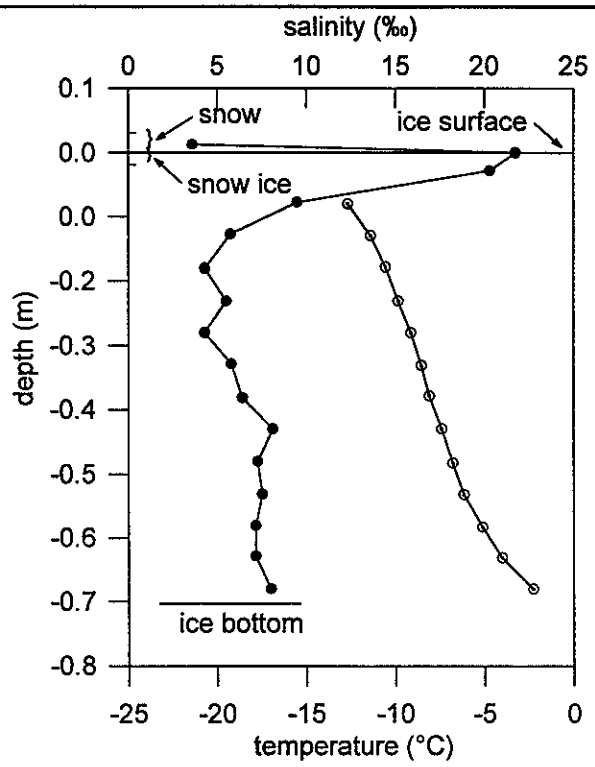

Figure 7. Snow-ice growth on sea-ice surface. (b) Salinity and temperature profile for core in (a); salinity 2, temperature /; note scale change on salinity between (7b) and (6b).

Ice grown from snow mixed with sea-water is characterised in Figure 6(b) and there is no sharp change in salinity at the depth where columnar ice formation occurs. There is a similar range of salinity and temperature values compared to columnar ice in Figure 3(b) but much different than the profiles for frazil ice in Figure 5(b).

Figure 7(b) is the salinity and temperature profile for snow that has been formed into ice by melting and refreezing conditions. This may be from solar radiation melting the snow or from the weight of the snow causing the sinking of the ice it is on and coming into direct contact with the sea water. The salinity range is less than for the slush-ice case but the temperature profile is similar (see Figures 6(b) and 7(b)).

The author states that "the brine drainage systems form between the crystal boundaries with feeder channels coming between the platelet boundaries. To illustrate the spatial frequency of brine channels, Figure 8 shows a previously unpublished observation made by Robert Lake of the brine-tube distribution at the bottom of a piece of first-year ice 1.6 m thick taken in February 1968 at Cambridge Bay, Northwest Territories, Canada; the brine channels have a characteristic spacing on

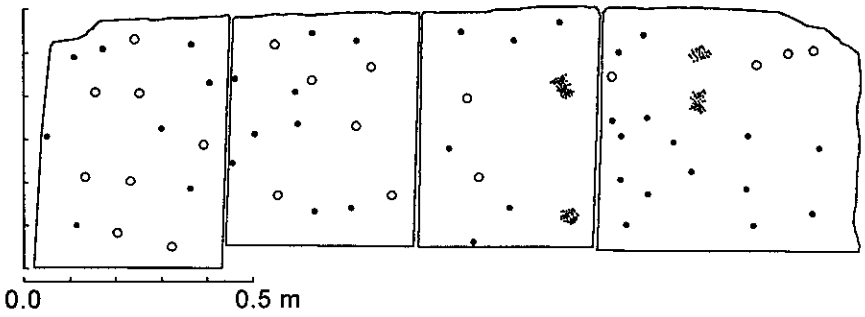

Figure 8. Sketch of brine channel distribution on the bottom of first-year ice made in February 1968 by Robert Lake. Large circles have a diameter of about 10 mm, large dots about 5 mm, and small dots about 1 mm.

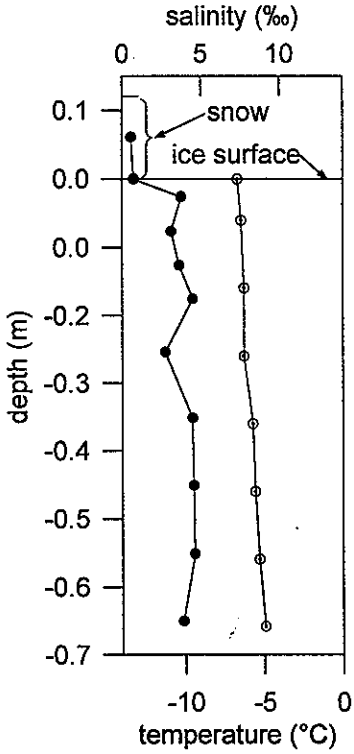

Figure 9. Brine drainage channels in the spring. (c) Salinity and temperature profile for (a); salinity 2, temperature /.

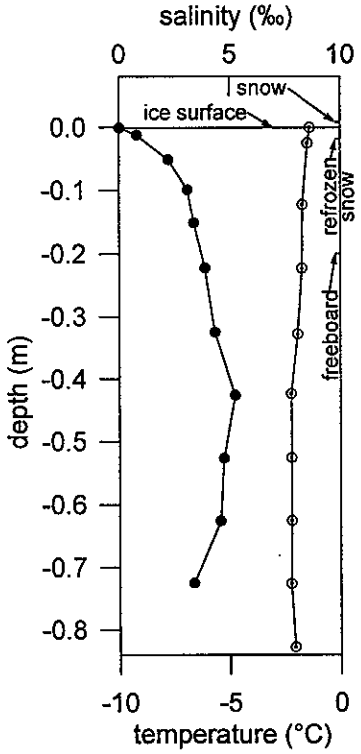

Figure 10. The salinity and temperature profile of a very warm core taken on 26 May 1976; salinity 2, temperature /. The freeboard of this core was determined from a nearby auger hole.

a rectangular grid of about 0.1 m. In this 1.6 m thick ice, these channels extended 0.1 to 0.5 m up into the ice."

The author has stated that the brine channel growth occurs in the spring and that the surface salinity will be much lower as reflected in the salinity profile illustrated in Figure 9(b) for a core removed 21 May 1976. The author states that the crystal structure of the core starting at the top was frazil ice (0-20 mm), columnar and frazil (20-150 mm) and columnar (below 150 mm). There were air bubbles trapped in the ice and the author believes this occurs when sea water travels up the brine channels or void spaces in the ice and due to coming in contact with cold air, freezes and the air entrapped in the water is encapsulated. He also suggests that oil, that has been released under the ice, can become entrapped in the ice in a similar manner.

The author states that, as in the case with the core profiled in Figure 10, when the ice becomes further desalinated the surface value approaches zero. The ice core was almost entirely columnar ice with an the air temperature of -1.5 °C, an ice temperature of -2 °C and a surface ice salinity of 0‰. Therefore, an increase in temperature would result in melt ponds.

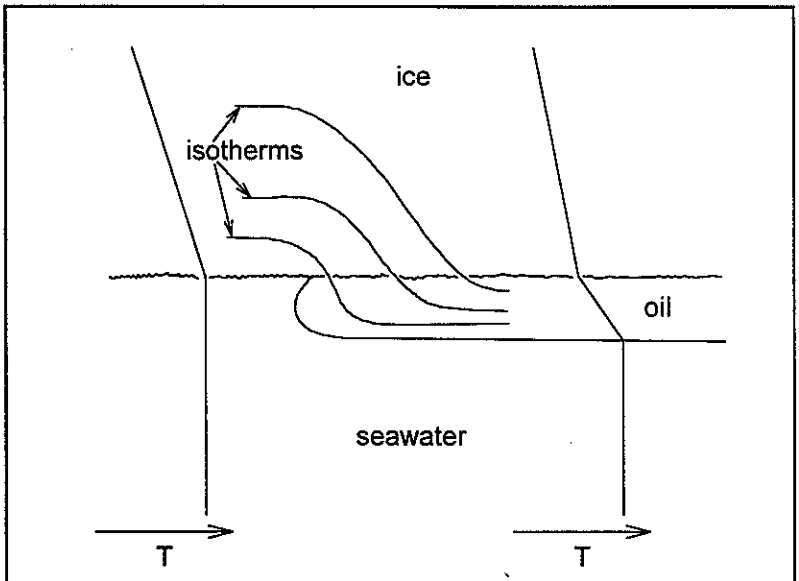

Figure 11. A sketch of the temperature profile and the location of isotherms both inside and outside of an oil lens.

The author states that when oil is released under sea ice, it collects in pools and droplets. He further states that the oil is cooled from above and heated from below. The heat transfer across the oil layer is a function of the Raleigh number which is proportional to $h^3\Delta T$, with h being the oil thickness and ΔT being the temperature difference across the layer. The author also states that if $h \leq 10$ mm, then heat transfer takes place via conduction and if $h > 10$ mm then convection takes place in the oil layer and the heat transfer might be much larger than the conduction value. This is illustrated in Figure 11 and the author states that the oil is 20 times less conductive than the ice, and so the oil is colder than the surrounding sea water causing ice formation first at the edges of the oil lens and eventually, encapsulation. The author has illustrated this with photographs taken of an ice core with just such a lip formation and those photographs (Figure 12 (a) and (b)) are not reproduced

here.

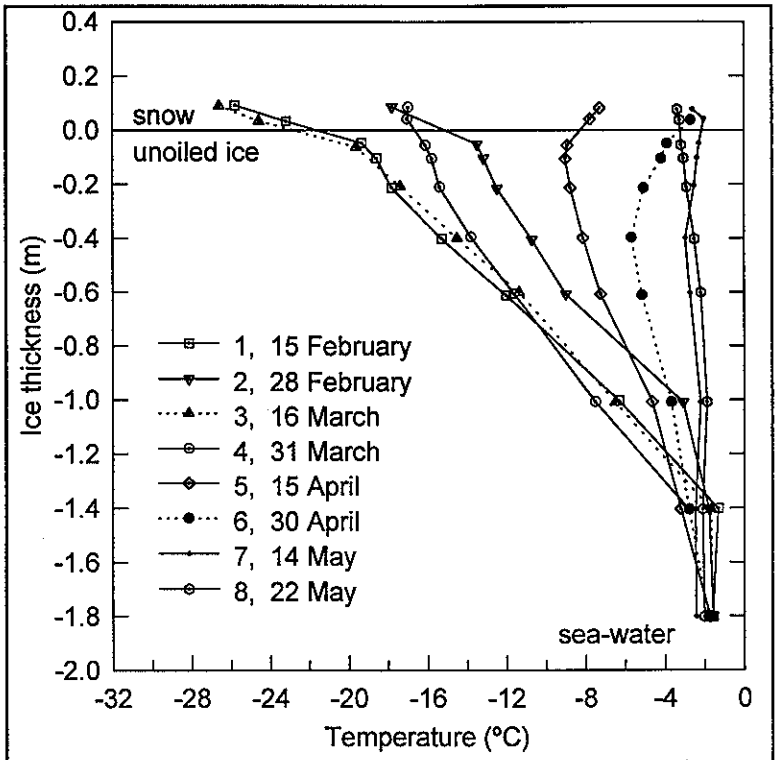

Figure 13. Temperature profiles from the 1975 Balaena Bay test site.

A selection of temperature profiles, obtained from a control chain of thermistors, are displayed in Figure 13, and are for a period of time from 15 February to 22 May, 1975. The author restates that because of the strong warming, after the end of April, the brine channels are opened and observers saw oil on the surface of spill sites in early May.

The author then describes the early May oil spill experiments. Forty-five minutes after the discharge, of 0.43 m^3 of Norman Wells crude, a single oil droplet appeared (1 mm diameter) on the ice surface and was marked. The author states that the oil subsequently invaded the surrounding area with a pattern similar to that illustrated in Figure 8. The oil filled brine channels of ice cores from the region were photographed by the author and were displayed in Figures 14, 15, and 16 which are not reproduced here. The following discussion is taken directly from the author's manuscript.

" To examine the details of this layered structure, Figure 16a shows the top 0.6 m of a 1.60 m long core which was pulled on 16 May from the Swan Hills crude spill on 12 April 1975; this core shows that the more viscous Swan Hills crude oil is also entrained in horizontal layers in the upper part of the ice. Figure 16b shows a 20 mm thick section of Figure 16a taken by transmitted light together with an adjacent schematic diagram. The figure shows the following four separate layers:

a. 0-15 mm. This layer of nearly clean ice lie above an oily layer. A similar clear zone occurred at the top of many of the cores which we pulled in May, including the surface spill discussed below. The reason this clear ice grows is that once oil rises to the ice surface under the snow, the solar radiation absorbed by the oil causes

melting and collapse of the overlaying snow layer shown in Figure 7a. Further, for the core shown in Figure 15a, where the oil was only on the surface for one day, this clear layer is absent.

b. 15-80 mm. The oil in this zone is trapped within spherical bubbles with the layer of darkest oil within this zone having a thickness of 35 mm. This may either be snow ice which is oil-saturated, or else the result of oil filling the voids left by the brine drainage.

c. 80-180 mm. This clear ice is either frazil or slush ice; as evidence, when we held the core segment up to the Sun, we saw within this zone reflections from randomly oriented crystals. We discuss below why this ice is oil free.

d. Below 180 mm. The oil which outlines the individual platelets at the top of this layer shows that this ice is clearly columnar. Also, the abrupt beginning of the columnar growth at 180 mm resembles the transition from frazil to columnar ice and slush to columnar ice shown respectively in Figures 5a and 6a."

The author states that the formation of oiled and unoiled horizontal layers is due to the percolation of melt water from above and rise of sea water from below. The author states that as the brine is drained out of the ice it is replaced with melt water from above and rising sea-water from below thus resulting in clear ice formation.

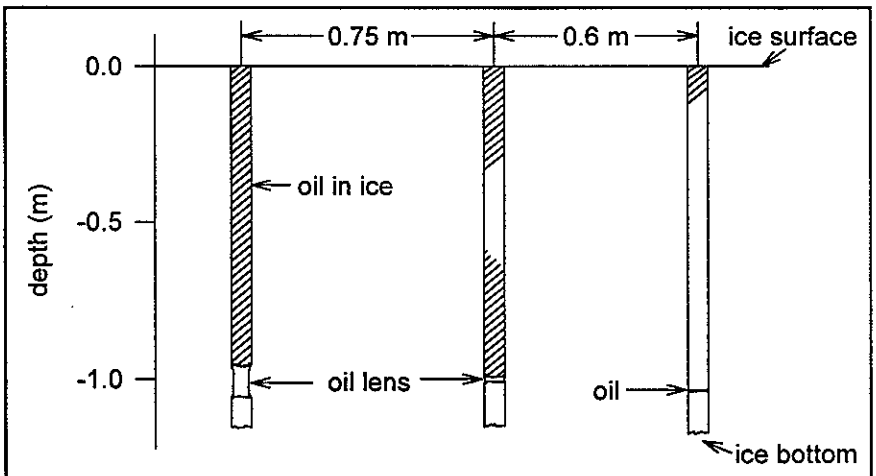

Figure 20. Sketch of the configuration of the three cores pulled near the pressure ridge.

Divers observed that oil was trapped under a weathered pressure ridge to a depth of 0.1 m, in a cavity near the ridge keel. Coring of this site, on May 30, 1975, is illustrated schematically in Figure 20 and the author states that this illustration backs up the diver's observations.

"The blackest core observed in the filed experiment is the core in Figure 21c. When we melted down that core segment which is just above the first break down from the top in the figure, we found 30 ml of oil in 910 ml of total liquid or an oil concentration of 3.3 % , so that again, a relatively small amount of oil produces very dark cores. This particular core was over an oil lens 100 mm thick and, after taking the core, pure oil from the lens flowed up to the surface. At the adjacent holes oil did not rise to the surface; rather the thin oil lenses were frozen into the cores.

Figure 21 also shows that the new ice growth beneath the oil lenses appears clean and free

of oil. For the black core in Figure 21c, Figure 22, a close-up photograph of the ice surface which grew beneath the oil, shows that a fine wave-like fluting covers the surface. Because this ice formed beneath h=100 mm of oil, the Raleigh number within the layer was probably large when the new ice formed. The fluting on this new ice surface, then, was probably caused by turbulent convection associated with the large Raleigh number within the oil layer."

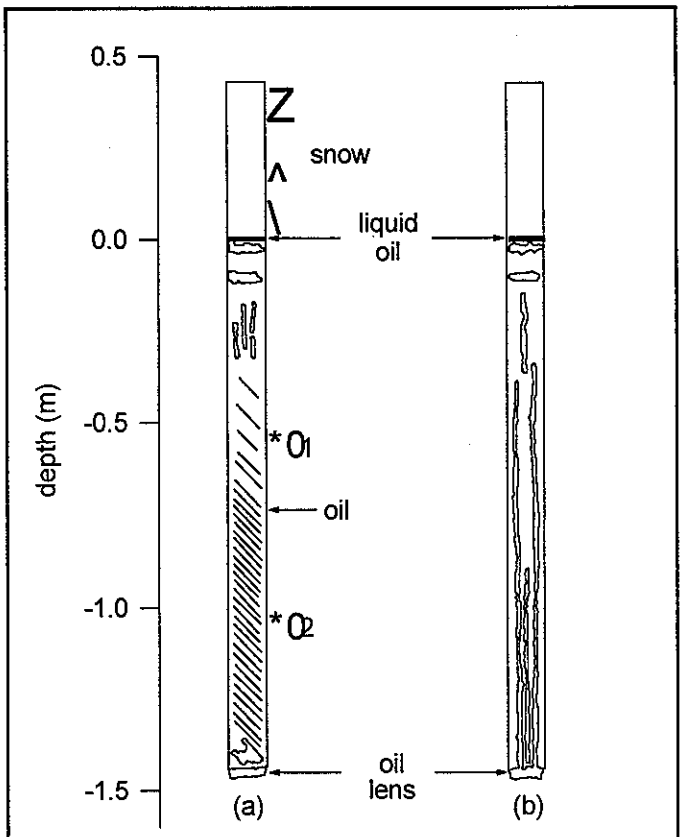

Figure 23. Schematic diagram of the feeder-channel distribution for the core pulled on 21 May 1975. View in (a) is at 90° to the view in (b).

The author states that Weeks and Gow ("Preferred crystal orientation in the fast ice along the margins of the Arctic Ocean," *Journal of Geophysical Research*, Vol. 83. No. C10, pp 5105-5122, 1978) have reviewed the literature and describe a field study of cases where the *c*-axes of the columnar ice platelets are predominantly aligned parallel to the coast (of Alaska). This is attributed to the ice response to long-shore currents. The author found this type of orientation from a core pulled in Balaena Bay and the oiled core that was pulled had a very high concentration of oil at 5.5% by volume.

"Figure 23 shows two schematic drawings at right angles to one another of the core which was pulled on 21 May 1975 under 0.43 m of snow from the Norman Wells oil spill of 15 April 1975. The approximately 60 mm of new growth beneath the oil is not shown. The photographs in Figure 24 show a view of the core perpendicular to the platelets; between the depths of 0.6 and 1.45 m,

plane parallel diagonal feeder channels fill the core. These feeders have a vertical spacing of 5 to 10 mm and lie at an angle to the horizontal of approximately 40°. Also, the top 150 mm of the core again show the alternating layers of clear and oil-soaked ice, with the top 50 mm being very dark."

BOSS Critique

The author has presented a very good selection of photographs which give the reader an understanding of the effect ice type has on oil location after a spill and depending upon ambient temperature.

There are estimates made about the oil content in the ice and the author does state that the oiled ice is melted down and the oil is separated. However, there is no exact description of how well the oil is separated before the oil volumes were measured nor how accurately the volumes were measured. Thus the reader is not told how approximate this method is, such as $5.5 \pm 0.5\%$.

Review of a manuscript by NORCOR Engineering and Research Ltd., entitled *The Interaction of Crude Oil with Arctic Sea Ice*, Beaufort Sea Project, Department of the Environment, Victoria, B.C., Beaufort Sea Technical Report #27, 1975.

Technical Summary

"The principal objectives of the study were to assess the impact of an offshore oil well blowout on the thermal regime of the Beaufort Sea, and to evaluate potential countermeasure techniques.

The main program, which consisted of nine controlled discharges involving 54 m^3 (11,900 gallons) of crude oil, was undertaken in a small bay 20 km to the south west of Cape Parry (70°02' N, 124°53' W). Two types of crude were injected under the ice at various stages of growth, between October 1974 and May 1975. The initial spreading and entrainment was documented by means of divers and a remote video system. An array of eleven point thermistor chains was logged hourly to assess the rate of migration and the effect of the oil on the thermal regime of the sheet. Oil, water and ice samples were recovered at regular intervals to determine the degree of weathering and dissolution of the oil. Detailed radiation studies were undertaken in the spring to assess the impact of surface oil on ice depletion. As well, two small discharges were conducted 30 km north of Cape Parry in April 1975, to determine the importance of currents on the transport of oil under solid ice cover. The oil was injected under the ice in the presence of a 10 cm sec^{-1} current, and the movement documented by means of divers.

When oil is released in the water column, it rises towards the surface in a conical shaped plume. The oil tends to be unstable, and breaks into small spherical particles of about 1 cm in diameter or less. On striking the underside of the ice, the oil radiates outward, progressively filling depressions in the sheet. Since most crudes naturally form sessile drops at the ice-water interface, the minimum oil film thickness is about 0.8 cm. Spherical drops of a lesser diameter can exist, but this normally only occurs near the periphery of the contaminated area, where the probability of collisions with other drops is small. The maximum film thickness is controlled by the depth of the depressions, or variation in ice thickness, which is typically about 20 percent of the average thickness. Within a matter of hours of the oil coming in contact with the ice, a lip of ice forms around the lens, preventing horizontal movement. During the depth of winter, a new layer of ice forms beneath the oil within several days. Once entrapped, the oil is stabilized until spring. The properties of the oil remain unchanged and there is little evidence of weathering or degradation.

Throughout the winter, the oil only penetrates between 5 and 10 cm into the loose skeletal layer. As the sheet begins to warm in the spring, activity intensifies in the brine channels and the oil begins to migrate upward. Initially the movement is slow; typically in the range of 15 to 20 cm during the months of February and March. The rate of migration increases with the level of solar radiation and the ambient air temperature. Oil released in late April under 150 cm of ice, was detected on the surface within one hour.

On reaching the surface of the ice, the oil saturates the snow cover, and substantially reduces the albedo. This causes an increase in the level of absorbed solar radiation, which accelerates the process. Oiled melt pool quickly develop. The albedo of an oil film on water is about one quarter that of oiled snow, and consequently the melt is further accelerated. Oil is splashed on the

surrounding snow by wind and wave action, and the pools gradually enlarge until interconnected. New oil is continually being released until the melt reaches the initial level of the oil lens. Once melt holes develop and surface drainage patterns are established, the sheet rapidly deteriorates. Depending on the nature and location of the sheet, oiled areas are likely to be free of ice between one and three weeks earlier.

A variety of clean-up techniques were investigated and in situ burning was found to be both the most efficient and effective. A minimum film thickness of a bout 0.5 cm was required to sustain combustion. Even when heavily weathered, most films could be ignited by sprinkling gasoline on a piece of paper towel. Between June 7 and July 17, 1975, four burns were conducted in the study area. On the first burn approximately 20 m^3 or 90 per cent of the oil on the surface was removed. The effectiveness of successive burns decreased, due to the reduction of film thickness. Of the 54 m^3 of oil discharged, approximately 15 m^3 evaporated naturally, and 33 m^3 was removed by burning. About 5 m^3 of residue was manually recovered from the ice. This proved to be a very costly and labour intensive operation. Less than three per cent of the oil reached the shore, of which one third was recovered.

In an effort to determine the impact of the tests, detailed physical and biological studies were conducted prior to the first discharge, and after the clean-up. With the exception of a very light oiling of the shingles in the tidal zone over about 900 m of shoreline, there was no evidence of oil in the water column, or deleterious effects on the marine eco-system."

Objective

"The principal objectives of the study were to determine:

- The areal extent of contamination and the disposition of oil released beneath solid ice cover;
- The role of advection currents in the transport of oil along the underside of an ice sheet;
- The effects of relief at the ice-water interface on the transport and pooling of oil;
- The factors controlling the entrainment and migration of crude oil in first year sea ice at various stages of growth;
- Mechanism by which free oil is transported to the surface of an ice sheet;
- Effects of entrainment and free oil on the surface heat exchange and the energy balance of the sheet, with particular emphasis on modifications to freeze-up and break-up;
- The importance of the physical and chemical properties of the oil, ice and water to the various processes;
- The rate and nature of aging of oil in, on and under the ice;
- The suitability of existing methods and techniques for the clean-up of an oil spill in ice covered and ice infested waters; and
- The biological impact of the tests and the possible relevance to other areas."

Theory

The authors have combined some of the experimental procedure, method and theory into each section and therefore this is the process followed in this review. However, the authors also have an experimental section and parts of this are reproduced here.

Method

" 5.0 EXPERIMENTAL TECHNIQUES

5.1 Schedule and Size of Discharges

The principal factor in determining the number and timing of controlled discharges for the entrainment study was thermal fluctuations within the ice sheet. In general, the effects of changes in ambient air temperature, absorbed solar radiation and snow cover are far more pronounced in the upper levels of the sheet. Conditions tend to stabilize with depth, due to the thermal inertia of the ice and the enormous heat sink provided by the sea water. During the depth of winter, which typically extends from early December to late March, the ice structure is relatively constant. With the exception of the immediate vicinity of the skeletal layer, the brine channels tend to be blocked, thereby limiting the movement of oil upward through the ice. The sheet is cooling from initial formation until about mid February, and warming thereafter. Although diurnal variations and other short period disturbances can be detected near the surface, in general the thermal gradient tends to be linear during the fall and winter. During the melt phase, there is a reversal in the gradient, with the coldest temperatures being located near the centre of the sheet.

The timing of discharges was designed to encompass the dominant stages in the ice growth and depletion cycle. Because conditions tend to be stable during the depth of winter, emphasis was placed on the freeze-up and break-up periods. The initial program called for the first discharge in open water, immediately prior to freeze-up, and the second at an ice thickness of 15 cm. However, due to delays in obtaining the necessary approvals to discharge oil, the tests had to be rescheduled. The open water test was simulated by clearing an area of ice approximately 36 m^2. The average ice thickness at the time was 43 cm. Although the results are not truly representative of conditions at freeze-up, they provided some indication of the behaviour of oil on water in the presence of growing ice. The final discharge was to be conducted immediately prior to break-up. As a result of other related studies being undertaken at Balaena Bay at the same time, it was felt that a full discharge posed too great threat, and two small tests were conducted instead. Because there was very little information on the properties of the crude likely to be found in the Beaufort Sea, two types of crude, which spanned the probable range of properties, were used in the tests. Norman Wells (NW) crude, which has a pour point of about -45 °C was used on all but two of the tests, due to its availability and ease of handling at low temperatures. Swan Hills (SH) crude, which has a pour point of about -4 °C was used for tests in December and April. These discharges were conducted simultaneously with discharges of Norman Wells crude, for the purposes of comparison. The date of each test, the type and quantity of crude, and average ice thickness is shown in Table 5-1.

Table 5-1. Schedule of Discharges

Date	Test	Quantity (m^3)	Ice Thickness (cm)	Date	Test	Quantity (m^3)	Ice Thickness (cm)
Oct 24	NW#2	7.3	38	Apr 8	NW - Offshore	1.5	122
Nov 1	NW#1	0.4	open water (43)	Apr 12	SH#2	6.4	154
Nov 14	NW#3	8.3	53	Apr 15	NW#7	8.2	154
Dec 7	SH#1	7.3	64	May 15	NW#8	0.4	195
Dec 9	NW#4	8.2	64	May 21	NW#8	0.2	195
Feb 15	NW#6	7.7	118				

Note: Ice thicknesses tabled here are representative values. A deviation of approximately 20 percent can be expected depending on sampling location and date (Figure 7-4a).

The size and volume of the test spills depended largely on environmental and physical

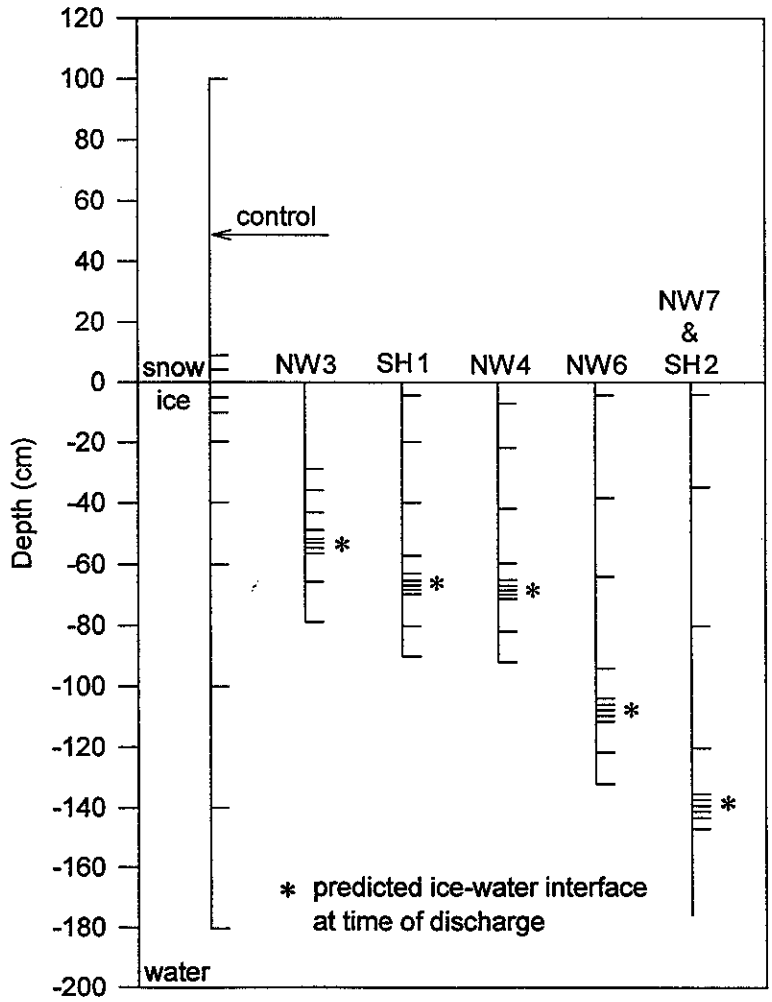

Figure 5-1. Thermistor spacing.

constraints. The concept of a free flowing spill was environmentally unacceptable. A containment area of 30 m in diameter was selected for each test. This size was considered large enough to avoid scale effects from the containment boundary itself, and to encompass meaningful cross section of natural ice thickness variations within a single test. Approximately 7.3 m^3 (1620 gal) oil, or enough to cover the total test area to an average thickness of 1 cm, was used on each test.

The specific day of each test was governed by a number of factors. Primarily, the thermistor chain spacing set close limits (±2 cm) on the ideal ice thickness and hence the day for the test. Figure 5-1 shows the probe spacings selected for each test. As the chains required a minimum of 10 days to freeze in properly, these spacings had to be fixed at the time of chain assembly, 2 to 3 weeks prior to the test. The spacing was designed so that the ice-water interface on the day of the test would fall on a dense array of 5 probes. On the basis of ice growth trends to that point, a prediction was made of ice thickness on the test day and the chains designed accordingly. By monitoring the chains for 2 to 5 days prior to the test, the probes reading water temperature would indicate when the interface was in the ideal position for a discharge. Snow cover variations made accurate chain placement difficult. However, attempts were made to install the probes in areas of equal snow cover, and after the first few tests, experience dictated ice variations to be corresponding to different snow covers. Some natural variation in the ice thickness between the chains was always present, and some probes were closer to the ideal position than others. Most of the chains were within 2 cm of the selected depth on the test day.

5.2 Oil Containment and Handling

5.2.1 Containment - Skirts

In selecting the oil booms, the following factors were considered: design, durability, cost, transportability, and ease of installation. In terms of performance, the most critical factor was that the skirt be intact at the ice-water interface for the duration of the test.

All existing techniques had major limitations for this application. A simple skirt embedded in the ice sheet was considered best suited for the Balaena Bay site. The design consists of three components, a Dupont 'Fabrene' membrane, a flotation collar, and cable ballast. Depending on what spill they were designed for, the skirts had lengths varying from 60 cm to 274 cm. The minimum skirt length available below the ice for any discharge was 22 cm.

Assembly was undertaken at the site using prepared lengths of 'Fabrene', sized according to the projected ice thickness at the time of discharge. The collar was constructed of 5 cm diameter PVC tubing, which was inserted into a pre-stitched sleeve along one edge of the 'Fabrene' strip. Sections of tubing were joined with sealed insert couplings and clamps. Similarly, the 1.0 cm diameter cable used as a ballast, was insert into a smaller sleeve on the bottom edge of the skirt. A two man crew assembled eight 30 m diameter booms in this manner at the rate of 3 per day. Once assembled, the complete strip was dragged out on to the ice sheet by skidoo and laid out in a circular shape. With standard chain saws, a 10 cm wide slot was cut 97.5 m in circumference. The ice in the slot was pushed underneath, and the skirt was inserted through the slot.

After joining the ends, the boom was left to freeze in. A two man crew was capable of installing 3 such skirts through 28 cm of ice in a six hour shift. This rate dropped to one per day as the ice thickness reached 44 cm.

A total of 8 skirts were installed through the ice in this manner. The booms were packed tightly together to locate the test area between the 6 and 9 m water depth contours (Figures 5-2, D-6),

and to avoid running long branch-cables from the main data cable to each test area (Sections 5.3, 5.4). The range of water depths was originally selected to provide enough water under 1.8 m of ice for a realistic test, and to allow operation of a camera scissor boom mast.

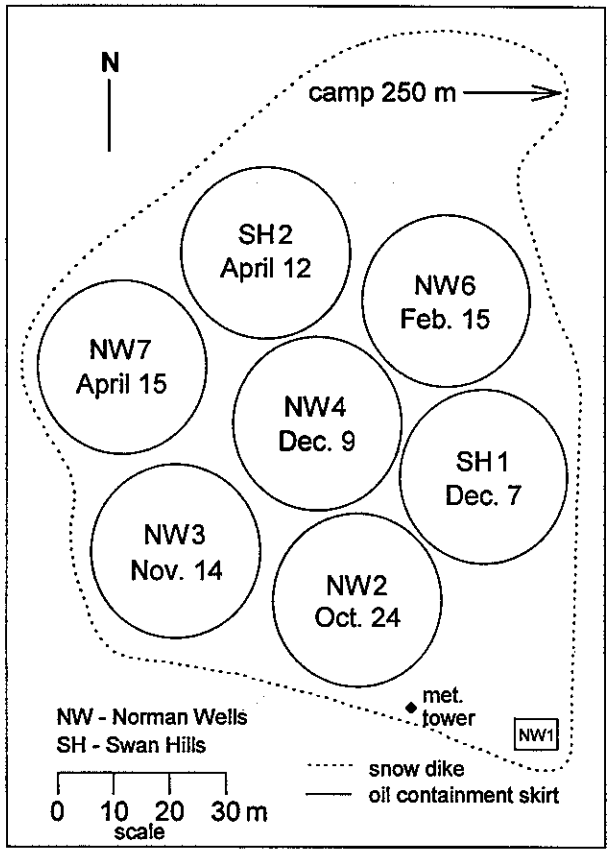

Figure 5-2. Test Layout.

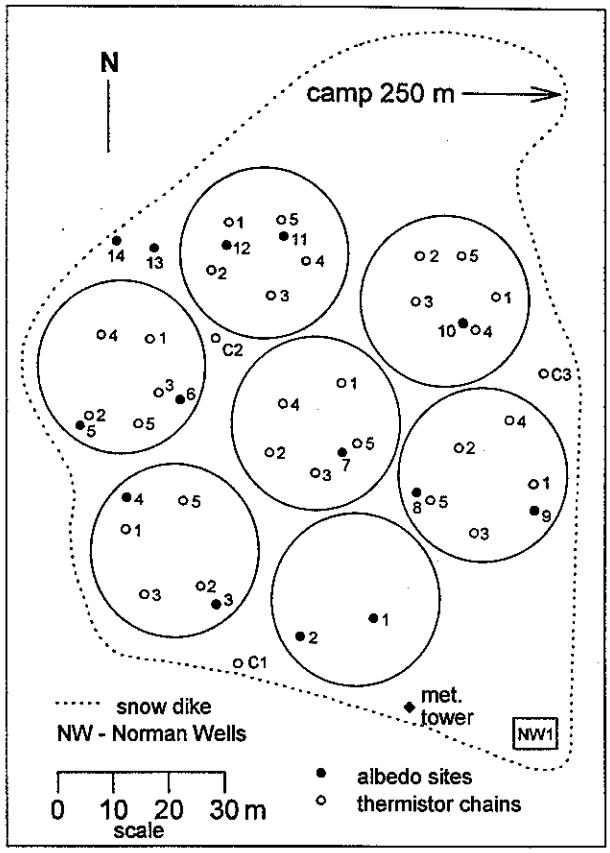

Figure D-6. Albedo sites and thermistor chain locations.

The 10 m diameter skirt for the open water test was installed from a small boat while the ice was less than 5 cm thick. The unit froze in place within 24 hours.

The boom scheduled for the NW8 test, incorporated a different collar designed to enable installation by a diver from under the ice. In place of the PVC pipe, solid styrofoam strips were used to eliminate the problems with sealed joints and brittle fracture at low temperatures. Also, the foam was extremely flexible, facilitating installation through a 2 by 3 m dive hole.

This skirt had a 'Fabrene' flap designed to float up against the ice and provide a better seal while freezing in. After the skirt was pushed through the dive hole, the diver was use to swim four lines attached to the skirt over to the quarter points of the circle. There, the lines were passed through a drill hole to the surface and used to drag the skirt into a rough circular shape. The diver completed the installation in about 45 minutes by hooking the flotation collar around wood stakes frozen into the ice.

The 'Fabrene' membranes served as an effective barrier throughout the winter. Although the

predominant thickness of the oil lenses was 2 to 5 cm in most locations, the skirt held lenses up to 20 cm thick. However, the ice did not adhere well to the 'Fabrene' and in some locations small quantities of oil migrated up the joint between the ice and the skirt. This problem would likely be encountered with any barrier extending through the ice sheet. In June, as surface melt increased, the collar pipes formed partial barriers to surface movement of oil on melt pools. ...

5.2.2 Containment of Snow

A snow dyke, approximately 400 m in circumference, was constructed around the entire test area, to restrict the movement of free oil on melt pools in the spring. A number of techniques employing cut snow blocks were attempted, but due to the limited snow cover generally proved ineffective. Finally, empty oil barrels were used to create a wind break, and the snow naturally drifted to form a barrier about 1 m high and 3 m wide. On average, it took between one and two days for the drift to stabilize. Attempts were made to flood sections of the dyke, but this proved to be time consuming and of little value.

The snow dyke was very effective in containing surface oil, and remained intact until late June. As a rule, the oil did not penetrate more than 15 to 20 cm into the snow. ...

5.2.4 Discharge Operations

The crude oil and support fuels, contained in palletized drums arrived by barge on August 28, 1974. Unusually heavy ice conditions at the mouth of Balaena Bay prevented the shipment from reaching the test cove as was originally planned, and the 136 metric tons of supplies were cached on the shore 0.7 km NE of the test site. Enough oil for the first three tests was slung by helicopter coincident with the camp move, and the remainder was transferred by skidoo to the test site during the winter.

At camp, a 9 m^3 (2,000 gal) capacity insulated wooden holding tank was constructed 50 m from shore. Several days before each test, oil was transferred from 45 gal drums to the tank. This transfer was accomplished in 2 to 8 hours using a centrifugal pump, with a standpipe transferred manually between drums. Even Swan Hills crude was successfully pumped at temperatures as low as -35 °C. Approximately 0.7 m^3 (155 gal) was pumped in excess of the quantity required for the tests, to allow for line losses and residue at the bottom of the tank.

The oil was heated to within approximately 1 °C of ambient water temperature, by means of a single immersed hot water radiator. The 8.6 m^3 of oil could be raised from ambient air temperature to about 0 °C in less than 24 hours, even in February. Once heated to the required temperature, the oil was pumper through a 5 cm diameter neoprene line approximately 250 m to the test area. A 7 m length of 5 cm diameter steel pipe was used to inject the oil under the ice. On the average, the discharge was completed in 50 minutes, yielding a flow rate of 0.15 m^3 min^{-1} (32 gal min^{-1}).

Divers were employed on all the fully instrumented discharges. Initially, their main function was to document conditions and inspect the containment skirt prior to each discharge. Due to the possible effects of released air, the divers were prohibited from entering the test area within 48 hours of a discharge. A remotely controlled scissor boom, which could be extended up to 15 m, was employed to move the underwater video system and transducer for the first three tests. However, for full coverage the boom had to be inserted in the centre of the test area, and a variety of techniques were attempted to prevent oil from seeping into the well without success. For the discharge in February, the video system was mounted on a rigid boom, which was inserted through the ice from

outside the test area. This unit permitted full rotation of the camera, but due to the low light levels, visibility was limited to about 10 m. A diver equipped with a closed circuit breathing system was employed on subsequent discharges. The entire operation was monitored from the surface, and the movements of the diver controlled by means of a surface communications system. This approach also permitted still and 16 mm photography. Since the diver had a range of approximately 40 m, it was possible to locate the dive hole outside the test area.

Two procedures were used to introduce the oil under the ice. For the first tests, the discharge pipe was inserted in a SIPRE hole angled into the test area from a point about 1 m outside of the skirt. The pipe end then projected 3 m into the test area at a depth of about 2.5 m below the ice sheet. Commencing with the NW3 test, an effort was made to provide more opportunity for plume spreading, by inserting the pipe section vertically though the ice sheet near the centre of the test area. The oil was then discharged from a depth of about 6 m. This procedure was used for tests NW3 to NW6. A small quantity of oil sometimes rose through the auger hole used to place the discharge pipe. Packing with snow and sorbent usually halted the flow of oil in a matter of minutes. Following the NW6 test, a decision was made to eliminate further surface contamination of the rest area, by reverting to the original side insertion of the discharge pipe near the skirt edge. This technique was used for NW7 and SH2, accompanied by a dive hole outside the spill area. ...

5.3 Instrumentation

"APPENDIX 27A
Equipment Specifications

I Sampling and Analytical Instruments

a) Multimeter: manufactured by Hewlett Packard
Display Model #34740A
Multimeter Model #34702A
Battery Pack Model #34720A
Accuracy at 23°C ± (0.01% of reading + 0.005% of range)
Temperature Coefficient ± (0.0035% of reading + 0.001% of range) /°C

b) Salinity Meter: manufactured by Yellow Springs Instrument Co., Model 33
Accuracy: Salinity: Above 4°C ± 0.9‰ at 40‰
± 0.7‰ at 20‰
Below 4°C ± 1.1‰ at 40‰
± 0.9‰ at 20‰

II Radiation Instruments

a) Solarimeter: manufactured by Kipp and Zonen, Model CM6
Effective wavelength band measured: 300 nm to 2.5 μm
Sensitivity: 1 g cal cm^{-2} min^{-1} has potential of 8.4 mV
Accuracy: within 1%; temperature coeff... 0.15% per °C

b) Albedometer: manufactured by Kipp and Zonen, Model CM7
Effective wavelength band measured: 300 nm to 2.5 μm
Sensitivity: 1 g cal cm^{-2} min^{-1} has potential of 8.0 mV

c) Net Radiometer: (Fritschen Type) manufactured by Mircomet Instruments, Model MNR
Effective for all wavelength bands

Sensitivity: 1 g cal cm^{-2} min^{-1} develops potential of 3.05 mV

III Surface Weather and Ice Temperatures

a) Anemometer: manufactured by Texas Electronics Inc., Model #446
b) Barometer: recording type manufactured by Taylor Instruments
c) Telethermometer: manufactured by Yellow Springs Instrument Co., Model #47
Absolute accuracy: ± 1% of scale
Sensitivity and readability: ± 0.4% of scale range
d) Thermistor Beads: manufactured by Yellow Springs Instrument Co., part # 44005X
Time Constant (time for a thermistor to indicate 63% of a newly impressed temperature) = 1 sec.
Dissipation Constant (power required to raise a thermistor 1°C above surrounding temperature) = 8 mW/°C
An error of 10^{-5} °C was introduced by electrical heating of the bead
Accuracy: ± 0.01 °C at 0 °C
± 0.03 °C at -20 °C and -40 °C
add ± 0.02 °C up to 20 °C on either side of known point (calibrated at 0 °C, -20 °C, -40 °C)
Repeatability error - negligible

IV Recording Instruments

a) Scroll-Chart recorder: manufactured by Rustrak Instruments and modified by Texas Electronics Inc., Model #446
b) Two-pen Recorder: manufactured by Fischer Scientific Instruments Ltd. Model # 5000
c) Underwater Television Camera: manufactured by Hydro Products, Model TC-125
d) Colour Videocorder: manufactured by Sony Corporation
Colour Videocorder Model AV-8400
AC Adaptor Model AC-1000
e) Datalogger with Scanner, Integrator, and Output Mechanisms: manufactured by Vidar Data Acquisitions Systems, Model 5400 DAS
which included the following components:
100 channel scanner
Digital Voltmeter: Non-linearity : ± 0.015% full scale
Resolution : ± 0.01% full scale
Time Stability: ± 0.01% per month
Ohms Converter: ±0.026% for worst case
Digital Printer
Tape Punch
10 Integrators

MEASUREMENT ACCURACY

Solar Radiation - combined error of Instrument Calibration, VIDAR DVM, and Integrator < 8% of reading

Albedo - combined error of Instrument Calibration and HP multimeter < ± 10% of Albedo Value (Albedo > 0.2)

	< ± 13% of Albedo Value (Albedo > 0.2)
Net Radiation	- combined error of Instrument, VIDAR DVM and Integrator Drift. Difficulty to quantify, owing to unstable integrator drift of approximately 80 $\mu V\ h^{-1}$ approaching the magnitude of the instrument output. Generally the possible error exceeded ±50%. For this reason, Radiometer values were discounted in the analysis.
Air Temperature	- ≤ ± 0.5 °C at 5 m and ≤ ± 0.05 °C at 1 m
Water Temperature	- ≤ ± 0.02 °C; Ice Temperature - ≤ ± 0.04 °C"

5.3.1 Surface Weather

Detailed observations of surface weather were made four times daily commencing on September 30, 1974 and continuing for the duration of the project, until July 22, 1975. All observations were taken at the following approximate times: 0900 hours, 1300 hours, 1800 hours, and 2300 hours. Visual estimates were made of cloud cover, the height of the cloud ceiling and the visibility. Barometric pressure was recorded. The wind speed and direction were measured and recorded with a Texas Instruments Model 446 system. Basically, this system consisted of a cup anemometer and wind direction indicator mounted on a tower free of obstructions at a hight of 8 m above ground level. For the period of March 6 to June 7, the wind speed and direction signals were fed into the data logging system integrator package to obtain average hourly values for wind speed. It was considered adequate to take hourly spot reading of wind direction.

Air temperature was measured using a YSI Model Telethermometer with the thermistor mounted in a radiation shield at a height of 5 m. A similar shielded thermistor on each control chain measure air temperature at a height of 1 m. From November 13 to June 7, these temperatures were recorded hourly on the main data logging system.

5.3.2 Radiation

Measurements relating to the radiation balance of the test area were undertaken from February 12 to June 6. To measure the total short wave radiation that was incident on the test area, a Kipp and Zonen CM-6 Solarimeter was mounted on a 3 m tower near the NW2 test area (Figures 5-2, D-6). A Fritschen type net radiometer at a height of 1 m was cantilevered 1 m out from the solarimeter tower. Both the solarimeter and net radiometer were connected to the data logging system. Hourly averages are available for the period March 6 to June 6. The albedo of the test site was measured for the period May 9 to June 4, using a Kipp and Zonen Model CM-7 Albedometer mounted on a mobile cantilever beam, 1 m above the ice surface. The DC voltage output signals were hand-logged every second day at 12 specific locations in the test area and 2 control sites using and H.P. 34702A Multimeter. Errors introduced by instrument limitations are outlined in Appendix 27A

5.3.3 Ice-Water Temperatures

All ice and water temperatures were measured using precision thermistors, Model #44005X manufactured by Yellow Springs Instruments. Over 450 thermistors were supplied for use in this project. Each thermistor bead was calibrated at -40 °C, -20 °C and 0 °C, the range most likely to be encountered between air and water temperatures over the 9 month period. At 0 °C, the average thermistor resistance was 9796 ohms. At this temperature, the line resistance of 29 ohms was 0.23%

of the reading. This error was substantially less for lower temperatures. The manufacturer considers that the worst case error of a single thermistor calibrated at the three points mentioned above is ±0.05 °C over the range -40 °C to 0 °C. Using a probe spacing of 5 cm and a temperature gradient of 0.2 °C cm^{-1}, the error in establishing the gradient would be ± 8 %. A total of thirty-three chains with 11 thermistors on each chains were constructed for six tests and three controls, which were installed on November 12. The thermistor chains consisted of a 2.4 m length of hardwood drilled to receive 11 clear acrylic tubes (0.635 cm OD), arranged in a ladder network. The beads were embedded in the tip of each tube which projected about 5 cm out from the wood stem. The leads were run up a slot in the back of the hardwood to a 12 pair connector on top, and the whole assembly potted with silicone rubber. ...

The rationale behind the spacing of probes is discussed under Section 5.1. Basically, the probe spacings were tailored to suit each spill (Figure 5-1). The control chain spacing was designed to have 3 probes 4 cm, 8 cm, and 100 cm above the ice surface to continuously monitor snow and air temperatures. Also, on the controls, probes projected 180 cm below the snow-ice interface so that even in May at least one probe remained to measure water temperatures.

5.3.4 Data Logging

A Vidar 5400 Data Acquisition System was used to log all ice-air-water thermistors and meterological instruments, as outlined above. The Vidar system consisted of a 100 channel reed scanner interrogated hourly by a precision DVM. Scan rate and sequence were variable, and controlled by a crystal clock. Data in the forms of ohms for the thermistor readings and DC volts for meterological instruments were recorded on printer paper and IBM compatible paper punch tape. Total scan time for the 92 active channels took less than 1 minute. The normal configuration consisted of 8 thermistor chains, each with 11 beads, and four channels for net radiation, short wave solar radiation, wind speed and wind direction. Integrator capability was added to one 10 channel batch on March 6, 1975. This enabled hourly average reading for appropriate instruments. The signals were fed through a 22 conductor branch cable to a 200 conductor trunk cable, which ran from the centre of the test area to the Vidar data acquisition system, located in the office parcol. The branch cables were 60 m in length, while the trunk cable was 220 m long. All cables were vinyl wrapped with solid shields, while the conductors were 20 AWG, solid and braided. Twenty-four pin connectors were installed on all cables to permit rapid switching and manual scanning.

Although the operating conditions were less than ideal, the DAS functioned reliably for the eight-month period it was on line. Over 600,000 pieces of data were recorded in total. Initially, some problems were encountered due to unstable power, but these were corrected by inserting a crystal clock. The Vidar was shut down prior to the first but on June 6, 1975, and the surviving thermistor chains hand logged until June 23. All data has been converted to engineering units and is available on magnetic tape.

5.4 Sampling and Analytical Procedures

5.4.1 Oil Sampling and Analysis

The purpose of the oil sampling program was to identify and quantify any changes in the oil's physical and chemical properties occurring from the time of the oil discharge to the end of the clean-up operation. The sampling program was arranged so that oil from each spill would be collected at regular intervals. Ultimately, the oil was sampled in four different situations: (1) immediately prior

to each discharge; (2) while entrained in the ice; (3) on the ice surface during the melt period; and (4) upon completion of the clean-up.

The sampling program outlined in the original proposal underwent extensive revision during the testing period. Original proposals suggested a sampling program requiring a sample size of one litre. Sampling performed very early in the program indicated that a size of ten ml was more realistic. A sample of about ten ml permitted more extensive coring without destroying the test area.

The approach adopted in the new schedule was to place more emphasis on deriving as much information as possible from the small oil samples that could be collected. This led to increasing the number of gas chromatographs (GC's) done per test from two to about seven for the earlier spills and three to four for the later ones. For a selected number of these samples, the density and viscosity of the oil were measured at the site. These measurements served as a standard for the work done in the laboratory in Toronto. There, tests were done to relate the viscosity, density, pour point, and solubility of the GC profile from the oil sample. This meant that oil samples as small as 20 ml could be collected and the oil properties derived from the GC done on the sample. In all 57 GC's were done on oil samples. In total, there were about 70 oil samples taken, however, some were used exclusively for site tests and some were damaged in transit.

Two composite oil samples were taken from Swan Hills and Norman Wells crude oil barrels at the start of the program. Each sample contained oil drawn from several stirred oil barrels and served as a baseline to compare later samples. A pole was used to mix the contents of each barrel thoroughly to ensure that when the oil was withdrawn, it would be of uniform composition. Two litres of each oil type were used for baseline GC's, and ASTM distillation, metal and sulphur content tests, refractive index, and pour point tests.

While the oil was beneath or within the ice sheet, three possible oil-ice configurations could occur. Immediately after a discharge, the oil formed pools or lenses the ice-water interface. As the ice sheet grew, the oil became entrained within the sheet (Section 6.2). As the ice deteriorated prior to breakup, the oil migrated upwards into the brine channels.

The bulk of the oil samples were recovered during the second phase, while the oil was entrained in the ice sheet. Sampling was avoided during the first phase, when coring operations could drain large areas of oil. Samples taken from oiled brine channels indicated oil properties to be the same as those of oil from lenses, reducing the requirements for sampling of this phase. The results are discussed in Section 8.1.

For all three situations, the following procedure was used, where applicable. The actual sampling schedule shown in Appendix 27B was keyed to other ongoing tests, principally the ice coring. An area within a particular spill was selected according to past experience and the probability of finding oil at that particular location. A standard 8 cm diameter SIPRE corer was used to obtain the ice cores.

After the core was withdrawn, any oil present in the vicinity of the hole would float to the surface of the water in the hole. A one litre glass bottle would then be lowered into the hole until the bottle lip was just below the surface. When withdrawn, the full bottle would contain from 2 to 500 ml of oil, depending upon the thickness of the oil layer. The oil was then transferred into smaller containers. Information as to the thickness of the oil lenses, and their location in the ice sheet was then obtained using an L-shaped probe and this data added to the coring reports. In the third situation, that of oil within the brine channels, the above procedure was followed up to the extraction of the ice core. After the core had been logged, the oil bearing ice section was cut out and

put in a glass jar to melt.

Surface sampling of the oil during the melt period took several forms, depending on the condition and location of the oil. In general, the oil could be found: (1) in open pools, usually on top of melt water; (2) beneath the snow cover but on the ice surface, as a layer; and (3) as a discolouration of the snow cover. The second condition usually preceded the first condition, and occurred just after the oil began surfacing in that particular area. The third condition usually occurred concurrently with the second, as oil spread through the snow column in a capillary action.

For collecting oil from open pools, the sample bottle was submerged in the melt pool and the oil allowed to flow into the bottle. For more viscous material, such as remained after the burning operation, a 12 cm diameter jar was used and a piece of the material was scooped up with a spoon, or by hand, and placed in the jar. The same type of jar was used to collect the oiled snow.

After breakup, oil that had been left on the ice drifted into shore on ice chunks and was then washed up onto the beach. Samples of this residue were collected just before the shore clean-up began on July 7.

Since the degree of weathering of the oil was of particular interest, the handling and storage of samples posed special problems. Oil samples were placed in glass bottles of appropriate size, leaving only sufficient air space for thermal expansion. The snow and ice samples were stored in 200 ml jars. A considerable air space was left when the sample melted, which likely introduced some error. All containers were sealed with silicone rubber and polypropylene tape, then sealed in plastic bags.

Camp Analysis

The viscosity measurements were made with Standard Ostwald viscometers, calibrated with water at the site at +15 °C and 0 °C. Benzene was used for calibration at temperatures below 0 °C. Five to eight tests were in the viscometer were made for each sample measured, and the result analyzed. For density measurements, two 50 ml volumetric flasks were used per sample, where possible, and the measured volume of oil weighed on a two-pan balance. For oil volumes less than 50 ml, the oil was transferred to the flask with a graduated pipette. The measurement of water in oil was done according to the ASTM D95 standard, using 200 ml oil samples.

Oil Evaporation Studies

To asses the effect of evaporation on oil at the surface during the winter, 300 ml samples of both Norman Wells and Swan Hills crudes were placed in evaporation pans December 24. The pans, which measured 20 cm in diameter with a 1 cm lip, were located at an elevation of 1 m to avoid ground effects. One ml samples were recovered on January 4 and 20, and February 26.

5.4.2 Ice and Snow Sampling

To fully understand the effect of included oil on the ice sheet, it was necessary to monitor the condition of both contaminated and uncontaminated ice throughout the winter. Since excessive coring would tend to alter conditions, a number of in situ monitoring techniques were tried.

Clear plexiglass tubes which were 2.5 m long with and inside diameter of 5 cm, were installed vertically through the ice early in the season. The lower end of the tubes were sealed, while the tops extended about 0.5 m above the ice. A specially designed borescope, or inverted periscope, was inserted in the tubes periodically to examine conditions adjacent to the wall. The unit was

equipped with variable intensity light source, and a splitter at the surface to permit photography simultaneously with viewing. Despite various attempts at insulating and sealing the tubes, frost build-up on the inside generally reduced visibility to an unacceptable level. In places where the tube was frost free, lack of contrast in the ice, as seen through the borescope made inspection difficult. Although this approach has potential, several major refinements are necessary for general field application.

Weighted hot resistance wires were installed at a number of locations throughout the test area, for measuring ice thickness. These units worked well in undisturbed ice. However, in contaminated areas, the small melt channel around the wire provided a drainage path for the oil. To avoid disturbing the oil lenses, this method was discontinued.

Full emphasis was then placed on the SIPRE coring program. Although coring is the most disruptive technique, it provides the maximum level of information. Early in November the sampling program was redesigned to ensure all necessary information was generated without unduly disturbing the test areas. As well, a SIPRE corer was used to cut all holes, regardless of the ultimate purpose. The location, snow cover, ice thickness, depth of oil lens, extent of migration and ice structure were logged (Appendix 27 C), and the cores immediately photographed. Small sections of core, generally from the region of the oil lens were retained for detailed study.

At regular intervals during the winter, and intensively during the melt phase, salinity profiles were made on representative cores. Each core was cut into 4 cm long slices, as soon after removal from the sheet as possible. The slices were then placed into labelled plastic bags that were sealed until the ice melted. Sorbent was used to remove oil from contaminated samples. The salinometer was routinely calibrated with prepared solutions, and a series of test were conducted to ascertain the effect of oil in the sample on the sensor.

5.4.3 Water Sampling

The non-biological water sampling program comprised measurements of salinity and temperature profiles, and dissolved hydrocarbon content, at various locations throughout the year.

During the initial site selection survey in August 1974, salinity and temperature profiling of the water column confirmed the similarity of the test bay to other areas along the coast. Measurements were repeated throughout the winter. Once ice cover was present, the profiling was done via SIPRE core holes through the ice. Most of the profiling was performed in unoiled locations so that reliable measurements could be taken. When measurements were done in oiled areas, care was taken to ensure that the probes did not come in contact with the oil.

Measurements of the dissolved hydrocarbon (HC) content proved difficult in the depth of the winter period. Of three proposed sampling methods, only the simplest one proved feasible. As contamination of a sample by trace amounts of undissolved oil would invalidate the results, sampling locations were located just outside of oiled ares. Samples were recovered by lowering a one litre glass bottle through a SIPRE core hole. The bottle then filled with water from just beneath the ice sheet, and was immediately withdrawn and rushed back to camp before freezing occurred. Glass bottles were necessary to prevent the possible evaporation of the highly volatile components during the extraction phase after adding five millilitres of n-pentane to the water sample. The bottle was capped, shaken, and left for twenty-four hours. After occasional shaking during that period, the pentane was drawn off and placed in a tightly sealed glass vial for shipment south for analysis by gas

chromatography. The sampling schedule is presented in Table 8-3.

...

5.5 Photographic Techniques

5.5.1 Underwater

A Hydro Products TC-125 underwater TV camera was used to document all controlled discharges, and to continuously monitor conditions both at the ice-water interface and in the water column. Since the camera measured less than 9 cm in diameter, it could be inserted through a SIPRE core hole. The unit maintains a nearly constant video output level over a dynamic range of illumination of 10,000 to one. Focusing was controlled from the surface. The signal was fed simultaneously to a Sony AV8400 video recorder and a Conrac monitor to permit selective recording. Positional data and information on the discharge were recorded on the sound track. Through the use of a constant current source, the entire system could be operated effectively from one 300 W portable generator.

During the depth of winter, lighting proved very difficult. Although the contrast between the oil and ice permitted high resolution around the edges of lenses or drops, the general lack of relief and the automatic compensation of the camera made the examination of fine details almost impossible, if the entire field of view was either all oil or all ice. A variety of lighting systems were tried, including tungsten, quartz halogen and quarts iodide. It was found that the spectral density was not as critical as the angle. In general, the more oblique the angle, the better the resolution. This was difficult to achieve, since in many cases it meant that the lighting system had to move independently from the camera. The problem was naturally resolved in spring. Even with up to 2 m of ice and 40 cm of snow, there was sufficient diffused light to permit viewing through 15 to 20 m of water.

For the initial test the camera and a narrow beam transducer were mounted in a telescopic scissor boom. The unit could be raised and lowered on an aluminum mast, rotated through 360 degrees and extended up to 15 m. However, to obtained full coverage, it was necessary to install the boom in the centre of the test area. A number of different barriers were tried in an effort to prevent oil from flowing into the well constructed for the boom. The only effective method was to thicken the ice around the well, which was equally disruptive to the test. For the NW6 test in February, the camera was mounted on a rigid boom, which was inserted through the ice from outside the test area. The extended distances limited the effectiveness of the system, and on all subsequent tests the camera was hand held by a diver wearing a closed circuit breathing system. The entire operation was monitored on the surface, and the movements of the diver controlled by means of a surface communications system. This approach provided the maximum recovery of data, and the greatest flexibility.

A Nikonos 35 mm camera with a 21 mm corrected lens was used for underwater still photography, and a 16 mm Bolex in an underwater housing for moving photography. Even with the use of flash and flood systems, lighting proved difficult. As a rule, all critical details were shot at a minimum of five exposures. The best results were obtained by pushing High Speed Ektachrome to 1000 ASA. The resulting grainy finish was not a great disadvantage in that the subject matter was largely high contrast in nature.

5.5.2 Time Lapse - Surface

From May to July 1975, two 8 mm time lapse move cameras were used to document site conditions. One camera was mounted in a weather proof housing and positioned on the top of a hill

to the north of the test area, at an elevation of approximately 30 m. This unit exposed a frame every 60 seconds. The second camera was mounted at the 15 m level on the anemometer tower and exposed a frame every 22.5 minutes.

5.5.3 Stills - Surface

Over 450 35 mm still pictures were taken throughout the project, covering surface conditions of the test sites, experimental techniques and ice cores. To ensure consistent quality and to accent internal features, all cores were photographed in specially designed light box, which had controlled back lighting.

5.5.4 Movies - Surface

The discharge operation, ice and surface conditions, the initial burn on June 7, and subsequent phases of clean-up were documented on 16 mm movie film. Altogether, some 5000 feet of film are available through NORCOR Engineering and Research Limited, the A.P.O.A., and the Department of the Environment."

Results

" 6.0 OIL AND ICE INTERACTION

Since all crude oils are less dense than sea water, they will rise towards the surface in a plume if released at depth. Enroute, the oil generally breaks into small droplets. If the area is ice-covered, the oil will collect on the bottom of the ice. The bulk of the oil will coalesce into pools or lenses, the size of which is controlled by the physical properties of the oil and irregularities along the bottom of the ice. Even with "smooth" first year ice, the variation can be considerable. The oil only penetrates several centimetres up into the skeletal layer and soft ice at the bottom. If the ice is still growing, new ice will begin to form beneath the oil, and the oil will be completely encapsulated or entrained in a mater of days. Once the oil is locked in the ice, further movement is limited until the ice begins to warm in the spring.

As sea ice freezes, approximately 80 percent of the salt or brine is rejected downward through the ice, while the remainder is trapped in small pockets in the ice. In response to increased solar radiation and a higher ambient air temperature in the spring, these isolated pockets of brine begin to etch their way through the ice. As they intersect voids left by the rejected brine, they form a continuous channel referred to as a brine channel. The oil migrates or moves towards the surface by means of these channels. Once oil reaches the surface, it greatly reduces the albedo and an increased quantity of solar radiation is absorbed. This causes an increase in activity in the brine channels and the process becomes self-accelerating. The various processes associated with spreading, entrainment, migration and surface effects of oil are detailed in subsequent sections.

6.1 Oil Plume and Spreading

The disposition of oil under solid ice cover is controlled primarily by three factors; the nature of the discharge, the condition of the ice, and the physical variables associated with the discharge of oil during a blowout. For example, well head temperature, pressure, the quantity of gas and oil, water depth and currents will all influence the plume, and ultimately the disposition of the oil. Due to the limited value of conducting a test under one particular set of conditions, and the probable

difficulty in controlling a large volume of oil, no attempt was made to simulate a blowout. Instead, the oil was heated to close to the ambient water temperature and injected under the ice in a manner designed to permit the best documentation.

Depending on atmospheric conditions and operational constraints, the oil was heated to between -4 °C and 1°C in a holding tank on shore. It was then pumped approximately 250 m out to the test area and injected under the ice. The discharge operation is detailed in Section 5.2.2. Although the minor variation in temperature had little effect on the physical properties of the oil (Table 6-1), on the several occasions when the oil was below approximately -1.8 °C, crystallization occurred in the water column. The oil quickly assumed the water temperature, and a maximum variation recorded by a thermistor was about 1.0 °C. The discharge rate varied from 0.13 to 0.19 m^3 min^{-1} (28.6 to 41.8 Imp. gal min^{-1}), yielding an exit velocity of 1.1 to 1.6 m s^{-1}. The projected discharge rate for a blowout in the Beaufort Sea is 0.27 m^3 min^{-1}, decreasing to 0.11 m^3 min^{-1} after one month.

Table 6-1. Variations in Physical Properties of Test Crudes with Temperature

	Temp (°C)	Norman Wells Crude	Swan Hills Crude
viscosity (g cm^{-1} s^{-1})	0 -15	0.12 0.18	0.34 0.45
density (g cm^{-3})	0 -10	0.845 0.855	0.837 0.845
thermal conductivity (cal cm^{-1} $°C^{-1}$ s^{-1} x 10^{-4})		≈ 3.0	≈3.0

A number of discharges were recorded on video tape and 16 mm film. In general, the oil rose in a conical plume, which had a half-angle of about 25 to 30 degrees. Flow tended to be unstable, and the oil broke into small particles within 0.3 m of the standpipe. The particles, which varied in diameter from about 0.2 to 1.0 cm, were close to spherical. Smaller particles were subsequently located in the ice, but these could not be detected in the plume. The movement of a number of particles was documented by means of the stop-action facility on the video system. The average upward velocity of five representative particles was 27 cm s^{-1} ± 6 cm s^{-1}. On the basis of the behaviour of the oil on contacting the bottom of the sheet, it was apparent that a considerable quantity of water was entrained in the plume. The upward movement of jelly fish near the periphery of the plume confirmed this observation. In general, the plumes closely resembled the deep water gas plumes documented by the Frozen Sea Research Group (Topham, 1976).

The behaviour of the oil striking the bottom of the sheet depended very much on ice topography. If there was a depression (or thin ice section) in the ice immediately above the standpipe, the oil would initially be confined to a single pool. Clear, uncontaminated ice could be observed in the splash zone created by the ascending particles. There was no appreciable movement of the oil outside of the splash zone. As additional oil was added, the pool or lens would slowly grow in size and depth until it reached the level of a channel which would permit flow into an adjacent depression. If the standpipe happened top be below a dome, or thicker section of ice, the droplets would radiate out from the centre after striking the ice. As the droplets decelerated, they tended to coalesce into concentric waves of oil, which radiated outward, but at a reduced velocity.

There was a distinct surging action, and clear bands of ice could be observed between rings of oil. Within several metres the wave would break down and the oil would flow outward in a dense array of small streams or rivulets. The widths of rivulets varied from about 2 to 10 cm.

In general, flow was unstable, and tended to pulsate in response to the wave action. There were periodic breaks in the oil, but the rivulets repeatedly followed the same course, suggesting that a path had been cut through the skeletal layer. Ice crystals were observed floating immediately below the oil. Occasionally, a surge of oil would flush over the entire area. On passing, the rivulet pattern would quickly re-establish while the ice in between showed no signs of contamination other that the occasional drop of oil. This would indicate that either time or pressure exerted by a new layer of ice below a lens is required for the oil to penetrate up into the skeletal layer.

The areal extent of spreading along the underside of the ice sheet is controlled by a number of factors. Most crude oils will naturally coalesce at an ice-water interface to form a sessile drop, which is similar in shape to mercury on glass. The process has been documented recently by a number of investigators (Lewis, 1975, Mackay 1975), and therefore will not be detailed herein. The minimum stable drop thickness is dependent on the properties of the oil, and is typically about 0.8 cm. A very small quantity of oil was deposited on the ice in the form of small spherical particles, which had a diameter less than the minimum film thickness. These normally occurred near the periphery of the contaminated ice, in areas where the currents were feeble, and the chance of collision with other oil particles was small.

The maximum film thickness is determined by variations in ice thickness, which take two basic forms. Due to differential growth at the skeletal layer, there is a small scale variation which is randomly oriented, and produces pockets about 5 to 10 cm wide and up to several centimetres deep late in the season. It is this pattern which likely accounts for the meandering in the oil rivulets. Consequently, although lenses as thin as 0.8 cm are possible, the minimum thickness tends to be in the range of one to two centimetres. The second form of irregularity is of much larger scale and is caused by variations in snow cover. Due to the insulating effect of the snow, the ice thickness varies inversely with snow depth. As a result, depressions tend to be created under drifts, and domes under more exposed areas. The size, orientation and stability of drifts is influenced by local climate and topography. In Balaena Bay, the drifts tended to be stable throughout most of the growth season. Plots of ice depth vs snow thickness made in November and January confirmed a well defined relationship between heavy snow cover and thin ice. Once the sheet exceeded about 50 cm, the maximum variation in thickness was approximately 20 percent of the average ice thickness. This yielded a maximum variation at the end of the season of 35 cm. For analysis of variations in ice thickness, see Figure 7-4a.

These large scale variations effectively contained the oil and controlled the maximum lens thickness. With the exception of the early tests 7.3 m^3 (1620 gals) was insufficient to fill even a single depression. On NW4, when the ice was about 64 cm thick, the oil covered approximately 400 m^2 for an average lens thickness of 2.0 cm. With NW7, when the ice was 154 cm thick, 180 m^2 was covered, yielding an average lens thickness of 4.5 cm. The maximum oil thickness measured was 20 cm, while the average oil thickness for all tests was 2.1 cm.

6.2 Oil Inclusion

The disposition of oil along the underside of the ice sheet has considerable bearing on the nature and rate of inclusion. As described in Section 6.1, the oil can be deposited in various

configurations, ranging from very small drops to large pools or lenses, depending on the characteristics of the plume and the roughness of the ice sheet. Although drops and small pools can be scattered over an appreciable area, they tend to contain an insignificant quantity of oil. In the tests at Balaena Bay, over 95 percent of the oil was contained in pools larger than one metre. The average depth of all pools was 2.1 cm, while the maximum observed depth was 20 cm. Because oil forms sessile drops at an ice-water interface, the minimum possible thickness of oil is about 0.8 cm.

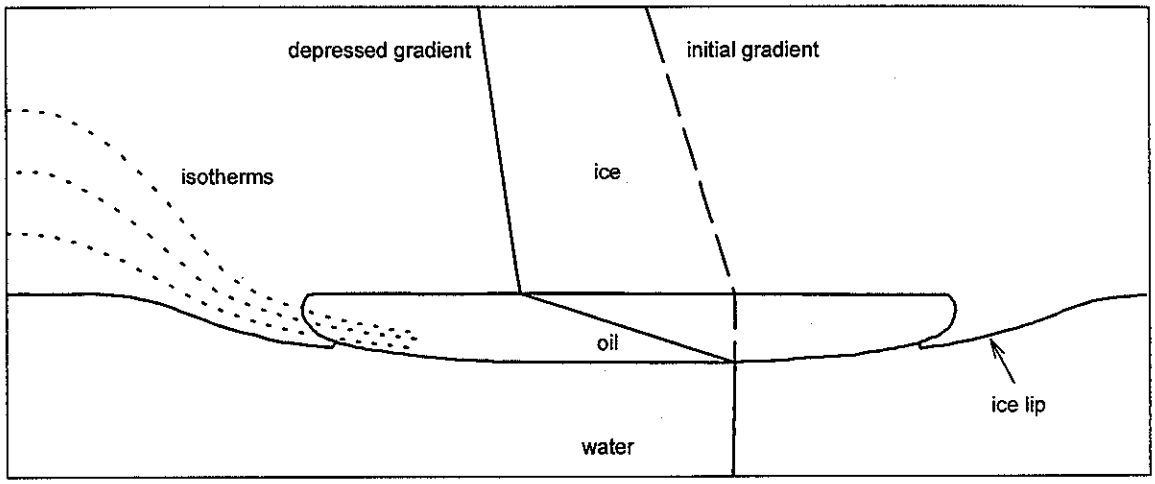

Figure 6-1. Initial effects of oil lens.

If the temperature of the oil is close to the ambient water temperature, which was the case for the tests and would likely be the case for most blowouts, the various processes associated with inclusion come into play shortly after the oil stabilizes on the bottom of the ice. The thermal conductivity of most crudes is about one fifteenth that of natural sea ice, and the insulating effects is detectable within hours. Although free convection could be significant in very thick oil lenses (Section 7.2.3), the required conditions are rarely encountered in the natural environment. For the more typical lens thickness encountered in Balaena Bay, the added thermal resistance of the oil caused a depression in the thermal gradient through the ice. Temperature drops of over 1.0 °C were observed immediately above the oil within 24 hours. The horizontal transition from a normal temperature gradient through the uncontaminated ice to a depressed gradient above the oil, caused sub-freezing temperatures at the edge of pools, which resulted in the formation of an ice lip. Figure 6-1, shows schematically the depresses thermal gradient and the realignment of isotherms.

The ice lip is a major feature of the inclusion process. Once it was formed, there is no possibility of further horizontal movement. This could be particulary important in areas with high currents or if there were continuous flow of oil. During the depth of winter, several ice lips were detected within hours after the oil was released, and in all cases a lip could be observed within 24 hours. ...

The time required for a new sheet of ice to form underneath an oil pool is primarily a function of the thermal gradient and the thickness of the oil. Due to the discrete spacing between thermistors, and gradual change from water to loose crystals then solid ice, it was difficult to ascertain the precise time at which a new sheet was formed. However, by continuously monitoring chains and extrapolating between beads near the water-oil interface, a reasonable approximation was possible. During late fall, when the ice and oil lenses tended to be relatively thin, the oil appeared to be

incorporated within about five days. This period increased to about seven days for a typical lens during the depth of winter and over ten days in the spring. As well as altering the thermal gradient, the oil also altered the system of brine drainage within the ice. In the normal brine rejection process, the freezing skeletal layer at the ice-water interface produces platelets of ice that are of lower salinity than the water. The brine that is rejected from the platelets during freezing flows downward through the forming ice. The rate of ice growth controls the amount of brine that is trapped in the ice sheet. When ice growth is slow, less brine is trapped within the ice.

Coincident with the drop in temperature, there is an increase in salinity in the ice immediately above an oil lens. This could be due to two factors. Firstly, the oil serves as a barrier to brine rejection, and the brine draining through the ice accumulates above the oil. Since the brine is denser than oil, other physical characteristics must come into play. Secondly, the depressed temperature would naturally cause a somewhat higher concentration of brine. However equally high salinity peaks could not be detected at other locations within the sheet, suggesting that a drop in temperature alone did not account for the entire accumulation of brine. The salinity in the new ice immediately below the oil tended to be lower than normal. This was likely due to the slow rate of growth and the barrier to brine drainage from ice above, imposed by the oil. In many respects, the ice which is formed beneath an oil lens resembled a sheet grown at the surface under controlled temperatures. ... The discharges which were conducted early in the year, when the sheet was growing rapidly, exhibit a far more pronounced jump in salinity above the oil, than do the later discharges. ... The temperature at which the brine channels will begin to open in the spring is dependent on brine concentration. The high salinity immediately above the oil will likely cause the brine channels to open somewhat earlier than normal, and thereby permit the upward migration of oil.

In most cases, a distinct band of clear relatively fresh ice could be detected immediately below the oil. The band was typically two to three centimetres thick, and consisted of small, randomly oriented crystals. The band was likely caused in part by the reduced salinity below the oil and the slow growth rate. Similar, but less pronounced bands were located at several levels in uncontaminated ice. These bands were also of lower salinity than the rest of the core. An attempt was made to correlate these features with temperature fluctuations, but due to variations in snow cover, and thermal lag in the sheet, no firm relationship could be established. There is also the distinct possibility of a periodic influx of fresh water with the tidal flush, but this would not explain the repeated reoccurrence of the band below oil pools.

Frequently, the new ice interface was very smooth, conforming with the underside of the oil lens. ... The surface appeared to be polished and did not contain large brine channels or crystals, common to uncontaminated ice at that depth. Occasionally flecks and small patches of oil were observed at the lower interface, but they did not penetrate more than a few millimetres into the ice. The effect of the oil at the upper interface was far more pronounced. Within a matter of days, the oil had penetrated several centimetres into the loose skeletal layer. The surface was very rough and irregular, and individual crystals and brine channels could be easily identified. The ice immediately above a lens tended to be saturated with oil, and plugs of oil could be seen in the brine channels.

6.3 Oil Migration

The migration, or upward movement of oil through the ice is controlled primarily by the condition of the ice, and to a lesser extent, the physical properties of the oil. The process can be reasonably correlated with the dominant periods in the growth and depletion of the ice sheet. During

the depth of winter when the sheet is cooling and growing rapidly, the ice is relatively solid, with the exception of the skeletal layer. Although the oil is less dense than water or sea ice, there are very few passages for it to penetrate, and movement tends to be limited. As the sheets starts to warm in the spring, brine channels begin to open, and the oil slowly moves upward, filling the voids. As the oil approaches the surface, increased solar radiation is absorbed and the process is accelerated. Late in the spring, when the ice is very porous, the oil flows freely through the sheet.

Simultaneous tests were conducted with Norman Wells and Swan Hills crudes primarily to determine the importance of the physical properties of the oil in the incorporation and migrating processes. Swan Hills crude is a relatively heavy oil (Table 6-1), while Norman Wells crude is light, and about the same consistency as Number 2 heating oil. It was felt the crude to be found in the Beaufort Sea would likely fall between these two. Although minor variations were observed, no significant differences, which could be attributed solely to the type of oil, were detected. However, the pour point of both crudes was well below the freezing point of the ice, and generally below the temperature of the ice when migration occurred. The effects of viscosity and density would likely be far more pronounced with a very heavy oil such as Bunker C.

Coring was found to be the best method of documenting the migration of oil through the ice sheet." The cores are presented in Seeley Martin's paper reviewed earlier. "During the coring operation, oil would flow up inside the SIPRE barrel, and surface contamination was unavoidable. Prior to photographing a core, the surface was cleaned with sorbent and then polished. During the winter, when the ice was solid, this proved to be effective, however, once the ice became porous, it was difficult to determine the source of the oil.

Cores recovered from the open water test area (NW2) showed no signs of the oil having penetrated downward into the ice. The sheet, which grew completely beneath the oil, closely resembled the natural ice sheet. The first 15 to 20 cm of snow above the initial level of the slick was saturated with oil, and had recrystallized. The snow above this appeared to be uncontaminated. The oiled snow-ice remained stable throughout the winter, and was subjected to drifting.

During the late fall and early winter, the ice grew at an average rate of about one centimetre per day. During this period, very little difference could be detected between the various test sites. Although the thickness of the ice was increasing, the initial thermal regime at the ice-oil interface was very similar. In all cases, the oil saturated the loose skeletal layer, and penetrated several centimetres further up open brine channels. On the average, between 4 to 6 cm of ice was contaminated. Once the oil was incorporated, a further depression in temperature had no apparent effect. ...

By about mid February, the sheet began to warm and the effect was immediately detectable in the oil. With the increase in temperature, isolated pockets of brine which formerly blocked brine channels began to melt and open short passages through the ice. The high salinity layer, immediately above the oil, was likely a significant factor in accelerating this process. The oil began to migrate upward as the channels cleared. By February 22, oil in the NW2 test site had penetrated some brine channels over 16 cm. The brine channels increased in size and became better defined. Initial movement appeared to be confined principally to the high salinity zone. A core recovered from the NW4 test area on March 1, displayed similar characteristics. The average diameter of major brine channels was about 0.1 cm. ...

During the initial stages of the migration, the location, or depth of the oil in the ice did not appear to influence its behaviour. The early discharges, which were close to the surface, exhibited

similar characteristics to the oil lenses near the bottom of the sheet. This is likely due to two offsetting factors. While temperature increases with depth, the level of absorbed solar radiation decreases. On the average, the radiation level is about six times greater at the 30 cm depth than at 60 cm depth. Since oil is an effective barrier to radiation, it is not unreasonable to assume that all radiation reaching the level of a lens will be absorbed by the oil. This could cause preferential localized warming of the lenses near the surface, and thereby enhance, movement in a depressed temperature field. No differences were detected between the Norman Wells and Swan Hills crudes.

During March and April the brine channels network became more pronounced, and the oil slowly progressed upward through the ice. By early May oil had reached the surface in most test areas. ... The oiled brine channels extended from the initial level of the lens to within 10 to 15 cm of the surface. The average diameter of the channels had increased to about 0.4 cm, and they tended to be interconnected by smaller feeder channels. At the surface there was normally a band of clear frazil ice. This layer did not have an established brine network, and was subject to repeated refreezing, in response to diurnal fluxes.

The rate of migration was controlled primarily by the condition of the ice. On May 15, 0.4 m^3 of Norman Wells crude oil was released under 195 cm of ice. The air temperature varied from -1.5 to -3.0 °C, while the internal temperature of the ice was about -4.0 °C. Special care was taken to ensure that the snow cover was not disturbed prior to the test. Within one hour traces of oil were detected on the surface of the ice. Initially small pools of oil formed around isolated brine channels, which penetrated the surface layer. The average spacing between pools was about 20 to 30 cm. The pools quickly spread, covering the entire surface with oil. Upon coring in the area, the brine channels were found to be completely filled with oil, and the conditions identical to the other test areas, where the oil had been incorporated in the ice for a number of months. Similar results were observed in a test conducted for Panarctic Oils on May 5.

As the ice continued to deteriorate, the oil progressively saturated the interstices between platelets. The average concentration of oil increased to about 4.5 percent. The maximum concentration recorded in a 4 cm section of core was 7 percent. Although the oil continued to flow up through the ice during the entire melt phase, all the oil was not released until surface melt actually reached the initial level of the oil lens."

"6.4 Effects of Surface Oil

Oil was first detected on the surface of the snow in the SH2 test area on May 9. Initially, the snow appeared to be slightly discoloured. Within 24 hours, the oil had formed a pool about 1.5 m in diameter. By May 12, approximately 10 percent of the entire test area was covered by either surfaced oil or darkened snow. For the preceding eight days the air temperature was above freezing, and a record high of 12 °C was recorded on May 5. Between May 9 and May 12, the average albedo to the test site dropped from 0.7 to 0.6.

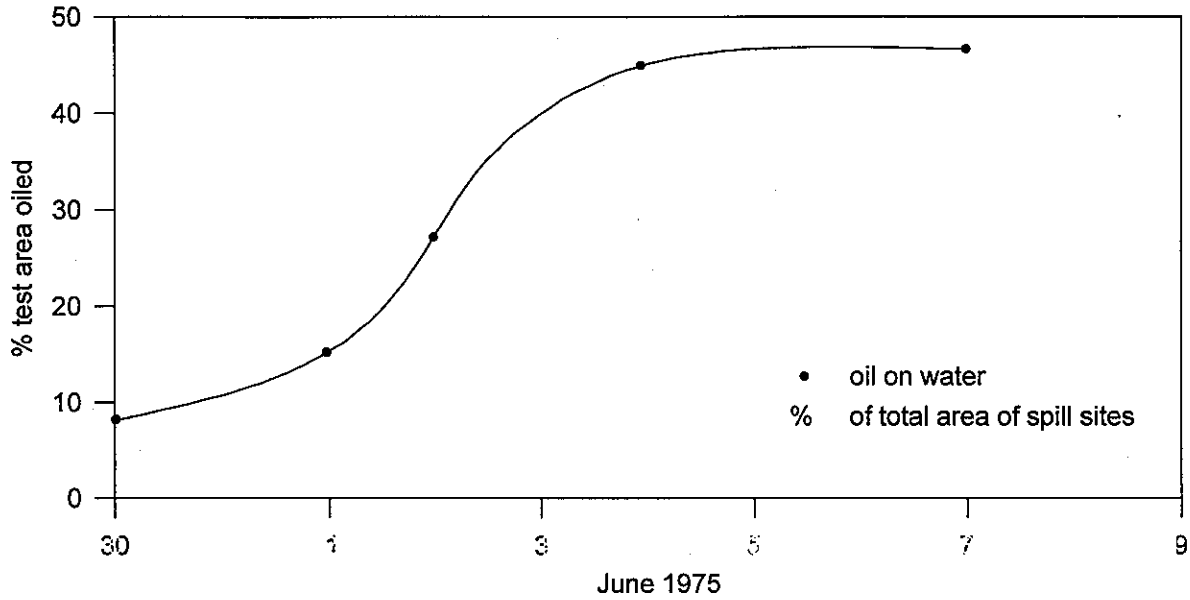

Figure 6-8. Oiled area coverage *vs* time.

A total of 7.5 cm of snow fell between May 13 and May 21 and there was an accompanying drop in temperature. The snow completely covered the test area, and the surface appeared similar to that prior to May 9. On May 24, oil was again detected on the surface. Conditions quickly deteriorated. The average albedo dropped from 0.76 to 0.27 by June 4. Within five days a number of well defined melt pools had developed. These pools progressively grew in area and depth, until about June 4, when they became interconnected and a common water level was achieved. At this point over 45 percent of the total surface area was covered by oiled melt pools. The pools ranged in depth from several centimetres to a maximum of 50 cm. Although the snow was very wet, melt pools had not developed in the uncontaminated snow outside the test area. The rate of change in surface conditions for the first seven days of June is shown in Figure 6-8."

...

"Throughout the melt period, incoming short wave radiation and net-radiation were monitored continuously. Albedo measurements were made every second day at a total of 14 stations. Twelve of these stations were located within the test area, while the two controls were at undisturbed sites (Appendix 27D). Care was taken in selecting the sites to ensure the full spectrum of conditions was covered. In most cases, a simple arithmetic mean of the twelve values was a reasonable approximation of the average albedo for the entire test area.

To minimize surface disturbance, the albedometer which consisted of upward and downward facing solarimeters, was mounted on a cantilever, which could be extended up to 3 m into the test area. The maximum error of the system was ± 10 percent of the measured value (Appendix 27A). Although the albedo of most surfaces is not sensitive to zenith angle, measurements were always taken at approximately 1930 G.M.T. Each site was photographed at the same time, to permit the correlation of surface conditions with albedo. Representative albedos for typical conditions are shown in Table 6-3.

Table 6-3. Measured Albedos - Balaena Bay

Fresh Snow	0.85
Wet Snow	0.65
Oil on Snow	0.70 to 0.30
Thin Oil Film on Water	0.10
Thick Oil Film on Water	0.06 to 0.10
Water	0.08 to 0.15

The measured change in albedo for the period May 9 to June 6 is shown in Figure 6-13. Values from all twelve stations were used in determining the average albedo for the test area. The heavily oiled curve, was based on observations in the SH2 test area, and is a reasonable approximation of the extreme low. The control curve is representative of the uncontaminated area. The rapid rise in all three curves about the middle of the May corresponds with a series of snowfalls (for detailed weather summaries, see Appendix 27D). Of particular importance is the progressive divergence between the average albedo of the test site and the control areas after May 25.

By June 4, the average albedo of the test area had dropped from 0.7 to 0.25, while the albedo of the control areas had only fallen to 0.5. Since a substantial portion of the test area was uncontaminated, the actual albedo of oiled areas was considerably less than the average for the site. The albedo of the heavily oiled SH2 location was only 0.09. From May 8 to June 6, the total daily incoming short wave radiation at ground level varied from 320 to 780 cal cm^{-2}, depending on atmospheric conditions (Figure 6-14). The average level for the period was 554 cal cm^{-2} day^{-1}.

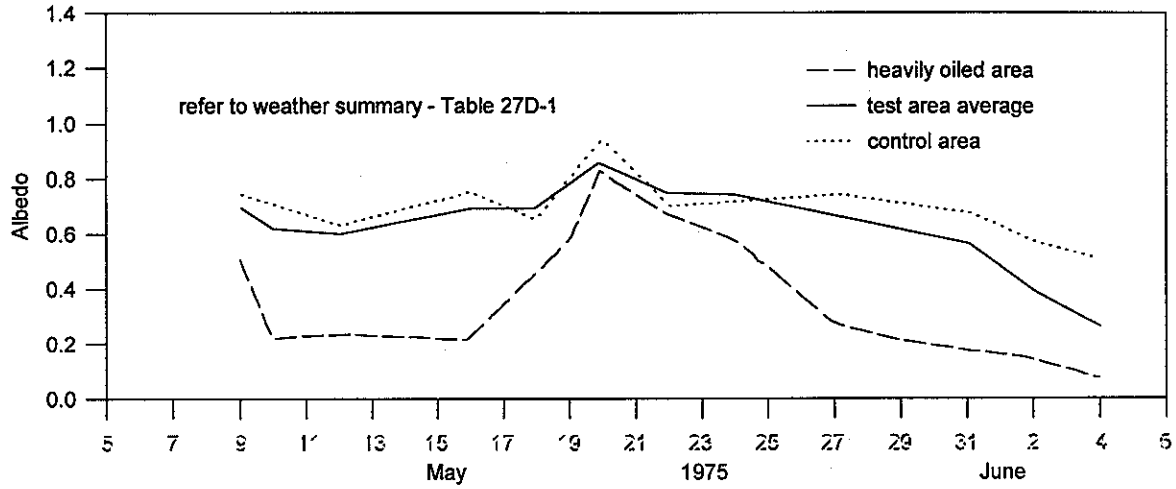

Figure 6-13. Albedo May 5 to June 6, 1975.

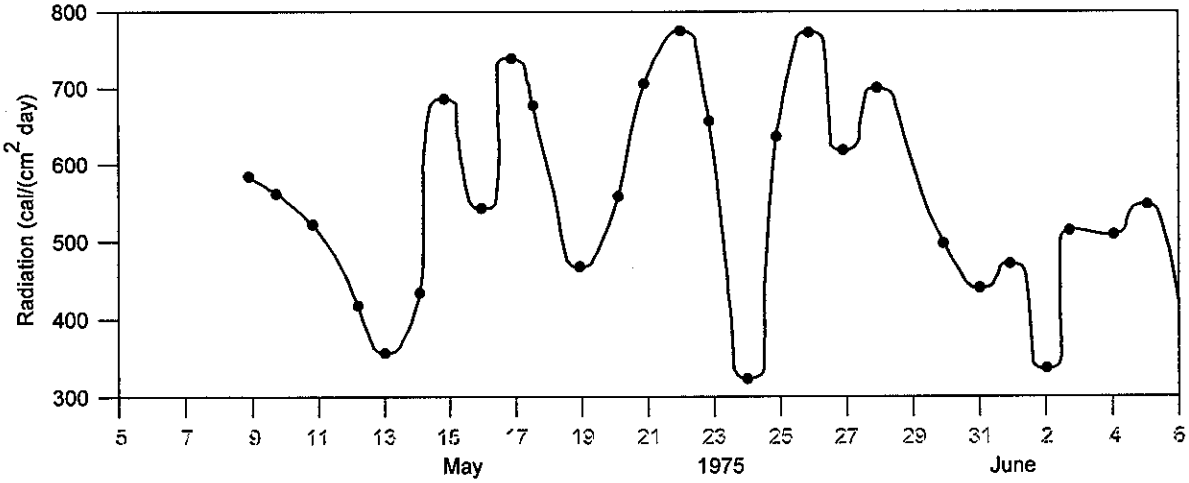

Figure 6-14. Incident solar radiation.

In the ten day period preceding June 6, 1730 cal cm^{-2} were absorbed in the control areas, and an average of 2510 cal cm^{-2} in the test area. A total of 3690 cal cm^{-2}, or sufficient energy to melt over 40 cm of ice, were absorbed in one heavily oiled area. The depth of an adjacent melt pool was 50 cm. The effect of the increased absorption was very pronounced. The location of melt pools closely corresponded to the initial disposition of oil lenses under the ice.

Although the albedo of a thick oil film on water and a clear melt pool are about the same, the thermal regime can be quite different. Because the oil serves as an effective barrier to radiation, most of the energy is absorbed by the oil. However, the radiation passes through a clear melt pool and is absorbed by the ice. ... The average spread in temperature between oil and the underlying water was between 8 and 10 °C."

" 7.0 THERMAL ASPECTS OF OIL-ICE INTERACTION

7.1 Principal Components of the Energy Balance"

The authors state that the ice sheet energy balance is expressed by:

$$G = (S + s)(1 - a) - L\uparrow + L\downarrow + Q_s + Q_l \qquad (1)$$

where G = change in heat content of the sheet,
S = direct solar radiation incident at surface,
s = diffuse solar radiation incident at surface,
a = albedo of surface,
$L\uparrow$ = outgoing long wave or terrestrial radiation,
$L\downarrow$ = incoming terrestrial or counter radiation,
Q_s = net sensible heat flux,
Q_l = net latent heat flux.

The authors state that sensible heat (reflected by a change in thermal regime), and latent heat (growth or depletion of the ice sheet) are the two components that determine the change in heat content of the ice. The thermal regime is measured using thermistors embedded in the ice sheet and growth and depletion by measuring ice thickness.

The solar flux is measured by pyranometers which have a range of 300 to 3500 nm.

Albedo is the ratio of reflected to incident short wave radiation and is typically 0.9 for new snow, 0.4 for oiled snow, and 0.1 for an oil lens or open water. The ratio is determined by measuring upward and downward components with a pyranometer.

The authors state that the earth is assumed to emit and absorb energy as a gray body (in the infrared region) and obey's the Stefan-Boltzmann law:

$$L\uparrow = \varepsilon\delta T^4 \qquad (2)$$

where $L\uparrow$ = outgoing long wave or terrestrial radiation,
T = surface temperature,
ε = infrared emmisivity,
δ = Stefan-Boltzmann constant.

The authors state that the infrared emissivity of natural surfaces varies from 0.9 to 0.95 and therefore the outgoing long wave terrestrial radiation is primarily temperature dependent. However, the atmosphere is not transparent to this wavelength and therefore only about 9% of this radiation escapes to space. Part of the radiation absorbed by the atmosphere is radiated back as counter radiation ($L\downarrow$). Also the emissivity of ice and oil are expected to be about the same value.

The authors state that the latent heat flux is principally in the form of precipitation and evaporation (almost nonexistent in winter) and the decrease or increase is from drifting snow. They therefore state that the exact value is hard to determine.

The other components of the heat flux equation were measured but still analysis was not complete due to the intermixing of oil and water during the melt phase and the error of the instrument was of the same order as the measurement.

The albedo of the oil was a dominant component and resulted in ice depletion. The albedo measurements were made at a minimum of 14 stations.

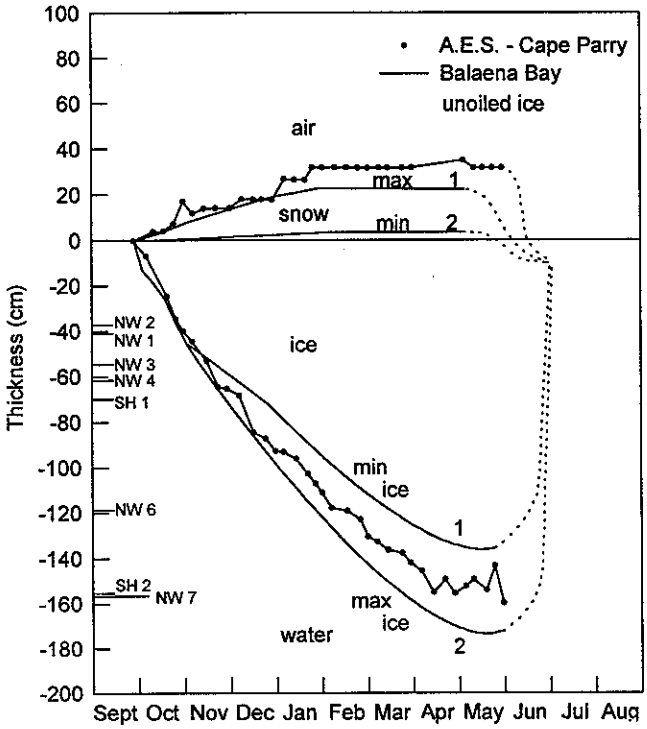

Figure 7-1. Ice growth 1974-75, Balaena Bay and Cape Parry.

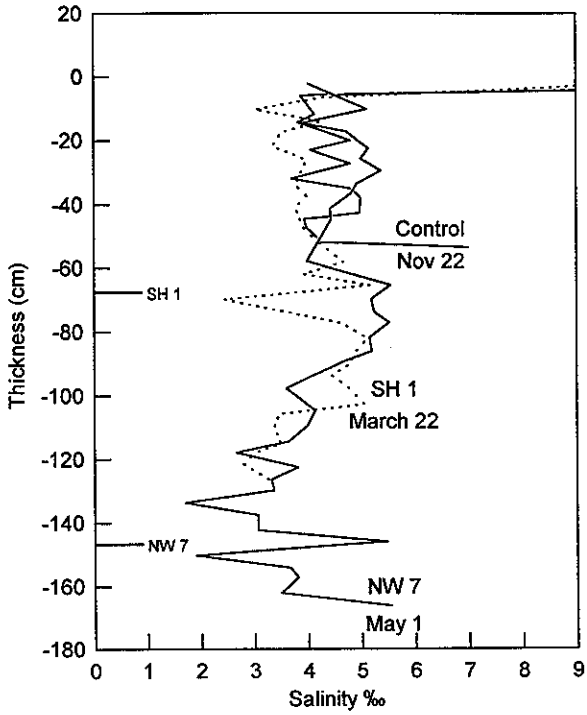

Figure 7-2. Representative ice salinity profiles.

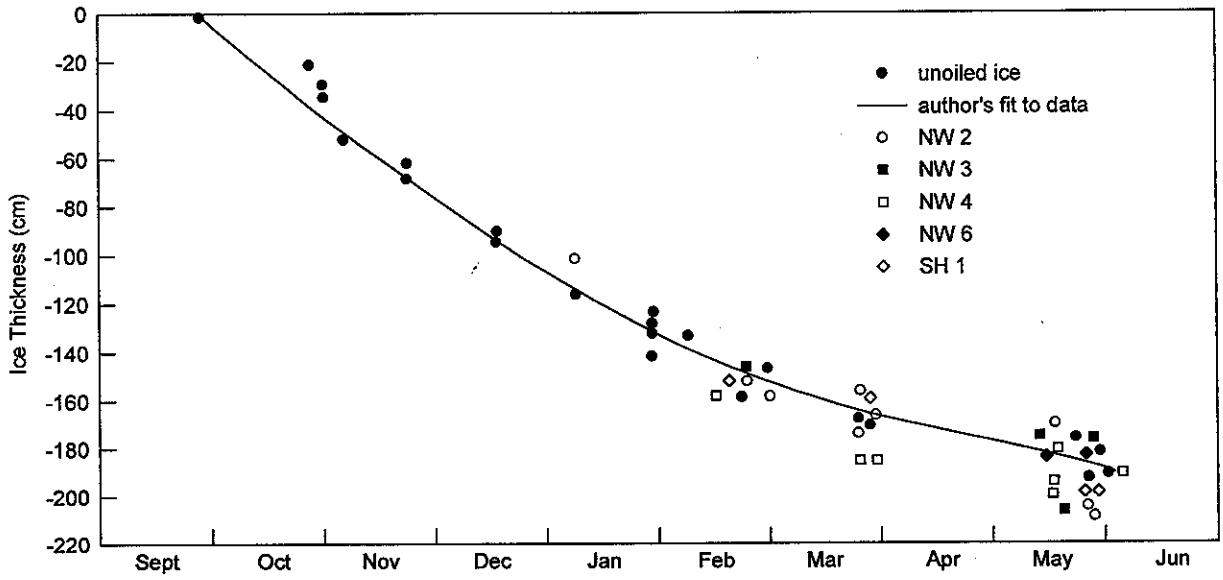

Figure 7-3. Ice thickness measurements in oiled and clean areas normalized to zero snow equivalent values.

" 7.2 Theoretical Considerations"

One of the main objectives of the work was to measure the effect of oil on ice growth. The thermal conductivity of sea ice is from 15 to 20 times that of oil and therefore an oil lens would be expected to reduce ice growth. Since the ice is not uniform the effect of an oil lens inclusion was reduced. The ice thickness and snow depth were measured, for September to July, and are presented in Figure 7-1. The lines marked 1 and 2 are the minimum and maximum thicknesses observed. The authors state that once the ice thickness exceeded 50 cm the average variation in thickness was 20%. They also state that there is an inverse correlation between ice thickness and snow coverage. Logically this makes sense since the snow acts as an insulator and therefore the ice remains thinner for thicker snow coverage.

The ice thickness is plotted versus ice salinity in Figure 7-2 and between November and June (for a total of 19 cores) the mean salinity was 4.56‰ with a standard derivation of 0.63%. In the upper 5 cm of ice, the salinity was 10‰ to 15‰ and in the skeletal layer the mean salinity was about 1‰ to 2‰ above the average.

The authors modified all ice thicknesses to a zero snow equivalent and this data is presented in Figure 7-3. No differences is noticeable between oiled and unoiled data. The authors expected that if oil was to increase the thermal resistance of the ice sheet then these areas should have had thinner ice, however, this was not the case.

The authors state that the oil ice interface is indistinct in nature and the oil fills voids in the ice up to a height of 2 to 5 cm into the skeletal layer. The authors also note that the core observations indicated that the lower oil-ice interface was smooth where ice had formed below the oil and there was no migration of the oil across this interface.

The authors state that the mode of heat transfer through ice is solid body conduction. In the oil lenses free convection may occur. Free convection result when a normal fluid whose density varies inversely with temperature is placed between plane surfaces and cooled. Free convection is is described in terms of two dimensionless variables, Grashof (Gr) and Prandtl (Pr) numbers. The Nusselt modulus (Nu) is a ratio of convective heat transfer coefficient ($\bar{h}$) to conductive heat transfer coefficient (L_{oil}/k_{oil}) where L_{oil} is oil lens thickness. For a fluid contained between two surfaces, the upper one being at a lower temperature, causes an unstable density stratification. Once the Gr Pr product reaches 1700 a free convection flow pattern, called a Bernard cell, occurs. For a laminar flow ($1700 \leq Gr \cdot Pr \leq 47{,}000$), $Nu = 0.107(Gr \cdot Pr)^{0.3}$. The Gr•Pr (Rayleigh Number) is a critical number for establishment of turbulent flow in free convection cases. Irregular turbulence is considered to be fully established for Rayleigh Number of 3×10^5. The authors refer to the data present in Table 7-1 and note that the viscosity of Swan Hills crude is about 2.5 times the viscosity of Norman Wells crude, at the same temperature. The authors also state that density and viscosity of crude oils will cause Nu to vary by <10% over a temperature range of -15 to 0 °C but there will be 25% less convective heat transfer across a Swan Hill oil lens than a Norman Wells oil lens. However, the authors also point out that the uncertainties in the other measured quantities in Table 7-1 can cause as much error in Nu. The authors calculations were performed using Norman Wells crude and the laminar flow regions were for Nu range of 1 to 2.7 and the turbulent regime were from a Nu of 6.58 to 187.

Table 7-1. Material Properties used in Heat Transfer Calculations

Material	Specific Heat, C_p (cal g^{-1} $°C^{-1}$)	Thermal Conductivity k(cal cm^{-1} $°C^{-1}$ s^{-1}) x 10^{-4}	Density ρ(g cm^{-3})	Viscosity μ(g cm^{-1} s^{-1})	Coefficient of Thermal Expansion $\beta(°C^{-1}) \times 10^{-4}$
Snow		5.33 - 9.8 [1]			
Sea Ice	0.46 [4] 0.50 [3]	43 to 47 [4] 60 [3]	0.915 [3]		1.1 [6]
Norman Wells Crude	0.41 [6]	3.0 [6]	0.845 [5] (0 °C) 0.855 [5] (-10 °C)	0.12 [5] (0 °C) 0.18 [5] (-15 °C)	9. [6]
Swan Hills Crude	0.41 [6]	3.0 [6]	0.837 [5] (0 °C) 0.845 [5] (-10 °C)	0.34 [5] (0 °C) 0.45 [5] (-15 °C)	9. [6]

Sources: 1. For snow $k = 0.0068 \rho^2$ (Anisimov, 1961) 2. Snow density as measured at Balaena Bay and quoted for Cape Parry in Burns, 1974 and Williams, 1958.
3. Lewis. 4. Weller, 1967. 5. Mackay, 1975. 6. From handbooks.

The Grashof (Gr) number is a function of $\forall T L^3$ ($\forall T$ is the temperature differential across the oil lens) and the authors state that the Nu modulus can be expressed in terms of $\forall T$ and L_{oil} for both laminar and turbulent flow. The authors also state that for natural first -year ice there are upper and lower limits for $\forall T$ and L_{oil}. (These are not stated but the implication is that they are used to calculate data for the plots.) Measured ice thickness variation is plotted versus measured mean ice thickness in Figure 7-4a. The authors state that the ice variation gives a maximum value for the oil lens size. They also state that $\forall T$ of the oil lens will be controlled by the overall temperature gradient of the ice sheet , the oil lens thickness and Nu modulus. For simple conduction the ratio of $k_{oil}/k_{ice} = 1/15$, however, if there is convection heat transfer across the oil, the gradient across the oil will decrease as the effective thermal conductivity of the oil lens increases.

The authors state that if the two types of heat transfer (conduction and convection) occur in parallel, then the total thermal resistance of an oil lens can be expressed as:

$$R_{oil} = \frac{R_1 R_2}{R_1 + R_2} \qquad (1),$$

where R_1 is the thermal resistance due to conduction ($= L_{oil}/k_{oil}$), and R_2 is the thermal resistance due to convection ($= L/\bar{h}$). Where $\bar{h} = Nu\, k_{oil}/L_{oil}$ and therefore $R_2 = L_{oil}/(Nu\, k_{oil})$. This then translates back to the original equation to give:

$$R_{oil} = \frac{L_{oil}}{(Nu + 1)k_{oil}} \qquad (6)$$

The authors state that if the temperature gradient (Grad) through the ice sheet is known then the thickness of the oil lens can be expressed in terms of $\forall T$, Nu Grad, and the ratio k_{ice}/k_{oil}. In Figure 7-4b, a representative ice temperature gradient is plotted versus the mean ice thickness. These values were collected from control thermistor chains over the winter (November to May). The authors

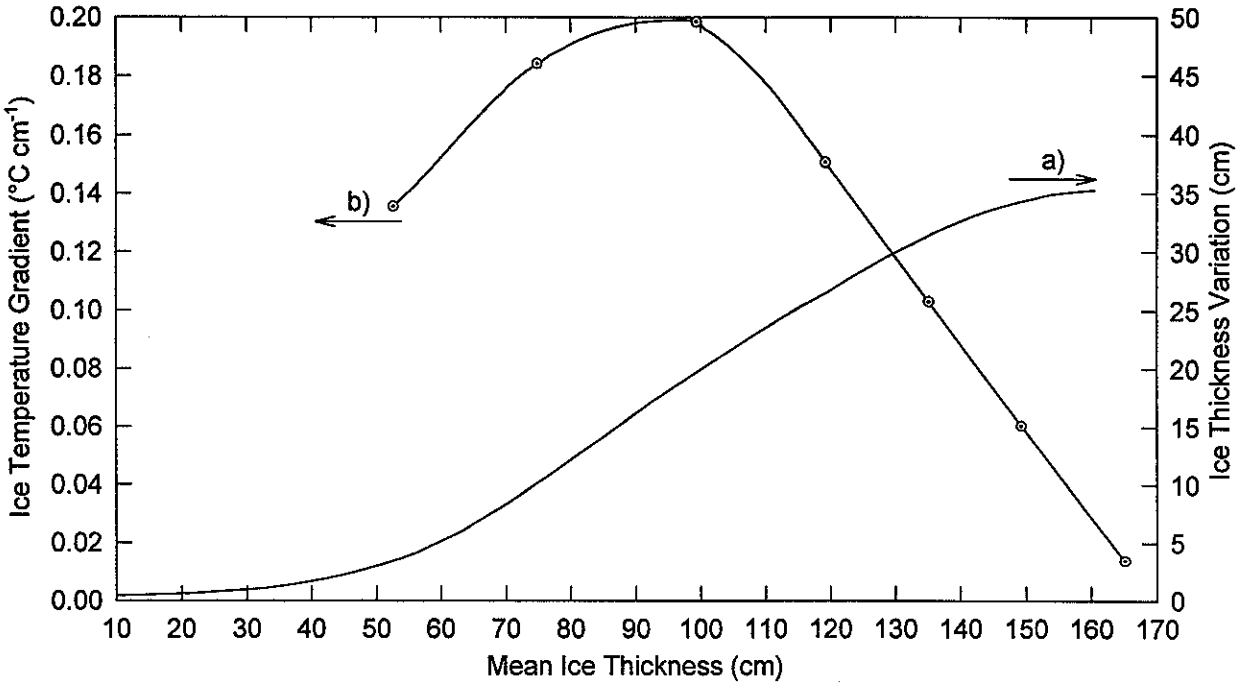

Figure 7-4. a) Natural variation in ice thickness. b) Typical natural ice temperature gradient.

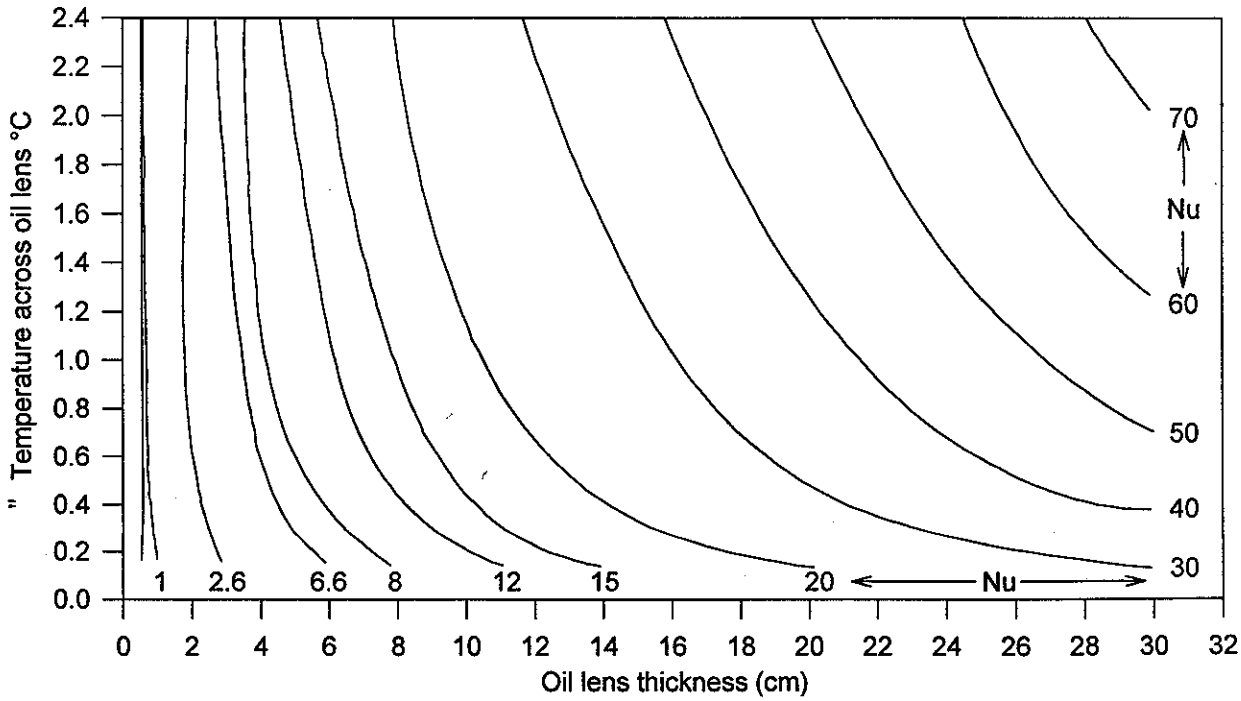

Figure 7-5. Oil lens temperature differential vs oil lens thickness.

calculated that since $\forall T_{oil}$ = f(Nu, Grad) they determined values for the laminar and turbulent regions.

Laminar $1 < Nu < 2.6$ $\Delta T_{oil} = (0.38\,Grad\,Nu^{0.1})^{0.83}$ (8)

Turbulent $6.58 < Nu < 187$ $\Delta T_{oil} = (0.29\,Grad\,Nu^{0.01})^{0.76}$ (9)

which the authors state results in a temperature drop of 0.6 to 1.5 °C for the laminar case and 0.54 to 1.33 °C for the turbulent case. (This is for an ice temperature gradient observed at Balaena Bay of 0.06 to 0.2 cm^{-1}.) The authors used these parameters for ΔT and L_{oil} and they generated data which was plotted in Figure 7-5, for Nu modulus versus temperature drop across an oil lens.

The authors state that their theoretical treatment would give a Nu = 50 for an extremely thick oil lens of 25 to 30 cm. The temperature gradient across the oil lens would be 1/4 that of the ice. However, the thermistor chains indicated that the oil lens was never greater than 2 cm. The experimental profiles in 7-12 and 7-14 show a temperature gradient through an oil lens of about 6 times that of ice which agrees with a theoretical (Figure 7-5) Nu modulus of 2.2.

The authors then define an overall heat transfer coefficient (U) and for a one component system with no oil or snow, $U_{ice} = k_{ice}/L_{ice}$. However it can be changed to incorporate oil, snow and ice and is simply the inverse of the sum of the individual thermal resistances:

$$U_{ice+snow} = \frac{1}{\frac{L_{ice}}{k_{ice}} + \frac{L_{snow}}{k_{snow}}} \quad (10)$$

$$U_{ice+oil} = \frac{1}{\frac{L_{ice}}{k_{ice}} + \frac{L_{ice}}{(Nu+1)k_{oil}}} \quad (11)$$

The ratio of $(U_{ice+snow})/U_{ice}$ versus mean ice thickness is plotted in Figure 7-6 for snow depths of 4, 10 and 30 cm. For the 10 cm snow cover in Figure 7-6, the overall heat transfer coefficient is reduced by 50% over the growth period.

The ratio of $(U_{ice+oil})/U_{ice}$ versus discrete oil lens thickness (0.75 to 30 cm) is plotted in Figure 7-7. The Nusselt (Nu) modulus (degree of heat transfer) and ΔT_{oil} are tabulated for each curve. The authors introduced a constraint to enhance the comparative nature of the plot. This was done by setting the thickness of $L_{oil} + L_{ice}$, that was used to calculated $U_{ice+oil}$, to the clean ice thickness used to calculate U_{ice}. The authors state that this was done since the oil would naturally seek out the points of minimum ice thickness. It becomes more important for large oil lens thicknesses. Figure 7-7 curves show that a maximum decrease in ice growth is caused by the thinnest (0.75 cm) oil lens, since there is no convective heat transfer present. This is a 15% reduction in heat flux over the non-oiled ice and the authors state that this is insignificant when compared to the 50% variation in flux due to changes in snow cover. The authors state that only when the oil lens is 10 to 20 cm thick is there a large change in heat flux (due to large Nu numbers). The authors further state that the theoretical treatment agrees with the field observations and that the large change in heat flux is due to snow coverage changing not oil lens formation.

The authors also state that the insulating effect of the oil lens decreases as the lens thickens

Absolute thermistor error ± 0.01 °C at 0 °C.
± 0.03 °C at -20 °C, -40 °C
add ± 0.02 °C up to 20 °C on either side of a known point.
Repeatability error involved in comparing 1 probe over a short time period - negligible.

Table 7-3. Control chain 1, Dec. 10

Depth (cm)	Temperatures (°C)					
	0100 h	0600 h	1000 h	1300 h	2000 h	Absolute Change
+100 Air	-29.60	-30.02	-29.93	-30.00	-31.49	1.89
+8.2 Snow	-25.29	-25.16	-24.72	-24.55	-26.99	
+4.1 Snow	-20.23	-20.36	-20.12	-20.02	-21.11	0.34
-5.1 Ice	-12.34	-12.39	-12.41	-12.42	-12.59	0.25
-10.1 Ice	-11.53	-11.59	-11.64	-11.64	-11.78	0.25
-20.0 Ice	-9.71	-9.82	-9.88	-9.90	-10.02	0.31
-40.00 Ice	-6.21	-6.29	-6.26	-6.40	-6.50	0.29
-59.2 Ice	-2.67	-2.71	-2.73	-2.76	-2.81	0.14
-99.2 Water	-1.12	-1.12	-1.11	-1.10	-1.10	0.02
-139.2 Water	-1.54	-1.53	-1.52	-1.52	-1.50	0.04
-179.2 Water	-1.38	-1.38	-1.37	-1.37	-1.35	0.03

Clear sky, 0 hr daylight.
Ice depth 68 cm.

Table 7-4. Mean monthly water temperature and standard deviation (°C)

Depth Below Ice Sheet (cm)	Nov	Dec	Jan	Feb	March	April	May
20-30		-1.11 (0.08)		-1.32 (0.17)		-1.22 (0.16)	-1.46 (0.11)
40-65	-1.25 (0.12)	-1.54 (0.10)	-1.54 (0.10)	-1.56 (0.13)	-1.27 (0.17)		
80-105	-1.51 (0.09)	-1.36 (0.12)	-1.57 (0.10)				

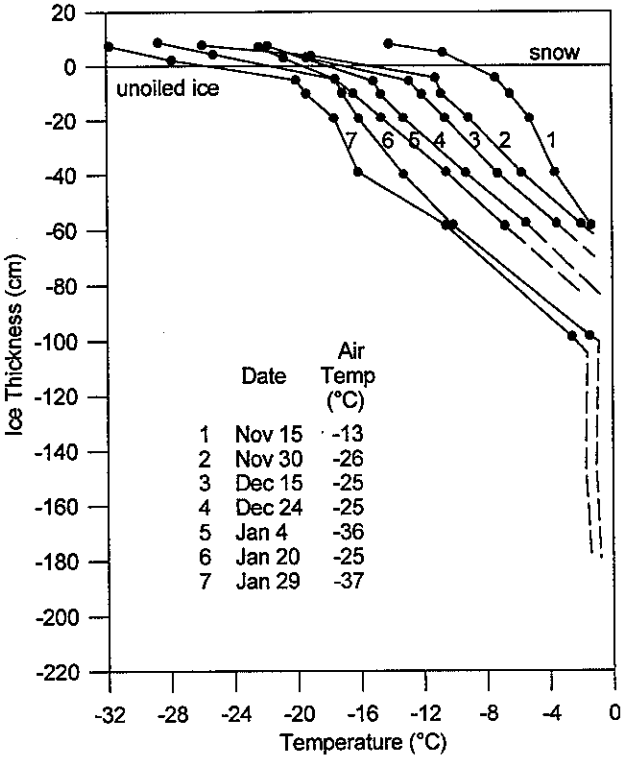

Figure 7-8. Control ice temperature profiles.

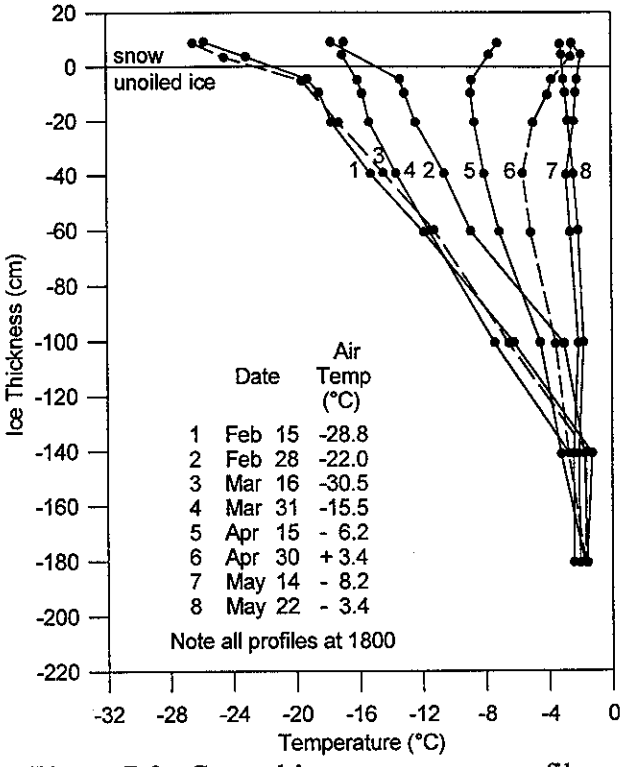

Figure 7-9. Control ice temperature profiles.

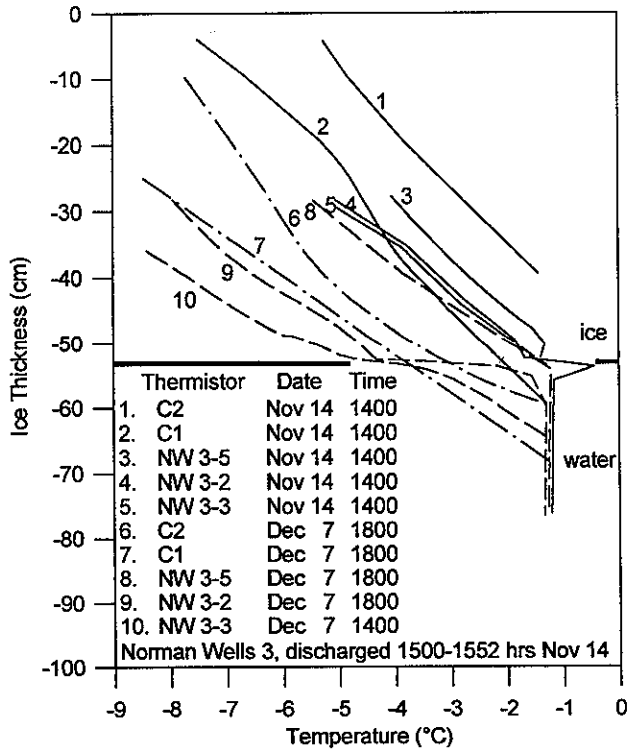

Figure 7-10. Control and NW3 temperature profiles.

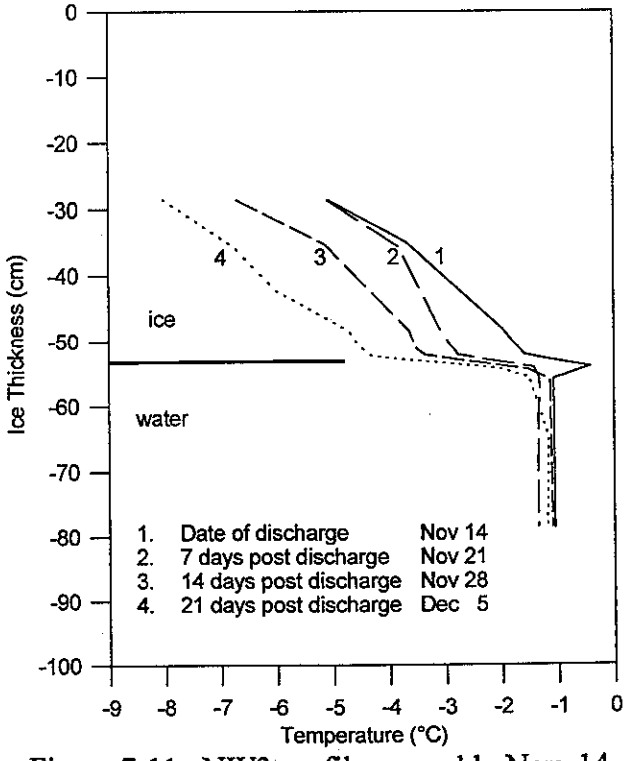

Figure 7-11. NW3 profiles - weekly Nov. 14 to Dec. 5.

The temperature profiles for control chain C1 are presented in Figure 7-8 (Nov 15 to Jan 29) and in Figure 7-9 (Feb 15 to May 22). All measurements were recorded at 1800 hrs to minimizes diurnal effects. The internal temperature of the ice was lower than air temperature at the end of April, however, the ice continued to grow until the end of May. The authors state that the thickness was approximated by extrapolating the thermal gradient near the bottom of the ice. The skeletal layer of ice on the bottom of the sheet was fragile and indistinct and thus the resolution of the ice measurements was ± 2 cm.

" 7.3.1 Late Fall"

The temperature profiles for the NW3 discharge (Nov 14) are depicted in Figure 7-10. The authors state that the growth rate during November was 0.7 cm per day and the average thickness was 55 cm. Controls C1 and C2 are included in Figure 7-10 and the snow coverage on C2 was 30 cm compared to 12 cm on C1. This is reflected in the decrease of the ice temperature by 2.0 °C and an ice thickness increase of 20 cm. The December 7 values indicate that the ice thickness at C1 had increased by 20 cm and at C2 by 10 cm and the temperature difference at 45 cm was 0.5 °C. The NW3-2 and NW3-3 thermistor chains were oiled and the NW3-5 thermistor chain was not. The oiled thermistor chain temperature profiles exhibited plateauing on December 7. Both oiled thermistor chains temperatures were 0.5 °C lower than C1, 1.3 °C lower than C2 and 2.8 °C lower than NW3-5. Less than 10 cm of new ice formed under the oil lens of NW3-3 and 4 cm under the oil lens at NW3-2 while the thickness at C1 and C2 increased an average 15 cm. The authors state that these differences could be due to differences in snow cover as well as oil pool thickness and size differences. In Figure 7-12 the temperature profiles of NW3-2 for 1 hour prior to the discharge, at discharge, 1 hour after the discharge and 24 hours after the discharge, are displayed. The authors state that the water temperature increased during the discharge and that after 24 hours had passed not only had the water temperature dropped back but there was a oil lens temperature gradient effect. The authors state that they judged the oil lens to be 2 cm thick from the slope change. The temperature gradient ratio (oil lens and ice) was 12 and was expected to be 15. This was due to little convective heat transfer taking place. The oil had the immediate effect of reducing the local heat flux by a factor of 2.5. Figure 7-11 is a plot of temperature profiles for the day of the discharge, and 7, 14, and 21 days after the discharge of oil. The profile for the day of the discharge has a spike as seen in Figure 7-12. The other profiles have the plateauing effect of an oil lens. The authors state that by extrapolating the temperature above the oil lens to intercept the water temperature they believe that the oil lens caused a 3 to 5 cm reduction in ice growth for the 21 days. This was a 20 to 30% reduction in heat flux and the theoretical curves (Figure 7-7) would have predicted only a 10 to 20 % reduction at the ice thickness of 55 cm.

The following text is directly quoted from the report.

" 7.3.1 Depth of Winter

Temperature profiles associated with the double discharges, SH1 on December 7 and NW4 on December 9, display short and long term responses similar to NW3 (Figures 7-13, 14).

Considering SH1-3 one hour prior to discharge, the ice-water interface is seen to fall on the dense array of probes at 68.5 cm (Figure 7-13). Snow depth around the chain on December 7 was 12 cm. One day after the test, the temperature in the lower 10 cm of the sheet had been depressed

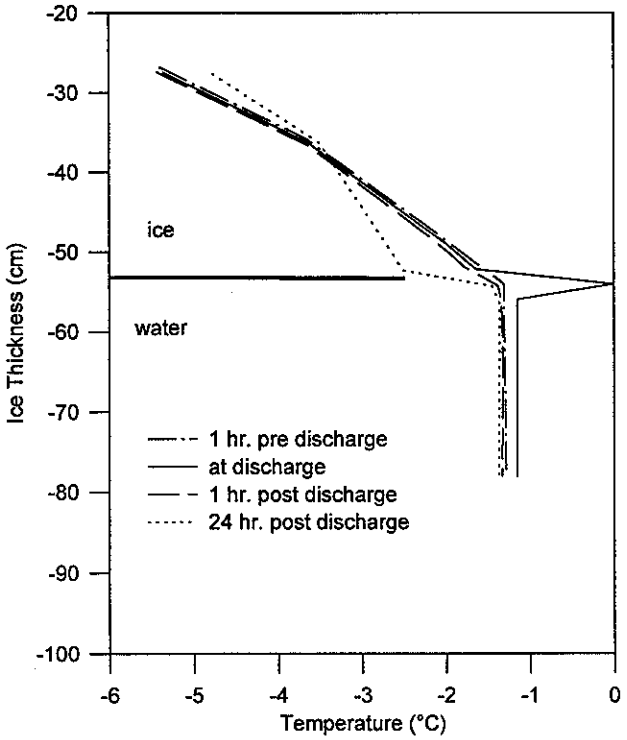

Figure 7-12. NW 3 profiles Nov. 14 - Nov. 15.

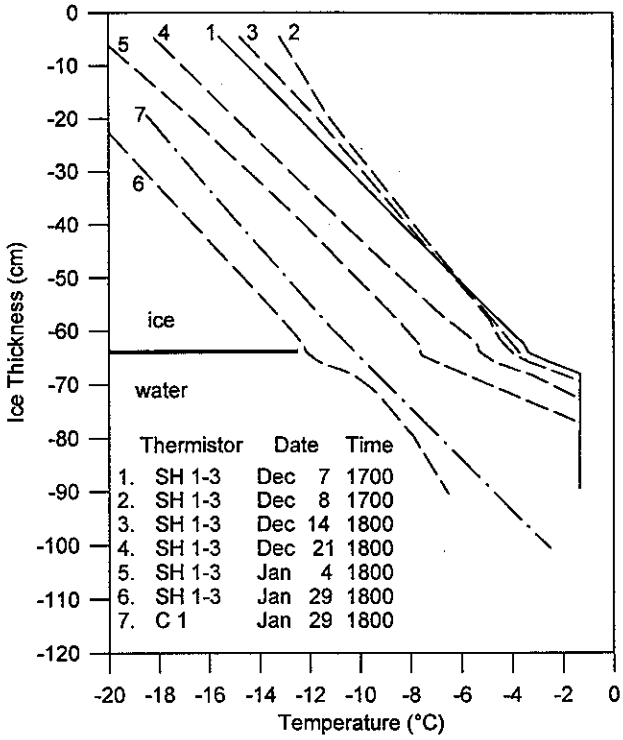

Figure 7-13. Control and SH 1 temperature profiles.

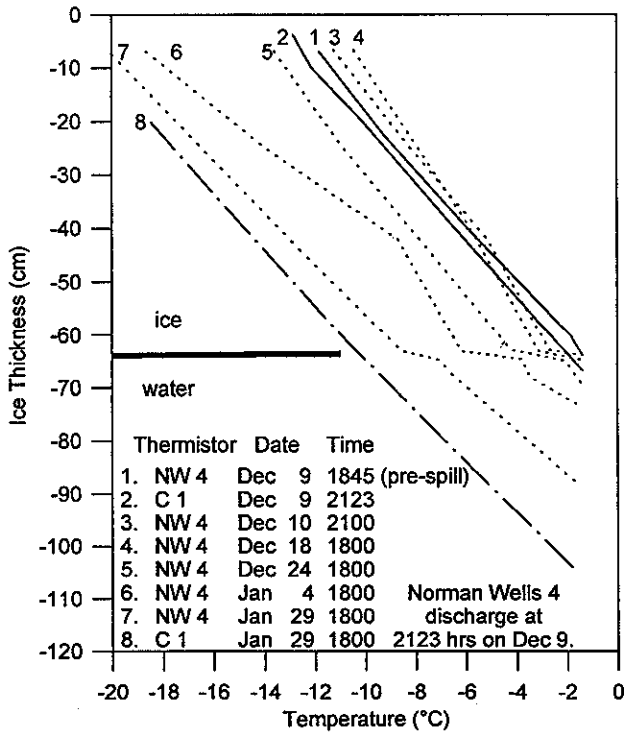

Figure 7-14. Control and NW 4 temperature profiles.

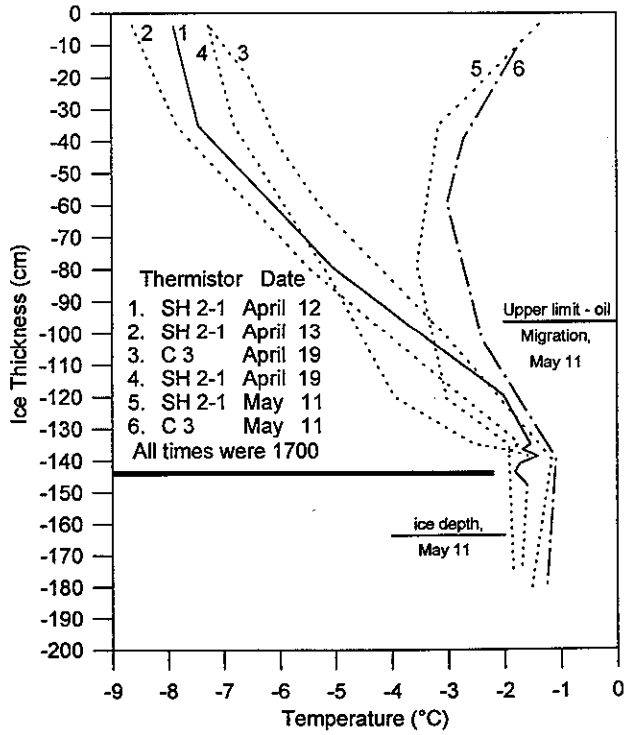

Figure 7-15. Control and SH 2 temperature profiles.

by about 0.9 °C while the upper 58 cm had experienced a temperature rise of up to 1.2 °C at a depth of 20 cm. It is doubtful if the increase reflected by the probe at the 4 cm level was due to the oil but rather fluctuations in the ambient air temperature.

By December 18, the temperature gradient was almost parallel to that prior to discharge. The presence of the oil lens was indicated by a sharp temperature drop of up to 1.1 °C between 66.5 and 68.5 cm. By December 18, there was definite evidence that a new ice interface had formed below the oil lens. Allowing for 1 to 1.5 cm of oil, a new ice-water interface position of 71.5 cm on December 18 would indicate that less than 2 cm of new ice had formed in the preceding 11 days, yielding an average growth rate of approximately 0.16 cm per day. By December 21, the ice had grown to 72.5 cm. In the period December 7 to December 21, control profiles with similar snow cover indicated a growth of about 10 cm. A profile from C1 on January 29 has been included to demonstrate that the oil lens did not have a significant effect on either the thermal regime of ice thickness after seven weeks.

Norman Wells 4 discharge took place at 1900 hours December 9. Considering the NW4-4 chain over the same period as SH1-3, no substantial difference between the two types of oil can be seen (Figure 7-14). Detailed temperature trends through the lens are not available on NW4-4 as the ice on discharge day had not yet grown to include the dense array of probes. Consequently, the localized steepening of the temperature gradient seen on SH1-3 is not seen on NW4. Ice thickness at spill time was 63 cm. The plot on December 10 shows the characteristic clockwise rotation of the profile to warmer temperatures above and cooler below the 40 cm level. This trend continued until December 18. Then, between December 18 and December 24, the temperature gradient rapidly smoothed out and returned closely to its pre-spill shape. As with SH1-3, the recovery of the temperature profile about ten days following the spill coincided with the formation of a new ice interface below the oil lens. Between December 21 and 24, the temperature of the probe immediately below the oil lens fell from -1.5 °C to 2.1 °C, indicating that about 1 cm of new ice had formed.

The immediate reduction in heat flux throughout the sheet following the introduction of oil is clearly demonstrated by the reduced gradient in the ice. The increased thermal resistance of the oil, and the enhanced heat exchange at the relatively smooth oil-water interface, tend to retard ice growth. Once a layer of ice has formed beneath the oil, the temperature profile quickly assumes its initial gradient.

On the basis of the SH1-3 and NW4-4 chains, there would appear to be only minor differences between the Norman Wells and Swan Hills crudes. However, a detailed comparison is difficult because of the limited number of chains actually in contact with oil. As well, variations in oil lens thickness and snow cover severely limit the significance of apparent deviations.

The oil lens thickness derived from thermistor plots are not precise. However, to core beside a chain would alter or destroy a lens. With probes spaced at 2 cm intervals, the probable error in estimating the thickness of a lens was likely within 1 cm. Laboratory and theoretical studies of the pooling characteristics of the two crudes indicate a minimum practical lens thickness of about 0.8 cm. From video observations at the time of discharge, the oil covered between 30 to 40 percent of various test areas, yielding an average oil thickness of about 3 cm. Aided by adjacent cores and diver observations, the error of most chains could be reduced to about 0.5 cm.

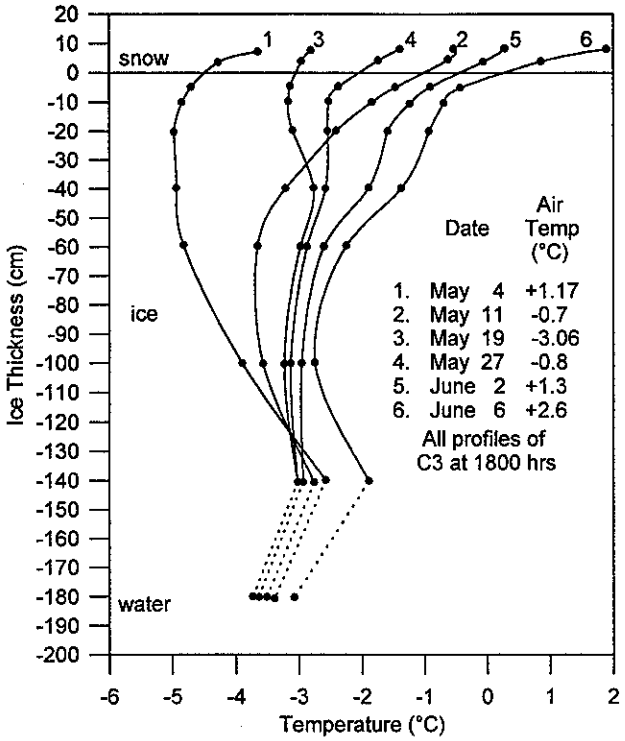

Figure 7-16. Control temperature profiles May 4 to June 5, 1975.

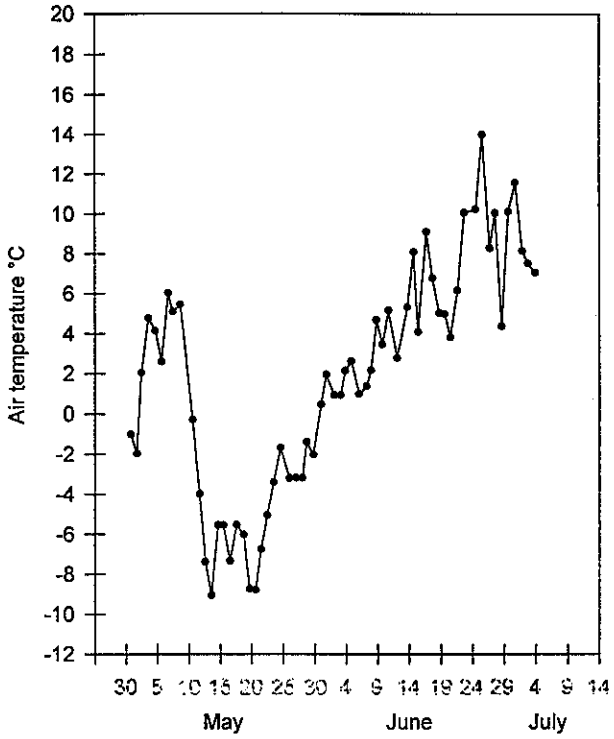

Figure 7-17. Daily mean air temperatures May 1 to July 1.

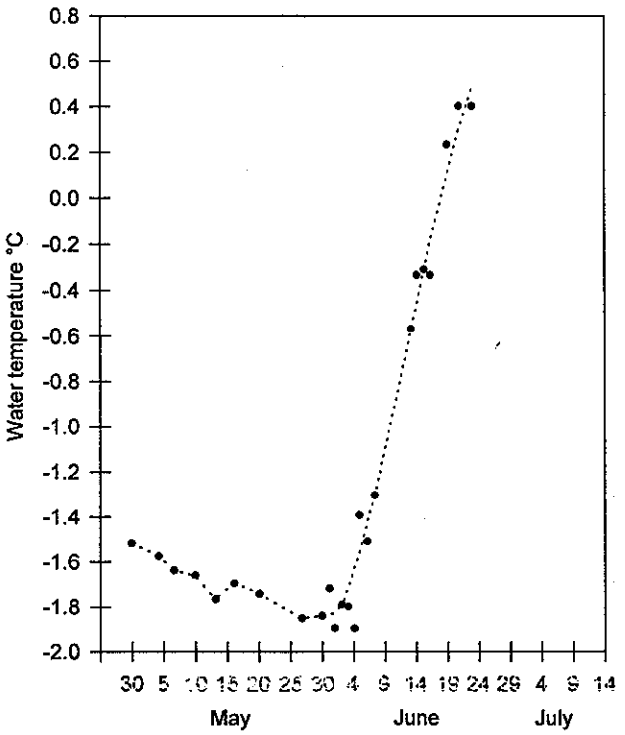

Figure 7-18. Daily water temperatures May 1 to July 1.

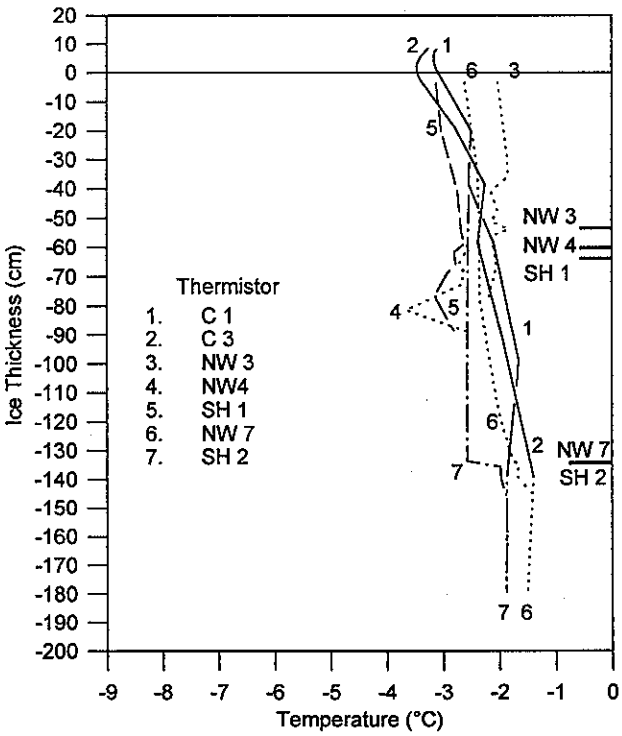

Figure 7-19. Comparative temperature profiles May 22.

7.3.3 Early Spring

The two discharges, SH2 and NW7 were undertaken on April 12 and 15, at an ice thickness of approximately 150 cm. The sheet was rapidly warming, and the average ice growth subsequent to the tests was less than 15 cm. After about the middle of April, it became difficult to estimate growth from the thermistor chains, as the temperature of the ice below the 140 cm level was very close to the water temperature, and on occasion higher. Although growth was not always apparent from the chains, it was confirmed by coring. As well, the profiles became transient in nature, and no longer displayed the linear or near steady state behaviour, characteristic of the late fall and winter.

Profiles from the SH2-1 and the C3 chains were very similar at 1700 hours on April 12, just prior to the discharge (Figure 7-15). The sharp temperature fluctuation of about 0.4 °C immediately above the interface, was likely due to density currents in the water column. Twenty four hours after the test, C1 had uniformly warmed by about 0.3 °C, while the test chain decreased approximately 0.5 °C over its entire depth. By April 19, seven days after the discharge, the control had continued to warm evenly, while SH2-1 exhibited the characteristic rotation, with a depression in temperature in the lower 30 cm of ice. The time taken to adopt this profile was considerably longer than in earlier discharges, where it was observed within 24 hours. However, the effects of the oil were still very pronounced.

Although the entire sheet was warming, the gradient had not recovered after three weeks. The temperature was depressed relative to the control, and 17 cm of new ice had formed beneath the oil. It is difficult to isolate the external factors, but the slow recovery could in part be due to upward migration of the oil. By May 11, oil was detected at the 93 cm level, or about 50 cm above the lens.

The NW7-2 chain was interesting, in that a distinct warm wave that was detected in C3 at the 60 cm level on April 15, appeared on the test chain a week later. This transient temporarily masked fluctuations due to the oil. By May 11, the shape of the profile was similar to SH2-1, but the temperatures were not as depressed. The general instability in the spring makes direct comparisons difficult, but no marked variations could be detected between the Norman Wells and Swan Hills crudes.

The compared study of oiled and unoiled temperature profiles demonstrated a number of interesting features. Firstly, the temperature gradient in the ice immediately above the oil is sharply reduced. In the case of the NW3 test, a reduction in the temperature gradient of 56 percent was observed within 24 hours after the discharge, while a reduction of 32 percent was observed in the same period after NW4 discharge. This reduction could be due to a number of factors, including the added thermal resistance of the oil, alterations in brine drainage, and enhanced heat exchange at the oil-water interface. Until suitable conditions develop for the formation of a new sheet below the oil, the heat of fusion, which is typically about 70 cal g^{-1}, is not available, causing a further depression in the temperature. Studies by the Frozen Sea Research group indicated that the heat of formation may account for between 50 and 60 percent of the total heat input into a growing sheet.

Norman Wells and Swan Hills crudes tended to have a similar impact on the thermal regime of the ice. For the oil lens thickness of 2 to 4 cm commonly encountered in Balaena Bay, the insulating effect of the oil was partially offset by convective transfer within the lens. The net reduction in heat flux through the ice as a result of the oil lens was less than 10 percent. Although the convective transfer might be as much as 25 percent lower in the more viscous Swan Hills crude, the effect was insignificant in comparison to natural variations.

There was no evidence of a substantial modification in temperature profiles as the oil

migrated upward through the ice. However, the brine channels represent no more than 3 to 5 percent of the ice by volume, even late in the melt phase.

7.4 Observed Effects of Oil on Ice Depletion

Ice growth in Balaena Bay ceased by about May 20. Signs of surface were already evident in a number of oiled areas. The progressive change in surface conditions is detailed in section 6.4. Consequently, only the thermal aspects, as reflected by temperature profiles, ice thickness measurements, and radiation levels, will be considered in this section.

The general trend in contaminated ice is best demonstrated by control chain C3. By May 4 the surface was warming faster than the ice could respond, and the profile was beginning to curve (Figure 7-16). Prior to this date the profiles had been essentially linear. The surface continued to warm until May 11, at which time the internal temperature of the ice was approximately 2 °C cooler than either of the interfaces. Between May 9 and May 14 the ambient air temperature dropped from +5 to -9 °C (Figure 7-17), causing a corresponding depression in the temperature in the upper levels of the ice. By May 19 the temperature profile through the ice was close to linear, and remained this way until about May 27. From May 21 onward the air temperature was progressively warming, reaching a high of 14 °C by June 26. Diurnal variations of over 6 °C were common during this period. On June 6, the day prior to the first full scale burn, the coolest observed temperature in the ice was -1.8 °C, while the water temperature was -1.4 °C, and the air temperature 2.6 °C. The water temperature remained close to winter average of about -1.8 °C until June 4, then began to warm at the rate of about 0.1 °C per day (Figure 7-18).

By May 22 there was no significant difference between the thermal regimes of oil and unoiled ice. Representative profiles from five of the test areas and two control sites are shown in Figure 7-19. Substantial oil migration had occurred, and the brine channels were saturated with oil to within 15 cm of the surface. The SH2 chain is the only location where an oil lens could be positively identified. There was a distinct drop of about 0.7 °C across the lens. Since convective heat transfer in the oil is part dependent on the temperature gradient, it was felt that convection would be relatively insignificant in comparison to conduction, and the insulating effect of the oil would be more pronounced. The disturbances in the NW4 and SH1 chains at the 80 cm level were transient. The warmer temperatures exhibited by all oiled chains near the surface, was likely a direct result of increased radiation being intercepted in the upper levels of the sheet.

Once the oil began to surface it had a marked effect on the ice depletion. Initially the oil appeared as a slight discolouration in the snow. Although barely detectable, it reduced the albedo by between 30 and 50 percent (Section 6.4). Since the level of absorbed solar radiation varies inversely with albedo, the contaminated areas melted much more rapidly than did the surrounding snow. As the underlying snow melted, the oil formed in small enclosed melt pools. In most areas the snow effectively contained the oil, and horizontal migration was limited to about one metre. Since the albedo of an oil lens on water is about 0.1, or less than 20 percent that of uncontaminated snow, the melt rapidly accelerated once the pools formed. Oil was splashed up on the surrounding snow by wind and wave action, and the pools grew in size, finally becoming interconnected. By early June a number of melt holes had developed in the oiled areas. The significance of these holes is questionable, since they tend to form at old core holes. However, similar melt holes did not develop in the uncontaminated ice, which had also been cored. By June 27, the NW3 and NW4 test areas were essentially free of ice, and the entire test area was open by June 30. The surrounding ice

sheet remained intact until July 6, when it was driven onshore by high wind. The average ice thickness at the time was 15 cm.

The most significant factor in advancing the melt was the reduction in albedo caused by the oil. At the beginning of May there was no evidence of oil on the surface, and the average albedo was 0.78. By May 9 small oiled patches of snow were starting to appear and the average albedo of the test sites dropped to 0.70, as compared to 0.75 for the control areas. The spread continued to increase until June 6, when the average albedo of the test site was 0.15, or less that 34 percent that of the uncontaminated snow. The albedo in one of the more heavily oiled areas was 0.03. Consequently the energy input in to the oiled areas was substantially greater. The cumulative absorbed solar radiation for both the average and extreme conditions in the test area are shown in Figure 7-20. The curves are the cumulative product of the integrated direct and diffused incoming solar radiation and the average daily absorptivity. Measurements at 14 stations were used in determining the average absorptivity (1.0 - albedo) for the test area.

Between May 9 and June 6 an average of 6000 cal cm^{-2} was absorbed over the test area, while only 4800 cal cm^{-2} was absorbed at the control sites. In the same period 10,000 cal cm^{-2} was absorbed in one of the more heavily oiled areas. The limited divergence between the control and test areas until the of May, directly reflects the percentage of total area contaminated. On June 1, melt pools and oiled snow represented only 15 percent of the surface areas (Figure 6-9). By June 6, oil was exposed over 47 percent of the site. It is unrealistic to extend the comparison beyond this date, due to fallout and other disturbances with the cleanup.

The distribution of absorbed solar energy within the ice sheet is considerably affected by the oil. With natural ice, approximately 40 percent of the energy penetrates to the 30 cm level (Hobbs, 1974). However, much of the energy is intercepted by the oil in the brine channels, causing a higher energy level near the surface. As well, even a very thin oil film on a melt pool serves as an effective barrier. During periods of high radiation, oil film temperatures as much as 10 °C higher than the underlying water were recorded (Section 6.4). The average temperature difference was about 7 °C. In accordance with the Stefan-Boltzmann Law, the longwave out going radiation is proportional to the fourth power of the absolute temperature, and consequently the flux from the oiled melt pools was approximately 10 percent larger than from the melting ice surface. The average emitted long-wave radiation from melting ice during the month of May is 625 cal cm^{-2} day^{-1}. On this basis, an additional 1750 cal cm^{-2} would have been radiated from the heavily oiled areas between May 9 and June 6, yielding a net gain of 3450 cal cm^{-2} relative to the control areas, or sufficient energy to melt an additional 50 cm of ice.

On June 11, six cores were recovered from the control sites, and two from heavily oiled areas. The average thickness of the natural ice was 157.5 cm, while the average thickness of the oiled ice was 107.5 cm. The precise agreement between the observed and theoretical enhancement of ice depletion caused by oil is somewhat coincidental, considering the broad assumptions made regarding surface heat exchange. However, it does suggest that the order of magnitude of the principal energy components is correct.

Although some general patterns would appear to exist, it is impossible to draw any firm conclusions as to the significance of the location of the oil in the ice on ice depletion. Measured ice thicknesses from the middle of May to the break-up of the sheet on July 6, are shown in Figure 7-21. Until about the end of May, the variation between oil and control areas appeared to be random. In general, the thickness of the ice varied directly with the depth of the lens. Ice thicknesses in the

NW3 and NW4 test areas were consistently thinnest, and the NW7 and SH2 test areas thickest. Although oil was first detected on the surface in the SH2 test area, it was not released as rapidly as was the oil in lenses closer to the surface. By June 7, most of the oil had been released in the NW3 and NW4 test areas. Oil continued to flow from the ice in the SH2 test area until about June 20. The fact that the NW4 and SH1 tests were conducted at the same time yet the ice was consistently thicker in the SH2 area, would suggest that the properties of the oil might have some bearing on depletion.

The clean-up activities, which commenced on June 7, disturbed the natural processes. By removing the oil, the absorptivity of the contaminated areas was substantially reduced, while traffic and fallout increased the absorptivity of the surrounding ice. If undisturbed, the oiled areas would likely have been free of ice between two and three weeks prior to the break-up of the sheet.

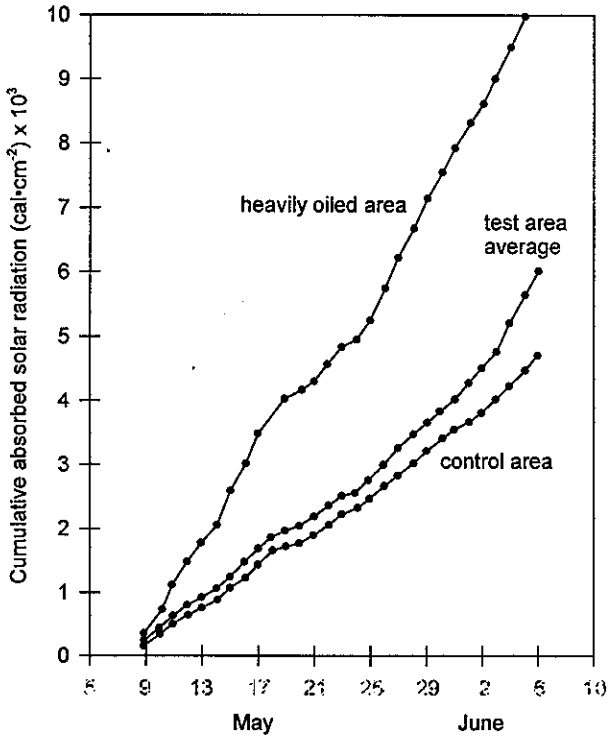

Figure 7-20. Cumulative radiation May to June, 1975.

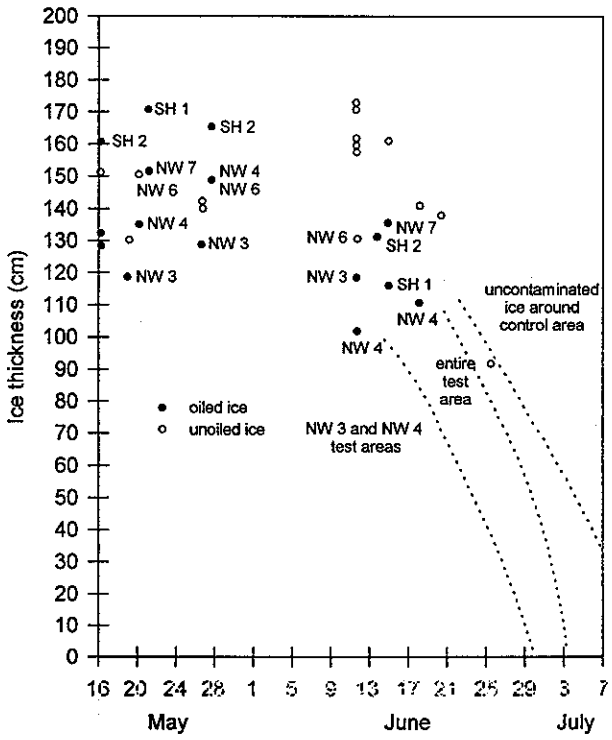

Figure 7-21. Ice depletion May to July.

8.0 PHYSICAL AND CHEMICAL PROPERTIES OF OIL

8.1 Weathering of Oil

Due to the large number of samples involved, chromatographic analysis was found to be the best technique for assessing changes in the properties of the crudes. Through gas chromatography (GC), it is possible to separate, identify and then quantify the various components of an oil. On the basis of changes in composition, not only the extent , but also the nature of weathering can be

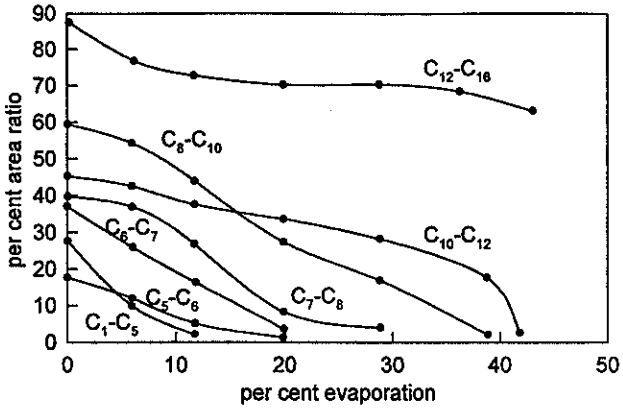

Figure B-1. Norman Wells crude oil composition *vs* per cent evaporation at 25 °C.

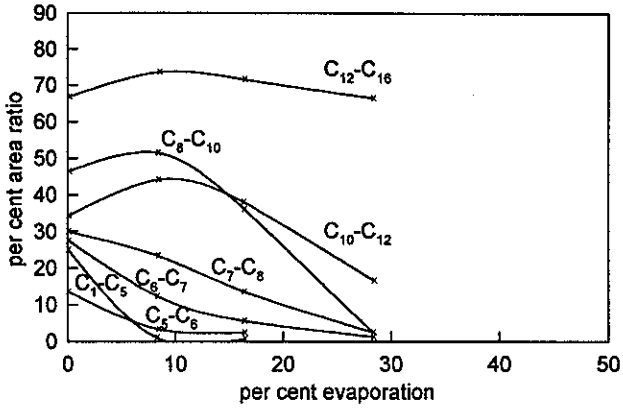

Figure B-2. Swan Hills crude oil composition *vs* per cent evaporation.

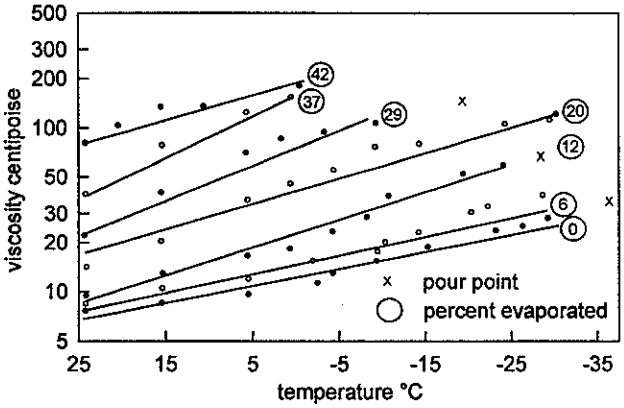

Figure B-3. Viscosity of Norman Wells crude oil.

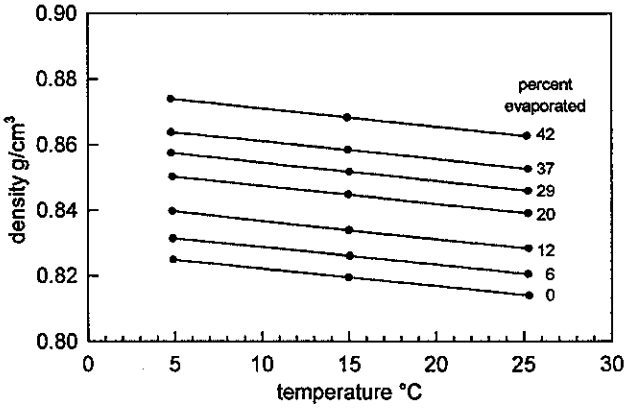

Figure B-4. Density of Norman Wells crude oil.

determined. With additional tests, this information can be correlated with changes in physical properties.

The results of the gas chromatography were presented in the form of percent area covered by a specific hydrocarbon group. For this analysis the following groups were selected; C_1 to C_5, C_5 to C_6, C_6 to C_7, C_7 to C_8, C_8 to C_{10}, C_{10} to C_{12} , C_{12} to C_{16}, and C_{16} to C_{24}. The chromatogram was stopped at carbon number 24. Under normal conditions, hydrocarbons above hexadecane do not evaporate significantly (Mackay 1973, Scott 1975), and therefore the C_{16} to C_{24} group was employed as a reference, to assess the relative evaporation of other components. Initially, fresh samples of both Norman Wells and Swan Hills crude oil were weathered under controlled conditions in a laboratory. This was done by placing trays of oil in a wind tunnel at a fixed temperature. Periodically, each sample was weighed in situ, and a small quantity of oil was recovered for GC analysis and the measurement of selected properties. The ratio of the area of each hydrocarbon group to the area of the C_{16} to C_{24} group was expressed as a percent (percent area ratio) and plotted against the percent evaporated by weight for the total sample (Figures B-1, B-2). A series of curves relating the physical properties to the percent oil evaporated was also developed (Figures B-3 to B-8).

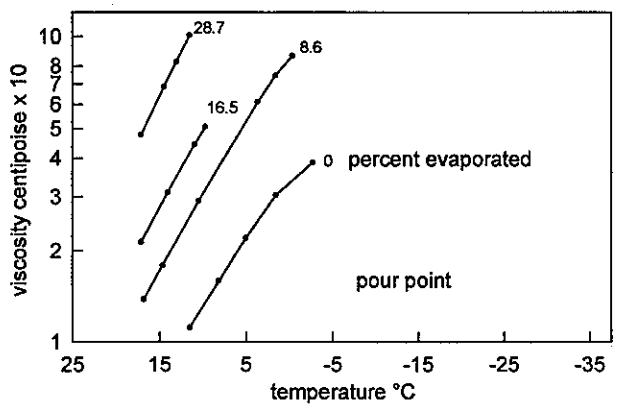

Figure B-5. Viscosity of Swan Hills crude oil.

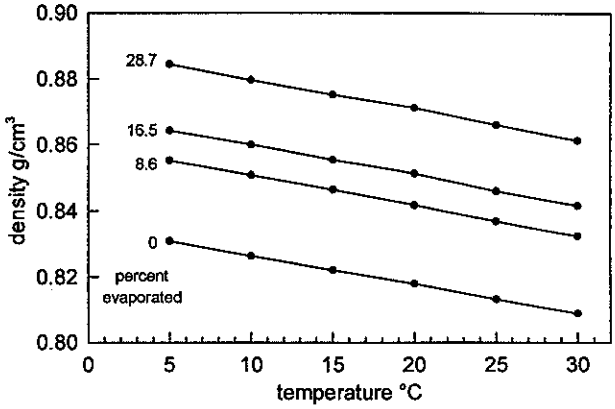

Figure B-6. Density of Swan Hills crude oil.

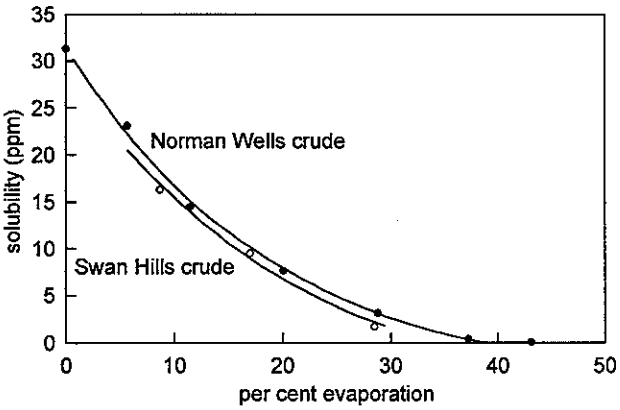

Figure B-7. Crude oil solubility *vs* per cent evaporation at 25 °C.

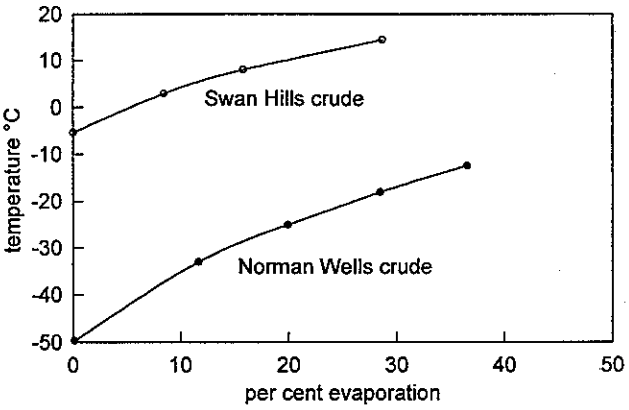

Figure B-8. Crude oil pour points *vs* per cent evaporation at 25 °C.

The following procedure was employed in analyzing subsequent samples. A GC was run and the percent area ratio determined for each hydrocarbon group. Then, depending on the type of crude, either Figure B-1 or Figure B-2 was used to estimate the percent evaporated or the degree of weathering. Theoretically, each hydrocarbon group should indicate the same percent evaporated for the entire sample. In fact, this is not the case. There are normally variations of several percent between the groups, and care was necessary in interpreting the data, particularly in the early stages, when weathering was relatively small. There are two basic causes for the apparent discrepancy. Firstly, crude oil is not perfectly consistent. Variations in composition were detectable between successive drums. To minimize this effect, a composite sample was used in preparing the curves. Secondly, there are a number of limitations associated with the experimental technique.

The rate of evaporation of a complex mixture of hydrocarbons, such as a crude oil, is very difficult to quantify. The rate is dependent on the turbulence characteristics of the atmosphere, or the mass transfer coefficient, as well as the properties of the oil. The rate of evaporation of a specific compound or group of compounds depends primarily on the concentration, vapour pressure, and the activity coefficients of the hydrocarbons in the liquid phase. Generally, lower carbon number compounds have a higher vapour pressure, and evaporate faster. Evaporation also increases with

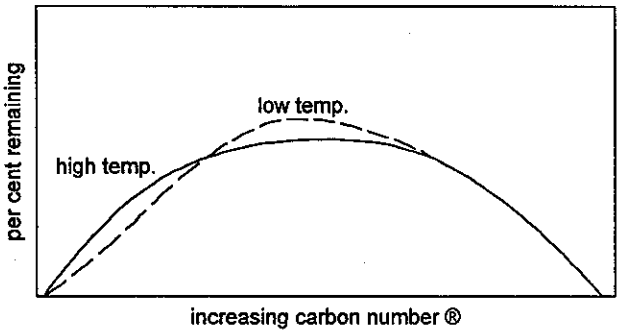

Figure 8-1. Effects of temperature on weathering.

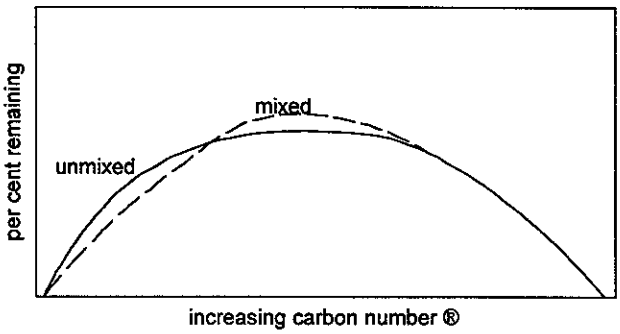

Figure 8-2. Effects of mixing on weathering.

temperature, and the ratio of vapour pressures for various components does not remain constant. Thus, the nature of evaporation at 25 °C may be different from that at 0 °C. Scott (1975) has quantified these processes by calculating first-order evaporation rate constants and Arrhenius activation energies for the components of Arctic diesel oil. This work demonstrates the complex nature of the temperature dependence of oil evaporation. At low temperatures, there is a tendency for better fractionation during evaporation. The low carbon number compounds are lost preferentially, producing GC's as shown in Figure 8-1. However, if the oil is unmixed, some of the components which would otherwise evaporate will be shielded, and there will be a preferential retention of the lower carbon numbers (Figure 8-2).

To allow for these considerations greater emphasis was placed on values for percent evaporated derived from the mid range carbon number groups that appeared consistent with each other and the aging history of the sample. The derived percent evaporated and changes in the physical properties for all samples are shown in Tables B-1 to B-4. Typical evaporation rates for oil samples in ice and on the surface are presented in Tables 8-1, and 8-2.

Table B-3. Derived Properties of the Norman Wells Crude Samples (At 0 °C).

Sample Number	Sample & Date	% Evap.	Derived			
			Viscosity (cp)	density g/cm^3	pour point °C	solubility ppm
14	NWC, Dec 8	3	11	0.850	-45	26
15	NW1, Dec 10	17	28	0.880	-27	10
16	NW1, Jan 22	19	32	0.882	-25	8
17	NW2, Oct 23	2	11	0.848	-47	27.5
18	NW2, Nov 15	3	11	0.850	-45	26
19	NW2, Dec 10	5	12	0.853	-42	23
20	NW2, Jan 21	2	11	0.848	-47	27
21	NW2, Feb 21	2	11	0.848	-47	27

Sample Number	Sample & Date	% Evap.	Derived			
			Viscosity (cp)	density g/cm^3	pour point °C	solubility ppm
22	NW2, May 9	5	12	0.853	-42	23
23	NW2, May 10	37	180	0.407	-11	0.25
24	NW3, Nov 14	4	12	0.852	-43	25
25	NW3, Dec 10	7.5	13	0.858	-38	20
26	NW3, Jan 22	3.3	11	0.851	-44	26
27	NW3, Feb 21	2.2	11	0.849	-47	27.5
28	NW3, May 12	4	12	0.852	-43	25
29	NW3, May 26	41	220	0.920	-7	0
30	NW3, Jun 6	34	160	0.903	-13	1
31	NW3, Jun 10	6	12	0.855	-40	22
32	NW4, Dec 9	3.5	11	0.851	-44	25
33	NW4, Feb 5	3	11	0.850	-45	26
34	NW4, Feb 21	2.5	11	0.874	-46	27
35	NW4, May 13	6	12	0.855	-43	25
36	NW4, May 27	4	12	0.852	-43	25
37	NW4, Jun 6	26	50	0.892	-20	4
38	NW4, Jun 13	43	300	0.923	-5	0
39	NW6, Feb 15	5	12	0.853	-42	23
40	NW6, May 10	23	45	0.888	-22	6
41	NW6, May 15	12	18	0.869	-32	14
42	NW6, Jun 12	43	300	0.923	-5	0
43	NW7, May 10	20	35	0.885	-25	8
44	NW7, Jun 6	27	60	0.894	-11	3.8
45	NW7, Jun 11	36	170	0.904	-13	0
46	NW7, Jun 12	>50	>400	>0.94	>0	0
47	NW7, Jun 13	>50	>400	>0.94	>0	0
48	NW3, Jun 26	42	300	0.922	-8	0
49	Resid., Jul 7	42	300	0.922	-8	0

Sample Number	Sample & Date	% Evap.	Derived			
			Viscosity (cp)	density g/cm^3	pour point °C	solubility ppm
50	Resid., Jul 7	>50	>400	>0.94	>0	0
51	Evap. Dec 24	7.1	13	0.858	-39	20.5
52	Evap. Jan 11	20	35	0.885	-25	7.5
53	Evap. Jan 20	26	55	0.892	-20	4
54	Evap. Jan 24	24	50	0.890	-22	5
55	Evap. Feb 6	33	90	0.901	-14	1

Table B-4. Derived Properties of the Swan Hills Crude Samples (At 0 °C).

Sample Number	Sample & Date	% Evap.	Derived			
			Viscosity (cp)	density g/cm^3	pour point °C	solubility ppm
1	SHC, Dec 7	0	32	0.837	-5	29
2	SH1, Dec 10	0.5	32	0.838	-5	28
3	SH1, Dec 30	<1	33	0.838	-5	27
4	SH1, Jan 22	<1	33	0.838	-5	27
5	SH1, Feb 18	1	34	0.839	-4	27
6	SH1, May 13	1.5	36	0.840	-3	26
7	SH1, Jun 3	18	200	0.870	+9	8
8	SH1, Jun 13	28	400	0.888	+15	2
9	SH2, May 10	26	350	0.883	+13	3
10	SH2, May 27	8	80	0.860	+3	17
11	SH2, May 29	28	400	0.888	+15	2
12	SH2, May 29	24	300	0.880	+12	4
13	SH2, Jun 12	33	500	0.89	+17	0
56	Evap. Dec 29	1.5	36	0.840	-3	26
57	Evap. Jan 4	9	95	0.862	+4	16
58	Evap. Jan 20	7	70	0.858	+2	17
59	Evap. Feb 26	19	210	0.874	+13	8

Table 8-1. Oil evaporation in ice.

NW 2	Oct 23	Nov 15	Dec 10	Jan 21	Feb 21	May 9	May 10
percent evaporated (%)	2	3	5	2	2	5	37*
SH 1	Dec 7	Dec 10	Dec 30	Jan 22	Feb 18	May 13	Jun 3
percent evaporated (%)	0	0.5	1	1	1	1.5	18

* surface sample.

Table 8-2. Oil evaporation on surface.

NW C	Dec 24	Jan 11	Jan 20	Jan 24	Feb 6
percent evaporated (%)	7	20	25	24	28
SH C	Dec 24	Jan 4	Jan 20	Feb 26	
percent evaporated (%)	1.5	9	7	19	

While the oil was incorporated in the ice very little evaporation occurred. This is reasonable, when it is considered that the ice is relatively solid during the depth of winter, and serves as an effective barrier to weathering. However, surface evaporation was pronounced when at sub-freezing temperatures. Within 24 hours of being exposed, the oil samples shown in Table 8-2 were covered by a layer of snow 1 to 2 cm thick. Some of the oil was absorbed by the snow. The snow remained in place for the duration of the tests. In spite of this, evaporation rates as high as 25 percent were recorded within one month. Considerably higher rates would likely occur if the oil were exposed to the atmosphere.

A comparison between derived oil propertied and those measured in the field is presented in Table B-5. In general, there is close agreement. The field viscosity readings are suspect, in that the oil was thought to contain traces of ice crystals. This was indicated by the non-Newtonian behaviour of the oil, and the difficulties in obtaining consistent values for the sample. Water in oil analyses conducted at the site indicated only trace quantities of water. However, tests were not done on all samples, due to the limited sample size. A Fann type viscometer, which measures viscosities at a constant shear rate, was used in the laboratory tests, and as a rule should produce more accurate values than the Ostwald viscometer used in the field.

Table B-5. Measured and Derived Densities.

Sample Number	Sample & Date	Density		
		derived @ 0 °C	measured	
			at temp. (°C)	corrected to 0 °C
16	NW1, Jan 22 NW2, Oct 24	0.882 0.848	0.872 @ 15 0.831 @ 15	0.882 0.844
18	NW2, Nov 15	0.850	0.832 @ 15	0.845
19	NW2, Dec 10	0.853	0.839 @ 15	0.850
20	NW2, Jan 21	0.848	0.829 @ 17	0.843
21	NW2, Feb 21	0.848	0.831 @ 15	0.844
24	NW3, Nov 14	0.852	0.836 @ 20	0.850
26	NW3, Jan 22	0.851	0.838 @ 15	0.849
27	NW3, Feb 21	0.849	0.835 @ 15	0.848
32	NW4, Dec 9	0.851	0.834 @ 15	0.846
34	NW4, Feb 21	0.849	0.836 @ 15	0.849
1	SH1, Dec 7	0.837	0.823 @ 15	0.836
3	SH1, Dec 30	0.838	0.822 @ 17	0.838
4	SH1, Jan 22	0.838	0.819 @ 20	0.838
5	SH1, Feb 18	0.839	0.819 @ 20	0.839

A number of the early gas chromatograms were examined to determine if there was significant dissolution of the oil, while in contact with the water. Three peaks, benzene, methylcyclopentane (MCP) and n-heptane were considered. The solubility of these compounds decreases from benzene to MCP to n-heptane, while the vapour pressure decreases from MCP to benzene to n-heptane (Table 8-3). If the weathering of a crude oil were due solely to evaporation, then the relative ratios of these components in the oil would change in accordance with their vapour pressures. If for example, the peak area of these compounds from the GC, were originally 10:10:10, for MCP, benzene, and n-heptane, a weathered ratio might appear as 8:9:10, indicating that relatively more MCP had evaporated than the less volatile benzene. The ratio also shows that the benzene has evaporated more that the n-heptane. Similarly, due to other difference in solubilities, the same ratio of 10:10:10 may be expected to change to 9:7:10 if there were significant dissolution occurring.

Table 8-3. Solubility and vapour pressure of control compounds.

Compound	vapour pressure (atm) at 25 °C	solubility mg/L
Benzene C_6H_6	0.125	1780
Methylcyclopentane C_6H_{12}	0.181	42
n-Heptane C_7H_{16}	0.060	2.9

A simple method of discriminating evaporation from dissolution is thus to compare the three peak areas before and after exposure to environmental conditions, and look for evidence of evaporation or dissolution. If the peak areas of the original oil are MCP_0, B_0, and nH_0, and after weathering are MCP_1, B_1, and nH_1, for MCP, benzene, and n-heptane, then if there is only evaporation, the benzene value will tend to remain roughly proportional to the mean of the other two. Expressed in symbols:

$$\frac{MCP_1 + nH_1}{B_1} = \frac{MCP_0 + nH_0}{B_0}$$

If dissolution takes place (alone or in addition to evaporation) this ratio should rise. If half the benzene dissolves, the ratio should double. Table 8-4 gives values for this ratio for some early samples. To establish a basis for comparison, ratios from samples that were not exposed to water were used to compare with later samples. The unweathered samples ranged from 4.38 to 5.41 with and average of 4.98. A ratio of 6 or higher might be expected to indicate some dissolution. The ratios of samples that had been in contact with the water did not go above 5.68. A "t" test for the null hypothesis using the unweathered samples as one group, and the other samples as the second group, gives "t" as 0.7, when the degrees of freedom equals nine. The level of significance at the 10% probability is 1.83, indicating that the null hypothesis cannot be disproven, or that the extent of dissolution is below the level of detectability in terms of oil composition.

Table 8-4. Oil sample dissolution ratios.

sample number	sample and date	peak areas			ratio (MCP + n-heptane)/(benzene)
		benzene	MCP	n-heptane	
14	NW C Dec 8	2011	4010	4797	4.38*
17	NW 2 Oct 23	1857	4410	5254	5.20*
24	NW 3 Nov 14	1845	4238	5128	4.94*
32	NW 4 Dec 9	1691	4085	4067	5.41*
					4.98 Avg. *
15	NW 1 Dec 10	562	968	2217	5.67
18	NW 2 Nov 15	1860	3873	4558	4.53
19	NW 2 Dec 10	1512	3425	4328	5.13
24	NW 3 Dec 10	1304	2586	3571	4.70

sample number	sample and date	peak areas			ratio (MCP + n-heptane)/(benzene)
		benzene	MCP	n-heptane	
	ICE CORE NW 3 Dec 10				
	0-5 cm	1481	3454	4964	5.68
	5-10 cm	1777	3754	5442	5.17
	10-18 cm	1698	3849	5258	5.36

* Original samples from barrels prior to discharge.

Metal analysis performed on samples of unweathered Norman Wells and Swan Hills crudes are presented in Table B-6. Because the sulphur content of both crudes was significant, 1.76 and 2.90 percent respectively, it was decided to analyze both weathered and burned samples, to determine if the sulphur was being concentrated in the oil, or being released to the environment. The evaporated sample of Norman Wells crude had a sulphur content of 1.9 percent, while the burned sample had a sulphur content of 2.1 percent. These results indicate that the sulphur content of the oil remains relatively constant. Assuming that approximately 95 percent of the oil either evaporated or burned, then about 2000 kg of sulphur was released into the atmosphere.

Table B-6. Metal Analysis of Unweathered Crude Oil Samples

	NORMAN WELLS	SWAN HILLS
Sulphur	1.76%	2.90%
Aluminum (Al_2O_3)	<0.5 p.p.m.	<0.5 p.p.m.
Barium	<0.5 p.p.m.	<0.5 p.p.m.
Calcium (CaO)	<0.5 p.p.m.	5 p.p.m.
Copper	<0.5 p.p.m.	<0.5 p.p.m.
Iron (Fe)	0.3 p.p.m.	0.3 p.p.m.
Lead	0.5 p.p.m.	20 p.p.m.
Magnesium (MgO)	<0.5 p.p.m.	<0.5 p.p.m.
Nickel	1 p.p.m.	<0.5 p.p.m.
Silicon (SiO_2)	<0.5 p.p.m.	<0.5 p.p.m.
Sodium (Na_2O)	<1 p.p.m.	1 p.p.m.
Tin	<0.5 p.p.m.	<0.5 p.p.m.
Vanadium	3 p.p.m.	<0.5 p.p.m.
Zinc	-	20 p.p.m.

8.2 Hydrocarbon Content of Water Samples

The non-biological water sampling concentrated on measuring temperature and salinity profiles and dissolved hydrocarbon content in the water column.

The hydrocarbon content was measured using pentane extraction and gas chromatography analysis. Some problems were encountered in early samples as a result of loss of pentane by evaporation during shipping. However, this was remedied by improved bottling techniques with subsequent samples.

The total amount of hydrocarbon in the pentane sample was estimated using gas chromatography, and the aqueous concentration calculated from this number. Later samples were analyzed using helium vapour phase extraction, a more sensitive and accurate technique which also enabled the identification of individual compounds. For example, if 5 ml of pentane were used to extract the hydrocarbons present in one litre of water, and a GC injection of 10 microlitres (µl) of pentane gave a peak area corresponding to 1 microgram (µg), then by proportion, the amount of hydrocarbon in the pentane sample is 500 µg or 0.5 mg. The aqueous concentration is then calculated to be 0.50 µg l^{-1}.

An upper limit exists as to the concentration in water of a particular dissolved hydrocarbon. This limit is the saturation concentration and, for practical purposes, cannot be exceeded. In theory, this means that only so much of a particular hydrocarbon can be dissolved in a particular quantity of water, and beyond that level, that hydrocarbon will no longer dissolve. This limit of saturation value is quite small. The limit for one of the most soluble crude oil component, that of benzene is 1,780 mg l^{-1} in distilled water, and 1,391 mg l^{-1} in sea water (Mackay, 1975). This is a very soluble component and other relatively soluble components such as toluene and xylene have solubilities of only 515 and 175 mg l^{-1} respectively. The majority of crude oil components have a solubility under 10 mg l^{-1} and can be ruled out so far as significant dissolution is concerned. A high solubility does not necessarily mean that a hydrocarbon will dissolve to the solubility limits. The rate of formation of dissolved hydrocarbons is dominated by vertical eddy diffusivity drift and it appears that in these tests the eddy diffusivity was low enough to result in dissolved concentrations about a factor of 100 below saturation concentration.

Results of the water sampling program are shown in Table 8-5. Although the samples were recovered close to the exposed oil lenses, the oil concentrations were very low. At these concentrations, even a slight contamination of the sampling apparatus could have significant effect on the results. As well, small oil droplets were detected in the water column a number of days after the discharge. One of these droplets in a litre of water, would substantially alter the apparent hydrocarbon content. Initially, it was thought that contamination by undissolved hydrocarbon might be detected by close examination of the GC's, since undissolved crude oil retains a similar composition to the original oil, while dissolved oil reflects the solubility of the various components. This was not possible, due to the very low concentrations. However, as a result of the various sources of contamination, the measured hydrocarbon content, was likely higher than the average for the water column."

Table 8-5. Water samples.

Sample	Date	Dissolved hydrocarbon concentration (mg/L)
NW 2, S. Corner	Dec 23	0.5
NW 2, E. Corner	Jan 20	not detectable
NW 3, test + 20hr	Nov 15	1.3
NW 3, NW edge	Jan 21	not detectable
NW 4, test + 10hr	Dec 9	4.6
NW 4, S. Corner	Dec 23	0.2
NW 4, E. Side	Jan 21	0.2
NW 6	Feb 15	0.006
NW 7	Apr 15	0.0107
SH 1, pre spill	Dec 7	4.4
SH 1, test + 3 days	Dec 10	not detectable
SH 1, S. Corner	Dec 23	1.3
SH 1, E. Side	Jan 21	0.32
SH 1		0.054
SH 1	Feb 23	4.38
Surface water at tidal crack	Jun 4	0.119
Outside SH 2	Jun 6	0.110
Control from Bay 200 m from site	Jun 11	0.038
2 m below ice in centre of test area	Jun 16	0.14

BOSS Critique

The authors have supplied a detailed list of equipment as well as measurement error for data collected with the equipment. The experiments were described and diagrams presented to outline the process of oil containment and detection. The ice coring program had been presented in Seelye Martin' manuscript "A Field Study of Brine Drainage and Oil Entrainment in First-Year Sea Ice" and therefore less emphasis was placed on reviewing the coring program presented in the NORCOR 1975 report. The authors of the NORCOR 1975 report also gave a detailed description of the effect of the oil spills on biological systems and this review does not contain any of that information.

The section on the energy balance of the ice sheet is quite detailed, however, the authors point out several times that the changing of snow cover is actually the most important aspect of the heat balance equation. Snow cover provides insulation to the ice (stops heat loss to the atmosphere), and if the wind clears snow from one location and piles it onto ice at another location the ice with the least insulation grows at the fastest rate. Once an oil spill has occurred, the oil is incorporated into the ice and does not have as great an effect on insulating the ice from heat transfer to the atmosphere as does snow cover. This is of course a relative effect and therefore if the oil spill was of a much larger scale then the insulating effect of the oil might be as important as the insulating effects of snow cover. The authors have claimed that heat transfer occurs through two "parallel" processes (convection and conduction). However, there are no references made to publications that discuss these processes in detail. The authors do note that the heat transfer theory that they discuss is not backed up by the experimental results measured at the thermistors buried in the ice, oiled and unoiled.

The results of the NORCOR 1975 program are that once oil is spilt under ice it stays in the ice until there are defects in the ice through which the oil can migrate to the surface. This usually happens through the naturally occurring brine channels that open in the spring. Therefore the quality of ice that appears in the sea is an important aspect of oil-in-ice behaviour.

The authors do note that the salinity of the ice directly above an oil lens was greater that for ice at the same depth but with no oil lens present. They believe the increased salinity lead to the brine channels clearing sooner in these areas and therefore the oil migrated to the surface sooner than would be expected if only regular brine channels were present. The authors also state that oil lenses near the surface would be heated more quickly by absorbing radiation coming through the ice which again results in the brine channels clearing sooner.

Review of a manuscript by Richardson, P., entitled "ABSORB Tests Oil/Ice Interaction", in *Alaska Construction & Oil*, pp 18-20, 1980.

Technical Summary

This author stated that the ABSORB (Alaska Beaufort Sea Oilspill Response Body) managed by Alan A. Allen working in conjunction with Dr. Will Nelson, of the University of Alaska-Anchorage, designed an experiment to measure the effect of oil spilled under ice, on ice growth. The experiment was also to monitor the chemical change of the oil entrained in the winter ice. This was a preliminary manuscript for distribution to the oil industry and no actual results are presented.

Objective

The author stated that two major objectives of the ABSORB experiment were to measure the growth rate of ice under oil spilled under ice and the analyze the chemical change of the oil after being entrapped in ice for a winter.

Theory

No theory is presented by this author but the theory of this work was presented in the Nelson and Allen manuscript reviewed in an earlier section.

Method

The apparatus, displayed in Figure 1 of Nelson and Allen's manuscript, was used to keep the injected oil in place and to measure ice thickness. Two types of oil, crude and arctic diesel, were injected under ice in the barrels. The oil was injected to an initial layer thickness of one, six and twelve inches with the initial ice thickness varying from six to 24 inches. The thicknesses were measured on a two to three weeks bases. Foam insulation was placed at other locations to measure the effect insulating the ice would have on the actual ice growth.

Results

The oil barrels were removed and the ice was inspected for oil migration and oil content but detailed data were not presented. The author states that the foam insulation caused a contour effect to the ice grown under it. This was described as being a useful effect to stop spreading of the oil.

BOSS Critique

The author has presented information about the ABSORB tests for the general consumption of the oil industry and data was not presented. The results are qualitative at best. Other authors have reported that using the hot wire type of apparatus allowed oil to migrate to the surface since the wire, once heated, melted a channel for oil migration and therefore interfered with the results.

Review of a manuscript by Reimer, E.M. entitled "Anticipated Oil Dispersion Rates in Pack Ice", in *Proceedings of the 1981 Oil Spill Conference*, pp 199-201, 1981.

Technical Summary

"As petroleum exploration and transportation systems move into increasingly difficult operating environments such as the Labrador Sea, there is a need for more sophisticated oil spill countermeasures and for new cleanup technology. The design of countermeasure systems compatible with pack ice conditions cannot be undertaken without some preliminary investigation of oil interaction with ice and, perhaps more crucially, without an estimate of oil dispersion processes in moving pack ice.

The characterization of dispersion processes os complicated by seasonal and geographic variations in the physical and dynamic nature of the Labrador ice pack. Nevertheless, on the basis of field observations over the past two winters, it has been possible to generate order-of-magnitude estimates of the probable dispersion and mixing processes. These processes are low compared with open water dispersion processes."

Objective

The author stated that major objective was to be able to predict the fate of oil spilled in pack ice.

Theory

The only theory presented by the author is the definition of landfast ice (attached to the land), the interior zone (right next to the landfast ice) and the skin zone (which is next to the interior zone). The skin zone has high dynamic energy levels, small floe size, and large volumes of brash ice. The interior zone has large floe sizes and static forces but the dynamic energy levels are relatively low. The author states that the dynamic energy level is of more importance in oil spill countermeasures.

Method

In the observations section the author states that dyes and photographic recording devices were used to determine the process of separation of the floes and the process of surface water/brash diffusion in the floe interstices. The dye fluorescein was mixed in sea water (cut with alcohol) and sprayed onto the melt water in the interstitial cell of a chosen floe.

Results

The states that the Centre for Cold Ocean Resources Engineering (C-CORE) followed the *Kurdistan* oil which was spilled in March 1979 and flowed up into in a skin zone ice North of Cape Breton. The author states that the Centre followed the oil dispersion in the ice for two weeks during which time the ice field travelled 100 km and underwent several compressive cycles. The author states that even though the dynamic level of the ice was large the dispersion was slow compared to open water process.

The author states that initially the oil was in a 10 square kilometre region of 1,000 km^2 of pack ice. The author states that the Bunker C concentration was 200 ppm oil-in-ice and that at the

end of one week with 80 percent of the ice melting the oil contamination was on 5 km^2 and still at a concentration of 200 ppm. The author states that there was mixing and dispersion but the ice was ablating and reducing the volume but still keeping the oil entrained.

In case 1 and 3 (see Table 1) the floes were in continuous motion with a period of about 20 to 30 minutes and the author further states that this motion flushed water and brash ice back and forth in the interstitial spaces. This dispersed the dye and complete mixing within a cell was rapid but there was little transport between adjacent cells.

Table 1. Dispersion Process in Adjacent Floes and in Their Interstices.

	Floe		
Parameter	1	2	3
Ice cover	8/10	8/10	8/10
Wind	0 to 10 km/hr	nil	10 km/hr
Time Span	20 hr	20 hr	6 hr
Floe Dimension	150 m	500 m	50 m
Divergence	180 m	1,000 m	50 m
Interstitial Cell Size	250 m^2	> 10,000 m^2	300 m^2
Interstitial Mixing Time	4 to 6 hrs (South side) 0.5 hr (West side)	-----	0.5 hr (West side)
"Breakout" Interval	3 hr (West side)	-----	4 hr (West side)

BOSS Critique

The author does not outline the error in the measurements made how ever he does state that the experiment was biased to a fair weather case. The author does not explain why fluorescein dye was used instead of another dye nor what range of emission is followed with the photograph equipment. There is no discussion on how ppm measurements of oil in ice were made. There is also no discussion of the state of the oil in the ice such as evaporation of lighter components.

Review of a manuscript by Mackay, D., M. Medir, and D. Thorton, entitled "Interfacial Behaviour of Oil Under Ice", in *The Canadian Journal of Chemical Engineering*, pp 72-74, 1976.

Technical Summary

"There are several important implications of the observed behaviour. First, since oil drops do not "wet" ice they may tend to remain mobile and may be subject to movement by currents until restricted by the growing ice. There is a possibility that oil removal from under ice may be facilitated by inducing a water current if the under-ice topology does not dominate the oil configuration. Second, surface tension forces will act to retard spreading of oil under ice and it is unlikely that oil films will be thinned appreciably below 1 cm. This permits a maximum area to be estimated of about 16 m^2 per barrel of oil spilled ... .

The general conclusion is that oil behaviour in water under ice is significantly different from that on water or on ice in that surface forces tend to restrict spreading and prevent "wetting". Clean-up technologies must be devised to use this behaviour to advantage, but this requires a new approach to oil containment and removal rather than a modification of established techniques."

Objective

To determine the role of interfacial tension in assisting or retarding the spread of oil under ice.

Theory

"We are concerned here with one aspect of this issue, namely the role of interfacial tension forces in assisting or retarding the spread of oil under ice. These forces are believed to be unusually significant in this regime because of the relatively small density difference between oil and water which provides the buoyancy or hydrostatic driving force for spreading and high contact angle between oil and ice in a water environment which retards spreading.

When oil is spilled on a solid or fluid medium its spreading rate is controlled by a balance between gravitational forces (which tend to cause the spill to become thinner) and retarding forces which vary according to the spill history.

The principal retarding force is initially the oil inertia followed by viscous forces as laminar flow develops. As the oil spill thins to about 1 mm in air the gravity forces are correspondingly reduced and become of the same order of magnitude as the surface tension forces. Depending on the direction of the interfacial tension forces the spill may stop or continue spreading to become very thin at the leading edge.

Generally, interfacial tension forces assist spreading on water. On ice the spreading effect of interfacial tension is not as large, possibly as a result of difference in surface forces but also as a result of the higher oil viscosities and the rigidity of the ice compared with the fluidity of the water. Oil spreading on wet ice is presumably akin to spreading on water as far as surface effects are concerned.

Oil spreading under ice in water presents a different situation in several important respects. First, the gravitational forces are only about 15 to 20 % of those in oil-air-ice systems since the density difference between the oil and the continuous fluid is typically 0.15 g/cm^3 compared with

0.85 g/cm^3 in oil-air systems. Interfacial forces can thus be expected to become significant at oil film thicknesses of 5 to 10 mm instead of 1 mm in air systems. Second, in air the viscous drag of the air on the oil can be neglected whereas in oil-ice-water systems the drag of the water on the oil may be significant. Third, the interfacial forces may be different in direction because of different "wetting" behaviour between oil on ice in air systems and oil under ice in water systems."

The authors state that if the drop is large (horizontal >> vertical) then the oil-water interfacial tension can be describe by:

$$\gamma = \Delta\rho\, h^2 g/2 \text{ and } \cos(\theta) = 1 - (H/h)^2$$

where γ is the oil-water interfacial tension, $\Delta\rho$ is the oil-water density difference, h is the vertical distance between the lower horizontal plane of the drop and the horizontal plane passing through the points on the edge of the drop (see Figure 2), H is the drop depth, g is acceleration of gravity, and θ is the contact angle.

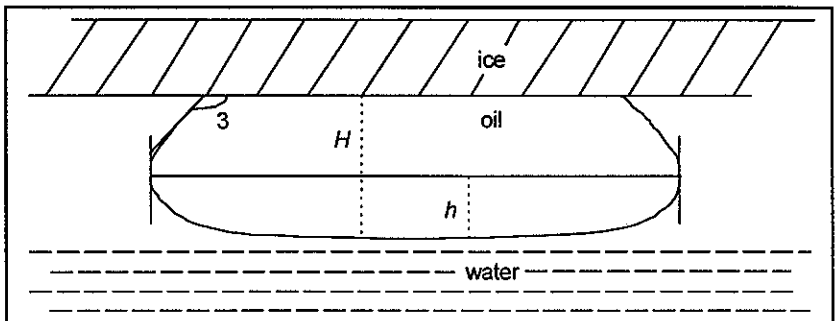

Figure 2. Diagram of sessile drop in water under ice.

Method

The authors state that a test chamber 20 cm x 20 cm x 10 cm was constructed from 0.64 cm thick plexiglass. The tank had a removable and sealable lid that was 10 x 20 cm. Deaerated water was frozen is this tank and then a piece of flat hot metal was placed on top of the ice to produce a flat surface on the ice. Water was then added to the tank, the top sealed in place and the tank inverted. Thus a flat ice face was exposed to the water in the tank. Crude oil was injected through a septum and formed a drop on the underside of the ice. The drop was photographed and the dimensions of the drop were determined from the photograph by using the needle diameter (1.75 mm) as a known scale.

The authors state that various volumes of oil (Prudhoe Bay and Norman Wells) were injected as well as distilled water and sea water. The density of the Norman Wells crude was 0.847 g/cm^3 and Prudhoe Bay was 0.911 g/cm^3 at 0 °C.

Results

The mean value (no other data are give) for Norman Wells crude was an H of 0.86 cm, θ = 138°, and γ = 31 dynes/cm and for Prudhoe Bay H = 1.2 cm, θ = 160°, and γ = 33 dynes/cm. No actual values are given for sea water, however, the authors state that the results are similar.

The authors state that because of the way that the equation is set up γ is overestimated and

θ is underestimated. The errors are linked to the determination of θ, and θ ranged from 155° to 165°. The authors believe that a more sophisticated technique would be needed to reduce the error, however, no such technique is presented.

The authors stated that the results lead them to believe that oil spilled under ice would adopt a thickness of 0.8 to 1.2 cm with a contact angle of 140 to 170°.

"There are several important implications of the observed behaviour. First, since oil drops do not "wet" ice they may tend to remain mobile and may be subject to movement by currents until restricted by the growing ice. There is a possibility that oil removal from under ice may be facilitated by inducing a water current if the under-ice topology does not dominate the oil configuration. Second, surface tension forces will act to retard spreading of oil under ice and it is unlikely that oil films will be thinned appreciably below 1 cm. This permits a maximum area to be estimated of about 16 m^2 per barrel of oil spilled ... ."

BOSS Critique

The authors make a point of stating that the "wetting" condition of the oil is important but they fail to explain this process. They do not describe in anyway the angle of interaction to the surface that the drop has to have in order for the interaction to be considered "wet". The authors do acknowledge that in real ice conditions the underside of the ice is not flat and therefore the topology of the underside of the ice will be of more importance than the interfacial tension.

Review of a manuscript by Goodman, R.H., A.G. Holoboff, T.W. Daley, P. Waddell, L.D. Murdock, and M. Fingas, entitled "A Technique for the Measurement of Under-Ice Roughness to Determine Oil Storage Volumes", in *The Proceedings of the Tenth Oil Spill Conference*, pp 395-398, 1987.

Technical Summary

"To plan an oil spill response in ice-covered regions it is vital to know the area of ice exposed to oil and the spatial extent of the spill. The parameter that characterizes this spatial extent is the storage volume, which has units of m^3/m^2, and is the average oil thickness under the ice. The critical parameters controlling this thickness are oil properties, the under-ice microlayer current regime, and the spatial roughness of the ice-water interface.

The polysulphide molding technique worked well and produces a high-quality replicate of the under-ice surface. Initial observations indicated that there was significant structure and hence oil storage volumes in Arctic sea ice at size and length scales of a few centimeters. The storage volume associated with the fine-scale roughness should be added to the storage volume associated with macro-scale thickness variations and ridge features (which had been the focus of previous ice roughness and storage volume estimates)."

Objective

To provide a reasonably accurate method of estimating oil storage volumes for under sea ice surfaces.

Theory

"A number of workers have measured ice thickness and hence deduced ice roughness. ... From this data, ice thickness and hence oil storage volumes have been calculated (Table 1). It can be seen that there is great variation in storage volume. There is likely to be a great variation in ice roughness, which occurs naturally from area to area and this may account for some observed variance. However, another factor is the length scale over which the roughness is measured. This is equivalent to the aliasing frequency of a digitizing system and, for most of the above measurements, this length is on the order of a few meters. Observations by divers and underwater photographic evidence indicates that there is a considerable ice structure at a size scale of a few centimeters. This is known as the skeletal layer and has been extensively described in laboratory studies. Features of such a scale would not have been seen in the field measurements or at best would have contributed to the variance of this data. Since roughness at this scale would contribute substantially to oil storage volume, especially in first-year ice, in which macro-roughness variation is small, it must be considered in any calculation of storage capacity. To provide a reasonably accurate estimate of oil storage volumes, a method of measuring ice roughness on a size scale of a few centimeters over an area of several square meters is required."

Table 1. Calculated oil storage volumes under ice.	
Location	Storage volume (m^3/m^2)
Tigvariak Island	0.032[1]
West Dock Site	0.0605[1]
Reindeer Island	0.010[1]
(flat smooth ice)	
Site A	0.0248[1]
Site B	0.0239[1]
Site C	0.0574[1]
Seal Island	0.130[2] 0.023[2]
Thunder Bay Harbour	0.062[2] 0.022[2]

[1] Values taken from Kovacs, 1981.
[2] Values taken from Comfort, 1986.

Method

A compound that could be used to take on the shape of the under sea ice surface was needed and the material that had been used to find the topology of archeological artifacts was proposed. The material was expected to not release heat (therefore not melt the micro surface detail) while hardening and a polysulphide compound at a ratio of 20:1 (rubber to catalyst) was used in the

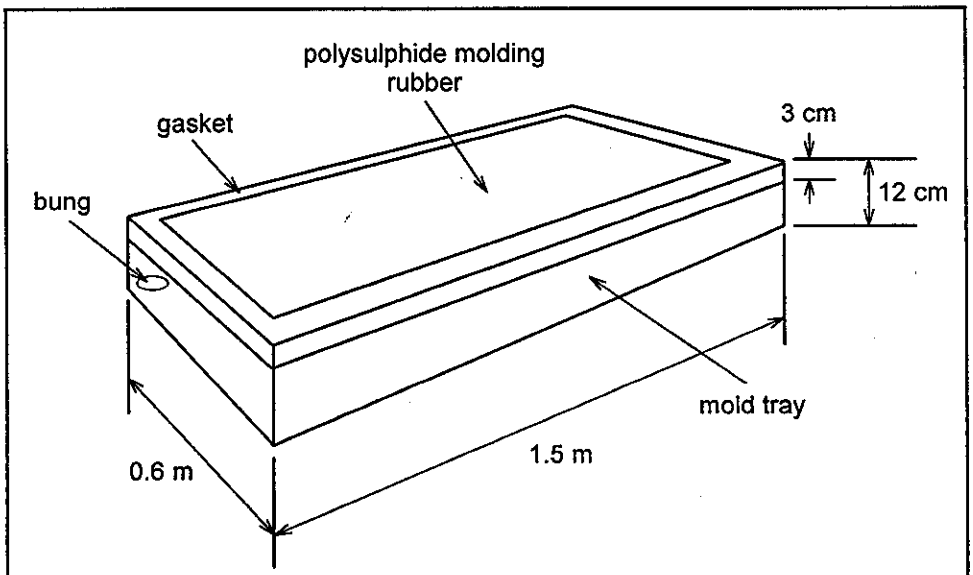

Figure 1. Mold for replicating ice surface.

experiments. The mold that was used to keep the polysulphide rubber in place is illustrated above in Figure 1.

The polysulphide rubber compound was kept in place by an air pressure flotation system. (see Figure 1 and 3.) The gasket depth (3 cm) is the maximum ice feature that can be recorded with the apparatus as presented by the authors.

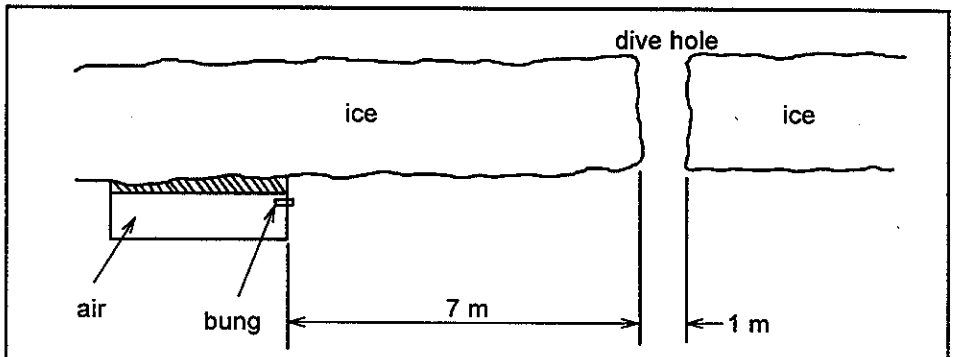

Figure 3. Mold under ice.

"The ice thickness was about 2 m, and the water depth varied from 3 to 6 m. Three sites were used, and four molds were made at each hole.

For each mold, the following procedure was used:

1. The rubber was mixed on site with the catalyst and applied to the mold in a uniform layer approximately 3 cm thick.
2. The mold was lowered into the hole, where two divers carefully transported it to a previously selected sample site. The direction of the mold was mapped and subsequently marked on the replicate.
3. Air from the divers' tanks was used to fill the buoyancy chambers, and hold the mold at the under-ice interface.
4. Additional buoyancy, in the form of 12 L (3 gal) plastic pails, was placed under the mold to ensure a good replication of the under-ice surface. Placement under the ice is shown in Figure 3.
5. Four molds were set out at each dive site.
6. After 12 to 16 h, the molds were recovered by the divers. The air in the buoyancy chamber was expelled by removing the bung, and then the mold was removed from under the ice surface.
7. The twelve molds were wrapped in plastic, and shipped to the Esso Resources Canada Limited research laboratory in Calgary."

Results

"The polysulphide rubber molds produce a negative impression of the under surface of the ice. To analyze the under-ice roughness, a more robust positive mold is required. This was made by mounting the polysulphide rubber negative on a rigid flat surface, and then imaging the mold with fibreglass and resin mixture. After the resin had cured, the rubber mold was removed, leaving the fibreglass positive. This positive was used for all further analysis of ice roughness.

To measure the surface roughness of the positive replicates, stereo photographic pairs were taken of each mold, and the roughness computed using techniques developed for terrestrial photogrammetry. ...

A second experiment using the positive molds involved the progressive flooding of the positive molds with fixed volumes of fluid. After each addition of fluid, high-contrast photographs were taken. The area covered by fluid was subsequently measured using automatic video-processing equipment.

The initial observations in the filed revealed a fine microstructure in the ice, whose amplitude appeared constant in all the molds. ... The molds did not completely replicate the ice surface, which was recognized by the absence of the fine structure. On most of the molds, large scale features were present. These included long, narrow peaks and complex hemispheric structures. The final analysis of the molds using the stereo photographs had not been completed."

BOSS Critique

The authors have presented a new method for measuring the underside roughness of sea ice and it would be more useful if errors in the method were presented with the method. The method allows for an increase in estimates of oil spills but no actual comparison of volumes is presented. If the results were presented in some other venue the authors should state this in the manuscript.

The contour map that was displayed in the original manuscript (and was not reproduced here) was presented with no errors associated with the contours. The stereo photographic systems has errors associated with the it and these should be either explained or a reference should be made to a manuscript that does explain all associated errors in the method.

The areas that were determined with the automatic video-processing equipment will have some range of error which is not presented in this manuscript. It is difficult to evaluate a method when no errors are given.

Review of a manuscript by, Welsh, J.P., O.M. Lissaer, G.L. Hufford, T.S. Ellis, B.D. Thompson, L.D. Farmer, and R.R. Hiltabrand, entitled "Some Dynamics of Spilled Oil in a Fractured Ice Field in Buzzards Bay, Massachusetts", in *Ocean Engineering*, Vol 4, pp 197-203, 1977.

Technical Summary

"A spill of #2 fuel oil occurred 28 January 1977 in a dynamic ice field in Buzzards Bay, Massachusetts. An oil budget study revealed that within four days after the spill occurred, approximately 60% of the oil was incorporated into the fractured ice zones and onto the ice surface. The movement of the oil (initially spilled under the ice) into the fracture zones appears to be the result of water current below the ice and buoyancy spreading mechanisms. Areas of fracture zones and leads provided a surface outlet for the less dense oil as it moved under the ice. When the leads closed, the oil was trapped into pools on top of the ice at the floe edges. The further spread of the oil onto the surface of the ice floes appears to have been caused by the wind. ... The fast ice formed an effective barrier to the shoreward movement of the oil."

Objective

To use the Bouchard Barge #2 fuel oil spill to study the dynamics of spilled oil in a changing ice field.

Theory

The theory was included in the overall discussion of the manuscript.

Method

"... In two days of data collection (January 29 and February 1), fourteen sites were sampled in the area. The field measurements consisted of air/ice temperature, ice thickness, water temperature and water velocity (at a depth of 0.3 m and 3 m below the ice cover). The results are summarized in Table 1. Samples of oil from in and on the ice were collected and transported to the laboratory where they were melted down and the volume of oil and water was measured in a graduate cylinder. Also, the thickness of the oil layer was measured for use in estimating oil in ice budgets for the entire spill area.

In addition to the field measurements, aerial photographs were taken of the spill area. These photographs and the measured thickness of oil were used to produce an estimate of the amount of oil incorporated into and onto the ice four days after the oil was spilled."

Results

The authors used the information in Table 1 (the oil thickness in the fractured zone was 0.25 cm and 0.30 cm for the ice floes) and aerial photographs to determined that the volume of oil in the fractured zone was 141.20 m^3 and for the floes it was 44.67 m^3. The sum of these is 185.87 m^3 which is 60% of the reported volume of the spill. The clean up crew estimated that they recovered 37.85 m^3 and the authors believe that the remaining 83.64 m^3 was trapped under the ice or floating in leads accounting, for 307.36 m^3 of the spilled 307 m^3 of # 2 fuel oil.

Table 1. Summary of Buzzards Bay Data									
Sample			Air/Ice Temp. (°C)	Volume (ml)		Salinity (‰)	Ice Density (g/cm^3)	Description	% Oil by Volume of Sample
No.	I.D.	Date		Oil	Water				
1	A12	1/29	-8.8/-9.2	138	142	32.2	----	Oil on top of ice	49
2	A6	1/29	-9.2	286	82	16.0	----	Oil/water in slush	78
3	C3	1/29	-9.2	12	46	14.9	----	Ice needles in oil	21
4	C9	1/29	-9.2	12	330	8.7	----	Oil/snow ice	4
5	29	1/29	-9.2	4	362	3.2	----	Ice block edge ice/oil	1
6	C16	1/29	-9.2	5	261	0.03	----	Surface oil on ice	2
7	B14	1/29	-9.2	18	313	18.3	----	Slush /oil	5
8	A1	2/1	-3.5	0	347	5.9	0.91	Top of ice core (D5 is bottom)	0
9	A16	2/1	-3.5	0	368	5.3	0.92	Top of ice core (#18 is bottom)	0
10	B13	2/1	-3.5	12	479	7.3	1.08	Bottom of ice core (A10 is top)	0.2
11	D5	2/1	-3.5	0	369	7.0	0.97	Bottom of ice core (A1 is top)	0
12	C10	2/1	-3.5	1	358	6.0	0.95	Bottom of ice core (C14 is top)	0.3
13	C14	2/1	-3.5	1	327	5.0	0.98	Top of ice core (C10 is bottom)	0.27
14	A10	2/1	-3.5	----	----	----	1.04	Top of ice core (B12 is bottom)	----

"Ice cores were taken from several floes. Quantitatively, very little oil was observed from the bottom of these cores. It appears that incorporation of oil into the underside of the ice was minimal. The oil on top of the ice floes was deposited there by ice rafting, flooding from the floe collision and the wind. The mechanism appears to be that when leads opened, oil trapped under the ice moved to the open water surface. Pools of oil were then transferred onto the ice primarily by flooding associated with ice motion and ridge making. These pools of oil were then blown over the ice floes and frozen into the upper 2.5 cm of the surface as the ice melted and refroze.

Oil was not found in the fast ice zone even though the tidal forces and winds during the first few days could have transported the oil into these areas. The fast ice acted as a barrier to oil dispersion toward the shoreline areas. It is expected that some oil did move under the fast ice but did not progress very far because the majority of the fast ice was grounded."

BOSS Critique

The authors do not discuss the errors involved in the measurements they reported nor the exact method of aerial photography and area measurements of fractured ice and ice floes. These numbers are important in order to determine the exactness of the reported volumes.

Review of a manuscript by, Sayed, M., and S. Løset, entitled "Laboratory Experiments of Oil Spreading in Brash Ice", in *The International Journal of Offshore and Polar Engineering*, pp 306-312, 1993.

The identical paper appears in the *Proceedings of the Third International Offshore and Polar Engineering Conference*, International Society of Offshore and Polar Engineers, Colorado, pp 224-231, 1993.

Technical Summary

"Experiments were conducted in an ice basin to examine the behaviour and spreading rates of oil in brash ice. Sea water was used to grow ice sheets which were broken to produce the required ice cover. Two types of North Sea crude oils (Gullfaks and Oseberg) as well as Bunker fuel were used. Oil samples were spilled on the broken ice/slush covers at an approximately constant flow rate. Analysis of the video records gives maximum spill dimensions, spreading rates, and ratio of the oil-covered area to total area of the spill. The results show that oil always flowed over the brash ice, and that surface tension plays a more significant role than viscosity in decreasing oil spreading. Measured slick dimensions were used to develop empirical expressions for the balance of gravity, surface tension and viscous forces."

Objective

To examine the spreading rates and maximum extent of oil spills in brash ice with sea water, North Sea crudes and Bunker fuel.

Theory

"In order to choose the appropriate expressions for the various forces in the present analysis, the simple idealization of the slick as an expanding disc was considered. This idealization was used by Yapa and Chowdhury (1991) to model oil spreading under ice. Considering the equilibrium of forces on a sector of the disc of angle $d\theta$ and radius R, gravity would be:

$$dF_g = \frac{1}{2}\gamma R h^2 d\theta \qquad (1)$$

The surface tension force acting on the perimeter of the sector would be:

$$dF_s = \sigma R d\theta \qquad (2)$$

where σ is the surface tension. It should be noted again that Eq. 2 gives a reference surface tension force, which may be different from the actual resultant force that acts on the slick. Assuming that the viscous shear stress is proportional to an average velocity gradient u/h, where u and h are average velocity and oil thickness, the viscous force becomes:

$$dF_v = \mu \frac{u}{h} R^2 d\theta \qquad (3)$$

Considering that oil volume V is constant, h can be expressed in terms of R and V using the relationship : $V = \pi R^2 h$. The average velocity, u, is also assumed to be proportional to the time

derivative of the radius, $\dot{R}$. Yapa and Chowdhury (1991) further assumed that the time derivative $\dot{R}$ is proportional to R/t, where t is the elapsed time. The resulting ratio of surface tension to gravity force becomes proportional to $\sigma R^4/\gamma V^2$, and that of the viscous force to gravity force becomes $\mu R^8/\gamma V^3 t$."

Method

"The experiments were conducted in an ice basin at SINTEF NHL in Trondheim. The basin is 7.7 m long, 4.7 m wide and 1.2 m deep. Sea water, approximately 24 m^3, was transported from a nearby fjord to the basin. Water depth in the basin was 0.65 m. Water salinity was 12 ppt. Ice was grown without seeding the water at temperatures of approximately -10 °C. Room temperature was raised to 0 °C when the required ice thickness was reached. Ice strength then gradually decreased because of the raised temperatures. The ice sheet was manually broken in order to prepare the required brash ice cover. In the case of small ice thickness (up to 20 mm), the ice was usually very weak and broke into slush with no distinct ice blocks. For thicker ice sheets (>25 mm), the brash ice cover consisted of distinct ice blocks with slush between them. All of the ice covers used in the experiments had no open water areas within the brash ice.

After preparing the ice cover, a grid of markers was placed a few centimetres above the ice surface for a scale. The grid consisted of strings attached to two steel bars at 0.5 m spacings. The steel bars were in turn mounted on the side walls of the basin. Small tape markers were then attached to the strings at 0.5 m spacings. Thus, a 0.5 m x 0.5 m grid was constructed. This type of grid was used for all oil spills of 4 litre volumes. Three types of oil were used in the experiments: two North Sea crudes (Gullfaks and Oseberg) and Bunker fuel IF-30. Properties of these oils are listed in Table 1."

Table 1. Oil properties

Type	Viscosity μ (Pa. s)	Surface Tension, σ (N/m)	Pour point (°C)	Specific gravity
Bunker	1.240	0.026	-6	0.936
Gullfaks	0.041	0.013	<-34	0.878
Oseberg	0.024	0.021	-24	0.853

"Temperatures of the oil samples were measured immediately before spilling and were always between -2 °C and +1 °C. These temperatures are above the pour points (Table 1). For each test, a 4 litre sample was spilled at an approximately constant flow rate. The oil sample was placed in a cylindrical Perspex container of 0.3 m in diameter. The container had a valve-controlled orifice that connected to a 3 m long, 20 mm inner-diameter flexible hose. At the end of the hose, a sprinkler with 1 mm diameter holes was used for Gullfaks crude samples. The sprinkler was removed when the slower flowing Oseberg crude and Bunker fuel were tested. The cylindrical container was held at heights between 0.6 m and 1.0 m above ice level. The container height was gradually raised during oil discharge in order to maintain a nearly constant flow rate. Oil was discharged only a few millimetres above the ice surface. Smaller oil samples (less than 4 litres) were poured directly from a beaker, again just over the ice surface.

Spreading of the 4 litre oil spills was monitored by two video cameras. One camera was mounted directly over the centre of the spill. That camera provided accurate visual records of the initial stages of spreading, but slick dimensions usually went out of the camera's range in the latter stages. The other camera was mounted further away from the spill at an oblique angle to the vertical direction. That camera had a sufficiently wide range of view to cover the slicks throughout the tests. The small oil spills were not monitored by the video cameras. Instead, their dimensions were directly recorded during the tests at several time intervals. Subsequent measurements from the video records were based on the grid, which was placed immediately above the ice cover. This procedure eliminates any distortions due to the camera's angle.

Test runs were chosen in order to examine the dependence of spreading rates and the maximum extent of a slick on oil volume, oil properties and ice cover type. A list of all test parameters is given in Table 2. Spilling time of each sample is listed in the table. For Tests 1 ~ 4, the ice cover consisted of slush. Ice covers of Tests 5 and 6 consisted of ice blocks with lengths up to 0.2 m, with slush between them. Ice blocks of Tests 7 and 8 were larger, with lengths up to 0.45 m. For Test 8, 40% of the ice blocks were removed from the basin. Slush, however, filled all the spaces between the remaining ice blocks, i.e. there was no open water."

Table 2. List of test runs

Test	Oil	Volume (litre)	Spilling time	Ice thickness (mm)	Remarks ice cover
1	Gullfaks	4	120	10 to 17	slush
2	"	4	150	6 to 12	"
3a	Oseberg	4	185	20	"
3b	"	1	65	"	"
3c	"	0.5	44	"	"
4a	Gullfaks	4	150	"	weak ice, slush
4b	"	1	19	"	"
4c	"	0.5	17	"	"
5a	"	4	175	25 to 35	distinct blocks
5b	"	1	35	"	"
5c	"	0.5	23	"	"
6a	Bunker	4	245	"	"
6b	"	2	115	"	"
6c	"	1	35	"	"
7a	Gullfaks	4	148	60 to 70	large blocks
7b	"	1	13	"	"

Table 2. List of test runs					
Test	Oil	Volume (litre)	Spilling time	Ice thickness (mm)	Remarks ice cover
7c	"	0.5	--	"	"
8a	"	4	150	"	60% of ice
8b	"	0.5	30	"	

Results

"An oil slick usually had a central region where oil almost entirely covered the brash ice surface. In the outer region of the slick, oil had smaller thicknesses and covered only the depressions of the ice surface. Spreading was approximately axisymmetric, but in some cases the difference between the dimensions along the length and width of the basin was up to 20%. ...

The outer region of the slick which was partially covered with oil was more pronounced for the Gullfaks crude than for the Oseberg crude and Bunker fuel. The latter two oils appeared to spread much more slowly than the Gullfaks crude, and with larger thicknesses that totally covered the ice surface. This observation indicates that the larger value of the surface tension of the Oseberg crude and the Bunker fuel may be responsible for retarding the speed of spreading and for producing the relatively large slick thicknesses. Viscosity could not have caused these effects because Gullfaks crude has a higher viscosity than that of Oseberg crude. As will be discussed later in the paper, we refer here to the surface tension between each oil and its vapour as a reference value. This value would be different from the force due to the interfacial tension among oil, water, ice, and air.

...

The video measurements (for the 4 litre spills) are in agreement with the values recorded during the tests. Accuracy of the measured dimensions appears to be within 0.1 m. Measured dimensions for Tests 3 ~ 8 are plotted versus time on logarithmic coordinates in Figures 3 ~ 8. The two lengths of the 4 litre spill shown in each figure were measured along two perpendicular directions. Orientation with respect to the basin had no effect on these lengths. Some dimensions of spills with volumes smaller than 4 litres are also noted on the plots. The vertical dashed lines indicate the times when oil discharge ended, i.e. slicks spread at a constant volume past those times.

Figure 3 shows that the Oseberg crude spreading in Test 3 decreased rapidly and slick dimensions reached constant values immediately after oil discharge stopped. In Test 4 (Figure 4), Gullfaks crude of the same volume (4 litres) as Test 3 was spilled over the same type of ice cover. Spreading of Gullfaks crude, however, continued to increase after oil discharge had stopped. The average diameter (or length) of the Gullfaks slick after 5500 s reached approximately twice that of the Oseberg slick. Oil properties in Table 2 show that Oseberg crude has higher surface tension but

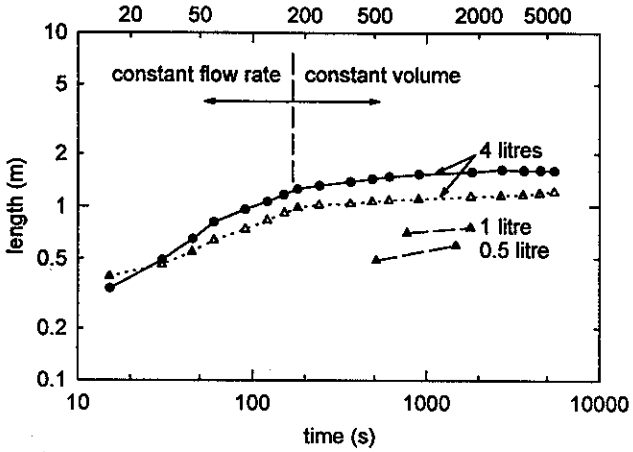

Figure 3. Oil slick dimensions, Test 3. 4-litre slick measured along two perpendicular directions.

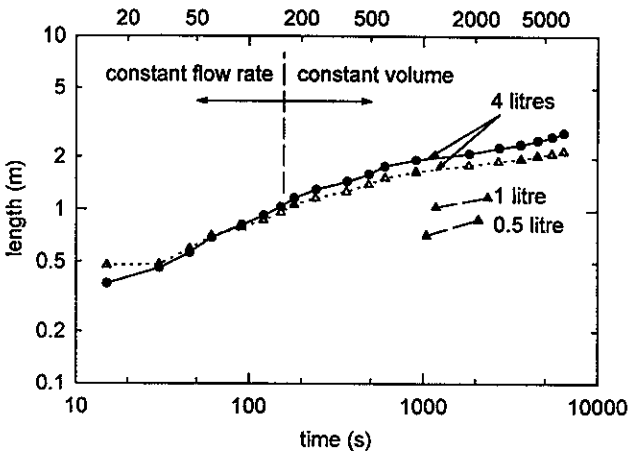

Figure 4. Oil slick dimensions, Test 4.

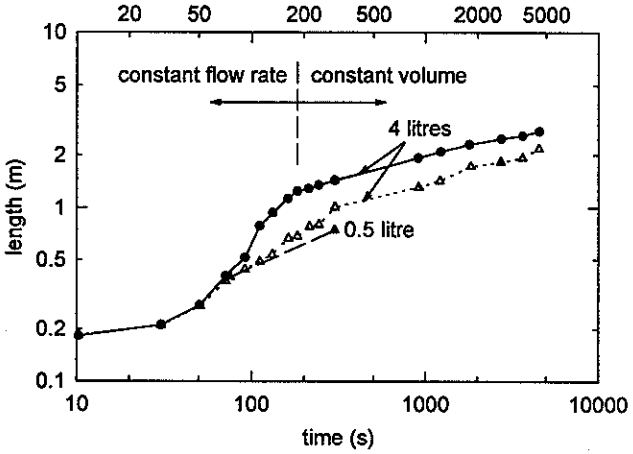

Figure 5. Oil slick dimensions, Test 5.

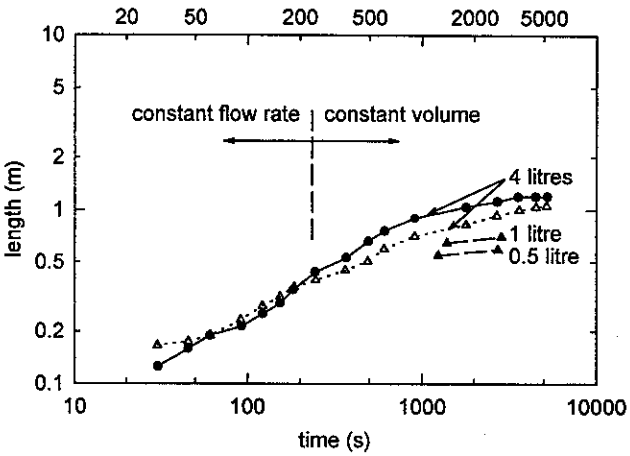

Figure 6. Oil slick dimensions, Test 6.

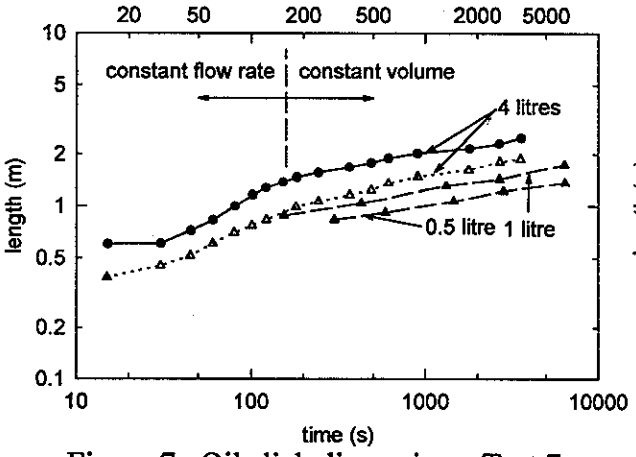

Figure 7. Oil slick dimensions, Test 7.

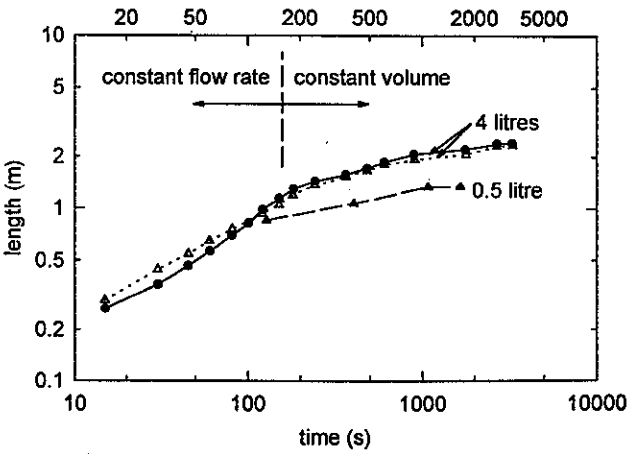

Figure 8. Oil slick dimensions, Test 8.

lower viscosity than Gullfaks crude. Consideration of these oil properties and comparison of Figures

3 and 4 clearly confirm the observation mentioned above: The surface tension role in limiting oil spreading in this case is more significant than viscosity.

The influence of ice cover on spreading may be examined by comparing Figures 4, 5, 7, and 8. These figures show the dimensions for spills of Gullfak crude over varied ice covers. ... Dimensions of the slicks were close for all ice covers. Therefore it may be concluded that, for the present range of ice covers, spreading are similar. Oil coverage within the slicks, however, varied between ice covers. Oil coverage is defined here as the ratio of oil-covered area to the total area of the slick. The total area of the slick is taken as the area within the slick's boundary, which was measured from the video tapes. Larger ice blocks within the slick remained clear of oil. Thus, the ratio of oil-covered area to the total area of a slick decreases with increasing ice block size. It follows that oil thickness increases with increasing ice block size. As an example, the oil covered area and the total area for Test 8 are plotted versus time in Figure 9. Oil thickness was calculated by dividing oil volume by the oil-covered area. Oil thickness at the end of each test and the ratio of oil-covered to total are listed in Table 3."

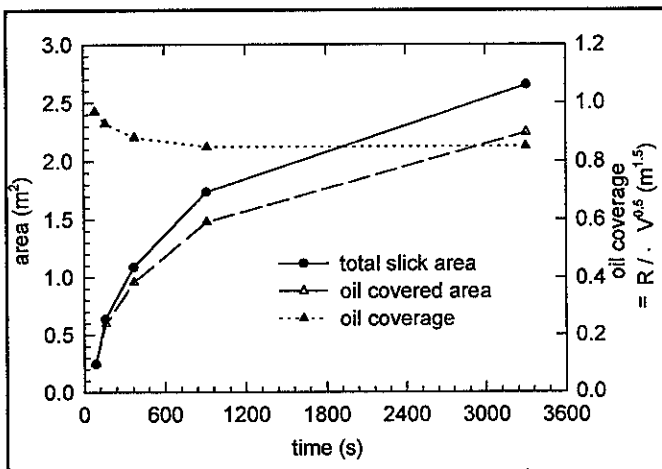

Figure 9. Total slick area, oil-covered area, and oil coverage (ratio of two areas); Test 8.

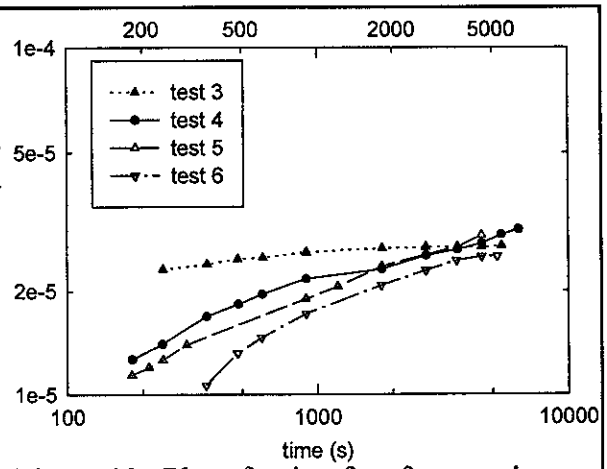

Figure 10. Plot of ratio of surface tension force to gravity force versus time.

Table 3. Oil thickness and oil coverage (ratio of oil covered area to total slick area)		
Test	Oil thickness (mm)	Oil coverage
3	3.7	0.96
4	1.6	0.91
5	2.4	0.82
6	3.8	0.98
7	2.7	0.85
8	1.8	0.85

"Oil spreading over brash ice is very complex. Even the simpler case of oil spreading over open water is too complex to model analytically .... To date, the dimensional analysis of Fay (1969) has been used in most studies of oil spreading. Fay assumed that gravity and surface tension forces induce spreading, and that they are resisted by inertia and viscous forces. Furthermore, by considering regimes where only pairs of these forces are significant, he obtained expressions for spreading rates. The present experiments, however, show that surface tension resists spreading. ... Surface tension was also considered to resist spreading by Yapa and Chowdhury (1991) for oil under ice, and by Belaskas and Yapa (1991) for oil in broken ice.

For oil in brash ice, it is difficult to determine the resultant force due to the interfacial tension among oil, air, ice and water. Evaluating such forces is further complicated by the complexity of the geometry of slick boundaries. We have not addressed this problem in the present experiments. Instead we simply use the oil/air surface tension here as a reference value.

The current measurements can be presented by considering that gravity force acts to spread the oil, and it is resisted by both viscous and surface tension forces. In the present tests, as in most field cases, oil spilling occurred over relatively short periods. Spreading took place over much longer durations. For example, the 4 litre samples were usually spilled over periods close to 150 s, while spreading continued for over 5000 s. In the following analysis, we will consider the case where oil volume is constant (discharge has stopped), since it covers the range of practical interest, at least from our point of view. Inertia of the oil is neglected in the following analysis because it always appeared to be negligible. Estimates using typical values for velocity and oil thickness showed that inertia forces are several orders of magnitude smaller than gravity forces. For example, consider a small part of the slick of unit length, unit width and average height h. The average velocity is taken as u, oil unit weight is γ and oil density is ρ. Gravity force would be of the order of $\gamma h^2/2$, and inertia force would be of the order of $\rho u^2 h$. Typical values from the present experiments can be taken as : h = 1 mm to 5 mm, and $u < 5$ mm/s. These values give a ratio of inertia force to gravity forces of the order of 10^{-4}."

The authors found that the expressions outlined in the theory section (equations 1 to 3) did not fit the preliminary results.

"Evidently the uniform disc idealization cannot adequately account for the complexities of the present oil flow patterns and boundaries. Changes were then attempted in order to empirically develop expressions that are applicable to the present problem. Consider first the equilibrium between surface tension and gravity forces when spreading stops. Comparison of the final dimensions of slicks of varied volumes showed that the radius R_f (taken as half the average length) is proportional to the square root of the volume V, as shown in Table 4."

Table 4. Ratio of final slick radius to square root of oil volume

Test	Oil volume (litre)	$R_f/\sqrt{V}$ ($m^{-0.5}$)
3	4	0.35
"	1	0.38
"	0.5	0.39
4	4	0.63

Table 4. Ratio of final slick radius to square root of oil volume		
Test	Oil volume (litre)	$R_f/\sqrt{V}(m^{-0.5})$
"	1	0.65
"	0.5	0.68
5	4	0.56
"	1	0.50
"	0.5	0.53
6	4	0.28
"	2	0.25
"	1	0.30
7	4	0.55*
"	1	0.9
"	0.5	1.0
8	4	1.0*
"	0.5	0.96

"Comparison of the different oil types indicated that the ratio $R_f/\sqrt{V}$ is proportional to γ/σ. Therefore the ratio of surface tension to gravity forces may be considered to be proportional to $\sigma R_f/(\gamma\sqrt{V})$. This ratio is plotted versus time for Tests 3 ~ 6 in Figure 10. As times increases, this ratio of surface tension to gravity force increases until the slick reaches its maximum dimensions. This behaviour is expected since oil thickness, and consequently gravity forces, decrease with time. Also, surface tension forces are expected to become more significant with increasing time because the length of the oil/ice interface increases. Results of all test of Gullfaks crude are very close to the shown values of Tests 4 and 5, but are not included to avoid clutter. The results of Test 3 in Figure 10 initially show high surface tension forces because that spill reached its maximum dimensions shortly after oil discharge had stopped. Figure 10 shows that as oil slicks approached their maximum dimensions, the ratio of surface tension force to gravity force for all tests approached a narrow range of values. Therefore, the equilibrium between the surface tension force and gravity force can be expressed as:

$$\frac{B\sigma R_f}{\gamma\sqrt{V}} = 1 \qquad (4)$$

where B is a parameter that depends on ice cover type and has dimensions of $(\text{length})^{-1.5}$. The present tests give values of B ranging from 3.3×10^4 to 4×10^4 $m^{-1.5}$. The narrow range of B values indicates that the difference between the present ice cover had little effect on the maximum dimensions of the slicks.

For the ratio of viscous to gravity forces, the data were found to best agree with the

expression $\mu R^3 \dot{R}/(\gamma V)$. The derivative $\dot{R}$ is not substituted for by R/t because $\dot{R}$ was found to give a better fit. The value of $\mu R^3 \dot{R}/(\gamma V)$ also decreases to zero when spreading stops, and therefore it may be a better representative of viscous forces than R/t. The resulting ratio $\mu R^3 \dot{R}/(\gamma V)$ is plotted versus time for Tests 4 and 5 in Figure 11. This ratio decreases slightly with increasing time until spreading stops, where it falls to very small values. Obviously gravity forces decrease with increasing time, but viscous forces apparently decrease faster. The term $\mu R^3 \dot{R}/(\gamma V)$ has dimensions of (length)^2. A parameter representing ice cover properties is required to make this term dimensionless.

The balance between gravity forces and the sum of the viscous and surface tension forces is examined by plotting $\mu R^3 \dot{R}/(\gamma V)$ versus $\sigma R/(\gamma V)$ in Figure 12. The curves representing all tests fall within a relatively narrow range (Figure 12). The agreement between the various tests indicates that the difference between the ice covers used in the experiments did not have significant effect on oil spreading. The results of Test 3 in Figure 12 all fall near the maximum dimensions of the slick, because spreading slowed down rapidly after oil discharge stopped.

The plots in Figure 12 can be approximated by the following equation:

$$\frac{k_1 \mu R^3 \dot{R}}{(\gamma V)} + \frac{k_2 \sigma R}{\gamma \sqrt{V}} = 1 \qquad (5)$$

Values for k_1 of 0.25 x 10^7 m^{-2}, and for k_2 of 0.25 x 10^5 m$^{-1.5}$ corresponding to a line representing an approximate average of the data. The value of k_2 is different from that of the parameter B of Eq. 4. The parameter k_2 corresponds to a spreading slick, where both viscous and surface tension act against gravity force. Alternatively the parameter B corresponds to a slick that reached its maximum dimensions, where only surface tension force is in equilibrium with gravity force. Results from one test from Belaskas and Yapa (1991) experiments are also presented in Figure 12. They show good

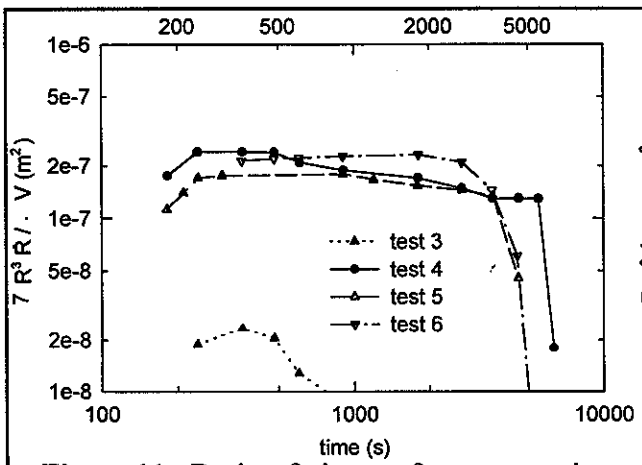

Figure 11. Ratio of viscous force to gravity force versus time.

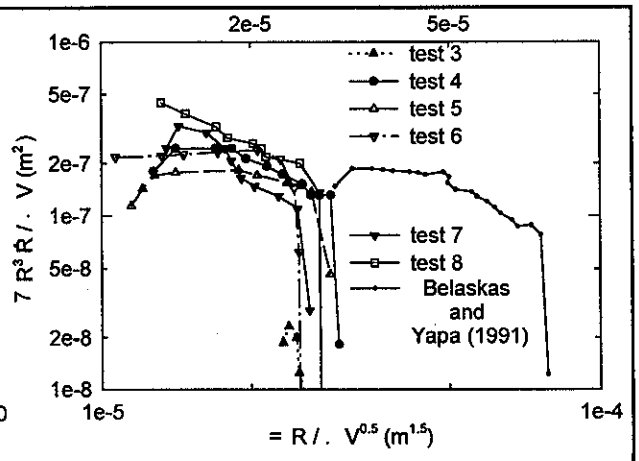

Figure 12. Ratio of viscous force to gravity force versus ratio of surface tension force to gravity force.

agreement with the present values of viscous/gravity force ratio. The surface tension/gravity force ratios are somewhat larger, although of the same order of magnitude as the present results. This small discrepancy could be attributed to the difference in ice cover geometry and type of ice, in

addition to the uncertainty in evaluating the actual resultant surface tension forces. The preceding presentation doe not provide a definite proof that the chosen ratios are those of surface tension to gravity forces and viscous to gravity forces. The justification is their analogy to the terms obtained from the expanding disc idealization, and their agreement with the present results.

The results in Figure 12 as well as Eq. 5 can be used to estimate the spreading rates of an oil spill in brash ice. It is simple to numerically integrate Eq. 5 to determine the values of the radius at various time intervals. Integration should start from an initial (nonzero) radius, which corresponds to the end of oil discharge. Note that there is a singularity in Eq. 5 at $R = 0$. Eq. 5 was obtained by fitting a line through the data shown in Figure 12, but does not include the end on the right side of the plots which corresponds to the drop in viscous forces when the slicks reach their maximum dimensions. Therefore, Eq. 4 should be used to determine the maximum radius of the slick."

BOSS Critique

The authors state that the grid was 0.5 m x 0.5 m and they then state that the accuracy of the measurements was 0.1 m. The authors do not explain how they reached this conclusion and they should have since the grid would only allow a 0.25 m interpolation.

The authors have made an effort to use the data that was collected from the experiments to improve the equations that are presented which is a distinct improvement over the usual approach of keeping the equations no matter whether the experimental data proves the theory to be true or not.

There still may be scaling effects that are needed to be included and the authors should have done so considering the time frame that the experiments are done in.

Review of a manuscript by, Sayed, M., L.S. Kotlyar, and B.D. Sparks, entitled "Spreading of Crude Petroleum in Brash Ice; Effects of Oil's Physical Properties and Water Current", in *Proceedings of the Fourth International Offshore and Polar Engineering Conference*, pp 225-232, 1994.

Technical Summary

"Experiments were conducted in a refrigerated, circulating current flume to examine crude oil spreading in brash ice. Amauligak, Hibernia, and Norman Wells crudes were tested. Measurements of the physical properties of the oils were also conducted, including: surface and interfacial tensions as well as viscosities. Spreading coefficients were calculated from measured surface and interfacial tensions. Results were obtained for original and weathered oils. For the spreading tests, spill volumes up to 3 litres and water currents up to 0.55 m/s were used. Tests were done using both fresh water ice and saline ice. Slick dimensions were measured, and modes of oil spreading were observed. Slick dimensions depended on oil type, but were not influenced by water current. Oils of high spreading coefficient and low viscosity spread over larger areas than those with low spreading coefficient and high viscosity."

Objective

To evaluate the effect that physical properties of the oil, volume of oil spilled, water current, and ice cover (block size and salinity) have on the behaviour of oil in brash ice.

Theory

The authors have interspaced theory with method and results. The following is quoted directly from the paper for the preliminary work done prior to the slick spreading work.

"**OIL PROPERTIES**

A set of experiments was performed in order to measure some of the physical properties of the three types of oil which were used in the spreading test. Measurements of oil properties included surface and interfacial tensions, as well as viscosities. Also, since exposure of the oil slicks to air and water was expected to affect oil properties, measurements were done using both original and weathered oil samples.

Weathering:

In spreading tests, oil always flowed over the wet surface of slush and ice. In order to obtain weathered samples for characterization, oil layers were placed on a water surface. Tap water and saline water (prepared by dissolving 30 ‰ sea salt) were used. The oil samples were placed on the water in trays, and were kept in a cold room. Weathering would occur in this case due to evaporation from the oil sample's surface which is exposed to air. It was not clear if the water beneath the oil will play any role. This arrangement, however, was used because it simulates the conditions of oil slicks in the spreading tests. Oil thickness was approximately 10 mm. The surface area of the oil which was exposed to the air was 0.0504 m^2 in most tests. In two tests (Norman Wells and Amauligak crudes over saline water), a surface area of 0.042 m^2 was used. Specific gravities were

not measured, but values given by Whiticar *et al* (1992) are: 0.9014 for Amauligak crude, 0.8773 to 0.843 for Hibernia crude and 0.84 to 0.8581 for Norman Wells crude.

The original weights of the oil samples were between 0.32 kg and 0.43 kg. Weight losses were monitored for 3 hours, which is close to the duration of the spreading tests. A few weathering tests were also carried out for 100 hours durations. The resulting percentage weight losses are given in Table 1.

The results indicate the water salinity has a negligible effect on the weight loss of oil samples. Also the rate of weight loss decreases with time. Figure 1 shows plots of the cumulative percentage weight loss versus time for the tests carried out over 100 hours."

Sample type	Table 1: Weight loss of oil sample during weathering tests.		Table 3: Interfacial tension between crude oils and water.		Table 4: Spreading coefficients of oil on water.	
	Weight loss, 3 hours, %	Weight loss, 100 hours, %	Interfacial tension, $S_{o/w}$ (N/m) x 10^{-3}		Spreading coefficient, $\gamma_{o/w}$ (N/m) x 10^{-3}	
			Original oil	Weathered for 3 hours	Original oil	Weathered for 3 hours
Amauligak/fresh water	6.06	26.33	24.8	24.1	17.9	17.6
Amauligak/saline water	5.91	-	22.8	22.2	17.6	17.6
Hibernia/fresh water	1.89	-	21.7	21.8	16.7	15.9
Hibernia/saline water	2.17	9.68	21.8	21.1	14.4	14.6
Norman Wells/fresh water	4.21	-	21.1	20.8	20.8	20.8
Norman Wells/saline water	5.21	7.77	21.2	20.2	18.6	19.4

"Spreading coefficients:

Surface and interfacial tensions were measured in order to determine the spreading coefficients, a du Nouy tensiometer was used. This approach is based on suspending a ring in the oil, then lifting it by a lever and counter-weights. The force which is required to lift the ring from the oil surface is used to determine the surface tension. A summary of the test cases is presented below. Values of the surface tension are given in Table 2, and those of the interfacial tension between oil and water are given in Table 3. Temperature during all tests was 1 °C. Other available surface tension values (Whiticar *et al* 1992) are slightly lower that the present values. Most differences are less than 5%, and the maximum difference is 25%."

Table 2: Surface tension of crude oils and water.	
Sample	Surface tension, S(N/m) x 10^{-3}

	Original	Weathered for 3 hours
Fresh water	72.4	-
Saline water	70.2	-
Amauligak	29.7	30.6
Hibernia	34.0	34.7
Norman Wells	30.5	30.8

"The spreading coefficient of oil on water, $\gamma_{o/w}$ is given by

$$\gamma_{o/w} = S_w - S_o - S_{o/w} \quad (1)$$

where S_w is the surface tension of water, S_o is the surface tension of oil, and $S_{o/w}$ is the interfacial tension between oil and water. The resulting spreading coefficients at 1 °C are given in Table 4.

Spreading coefficients of oil on saline water are lower than those for oil on fresh water. Differences between the spreading coefficients for original and weathered oil samples, however, were less than two standard deviations in all cases.

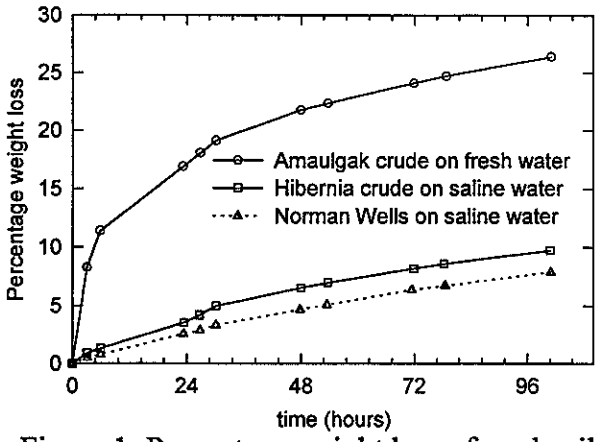

Figure 1: Percentage weight loss of crude oils over 100 hour durations.

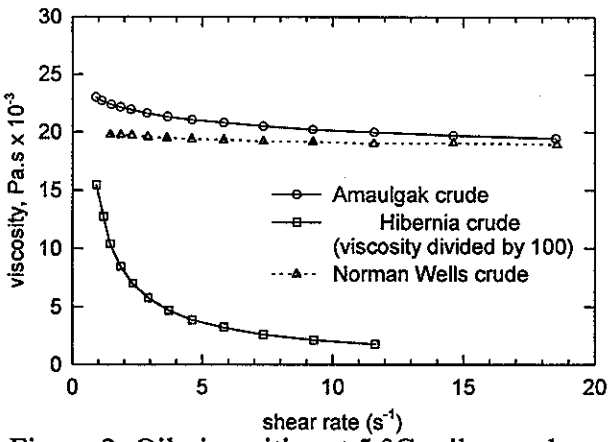

Figure 2: Oil viscosities at 5 °C; oils weathered for 3 hours.

Measurements were also made at 21 °C in order to examine the role of temperature. Spreading coefficients of oil on saline water increased for the higher temperature. Spreading coefficients of oil on fresh water, however, did not change with temperature in most cases. Only Hibernia crude on fresh water showed an increase of spreading coefficient with increasing temperature.

Viscosity:

AS Bohlin VOR rheometer was used to measure the dynamic viscosities. The apparatus consists of two co-axial cylinders. The outer cylinder rotates, thereby providing the required shear rate to the oil which fills the gap between the two cylinders. Measurements were taken for original

and weathered (over 3 hours) oil samples, using shear rates between 1 s^{-1} and 20 s^{-1}. Testing was done at constant temperature. Resulting viscosities were non-liner; they decreased with increasing shear rate. Figure 2 shows plots of viscosities for the three oil types versus shear rate at a temperature of 5 °C."

Method

"SLICK SPREADING

Experimental set-up and procedures:

The spreading experiments were conducted in a refrigerated circulating-current flume. The flume is constructed of steel plates and frames. The length and width of the flume are 4.73 m and 2.2 m, respectively. The maximum water depth is 0.24 m. The flume is longitudinally divided by a steel plate. A paddle wheel is mounted on one side to generate the water current. The paddle wheel is driven by an electric motor through an arrangement of gears and belts in order to reduce the rotation rates of the motor. Vanes are installed at each end of the flume to insure that water velocities are uniform across the test section. Velocity distributions across the test section of the flume were measured at two speeds of the paddle wheel. Baffles were placed between the vanes, and readjusted until velocities became as uniform as possible. The test section of the flume is 2.4 m long and 1.1 m wide. Three transparent windows, each 0.24 m by 0.24 m, are installed in the wall along the test section to provide a vertical view. A vertical screen was lowered at the end of the test section to support ice covers in place while permitting water flow and oil spreading to take place.

...

Ice was grown in a separate cold room at -10 °C. Ice sheet thicknesses were between 50 mm and 100 mm. Saline ice was grown from water of 12 ‰ salinity in a similar manner. The ice sheets were broken into blocks and placed in the test chamber for several hours prior to testing. This procedure ensured that the temperature of the ice blocks was equal to the ambient air temperature. Block shapes were irregular. Their dimensions varied between 50 mm and 150 mm. Commercial fresh water ice blocks of approximately cubical shapes were also used. Their dimensions were between 20 mm and 35 mm. Air temperature in the test cold room was kept at -2 °C during fresh water tests. Water temperatures were close to 0.5 °C. For saline ice tests, water of 30 ‰ salinity was used. During those tests, room temperature was -2.5 °C, and water temperature was -1.5 °C. When the ice blocks were placed in the test section of the flume, an ice cover with approximately uniform thickness formed. Spaces between the ice blocks at the surface were always covered with slush (i.e. no open water areas were present).

Oil samples were kept in the test cold room in order to maintain their temperatures close to the ambient air in the cold room. Volumes of spilled samples ranged from 0.5 litre to 3 litres. A list of all test parameters is given in Table 5. Oil samples were manually poured from a beaker, while attempting to maintain constant flow rate. Spreading of the oil slicks was monitored by a video camera, mounted vertically over the centre of the test section of the flume. Markers were placed along the sides of the test section for scale. The video records were used to determine the evolution of slick dimensions. Manual measurements were also taken at several time intervals during each test."

Table 5: List of test runs.

No.	Water Current (m/s)	Oil	Volume of oil sample (litre)	Ice block size	Water	Maximum length of slick (m)	Maximum width of slick (m)
1	0.35	Amauligak	0.5	Large	fresh	0.9	1.0
2	0.35	Amauligak	0.5	Large	fresh	0.8	0.89
3	0.35	Amauligak	1	Large	fresh	1.0	1.05
4	0.35	Amauligak	1	Large	fresh	0.7	1.0
5	0	Amauligak	1	Large	fresh	0.85	0.85
6	0.35	Amauligak	1	Large	fresh	0.9	0.9
7	0	Norman Wells	1	Large	fresh	1.2	1.0
8	0.35	Norman Wells	1	Large	fresh	1.2	1.0
9	0.55	Norman Wells	1	Large	fresh	0.7	1.0
10	0.35	Hibernia	1	Large	fresh	0.7	1.0
11	0.35	Amauligak	1	Small	fresh	0.8	1.0
12	0.35	Hibernia	1	Small	fresh	1.0	0.95
13	0	Hibernia	1	Small	fresh	0.85	0.85
14	0	Amauligak	1	Small	fresh	0.76	0.62
15	0.35	Norman Wells	1	Small	fresh	1.07	0.95
16	0	Hibernia	2	Small	fresh	1.36	1.0
17	0	Hibernia	0.5	Small	fresh	0.65	0.62
18	0	Hibernia	3	Small	fresh	0.9	0.85
19	0.35	Hibernia	2	Small	fresh	1.1	1.0
20	0	Hibernia	2	Small	fresh	1.0	0.95
21	0	Hibernia	1	Small	fresh	0.64	0.68
22	0	Hibernia	0.5	Small	fresh	0.5	0.48
23	0	Hibernia	3	Small	fresh	0.95	0.9
24	0	Norman Wells	1	Small	fresh	1.04	1.0
25	0.35	Amauligak	1	Large	fresh	0.80	0.87
26	0	Hibernia	1	Large	fresh	0.65	0.82

Table 5: List of test runs.

No.	Water Current (m/s)	Oil	Volume of oil sample (litre)	Ice block size	Water	Maximum length of slick (m)	Maximum width of slick (m)
27	0	Hibernia	2	Large	saline	1.18	1.0
28	0	Hibernia	0.5	Large	saline	0.7	0.57
29	0.35	Hibernia	2	Large	saline	1.27	1.0

Results

"Ice cover thickness profiles were mostly uniform, but were affected by water current in a few cases. The large ice blocks always had an average thickness of 100 mm, which was uniform for water currents of up to 0.35 m/s. At 0.55 m/s water current, blocks were dislodged from the upstream edge of the ice cover. Those blocks were carried downwards which resulted in a deeper keel immediately at the edge of the ice cover. The thickness of the ice cover was usually 150 mm at the upstream edge, and decreased to the uniform value of 100 mm after a horizontal distance of 0.5 m. The small ice blocks were used with water currents of up to 0.35 m/s. At that water current, the ice cover thickness was 85 mm at the upstream edge, and decreased to a uniform value between 35 mm and 45 mm after a horizontal distance of less than 0.5 m.

Visual observations:

Oil sticks spread on top of the ice covers during all tests. Slush always formed between the ice blocks, and thus isolated the oil from open water. The oil flowed over the apparently wet surface of the ice and slush. In all tests, a very thin layer of oil extended from the edges of the slick. Such "leading zones" were light coloured and meandered between the ice blocks. The oil formed droplets within those parts of a slick. The droplets would gradually grow and eventually coalesce, thereby spreading the stick further. This mechanism of stick spreading was observed under all test conditions. ...

Norman Wells crude had the largest "leading zone", while Hibernia had the smallest. Norman Wells crude has the lowest viscosity and gave the highest spreading coefficient values. Note that Hibernia crude has the highest viscosity and lowest spreading coefficient values. Oil type also appeared to influence oil coverage in the stick which is defined here as the ratio of oil covered area to the total area. Norman Wells crude appeared to give the lowest oil coverage, while Hibernia crude gave the highest.

The "leading zone" of a slick showed no dependence on the block size of the ice cover. It appeared to increase, however, when saline ice and water were used. Salinity decreased the spreading coefficients of oil on water, which evidently increased the size of the "leading zones". Still the manner in which the spreading coefficient affects the formation of the leading zones is not clear.

Slick Dimensions:

Slicks were approximately axisymmetric until the oil reached the side walls. This axisymmetric spreading covered the range of most tests, including those with water current. Slick shapes were irregular; in many instances far from circular. Spreading was anisotropic in some cases. The preferred direction of spreading in such cases appeared to have random orientations. The irregularity of slick shapes and anisotropy of spreading may be attributed to the relatively large ice block sizes compared to the dimensions of the slicks.

Edges of the slicks were difficult to define because of the "leading zone" which preceded the slick as mentioned above. It was decided to define the edge of a slick as that corresponding to the furthest point (along the length or the width of the flume) reached by the dark, thicker oil. This definition ignores the light coloured thin "leading zone". The records begin 30 s after the start of spilling, and continue for approximately 2.5 hours (9000 s). Most of the spreading took place over the first 100 s to 500 s. Afterwards, spreading rates dropped, and the slicks appeared to approach their maximum dimensions. The following factors should be considered in interpreting the results:

- The relatively high water current of 0.55 m/s deformed the upstream edge of the ice cover. The water current also compressed the ice cover along the direction of the flume's length.
- The slick's width was larger than the length in some cases. A water current of 0.35 m/s apparently compressed the ice cover in a few cases, and thus increased the spreading in the direction of the flume's width. Anisotropy of the ice covers could have also contributed to producing larger widths.
- Several tests were repeated under similar conditions in order to examine reproducibility of the results. Variations in measured slick dimensions were usually within 0.25 m. The variations are most probably the result of differences in ice covers, which are difficult to reconstruct with exactly the same details.

To summarize the results, the final slick dimensions are listed in Table 5. Oil coverage and thickness were estimated at the end of a few tests, and are listed in Table 6. They appeared to depend on ice cover type and oil type. Therefore, these estimates, which are time consuming to do manually, were not repeated for all tests. The range of oil thicknesses agrees with other observations (Ross and Dickens, 1987, and Sayed and Løset, 1993). Hibernia crude gave the largest thicknesses, while Norman Wells crude gave the lowest."

Table 6: Oil coverage and thickness.

Test No.	Oil coverage (%)	Oil thickness (mm)
5	51	2.7
6	44	2.8
14	64	3.3
21	75	3.0
24	66	1.5
26	43	4.4
27	26	6.5

"Slick length is plotted versus time in Figures 5 to 8. Those plots compare slick dimensions for tests done using similar conditions except for oil type. Those figures correspond to an oil volume of 1 litre. Each figure, however, represent a different set of values of water current (0 m/s and 0.35 m/s), and ice block sizes (large or small). The comparisons show that Norman Wells crude corresponds to the largest slick dimensions, followed by Amautigak crude, and finally Hibernia crude yielded the smallest slick dimensions. Norman Wells crude also has the highest spreading coefficient and lowest viscosity, while Hibernia crude has the lowest spreading coefficient and highest viscosity. This indicates that slick size increases with increasing spreading coefficient, and decreasing viscosity. It is difficult to determine the separate roles of spreading coefficient and viscosity from the present tests. Nonetheless, it is likely that spreading coefficient is the oil property which determines the maximum size of a slick, since viscosity would only act when there is a velocity gradient in the oil. This argument agrees with the results of Sayed and Løset (1993) which

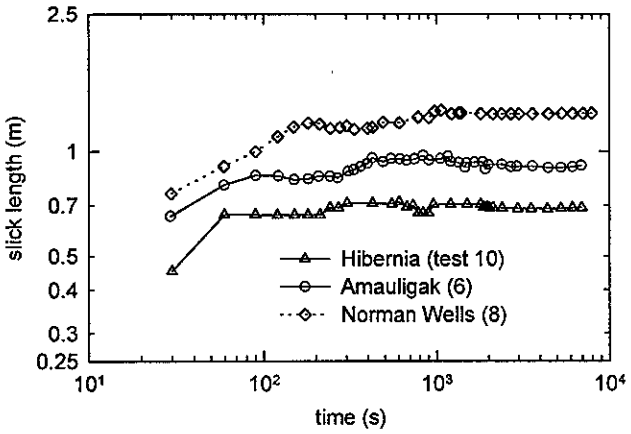

Figure 5: Slick length for different oil types; water current = 0.35 m/s, oil volume = 1 litre, ice cover: large fresh water ice blocks.

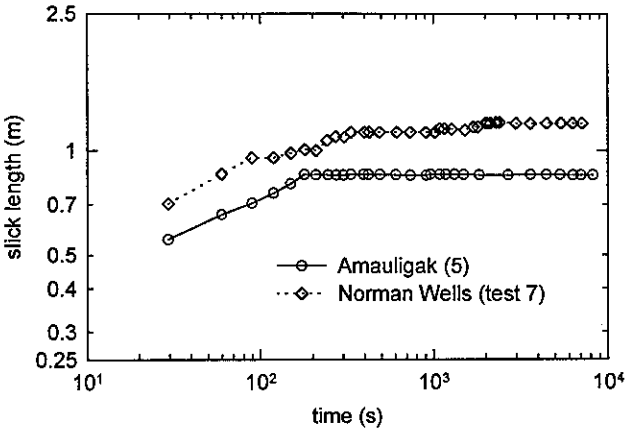

Figure 6: Slick lengths for different oil types; water current = 0 m/s, oil volume = 1 litre, ice cover: large fresh water ice blocks.

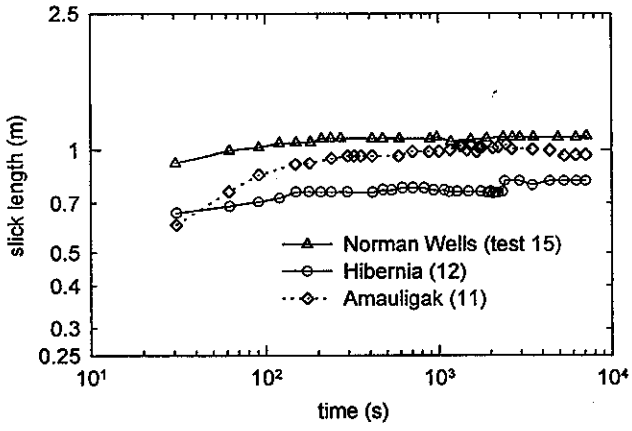

Figure 7: Slick lengths for different oil types; water current = 0.35 m/s, oil volume = 1 litre, ice cover: small fresh water ice blocks.

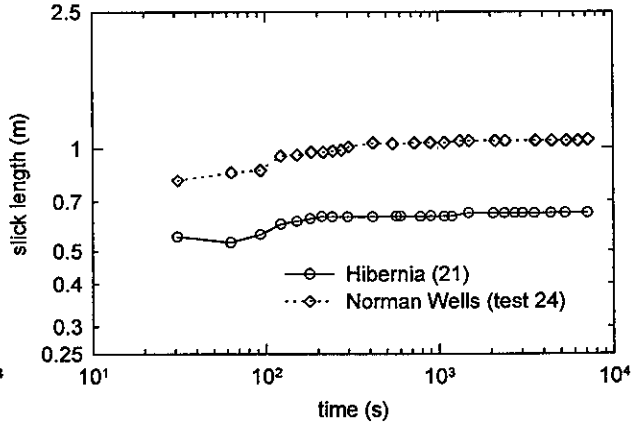

Figure 8: Slick lengths for different oil types; water current = 0 m/s, oil volume = 1 litre, ice cover : small fresh water ice blocks.

have shown that surface tension, not viscosity, determines the final dimensions of oil slicks."

'Comparisons between test results which examine the roles of ice cover type (ice block sizes) are shown in Figures 9 to 11. The comparisons show that stick dimensions are to close to detect any changes. Figure 12 shows a comparison between slick sizes on saline and fresh water ice covers. Slicks on saline ice covers have slightly larger dimensions than those on fresh water ice covers (note that spreading coefficients of oil on saline water are lower than those on fresh

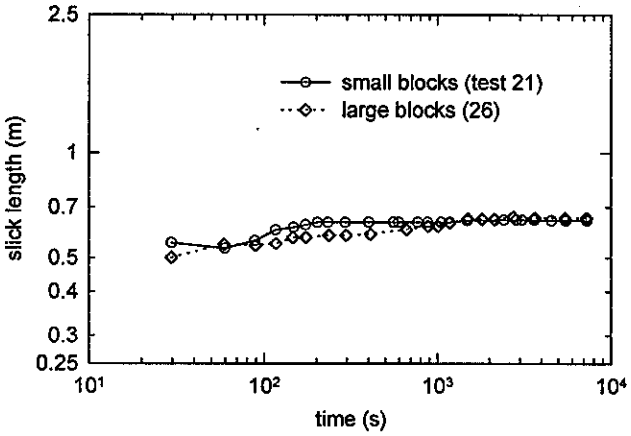

Figure 9: Slick lengths for different ice cover types; water current = 0 m/s, oil: 1 litre Hibernia crude, fresh water ice cover.

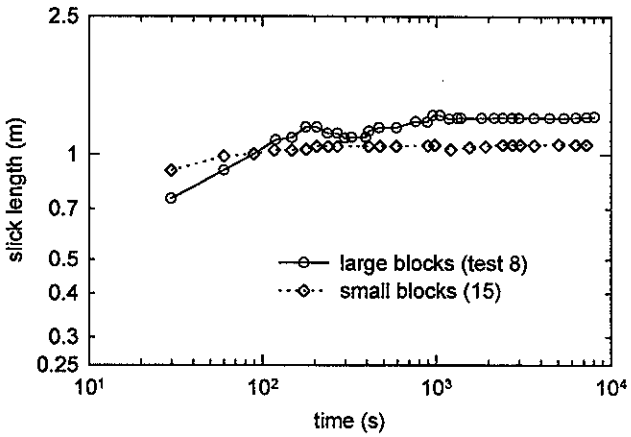

Figure 10: Slick lengths for different ice cover types; water current = 0.35 m/s, oil: 1 litre Norman Wells crude, fresh water ice.

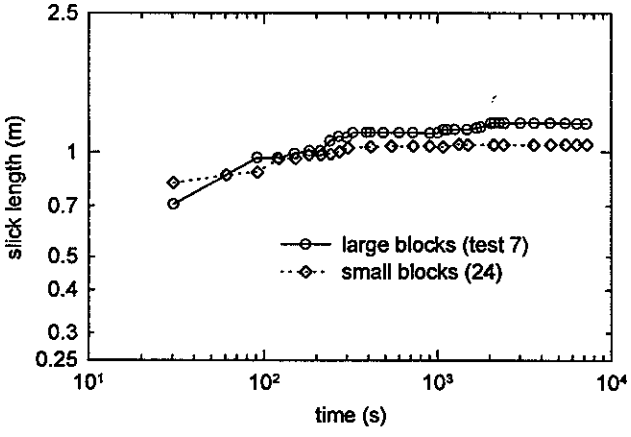

Figure 11: Slick lengths for different ice cover types; water current = 0 m/s, oil: 1 litre Norman Wells crude, fresh water ice cover.

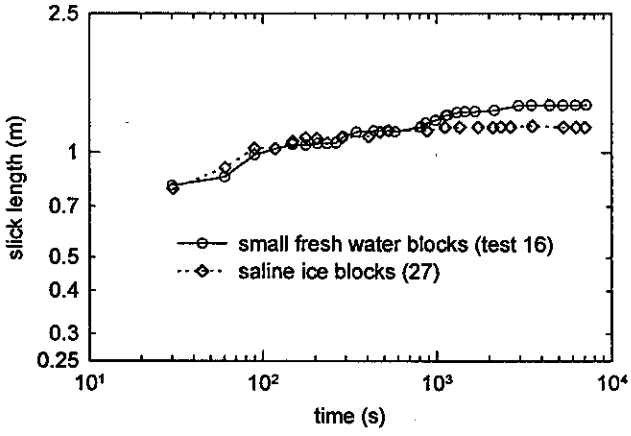

Figure 12: Slick lengths for different ice cover types; water current = 0 m/s, oil: 2 litres Hibernia crude.

water). This result is a further indication of the increase of slick size with increasing spreading coefficient.

Slicks from tests done using different values of water current are compared in Figure 13. Several such comparisons showed that water current had negligible effect on slick dimensions. At first however, this result may be somewhat surprising. It may be explained, however, as follows. In all tests, slush filled the spaces between the ice blocks. There were no open water areas within the ice cover. Oil simply flowed over the ice/slush mixture. Thus, slicks were isolated by the water current, which did not affect oil spreading.'

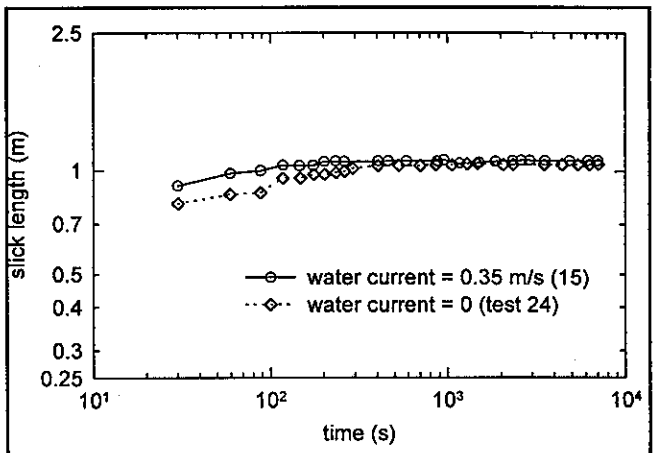

Figure 13: Slick lengths for different values of water current; oil: 2 litres Hibernia crude, small fresh water ice blocks.

"Tests done using various oil volumes are compared in Figures 14 and 15. There is a clear increase of slick dimensions when volumes increase from 0.5 litre to 2 litres. In that range, slick length was proportional to the square root of oil volume. Larger spill volumes of 3 litres (Tests 18

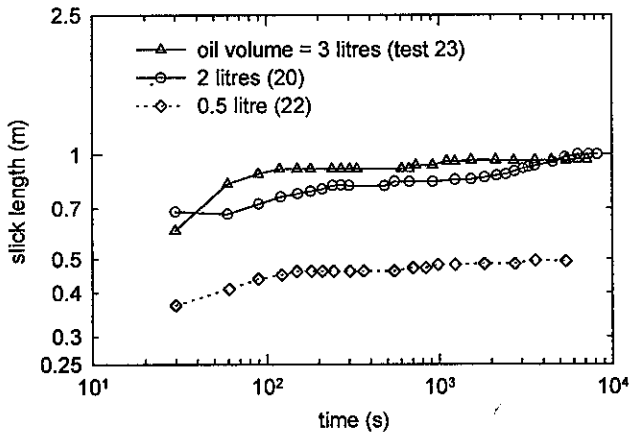

Figure 14: Slick lengths for different oil volumes; water current = 0 m/s, Hibernia crude, small fresh water ice blocks.

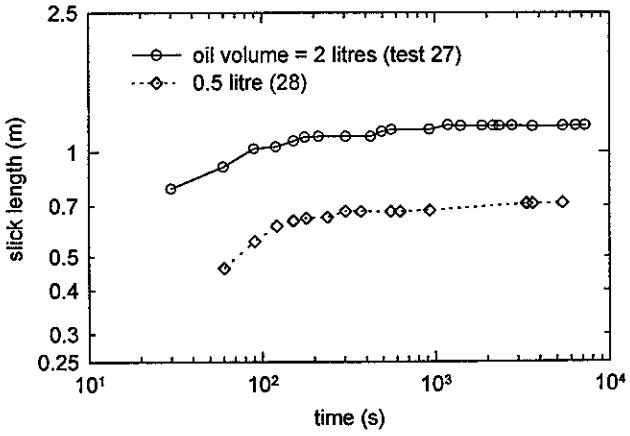

Figure 15: Slick lengths for different oil volumes; water current = 0 m/s, Hibernia crude, saline ice blocks.

and 23), however, did not correspond to appreciably larger dimensions. In the 3 litre volume tests, oil penetrated the ice cover to larger depths during the early stages of spreading. This behaviour occurred in spite of the care taken in pouring the oil close to the ice surface. It is probably the weight of the oil which caused it to reach deeper inside the ice cover compared to smaller oil volumes.

The preceding data was presented in a dimensional form for clarity. Previous studies (Yapa and Belaskas 1993, and Sayed and Løset 1993) used nondimensional groups based on assuming oils' viscosities to be Newtonian, and using oils' surface tension (instead of spreading coefficients).

Those assumptions, however, do not agree with the present results which indicate that oil properties spreading behaviour can be much more complex. Therefore, it was decided to present the data without nondimensionalization, although that may be inconvenient for comparison with other experiments. Further analysis of the data is required in order to develop formulas that describe spreading rates and the maximum extent of a spill."

BOSS Critique

Errors for surface and interfacial tensions are not discussed by the authors and these errors will determine the accuracy and reproducibility of the spreading coefficient, $\gamma_{o/w}$. The authors use this parameter to determine the extent of the oil spill and therefore errors must be included in the discussion of the values in order to determine how useful this parameter will be in full scale spills. The authors also failed to explain the reasons they had for determining spreading coefficients at 1 °C while the viscosities were measured at 5 °C.

The authors have made an important distinction between two types of "leading zones". The lighter coloured "leading zone" may be as important as the darker "leading zone" in determining the spreading of oil spilled in brash, or other types of, ice cover. It would be prudent to identify the carbon groups in these different "leading zones" and hopefully the authors will do this in future experiments.

The authors have also pointed out an important fact that the theory before this use viscosities that are Newtonian and the measured viscosities and other results in this paper indicate that the oils act in a non-Newtonian fashion. This distinction should be explored further and tied into the nonlinear behaviour of ice and water.

Review of a manuscript by, Puskas, J.K., and E.A. McBean, entitled "The Transport of Crude Oil Under Saline Ice", in *Proceedings of the Fourth International Conference on Cold Region Engineering*, American Society of Civil Engineers, New York, pp 670-684, 1986.

Technical Summary

"A mathematical model was developed to describe the forces acting on an oil slick under saline ice in the presence of water current. The model was verified through a set of laboratory experiments conducted in a recirculating flume located in an "ice room" facility. The results were also compared to similar experiments conducted under fresh water ice. It was found that oil slicks moving under saline ice experience an increase in frictional resistance due to the small scale roughness of the ice undersurface. The friction force can be approximated by assuming "no-slip" at the oil-ice interface and a linear velocity distribution in the slick."

Objective

The authors developed a mathematical model and a set of experiments to test the effect of resistance (of the ice surface) to the movement of an oil slick under the ice.

Theory

"An oil slick moving under ice in the presence of a water current is acted upon by three external forces:

1. Oil-ice friction force;
2. Shear force at the oil-water interface; and,
3. Form drag force,

as per Figure 1.

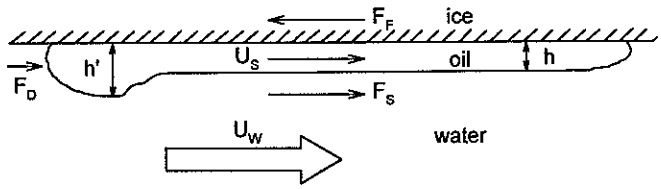

Figure 1. Forces Acting on a Moving Oil Slick Under Ice.

Oil-Ice Friction Force

Through an extensive set of experiments, Malcolm and Dutton, 1979, determined that the contact angle for an oil drop under smooth ice is always 180 degrees. This means that an oil slick is separated from the ice by a thin film of water. Malcolm and Dutton estimated the thickness of this water film to be less than 5×10^{-6} m.

The existence of this water film plays an important role in the friction force exerted on a moving oil slick under smooth ice. Puskas (1985) found that oils with high viscosities slid along the ice sheet almost as a solid mass, with the majority of the velocity variation taking place within the water film. However, for oils with low viscosities, the friction force could be modeled by assuming

no slip at the oil-ice interface.

With small scale roughness, such as found under saline ice, the role of the thin water film is reduced. The magnitude of the individual roughness elements are larger than the expected thickness of the water film and will tend to retard the velocity of the oil at the interface.

Therefore, the no-slip approximation should be applicable to both oils with high and low viscosities. As a result, the presence of small scale roughness will have a greater effect on oils with higher viscosities.

Assuming no-slip at the oil-ice interface and a linear velocity distribution in the oil, the stress at the interface can be expressed as

$$\tau = 2\mu_o \frac{u_s}{h} \tag{1}$$

where μ_o is the viscosity of the oil. u_s is the mean velocity and h is the thickness of the oil slick.

The magnitude of the friction force is then given by

$$F_F = 2\ell w \mu_o \frac{u_s}{h} \tag{2}$$

where ℓ and w represent the respective length and width of the oil slick.

Shear Stress at the Oil-Water Interface

The shear stress F_s at the oil-water interface can be treated in a manner similar to flow over a flat plate (as per Schlichting, 1955) as

$$F_s = \frac{1}{2} C_s \rho_w u^2 \ell w \tag{3}$$

where C_s is the shear stress coefficient , ρ_w is the density of the water and u is the related water velocity between free stream and the interface.

From Schlichting (1955), C_s is

$$C_s = 0.074 R_\ell^{-1/5} \tag{4}$$

where R_ℓ is the Reynolds number based on the length of the slick

$$R_\ell = \frac{u \ell \rho_w}{\mu_w} \tag{5}$$

Form Drag Force

When the water impinges on the trailing edge of the moving slick, its loss of momentum results in a thickening of the oil slick, as illustrated in Figure 1. This agrees with the findings of Wilkinson (1972) for oil slicks trapped upstream of a fixed barrier.

The magnitude of the form drag force can be expressed as

$$F_D = C_D \rho_w (u_w - u_s)^2 wh' \tag{6}$$

where wh' is the thickness of slick's "head" region, and C_D is the coefficient of drag."

Method

"Recirculating Flume

The experiments were conducted in a 50 cm x 61 cm x 670 cm recirculating flume, illustrated in Figure 2, which is located in a "walk-in" freezer. The sides of the flume were insulated to permit freezing of the water from the surface only.

Water Velocity Measurements

Velocity profiles in the flume were measured by a visualization technique which utilizes the electrolysis of water to produce rows of hydrogen bubbles that act as tracers. A length of 0.0025 cm diameter platinum wire with 13% Rhodium serves as the cathode in the electrolytic process. The wire was placed in the flow field and supplied with a pulsing voltage to produce the hydrogen bubbles. The hydrogen bubbles were then photographed and the velocities determined by knowing the time between pulses and measuring the distances between the bubble rows. A detailed description of this apparatus is given by Puskas (1985).

Experimental Procedures

A salinity of 30 ppt (parts per thousand) was used, representative of water in the Beaufort Sea. The density of the water at T = -1.0 °C was found to be 1025 kg/m^3.

Once the ice cover had acquired a thickness of approximately 5 cm, a length of styrofoam insulation was placed down the middle of the flume. The ice cover was allowed to continue growing and develop a slight curvature transverse to the flow direction. This slight curvature was required to ensure the oil would be transported down the centre of the flume.

Holes were made in the ice at both ends of the flume to permit release and removal of the oil. A boom was placed across the flume at the downstream hole to capture the oil.

Prior to each oil release, photographs of the flow field were taken with the velocity measuring apparatus in operation. Photographs were also taken as the oil passed the velocity measuring station to be used in determining the oil slick thickness.

Times were recorded as the oil slick passed prescribed locations along the flume. The slick length and width were measured directly from the surface as the oil could be observed through the ice.

Flow conditions in the flume were varied by using different water depths. The water velocities used in this study ranged from 10 cm/s to 18 cm/s."

Results

..."Measurements taken from the photographs allowed determination of the resulting velocities versus distance from the ice. A typical plot is given in Figure 4. Due to the turbulence in the water and measuring error within the boundary layer, uncertainty exists in the velocity profile close to the ice. However, the free stream velocities were consistent.

Properties of the Oils

The important physical properties which affect the transport of oil under ice are considered

to be the density, viscosity, surface tension and contact angle.

The thickness of large oil drops under smooth ice in ambient conditions is given by Malcolm and Cammaert (1981):

$$h = 2\ (\sigma/(\rho_w - \rho_o))^{1/2} \qquad (7)$$

where σ is the interfacial surface tension. This expression was determined assuming the contact angle between the oil and ice was 180 degrees. The effect of the surface roughness of saline ice on the contact angle is unknown. Puskas (1985) found that the thickness of oil slicks moving under smooth ice do not always adopt the equilibrium thickness provided by Equation 7 with the result that measurements of surface tension and contact angle were not attempted.

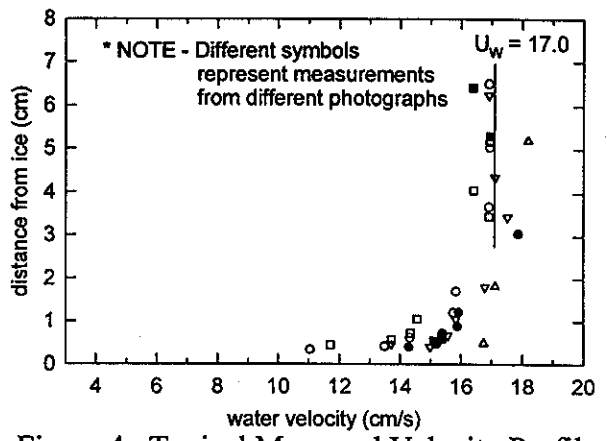

Figure 4. Typical Measured Velocity Profile Under Ice.

The density and viscosity of the oil samples used in this study are presented in Table 1.

Table 1: Table of Oil Properties at T = 1.0 °C.

Oil Type	Density (kg/m)	Viscosity (c)
Norman Wells	844	13.7
Adgo	960	209.0
Itiyok	938	368.5

From photographs of the saline ice cover, it was observed that both the amplitude and spacing of the roughness are approximately equal to 0.5 mm.

Ice Roughness

To extend the applicability of the laboratory results, the roughness of the saline ice cover used in the experiments must be quantified, although this is a difficult exercise.

In the development of Equation 2, it was assumed that the ice roughness was sufficiently large to eliminate the effect of the thin water film separating the oil and ice. For this assumption to be valid, the roughness elements must be larger than the thickness of the water film. On the other hand, for the assumption of a one-dimensional linear velocity distribution in the oil slick, the roughness must not be an appreciable portion of the oil slick thickness. A check of the estimated roughness (0.5 mm) to water film thickness (5×10^{-7} m), and oil slick thickness (1.0 cm) ratios are 1,000 and 0.05 respectively.

Although the limits of application as presented above are not completely definitive, the roughness of the ice used in this study appears to satisfy the criteria for validity of Equation 2. As a fairly broad range of roughnesses will satisfy these criteria, and therefore be expected to present similar resistance, more accurate determination of individual roughness elements is not warranted.

Test Results

Similar to the behavior noted under smooth ice (after Puskas, 1985), the heavier oils were observed to orient themselves transverse to the direction of the water flow in short, wide slicks, while the light oil tended to form a long narrow slick, oriented longitudinally in the flow direction. However, on three occasions, both heavy oils formed long, narrow slicks. This probably resulted from the curvature of the ice under surface. In the absence of such curvature, the heavy oils can be expected to form short, wide slicks.

In contrast to the results for slicks under smooth ice (Puskas, 1985), it was observed that the light oil was transported at a higher velocity than the heavy oils under the same flow conditions. This is expected from the theoretical analysis where the presence of small scale roughness has a greater effect on the movement of the more viscous oils.

For comparison with slicks under smooth ice, the mean slick velocities measured by Puskas (1985) and those from this study were plotted against the free stream water velocity for the three oils in Figures 5 to 7. In addition, the results for the 4E oil (from Cox (1980)) are also plotted in Figures 5 and 6.

From Figures 5 and 6, several observations are noteworthy. Initially, it is noted that the presence of the small scale roughness greatly reduces the velocity at which the slick is transported. Also, where the orientation of the slick had a major effect on the slick velocity under smooth ice, its effect is reduced for rough ice.

The results for the 4E oil (Cox, 1980) closely approximate those for the Adgo oil. The density of the 4E oil (912 kg/m^3) is closer to that of the Itiyok sample, yet its viscosity (120 cp.) is closer to the value for Adgo. Therefore, it seems that the viscosity plays a more important role for oils with physical properties in this range.

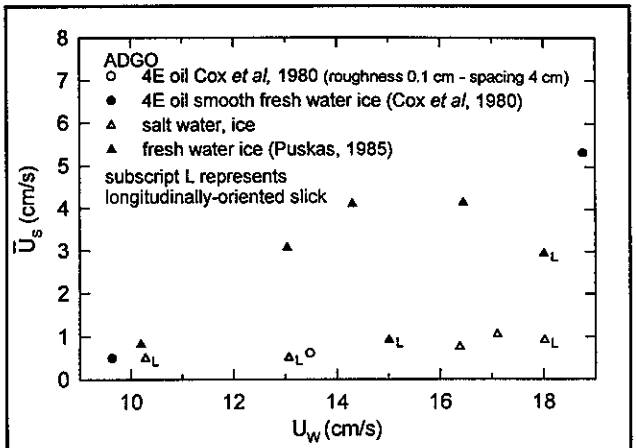

Figure 5. Plot of Slick Velocity Versus Water Velocity - Adgo Oil.

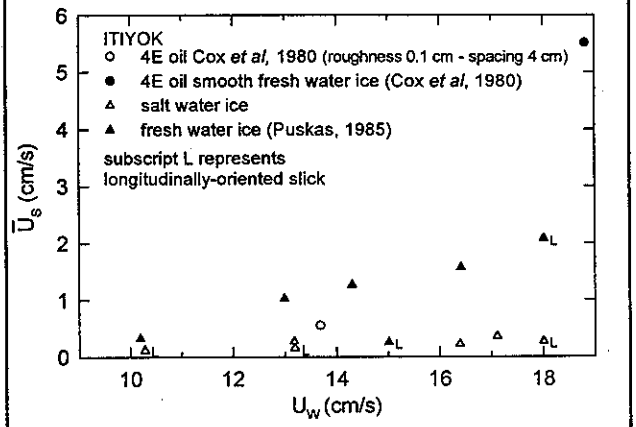

Figure 6. Plot of Slick Velocity Versus Water Velocity - Itiyok Oil.

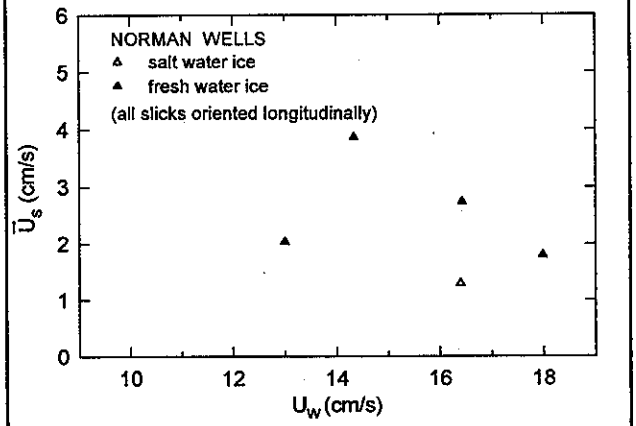

Figure 7. Plot of Slick Velocity Versus Water Velocity - Norman Wells.

However, it is also noted that the nature of the roughness was different in the two studies.

The results for Norman Wells oil in Figure 7 appear to be somewhat inconsistent. This is probably the result of the susceptibility of the light oils to small changes in the ice under surface. Due to its high buoyancy, small changes in ice thickness dominate the transport of light oils where the heavy oils move over these variations unaffected.

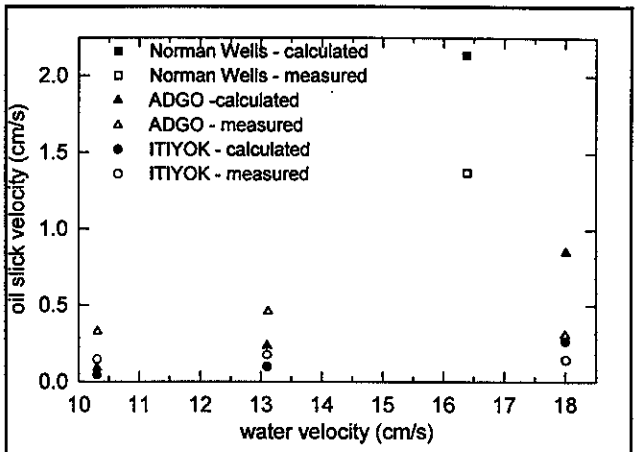

Figure 8. Plot of Measured and Calculated Slick Velocities Versus Water Velocity for Longitudinally Oriented Oil Slicks.

Quantitative Results

For slicks oriented longitudinally in the direction of the water flow, the dominant force is the shear force at the oil-water interface which is balanced by an equal friction force at the oil-ice interface. Although the heavy oils do not normally form long narrow slicks, the analyses of the heavy oil slicks in this configuration allows for verification of the expression for the friction force as described in Equation 3.

By equating Equations 2 and 3, and substituting Equation 4 for the shear stress coefficient, the following expression results:

$$u_s = 0.0185 \frac{h \rho_w}{\mu_o} R_t^{-1/5} (u_w - 2u_s)^2 \qquad (9)$$

From the free stream water velocity and the dimensions of the oil slick, the mean slick velocity can be calculated from Equation 9. The results for the longitudinally oriented oil slicks are presented in Table 2 and Figure 8. Included in the results are two test runs in which measurements for oil slick thickness and free stream water velocities were not obtained and had to be estimated.

Table 2: Results for Longitudinally Oriented Oil Slicks Under Salt water Ice.

Oil	Test #	Length ℓ (cm)	Width w (cm)	Thickness h (cm)	Free stream water velocity U_W (cm/s)	Measure slick velocity $U_{S_{meas}}$	Calculated slick velocity $U_{S_{calc}}$
ADGO	1A	50	27.5	1.30	13.1	0.45	0.21
ITIYOK	1I	75	22	1.10	13.1	0.19	0.095
Norman Wells	2NW	120	10	1.0	16.4	1.33	2.14
ADGO	4A	87	20	0.98	10.3	0.321	0.10
ITIYOK	4I	105	15	0.95	10.3	0.14	0.056
ADGO	5A	65	20	1.0*	18*	0.84	0.30
ITIYOK	5I	110	15	1.0*	18*	0.28	0.16

* estimated values (no measurements obtained because of equipment difficulties)

From these results, it is apparent that Equation 9 underestimates the mean slick velocity in all cases except for the Norman Wells Slick. This discrepancy may result from some "slipping" taking place at the oil-ice interface. However, Equation 9 does give order-of-magnitude estimates which agree favorably with the measured slick velocities.

For oil slicks oriented transverse to the water current. the primary driving force is the form drag force. When the water flows over the edge of the oil slick "head" region, the boundary layer separates from the slick and re-attaches a distance downstream. Experimental observations of Plate (1964) for flow over a fence on a flat plate concluded that the separated boundary layer will re-attach to the wall about 50 disturbance heights downstream. In this analysis, the point of re-attachment was assumed to be 50 times the difference between the thickness of the "head" region and the thickness of the remainder of the slick. Hence, the shear force was calculated by applying Equation 3 from this point to the end of the slick.

The friction force for slicks oriented transverse to the water flow was determined in the same manner as for the longitudinally-oriented slicks, by applying Equation 2. The drag force was then determined by subtracting the shear force from the friction force and the coefficient of drag, calculated from Equation 6. These results are presented in Table 3.

Table 3: Results for Transverse Oriented Oil Slicks Under Salt water Ice.

Oil	Test #	Length ℓ (cm)	Width w (cm)	Thickness h (cm)	Head Thickness h' (cm)	Free stream water velocity U_W (cm/s)	Slick velocity U_S (cm/s)	Friction Force F_F ($Nx10^2$)	Shear Force F_F ($Nx10^2$)	Drag Co-efficient C_D
ADGO	2A(a)	20	42	1.23	1.80	16.4	0.77	2.20	0	0.12
ADGO	2A(b)	30	40	1.41	2.15	16.4	0.74	1.76	0	0.08
ITIYOK	2I	35	43	0.86	0.98	16.4	0.26	3.35	1.54	0.16
ADGO	3A	35	35	1.10	1.38	17.1	0.98	4.56	0.90	0.28
ITIYOK	3I	38	30	0.83	2.14	17.1	0.35	3.54	0	0.19

From the results in Table 3 it is noted that this model gives reasonable estimates for the coefficient of drag. The main source of error probably results from the measurement of the thickness of the head region. This dimension was determined from photographs taken as the oil slick passed over the velocity-measuring station. Hence, this measurement represents the thickness of the head region midway across the width of the slick, at one instant in time. Such a measurement may not represent the average thickness of the head region over the entire experiment.

Also, Equation 2 overestimates the friction force for transverse oriented oil slicks as it applies only downstream of the head region. As the head region is typically 4 to 5 cm in length, this has a greater effect on the shorter slicks."

BOSS Critique

The authors do not describe the quantitative errors associated with the measurements performed in the recirculating flume. The errors for measurements performed on the photographs are not discussed.

The authors stated that the surface tension and contact angle (of the oil and ice) were important parameters but that they were too difficult to measure. The authors should then explain the what effect the lack of contact angle and surface tension parameters have on the interpretation of the experimental results and the limits this has on applying these results to a full scale spill.

Review of a manuscript by, Puskas, J.K., E.A. McBean, and N. Kouwen, entitled "Behaviour and Transport of Oil Under Smooth Ice", in *Canadian Journal of Civil Engineering*, 14, pp 510-518, 1987.

Technical Summary

"Mathematical and physical models are used in studying transport of oil slicks beneath ice in the presence of an ambient water current. The mathematical expressions for the relevant forces are developed by utilizing basic boundary layer theory and considering the physical properties of the oils and are verified from the laboratory experiments. Three different crude oils are utilized beneath freshwater ice under various flow conditions in the experiments.

The transport of oil slicks oriented longitudinally to the direction of the water flow are modelled by the summation of the shear force at the oil-water interface and the oil-ice friction force. Oil slicks oriented transverse to the direction of the water flow are subjected to an additional form-drag force acting as the primary force.

For oils with low viscosities, the oil-ice friction force can be approximately by assuming "no-slip" at the oil-ice interface. Oils with high viscosities move almost as a solid mass, with the majority of the velocity variation taking place in a thin water film separating the oil and the ice."

Objective

The authors developed a mathematical model and a set of experiments to test the effect of water current on the movement of an oil slick under the ice.

Theory

"Uzuner *et al.*(1979) conducted a series of laboratory experiments studying the transport of oil under smooth freshwater ice in the presence of a water current. Uzuner's analysis treated the transport of an oil slick under ice as a result of the summation of three forces (see Figure 1):

1. Form drag, F_D:

[1] $$F_D = \frac{1}{2} C_D \rho_w (\bar{U}_w - U_s)^2 wh$$

2. Shear force at oil-water interface, F_S:

[2] $$F_S = \frac{1}{2} C_S \rho_w (\bar{U}_w - U_s)^2 A$$

3. Ice-oil interfacial friction, F_F:

[3] $$F_F = C_F (\rho_w - \rho_o) gAh$$

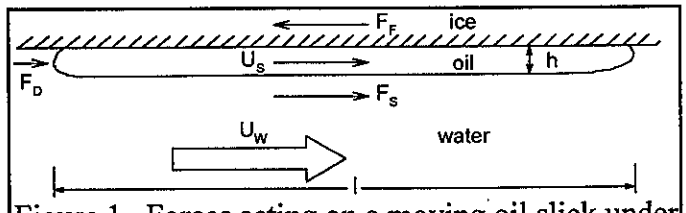

Figure 1. Forces acting on a moving oil slick under ice.

where U_S and $\bar{U}_w$ are mean oil slick and water velocities, C_D, C_S, and C_F are drag, shear, and friction coefficients. ρ_o and ρ_w are the densities of the oil and water, h is the thickness of the oil slick, and A is the plane area of the oil slick given by length x width.

...

Cox *et al.* (1980) conducted an intensive investigation to determine the transport and behaviour of oil spilled under ice. For smooth ice. Cox's theoretical formulation closely followed

that of Uzuner *et al.*, but allowed the interfacial shear stress coefficient to vary inversely with $\bar{U}_w^2$.

...

Both the Uzuner *et al.* and Cox *et al.* analyses have the same deficiency: all coefficients are lumped into one or two parameters, which are estimated by regression techniques. This method gives no insight into the actual nature of the forces involved, nor does it confirm the forces are correctly represented in the mathematical model. The mean water velocity does not appear to be the correct parameter to use in the force equation, as the oil slick is located in a region of reduced flow within the water's boundary layer. In the laboratory, the validity of using the mean water velocity is questionable as it is dependent on both the geometry and hydraulic roughness of the flume. In addition, Uzuner *et al.* and Cox *et al.* both ignored potentially important physical properties of the oils such as interfacial surface tension and viscosity. Therefore, there is concern with applicability of these results for conditions outside the laboratory.

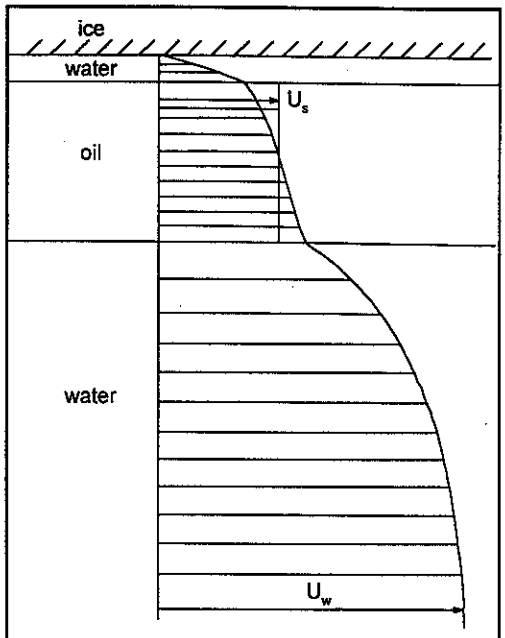

Figure 2. Velocity distribution in moving oil slick system.

Oil-ice friction

Malcolm and Dutton (1979) found the oil-water-ice contact angle to be 180 degrees, meaning that a thin layer of water separates the oil from the ice. Using this fact, a velocity profile through a moving oil slick can be expected to exist, as shown in Figure 2. The thickness of the intervening film of water between the oil and ice is expected to be less than 5×10^{-7} m (Malcolm and Dutton 1979). Therefore, it is reasonable to assume laminar flow and a linear velocity distribution in the water film.

Uzuner *et al.* (1979) and Cox *et al.* (1980) assumed the velocity within the oil slick to be constant. The degree to which the actual distribution differs from this assumption will depend on the viscosity of the oil. Oils with high viscosities will tend toward uniform velocity distribution and move as solid masses. In the analyses to follow, the flow in the oil slick is assumed to be laminar and have a linear velocity distribution, as illustrated in Figure 3.

From Newton's law of friction,

$$[4] \quad \tau = \mu_w \frac{U_2}{\lambda} = \mu_o \frac{(U_1 - U_2)}{h}$$

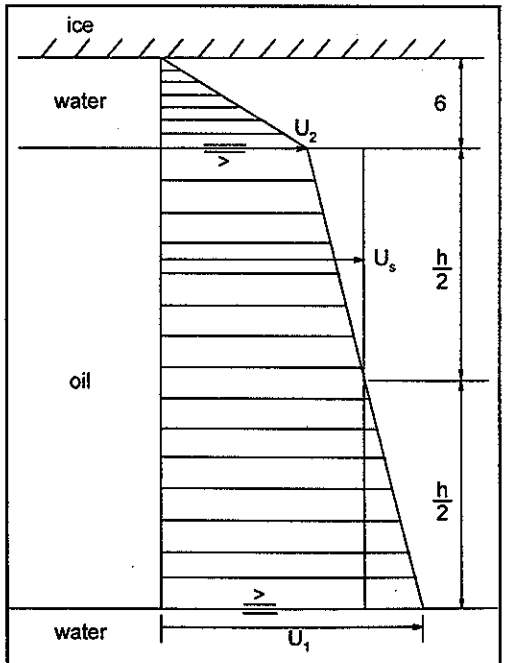

Figure 3. Assumed linear velocity distribution in oil slick and water film.

where τ is the stress at the oil-water film interface, U_2 is the velocity at the oil-water film interface, U_1 is the velocity at the oil-ambient water interface, μ_w and μ_o are the dynamic viscosities of the water and oil respectively, λ and h are the thicknesses of the water film and oil slick respectively. The mean velocity of the oil slick is equal to

$$[5] \quad U_S = U_2 - \frac{(U_1 - U_2)}{2}$$

For oils with low viscosities, U_2 can be set to zero, as the thickness of the water film is expected to be very small. This is the same as assuming "no-slip" at the oil-ice interface and [4] can be written as

$$[6] \quad \tau = 2 \frac{\mu_o}{h} U_S$$

Utilizing this assumption, the total friction drag on a moving oil slick can be expressed as

$$[7] \quad F_F = 2 \frac{\mu_o}{h} U_S A$$

where A is the plane area of the oil slick given by ℓ x w. However, [7] may be inadequate for oils with high viscosities. Oils with higher viscosities are expected to move almost as solid masses and therefore a more significant velocity variation is expected over the thin water film separating the oil and the ice.

Shear force

A common means of expressing shear drag is

$$[8] \quad F_S = \frac{1}{2} C_S \rho_w U^2 A$$

where U is the relative velocity $(U_w - U_1)$.

...

Since the Froude numbers for the oil-water systems to be studied in this research fall into this range," (0.03 to 0.8) "it is assumed that the shear stress coefficient is a function of Reynolds number only.

An approximate solution for the shear stress can be obtained from the momentum equation. Assuming $\partial p/\partial x = 0$ and following the procedure of Schlichting (1955), the shear stress coefficient, C_S, is given as

$$[9] \quad C_s = 0.074 (R_1)^{-1/5}$$

for a turbulent boundary layer and

$$[10] \quad C_s = 1.328 (R_1)^{-1/2}$$

for a laminar boundary layer where R_1 is the Reynolds number based on the length of the oil slick and the relative motion:

$$[11] \quad R_1 = \frac{U \ell}{\nu_w} = \frac{(U_w - U_1) \ell}{\nu_w}$$

Equation [9] is generally applicable for values of R_1 greater than 5×10^5.

Form Drag

The trailing edge of a moving oil slick under ice is very similar to the frontal region of an oil slick trapped upstream of a fixed barrier in free surface conditions as described by Wilkinson (1972). The edge is rounded and interfacial waves can be observed immediately behind (as illustrated in Figure 4).

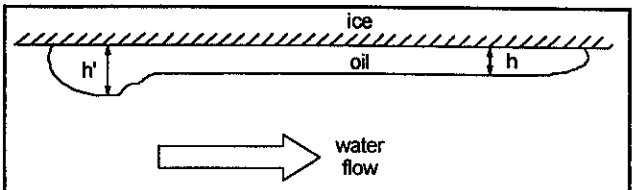

Figure 4. Frontal region of a moving oil slick.

The form drag force can be expressed as

[12] $F_D = C_D \rho_w (U_w - U_s)^2 wh'$

where h' is the thickness of the slick in the "head" region, C_D is the coefficient of drag, which is assumed to be a function of h'/δ, and δ is the water boundary layer thickness. The function for C_D must be determined experimentally.

Given the form of [7], [8], and [12], the model can only be verified by comparison with laboratory or *in situ* field data. The only data available are those of Uzuner *et al.* (1979) and Cox *et al.* (1980). However, Uzuner *et al.* (1979) and Cox *et al.* (1980) only report the average flow velocities for their experiments, whereas [7], [8], and [12] are based in the free-stream velocity. Therefore, it was deemed necessary to conduct a set of experiments to test the mathematical model."

Method

"*Cold room*

The experiments were conducted in a "walk-in" freezer with interior dimensions of 1.4 m in width, 2.2 m in height, and 6.9 m in length. The refrigeration system maintained a temperature of -10 ± 2 °C during experiments, with temperatures dropping as low as -25 °C during ice formation.

Recirculating Flume

The experiments were carried out in a 58 cm x 61 cm x 670 cm recirculating flume, schematically depicted in Figure 5, located inside the walk-in freezer. The sides and bottom are insulated with 5 cm thick styrofoam to permit freezing of the water from the surface only.

The flume is fitted with three 31 x 92 cm Plexiglas viewing windows—two along one of the sides and one in the bottom. These windows were covered with 5 cm thick styrofoam insulation during ice formation.

A 2 hp Baldor all-bronze centrifugal pump, located outside the freezer, recirculates water through the flume. The 7.5 cm ABS pipe, also located outside the freezer, is insulated with 1.25 cm thick foam rubber insulation.

Flow velocities were varied from 10 to 18 cm/s by using different water depths. To achieve higher flow velocities and at the same time maintain a submerged inlet and outlet, a working section with a "false bottom" was employed. This false bottom raised the floor of the flume by approximately 10 cm.

Baffles were positioned at both the inlet and outlet to produce uniform flow in the working section of the flume.

Experimental equipment

For interpretation of the experimental results, the following parameters were measured: water velocity profiles, water temperature, physical properties of the oils, oil slick dimensions, and oil slick mean velocity. Of these, only the water velocity and physical properties of the oils required specialized equipment and procedures.

Water velocity profiles

A flow visualization technique was utilized to measure the water velocity profiles beneath the ice. This method involved using electrolysis of water to produce small gas bubbles that act as tracers. ...

A small-diameter (0.025 mm (0.001 in.)) platinum wire placed in the velocity field serves as the cathode in the electrolytic process. The anode, a small length of aluminum rod, was placed against the flume wall to prevent interference with the flow.

Rows of hydrogen bubbles were produced at the wire by supplying a pulsing voltage to the electrodes. The bubbles were then photographed and the velocities quantified by measuring the distance travelled between pulse times.

The lighting of the hydrogen bubbles is critical in obtaining usable photographs. ..., this is best obtained by using a narrow plane of high intensity light to illuminate only the section of interest (i.e., the narrow plane containing the rows of hydrogen bubbles). This was achieved in the flume by cutting a narrow slot in the "false bottom" above the bottom viewing window. By recessing a small area around the slot, a piece of clear Plexiglas was fitted flush with the surface. Light from below the flume entered the flow region as a narrow plane aligned along the centre of the flume. The light source used for photographing the hydrogen bubbles was an electronic flash synchronized with a 35-mm camera.

Oil properties

The densities of the three oils used in this research (Adgo, Itiyok, and Norman Wells) were measured using an ASTM-approved hydrometer.

The viscosities of the heavy oils (Adgo and Itiyok) were determined by using a Brookfield rotation viscometer. As the viscosity of the Norman Wells crude oil was outside the range of this instrument, it was measured using a Cannon Fenske Routine capillary viscometer.

The surface tension (σ) of the oil-water interface was determined using a variation of the sessile drop technique developed by Malcom and Elliot (1980). Assuming a contact angle of 180°, the surface tension can be determined from the dimensions of a sessile drop.

The physical properties of the oils are indicated in Table 1.

Table 1. Oil properties

Oil	Density at 0 °C (kg/m^3)	Surface tension (μN/cm)	Viscosity (mPa · s)
Adgo	960	265	195
Itiyok	937	288	340
Norman Wells	844	224	13

Experimental procedures

Ice preparation

Prior to growing the ice cover, the platinum wire for hydrogen bubble generation was installed. In addition, a 11.5 cm diameter ABS cylinder was suspended in the water at the oil injection site. This cylinder, filled with foam insulation, was frozen into the ice cover and later removed, leaving a hole in the ice for oil releases.

An oil boom was also frozen into the ice immediately upstream of the outlet baffles. This boom consisted of a piece of 1.25 cm thick plywood placed across the flume at a 30° angle to the flow, and extended approximately 10 cm below the water surface.

The temperature in the cold room was brought to approximately -5 °C. When the water temperature neared 0 °C, the pump was turned on to mix the water and obtain a uniform temperature throughout the flume. The cold-room temperature was then reduced to approximately -10 °C and ice formation began. The ice cover was allowed to develop to a thickness of approximately 8 cm.

Immediately prior to running an experiment, the ice cover was removed from a small area on the upstream side of the oil boom. This allowed removal of the trapped oil.

Procedure

Once the flow had stabilized, the electrolytic process was commenced and several photographs were taken of the flow prior to the oil releases.

The oil injection apparatus consisted of a Plexiglas cylinder, 11.5 cm in diameter and 27 cm in length, and a plywood plunger with a brass handle. The cylinder was placed in the ice opening and filled with approximately 2.5 L of oil. The plunger was then inserted into the cylinder and the cylinder was raised while the plunger was simultaneously depressed.

The volume of oil was measured prior to placing it in the injection cylinder; however, some oil would remain in the injection port after the release. This remaining oil (typically about 0.50 L) was extracted and measured, allowing determination of the volume of the moving oil slick by simple subtraction.

The dimensions of the moving oil slick and the time transpired were recorded at prescribed positions along the flume. Photographs of the flow field were taken as the oil passed the measuring station. The oil was trapped at the oil boom, where it was extracted.

At the end of an experimental run, a hole was cut in the ice at the platinum wire and a steel scale was inserted and photographed. This provided scaling for all photographs taken during the experiment."

Results

"*Qualitative observations*

Several qualitative observations were made during the course of the experiments. Once the oil was released, it would quickly form a single pool and proceed to move downstream. Some small droplets normally travelled downstream ahead of the main slick, but their volume was insignificant.

The measured velocities and dimensions of the moving oil slicks remained essentially constant over the length of the flume, indicating that the system had reached equilibrium conditions.

The heavier oils formed short slicks, which were generally oriented transverse to the flow. On the other hand, the light oil (Norman Wells) always formed a long narrow slick oriented

longitudinally in the direction of the flow. ... However, there were exceptions, as both heavy oils formed long narrow slicks on two occasions. This may have resulted from a slight curvature in the ice surface.

It was noted that the short slicks were normally transported at a higher velocity that the long narrow slicks. Consistent with the findings of others, all the oil slicks exhibited a nonwetting characteristic. No traces of oil remained under the ice once the slick had passed.

Experiment durations were approximately 2 h. In that time, no visual deterioration in the ice sheet was detected other than a slight decrease in thickness. The water temperature never increased more than 1 °C during an experiment.

Velocity profiles

Water velocity profiles were measured prior to each oil release using the hydrogen bubble electrolysis system. ...

The distance measurements were obtained from slide photographs projected onto a grid. The measurement error resulting from this analysis is typically of the order of ±0.5 to ±1.5 cm/s. This error increases in the region of the boundary layer where the velocity gradient is large.

A logarithmic expression was fitted to data points within the boundary layer and the free-stream velocity (U_w) was estimated by averaging data points outside the boundary layer. The measured velocity profiles are shown in Figures 7–10, along with the best-fit regression lines.

From Figures 7–10, it is apparent that the boundary layers are not fully developed. However, over the relatively short working region of the flume, it is assumed that the flow conditions are constant. The velocity measuring station is located approximately 1 m downstream from the oil injection port.

Experimental results

For these analyses the slicks were separated into two groups:

1. Long, narrow slicks, whose primary driving force is the shear stress force.
2. Short, wide slicks, whose primary driving force is the form drag force.

The measured parameters for the slicks that formed longitudinally in the direction of the flow are presented in Table 2.

For long, narrow oil slicks the shear force is balanced by the friction force. Assuming no slip at the oil–ice interface and equating [7] and [8], the following expression for mean slick velocity is obtained:

$$[13] \quad U_S = \frac{1}{4} \frac{C_S h \rho_w U^2}{\mu_o}$$

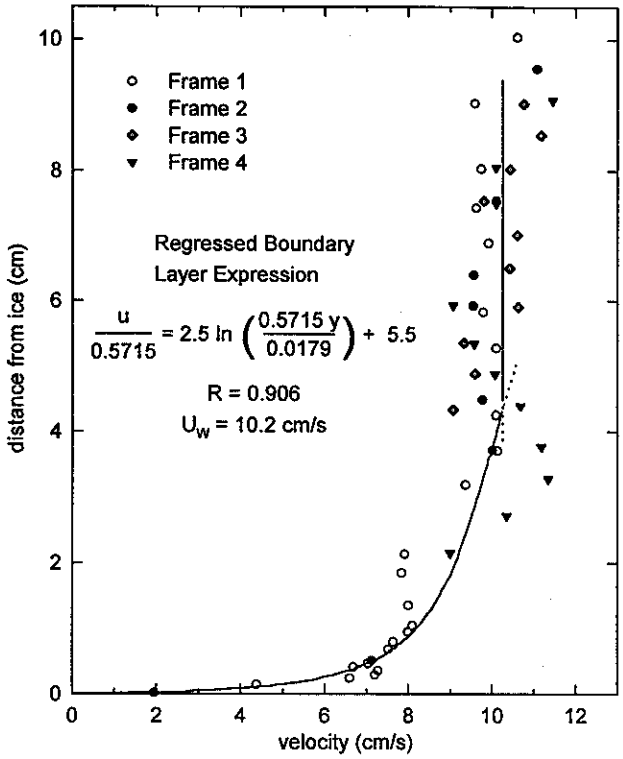

Figure 7. Velocity profile under ice–test 1, $U_w = 10.2$ cm/s.

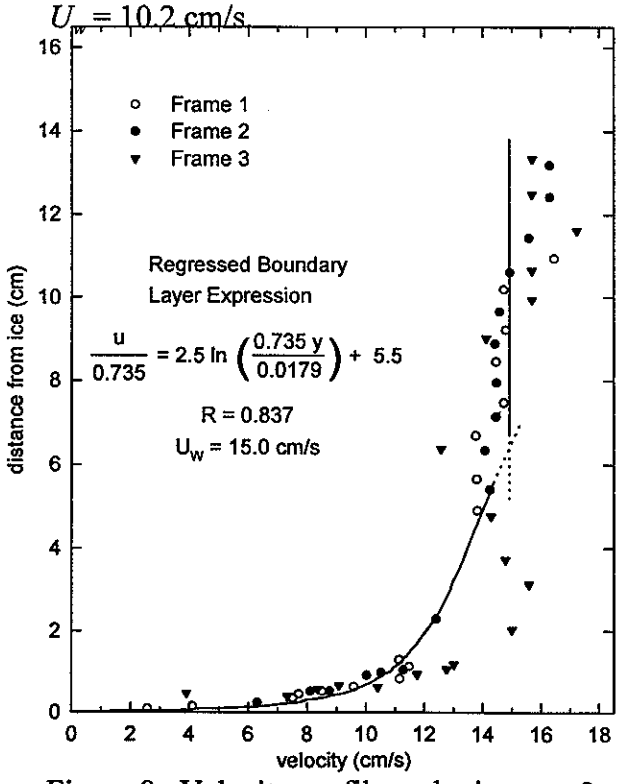

Figure 8. Velocity profile under ice–test 2, $U_w = 15.0$ cm/s.

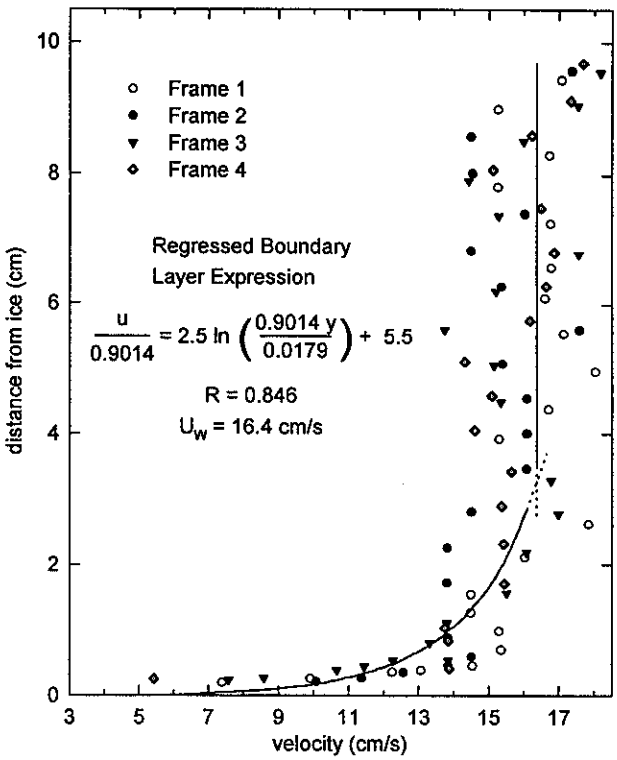

Figure 9. Velocity profile under ice–test 3, $U_w = 16.4$ cm/s.

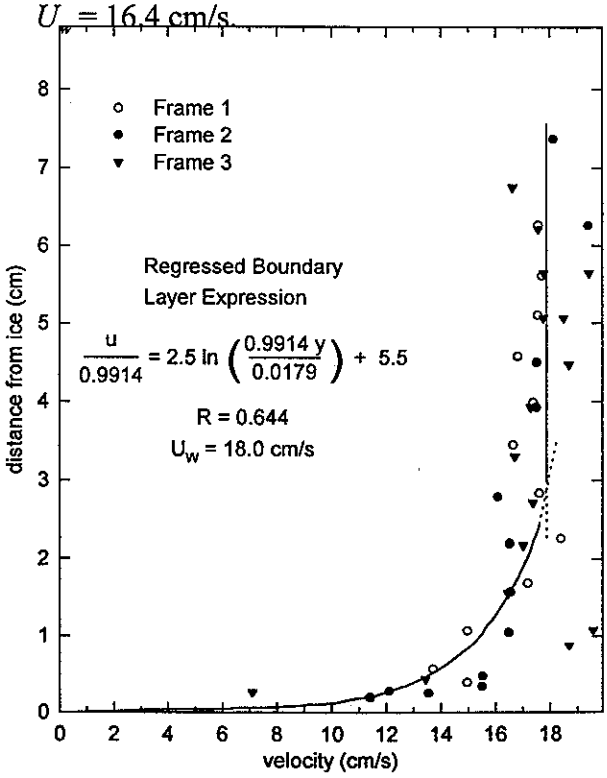

Figure 10. Velocity profile under ice–test 4, $U_w = 18.0$ cm/s.

Table 2. Results for longitudinally oriented oil slicks

Test no.	Free stream water velocity U_W (cm/s)	Oil	Slick length ℓ (cm)	Slick width w (cm)	Slick thickness h (cm)	Mean slick velocity (measured) U_S (cm/s)	Calculated shear stress coefficient C_S x 10^3	Mean slick velocity (calculated) U_S (cm/s)	Slick volume (mL)
1A	18.0	Adgo	90	15	0.97	2.86	4.46	0.17	1400
1I	18.0	Itiyok	60	30	1.20	2.06	5.45	0.15	1800
1NW	18.0	Norman Wells	137	17	1.04	1.75	4.03	1.9	1900
2A	15.0	Adgo	60	20	2.17	0.83	6.05	0.34	1900
2I	15.0	Itiyok	97	15	1.24	0.25	5.00	0.91	1800
3NW	13.0*	Norman Wells	120	10	1.07	2.0	5.03	1.3	1300
5NW	16.4	Norman Wells	80	10	0.74	2.7	5.43	1.5	600
6NW	14.3	Norman Wells	120	10	1.50	3.8	5.01	1.9	1800

* estimated velocity.

For all experiments presented in Table 2, the Reynolds number R_l is less than 5 x 10^5 and therefore the shear stress coefficient for laminar flow ([10]) was utilized in the analysis. Noting that $U_l = 2U_S$ and substituting [10] for the shear stress coefficient gives

$$[14] \quad U_S = 0.332 \frac{h \rho_w}{\mu_o} R_l^{-1/2} (U_w - 2U_S)^2$$

The free stream water velocities, as estimated using the velocity profiles, and the measured slick dimensions were substituted into [14] to determine the mean slick velocities. The mean slick velocities calculated using [14] are given in Table 2. From Table 2 it is immediately apparent that [14] does not adequately describe the motion of the oil slicks in tests 1A and 1I, as the predicted slick velocity is a full order of magnitude lower than the measured velocity. However, [14] does give order-of-magnitude results that compare favourably to the measured slick velocities for the other experimental results.

In the development of [7], the velocity variation in the thin water film separating the oil slick from the ice was assumed to be negligible. If this assumption is not made, and the velocity distribution in the oil slick is again assumed to be linear as per Figure 3, the velocity difference U_1 - U_2 can be determined by equating the equation for viscous friction:

$$[15] \quad F_F = \mu_o \frac{(U_1 - U_2)}{h_o} A$$

with [8] and substituting for the mean slick velocity using [5]. The thickness for the water film separating the oil slick and the ice surface can be determined as

[16] $F_F = \mu_w \frac{U_2}{\lambda} A$

The results of these calculations for the heavy oil slicks are presented in Table 3.

Table 3. Results for longitudinally oriented heavy oil slicks

Test no.	Free stream water velocity U_w (cm/s)	Oil	Slick length ℓ (cm)	Slick width w (cm)	Slick thickness h (cm)	Mean slick velocity U_S (cm/s)	Velocity variation $(U_1 - U_2)$ (cm/s)	Calculated water film thickness λ (cm)
1A	18.0	Adgo	90	15	0.97	2.86	0.28	0.083
1I	18.0	Itiyok	60	30	1.20	2.06	0.26	0.047
2A	15.0	Adgo	60	20	2.17	0.833	0.64	0.016
2I	15.0	Itiyok	97	15	1.24	0.25	0.31	0.0034

From Table 3, it is apparent that the majority of the velocity variation takes place in the water thin film and the heavy oil slick moves almost as solid masses. This effect is more pronounced for oil slicks moving at higher velocities, such as in tests 1A and 1I.

The thickness of the water film was found to be of the order of 3.4×10^{-5} to 8.3×10^{-4} m. This is substantially larger than for stationary oil drops, where the water film thickness is expected to be 5×10^{-7} m (Malcom and Dutton 1979).

It is noted that parameters σ and ρ_o are not included explicitly in [14]. However, they are important parameters in determining the slick thickness, h. Uzuner *et al.* (1979) and Cox *et al.* (1980) assumed that the thickness of the oil slicks moving under ice would be the same as under quiescent conditions. Using the expression for static oil slick thickness developed by Malcom and Cammaert (1981):

[17] $h = 2.0 \left(\frac{\sigma}{(\rho_w - \rho_o) g} \right)^{1/2}$

and the values for surface tension in Table 1, the following slick thicknesses are expected under quiescent conditions: Adgo, 1.65 cm; Itiyok, 1.38 cm; and Norman Wells, 0.77 cm. Comparing these values with the measured slick thickness in Table 2, the differences can obviously be substantial (as great as 100% in test 6NW). Since the equation for friction drag is a function of h, using the static equilibrium thickness can result in large errors. Unfortunately, no pattern for slick thicknesses is immediately apparent from the experimental results. The thicknesses of both Itiyok oil slicks were very close to that expected under quiescent conditions; however, the thicknesses of the other slicks varied significantly.

The measured parameters for the oil slicks that oriented themselves transverse to the flow are presented in Table 4. For oil slicks in this configuration, the primary driving force is the form drag force, given by [12]. For equilibrium, the sum of the driving and retarding forces must equal zero.

The friction force was calculated by assuming a constant velocity in the oil slick:

[18] $F_F = \mu_w \frac{U_S}{\lambda} w\ell$

The values for λ were selected using those calculated for the longitudinally oriented oil slicks as a guide. The results of these analyses are presented in Table 4.

Table 4. Results for transverse oriented oil slicks

Test no.	Free stream water velocity U_W (cm/s)	Oil	Slick length ℓ (cm)	Slick width w (cm)	Slick thickness h (cm)	Head thickness h' (cm)	Mean slick velocity U_S (cm/s)	Estimated film thickness λ (cm)	Calculated drag coefficient C_D
4A	10.2	Adgo	45	50	1.59	2.51	0.745	0.008	0.33
5A	16.4	Adgo	30	40	1.47	3.48	4.06	0.060	0.07
5I	16.4	Itiyok	40	40	1.42	2.50	1.54	0.020	0.10
6A	14.3	Adgo	20	35	1.93	4.00	4.04	0.060	0.06
6I	14.3	Itiyok	40	40	1.97	3.14	1.22	0.020	0.08

The values for the form drag coefficients are expected to lie in the range 0–1. Although the calculated drag coefficients for tests 5A, 5I, 6A, and 6I all appear to be quite low, it is noted that they are directly dependent on the value of λ, for which the uncertainty is large.

It is believed that the form drag coefficient varies with the dimensionless ratio h'/δ (Schlichting 1955), where δ is the boundary layer thickness and h' is the thickness of the head wave. Due to scatter of the measured velocities within the water boundary layer, it is impossible to predict the thickness of the boundary layer from the measured profiles with any degree of accuracy. This, coupled with the uncertainty associated with the calculated values for C_D, makes the relationship between C_D and h'/δ indeterminate from these data."

BOSS Critique

The authors clearly state the errors, and method, used to determine the velocity measurements from the photographs taken during the experiments. However, the authors do not explain the error in the measurement of the slick dimension (length, width, depth and head depth) nor the error in estimating the film thickness and the drag coefficients, all which will effect the usefulness of applying these measurements to full scale spills.

The authors have presented the theory in much greater detail than in their previous manuscript reviewed here. The determinate error of the water velocity measurement (the scatter) may be a much larger influence on the outcome of the laboratory experiments than the authors anticipated. Also, the under ice roughness of ice in a real spill situation may be a much large factor in determining how the oil spill behaves.

Review of a manuscript by, Metge, M. and A.S. Telford, "Oil in Moving Pack Ice-Laboratory Study", in *Proceedings of the Fifth International Conference on Port and Ocean Engineering Under Arctic Conditions (POAC),* pp 255-264, 1979.

Technical Summary

"There is a small risk that during offshore petroleum exploration in Canada's Eastern Arctic, a subsea blow out could release oil and gas under moving ice. Predictions of the potential environmental effects of the oil and development of oil spill countermeasures depend strongly on an adequate knowledge of the behaviour of oil in moving ice.

This paper describes a series of three laboratory tests, largely quantitative in nature, during which two different crude oils were released under moving ice. The moving pack ice was simulated by small ice floes, about 30 cm in diameter, confined in a 3 m diameter steel ring, in a basin, in a cold room, and agitated by the slow back and forth motion of the confined ring.

The main observations were:

-During interactions between ice floes, the oiled slush, being more viscous than either oil or slush alone, was squeezed up onto the edges of the floes. This is one of the many mechanisms by which oil can become encapsulated in the ice.

-A water-in-oil emulsion formed during the tests even though the agitation was rather gentle. Some emulsion may have formed during melting of the ice in the sun, where it appeared as a light brown scum on top of the ice.

Other observations, relative to the spreading of the oil, the effect of wind and waves, and countermeasures are also described."

Objective

"The experiments were conducted to help predict what would happen to crude oil released from a subsea blow out in moving pack ice on Canada's East Coast."

Theory

"It was not possible to model all aspects of the complex oil-ice interaction phenomenon in a small laboratory test. Therefore, the experiments were rather qualitative in nature. They were designed so that the important processes in oil-ice interaction could be observed and identified. Ice grown from sea water and crude oils were used in the experiment, therefore viscosities and surface tensions were not scaled down. While there was no attempt at making a scientifically accurate model of the oil-ice interaction, similarity with the real situation was the goal. As far as the ice and its motion were concerned, the test were roughly geometrically similar to Labrador pack ice conditions (ice floes about 10 m in diameter) with a scaling factor of about 1/30. Using Froude scaling, the velocity and time scaling factors would be about 1/5.5."

Method

"The test were performed in a cold room. A 2.7 m by 3.5 m by 0.6 m basin was installed in the cold room and was filled with fresh water to a depth of about 0.3 m. Evaporated California sea salt was mixed with the water up to a salinity of 34 parts per thousand to simulate sea water.

In order to agitate the ice floes and simulate the movement of real pack ice floes, a specially designed ice mixer was installed in the basin (Figure 1). The ice mixer consisted of 2.5 diameter galvanized iron ring, suspended over the water basin and capable of rotating. The ring was about 0.2 m deep and half submerged in the water. It served to confine both the oil and the ice floes. A series of small projections on the inside of the ring caught some of the ice floes as the ring rotated. A fixed center piece in the middle of the basin tended to stop some of the ice floes near the center, thereby creating relative motion between inner and outer floes. The ring rotated alternatively to the right and then to the left. Each cycle lasted 33 seconds; 14 seconds to the left, 2.5 seconds stop, 14 seconds to the right, then 2.5 seconds stop, etc. The rotation rate was about 0.01 turns per second, resulting in a 7.7 cm/s velocity at the outside ring. Assuming a model scale of 1/30 and Froude scaling, this velocity would correspond to 42 cm/s full scale.

A 16 mm movie camera capable of time lapse photography was used to record the experiments. A simple device with mirrors was used to observe the underside of the ice and the behaviour of oil particles under the moving ice.

Test Procedure

Before each test, the first task was to grow ice and form the floes. This was done differently for each of the three tests. For the first test, the floes were grown in separate tanks and stored for a week (possibly losing some brine) before being cut and shaped into roughly circular floes. For the second test, a solid ice cover was grown over the whole basin and floes were cut from this cover immediately before releasing the oil. For the third test, the floes were also cut from the ice cover on the basin but, after cutting, they were allowed to grow further while being agitated by the ice mixer. This third method resulted in ice floes with very realistic pancake-like shapes, including raised edges (Figure 2).

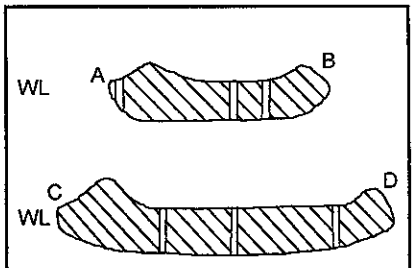

Figure 2. Comparison of ice floe shapes. (Actual profiles of Labrador ice floes)

Before each test the inside of the ice mixer was filled to capacity with ice floes which gave ice concentration of about 0.7 (70% ice and 30% open water). After some agitation, the ice concentration dropped to about 0.5 to 0.6 due to rafting and the space between the floes became filled with slush.

Oil was injected underwater beneath the ice floes using a pressurized system and a small nozzle. This provided a continuous release of relatively small oil droplets, about 2 to 3 mm diameter. Attempts at obtaining smaller droplets were unsuccessful, but it did not seem that the droplet size would have much effect on the behaviour of the oil in this type of experiment.

The volume of oil injected was kept constant at 1 litre for each test. For an ice concentration of 0.7, the 1 litre of oil caused an 0.7 mm thick slick between floes. Tests 1 and 2 used Atkinson Point crude oil, test 3 used Prudhoe Bay crude oil.

Each test was continued for 1 to 3 days during which films, pictures and observations were taken. At then end of the test, the ice floes were put in a bin to melt. After melting, the oil that had

been incorporated in or on the ice was recovered, measured and analyzed. The oil that remained on top of the water in the basin was also recovered and measured."

Results

"The results of the three tests are summarised in Figure 3. After being injected, the oil droplets rose to the surface. With slight agitation, the oil always percolated through any slush present between the floes. Oil droplets that rose under ice floes tended to be trapped there. Some of this oil migrated to the surface of the ice through brine channels, but only after a few hours. Within 10 minutes, the oil spread to cover about half the test basin and it took 20 to 40 minutes for the oil to cover the whole basin, depending on the oil. Prudhoe Bay crude spread much slower than the less viscous Atkinson oil. If the area between the floes was filled with slush, the slush tended to retain the oil. The oil-slush mixture was much more viscous than either oil or slush alone, forming a thick paste.

Figure 3. SUMMARY OF TEST CONDITIONS				
Average floe size		35 cm	25 cm	25 cm
Average floe thickness(at beginning of test)		7.5 cm	2 cm	3 cm
Ice Salinity		4‰	8‰	11‰
Air Temperature		-6 to -8 °C	-8 °C	-9 °C
Crude Oil used		Atkinson	Atkinson	Prudhoe Bay
Time of 25% oil coverage 50% 75% 100%		5 min. 10 min. 15 min. 20 min.	5 min. 10 min. 15 min. -	5 min. 10 min. 15 min. 20 min.
Duration of test		27 hours	42.5 hours	48 hours
Oil on the Ice:	% water Volume of oil	59% 351 ml	74% 217 ml	61% 79 ml
Oil between ice floes:	% water Volume of oil	24% 212 ml	27% 84 ml	36% 342 ml
Oil Loss:	By evaporation On sides of tank	about 300 ml 137 ml	about 350 ml 349 ml	about 300 ml 279 ml

During mixing, the ice floes behaved in a way that appeared similar to East Coast conditions. The motions were slow and there were no violent interactions between floes. Still, some rafting did occur as one would expect. Raised edges did form on the floes during each test and they looked very similar to raised edges of East Coast ice floes. In the tests, raised edges were formed when the slush and slush-oil mixtures were squeezed up onto the floes during floe movement and impact. Also, the movement, rotation, and contacting of floes resulted in oil being transferred from one floe to another and from one area to another, thus increasing the area of oil contamination.

Small waves were generated during part of one test and were found to have no significant effect on the oil-ice interaction processes unless the waves were so high that the ice floes became partially submerged. A fan was used to blow air across the surface of the basin to simulate wind conditions. The wind tended to move and herd the oil that was present in the areas between the floes.

At the end of a test, the oil between and on the ice floes was collected and measured and the amount lost by evaporation at cold room conditions was measured in a separate experiment. Water-in-oil emulsions were formed during the tests and on melting the ice floes in the sun, an emulsion which seemed to be an oil-water-gas mixture appeared as a light brown scum on the surface of the ice.

Several tests were also performed to determine how the oil spread in open water and slush (3 cm thick) under static conditions. A summary of the results is shown in Figure 4. The prime result of these tests was that the spreading of oil in slush is considerably less than in open water.

Figure 4. RESULTS OF SPREADING TESTS

	Open Water		Slush (3 cm thick)	
	Slick Size	Slick Thickness	Slick Size	Slick Thickness
(1) 50 ml Atkinson Oil after 1 minute after 1 hour (final)	3702 cm^2 16000 cm^2 (limited by tank)	0.13 mm 0.04 mm	120 cm^2 470 cm^2	4.2 mm 1 mm
(2) 50 ml Norman Wells Crude Oil after 1 minute after 1 hour (final)	390 cm^2 390 cm^2	1.3 mm 1.3 mm	230 cm^2 310 cm^2	2.2 mm 1.6 mm
(3) 50 ml Prudhoe Bay Crude Oil after 1 minute after 1 hour (final)	390 cm^2 390 cm^2	1.3 mm 1.3 mm	Prudhoe Bay crude oil did not percolate through 3 cm of slush without some agitation and then it did not spread.	

"

BOSS Critique

The authors have stated that the work report in this paper was of a qualitative nature, however, size measurements were reported in cms and mms and therefore errors should be stated for these measurements. The reproduction of field conditions is important and stating how this is done in exact terms allows other researchers to reproduce the experimental conditions. Therefore the existing experiments can be used as a bases for future work with improved apparatus or improved theory.

Review of a manuscript by, Malcolm, J.D. and C. Dutton, "The Interfacial Tension and Contact Angle of Crude Oil Under Ice", in *Proceedings of the Fifth International Conference on Port and Ocean Engineering Under Arctic Conditions (POAC)*, pp 771-778, 1979.

The same information is also presented in a manuscript by Malcolm, J.D., entitled "Studies of Oil Spill Behaviour Under Ice", in *Proceedings of a Workshop on Oil, Ice and Gas*, EE-14, Institute For Environmental Studies, University of Toronto, Toronto, Ontario, pp 47-53, 1979.

Technical Summary

"The wetting behaviour of oil under ice in water surroundings is characterized by the contact angle between the fluid interface and the solid, and the interfacial tension between the oil and water. An improved sessile drop analysis has been applied to laboratory measurements on two crude oils under ice in both fresh water and sea water.

The interfacial tensions of all crude oil/water systems tested were found to be in the relatively narrow range 20 ± 5 dynes/cm. The contact angles were found to be 180° in every case. It is expected that a thin film of water exists between the oil drop and the ice, which would account for the apparent lack of wetting."

Objective

To provide accurate measurements of two physical properties (interfacial tension and contact angle) which govern the extent and distribution of crude oil spilled in water under a solid ice cover.

Theory

"The two most important properties directly related to oil-ice interaction are contact angle and interfacial tension of the oil-water-ice system. Oil-ice interaction here includes such factors as wettability, spreading, spill homogeneity, and spill thickness, as well as capillary action which allows oil penetration into ice surface cracks and brine drainage channels.

The sessile drop method is the only in-situ method for determining contact angle and interfacial tension on an oil-water-ice system. The sessile drop method however has been controversial because of two major problems, not completely resolved to this day. For example, Mackay *et al.* [4] assumed the crude oil formed sufficiently large sessile drops so as to be considered two dimensional and semi-infinite, an assumption which has been severely criticized since 1885 [6]. The assumption allows the use of an attractive but unrealistic analytical solution first provided by Laplace [7]. The fact that the errors incurred by this assumption are large has not eradicated completely its persistant application.

The second problem concerns the enormous emphasis placed by most analytical treatments of sessile drops on the location of the drop equator. The nonlinear variation of meridian curvature in the equatorial region makes the precise location difficult to resolve. This contributes to the wide variation in reported results. For example, Rosenegger [3] reported values of interfacial tension ranging from 5 to 50 dynes/cm on two crude oil-saline solution-ice systems. The problem of precisely determining drop equator location from photographs is coupled in Rosenegger's paper by the use of poorly fitted approximate formulae due to Staicopolus [8]. Padday and Pitt [9] have found

that Staicopolus' work is in error by at least two percent from the theoretical drop forms. The Staicopolus formulae are also unwieldy, since 13 parameters are required to determine interfacial tension, while 67 parameters are needed to estimate contact angle. Rosenegger chose not to report contact angle from his laboratory work. In what follows a novel sessile drop analysis [9] is briefly outlined which avoids both problems associated with the traditional methods.

ANALYSIS

The angle of contact, ϕ_c between a liquid and a solid is given by the Young-Dupré equation as:

$$\phi_c = \cos^{-1}\left[\frac{\sigma_{s1} - \sigma_{s2}}{\sigma_{12}}\right]$$

where σ is the interfacial tension and subscripts s, 1 and 2 denote the solid, first liquid and second liquid, respectively. Thus, contact angle ϕ_c is a function only of fluid and solid properties in the local region of the contact line between liquids and the solid, and is independent of liquid drop volume or shape. Similarly, the capillary length, $\underline{a} = [(\sigma_{12}) /((\rho_1 - \rho_2) g)]^{1/2}$ which is a property of the interface between the two fluids, and the density difference between the fluids $(\rho_1 - \rho_2)$, will be independent of drop shape and volume. The gravitational acceleration is denoted by g.

It has been found that measurements of drop height, H (from apex to solid substrate) and drop equatorial diameter, D on a series of drops of different volume can be used to compute accurate estimates of contact angle, ϕ_c, and capillary length. The following formulae apply

$$\begin{aligned} W &= 2(H/D) - 1 \\ Z &= W - W^2/\beta \\ M &= H^{9/4}/\alpha \end{aligned} \tag{1}$$

If the parameters α, β are specified, values of W, Z and M may be computed for each drop whose measurements of H and D are known. For a number of drops, N, of identical fluid on the same solid, a least squares approach yields:

$$\underline{a} = \left[\frac{\Sigma Z \; \Sigma M - N \Sigma(ZM)}{N\Sigma Z^2 - (\Sigma Z)^2}\right]^{4/9} \tag{2}$$

$$Y = \underline{a}^{-9/4}\left[\frac{\Sigma Z^2 \Sigma M - \Sigma Z \; \Sigma(ZM)}{N\Sigma Z^2 - (\Sigma Z)^2}\right] \tag{3}$$

where Σ denotes summation over N drops,
and

$$\phi_c = \cos^{-1}\left(-\frac{\beta}{2}\left[1 - \sqrt{1 - \frac{4Y}{\beta}}\right]\right) \tag{4}$$

$$\sigma = \underline{a}^2 (\rho_1 - \rho_2) g \tag{5}$$

The parameters α, β have been obtained by treating the tabulated drop shape profile coordinates of Padday [6] as data in a search program which optimizes the selection α, β for a given

contact angle. The range of contact angles from 90° to 180° in 10° intervals was covered in the search program. In practice, an initial guess for the contact allows selection of α, β to be used in equations (1) through (4). If the calculated value of contact angle from equation (4) differs from the initial guess by more that 5°, a rerun with new α, β is indicated. At $\phi_c = 180°$, α, β are found to be 4.34243 and 4.82141 respectively.

The parabolic formulae, equations (1) through (4), provide fairly close fit to the "perfect" drop data of Padday [10]. There is however a systematic difference between the parabolic formulae and the true data. This systematic variation may be accounted for by subtracting a correction quantity ZC from the value Z calculated in (1). For a large number of experimental H, D values the ZC corrections tend to cancel each other out, but for smaller number of experimental values, it was found worthy of consideration."

Method

"The analysis requires precise measurements of drop height and diameter on a series of drops of different volume. Silhouette photographs were taken with a Hasselblad 500C using an 80 mm lens and bellows extension mounted on a 3-axis stand. A variety of lighting arrangements were tried, using a ball bearing resting upon an optical flat as a calibration target. Dimensions on the photograph negatives were obtained using a Nikon Profile Projector. Back lighting through a ground glass diffuser was found to give excellent results, in combination with black paper shrouding the entire optical path from the light source to camera, to remove room lighting highlights on the drop surface. Alignment of the optical system was found to be a critical factor, but the use of a calibration object, such as a scale or ball bearing in each photo allowed compensation for inherent errors in the measurement system.

A 20 gallon aquarium was found to be large enough to allow a variety of solid supports to be mounted underwater for the oil-water-solid support studies. Although the case of oil under ice is of greatest interest, it represents the greatest experimental difficulties. In developing the technique, a glass plate was used instead of an ice surface. The 8 x 24 cm plate contained five evenly spaced holes (2 mm diameter) and a support arrangement for #20 gauge hypodermic needles to provide for oil injection through the glass plate.

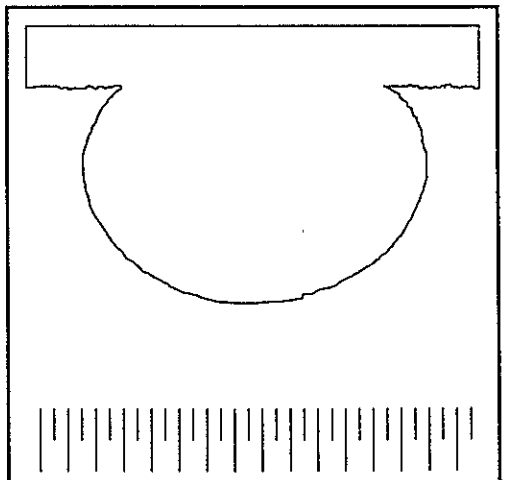

Figure 1. Guanipa Crude Oil Drop Under Glass Plate. One scale division = 0.5 mm.

An ice sheet was formed by chilling a brass plate in liquid nitrogen, then dipping the brass sheet into water. Typically, the ice layers that formed were about one cm thick, and relatively flat, except near the edge of the brass. No attempt was made to artificially flatten the ice, as in the method of reference [4].

To conduct an experiment, the aquarium was first filled with either fresh water (courtesy of St. John's water supply) or water obtained from the Atlantic Ocean (courtesy of Marine Sciences Research Laboratory, Logy Bay, Newfoundland). Either the glass plate or the chilled brass plate was mounted in a fully submerged position and aligned with the optical system. A precision steel scale or ball bearing of known dimension was included in each oil

drop photo for calibration purposes. A typical result is shown in Figure 1.

Two crude oil samples were examined. A Venezuelan crude called Guanipa was obtained from Imperial Oil Ltd. with a density of 0.8878 g/cc. Golden Eagle Canada Ltd. provided a sample consisting of Trinidad (24.8%), B.C.F. (56.2%), Leone (19.0%) which had a density of 0.9014 g/cc."

Results

"It was found that a thin film of water was retained between the upper solid surface (either glass or ice) and the liquid oil drops, and that the liquid oil drop was unlikely to come into direct contact with the solid support. Analysis of all drop data indicated that the contact angle is 180° in every case, confirming the lack of contact between oil and solid support. Tilting the plate or providing water motion caused the sessile drops to roll across the solid support, leaving no tracks behind. The results are summarized in Table 1.

Table 1. Contact Angle and Interfacial Tension Results

Oil	Water (source)	Drop Height (mm)	Oil Density (gm/cc)	Interfacial Tension (dynes/cm)	Contact Angle (degrees)	Capillary Length, a (mm)
Guanipa	Fresh (Lake Windsor)	4.925 - 7.919	0.8878	24.75	180.0	5.269
Guanipa	Atlantic Ocean (Logy Bay)	4.021 - 6.200	0.8878	15.94	180.0	3.344
Golden Eagle	Fresh (Lake Windsor)	4.762 - 7.526	0.9014	19.09	180.0	5.019
Golden Eagle	Atlantic Ocean (Logy Bay)	4.719 - 7.076	0.9014	20.80	180.0	4.011

...

Michael Faraday first proposed that the surface of ice, when not too far below the melting point, is covered by a thin liquid-like layer. More recent work" Fletcher, N.H., Phil. Mag. 18, 1287 (1968) "confirms this hypothesis of the totally hydrophilic nature of ice. There are thus substantial reasons for concluding that crude oil in water under ice forms sessile drops with a contact angle of 180°, indicating that the oil is separated from the solid by a water film.

The interfacial tension results for an individual crude oil/water system are very consistent. However, changing from fresh water to sea water has an apparently large effect with Guanipa, but little effect with Golden Eagle. The interfacial tensions of the two crude oils in both fresh water and sea water may be characterized by $\sigma = 20 \pm 5$ dynes /cm.

The capillary length of crude oil/water systems appears to be reduced by changing from fresh water to sea water. This has important consequences on the maximum height which may be expected by an oil spill pool. It is important to distinguish between the maximum height of sessile drops and the height reached by very large sessile pools, which is less than the true maximum height. As volume is added to a sessile drop, the height reaches a maximum value, then height declines to a limiting value as further volume is added. The maximum height is 2.107399 a and the limiting height is $2a$. Table 2 gives the heights expected by the oil/water systems in this study. A 250 cc sessile pool of Golden Eagle in fresh water reached a height of 10.2 mm in one test in our laboratory.

Table 2. Height of Sessile Drops and Pools Calculated from a Values of Table 1.			
Oil	Water	Maximum Height (mm)	Height of very large Pool (mm)
Guanipa	Fresh	11.104	10.538
Guanipa	Sea	7.047	6.728
Golden Eagle	Fresh	10.577	10.038
Golden Eagle	Sea	8.453	8.022

"

BOSS Critique

The authors have reported the drop height in mm to three significant figures even though they state that the scale for interpolating the photographs is 0.5 mm (shown in Figure 1) and therefore may be interpolated carefully to 0.1 mm. The authors do not state their reason for including the remaining significant figures in the reported data. The interfacial tension is reported in Table 1 to two significant figures however the authors' formula for calculating sigma is dependent directly on a and therefore cannot be more accurate then a which, from the information presented in the text, can not be more accurate than ±0.1 mm.

Review of a manuscript by, Kovacs, A., entitled "Sea Ice Thickness Profiling and Under-Ice Oil Entrapment", in *Proceedings of the Ninth Annual Offshore Technology Conference*, OTC2949, Offshore Technology Conference, Dallas, Texas, pp 547-554, 1977.

The same information is also presented in the following manuscripts:

Kovacs, A, entitled, "Oil Pooling Under Sea Ice", in *Outer Continental Shelf Environmental Assessment Program, Vol. VIII: Transport*, RK-8-0065, National Oceanic and Atmospheric Administration, Ocean Assessment Division, Alaska, pp 310-353, 1979. This contains a document (attachment A) by Kovacs, A. and R.M. Morey entitled "Anisotropic Properties of Sea Ice in the 50-150 MHz Range", *J. Geophys. Res.*, Vol 84, 1979.

Kovacs, A., R.M. Morey and D. Cundy, "Oil Pooling Under Sea Ice", in *Outer Continental Shelf Environmental Assessment Program, Vol. VII: Transport*, National Oceanic and Atmospheric Administration, Ocean Assessment Division, Alaska, pp 333-339,1980.

Kovacs, A., R.M. Morey, D.F. Cundy and G. Decoff, "Pooling of Oil Under Sea Ice", in *Proceedings of the Sixth International Conference on Port and Ocean Engineering Under Arctic Conditions (POAC)*, Vol. II, pp 912-922, 1981.

Technical Summary

"Results obtained with a unique dual-antenna impulse radar systems used to profile first- and multi-year sea ice near Prudhoe Bay, Alaska, are discussed. A description of the radar system is given along with representative field data. Continuous ice thickness profiles are required for studies related to modelling and understanding the dynamics of the sea ice cover, heat exchange between the ocean and the atmosphere and mass balance of the ice cover. Ice thickness profiles are also required for studies related to the determination of ice load distributions and force analyses, and the subsurface roughness as it pertains to under-ice sound propagation and to the quantity of oil that would be trapped in the undulating bottom relief of first-year and multi-year ice should an oil blowout occur in an ice-covered sea. From the radar impulse travel times obtained with the use of dual antennas, calculations of thickness, electromagnetic impulse velocity and effective dielectric constant of the ice were made. Ice thicknesses determined by direct measurement and those calculated using radar impulse travel times were found to be in good agreement. Continuous ice thickness profiles obtained with the radar were analyzed to provide representative cross sections of first-year and multi-year sea ice. These cross sections reveal the undulating bottom surface relief of both ice types. Calculations are presented that indicate a significant amount of oil could be trapped within this bottom relief should the oil be released under the ice from a sea-floor oil-production system."

Objective

To use a radar frequency between 10 and 500 MHz to measure sea ice thickness and using the profile obtained from this measurement, calculate the volume of oil that could be captured in the under ice pockets.

Theory and Method

"A very-high-frequency (VHF) impulse radar system that has demonstrated its ability to profile sea ice thickness is the electromagnetic subsurface profiler developed by Geophysical Survey Systems Inc. (GSSI). This system, described by Campbell and Orange (1974) and Morey (1974), consists of timing electronics that clock an impulse generator and sampling head. The impulse source generates 60- to 100-volt impulses with a band width of nearly 500 MHz at a repetition rate of 50 kHz. The impulse has a center frequency at 100 MHz, and frequencies of 50 and 150 MHz at the -3 db points. The impulse is fed to a transmitting-receiving antenna which radiates the signal into the underlying material. The radiated energy that is not scattered by the material is reflected back to the antenna.

The received signals are from the top surface of the material, from layers or anomalies within the material, and, in the case of ice, from the bottom surface of the material. The signals are fed to a sampling head which modifies them for display on an oscilloscope and a graphic recorder. When desired, the data may also be recorded on an FM tape recorder for later playback or data processing. The signal information recorded is the travel time to and from the various reflecting surfaces. In order to convert the two-way travel time of the signal from an interface to a depth scale, the velocity of propagation of the EM pulse within the intervening medium must be known. From the effective propagation velocity, the depth can be determined from:

$$D = V_e \frac{t_d}{2} \qquad (1)$$

where D = depth, V_e = effective velocity of EM signal, t_d = travel time from transceiver antenna to and from subsurface interface.

For certain homogeneous materials, such as fresh water and fresh-water ice, the velocity of propagation can be calculated from:

$$V_e = \frac{c}{\sqrt{e_r}} \qquad (2)$$

where c = velocity of EM in air = 3×10^8 m/s (0.9843 ft/ns ≈ 1 ft/ns), e_r = dielectric constant = 81 for fresh water ≈ 3.2 for pure fresh water ice.

Unfortunately, the dielectric constant, and in particular the effective dielectric constant of most earth material, is not known. This is due to the fact that the dielectric constant is affected, to varying degrees, by the moisture content, temperature, pressure, density, grain size and mineral composition of the material, impurities within the material, and the frequency of the system used. The standard GSSI impulse radar system must therefore be calibrated using drill hole log information. In addition, as material properties change along a route, e.g., when sea ice thickness changes, the instrument must be recalibrated using another depth measurement obtained by drilling.

In April 1976, a modified GSSI impulse radar was used in a preliminary study to evaluate its ability ti profile sea and lake ice thickness and to investigate in-situ features within permafrost. The CRREL radar system is unique in that it had been modified to use

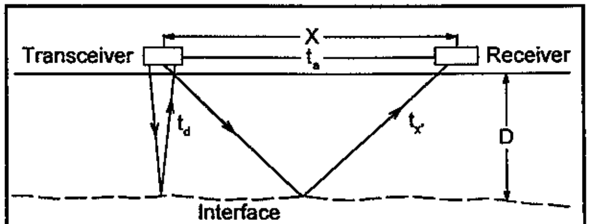

Figure 1. Schematic for dual-antenna EM pulse flight path.

two antennas. With this dual-antenna system, it is now possible to determine the velocity of propagation of the EM impulse and the effective dielectric constant at any time along a track, irrespective of changing material properties. One antenna operates in the standard transmit-receive mode and the second in the receive-only mode as depicted in Figure 1. The antennas are placed a fixed distance apart and moved as a unit over the surface. The effective propagation velocity of the EM pulse in the medium is given by:

$$V_e = \frac{X}{\sqrt{t_x^2 - t_d^2}} \quad \text{...} (3)$$

where X = distance between centers of two antennas, t_d = vertical travel time from transceiver antenna to and from subsurface interface, t_x = travel time from transceiver antenna to subsurface interface to receive-only antenna ($t_{x'}$) plus time t_a = air-wave travel time between antennas (Fig. 1)

The graphic recorder display for the dual-antenna profiling is similar to that depicted in Figure 2. The two-way travel time t_d in nanoseconds is measured from time zero (t_0). The travel time t_x in nanoseconds is also measured from t_0. To determine t_x the air-wave travel time ($t_a = X/c$) of the EM pulse radiated from the transceiver to the receiver antenna is added to the time $t_{x'}$ as shown in Figure 2. Thus, the first signal received by the receiver antenna after the transceiver antenna has radiated an EM pulse is that which arrives through the air at t_1. During 1976 field trials, the antennas were separated by 10 ft (~ 3 m). Therefore, 10 ns was added to the time $t_{x'}$ measured on the graphic recorder.

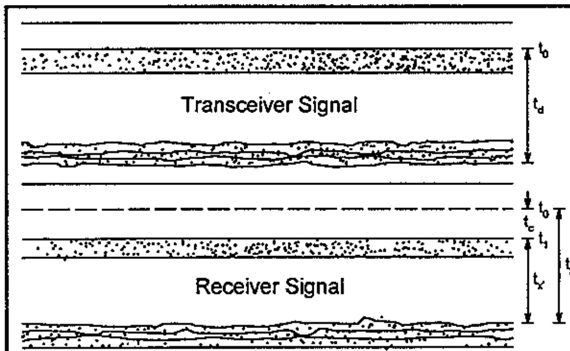

Figure 2. Simulated graphic recorder display for dual-antenna receive mode.

With the velocity of the EM pulse thus determined, it is then possible to determine the thickness of sea ice and its effective dielectric constant at any location on a continuous profile using equations 1 and 2."

Results

...

"The depth of the ice was determined at 11 stations by drilling and tape measurement. These measurements are shown in Table 1 along with ice thickness calculations made using the EM impulse travel times obtained from the graphic record. The average thickness determined by direct measurement was 1.87 m and that by radar travel time analysis was 1.91 m. The agreement is quite good.

Table 1. Comparison of ice thicknesses measured in drill holes and those calculated from radar impulse travel times. The calculated EM pulse velocity and effective dielectric constants for first-year sea ice are also given.

Station	*Measured Thickness*		*Radar Thickness*		*Calculated Velocity*		*Dielectric Constant*
	(m)	*(ft)*	*(m)*	*(ft)*	*(m/ns)*	*(ft/ns)*	
0	1.98	6.50	2.01	6.6	0.138	0.452	4.74

Table 1. Comparison of ice thicknesses measured in drill holes and those calculated from radar impulse travel times. The calculated EM pulse velocity and effective dielectric constants for first-year sea ice are also given.

Station	*Measured Thickness*		*Radar Thickness*		*Calculated Velocity*		*Dielectric Constant*
	(*m*)	(*ft*)	(*m*)	(*ft*)	(*m/ns*)	(*ft/ns*)	
1	1.93	6.33	1.96	6.45	0.140	0.461	4.70
2	1.70	5.58	1.83	6.02	0.139	0.455	4.70
3	1.80	5.92	1.88	6.16	0.142	0.465	4.48
4	1.83	6.00	1.88	6.16	0.142	0.465	4.48
5	1.98	6.50	1.96	6.43	0.140	0.459	4.58
6	1.80	5.92	1.83	6.02	0.137	0.450	4.78
7	1.80	5.92	1.91	6.28	0.142	0.465	4.49
8	1.93	6.33	1.97	6.47	0.138	0.454	4.71
9	2.01	6.58	1.98	6.50	0.138	0.452	4.74
10	1.80	5.92	1.83	6.01	0.140	0.458	4.61
Average	1.87	6.14	1.91	6.28	0.140	0.458	4.62
Std. error	0.098	0.32	0.064	0.21	0.0017	0.0055	0.11

Equations 1 and 2 were used to calculate the velocity of the EM pulse and the effective dielectric constant of the first-year sea ice at the 11 profile stations. These are also given in Table 1. Using the average velocity of 0.140 m/ns and the travel time of the EM impulse at several hundred points along the profile, a cross section of the ice was constructed (Fig. 6). This profile, or the digitised data thereof, can be used as input for many of the studies previously mentioned.

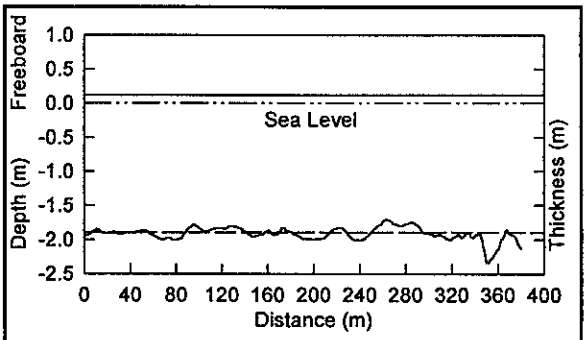

Figure 6. First-year ice cross section constructed from radar data. Dashed line represents mean thickness of 1.91 m determined for the first 345 m of the cross section.

Part of an exceptionally thick multi-year flow was also profiled from the ice surface. A portion of the graphic record is shown in Figure 7. The horizontal scale lines are 12.5 ns apart and the vertical hatched events are 15 m apart. To my knowledge, this is the first time this thickness of multi-year sea ice has been profiled in a continuous manner. Using the EM impulse travel times measured from the transceiver and receiver traces in Figure 7, the maximum depth of the ice was calculated to be 8.44 m, the average velocity of the EM impulse to be 0.152 m/ns, and the average effective dielectric constant to be 4.

Analysis has been done to construct the "true" cross section of the flow using ice freeboard

vs total thickness information obtained from over 100 drill hole measurements made through multi-year sea ice and data on multi-year ridge height vs keel depth. The drill hole data are presented in Figure 8. Two rectilinear curves, I and II, passing through the data were found to represent the data reasonably well. The slope of the line III was found to fit the data for multi-year pressure ridges (Kovacs 1976).

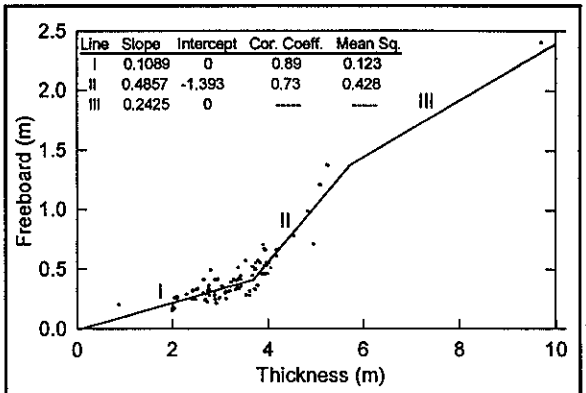

Figure 8. Freeboard versus total thickness for multi-year sea ice. (Line I, II and III represent multi-year sea ice freeboard to draft ratios of 1:8.26, 1:4.12 and 1:3.13 and effective specific gravities of 0.9, 0.82 and 0.775, respectively.)

Using the equations for these lines and the total ice thickness as calculated using the recorded flight times of the EM impulse, two cross sections of the multi-year floe were constructed (Fig. 9). These cross sections are considered a reasonable representation of the surface and subsurface relief of the floe. The mean elevation and depth of the floe were found to be 1.37 m and 4.31 m respectively. The resultant freeboard-to-depth ratio is representative of ice with a specific gravity of ~ 0.78. After these cross sections were plotted, another trip was made to the floe. At this time the thickness of the refrozen melt pond at station 650 on cross section 1 in Figure 9A was determined by drill hole tape measurement. The depth was

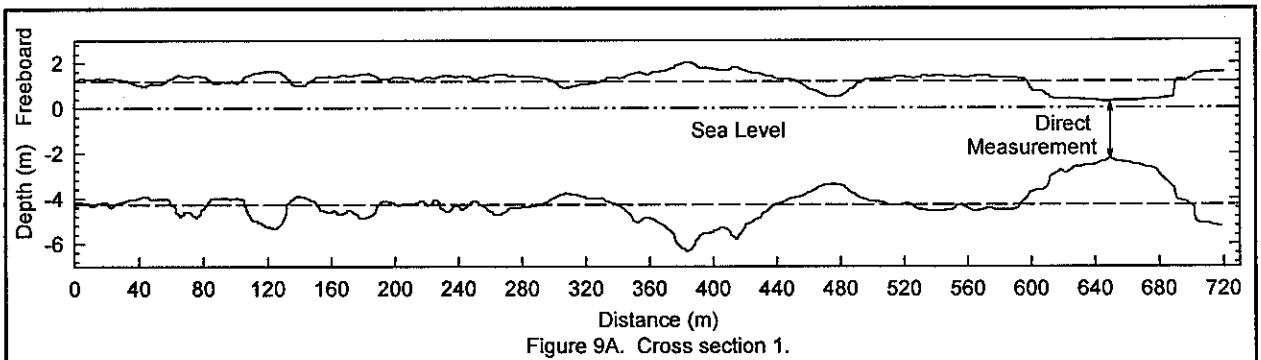

Figure 9A. Cross section 1.

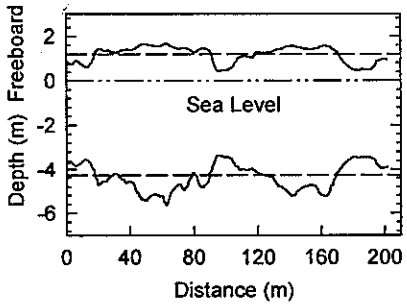

Figure 9B. Cross section 2.

Figure 9. Multi-year sea ice cross sections constructed from radar data. Dashed line above sea level represents their combined mean surface elevation of 1.37 m (4.49 ft.). The bottom dashed line below sea level represents their combined mean bottom depth of 4.31 m (14.14 ft.)

found to be 2.49 m, or 0.12 m less than the thickness calculated using the EM impulse travel times from the two antennas.

...

An estimate has been made of the quantity of oil which could accumulate in the pockets of the undulating relief under first-year sea ice should a sea bed oil-production gathering system rupture. The analysis assumed that the pockets existing above the mean depth are not interconnected and therefore will act as "catch basins" for oil spreading outward from the point of discharge. It also assumed that the first-year ice is part of the stable fast ice zone, that the under ice currents are negligible and that the gas released during the blowout is vented through rupture cracks in the ice above the blowout.

Using the digitised ice thickness data for the 382.5 m first-year sea ice cross section (Fig. 6) and the mean thickness of 1.91 m as determined from radar measurements, the area of the pockets above the mean thickness was found to be 10.5 m^2. This is equal to a pocket volume of 0.027 m^3/m^2 of ice cover. ...

For the multi-year sea ice floe profiled (Fig. 9A and B), the pocket area above the mean depth of 4.31 m, as determined over a total profile of 930 m, was 272.5 m^2. This is equal to a pocket volume of 0.293 m^3/m^2 of ice cover, or a volume of 293,000 m^3 (~1,843,00 bbl), over an area of 1 km^2."

Results from the author's second manuscript are as follows:

" Our studies have shown that where there is a preferred current direction under sea ice the crystal structure of the ice becomes highly ordered. This includes a crystal structure with a preferred horizontal c-axis that is oriented parallel with the local current. This ordered structure is a complex anisotropic dielectric which was found to be an effective polarizer of transverse electromagnetic waves. The reason for the polarization has been related to the ordered arrangement of the brine inclusions which are believed to create a unique array of parallel plate wave guides. This arrangement has been shown to reduce or eliminate radar signal reflection from the ice bottom when a linearly polarized radar antenna E-field is oriented perpendicular to the preferred crystal c-axis direction and to allow a maximum signal return when the antenna E-field is aligned parallel with the preferred c-axis azimuth.

Because current effects establish the preferred crystal alignment, the above radar signal phenomenon makes it possible to determine the direction of the preferred current under sea ice remotely. ...

Our sea ice profiling data from the Tigvariak Island runway site have been partially analyzed, with the following findings. From the ice thickness data we constructed ice thickness cross-sections showing the under-ice relief as depicted in Figure 1. The ice thickness data were also digitized. From this information a contour map of 150-m-long section of the profiled runway was made. This map is shown in Figure 2." Figure 2 of the second manuscript is

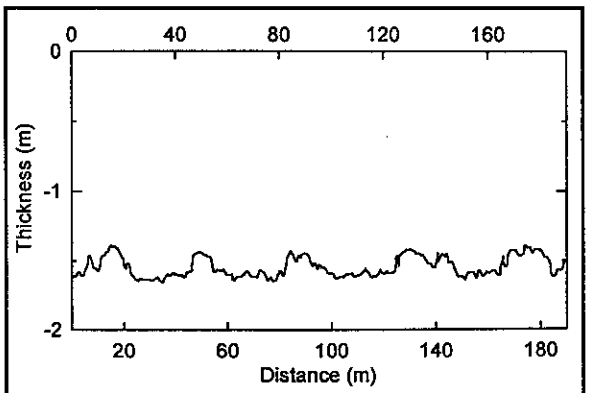

Figure 1 (second manuscript). Under-ice relief associated with snow cover thickness variation.

not reproduced in this review. "The contour intervals are 5 cm and show only the depth range from 1.5 to 1.65 m. This depth range varies around the mean depth which was found to be 1.56 m. The light shaded areas show relief which is under 1.55 m or areas where oil can be expected to pool up in pockets which are less than the mean depth. The darker shaded areas represent pockets which are less than 1.55 m deep but which may not fill with oil because they are surrounded by deeper ice relief. ...

From the digitized data we have determined that the mean depth for 18 parallel traverses 1.1 m apart and 150 m long was 1.56 m with a standard deviation of 0.03 m. We have also found that for the 20 m by 150 m area shown in Figure 2 the quantity of oil which could be expected to pool up in the under-ice pockets which exist above the mean depth is 0.0320 m^3/m^2 or 32,000 m^3/km^2 with a standard deviation of 1,580 m^3/km^2.

... An important finding is that a single traverse of only 30, 60, or 90 m long is not reliable for determining the surrounding area pocket volume above the mean depth as obtained for the single traverse.

...This mean of 31,000 m^3/km^2 represents the storage potential for these areas segments at about the 95% confidence level. The tabulated data"..."are graphically shown in Figure 3. From this graph one can infer that a single traverse profile of 150 m or more down the runway would provide data from which the under-ice storage potential of the are could be determined with a high degree of confidence. However, we do not recommend a single traverse at this time because we do not know the length of the individual under-ice pockets.

...

The profile information collected to date shows the strong effect of snow cover variation on under-ice relief and therefore oil pooling potential. In short, where a deep snow cover with varying thickness exists, the under-ice bottom relief is also significant, with large pocket areas above the mean ice thickness depth in which a significant amount of oil could pool should an under-ice oil release occur."

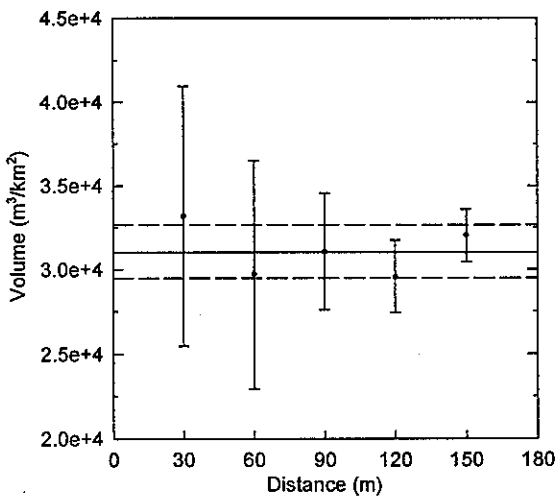

Figure 3 (second manuscript). Mean (·) and standard deviation (I) of oil pooling potential under sea ice as determined from 18 traverses 1.1 m apart of 30, 60, 90, 120 and 150-m-long. The solid line across the data is the mean of the means and the dashed line the related standard deviation.

BOSS Critique

The authors did not confirm the under-ice volumes with actual measured volumes of spilled oil. In fact the ice-water-oil interface may show up on the profile. If the gas goes through rupture cracks in the ice above the blowout it is also likely that the oil will as well.

Review of a manuscript by, Keevil, B.E. and R. Ramseier, entitled "Behaviour of Oil Spilled Under Floating Ice", in *Proceedings of the 1975 Conference on Prevention and Control of Oil Pollution*, American Petroleum Institute, Washington, D.C., pp 497-501, 1975.

Technical Summary

"Cold room experiments designed to simulate a hot oil spill demonstrated the basic behavior of crude oil under ice. Hot crude oil separates into particles 0.1 to 0.2 cm in diameter and rise to the ice-water interface. Under planar freshwater ice the particles spread in concentric rings at a radial rate of about 1.0 cm/sec. In still water the particles coalesce and form an oil lens about 1.0 cm thick which tends to become trapped in concavities on the ice bottom. If the ice continues to grow, the lens is sandwiched between layers of ice. A sandwiched oil lens does not significantly alter the ice growth rate.

Comparing cold room data with accidental oil spill data has verified that crude oil does separate into particles when released in cold waters. Pour point is important for predicting the initial behavior of spilled oil, especially when the pour point and spilled oil temperatures are about equal. As observed at Chedabucto Bay, oil (pour point -1 °C, oil temperature about 0 °C) escaping from small openings in the sunken tanker did not flow freely but surfaced as a discrete rope-like piece. Oil lens thicknesses varying between 1.0 cm and 2.0 cm have been reported. At many spills oil does not have an opportunity to spread under the ice. Since the specific gravity of most oils is between 0.8 and 0.9, which is less than water or ice, and as the rate of aging is greatly reduced at 0 °C, spilled oil could tend to flow over the ice. However, hot oil can melt through the ice, and as a natural ice cover floats with its ice surface above the water level, the oil is contained by the natural ice boom. In addition, the ice cover can be used as a working platform simplifying cleanup operations. The sources of a large percentage of oils spills under ice are unknown, and many spills occur that are not reported."

Objective

"In this study considerable care was taken to design cold room equipment that simulated a hot oil leak under floating freshwater ice. Although the experimental apparatus doe not duplicate exactly the spill conditions in a natural ice-covered water body, it nevertheless provides considerable insight into the behavior of crude oil under ice. In addition, the comparison of oil behavior in the cold room with oil behavior at accidental oil spills produces a realistic and inexpensive understanding of the mechanisms involved. The objectives of the study are, therefore, to: (1) conduct cold room experiments to determine the fate and behavior of spilled crude oil under floating ice; (2) correlate the behavior of spilled crude oil in cold room tests with accidental spills in the field."

Theory

The authors presented the theory with the results.

Method

"A circular aluminum basin, 1.5 m diameter and 0.7 m deep, was installed in a cold room capable of maintaining the air temperature at -15 ± 3 °C (figure 1). The cold room was equipped

with a fan to ensure uniform air flow and heat transfer in the basin. Heating tapes were glued to the outside of the tank and covered with 10 cm of polystyrene insulation. The heating tapes were connected to Variacs set at very low power to cancel out the bottom and side heat losses. This combination of heating tapes and insulation allowed one-dimensional freezing in the basin and effectively simulated the growth of natural ice similar to the type found in lakes, reservoirs, and rivers with low-flow velocities. In both the primary and secondary columnar ice layers, the crystallographic orientation of the c-axis is preferred vertical, and the grains are large to extra large with irregular shaped boundaries [6].

...

The ice thickness was measured with ice-thickness gauges [9]. The gauge is a small steel cylinder suspended by a wire under the ice. To measure the thickness, the cylinder is raised to the ice-water interface, and the distance from the ice-air interface is measured and subtracted from the total wire length.

An ice-water thermistor probe obtained a temperature profile with relative accuracy of ±0.2 °C. The probe contained 19 precision thermistors (YSI No. 44033) mounted in a plastic rod at a separation of 1 cm in the ice and 5 cm in the air and water. Each thermistor, solder joint, and wire was waterproofed with epoxy to ensure that no water could leak into the system. A multiconductor plug was installed at the top of the probe for connection of the bridge circuit. A rotary switch enabled each thermistor to be switched into the bridge, balanced, and the resistance recorded.

The importance physical properties of the oil to consider for the experiments are pour point, specific gravity, and viscosity. The physical properties of some northern crude oils are shown in Table 1. Pout point is the temperature below which the oil does not flow freely and is important for predicting the behavior of spilled oil under ice, especially when the temperature is low. Examining the table, it is reasonable to assume that most northern crudes will have a pour point in the range -10 ° to -50 ° C. Norman Wells crude oil was selected for these experiments.

Table 1. Physical properties of northern crude oils

Crude oil	Pour point °C	Specific Gravity at 16 °C	Viscosity at 16 °C centipoise
Prudhoe Bay, Alaska	-10	0.893	17 (at 25 °C)
Pembina, Alberta	-10	0.857	13
Atkinson Point, N.W.T.	-45	0.919	61
Norman Wells, N.W.T.	-50	0.833	6.5

Most oil spilled under ice will initially be hot, since the well head, tanker, and pipeline transit temperatures are between 40 °C and 80 °C. Because heating the oil in the laboratory cold room is too dangerous, the crude was injected at room temperature of about 20 °C. The oil injection system was a 25 litre plastic tank and gravity-fed electric pump. The system was portable and could easily be carried into the cold room and connected to the oil injection pipe.

The typical test procedure was as follows. At a cold room temperature of -15 °C, the basin was filled with water to a height of 60 cm. Two days later, a primary ice layer began to form. Its growth was predominately in the horizontal plane, forming a very thin ice layer. The secondary ice

grew parallel to the heat flow, perpendicular to the water surface, and reached the desired thickness (6 to 8 cm) three days later. The temperature gradient in the ice (about 0.5 °C/cm) was linear. Norman Wells crude oil (5 litres at 20 °C) was pumped for about 70 seconds through a 1.3 cm pipe and released 30 cm below the ice-water interface in the center of the basin. A plastic grid (2 cm reference lines) and clock were placed on top of the clear ice, and the oil behavior was photographed through the ice."

Results

"Oil behavior under floating ice in cold room

The circular basis tests investigated the basic behavior of crude oil under freshwater ice. Observations of oil particle formation, spreading under ice, and oil lens mechanisms were made.

Particles. The most significant observation of the behavior of hot crude oil released under ice is the separation of the oil into hundreds of small globs or particles 0.1 to 2.0 cm in diameter. When released from the injection pipe, the oil acts much the same way as water falling from a tap and is separated into particles by surface tension. Surface tension is the result of unbalanced molecular fields existing at the oil surface. Within the bulk of an oil particle the intermolecular forces are uniform, but at the oil surface the intermolecular forces pull the surface molecules toward the center. These centrally directed forces cause the oil particles to assume a spherical shape, thereby minimizing their surface energy and area. The crude oil particles are less dense than water and try to rise to the water surface. However, the ice sheet is a boundary and the particles are flattened on the under-ice surface by reason of their buoyancy. ...

Spreading under ice. Figure 3 illustrates the case of an oil lens and an oil particle at the ice-water interface. Oil particles at the ice-water interface may behave in one of two ways. First, they may remain as nonspreading particles. Second, they may coalesce with other particles and spread along the ice-water interface to form an oil lens. ...

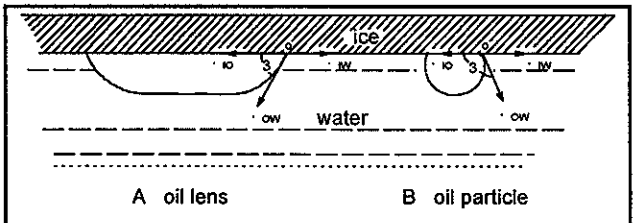

Figure 3. Oil at the ice-water interface.

Assuming that the various surface forces can be represented by interfacial tensions acting in the direction of the surfaces, then by equating the horizontal components of the tensions

$$\gamma_{IW} = \gamma_{IO} + \gamma_{OW} \cos\theta \qquad (1)$$

where γ denotes interfacial tension and subscripts *IW, IO,* and *OW* stand for ice-water, ice-oil and oil-water interfaces respectively. Before the oil particle touches the ice-water interface, the ice-water and oil-water interfaces are independent of each other. When the two are brought into contact, a new ice-oil interface is created while the ice-water and oil-water interfaces of equal area are destroyed. The energy expended in forming the ice-oil interface can be expressed as a spreading coefficient S

$$S = \gamma_{IW} - \gamma_{OW} - \gamma_{IO} \cdot \qquad (2)$$

Then combining (1) and (2),

$$S = \gamma_{OW} (\cos\theta - 1) \qquad (3)$$

For spreading, S is positive, and for nonspreading, S is negative.

The spreading rate of oil under ice depends on interfacial tension forces and hydrostatic forces derived from density differences between oil, ice, and water. In addition, the spreading rate depends on the injection rate, particle formation, ice roughness, and the ability of the oil to fractionate according to different solubilities of some components. As a result, the spreading mechanism is complicated and there is no simple realistic equation to predict spreading rate. In the circular basin tests the crude oil was injected at a rate of 70 cc/sec under smooth planar ice and the oil particles spread in fairly uniform circular rings. Clearly this can only occur in the absence of currents under smooth ice. Figure 4 shows four time-lapse photographs, taken at 5-second intervals, of oil spreading under ice. The separation between grid circles is 2.0 cm. A number of spreading experiments showed the oil spread radially at a rate of about 1.0 cm/sec.

Oil lens. At the ice-water interface the smaller particles of oil coalesce together and form larger particles, then most of the larger particles coalesce and form an oil lens. The time the oil particles rest at the ice-water interface before coalescing varied from seconds to several hours. Figure 5 shows and oil lens under 8 cm if ice 3 hours after a spill. Most of the oil has coalesced into a lens; however, a few particles remain independent. At the edge of the basin the heating tapes have melted the lower ice surface causing the oil to spread into the cavity. The oil lens does not adhere to the ice-water interface. Also the oil does not freeze or become semisolid, as the water temperature under the ice is about 0 °C and the pour point of the oil is -40 °C. The thickness of an oil lens is about 1.0 cm.

While the oil particles spread under the ice, coalesce, and form an oil lens, the ice continues to grow. First, the ice grows down around the sides of a lens and then underneath, sandwiching the lens between ice layers. Even with a slow ice growth rate (0.5 cm/day) or when the oil covers the whole ice-water interface, the oil is not pushed ahead by the growing ice. During one experiment, 5 litres of oil was sandwiched under 10 cm of ice. Two holes were drilled down to the oil, and almost all of the sandwiched oil was pumped into a storage drum. Examination of the lower ice-oil interface showed that it was rougher than the upper ice-oil interface.

The circular basin was divided into two halves with polystyrene to investigate the effect of a sandwiched oil lens in the temperature profile and ice growth rate of an ice sheet. Both halves had thermistor probes and ice-thickness gauges installed. One half was a control; in the other half oil was injected under 11.0 cm of ice and formed an oil lens about 1.0 cm thick.

To calculate the heat flux rate we assume that the sensible heat stored in the ice can be neglected and that all the latent heat of fusion liberated as a result of ice growth will pass upward through the ice sheet. The heat flux rate q is

$$q = \rho L \frac{\Delta h}{\Delta t}, \tag{4}$$

where ρ is the density of ice , L is the latent heat of freezing, Δh is the change in ice thickness, and Δt is the change in time. The heat flux rate in the circular basin is 110 cal/cm^2/day and compares with a heat flux rate of 120 cal/cm^2/day quoted by Williams [12] for a sheltered lake or ice surface under relatively still air conditions.

Figure 6 shows the ice thickness and typical temperature profile for each half of the basin 7 days after the oil spill. Below the sandwiched oil lens both temperature gradients (-0.3 °C/cm) were essentially the same. Above the oil lens, however, the temperature gradient remained constant but

decreased slightly in magnitude. It is clear that the temperature gradient in the oil (about -2.5 °C/cm) was much larger than in the ice as the oil is an insulating layer between the warm water below and the cold air above. Although it was impossible to measure the ice-oil-ice thickness until 3 days after an oil spill, the growth rate after that time was equal to the growth rate in the control. Ice is a better conductor of heat than oil, however, and the ratio of thermal conductivity for ice-oil is about 18:1. As a result, the thermal resistance of the oil lens could be considered equivalent to 18 cm of ice. This is illustrated in Figure 6 by extending the oil lens temperature profile down to 0 °C point, 18 cm below the actual ice-water interface. As the temperature drop across the ice is proportional to its thickness, the oil lens increased the temperature drop across the total ice thickness, but did not significantly alter the ice growth rate.

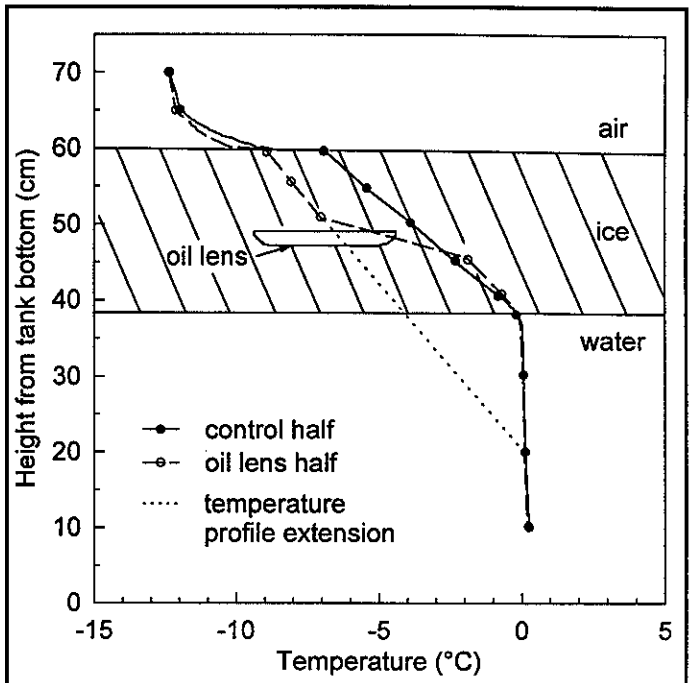

Figure 6. Temperature profile 7 days after oil spill.

Oil behavior under ice at accidental oil spills

...three accidental spills involving the behavior of oil under ice have been documented. At Deception Bay, Quebec, Canada, in June 1970, 427,000 gallons of No. 2 fuel oil and gasoline were spilled over permafrost and sea ice when a tank farm was destroyed by a slush avalanche [8]. At Chedabucto Bay, Nova Scotia, Canada, in February 1970, 2,000,000 gallons of No. 6 fuel oil, Bunker C, spilled from the wreck of a tanker into 0 °C to 2 °C water [7]. At Lake Champlain, New York, U.S.A., in March 1971, 44,000 gallons of No. 6 fuel oil overflowed from a storage tank and eventually flowed into the lake [4].

Particles. At the Chedabucto Bay Spill, Barber [1] reported that "chunks of oil varying from the size of a 50-cent piece to that of a hand-towel rolled up lengthwise" were coming from the wreck of the tanker. Divers also observed that oil leaking from small openings in the wreck generally surfaced in a "discrete piece like a rope 1 to 2 feet long." This chunk-like behavior results from the pour point temperature of the escaping oil (- 1 °C) being very close to the seawater temperature (0 ° to 2 °C) and demonstrates the importance of the pour point in determining the behavior of spilled oil.

Spreading under ice. Experience at Chedabucto Bay and Lake Champlain has shown that oil can be contained by a natural ice boom and it will not spread under the ice at all. At Lake Champlain the viscous fuel oil, which was stored at 55 °C in the tank, melted through 1.5 m of ice near the shore, cooled, and turned into a thick tar-like substance. The natural ice boom contained the oil from spreading further into the lake.

Lens. At Deception Bay oil spill, it was estimated that 75,000 gallons out of 427,000 spilled were contained under the shore-fast ice. The shore-fast ice had an average ice thickness of 0.9 m and

a very irregular under-ice surface. At low tide, holes were observed in the ice big enough to allow a man to enter the labyrinth of chambers below. It was difficult to judge the quantity of oil trapped under the shore-fast ice, although it was estimated that 2.5 cm of oil covered about half of the under-ice area.

While no oil under ice was actually observed at the Chedabucto Bay spill, it was suspected that oil was trapped under the ice in cavities and released when the ice cover melted. Barber [1] concluded that, away from intertidal zones and lagoons, oil did not accumulate under a uniformly flat ice cover. A 20-cm ice cover proved to be effective barrier to oil at the water surface and stopped the oil from spreading under the ice."

BOSS Critique

The authors state that transportation equipment such as pipelines or tankers will have oil temperatures between 40 and 80 °C but that the experiments were carried out at 20 °C for safety sake. Therefore, these experiments are not very close to reproducing the actual spill conditions of a tanker or pipeline and it should be noted that viscosity, as well as other oil parameters, are temperature dependent.

Review of a manuscript by, Greene, G.D., P.J. Leinonen and D. Mackay, "An Exploratory Study of the Behaviour of Crude Oil Spills Under Ice", Canadian Journal of Chemical Engineering, Vol. 55, pp 696-700, 1977.

Technical Summary

"An experimental spill of 0.38 m^3 of warm (55 °C) crude oil under the ice cover of a fresh water pond with an under water viewing port is described. Temperatures, dissolved hydrocarbon concentrations and oil slick behaviour and areas were determined. Some oil recovery and disposal methods were tested. An attempt has been made to quantify the rates of heat and mass transfer from the oil using reported values for transfer coefficients. The results indicate that the oil slick adopted a thickness of about 2 cm under the ice, that heat transfer from the oil was relatively fast and complete, that dissolution mass transfer is slow resulting in oil concentrations in the water of only 187 to 287 µg/l in the vicinity of the spill. Some recommendations are made for further studies to elucidate the nature and rates of the relevant physical processes and thus assist in assessing the environmental impact of under-ice spills."

Objective

The authors expected to experimentally determine, in a semi-quantitative way, the dominate process of oil movement under ice and leave the precise determination to future work.

Theory

The authors presented their theory in the paper's discussion section.

"**Heat and Mass Transfer**

A detailed experimental and theoretical description of heat and mass transfer from rising hydrocarbon drops in water has been given by Henkel[11] and Van Berg and Henkel[12] who showed that existing correlations for dispersed and continuous phase coefficients are adequate for circulating and oscillating drops. For present purposes, an order-of-magnitude analysis suffices to give estimates for the coefficients. Henkel[11] has given detailed data for transfer from an iso-octane drop into water during free rise. The following data apply which are probably also typical of values obtained in the experimental spill.

Drop diameter (based on volume)	d	0.61	cm
Rising velocity	v	16.7	cm/s
Overall heat transfer coefficient	U	0.0825	cm/s
Overall mass transfer coefficient	K	0.012	cm/s

This heat transfer coefficient U is equivalent to the conventional coefficient with units of W/m^2K divided by the oil heat capacity ($J/kg\ K$) and density (kg/m^3).

If, as the drop rises the temperature difference between it and the continuous phase falls from ΔT_1 to ΔT_2 in t during a rise of Z cm, it can be shown[11] that using Henkel's values for U and V,

$$\Delta T_1/\Delta T_2 = \exp(6Ut/d) = \exp(6UZ/dv) = \exp(0.050Z)$$

For the oil spill ΔT_1 was about 55 °C. Having risen 150 cm to the ice, the equation predicts a ΔT_2 of about 0.03 °C which is negligibly different from the water temperature.

...

An analysis can also be made of the mass transfer during the oil rising process. For

hydrocarbons dissolution from oil the mass transfer resistance lies almost totally in the continuous aqueous phase because of the high partition coefficient in favour of the hydrocarbon.

Assuming that the oil droplet is unchanged in concentration by mass transfer, the rate of mass transfer N can be calculated as

$$N = KA(C_i - C_\infty) g/s$$

where A is the drop area (here about 1.2 cm^2), C_i is the concentration of oil at the interface on the water side (here 30 mg/l or 30 g/m^3) and C_∞, the concentration in the bulk of the water can be assumed to be zero. The dissolution rate will thus be about 0.43 µg/s from each drop."

Method

"A pond 15 m in diameter and approximately 2.5 m deep at the centre was dug during the summer of 1974 at the Institute for Environmental Studies, University of Toronto, field station at Baie du Doré near Douglas Point, Ontario. ...

The under water viewing chamber, constructed from welded 45 gallon drums, was installed at one side of the pond so that the viewing ports were approximately 1 m below the water level when the pond was filled. A working platform was also constructed across the centre of the pond.

A one-inch diameter polyethylene pipe was buried in the pond bottom and connected to two drums of mixed sour blend Alberta crude oil of specific gravity 0.847 and approximate viscosity 10 mPa.s at 15 °C (supplied by BP Canada Ltd.). The drums were mounted on a stand approximately 1.5 m above the pond surface. The oil was to be discharged by gravity through the plastic pipe under the ice.

In order to follow the spreading and movement of the oil slick under the ice the pond was illuminated from below, enabling the oil silhouette to be viewed from on top of the ice. This technique, which eliminated the need for drilling exploratory holes to find the oil, was accomplished by installing six weighted 12 V automobile sealed beam headlight units at the bottom of the pond neat the oil discharge pipe prior to freeze-up.

Provision was made to sample the water column under the ice through four 6.4 mm (i.e. 1/4 inch) stainless steel tubes as illustrated in Figure 1. The water samples were taken from inside the recovery chamber.

When the pond ice was sufficiently thick, two vertical thermistor chains were placed through the ice. Temperature measurements were made during the spill with a YSI Telethermometer. An ice thickness gauge was also placed on the ice at this time. Unfortunately, the winter of 1975 was very mild in this location and the ice thickness at the time of the spill was only 20 cm with 2 cm of water on top of the ice. The ambient air temperature was 0 °C. Before the spill at 20:00 h February 19, 1975 the 0.38 m^3 (84 gal Imp.) of crude oil were heated to 55 °C using two 29 kW (100,000 BTU/hr) liquid propane burners applied directly to the drums. For safety, volatile hydrocarbons formed during heating were vented through a hose 15 m downwind from the drums.

The oil was discharged at a depth of 1.5 m below the ice in 10 minutes. The silhouette of the impinging and spreading oil was easily seen in the darkness. Monitoring continued for two hours after the spill and the following morning. Water and ice temperatures were also measured.

Water column samples were taken before the spill and periodically after the spill. The samples were taken in 60 ml amber glass bottles with aluminum foil-lined caps and were stored at 0°C until analysis.

The dissolved hydrocarbon content of the water samples was determined using the gas-stripping method and a Hewlett-Packard 5700A Gas Chromatograph equipped with a flame ionization detector and a 50 m x 0.25 mm ID squalane coated open tubular column. The gas stripping method which is described by Leinonen[9] and Mackay and Shiu[10] is only suitable for measuring the solubilities of the lower molecular weight hydrocarbons ($<C_9$) which have however the highest aqueous solubility and are regarded as being the principal components of the dissolved hydrocarbon."

Results

"It had been hoped that the rising oil column could be viewed and photographed through the under water observation port. This proved impossible because silt particles in the water reduced the visibility considerably. Other studies have shown that the rising oil disperses into droplets of varying diameter (typically 0.1 to 2.0 cm)[6].

The oil impinged on the under-surface of the ice and began to spread outward. The silhouette produced by the submerged lights allowed for easy timing of the oil movement during and after the spill. During the spill the spreading of the oil under the ice was characterised by a series of waves of oil emanating outward from the point of impingement. As viewed from the surface these appeared as concentric circles. This has been observed in the laboratory by Chen et. al.[6]. After about two minutes the outer boundary of the oil became more elongated as the oil began to follow the topography of the under-surface of the ice.

After the end of the spill the oil continued to spread and move, but the wave motion type of spreading stopped. Ultimately some of the oil reached as far as 5 m from the spill point but the coverage was not continuous.

...

An estimated 0.04 m^3 of oil reached the surface of the ice through cracks. The remaining 0.34 m^3 of oil spread to cover an area of 16 m^2, and thus achieved an average thickness of 2.1 cm after thirty minutes. During the next 15 h there was no further spreading and the oil appeared to be at equilibrium under the ice sheet at the ice-water interface.

The temperature records showed a rise at the ice-water interface of approximately 4.5 °C following oil impingement. This rise was believed to be due to contact with oil at the ice-water interface. The oil apparently had cooled considerably during its rise through the water column. The water temperature 20 cm below the ice rose by about 0.5 °C by oil heating. Within an hour after the spill, the water column had returned to its ambient temperature of 0 °C and the ice-water interface had fallen to within 0.5 °C of its initial temperature.

Analyses of pre-spill water sample showed only traces of volatile organics including methane which was probably formed by anaerobic degradation of organic matter in the pond. Table 1 gives the concentrations (in µg/l or parts per billion) of hydrocarbons in the post-spill samples. The total concentration ranged from 18 to 287 µg/l which is considerably lower (by a factor of 100 to 1600) than the equilibrium oil solubility of 30 mg/l. Benzene and toluene account for about half the total hydrocarbons present, in agreement with observations by Mackay and Shiu[10] of solubility of crude oil components in water. As expected, the highest values are encountered near the surface shortly after the spill. One week later concentrations had about halved, possibly by a combination of biodegradation and ground water flow through the pond.

Table 1. Hydrocarbon concentrations (µg/litre or parts per billion) after the spill at stated water depths below the ice surface.

Hydrocarbon	20 min after spill				12 hrs after spill		1 week after spill			
	50 cm	100 cm	140 cm	180 cm	100 cm	140 cm	50 cm	100 cm	140 cm	180 cm
C_3	93	84	20	--	56	30	58	42	10	21
C_4 (*n* and iso)	55	47	11	4	28	14	34	24	3	12
C_5 (*n* and iso)	16	12	12	3	12	6	12	9	11	3
other C_5 & C_6	8	2	2	--	3	2	2	2	--	1
benzene	71	82	16	11	52	15	27	18	1	4
toluene	44	43	7	--	24	8	19	7	--	2
Total	287	270	68	18	175	75	152	102	25	43

Although the principal aim was to study the behaviour of oil under ice, two cracks in the ice permitted the oil to reach the surface and provided an opportunity to examine the behaviour of crude oil spreading on a freezing water surface. Two surface oil slicks formed of areas 1 m^2 and 3 m^2 with an oil thickness of about 1 cm. These slicks stopped spreading within a few minutes of formation and did not spread further during the 16 hours of observation. The slicks appeared to have a stable edge about 0.5 cm thick which showed no tendency to become thinner. The slick was easily herded into a smaller area by light wave action but returned to their original coverage when the waves stopped. This is in contrast to behaviour on warmer water surfaces where some oils may spread to form very much thinner slicks, under the influence of surface tension and viscous forces. Whether the spreading behaviour is a function of temperature or oil composition or both is not known.

Overnight a thin film of fresh ice formed on the surface water and partly under the oil at the edges of the slicks. No ice formation occurred under the slick centres probably due to lower thermal conductivity of the oil. The easy herding and relatively thick oil slicks observed suggest that oil spills on near freezing water may be more easily contained than under warmer conditions."

From the discussion section of the manuscript.

"...The experimental oil temperature was about 4.5 °C suggesting that in the vicinity of the rising oil the water temperature had reached about this temperature. It thus appears that the oil drops will cool rapidly during the first few metres of rise essentially reaching the ambient water temperature which in turn is controlled by the relative enthalpies of the oil and water. In this case an interpretation of the data is that the oil enthalpy was only sufficient to raise about 1.3 m^3 of water in the vicinity of the rising oil about 4.5 °C because of the lower oil heat capacity. More heating will occur when the oil mass is high relative to the water mass and the water column may become quite warm. The extent of this heating will depend on the nature of the water currents induced by the rising oil. It can be concluded that the rates of heat transfer are fast and that the behaviour is dominated by enthalpies rather than rates.

It is noteworthy that although the oil may still be warm while under the ice the available enthalpy is small compared to that required to melt ice. For example, 1 m^3 of oil at 5 °C has an

enthalpy relative to 0 °C of about 6.3 MJ. The enthalpy of fusion of ice is about 305 MJ/m^3. Thus to melt one volume of ice requires the enthalpy contained in about 48 volumes of oil. Since the oil underlying the ice will lose heat both upwards to the ice sheet and downwards to the underlying water (probably at similar rates) it appears that the ratio of volume of ice melted to volume of oil spilled may be of the order 1 to 50. Accordingly, the thickness of the ice melted may be of the order of 0.01 to 0.1 mm. If the oil is continually flushed from the area and replaced by warmer oil, greater depressions may result but the stagnant oil pockets may effectively insulate the ice from further melting. It thus seems likely that depressions of a few *mm* or *cm* may form directly above the oil column but at radial distances of several metres from the centre only a few *mm* may melt. The temperature history of the oil after reaching the ice sheet indicates that within one hour after the spill it has essentially reached the ambient temperature.

... Since the drop mass is typically 0.1 g, the loss is a negligible fraction of the drop mass, thus justifying the earlier assumption that the oil composition change is negligible. During the rise of 150 cm in 9 s the mass dissolution will be about 3.9 μg of 0.004% of the drop mass. If all the oil behaved in this manner the total mass dissolved during the release of the 0.38 m^3 (approximately 300 kg) would be about 12 g. The water volume in the vicinity of the spill, i.e. over an area of 16 m^2 was of the order of 20 m^3, thus the maximum average concentration expected is about 0.6 g/m^3 or mg/l or about 2% of saturation. Clearly the oil concentration in the vicinity of the spill is controlled at a low fraction of the oil solubility by the rate of diffusional mass transfer in the aqueous phase in contact with the oil. The prediction is in satisfactory agreement with the experimentally observed values which were somewhat lower and in the range 0.07 to 0.30 mg/l.

In both the heat and mass transfer calculations the results are sensitive to the drop size and rising velocity which were not determined in this work. Clearly the approach must be to determine these quantities for an actual spill under realistic environmental conditions then use existing correlations for heat and mass transfer to calculate flues. The present results indicate that heat transfer is fast and that the dominant parameters are the relative oil and water masses and enthalpies brought into contact. In contrast, dissolution mass transfer is slow and the concentrations achieved in the water columns are only a small fraction of the equilibrium solubility. The extent to which aquatic biota are exposed to oil is thus controlled by the mass flux by both dissolution and emulsion formation.

... There is little information on oil to water transfer rates or on vertical eddy diffusivities under these conditions. Indications are that the rates are slow since concentrations of hydrocarbons dropped after the spill, suggesting that most of the dissolution took place during oil plume rise with relatively little occurring later from the stagnant slick. The relative contribution of these regimes and that of emulsion formation (with later emulsion dissolution) and dispersal requires further elucidation."

BOSS Critique

By allowing the volatile components to vent while heating the oil to be pumped under the ice, the under ice study has already been skewed to lower volatile (higher carbon number) components available to dissolution in the water column. This result is somewhat reflected in the results reported in the paper in that the some components in the water column were at a lower levels than expected. No measurement errors are mentioned here or referred to reference papers.

Review of a manuscript by, Deslauriers, P.C., "Observations of Oil Behaviour in Ice Floes and the 1977 Ethel H Spill", in *Proceedings of a Workshop on Oil, Ice and Gas,* EE-14, University of Toronto, Institute For Environmental Studies, Toronto, Ontario, pp 87-94, 1979.

Technical Summary

"From the Hudson River spill, the Buzzards Bay spill and laboratory experiments some general observations on the behavior of oil spilled in ice floes have been made. These conclusions were made from a limited amount of data and may not apply to other spill situations. More observations are needed to either support, change or add to these initial findings.

- The more porous the ice the greater the probability that oil will adhere to its surface. Therefore more oil will remain on the water for a spill in hard fresh water ice floes compared to a spill in decaying saline ice floes.
- Heavy ends of oil tend to adhere to porous ice floes while lighter ends are released on the surrounding water in a thin sheen. If there is enough interaction between the oil and ice, all of the heavy fractions of the spilled oil may adhere to the porous ice subsurfaces. This may have a great effect on cleanup procedures.
- Melt holes are formed in decaying ice where oil has come in contact with the ice. Therefore, the oil cannot easily be removed from the ice surface.
- When the ice is growing the oil which has adhered to the ice will become enclosed by ice.
- When the ice concentration is low, oil and ice tend to move in different directions and speeds. Also, at some increased ice concentration oil and ice movement occur together. It is not known at what ice concentration this transition of oil and ice movements occurs. This may be important for spill trajectory.
- When ice floes are very close together and stationary, high viscosity oil tends to accumulate to great thickness. The thickness of the oil appears to be dependent upon ice concentration, ice movement, oil viscosity, oil volume, and ice thickness. ...
- When ice floes are very close together and moving, the oil is spread amongst the ice. If there are waves present, the ice field will periodically compress and expand so that the oil will be progressively pumped along channels. If a channel is restricted and the film is sufficiently thick, the oil will be found on the ice surface.
- After ice breakup, oil in rafts, rubble fields, and ridges will travel with the moving ice floes until those ice formations decay.
- Oil incorporated in ice floes can travel considerable distances before being released. If those floes are beached or settle in sensitive areas the relatively fresh oil will be released in these areas, possibly increasing the environmental impact on these areas.
- Spill response in ice floes can be placed into three general categories; based on the oil behavior. Low Ice Floe Concentration, ... Medium Ice Floe Concentration, ... High Ice Floe Concentration, ... "

Objective

To present previously unreported observations on the *Ethel H* oil spill, and ice interaction, on the Hudson river.

Theory

None discussed or referenced.

Results

"On 4 February 1977, the barge Ethel H, with 2.7 million gallons of high-pour No. 6 fuel oil, ran aground on Con Hook Rock, two miles north of the Bear Mountain Bridge in the Hudson River. The barge leaked oil into the river for three days, until off-loading operations were complete. By that time 420,000 gallons of oil had been spilled into the icy waters of the Hudson.

At the time of the spill, ice covered up to 80% of the river surface, and averaged 15-25 cm in thickness. ... Ice floes, which for the purposes of this report are defined as free-floating ice, averaged 7 m in diameter, with some floes as large as 90 m. Transport and breakup of these floes was influenced primarily by strong river currents, and to some extent by shipping traffic and winds.

By 6 February, pockets of sheen and small amounts of oiled brash ice were visible as far as the George Washington Bridge, 30 miles south of the spill site. By 8 February, when the barge was finally off loaded and towed away, heavy concentrations of oil and oiled ice had spread to the George Washington Bridge. By 11 February, these oil concentrations had spread to the mouth of the river and into Upper and Lower Bays of New York. Over the next week, ice floating down the river gradually became cleaner, until by 16 February, little or no oiled ice or oil was visible in the river or bays.

One of the primary objectives of the researchers at the spill site was to determine if large amounts of oil were present in the shorefast ice region. Shorefast ice along the river had a very smooth underside. ... While the ice was not visibly stained with oil, chemical analyses of the ice samples revealed that the oil concentration in the ice to be from 0.7 to 0.8 ppm. The only oil detected under the ice was in the form if a very thin sheen. No evidence of heavy pooling was found.

The oil from the Ethel H became intermixed with the ice floes, while both were transported down river by the currents. It was observed that the black tarry oil adhered to many of the ice floes and, in some instances, the ice floe surface was as much as 60% covered with this oil. The ice melted more rapidly where the oil contacted the ice. The more heavily oiled ice pieces, therefore, had many cavities due to accelerated melting of the areas covered with oil. A thin sheen was observed streaming from some of the more heavily oiled ice pieces.

Ice floes appeared to flow down river in bands of closely packed floes stretching across the river. These bands were up to 100 m wide with up to 1 km separating each strip. The black tarry oil tended to stay within these bands while moving down river. Concentrations of oil were much higher within these packs of ice than in the ice free areas, although sheen was often visible covering most of the river surface. When the ice reached the mouth of the Hudson and flowed into the Lower Bay, it stretched out in long thin lines of floes with sheen streaming from the ice pieces. The sheen did not appear to be affected by the same wind and current parameters as the oiled ice, and was observed travelling in different directions and different rates that the ice."

BOSS Critique

This is a review of several spills and there is some qualitative discussion about oil and ice interaction and a statement about the oil not being observed in the ice after several days but that the actual measurements did show that there was oil present. No errors are mentioned for these measurements and no errors are given for the estimates of oil spilled and cleaned up.

Review of a manuscript by, Vandermeulen, J.H., B. Amero and T.P. Ahern, "Physical Weathering of Kurdistan Oil: Droplet Formation and Effect on Shore-Ice Melting", in *Proceedings of a Workshop on Scientific Studies During the Kurdistan Tanker Incident*, Bedford Institute of Oceanography, Dartmouth, Nova Scotia, pp 105-119, 1980.

The same information is presented in Vandermeulen, J.H., "Oil-in-Ice and Oil-Stranding Observations", in *The Kurdistan Oil Spill of March 16-17, 1979: Activities and Observations of the Bedford Institute of Oceanography Response Team*, Canadian Technical Report of Hydrography and Ocean Sciences, No. 35, pp 49-61, 1985.

Technical Summary

"1. Observations of inshore surface waters and of shore-ice stranded on St. Esprit Island, Cape Breton Island, showed the presence of numerous oil blobs and particles.

2. Particle size range varied from ca. one or two decimeter in length, down to numerous particles smaller than one centimeter in diameter. By far the largest proportion of oil particles was in the size range 500 microns and smaller.

3. The contamination by oil of the shore-ice enhanced the melt-rate of this shore-ice, through the heat gain of the oil droplets acting as black bodies. This effect was further enhanced by the spreading of the oil blobs during heat gain, thereby increasing the effective melting diameter of the oil drops."

Objective

The authors presented preliminary observations on the Kurdistan oil spill interaction with landfast and floating ice.

Theory

None stated by the authors.

Method

"Oil, water and ice samples were collected by helicopter on March 28, 1979, thirteen days after the tanker break-up. The samples were collected mainly from St. Esprit Island and from Pt. Michund. They were stored in an ice-chest aboard the aircraft, and were transported back to the Bedford Institute of Oceanography in Dartmouth for subsequent analysis. Samples of Kurdistan cargo oil taken from the deck near the ruptured # wing-tanks or directly from the #5 tank served as standards for comparison.

A number of methods have been used to determine particle size of oil in water (Cornillon, 1978). In the end we settled on two methods - direct observation by compound microscope, or indirect observation by projecting an image of the sample contained in a glass dish onto a screen by means of an over-head transparency projector. All particle counts were done in a refrigerated walk-in coldroom (ca. 5 °C). Water samples were examined directly. For ice samples a known volume was allowed to thaw in a shallow plastic petri dish. Prior experimentation had shown that under these conditions the oil particles or droplets did not coalesce, but remained apart and distinct, and could be readily counted and measured.

Oil concentrations in the various samples were determined by UV spectrofluorometry using the method of Gordon and Keizer (1974)."

Results

"OBSERVATIONS

At the time of the sampling trip patches and strips of floe-ice lay along most of the eastern coast of Cape Breton Island, down to and around Point Michaud at the entrance to Chedabucto Bay. Blobs of oil, ca. 30 to 60 centimeters in diameter, lay on the upper surface of some of the ice-floes. As well the edge of the ice-floes frequently were stained a faint brown coloring with smears of oil or smaller oil blobs.

Closer examination of the inshore surface water showed the presence of numerous small particles (Fig. 1 and 2). These appeared to be largely oil particles, distinguishable from other suspended matter both by their shape and by their tendency to stick to the walls of sampling vessels. The numbers of these particles increased the closer one sampled near the shore.

Onshore the surface of the shore-ice was contaminated generally with a fine cover or spray of oil blobs and droplets, ranging in size from hand-sized smears and splatters (Fig. 3) down to micro-particulate droplets or nodules a millimeter or less in diameter (Fig. 4). This oiling appeared to be restricted to the ice surface only, and was not found deeper within the one-half to two meter thick ice crust.

Morphologically there were three types or categories of oil contamination - the larger smears and blobs, the numerous fine droplets or particles, and a third group of "cratered" oily deposits (Fig. 5). The latter were almost invariably found within pits or depressions of varying depth, and were often surrounded by or consisted of a fine-veined network of oil particles spreading out over the ice surface (Fig. 7). In some cases these pits had penetrated through the ice (Fig. 8).

Table 1. Particle Size Distribution for Particulate Matter Extracted from Stranded Shore-ice

Mean Particle Diameter (μm)	Numbers/Litre	ppm (μl/l)
>1871	171.5	-
1871	514.6	1.8×10^3
1493	1,372.2	2.4×10^3
1128	6,861.1	5.2×10^3
892	2,058.3	0.8×10^3
691	15,094.3	2.6×10^3
489	107,375.6	6.6×10^3
<489	1,411,835.3	-

Table 2. Hydrocarbon Concentrations in Inshore Surface Seawater and in Stranded Shore-Ice

	Hydrocarbon Concentrations (μg/ml)	
un-oiled floe-ice[3]	0.307[1]	0.331[2]
seawater	908.23	812.98
shore-ice sample	2,145.45	2,304.00

[1]Referenced to #5 tank oil sample; [2]referenced to #3 wing-tank; [3]one-litre sample;

Particle size distribution of the fine particulate oil is shown in Table 1. Although there are a large number of particles in the range 1 to 2 mm diameter, the bulk of the particulate content of these samples consisted of particles smaller than 0.9 mm in diameter. The largest portion consisted

of particles smaller than 0.5 mm diameter. It should be noted here that no attempt was made to differentiate between normal suspended organic particulate matter and particulate oil.

A separate calculation of the total volume of micro-particulate matter in these shore-ice surface samples (based on Table 1) showed a concentration of 2.882 grams per litre of ice. This figure is in close agreement with the total hydrocarbon concentration of 2.15 grams per litre determined by chemical analytical means (Table 2).

DISCUSSION

...

The present observations on oil particles following the Kurdistan are essentially similar to Forrester's, differing only in that much larger numbers of particles were observed in the oiled shore-ice, due probably to the concentration effect of the shoreline with regard to inshore suspended material. This effect was pointed as well by Forrester.

As for the question of how these various particles were formed, there is the possibility that the presence of the ice at or near the site of the Kurdistan had something to do with this. Presumably an oil slick, through the shearing-grinding action of ice-floes, can be broken up into smaller and smaller blobs and particles. But it is still uncertain whether in fact the Kurdistan's spilled oil was contained within ice or if it escaped entrapment by the ice-field (viz. Trites et al., this volume). Certainly the weather conditions and sea-state at the time of the tanker break-up and for the two or three weeks following were violent enough that much of the particle and droplet formation can be accounted for just on the basis of wave action and water-column turbulence. Droplets can also be formed onshore by splattering of oil blobs onto ice or rock surfaces (Fig. 3).

While there was no attempt made to differentiate between normal suspended material and oil particles in the analysis there is little doubt in our minds that the bulk of the particles were in fact oil. Firstly there is close agreement between total volume of particulate matter (2.882 grams per litre of ice) and the total volume of hydrocarbons (2.15 grams per litre of ice), there being a circa 25% difference. Also the particle range, both with respect to size and numbers, was far greater than found normally in similar nearby waters (Strait of Canso, Nova Scotia, Kranck, personal communication).

A rather surprising aspect of this shoreline oiling by particulate oil is the unexpectedly large amount of oil that is represented by what, at first glance, appears to be a very fine cover of spray. If we assume that the oiled, shore-ice sample in Table 2 represents one square decimeter of ice surface then a beach 10 m wide and 1 km long can accommodate 2,250 kg of stranded oil in particulate form. This figure is at best a near guess of course, but it nonetheless serves to illustrate the amount of oil contamination that can occur due to particulate oil only. This also highlights the very significant role of droplet or particulate formation and potential contamination from this source during a spill.

The other more curious aspect of such particulate oil is the potential role such stranded oil may play in the melting rate of stranded ice. Most of the oiled shorelines examined had a heavily eroded pitted ice surface differing markedly from the smoother ice surfaces of non-oiled beaches. Probably this is a case of the oil particles and lumps acting as dark-bodies or heat-sinks for solar radiation, this in turn accelerating the melting rate of the underlying ice surface. This was observed out at sea as well, where large flattened blobs or discs of oil lying on floe surfaces were floating in a water-filled crater in the floe-surface. Occasionally one sees the same thing occurring under a piece of kelp or a sea-urchin skeleton, where with time the material becomes embedded within the

ice as it melts the ice underneath by reradiating absorbed solar heat.

There is one difference, however, between the melting effect of an oil droplet and that of a sea-urchin test, and that is the spreading effect of the oil droplet as it warms up under the sun. As the droplet spreads, its diameter increases and concomitantly its net heat gain (absorptivity minus emissivity) available for ice melt also increases. Therefore each of the oil droplets or particles act not as single point sources of constant area, but have to be treated as expanding black bodies with an area increasing as a function of time. This phenomenon is best illustrated by Figures 7 and 8, in which the network of oil 'veins' probably represents the greatest extent of oil droplet spreading before breaking up into smaller droplets. Taking this process on step further, it seems likely that some of these 'veins' will in time coalesce in turn, and again give rise to smaller droplets and particles (viz. Fig. 7). Thus this as well is a part of the microparticularization of spilled oil."

BOSS Critique

Although the oil concentrations method is referenced the authors should discuss the errors involved for the method. The authors do not include any errors for the other measurements. The manuscript does include a number of photographs of the oiled ice most with an internal scale of one kind or another.

Review of a manuscript by, Topham, D.R. and P.R. Bishnoi, entitled "Deep Water Blowouts" in *Proceedings of the Third Arctic Marine Oilspill Program Technical Seminar,* Environment Canada, Ottawa, pp 87-95, 1980.

In the manuscript written by Topham, D.R., entitled "The Interaction of Oil With Sea Ice in an Offshore Environment", in *Proceedings of Offshore Environment in the 80's*, 24 p, 1980, the author has summarised work done in the main title above and other work but does not present new data.

The manuscript by Topham, D.R., P.R. Bishnoi, and B.B. Maini, entitled "Laboratory Study of Behaviour of Oil and Gas Particles in Salt Water Relating to Deep Oil Well Blowouts" in *Proceedings of the Second Arctic Marine Oilspill Program Technical Seminar,* Environment Canada, Ottawa, pp 20-36, 1979 discusses the apparatus used for the main titled manuscript and work is performed on hydrate formation but not on oil in gas and gas hydrates.

Technical Summary (from the last section)

"From these laboratory tests it is possible to state that in oil well blowouts occurring at depths greater than 500 metres all the available gas will be converted to hydrate after about 200 metres of rise leaving the oil droplets to continue under their own buoyancy. These oil droplets will then be carried by cross currents during their rise. The water from the lower portion of the bubble plume will eventually find its equilibrium level and spread in a horizontal layer (the water at any level within the plume represents a mixture of entrained water from all depths below that point and has some intermediate density).

The gas saturated droplets do not appear subject to further shattering due to gas coming out of solution, although if the depths are greater than 800 metres, hydrates may form around the drops. Since their density is very close to that of water (sg 0.96) this will have little effect on their rise velocity.

The figures of depth given above depend on the gas composition, but are not expected to differ widely for gases associated with oil reservoirs."

Objective

To probe the interaction of gas hydrate and oil bubble formation during a simulated oil well blowout.

Theory

"The behaviour of oil well blowouts in shallow waters is largely determined by the large quantities of gas which are released along with the oil. The gas rises to the surface as a column of bubbles, acting as a very large scale pump transporting the oil, together with a quantity of water, rapidly to the sea surface. This is the case studied experimentally by Topham (1975) and occurred in nature during the recent Mexican blowout. The pumping action of the bubbles brings the oil to the surface in a concentrated plume and the surface release is confined to an area of a few hundred metres across. Normal ocean currents are small compared to the vertical velocities in the plume and have little influence on the oil during its journey from the seabed to the surface.

At higher hydrostatic pressures the gas can combine with water to form a solid substance similar in appearance to ice, whose density is very close to that of water. These crystalline formations are known as hydrates and if formed from the rising gas bubbles, the driving buoyancy of the rising plume is lost and the oil droplets are free to rise under gravity forces alone, and hence liable to be affected by cross currents during their rise.

Gas hydrates are non-stoichiometric crystalline solids formed under pressure when certain non-polar or slightly polar, low molecular weight gases are contacted with water. The pressure required for hydrate formation depends on the ambient temperature. The thermodynamic conditions are likely to be suitable for hydrate formation in most blowouts occurring below 300 metres of water if the water is within a few degrees centigrade of freezing point. However, the thermodynamic conditions alone are not sufficient for predicting whether or not the hydrates will form in a blowout. Other factors, such as water turbulence, presence of impurities and temperature history of the water can influence nucleation of hydrate crystals. The kinetics of hydrate formation are poorly understood at present which makes it difficult to estimate the rate of conversion of the gas bubble into hydrates.

Another consequence of the high pressure at the seabed in deep waters is that a considerable amount of gas is dissolved in the oil at its point of release. This raises the possibility that the gas, as it comes out of the oil drop during its journey towards the surface under the influence of reducing pressure, could form a layer of hydrates on the surface of the oil drop. It is also probable that such a drop would become super-saturated with gas. If this super-saturation should suddenly be relieved by nucleation of gas bubbles inside the drop, the resulting release of gas may shatter the oil drop into fine particles, thus aiding in their dispersion in water. The interaction of oil and gas particles could also have an influence on the formation of hydrates."

Method (from the Topham, D.R., P.R. Bishnoi, and B.B. Maini, manuscript listed above)

"In the present work, the objective was to develop an apparatus capable of holding gas bubbles of up to about 3 cm diameter in free suspension at pressures of up to 2000 psi (13790 kPa). The high pressure dictates the use of small windows for observing the bubbles. It is therefore imperative that the deviations of the bubble about its mean position should be very small. The pressure also makes the use of large diameter settling sections undesirable.

None of the reported equipments appeared to be totally satisfactory for building large bubbles in free suspension at high pressures. However, based on the experience of previous workers the hydrodynamic conditions necessary for holding a bubble in free suspension may be summarised as follows:

1. The drag on the bubble should be equal to the force of buoyancy.
2. To provide stability against vertical displacements, the axial velocity of the liquid should gradually increase with height in the liquid column.
3. To provide stability against lateral displacements, the velocity distribution over a cross-section of the liquid column should be axially symmetric with a local minima at the centre.
4. To prevent breakup of the bubble, the flow should be free of large scale turbulence.

Figure 1 shows a schematic diagram of the high pressure equipment used in this work. The details of its design have been described elsewhere (Bishnoi, P.R. and B.B. Maini, AMOP, 1978). The working section was fabricated from a 66 cm length of stainless steel bar of 28 cm diameter. The bar stock was bored through to make a tapered tube. The tapered section was fitted with three windows. The locations and dimensions of the windows are shown in Figure 2. The long windows

were made by incorporating Jerguson 5-T-20 series gage glass design. The circular window was fabricated out of plexiglass material. The flow modification section was made form a 120 cm length of 12.7 i.d. steel tube. The inside of the tube was Epoxy coated to prevent rust formation. The fittings inside the flow modifier were all made of stainless steel except for the honeycomb section, which was made from plastic drinking straws.

Auxiliary equipment attached to the water tunnel included the following:

1. Circulation pump: A Pioneer 575 series model P180 pump, with naval bronze bowl and impeller and 316 stainless steel shaft, was used for water circulation. The pump was driven by a Century 3 H.P. motor with stainless steel casing and a pressure equalizing diaphragm. The entire pump and motor assembly was enclosed in a steel can to enable operation at high pressures. The can was a 20.32 cm (8 in.) nominal diameter steel pipe, fitted with a top and bottom flange. The pump was attached to the top flange and it discharged into a 5 cm diameter stainless steel pipe. The bottom flange of the can was connected to the inlet pipe. The circulating water filled the can completely and thus caused the pressure on the inside and outside of the pump casing to be nearly identical.
2. Glycol Chiller and Heat Exchanger: The circulating water was cooled and maintained at low temperature (about 3 °C) by exchanging heat with chilled glycol in a shell and tube heat exchanger. A 2 ton refrigeration capacity glycol chiller and a 1/3 H.P. pump were employed for circulating the coolant. The temperature of the circulating water was monitored with a thermocouple connected to a digital voltmeter. The temperature was controlled within ±0.25 °C by an electronic controller and a control valve in the coolant line.
3. Pressurizing Cylinder: The water was pressurized by a piston and cylinder attachment. The piston was driven by high pressure nitrogen from a compressed nitrogen bottle.
4. Flow meter and Controller: The flow rate of the water passing through the tunnel was monitored by an orifice type flow meter with a digital readout. The flow could be changed either by operating the hand valve in series with the tunnel or by operating the control valve in the bypass line. An electronic controller was installed to maintain a constant flow rate through the tunnel. However, the set point of the controller had to be changed frequently to keep the bubble in view of the camera.
5. Bypass Filter: Though most of the equipment was made out of 316 stainless steel, the circulating brine did cause some corrosion and gradually became rusty in colour. A Balston "Type 50" filter was used to remove the rust particles and other suspended solids from the brine. The filter was operated only at low pressures during the initial cooling of the salt water. The brine was deaerated before filling in the system to reduce oxygen available for rust formation.
6. Video Camera and Recorder: A video cassette recorder was used for continuously recording the image of the stabilized bubble. The bubble was illuminated from the sides through the two long windows with the high intensity quartz halogen lamps."

Results

"The conditions under which hydrates can form are best described on a plot of temperature versus pressure. Figure 1 shows the equilibrium diagrams for three gases, ethane, methane and a typical natural gas mixture. Table 1 shows the composition of this particular gas. For hydrates to form, the temperature and pressure conditions must lie below the equilibrium line of the particular

gas considered. The equilibrium diagram refers to gas and water under saturation conditions and in cases where the concentration of gas in the water varies spatially, hydrate can only form where the concentration is above the critical level defined by the phase diagram.

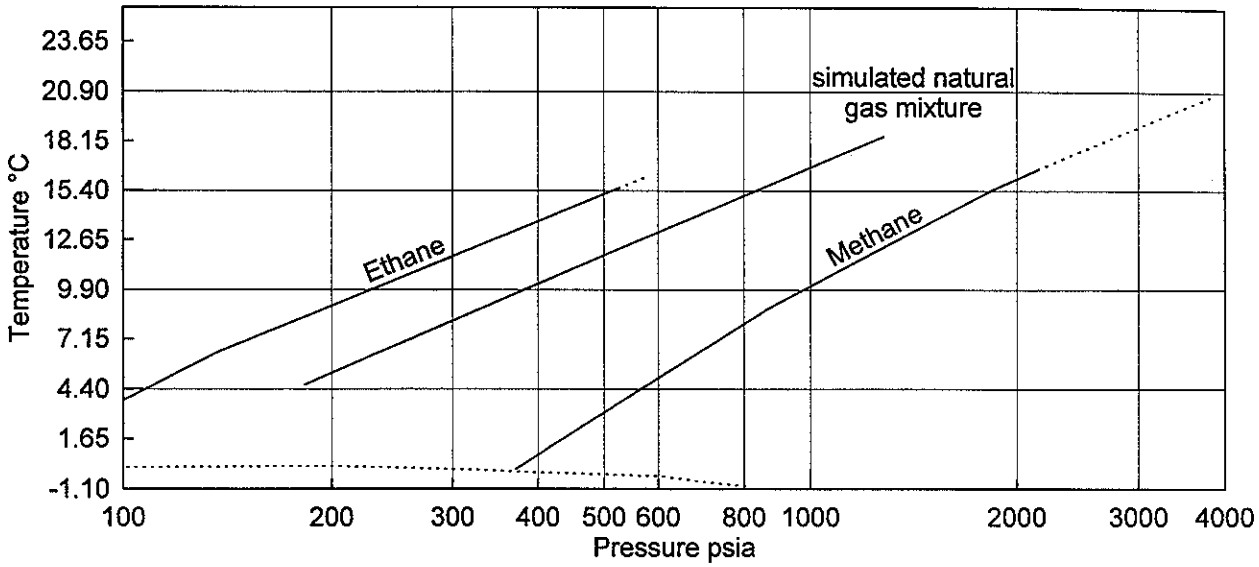

Figure 1. Hydrate formation from hydrocarbon gases in sea water (after Sze and Adams)

Table 1. Composition of simulated natural gas

Component	Methane	Ethane	Propane	I-Butane	N-Butane	I-Pentane	N-Pentane	N-Hexane
Mole Percent (%)	81.5	12.2	4.4	0.63	0.88	0.25	0.20	0.40

This is particularly relevant to the situation considered here, that of a bubble or cloud of bubbles, rising through a body of water having little or no dissolved gas. Here the concentration of gas in the water will be the saturation value only at the interface itself, falling off to the background level within the thickness of the diffusion/convection controlled boundary layer around the rising bubble. Hence the volume of the fluid available within which hydrate formation is possible will depend on the gas pressure over and above that defined by the equilibrium line on the phase diagram. For example if the gas within the bubble were at the equilibrium pressure for hydrate formation, the volume of water within which hydrate could form would be vanishingly small.

Having provided the conditions for hydrate formation, their actual formation depends on the presence of suitable nucleating centres to initiate the process. The time taken for the first occurrence of hydrates in a particular case is thus a statistical quantity depending on the density of nucleation centres and the volume of fluid of potential hydrate formation. The initial experiments with bubbles at constant pressure clearly illustrate this effect where gas pressures in excess of 500 psi above the equilibrium pressure were required to initiate hydrate formation when no gas had been previously injected into the water (simulated sea water at 3 °C, a mixture of Calgary tap water and sea salt). This can be taken to mean that no nucleation occurred within the time of the experiment, limited either by the bubble dissolving or being lost from the working section and distributed around the

circulating system.

Table 2. Hydrate formation results for simulated natural gas at 3 °C.		
Water tunnel pressure (psig)	Equilibrium pressure for pure water (psi)	Behaviour of the injected bubble in salt water
300	125	No hydrate formed.
500	125	No hydrate formed.
700	125	Hydrates formed on surface of the bubble. Shedding of small particles.
900	125	Hydrates formed on the surface. Shedding more rapid.
1130	125	Hydrates formed. bubble collapsed into hydrate flakes.
1300	125	Very rapid formation of hydrates.

It was found, however, that after several gas bubbles had been injected into the system, hydrates formed at lower pressures than with gas free water (see Table 2). The effect of the level of dissolved gas on the pressure at which hydrates formed during an experiment has now been explored further, and although the experiments are at the moment incomplete, it is apparent that the higher level of dissolved gas in the main body of water, the closer equilibrium conditions can be approached and form hydrates. Typical results would be that 45, 1-inch diameter hemispherical bubbles caused hydrate formation at 250 psi (the equilibrium pressure of the hydrate being 125 psi), whilst only three were required to cause instant hydrate formation at 900 psi. These amounts of gas correspond to concentrations far below the saturation level, so low in fact, their effect on the concentration profiles around the bubbles can be neglected. This suggests that their action is to provide an abundance of nucleation centres and this increases the probability for the first hydrate structure to form. Once the hydrate formation has been initiated, its rate depends on the complex exchange mechanisms around the hydrate covered bubble.

In the case of a well blowout it is likely that the sediment or fine suspended matter would enhance the nucleation and that one would not expect long induction times. ...

The results of gas bubbles under conditions of decreasing pressure, simulating their rise from depth were presented in a previous seminar, and in the present context it is sufficient to state that the decreasing pressure runs had a faster rate of hydrate formation. This was interpreted as the expansion of the bubble opening up fresh areas of gas/water interface which rapidly became coated with hydrate. This continual expansion accelerates the rate at which hydrate accumulates.

BEHAVIOUR OF GAS SATURATED OIL DROPS

... The behaviour of oil drops was observed by stabilizing a drop of oil in the water tunnel and subjecting it to controlled decompression. The oil was saturated with dissolved gas by mixing it with simulated natural gas in a rocking cell for about 24 hours prior to its injection in the tunnel. Two types of crude oil were used in these runs, namely Norman Wells and Imperial Judy Creek oil. The crude oil samples were supplied by Imperial Oil Limited of Calgary, Alberta.

Table 3. Summary of oil droplet runs

Type of oil	Pressure at which saturated with natural gas (psig)	Temperature of saturation (°C)	Temperature in the water tunnel (°C)	Pressure in the tunnel at time of injection psig	Were hydrate nuclei present in the tunnel at time of injection?	Behaviour of dissolved gas and oil droplet
Norman Wells	1050	25	3	1000	no	The droplet remained visually unchanged. Dissolved gas simply diffused out of the drop. No hydrates formed
Norman Wells	1250	25	2	1200	no	Some foam was observed on surface of the drop. No hydrates formed.
Norman Wells	850	1.5	2	800	no	Some foam accumulated on surface of drop. No hydrates.
Norman Wells	1200	25	3	1100	yes	A layer of hydrate formed on surface of the drop. Hydrates decomposed into gas bubbles as the pressure dropped during controlled decomposition
Judy Creek	1050	25	2	1000	no	
Judy Creek	1100	1.5	2	1000	no	No change on the drop could be detected visually.
Judy Creek	1250	25	3	1200	no	
Judy Creek	1250	25	3	1200	yes	A layer of hydrates formed on surface of the drop and soon enclosed the oil in a rigid structure. The structure broke down during the later parts of the run when pressure was around 300 psig.
Judy Creek	900	25	3	800	yes	A layer of hydrates formed on surface of the drop. It appeared to be less rigid than the above run.

It was observed in preliminary runs that the drop moved considerably in radial as well as axial direction. To keep the drop in view of the camera and to eliminate the possibility of the drop being lost during the run, it was decided to attach the drop to a metallic support. A stainless steel wire bent in the form of a hook was used for this purpose. The velocity of the flowing water was kept identical to that required for stabilizing a freely suspended drop. It is believed that the results obtained in this manner would be applicable to freely suspended drops.

The results of these runs are summarized in Table 3. The drops behaved differently

depending on whether or not previously formed hydrate nuclei were present in the tunnel at the time of the oil injection. When hydrate nuclei were not present the gas came out of oil mainly by diffusion. However, in some of the runs, an accumulation of foam on surface of the oil drop was observed. This would indicate that gas bubbles nucleated inside the oil. This nucleation did not lead to breakup or emulsification of the drop.

When hydrate nuclei were present in the tunnel at time of oil injection, the gas coming out of the oil formed a layer of hydrates on surface of the drop. The rigidity of this layer increased with time during the initial stages of a run. The time required to attain maximum rigidity decreased with increasing values of initial pressure. The extent to which the hydrate layer grew into a solid like structure also was a function of the initial pressure. The hydrate layer after attaining rigidity remained stable till the pressure dropped below hydrate decomposition level. The decomposition after that was fairly rapid and resulted in the production of gas bubbles. The gas bubbles eventually broke off from the suspended oil drop, carrying some of the oil with them. The type of oil used had some influence on the behaviour. Norman Wells oil formed a less rigid structure and the hydrate layer with this oil decomposed at higher pressure compared to Judy Creek oil.

The length of the oil decompression runs was primarily a function of the starting pressure. It was typically of the order of one hour.

Effect of Oil on Hydrate Formation in Bubble

Oil and gas were injected simultaneously from the same nozzle to see if a thin oil coating on the gas water interface changes the hydrate formation behaviour. The presence of oil appeared to cause a slight reduction in the rate of hydrate formation at a given pressure.

Interaction of Gas Bubbles and Oil Drops

Gas bubbles were forced to collide with an oil drop by releasing the bubbles directly below the suspended drop. The oil drop did not coalesce with the rising gas bubble even when the gas bubble was coated with a layer of oil.

Interaction of Hydrate Particles and Oil Drops

The interaction between hydrate particles and oil drops was not investigated systematically. However, some conclusions could be drawn on the basis of the runs in which oil was injected in the presence of hydrate particles. The oil appeared to become absorbed in the pores of hydrate flakes. It also acted as a weak binder for holding the hydrate particles together."

BOSS Critique

The mole percent values presented in Table 1 add up to 100.46% and since some of the component values are between 0.20 % and 0.88 %, 0.46% is a significant error in this calculation.

The authors do not explain the absorption of the oil into the hydrate pores. In fact the authors do not even discuss pore size of the hydrate layer never mind the absorption of the oil into the hydrate layer. The approach presented here was qualitative not quantitative and there were no errors mentioned for the measurements nor for the assumptions made.

Review of a manuscript by, Topham, D.R. entitled "The Disposition of Gas/Oil Mixtures Trapped Under Ice", *Canadian Journal of Physics*, Vol. 58, pp 1183-1190, 1980.

Identical results are presented in the manuscript by Topham, D.R., entitled "The Disposition of Gas/Oil Mixtures Trapped Under Ice", in *Proceedings of a Workshop on Oil, Ice and Gas*, EE-14, Institute For Environmental Studies, University of Toronto, Toronto, Ontario, pp 55-65, 1979.

Technical Summary

"A number of stable configurations which can be formed from mixtures of oil and gas trapped in water under a solid surface is examined. In particular, the problem of a lens of oil lying within a sessile bubble of gas is solved, and two forms of stable solution are found; a discrete lens of oil lying in the bottom of the gas bubble and a double sessile drop formation with the oil completely enclosing the gas. A comparison of the energies of the formation indicates the ranges of oil properties where each configuration is likely to be found. The results are applied to the specific case of crude oils trapped under ice and an appropriate existence diagram constructed."

Objective

"When considering their behaviour at a gas–water interface, oils can be divided into two types, spreading and non-spreading. As suggested by the terminology, the former tend to cover the available water surface, whilst the latter form discrete pools or lenses (1). The condition that an oil be non-spreading is that the sum of the interfacial tensions of the oil–gas and oil–water surfaces exceeds that of the gas–water interface.

The characteristics of the following configurations are now examined in detail: oil lying on the bottom portion of a trapped gas bubble (the sessile drop–lens configuration), a gas bubble encapsulated within a sessile drop of oil (the double sessile configuration), and separate sessile drops of gas and oil. An existence diagram is constructed from energy considerations which indicates the most probable configuration for a given set of oil properties. ..."

Theory

"2.0 The Sessile Drop–Lens Combination

The configuration under consideration is shown in Fig. 1*a* which details the outer edge of the system. The horizontal line through the meeting point of the three interfaces is taken as a reference point for the vertical distances.

In general the pressure difference across an interface with interfacial tension γ is given by the expression

[1] $$\Delta p = \gamma [1/R_1 + 1/R_2]$$

where R_1 and R_2 are the principal radii of curvature. The equation of such a surface under static conditions can be derived by equating the hydrostatic pressure forces to those deriving from the interfacial tension and the surface curvature. The problem can be considerably simplified by letting one of the principal radii of curvature become large, i.e., by considering large diameter systems. The mathematical problem then reduces to one of two dimensions in a plane. The case of single sessile

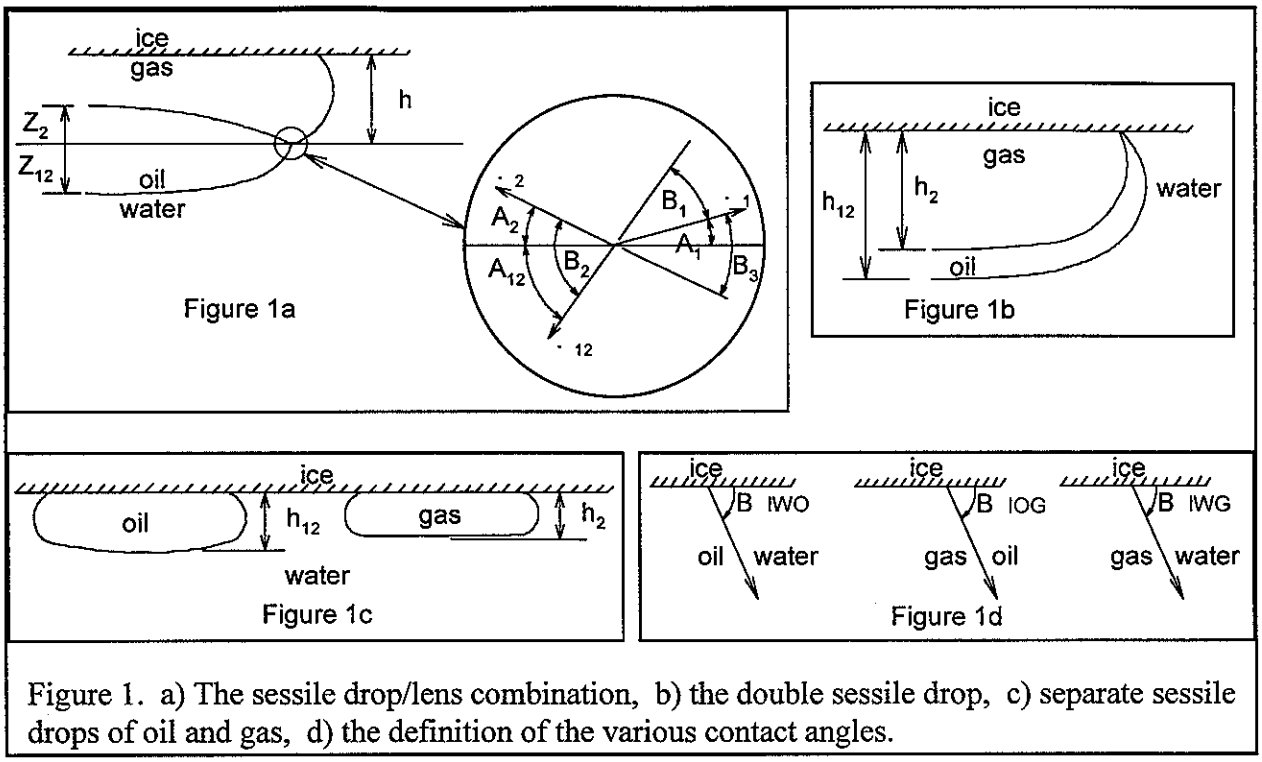

Figure 1. a) The sessile drop/lens combination, b) the double sessile drop, c) separate sessile drops of oil and gas, d) the definition of the various contact angles.

drops is well documented in elementary textbooks; see for example Champion and Davy (2).

The three surfaces making up the sessile drop–lens combination can all be represented by an equation of the form

[2] $$z^2 + 2(b - h)z + a^2(\cos\theta - \cos\phi) = 0$$

where z is the vertical coordinate measured from an appropriate origin and θ is the angle the local tangent makes with the horizontal. The constants a, b, h, and ϕ represent, respectively, the capillary length $(2\gamma/\rho g)^{1/2}$, the gas pressure inside the bubble, the hydrostatic pressure at the origin, and the angle of the tangent at the origin. In general, the surfaces described by [2] possess a single point of inflexion at $z = b - h$, at which point the surface has zero curvature and there is no pressure drop across it. The following quantities are defined:

$$a_1^2 = 2\gamma_2/\rho_1 g$$
$$a_2^2 = 2\gamma_2/\rho_2 g$$
$$a_{12}^2 = 2\gamma_{12}/(\rho_1 - \rho_2)g$$
$$m^2 = 2(\gamma_2 + \gamma_{12} + \gamma_1\cos\psi_{IWG})/\rho_1 g$$
$$b = p/\rho_1 g$$

where γ_1 = gas–water surface tension, γ_2 = gas–oil surface tension, γ_{12} = oil–water interfacial tension, ρ_1 = water density, ρ_2 = oil density, and p = pressure in the gas bubble. The various coordinates and angles necessary for a mathematical description are defined in Fig. 1 *a* and *d*.

By applying [2] to the three interfaces or, which is equivalent, by considering the force balance on the various elements of the system, the following set of equations can be derived:
Upper section of oil lens

[3a] $$z_2^2 = a_2^2(1 - \cos A_2)$$

Lower section of oil lens

[3b] $$z_{12}^2 - 2z_{12}z_2[\rho_2/(\rho_1 - \rho_2)] + a_{12}^2(1 - \cos A_{12}) = 0$$

Gas bubble

[3c] $$h^2 - 2bh + a_1^2(\cos A_1 + \cos\psi_{IWG}) = 0$$

Overall force balance

[3d] $$2b(h + z_{12}) + (\rho_2/\rho_1)(z_2 + z_{12})^2 - m^2 - (h + z_{12})^2 = 0$$

Pressure balance between centre and outside

[3e] $$b + (\rho_2/\rho_1)(z_2 + z_{12}) - (h + z_{12}) = 0$$

Simple geometry yields the following angular relationships at the gas–oil–water junction

[3f] $$A_2 = B_3 - A_1$$

[3g] $$A_{12} = B_1 + A_1$$

and a force balance gives

[3h] $$\cos B_1 = (\gamma_1^2 - \gamma_2^2 + \gamma_{12}^2)/2\gamma_1\gamma_{12}$$

[3i] $$\cos B_3 = (\gamma_1^2 + \gamma_2^2 - \gamma_{12}^2)/2\gamma_1\gamma_2$$

It can be shown (Appendix A) that real solutions to the above set of equations only exist when $b = h$. The is the requirement that there is no pressure difference across the gas–water boundary at the oil–water–gas junction point which, in turn, implies that this is a point of inflexion in the gas–water interface curve.

For conciseness in the presentation of results, it is convenient to work with nondimensional variables and, accordingly, the quantities a_1, γ_1, and ρ_1 are chosen as reference values of length, interfacial tension, and density, respectively. Setting $b = h$ in the set of equations [3] and performing some eliminations yields the following equation for the angle A_1 :

[4] $$\left[1 - \frac{\gamma_2^* \cos B_3}{(1 - \rho^*)}\right]\cos A_1 + \left[\frac{\gamma_2^*}{(1 - \rho^*)}\sin B_3\right]\sin A_1 + \left[\frac{\gamma_2^* \rho^*}{(1 - \rho^*)} - \gamma_{12}^*\right] = 0$$

where the starred quantities have the following nondimensional form

$$\gamma_2^* = \gamma_2/\gamma_1$$

$$\gamma_{12}^* = \gamma_{12}/\gamma_1$$

and

$$\rho^* = \rho_2/\rho_1$$

Once [4] is solved, the nondimensional forms of the oil thickness t^* and the depth h^* are readily

calculated.

Before considering the details of the solutions, the limits imposed by the form of the equations will be considered. The values of cos B_1 and cos B_3, must lie in the range -1 to +1 and [3*h*] and [3*i*] then yield the following conditions:

[5*a*] $$\gamma_{12}^* \leq 1 + \gamma_2^*$$

[5*b*] $$\gamma_{12}^* \geq 1 - \gamma_2^*$$

[5*c*] $$\gamma_{12}^* \geq \gamma_2^* - 1$$

A further condition is imposed by the shape of the gas–water interface. Negative values of the angle A_1 imply a minimum in the gas–water interface curve between the oil–water–gas interface junction and the solid surface. Since the triple interface point is a point of inflexion, hydrostatic considerations would dictate a second point of inflexion on the opposite side of the minimum. Since the equation of the curve only admits a single point of inflexion, it follows that the angle A_1 must be positive. In the limit of $A_1 = 0$, [4] reduces to the quadratic form.

$$\gamma_{12}^{*2} - 2(1 - \rho^*)\gamma_{12}^* + 2\rho^*\gamma_2^* + 1 - 2\rho^* - \gamma_2^{*2} = 0$$

which has solutions

[6*a*] $$\gamma_{12}^* = 1 - \gamma_2^*$$

[6*b*] $$\gamma_{12}^* = 1 + \gamma_2^* - 2\rho^*$$

Equation [6*a*] is identical with the limit implied by [5*b*], and [6*b*] represents a further restriction over and above those imposed by the cosine relationships, which solutions to [4] show to be a lower limit on γ^*_{12}. The conditions are best illustrated as an existence diagram with axes γ^*_{12} and γ^*_2 (Fig. 2). The region of real physical solutions lies within the open rectangle defined by [5*a*], [5*b*], and [6*b*]. Equation [5*b*] is the criterion dividing the spreading from the non-spreading oils.

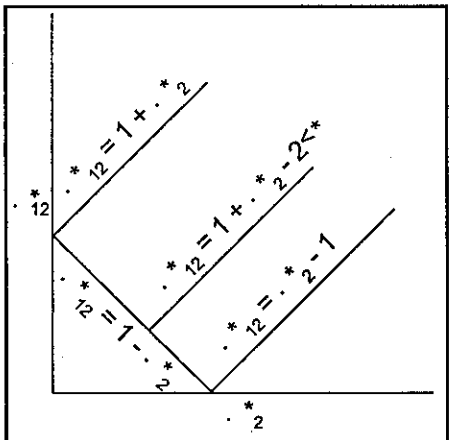

Figure 3. The configuration assumed for the energy analysis.

2.1 The Double Sessile Drop

Figure 1*b* shows the general form of the configuration where the gas is completely enclosed within a sessile drop of oil. Applying a simple pressure balance at the centre point gives the pressure at the oil–gas interface as

$$p = (\rho_1 - \rho_2)gh_{12} + \rho_2 h_2 g$$

When considering the equations of the gas–oil and oil–water interfaces, as far as the former is concerned, the term $(\rho_1 - \rho_2)$ gh_{12} is a constant applied pressure that does not affect the shape of the interface, since this only reflects pressure differences across it. Likewise, the term $\rho_2 h_2 g$ has no effect on the shape of the oil–water interface, and thus the two interface shapes can be calculated independently. The

thickness of the resulting oil layer is then given by the difference between the depth of a sessile drop of oil in water and that of a bubble of gas in an infinite body of oil.

The equations of the two interfaces can be obtained from [2] by setting $b = h$, $\phi = 0$. The depths of the sessile drops are then given by putting $\theta = -\psi_{IOG}$ and $\theta = -\psi_{IWO}$ for the gas in oil and oil in water cases, respectively.

Hence:

$$h_2^2 = a_2^2(1 + \cos\psi_{IOG})$$

and

$$h_{12}^2 = a_{12}^2(1 + \cos\psi_{IWO})$$

The resultant oil thickness is given by

$$t = h_{12} - h_2$$

The conditions for the double sessile drop to exist are that $t > 0$ and that suitable boundary conditions can be satisfied at the solid surface. The first of these can be expressed in nondimensional terms as:

[7]
$$\frac{\gamma_{12}^* \rho^*}{\gamma_2^* (1 - \rho^*)} \geq \frac{(1 + \cos\psi_{IOG})}{(1 + \cos\psi_{IWO})}$$

The second concerns the balance of various interfacial energies at the solid surface and will not be pursued further at this point.

2.2. Energy Considerations

The solution of the set of equations derived in Sect. 2.0 for the sessile drop–lens combination describes the equilibrium of a set of forces, but provides no information as to whether or not the equilibrium is stable. To answer this question it must be established that the solution obtained corresponds to an energy minimum.

To calculate the energy, a large diameter system is again assumed, but now the energy of the curved edges is neglected in comparison with that of the horizontal areas. The volumes of oil and gas are taken to be fixed and are denoted by V_O and V_G, respectively. The problem is to determine the thicknesses of oil and gas, denoted by t and h_2, respectively, which correspond to the minimum energy of the system, Fig. 3. In terms of the notation of Sect. 2.0, $t = z_2 + z_{12}$ and $h_2 = h - z_2$.

The total energy of the combined system, denoted by E_t can be written as the sum of the potential and surface energies as follows:

$$E_t = \frac{1}{2}Ag[(\rho_1 - \rho_2)(h_2 + t)^2 - (\rho_1 - \rho_2)h_2^2 + \rho_1 h_2^2] + A(\gamma_{IG} + \gamma_2 + \gamma_{12} - \gamma_{IW})$$

where γ_{IG} and γ_{IW} are interfacial tensions of the ice–gas and ice–water interfaces, respectively, and A is the horizontal surface area of the bubble. After some manipulation, we obtain

$$\frac{E_t}{V_G \rho_1 g} = \left[\left(1 - \frac{\rho_2}{\rho_1}\right)\frac{t}{h_2}\left(\frac{t}{h_2} + 2\right) + 1\right]\frac{h_2}{2} + \frac{(\gamma_{IG} + \gamma_2 + \gamma_{12} - \gamma_{IW})}{h_2 \rho_1 g}$$

Differentiation with respect to h_2, with the ratio t/h_2 fixed, to determine the minimum total energy,

yields the following relationship for the gas thickness h_2

$$[8] \qquad \left[\left(1 - \frac{\rho_2}{\rho_1}\right)\frac{t}{h_2}\left(\frac{t}{h_2} + 2\right) + 1\right]h_2^2 = \frac{2(\gamma_{IG} + \gamma_2 + \gamma_{12} - \gamma_{IW})}{\rho_1 g}$$

where $t/h_2 = V_O/V_G$.

By considering a balance of forces at the ice–gas–water interface, the ice–gas interfacial tension can be written in terms of the ice–water–gas contact angle ψ_{IWG}, Fig 1*d*, to yield

$$\gamma_{IG} = \gamma_{IW} + \gamma_1 \cos\psi_{IWG}$$

The sum of the interfacial tensions on the right hand side can then be written in terms of the ice–gas–water contact angle, ψ_{IWG} as

$$\gamma_{IG} + \gamma_1 + \gamma_2 - \gamma_{IW} = \gamma_{12} + \gamma_2 + \gamma_1 \cos\psi_{IWG}$$

Substituting this expression into [8] yields the relationship

$$[9] \qquad \left[\left(\frac{h_2}{t}\right)^2 + \left(1 - \frac{\rho_2}{\rho_1}\right)\left(1 + \frac{2h_2}{t}\right)\right]t^2 = m^2$$

This same relationship can be derived from [3*d*] and [3*e*] with b set equal to h and substituting $z_2 + z_{12} = t$, and $h = h_2 + z_2$. Hence, the conditions derived from the force balance correspond to an energy minimum. The energy of the system at the minimum condition is then given by

$$\frac{E_t}{V_G \rho_1 g} = \left[\left(1 - \frac{\rho_2}{\rho_1}\right)\frac{t}{h_2}\left(\frac{t}{h_2} + 2\right) + 1\right]h_2$$

when the energy is equally divided between the potential and surface energies. Making use of [9] and [3*e*] and writing $h_2 = h - z_2$ gives the form

$$\frac{E_t}{V_G \rho_1 g} = \frac{m^2}{t}\,\frac{1}{[h/t - (1 - \rho_2/\rho_1)]}$$

where values of h and t are derived from the solutions of the set of equations [3].

The relationship [8] applies equally well to the sessile drop–lens configuration of Fig. 1*a*, or to the double sessile drop of Fig. 1*b*, since only the nearly plane surfaces are considered. In the latter case, the group of interfacial terms on the right-hand side of the equation can be expressed in terms of ice–water–oil and ice–oil–gas contact angles. By the same token, it applies to both spreading and non-spreading oils. Equation [8] is satisfied for either system provided that appropriate values of t/h_2 are used.

We thus have three main configurations to consider, the sessile drop–lens combination, the double sessile drop, and separate sessile drops of gas and oil. A fourth possibility, that of a ring of oil lying at the base of the gas bubble, can also be shown to be a possible configuration, but for large diameter bubbles the volume of oil concerned is small compared to that involved when the whole lower surface of the gas bubble is oil covered.

It remains to compare the energies of the various systems considered and, on the basis of this and on the conditions for the existence, to predict the most probable configuration. Although each configuration corresponds to an energy minimum, and hence is locally stable, finite perturbations

may lead to a change to a different configuration having a lower total energy.

3.0 The Characteristics of the Ice–Oil–Water–Gas System

The general case of three fluids and a solid surface contains a total of nine independent parameters; six interfacial tensions and three densities, and a concise presentation of the characteristics of the system is not possible. However, for the case considered, one fluid is a gas and its density may be neglected, and this combined with recent measurements on oil–water systems (3) suggest that three parameters may be sufficient; the specific gravity of the oil and the ratios of the oil–gas and oil–water interfacial tensions to that of the water–gas surface tension, denoted ρ^*, γ^*_2 and γ^*_{12}, respectively. The relative interfacial tensions are always less than unity and typically range between 0.4 to 0.7 for both parameters for crude oils (4).

The interfacial tensions and contact angles of crude oils in an ice–water system have been measured with great precision by Malcom and Dutton (3), using the improved method of Malcom and Paynter (5). In all cases it was found that the angle of contact (as defined in Fig. 1*d*) of the ice–water–oil intersection was 0° the interpretation being that there is always a layer of water adjacent to the ice; similar results were found for glass surfaces.

Malcom and Dutton (3) suggest in a discussion of their results that it takes a pressure of 10^8 Pa to remove a thin film of water from glass, whilst the pressure exerted by a sessile drop of oil is of the order of 10^2 Pa. The results for ice suggest that it is of a similar hydrophilic nature. If this is the case, the pressure exerted by a gas bubble, at most 10^3 Pa is also insufficient to remove the water–ice interface and hence the contact angles of gas bubbles in water will also be zero. If this is the case the contact angles no longer appear in the analysis and we are dealing with free floating bubbles distorted by gravity and the surface properties of the solid do not appear in the system. In the present notation

$$\psi_{IWO} = \psi_{IOG} = \psi_{IWG} = 0$$

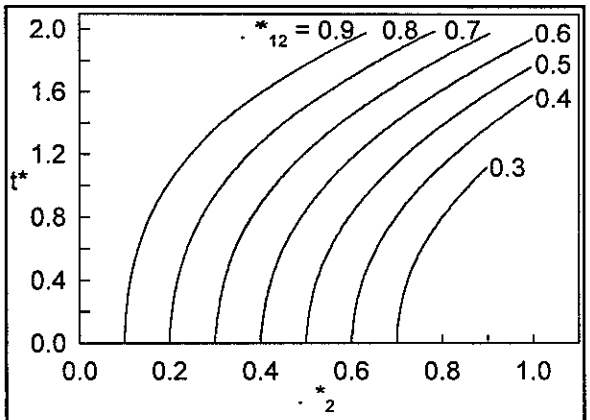

Figure 4. Normalized oil thickness for sessile drop/lens combinations, $\rho^* = 0.8$.

The sessile drop–lens configuration of Sect. 2.0 has been solved under these conditions and Fig. 4 shows the variation of oil thickness t^* for a range of values of γ^*_2 for the case of $\rho^* = 0.8$. The thickness of the oil layer is always greater than that which it would attain on open water (1). In practice it is approximately 1.4 times the open water thickness. The thickness of the oil layer for double sessile drops is shown in Fig. 5. Figures 6 and 7 show the ratios of oil to gas thickness (and hence volume ratios) for the two systems. For the sessile drop–lens this is the maximum quantity of oil that the configuration can contain, whilst for the double

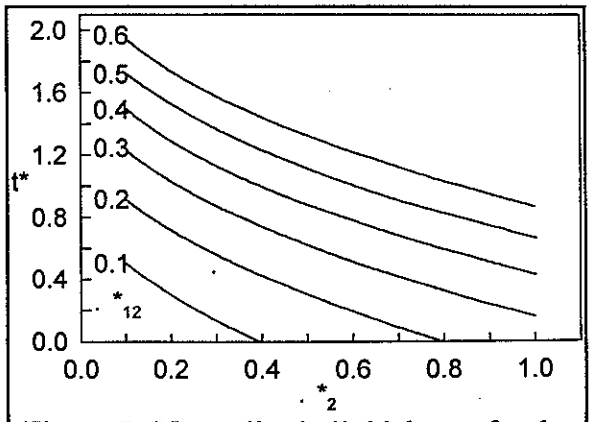

Figure 5. Normalised oil thickness for the double sessile drop, $\rho^* = 0.8$.

sessile drop it represents the minimum quantity of oil required for its formation.

Returning now to the problem of the most probable configuration, the energies of the various systems are compared and an existence diagram constructed on the basis of the lowest energy state in any particular region. The sessile drop–lens combination is taken as a basis for comparison and the oil–gas ratio V_O/V_G appropriate to this case is then used to calculate the energy of the same volumes of gas and oil, but disposed in the different configurations. The energies of the following sessile drop systems are required which can be derived from the classical results for infinitely large single component drops. The contact angles have been set to 0° and the parameters normalized.

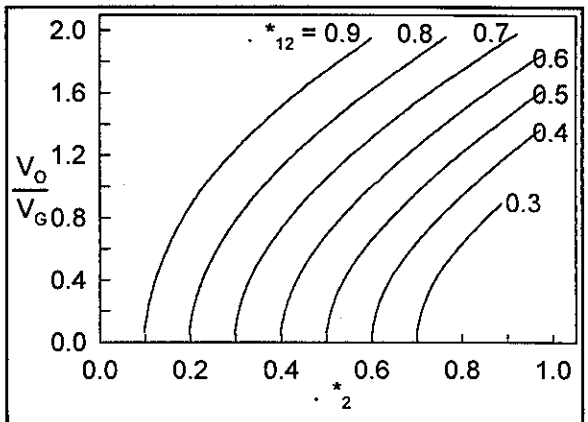

Figure 6. Maximum oil/gas ratio, sessile drop/lens combination, $\rho^* = 0.8$.

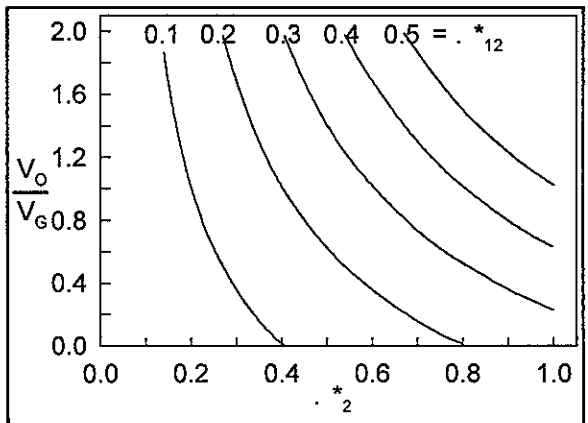

Figure 7. Minimum oil/gas ratio, double sessile drop, $\rho^* = 0.8$.

(*a*) Gas in water

$$E^*_{GW} = \frac{E_{GW}}{V_G (2g\rho_1\gamma_1)^{1/2}} = \sqrt{2}$$

(*b*) Oil in water

$$E^*_{OW} = \frac{E_{OW}}{V_G (2g\rho_1\gamma_1)^{1/2}} = \frac{V_O}{V_G} [2\gamma^*_{12} (1 - \rho^*)]^{1/2}$$

(*c*) Gas in Oil

$$E^*_{GO} = \frac{E_{GO}}{V_G (2g\rho_1\gamma_1)^{1/2}} = (2\gamma^*_2 \rho^*_2)^{1/2}$$

(*d*) The sessile drop–lens combination

The solution of Sect. 2.1 furnishes the result

$$E^*_t = \frac{E_t}{V_G (2g\rho_1\gamma_1)^{1/2}} = \frac{m^{*2}}{t^*} \frac{1}{[h^*/t^* - (1 - \rho^*)]}$$

The oil–gas volume ratio corresponding to the sessile drop–lens configuration is given by

$$\frac{V_O}{V_G} = \frac{1}{[h^*/t^* - (1 - \rho^*)]}$$

where h^*/t^* is obtained from the solution of the set of equations [3].

The following energy comparisons define boundaries on the existence diagram:

(*i*) The sessile drop–lens with separate drops of gas and oil

$$E^*_T \leq E^*_{GW} + E^*_{OW}$$

(*ii*) The sessile drop–lens with the double sessile drop

$$E_T^* \leq E_{OW}^* + E_{GO}^*$$

(*iii*) The double sessile drop with separate drops of gas and oil

$$E_{OW}^* + E_{GO}^* \leq E_{GW}^* + E_{OW}^*$$

which reduces to $\gamma^*_2 \rho^* < 1$.

In addition, the following physical conditions must be met.

(*iv*) The double sessile drop system can only form if the thickness of an infinite oil bubble in water exceeds that of an infinite gas bubble in oil, that is, above the line defined by the equation

$$\gamma_{12}^* = [(1 - \rho^*)/\rho^*]\gamma_2^*$$

obtained by setting $\psi_{IOG} = \psi_{IWO} = 0$ in [7]. This assumes that the forms of the interfaces are independent, i.e., 'thin' films are excluded. Spreading oils, however, can spread to molecular thicknesses and oil covered gas bubbles are expected to exist over the whole region to the left of the line $\gamma^*_{12} \geq 1 - \gamma^*_2$.

(*v*) In the case of the sessile drop–lens configuration a boundary exists beyond which the oil contained is not enough to form a double sessile drop, i.e., t(sessile drop–lens) < t(double sessile drop).

These conditions divide the existence diagrams into five distinct regions, shown in Fig. 8, which has been drawn for oils of specific gravity 0.8. The illustrations in each region indicated the energy hierarchy of the configurations, i.e., the configuration placed lowest in each set has the least energy.

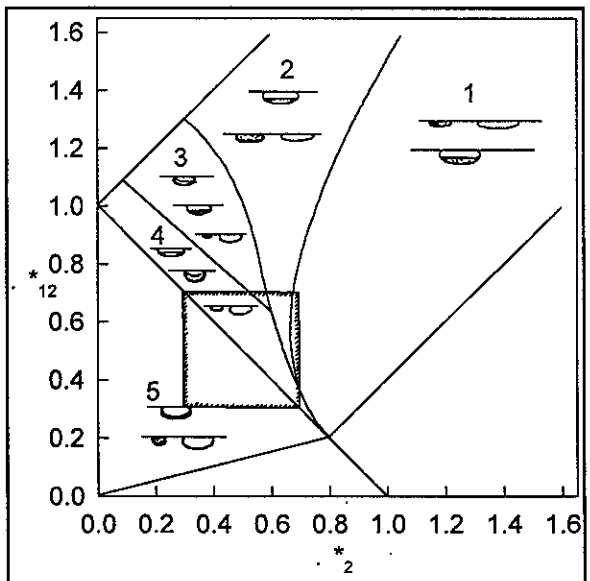

Figure 8. Existence diagram, $\rho^* = 0.8$.

It should be remembered that these calculations only refer to the ratios of oil and gas required for the sessile drop–lens configuration. In other words, given a sessile drop–lens configuration containing the maximum quantity of oil, what is the most likely configuration which would result from a finite disturbance in the system, or what would be the effect of a further addition of oil? In region 1, the sessile drop–lens configuration itself has the lowest energy and thus should be stable; further additions of oil would form isolated oil pools. In region 2, the situation is reversed, a finite disturbance of the sessile drop–lens combination would lead to a separation of gas and oil.

To the left of the line dividing regions 2 and 3 the double sessile drop can also be formed, but in region 3 it has the highest energy state. In region 4, the double sessile drop can be formed from the sessile drop–lens configuration, and in this case the quantity of oil involved is more than the minimum required for the double sessile drop, and the oil extends beyond the sides of the gas bubble. The gas bubble would suddenly appear to have been engulfed in oil. In region 5 only the

double sessile drop and separate droplets can exist with the latter having the least energy. Since the oils in this region are of the spreading type, gas bubbles will always retain a coating of oil of indeterminate thickness.

The probable range of normalized interfacial tensions for crude oil is between 0.3 and 0.7 (3,4), and the region of the existence diagram of practical interest lies within the small shaded square. At the present time there is little or no published quantitative information on the behaviour of mixtures of gas and oil beneath ice although some qualitative descriptions have been given (6). These indicate that all three of the configurations discussed above can exist in their own right, and that the presence of gas can greatly extend the area of potential oil contamination.

If the quantities of oil involved are substantially less than those required for the configurations discussed above, the non-spreading oils lie beneath gas bubbles at a thickness approaching the value for lenses on open water, given by Langmuir's (1) equation in normalized form :

$$t^* = (\gamma_2^* + \gamma_{12}^* - 1)/\rho^*(1 - \rho^*)$$

In the case of spreading oils, the whole gas–water interface will be covered."

Method

None stated

Results

"In some rather small-scale experiments, the present author was able to demonstrate that certain non-spreading oils collected in stable lenses on the bottom of gas bubbles, whilst others were unstable, slowly migrating upwards to the solid surface.

In practice, the appropriate characteristics of crude oil–water mixtures are difficult to determine, as complex diffusion processes take place across boundaries. In working with crude oils in water, the present author has found that a drop of oil in water can form a semi-rigid skin which can be left behind like a burst balloon skin (7). This is probably due to diffusion of light components from the oil–water interface leaving a skin of heavier components. "

BOSS Critique

The author does not state the errors resulting from the assumptions made during the evolution of the authors theory. The author does not seem to realize that the cosine of any angle has a value between -1 and +1. The discussion would have benefited from a more detailed description of the actual experiments and the quantitative experimental results.

Review of a manuscript by, Thomas, D.R. and R.S. Pritchard, "Oil Movement in the Ice Covered Beaufort and Chukchi Seas", in *1979 Workshop on the Physical Behaviour of Oil in the Marine Environment*, Princeton University, Princeton, New Jersey, pp 5.17-5.31, 1979.

Technical Summary

"Monthly means and variation of free drift ice trajectories are presented for the Beaufort and Chukchi Seas. Results are based on 25 years of historical atmospheric data. The method used allows separation of motion induced by winds and deep currents so that the results remain valid as more accurate estimates of the currents become available. Historical free drift motions conform to the know drift pattern for the area - a clockwise circulation about the Beaufort Gyre. By interpreting free drift as the limit of ice motion for one extreme of ice conditions (i.e., light ice), the results are useful for predicting the range of motions of oil-contaminated ice."

Objective

"... Unfortunately, our knowledge of the currents in the Beaufort/Chukchi Seas is limited. The general circulation pattern is known, but quantitative assessment of currents throughout the region is lacking. The best available estimated of currents comes from Newton's (1973) compilation of historical data providing a climatological mean dynamic topography for the Beaufort Sea. These data are not only incomplete in spatial coverage, but do not include more recent oceanographic observations. Because of the lack of complete and reliable information on the geostrophic ocean currents, we formulated the free drift model to allow a separate calculation of geostrophic current induced drift. In this work, we have concentrated on determining the component of ice drift caused by winds. We also show that mean currents and variations in the current may be superposed directly on the free drift statistics. Thus, the results of this work are independent of actual currents."

Theory

"During free drift, forces acting on the ice are air stress $\underset{\sim}{\tau}_a$, water stress $\underset{\sim}{\tau}_w$, Coriolis force $-mf\underset{\sim}{k}\times\underset{\sim}{v}$ and sea surface tilt $-mg\nabla H$ so that

$$\underset{\sim}{\tau}_a + \underset{\sim}{\tau}_w - mf\underset{\sim}{k}\times\underset{\sim}{v} - mg\nabla H = \underset{\sim}{0} \tag{1}$$

where H is the dynamic sea surface height, mg is the gravitational force on the ice and $\underset{\sim}{v}$ is the ice velocity. The air stress is determined from the geostrophic wind in the atmosphere as

$$\underset{\sim}{\tau}_a = \rho_a c_a \|\underset{\sim}{U}\| \underset{\sim}{B}_a \underset{\sim}{U} \tag{2}$$

$$\underset{\sim}{B}_a = \begin{pmatrix} \cos\alpha & -\sin\alpha \\ \sin\alpha & \cos\alpha \end{pmatrix} \tag{3}$$

where ρ_a is the air density, c_a is the atmospheric drag coefficient, $\underset{\sim}{U}$ is the geostrophic wind velocity as computed from gradient of the historical pressure fields, and where α is the atmospheric turning angle. The water stress satisfies a quadratic drag law similar to the atmosphere

$$\underset{\sim}{\tau}_w = \rho_w c_w \|\underset{\sim}{v} - \underset{\sim}{v}_g\| \underset{\sim}{B} (\underset{\sim}{v} - \underset{\sim}{v}_g) \tag{4}$$

$$\underset{\sim}{B} = \begin{pmatrix} \cos(\beta+\pi) & -\sin(\beta+\pi) \\ \sin(\beta+\pi) & \cos(\beta+\pi) \end{pmatrix} . \tag{5}$$

where $\underset{\sim}{v}_g$ is the ocean geostrophic current, ρ_w is the water density, c_w is the water drag coefficient and β is the turning angle through the oceanic mixed layer. The sea surface tilt defines the ocean geostrophic current in the form

$$mg\nabla H = - mf \underset{\sim}{k} x \underset{\sim}{v}_g \tag{6}$$

where m is the ice areal mass density and f is the latitude dependent Coriolis parameter.

This force balance relates air stress $\underset{\sim}{\tau}_a$, ocean currents $\underset{\sim}{v}_g$ and ice drift in a special way, namely, the ice velocity and current always appear as a difference

$$\underset{\sim}{G} = (\underset{\sim}{v} - \underset{\sim}{v}_g) \tag{7}$$

so the force balance may be written

$$\underset{\sim}{\tau}_a + \rho_w c_w \|\underset{\sim}{G}\| \underset{\sim}{B} \underset{\sim}{G} - mf \underset{\sim}{k} x \underset{\sim}{G} = \underset{\sim}{0} \tag{8}$$

By introducing the ice velocity relative to deep ocean current, it is seen that $\underset{\sim}{G}$ is the portion of the ice velocity that is driven by the wind. Therefore, contributions to ice drift due to air stress and to ocean currents may be calculated separately. Shear in the mixed layer of the ocean has been accounted for in our water stress model.

Values of density ρ_a, ρ_w, drag coefficients c_a, c_w, turning angles α, β used in this study were derived from AIDJEX data (McPhee, 1977, Albright, 1978 and personal communication). The ice mass per unit area, m, is $\rho_i \bar{h}$ where the average ice thickness ($\bar{h}$) is considered constant throughout the region of interest for a month. The values used are presented in Thomas and Pritchard (1979).

Integrating velocity throughout a day gives daily displacements. Let $\underset{\sim}{x}$ be the daily ice displacement relative to ocean currents and $\underset{\sim}{c}$ be daily displacements of currents. Total daily displacement is $\underset{\sim}{x} + \underset{\sim}{c}$. During a month of M days, the total monthly displacement, $\underset{\sim}{W}$, is

$$\underset{\sim}{W} = \sum (\underset{\sim}{x} + \underset{\sim}{c}) \tag{9}$$

which can be written as

$$\underset{\sim}{W} = (\underset{\sim}{X} + \underset{\sim}{C}) \tag{10}$$

where $\underset{\sim}{X} = \sum \underset{\sim}{x}$ is the monthly relative ice motion and $\underset{\sim}{C} = \sum \underset{\sim}{c}$ is the monthly ocean current motion. For a sample of N = 25 years, the mean monthly displacement is

$$\overline{\underset{\sim}{W}} = \frac{1}{N} \sum \underset{\sim}{W} \tag{11}$$

and the standard deviation of monthly displacements is

$$S_w = \left(\frac{1}{N-1} \sum \|\underset{\sim}{W} - \overline{\underset{\sim}{W}}\|^2 \right)^{1/2} \tag{12}$$

Using the relationship shown in equation (10) and some results of elementary statistics, we can write equations (11) and (12) as

$$\overline{\underset{\sim}{W}} = \overline{\underset{\sim}{X}} + \overline{\underset{\sim}{C}} \tag{13}$$

and

$$S_w = \left(S_x^2 + S_c^2 + 2\ \mathrm{cov}(\underset{\sim}{X}, \underset{\sim}{C})\right)^{1/2} \tag{14}$$

We see from equation (14) that the standard deviation of monthly ice motions is bounded by

$$S_w \leq S_x + S_c . \tag{15}$$

When ocean currents are nearly constant along the trajectory, then

$$S_w \cong S_x \tag{16}$$

quantifies the year-to-year variations."

Method

"At each grid point for each of the twelve months, the 25 year (1953-1977) means of ice displacement are formed. These are years for which we have reasonable confidence in the NMC pressure fields. Rectangular coordinates are used to avoid difficulties inherent in working with azimuths. The variance-covariance matrix at each point for each month is also computed. To show graphically the distribution of monthly displacements, equi-probability ellipses are constructed assuming a bi-variate normal distribution (Morrison, 1976). We present the monthly mean free drift ice motion fields and the 50 percent equi-probability ellipses based on 25 years of historical data in Figures 1 through 12." These figures have not been reproduced in this review. "The area within each ellipse is interpreted as the region of most probable ice location after drifting from the starting point for one month. These 12 monthly plots provide the expected ice drift component due to winds and can be accumulated to find longer term drift. To determine actual monthly drift, the mean ocean current must be added to this drift component.

The variability from year-to-year of the wind induced free drift component of ice motion is presented in Figures 13 through 16." Figures 13 through 16 are not reproduced in this review. "The months of January, April, July, and October are selected to show seasonal variations. Three points at widely separated locations are shown so that spatial variability is also indicated. The drift calculated for each of the 25 years is included to help the reader gain a feeling for the actual year-to-year distribution. The three ellipses represent the areas containing 50, 90 and 99 percent of the ice motions. The Central Limit Theorem leads us to expect a near normal distribution of ice motions, but several tests were made to confirm this. The quadrant test shows a nearly equal distribution of data among the quadrants with a possible skewness toward the west. A count of the data points within the 50-,90-, and 99 percent equi-probability ellipses indicates that the data might be more dense near the mean than normality predicts. Since no large and apparent deviations from normality are observed, our assumption of normality is not unreasonable. The 95 percent confidence region for the mean is an elliptic region about 45 percent the size of the 50 percent equi-probability ellipse. The 95 percent confidence limits for the equi-probability ellipses are the elliptical regions $0.64\ D \leq d \leq 2.24\ D$ where D is the distance from the mean to the equi-probability ellipse. A sample size of 25 is too small to ensure reliable statistics, but we feel some additional information is present in the data and in the results. This is the smooth variation over space and time of the results. The results

are also consistent with what is known about the general ice motion in the Beaufort Sea. We, therefore, feel that the region-to-region and month-to-month variations are real."

Results

"The monthly mean motion fields presented in Figures 1 through 12, show an obvious westerly trend to the motions throughout most of the year. During the summer months the motion exhibits a northerly component of motion with July being the extreme. In fact, the northern most grid points have an average motion almost due east in July. In general, the winter mean motions are larger than those in summer. This is due in part to the winds being more variable in direction during the summer, but an examination of the individual monthly trajectories shown in Figures 13 through 16 shows that more large winds occur during the winter. A pronounced east to west variation in the magnitude of the means is also evident. The larger means occur in the Chukchi Sea. During December and January and again during July, the means in the eastern Beaufort Sea are nearly zero. This appears to be a result of directional variability in the winds and motion during these three months. There also appears to be a slight reduction in magnitude of the means from south to north. In general, the greatest variability in motion occurs in the east-west direction. Northwest of Point Barrow during the summer is an exception with nearly circular distributions occurring. Our assumption of bi-variate normality appears to be justified. Some doubtful looking instances are to be expected with sample sizes of 25, but no extreme deviations from normal are evident.

To determine total monthly motion, some estimate of geostrophic ocean currents is needed.

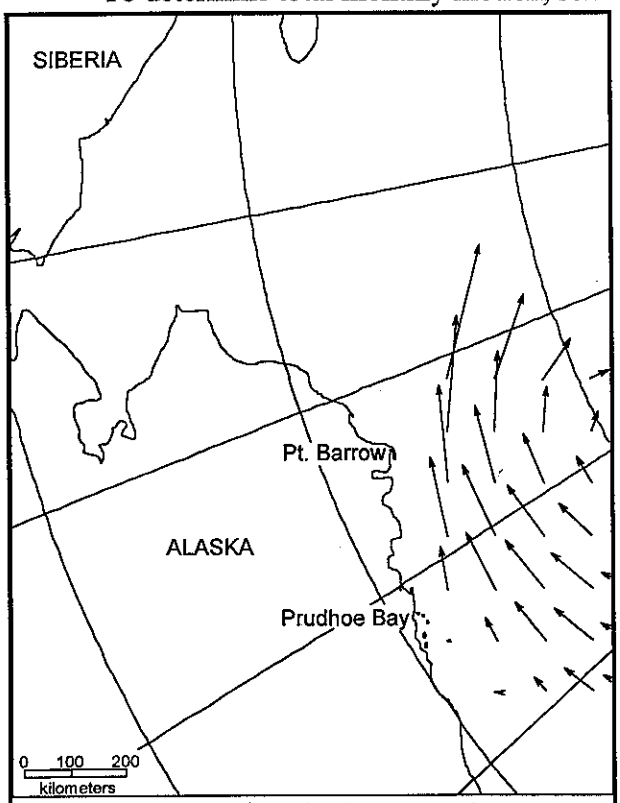

Figure 17. Monthly Displacement Due to Geostrophic Ocean Currents in Central Beaufort Sea.

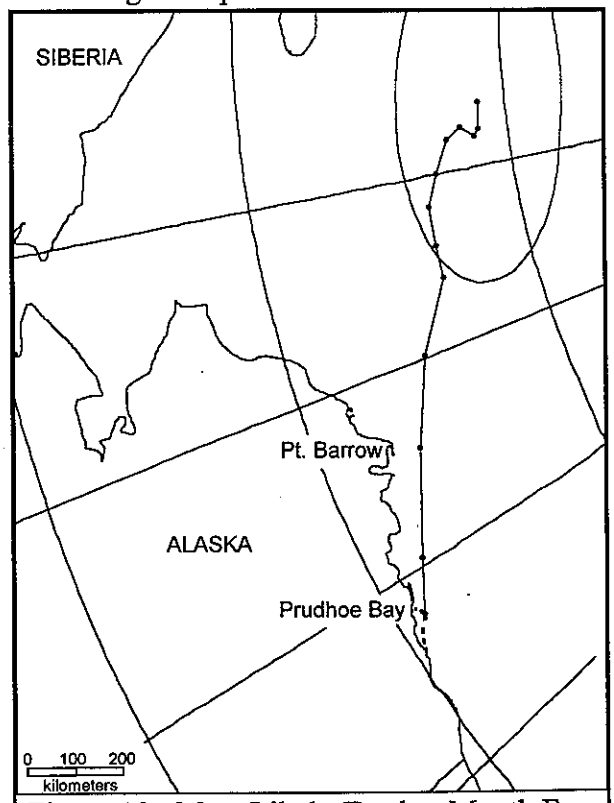

Figure 18. Most Likely Twelve-Month Free Drift Ice Trajectory (Including Currents) Beginning at Prudhoe Bay, October 1st.

We have used the geostrophic flow taken from a dynamics topography compiled by Newton (1973). These currents, expressed as km/month displacements, are shown in Figure 17. The blank area over most of the region of interest does not indicate zero currents, but lack of information. The accuracy of the currents presented may be questioned too. Nevertheless, the currents shown in Figure 17 represent the best available estimates of long-term average currents in the Beaufort Sea.

In Figure 18 we present the results of a twelve-month accumulation of mean free drift beginning October 1. The currents were included in computing the year long trajectory. The ellipse shown is approximately the 50 percent equi-probability ellipse assuming that the standard deviation of the sum of variables is accumulated in a mean-square sense. This final result is included to show how the information obtained in this work may be used to determine ice behaviour and to give a preliminary indication of the possible drift of oiled-ice that could occur after an oil spill near Prudhoe Bay."

BOSS Critique

The author has included errors by including the ellipse information on the graphs. A small error that is compounded can cause a large deviation from the expected trajectory, as seen in the Figure 18 ellipse.

Review of a manuscript by, Purves, F., *The Interaction of Crude Oil and Natural Gas With Laboratory-Grown Saline Ice*, EPS-4-EC-78-9, Environment Canada, Ottawa, Ontario, 18 p, 1978.

Technical Summary

"Norman Wells crude oil and natural gas were injected under 35 cm of saline ice in the laboratory, and 20 cm of additional ice was grown under the oil and gas. The oil was observed to spread in a thin layer on the under-surface of the gas bubble. When the sheet was thawed, the gas was observed to escape when the minimum temperature in the ice sheet rose to -3.6 °C, and this caused the release of a few drops of oil. The bulk of the oil, however, emerged at the same time as a pure oil spill in a control experiment. It was concluded that the presence of gas greatly increases the area over which spilled oil will surface, but does not affect the timing of its appearance."

The author's conclusions are also included:

"

a) Norman Wells crude forms a sessile pool on the underside of a methane bubble held under an ice sheet.
b) At gas to oil ratios of 60:1 or greater, the pool of Norman Wells will not coat the entire bubble surface.
c) Oil layers as thin as 0.2 cm will probably be encountered when well blowout products accumulate under ice.
d) The distribution of the oil phase varies markedly with oil properties.
e) Gas will be released much earlier than oil in the course of thawing a containing sheet.
f) The presence of gas has little or no effect on the release timing of oil trapped under first-year ice.
g) The presence of gas under an ice sheet greatly increases the area contaminated by oil spilled under the ice.
h) The release timing of both gas and oil can possibly be predicted on the basis of ice thickness, salinity profile, and meteorological data."

Objective

The author wanted to study the interaction of oil and gas under and encapsulated in an ice sheet, to simulate the effects of a blowout under ice.

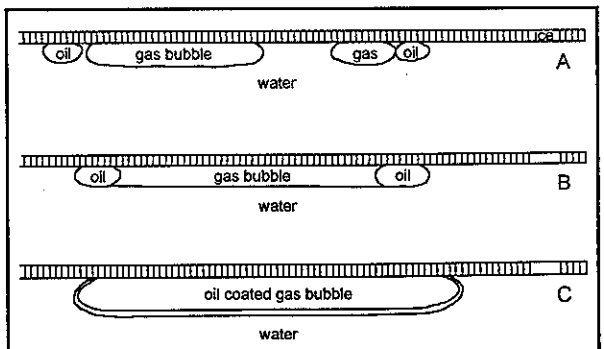

Fig. 1 - Possible Configurations of an Ice/Oil/Gas/Water System.

Theory

"... In the case of a well blowout the oil residue is mixed with 100 times its own volume of natural gas. This natural gas can be expected to significantly alter the results of these pure oil studies in two ways. First, the gas will preferentially fill the under-ice topography and present to the oil, not an undulating ice surface, but the perfectly level under-surface of a gas bubble. The oil can spread on this gas-liquid interface

much as it would floating freely on calm water. In this case, the concentrating effect of the rough ice under surface would be largely lost.

Figure 1 shows three possible schematic configurations for the resulting ice/oil/gas/water system. Configuration A results in the minimum area of oil/gas interface. Configuration B minimizes oil/water interfacial area, while Configuration C minimizes the area of gas/water interface. The various interfacial tensions determine which of these configurations will be energetically favoured.

A second effect of the gas might be in pioneering a route to the surface for the oil. All of the work cited above discusses oil as penetrating the ice through brine drainage features enlarged by the oil as it absorbs solar radiation. Rosenegger discusses the pore diameter required for this sort of permeation, and Milne models the process on this basis. The lower-density, lower-viscosity gas should be capable of penetrating less porous ice (in other words, colder ice earlier in the spring). Once cleared in this way, the channels might be penetrated by oil more easily than if the oil alone cleared the channels."

Method

"2 **EXPERIMENTAL WORK**

Field studies (e.g. Lake and Lewis 1970) have shown that the brine drainage features in first-year sea ice are spaced, on average, about 13 cm apart. On this basis, an experiment 1 meter in diameter was considered somewhat representative of field conditions. Ice sheets of this size were thus grown and thawed in an environmental room under controlled conditions of temperature and illumination.

2.1 Apparatus

The experiment was conducted in two cubical tanks 1.2 m on a side. Each tank was fitted with two 25 x 60 cm viewing windows - one in the bottom and one set vertically in the side. ... These were mounted in an environmental chamber on a platform 41 cm high to permit access to the bottom viewing port. The tops were left open but the other 5 faces of each tank were insulated with 21 cm of glass wool insulation which could be removed for access to the viewing ports.

Each box was equipped with an injector system for inserting gas bubbles and/or oil drops under the ice. A 60 cm length of 4 mm ID glass tubing was tapped through the wall of each tank to provide an injection point at the center 15 cm above the bottom viewing window. Once an ice sheet had been grown in the tank, gas and/or oil could be forced through this tube to escape in the center of the tank and rise to the center of the ice sheet.

One of the two tanks was fitted with a string of 9 thermistors mounted vertically 12 cm from one corner. The top-most thermistor of the string was above the ice surface while the others relayed temperatures down through the sheet to a depth of 50 cm.

During the thawing phase of the experiment, both tanks were covered with polyethylene covers to confine a volume of approximately 0.4 m^3 over the surface of the ice sheet. A Westinghouse 75w "Agro-Lite" was set into the center of each cover to roughly simulate the spectral distribution of solar illumination and each light was equipped with a rheostat to adjust the illumination level. The covers were also fitted with mercury-in-glass thermometers to monitor the temperature of the enclosed volume.

The escape of gas through the ice sheet was monitored by measuring the concentration of methane in the air space beneath each cover with a Drager Model 31 gas detector. This detector was

capable of detecting gas concentrations as low as 0.5% by volume which corresponds to an escape of 27% of the injected gas bubble.

2.2 Methodology

Each of the tanks described above was charged with 1134 kg of tap water in which had been dissolved 34 kg of Windsor "High Grade" granulated salt to give a salinity of 30‰. With the environmental room at -5 °C, the two tanks were equilibrated at the freezing point, and the insulation was installed. The room temperature was then lowered to -45 °C.

The growth of ice in both tanks was observed through the side windows. In 165 hours, 34 cm had formed, measured at the center of each basin. The sheets were not pierced for these measurements, and the underside was slightly concave, so the thickness is accurate to only ±1 cm. From above and through the windows both sheets appeared uniform with no large included bubbles. ...

The room was then brought to -5 °C for 8.25 hours during which time oil and gas were inserted under the ice sheets. A 1 m length of 1.4 cm ID clear plastic tubing was attached to each injector fitting. Initially, the first few cm of the glass injection tube was frozen in the proximity of the tank wall. This was thawed by placing a few cc of hot tap water in the plastic tubing. This, plus the hydrostatic pressure differential quickly unblocked the injector.

The injector line of the experimental tank was then connected to a cylinder of methane, and this was gradually bubbled through the injector tube to rise in the center of the slightly domed ice sheet. The bubbles immediately coalesced to form a single large bubble, and this was observed through the windows until its diameter was estimated to be 1 meter. ... It had been intended to meter the amount of methane added, but this system failed to function as expected. Instead the volume of the bubble was estimated to be 7.5 liters on the basis of the observed concavity of the ice surface and the bubble's observed diameter. The bubble was quite circular, and no small outlying bubbles remained. Its meniscus edge had a diameter of about 0.5 cm.

The methane injection just described was in the experimental tank only. Norman Wells crude oil was then injected into both the experimental and control tanks. A 125 cc charge (1.7% of the gas volume in the experimental tank) was added to both injector lines and pressured into the tanks with methane. In the control tank, the oil entered smoothly in large drops. In the experimental tank, the injector had initially refrozen, and the first charge of oil escaped from the bulkhead fitting at the tank wall and was caught in the ice on the tank wall at that point. None rose to the underside of the ice sheet, although later in the experiment this lost oil melted up the wall in front of the window and surfaced at the side of the sheet. It was always confined at the wall with a barrier and not confused with the oil at the center. After this false start, the injector of the experimental basin was again cleared with hot water, and another 125 cc charge was injected. These drops rose in the center of the basin and immediately coalesced in a sessile-appearing pool on the under-surface of the gas bubble. ...

The room temperature was then lowered to -45 °C for a further 128.5 hours. The total thickness at this point was 59 cm ±2. The room was then adjusted to -8 °C for 106 hours, during which time the tank covers and lighting systems were installed.

The light intensity at the center of the sheet over the inclusions was adjusted to 555 cal/cm^2 -day using the rheostat control and a Gossen "Lunasix 3" light meter. The air temperature was adjusted to a target temperature of +10 °C under both covers as measured by a mercury-in-glass thermometer. The thawing process was then observed every two hours."

Results

"3.1 Oil and Gas Geometry Under the Ice

The gas injected under the experimental sheet rose in bubbles of mixed sizes mostly from 0.5 - 4 cm in diameter. These impacted the underside of the ice over an area approximately 20 cm in diameter at the center of the sheet and immediately fused into a single circular bubble with a sessile-appearing edge. The large bubble almost covered the ice sheet; its diameter was estimated at a meter and it was confined by the domed shape of the sheet in a pool approximately 2 cm deep at the center. The edges of the bubble appeared typically sessile with meniscus-like edge about 0.5 cm in diameter. The edge of the bubble was about 10 cm from the tank wall on all sides. The volume of the bubble was estimated at 7.5 liters based on the volume of a spherical segment 2 cm deep. The injection process took about 5 minutes.

The oil drops arrived under the gas bubble or under the ice sheet (in the control tank) in a small area < 10 cm in diameter. They thus impacted an existing oil pool and immediately fused to form a single, sessile-appearing oil body. Against the ice interface (in the control tank) this circular pool simply grew in diameter with each drop until the 125 cc formed a pool approximately 15 cm in diameter. ... Under the gas bubble the large sessile pool was resting against a flat interface, and gradually spread in area with each drop. This pool was not circular. It grew in lobes and tentacles to eventually coat an estimated 80% of the gas bubble surface. Figure 10 shows the final configuration. The thickness of the oil layer was not measurable without a reference length but the curved edge of the drop was clearly visible.

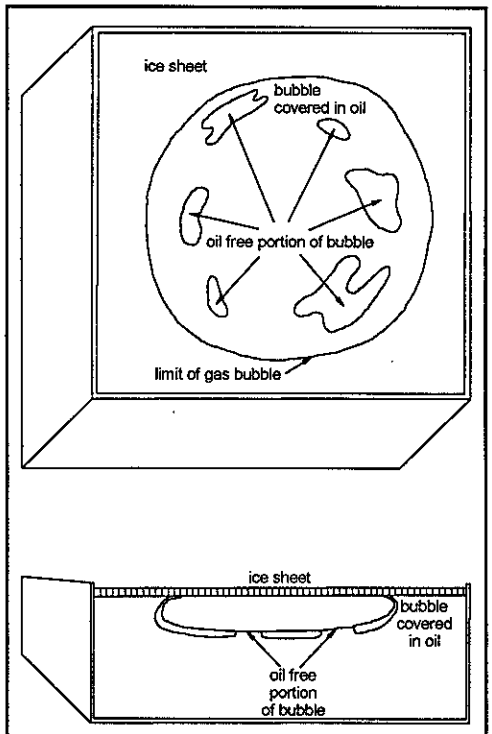

Fig.10 - Distribution of Oil under a Gas Bubble.

3.2 Release Timing - Gas

As the air temperature over the two sheets was gradually raised, and particularly in the center under the lights, melt pools began to form within 24 hours. To highlight escaping gas, 3 drops of Palmolive dish washing liquid were added to the melt pool on the experimental sheet. After a further 3 hours (at 124.4 thawing degree-hours) 5-10, 0.5-1 mm diameter bubbles were observed in a small cluster on the melt pool. The minimum temperature in the sheet at this point was -3.6 °C at the mid-plane. Both surfaces were at -2 °C.

At 147.8 thawing degree-hours bubbling became rapid enough that bubbles could be observed emerging within a few minutes of observation. At 162.6 thawing degree-hours, 31 of these small bubbles were observed in 90 seconds emerging from approximately 31 different points on the sheet. Some of these points were on the wet, bare surface of the sheet; others were at the edges of melt pools; but no bubbles emerged in melt pools deeper than 0.7 cm. At 174.6 thawing degree-hours, the rate had become sufficient that bubbles could be counted through a 65 cm^2 mask. Based on bubbles 0.75 mm in diameter, the flow was 10^{-5} cc/cm^2 -min. The sheet center temperature was -2.2 °C.

Shortly thereafter, at 204.2 thawing degree-hours, the flow became concentrated at a single channel in a steady stream of one 1 mm diameter bubble every 7 seconds. This evolved to a pulsing flow of approximately 200 bubbles (4 slugs of 50) in 90 seconds. Then, at 250 thawing degree-hours, the bubbling tapered off quickly, and no further gas escape was observed apart from very occasional bubbles which might have been air trapped in the ice sheet on freezing.

In clock time, the 1 m bubble of 7500 cc of gas was released over a period of 22 hours starting 76 hours after the onset of thawing. The atmosphere over the sheet was sampled with a gas analyzer during this period, but concentrations greater than 0.5% were never obtained. As a result, no rigorous mass balance was possible.

3.3 Release Timing - Oil

Within two hours of the last bubbling (at 266.4 thawing degree-hours) oil appeared on the experimental sheet. The oil in the form of drops 5×10^{-4} cc to 7 cc in volume widely distributed over the surface melt pools. By 637 thawing degree-hours about 100 of these were apparent, but by 675 thawing degree-hours evaporation and dissolution had reduced the population to 3 or 4 drops of about 5 cc each. This situation remained stable until the eventual complete rotting of the sheet.

In clock time the first oil drops appeared on the experimental sheet 55 hours after the onset of thawing, 2 hours after the end of gas release. The population of oil drops rose to about 100 over 68 hours, then the initial release of oil slackened and the population stabilized at less than 10 drops for the next 160 hours. During this period, oil release was not observed but was indicated by the persistence of oil in the face of evaporation and dissolution and by changes from day to day in the positions of the drops on the melt water pool.

Everything described to this point took place in the experimental tank. The first occurrence of note in the control tank occurred at 1768 ±20 thawing degree-hours when a single 1-5 cc drop of oil appeared on the melt pool. This was almost coincident with a resurgence of oil flow in the experimental basin at 1711 ±188 thawing degree-hours. Thereafter, both sheets released all of their oil over a period of 24 hours.

The release took the form of individual drops 3 mm in diameter which, at the height of release, rose at 1.5-3 second intervals through the melt pool. In the experimental sheet this flow was dispersed over an array of points about 1 cm apart. In the control basin, with its limited oil pool diameter, the flow was concentrated at a single spot. The oil rising in the experimental sheet could be observed as individual drops. The pattern in the control sheet was unobservable as the ice was heavily oiled throughout in the area of the oil pool.

3.4 Redistribution of Oil After Gas Release

It was impossible to discern the oil configuration through either of the viewing ports in the experimental vessels. Nevertheless, the pattern of oil release clearly indicated that the oil originally spread under the gas bubble remained spread over the bubble area after release of the gas."

BOSS Critique

The author uses terms, such as thawing degree-hour, without ever presenting a definition. Sizes of bubbles are given as ranges but the author states that no actual measurement grid was in place so these measurements are very qualitative not quantitative.

Review of a manuscript by, Scott, B.F. and R.M. Chatterjee, *Behaviour of Oil Under Canadian Climatic Conditions: Part 1. Oil on Water Under Ice-Forming Conditions*, Scientific Series No. 50, Environment Canada, Ottawa, Ontario, 21 p, 1975.

Technical Summary

"Oil was poured onto a water surface under ice-forming conditions. Weather conditions were monitored continuously, as were the physical properties of the oil and the effect of the oil on its physical environment. Properties of the oil were investigated by gas chromatography and the following forms of spectroscopy: neutron activation (γ-ray), infrared, ultraviolet, visible and fluorescence. The weathering of the oil and its influence on its environment were correlated with the weather parameters. An estimated 50% of the oil had evaporated before the oil was covered with snow, as determined by gas chromatographic analysis and supported by neutron activation analysis. A biological assessment was conducted during the following summer where the effect of the oil on one pond was compared with the control pond. In the oiled pond, the variety of biological species was substantially less than in the control pond."

Objective

The authors wanted to investigate the fate of oil under ice forming conditions.

"The spill was carried out near Ottawa at the Shirleys Bay Quiet Site where four large ponds were constructed. The site was selected because of the following considerations:

(1) these quiescent ponds simulate typical lakes found in the Mackenzie Delta area,
(2) better control of the spilled oil is allowed by the ponds to prevent the increase of environmental pollution,
(3) these ponds are easy to clean up,
(4) in case of an emergency, service is available from our support personnel since the ponds are close to our laboratories, and
(5) these ponds, close to Ottawa, experience the severe weather conditions common to Ottawa that can be used to approximate arctic conditions."

Theory

Theory, when it was presented, was in with the method and results.

Method

"**Field**

Field Site Facilities and Preparation

The location of the ponds is shown in Figure 1" (which is not reproduced here) "and a plan of the ponds is indicated in Figure 2. Each pond was doubly lined with polyethylene sheets with the ends buried under the earth and with the linings between adjacent ponds overlapping and buried so that the complete filling of the ponds would form one large pond without leaks. This was tested by filling each pond with water and observing that the water levels were constant. A trailer serviced with electricity was located near the ponds to provide a field headquarters.

Three sets of monitoring cells were positioned in each pond. Each set composed of a

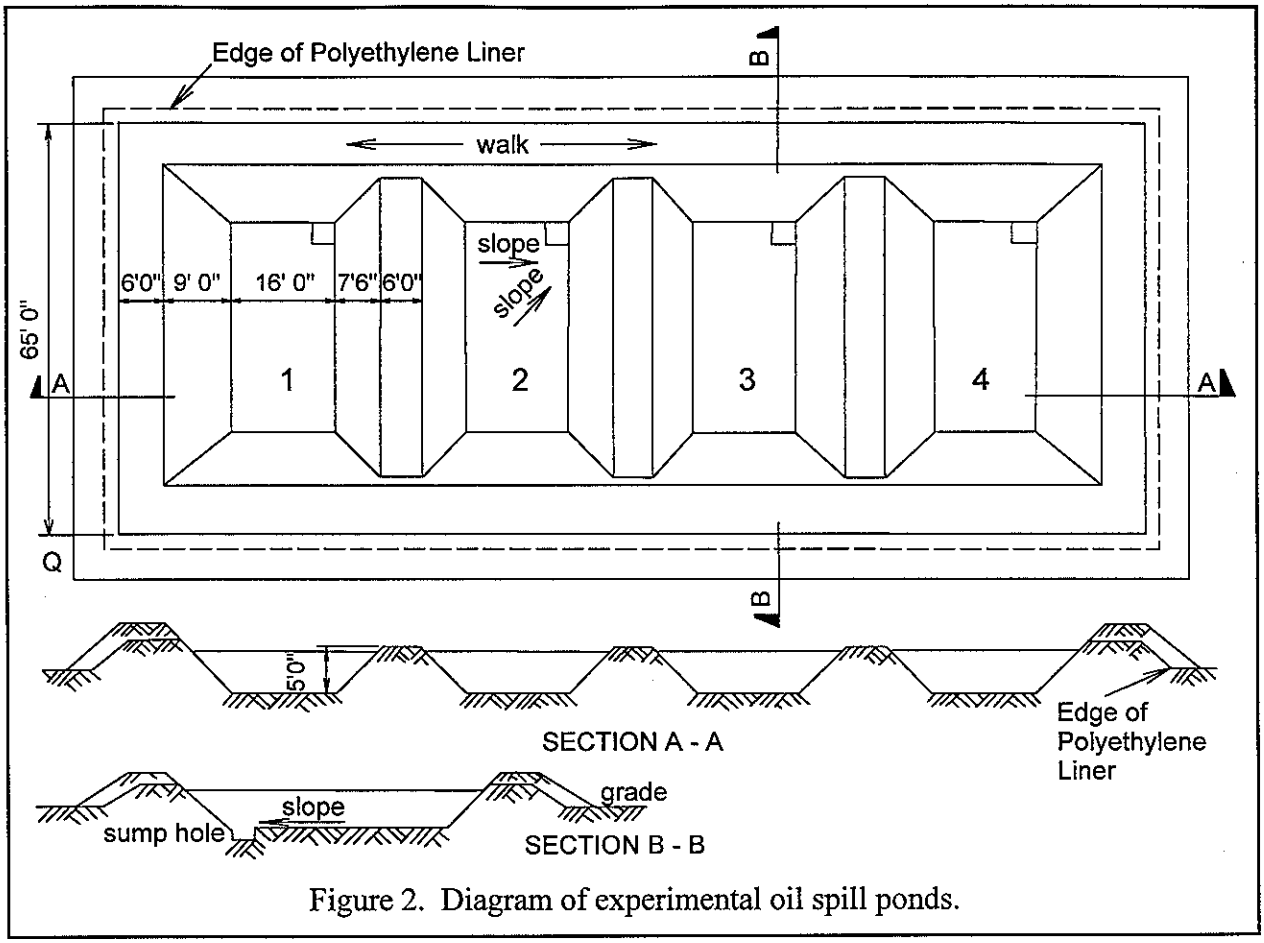

Figure 2. Diagram of experimental oil spill ponds.

calibrated thermistor for temperature readings and a capacitance cell for conductivity measurements. One set was positioned near the top of each pond, one at mid-depth and the third at the bottom. A schematic diagram of this arrangement is shown in Figure 3." (which is not reproduced here) "... The pond at the extreme right in Figure 2 was used as the control pond for this and subsequent spills.

Oil Used

Norman Wells crude oil, supplied by Imperial Oil of Canada Limited, was used for this and subsequent spills. ... It has a pour point of -51 °C and a low residuum carbon value (Charbonnier *et al*, 1969). The results of a partial Hempel distillation (United States Bureau of Mines, 1951) are shown in Table 1, and a complete distillation conducted several years ago is shown in Table 2. The low pour point of this oil is similar to that of the oil found at Atkinson Point (-43 °C), and both of these oils have lower pour points than that of the oil from Prudhoe Bay (-9 °C) (Parker, 1968). These three oils are found in the Arctic and Subarctic.

Table 1. Partial Analysis of Norman Wells Crude oil Used in this work (United States Bureau of Mines, 1951)					
Fraction cut at °C	Percent (volume)	Cumulative percent (volume)	Specific gravity	Percent (weight)	Cumulative percent (weight)
50	2.7	2.7	0.635	2.12	2.1
75	2.8	5.5	0.664	2.3	4.4
100	5.8	11.3	0.710	5.0	9.4
125	8.2	19.5	0.738	7.3	16.7
150	5.9	25.4	0.759	5.4	22.1
175	5.2	30.6	0.779	4.9	27.0
200	4.9	35.5	0.795	5.2	32.2
225	5.4	40.9	0.811	5.3	37.5
250	5.2	46.1	0.824	5.2	42.7
275	6.2	52.3	0.838	6.3	49.0

Table 2. Complete Distillation Analysis of Norman Wells Crude oil (Charbonnier *et al*, 1969; United States Bureau of Mines, 1951)			
Fraction cut at °C	Percent cut	Cumulative percent	Specific gravity cut
50	2.7	2.7	0.657
75	3.1	5.8	0.673
100	4.7	10.5	0.712
125	7.9	18.4	0.742
150	5.7	24.1	0.764
175	6.1	30.2	0.781
200	5.4	35.6	0.801
225	5.7	41.3	0.815
250	5.4	46.7	0.828
275	6.2	52.9	0.842
Distillation continued at 40-millimetre of Hg pressure.			
200	4.6	57.5	0.856
225	6.0	63.5	0.865

Table 2. Complete Distillation Analysis of Norman Wells Crude oil (Charbonnier *et al*, 1969; United States Bureau of Mines, 1951)			
Fraction cut at °C	Percent cut	Cumulative percent	Specific gravity cut
250	5.0	68.5	0.880
275	3.8	72.3	0.894
300	5.2	77.5	0.902
Residuum	21.5	99.0	0.948
Carbon residue of residuum–6.5%; carbon residue of crude – 1.4%			

Weather Monitoring

A Rimco 5-inch (123-millimetre) cup contact anemometer and a wind vane attached to a Summer Mark III recorder were installed at position Q shown in Figure 2. Temperature readings were taken daily and correlated with those at the Ottawa Weather Station located at the airport, and with those recorded at the Central Experimental Farm. It was found that the temperature readings at the site agreed to within 1 °C with those at the other two federal installations.

Spills

On November 20, 1972, we made our first spill on pond no. 3. This spill simulated oil on water under ice-forming conditions. At this time, freeze-up had commenced in the Ottawa area and 40 mm of ice covered each pond. An approximate 3.6 by 3.6 m area of ice was removed from the centres of ponds no. 3 and no. 4, but on pond no. 3 an additional area was removed from the southeast side of the pond (Fig. 4). The barrel containing the oil was shaken. Homogenized by agitation, 23 gallons of the oil were then delivered to the exposed water area of pond no. 3 by a mechanical pump and hose. Pumping commenced at 1500 hours and ended at 1530 hours. ...

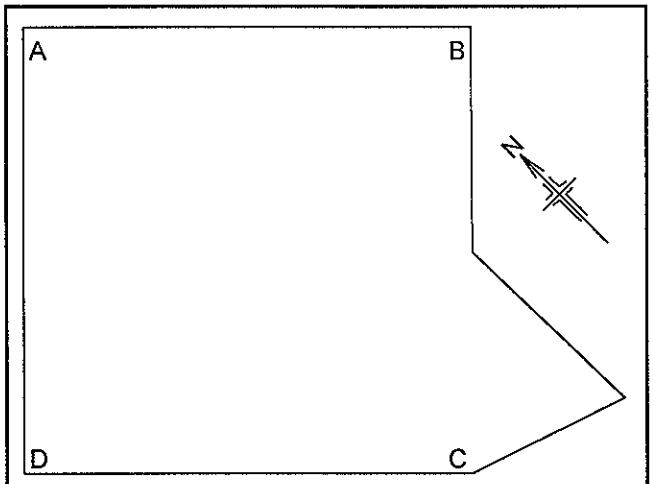

Figure 4. Ice-free area in pond no. 3.

Sample Collection and Treatment

All of the samples were identified by the date, time and location of sampling. Samples of 10 ml were removed daily as shown in Figure 6" (Figures 5 and 6 are not reproduced here) "and transferred to clean, glass storage bottles previously purged with nitrogen. These samples, which were transported in the dark and stored in refrigerators at -5 °C in our laboratories, were used for gas chromatographic, infrared, visible and ultraviolet, and fluorescence spectroscopic analyses. No special pretreatment was given to these samples other than to prevent any water collected with the sample from being withdrawn with the oil prior to analysis.

Less frequently, additional samples of about 20 ml were removed for neutron activation analysis. Surface samples were collected by a polyethylene scoop and transferred to Teflon-gasketted, Nalgene sample bottles for storage under nitrogen in the refrigerator.

Laboratory

Neutron-Activation-Analysis

Sample Treatment—Samples were transferred from the Nalgene bottles and washed individually with deionized doubly distilled water. Each sample was then centrifuged to separate the water from the oil. The choice of the material of the centrifuge tubes was restricted to polyethylene that had been cleaned with detergent and thoroughly washed with deionized water. No heating of the centrifuge tubes, of their shielding or of the oil samples was necessary, since viscosity of the Norman Wells crude oil and the weathered oil samples did not cause any special problems. After a few minutes of centrifugation, the denser water phase in the tube was removed by disposable syringe. After centrifuging for an additional few minutes, any residual water was withdrawn, and the oil was poured directly into tared polyethylene snap-top irradiation vials. After capping and before heat-sealing, the vials were weighed.

Irradiation and Counting Procedures—The samples were irradiated in the sealed polyethylene vials for 1 hour at a thermal neutron flux of 2.5×10^{12} neutrons cm^{-2} sec^{-1}, in the SLOWPOKE nuclear facility at the Atomic Energy of Canada Limited (AECL), Commercial Products Division, Ottawa. Following irradiation, the samples were transferred from the irradiation vials and counted after a decay period such the ^{24}Na activity had sufficiently diminished. The counting facility used was a 35 cm^3 Ge(Li) detector coupled to an 800-channel pulse-height analyzer. Standards were irradiated and counted using the same technique. An Au-Al flux-monitor wire was employed with each irradiation to monitor the actual neutron dose.

For ^{51}V, a short-lived isotope ($t_{1/2}$ = 3.8 min), a short irradiation of 1 minute followed by a radioactivity measurement was carried out. Vanadium was detected in all of the samples and its abundance masked the detection of other short-lived isotopes. Aluminum (^{28}Al, $t_{1/2}$ = 2.3 min) was detected in all of the samples. For this short-lived isotope it was necessary to delay its measurement in order for the ^{51}V activity to decay. The levels, however, were too low for quantitative determination. For the other elements, the standard procedure was then followed.

Some samples were also irradiated in the NRX and NRU high-flux research reactors (maximum flux = 5×10^{14} neutrons cm^{-2} sec^{-1} and 10^{14} neutrons cm^{-2} sec^{-1}, respectively) at the Chalk River AECL Nuclear Laboratories. A neutron flux of 5×10^{12} neutrons cm^{-2} sec^{-1} was used and the samples irradiated for 75 hours. For certain irradiations the concentration level of desired elements producing relatively long-lived isotopes made it necessary to use quartz capsules as irradiation containers. A number of the samples were irradiated together in the reactor, and the irradiated samples were transported to Ottawa for counting measurements. The total activity had a large contribution from the ^{24}Na isotope, and therefore it was necessary to wait for the activity to decay before counting for the other isotopes.

Gas Chromatography

Chromatographic conditions are shown in Table 3. To protect the SCOT column, an empty 1.8 metre precolumn was placed in front of it. Heavier ends of the oil, which would not pass through the column, remained in the precolumn. This arrangement with its resulting dead-space did not

seriously affect the retention times.

Table 3. Chromatographic Conditions for Oil Analysis on Perkin-Elmer 900.

Parameter	Dexsil-300 SCOT column	OV-1 SCOT column
Sample size (µl)	0.45	0.45
Injector temperature (°C)	350	300
Split ratio	10:1	10:1
Carrier gas	He	He
Flow rate (ml/min)	10	10
Initial temperature (°C)	60	35
Initial temperature hold (min)	0	6
Final temperature (°C)	300	210
Final temperature hold (min)	32	32
Program rate (°C/min)	4	4
Detector	FID	FID
Detector temperature (°C)	350	300
Hydrogen pressure (kg/cm^2)	1.8	1.8
Air pressure (kg/cm^2)	2.1	2.1
Column diameter (mm internal)	0.5	0.5
Column length (m)	15.6	15.6
Precolumn length (m)	1.9	1.9
Coating of precolumn	empty	empty

Table 4. Wind conditions at the Shirleys Bay site during the first spill.

Date (1972)	Average wind speed		Direction
	(mph)	($km\ h^{-1}$)	
November 20	4.5	7.2	NE
November 21	5.9	9.5	E to N to E
November 22	5.7	9.1	NE to N to E
November 23	4.4	7.1	NE to N to W
November 24	4.0	6.4	NW to N
November 25	4.2	6.7	NE to N to E to N
November 26	3.8	6.1	N to W
November 27	10.4	16.7	W to N to NW to N
November 28	7.1	11.4	N to NW
November 29	3.1	5.0	NW to N to NE
November 30	3.6	5.8	NE to N to NW to W
December 1	5.4	8.7	W to NW to N
December 2	5.7	9.1	E to ENE to NE to N to W
December 3	4.9	7.9	W to NE to N to NE
December 4	4.3	6.9	NE to N to SE
December 5	6.9	11.1	SE to W to S to E to N
December 6	5.1	8.2	N to W to NW
December 7	8.1	13.0	E to NE
December 8	4.7	7.1	NE to W

Infrared Spectroscopy

A Perkin-Elmer (Model 357) grating infrared spectrophotometer was employed for these measurements. Cavity cells were used to hold the samples and chloroform or carbon disulphide was used as solvent.

Visible and Ultraviolet Spectroscopy

A recording Beckman DBG, double-beam, grating spectrophotometer was used to record the

spectra, and occasional replicate samples were run on a Cary Model 14 spectrophotometer. Fused quartz, 10-millimetre cells were employed. Oil samples (0.02 µl) were diluted to 10 ml by n-hexane.

Fluorescence Spectroscopy

A Perkin-Elmer MPF 2A recording fluorescence spectrophotometer was used. The solvent of choice was spectro-analyzed n-hexane. Samples in the 1-microlitre size range were added to 10-millilitre volumetric flasks and these solutions were analyzed by first determining maximum absorption regions in the ultraviolet (ca 256 mµ) and then using the wavelength as the excitation line. A calibration was performed each day. Efforts were made to resolve the spectra obtained from the fluorometer by a Dupont Model 310 curve resolver."

Results

"**Field**

Weather Data

Pertinent weather factors influencing the behaviour of the oil are wind speed, temperature, sunlight or cloud conditions and precipitation. These are shown in Tables 4, 5 and 6, respectively. As noted in Table 4, the wind speed is generally constant at 2.0 m/sec, but the wind direction continually changes. Temperatures generally were about the freezing point of water up to November 28, 1972, when the weather turned colder. The cold weather persisted until December 6, 1972, when the temperature again reached 0 °C, but then went back down to seasonable averages. There were approximately 12 hours of sunlight from November 20 to December 2. From December 2 to December 8, there was about 8 hours of sunlight at the field site. ...

Table 5. Hourly air temperatures (°C) for duration of first spill.

	Temperature (°C)															
	November, 1972											December, 1972				
hour	20	21	22	23	24	25	26	27	28	29	30	1	2	3	4	5
00	-0.6	-4.4	-8.3	-12.2	0.0	1.7	1.1	2.8	1.1	1.7	-3.3	0.0	-13.3	-10.0	-13.9	-13.3
01	-1.1	-3.9	-8.9	-12.8	0.0	1.7	0.6	2.2	1.1	1.1	-2.8	0.0	-13.9	-9.4	-14.4	-13.3
02	-1.1	-4.4	-11.1	-13.3	0.6	1.7	0.6	2.2	1.1	0.0	-2.8	-2.2	-14.4	-8.9	-15.6	-13.3
03	-1.1	-3.3	-10.6	-13.9	0.6	1.7	0.6	2.2	0.6	-0.6	-2.8	-2.2	-16.1	-8.3	-15.6	-12.8
04	-1.1	-3.9	-10.0	-13.9	0.6	1.7	0.6	2.2	0.6	-1.7	-4.4	-2.2	-16.1	-8.3	-16.7	-12.2
05	-0.6	-5.0	-11.1	-14.4	1.1	1.7	0.6	1.7	1.1	-0.6	-3.3	-2.8	-17.2	-8.3	-17.8	-11.7
06	-0.6	-6.1	-11.7	-14.4	1.1	1.7	0.6	1.7	0.0	-0.6	-3.3	-2.8	-17.2	-8.3	-17.8	-11.1
07	-0.6	-6.1	-11.7	-14.4	1.7	1.7	1.1	1.7	0.6	-1.1	-2.8	-2.8	-17.8	-8.3	-17.8	-10.6
08	-0.6	-7.2	-11.7	-13.9	1.7	1.7	1.1	1.7	2.2	-1.7	-2.8	-2.8	-17.8	-8.3	-17.8	-10.0
09	-0.6	-6.7	-11.7	-10.0	1.7	1.7	2.2	2.8	2.2	-1.7	-1.7	-2.8	-16.1	-8.9	-17.8	-9.4
10	0.0	-6.7	-10.6	-9.4	2.2	2.2	2.2	3.3	2.8	-1.7	-1.1	-2.2	-15.6	-8.9	-16.1	-9.4

Table 5. Hourly air temperatures (°C) for duration of first spill.

	Temperature (°C)															
	November, 1972											December, 1972				
hour	20	21	22	23	24	25	26	27	28	29	30	1	2	3	4	5
11	0.0	-6.1	-9.4	-7.2	2.2	2.2	1.7	3.9	3.3	-1.1	-0.0	-1.7	-14.4	-8.9	-16.1	-8.3
12	0.0	-5.6	-8.3	-5.6	2.8	2.2	1.7	3.3	2.8	-1.1	-1.1	-1.1	-12.8	-8.9	-15.6	-7.8
13	0.0	-5.0	-7.2	-4.4	2.8	2.8	2.2	3.3	2.8	-0.6	2.2	-0.6	-11.7	-8.3	-15.0	-7.8
14	0.0	-4.4	-6.7	-2.2	2.2	2.8	1.7	3.3	2.2	-0.6	1.7	0.6	-10.6	-8.3	-15.0	-7.2
15	0.0	-4.4	-5.6	-1.1	2.2	2.8	2.2	3.3	2.2	-0.6	1.1	1.1	-11.1	-7.8	-15.0	-7.8
16	0.0	-5.0	-6.1	-0.6	2.2	2.2	2.8	3.3	1.7	-0.6	1.1	-1.1	-11.7	-8.9	-15.0	-7.8
17	-1.7	-6.7	-7.2	0.0	2.2	2.2	3.3	2.8	1.7	-1.7	-0.6	-2.8	-11.1	-10.0	-15.0	-7.8
18	-1.7	-7.2	-7.2	0.0	2.2	2.2	3.9	2.8	1.7	-2.8	-1.1	-5.6	-11.7	-10.6	-14.4	-7.8
19	-2.8	-7.2	-9.4	0.0	2.2	1.7	3.9	2.8	1.1	-2.8	-1.7	-7.8	-11.7	-10.6	-14.4	-7.2
20	-3.3	-7.2	-9.4	0.0	1.7	1.7	3.3	2.2	1.1	-5.0	-6.7	-8.9	-11.7	-12.2	-13.9	-7.2
21	-4.4	-8.3	-10.0	0.0	1.7	1.7	3.3	2.2	1.1	-4.4	-2.2	-9.4	-11.7	-12.8	-14.4	-7.2
22	-3.3	-7.8	-10.6	0.0	1.7	1.1	3.3	1.7	0.6	-3.9	-1.7	-11.1	-11.1	-12.2	-14.4	-7.2
23	-4.4	-8.3	-10.6	0.0	1.7	1.1	2.8	1.7	0.6	-4.4	-1.7	-12.2	-10.6	-13.9	-13.9	-7.2

Table 6. Cloud conditions and precipitation

Date (1972)	Sunlight	Precipitation
November 20	Sunny during afternoon	Snow in morning
November 21	No cloud cover	
November 22	Intermittent clouds	Trace of snow
November 23	Overcast	Trace of snow
November 24	Overcast	
November 25	Overcast	Wet snow during evening and night
November 26	Overcast	Snow and rain (3 in.)
November 27	Overcast	Freezing rain and snow (trace)
November 28	Overcast	
November 29	Intermittent clouds	

Table 6. Cloud conditions and precipitation		
Date (1972)	Sunlight	Precipitation
November 30	Overcast	Snow in afternoon (1 in.)
December 1	Overcast	Snow (4 in.)
December 2	Sunny in morning, Cloudy in afternoon	Snow in afternoon (4 in.)
December 3	Cloudy in morning, Clear during afternoon	Snow in morning (4 in.)
December 4	Sunny	Snow in evening (trace)
December 5	Overcast	Freezing rain and snow (trace)
December 6	Overcast	Freezing rain and snow (trace)
December 7	Clear	
December 8	Overcast	Snow (1 in.)

Behaviour of Surface Oil—For the first few days after the spill, the oil stayed contained within the area cut out of the ice for this spill, as denoted by the illustrations mentioned in the previous section. Small ridges formed on the exposed ice near point C along side BC (Fig. 4) within two days after the spill. At their maximum height these ridges were 20 mm high (Fig. 9)." (Figures 7 through 11 are not reproduced here) "By the fifth day after the spill, these ridges began to lose their structure. On November 27, the ridges were no longer visible, but there were furrows only in the ice as recorded in Figure 10. The disappearance of this structure was aided by the higher air and oil temperatures occurring at that time. No similar structures were noted in the control pond or in other areas of the pond where the spill occurred. This area was originally bounded, in part, by the polyethylene liner.

By November 24, the ice edge between B and C (Fig. 4) resulting from removing the ice layer for the spill began to lose its sharp definition. It is known that the oil is usually at a higher temperature than its surrounding because of solar radiation (McMinn, 1972; Adams). This is reinforced by the fact that samples collected prior to December 1 contained water that came from a water layer formed between the ice surface and the oil. During this time, no water was visible on the surface of the adjacent control pond. When the oil cooled during the night, the water under the oil layer could solidify of the temperature went below freezing. This effect was the most noticeable between points B and C (Fig. 4). As the new ice layer formed, it appeared preferentially near the sides of the section removed to contain the oil; point C (Fig. 4) was near the edge of the ice surface of the pond. Therefore a thicker ice layer would form causing an uneven surface and the oil flowed to a lower surface. It appeared that the prevailing winds did not affect the position of the oil while it was contained within the original spill area at this time.

On November 25, very little oil was observed on side BD (Fig. 4). The increase in the height of the ice surface at BC and the prevailing winds caused the oil to flow in the direction of AD (Fig. 4). From November 25 to November 29, the oil movement on the pond depended on the wind direction. Prior to the snowfall of December 2, the oil was always exposed to solar radiation and consequently had a temperature higher than that of its surroundings. Before that time, any snow that fell onto the oil was melted by the internal heat of the oil. With the decrease of temperature on

December 2, any water under the oil was solidified, and part of the oil became embedded in the ice. A trace of free oil could still be observed on the northeast side of the pond. The snow on December 3 completely covered the oil, and the temperatures on this day were well below freezing. These conditions prevented further melting of the snow cover by the oil.

On December 6, only a small amount of oil was found on the surface of the slush-like mixture which extended down 50 mm. If the oil was contained only within the snow that covered it, more oil would be expected rather than the small amount that was later found. Therefore the oil must have been embedded in the ice that eventually formed from the melted snow that fell prior to December 3. When the slush layer had frozen the next day (December 7) only a small area near line AB had free oil. On inspection, however, oil was observed beneath the ice surface and was concentrated in the area where oil was observed on December 2. From December 9, 1972 to January 9, 1973, 750 mm of snow fell and the ponds were covered. On January 9, there was an ice cover on the pond as well as the control pond and the ice level had increased by about 200 mm over that observed on December 8. During the visit to the site, the ice surface was inspected. The pressure on the ice caused by walking on it resulted in cracks occurring in the ice. About 2 hours later, a small amount of oil oozed to the top of the ice surface through the cracks as shown in Figure 11. On the following days, very little oil came out of the cracks. The oil was observed in the vicinity of point A.

Laboratory Studies

By applying the techniques outlined in the experimental section, the composition of the oil remaining from the spill was monitored. Some of the methods employed yield more information than others.

Gas Chromatography

This technique involves the separation of the components of a sample by a simulated distillation. This distillation occurs in columns contained in a programable heating chamber. The length and internal coating of the column determine the degree of separation of the components in the sample of interest. For the present investigations, SCOT columns, 50 ft x 0.02 in. (15 m x 0.5 mm) i.d., were used, as they give a better separation of components relative to shorter thicker columns. Since the technique is essentially a distillation, only those components that are in their vapour state in the column can be detected. In addition the type of material used as the liquid phase in the columns defines the upper temperatures that may be used. For this investigation, two types of SCOT columns were used. One contained Dexsil 300, a material that allows high temperatures to be used (+400 °C), but at temperatures below 125 °C it is a solid. Accordingly below this temperature solid vapour chromatography was being performed and the peaks under these conditions were not too well resolved (typical of this type of chromatography). These columns were used to monitor the higher boiling fractions of the weathered oils. A second type of SCOT column with OV-1 liquid phase was used to investigate the lighter ends.

Figure 12. Chromatogram of Norman Wells crude oil using (a) Dexsil-300 SCOT column and (b) OV-1 SCOT column.

Chromatograms of the original crude oil, run on the two types of columns, are shown in

Figure 12. As can be seen from these two chromatograms, there is a distinct difference in the resolving power of the two columns, but both columns indicate there is an abundance of high vapour-pressure components. A sample, taken from the aqueous surface just after the spill, had a slightly different pattern of peaks at the beginning of the chromatogram relative to the original oil. This resulted from the evaporation of the extremely volatile fraction.

The sample taken on the morning of November 21 did not contain those components with vapour pressures greater than that of n-heptane. Significant changes were noted in the chromatogram of the afternoon sample of the same day, but some octane was still present. The sample collected on November 24 showed that all of the octane had disappeared and the amount of nonane was low. The sample removed on November 28 contained no nonane; decane was greatly depleted in the sample of November 30 (Fig. 13). The amount of decane in the sample taken on December 1 was about the same as that in the sample of November 30, and the concentration of undecane was also low. Analysis of the sample collected on December 8 did not differ greatly from that taken on December 1 nor did the chromatogram of the sample taken on January 9, 1973. All of the samples had similar chromatographic traces between tetradecane and hentricosane. This indicates that very little alteration of this fraction of the oil occurred.

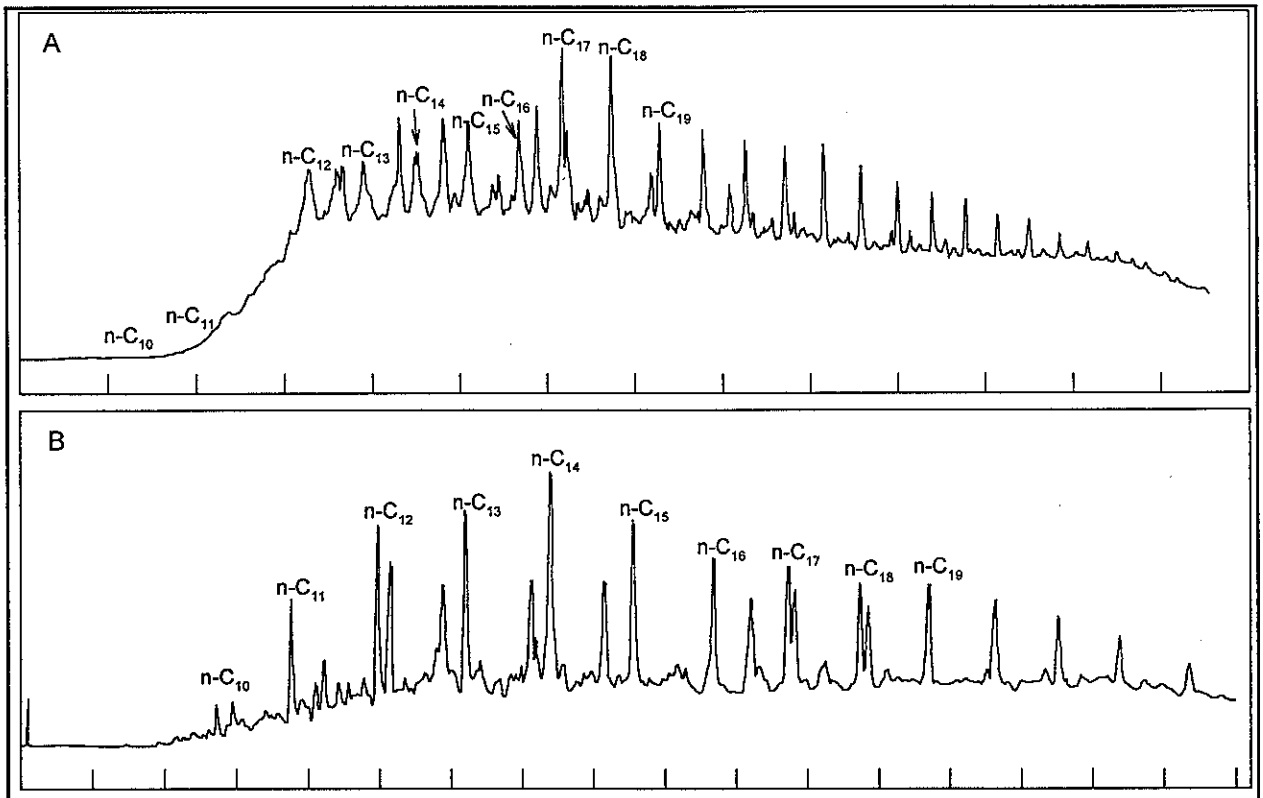

Figure 13. Chromatogram of weathered oil sample taken November 30 by (a) Dexsil-300 SCOT column and (b) OV-1 SCOT column.

In Table 7, the boiling points of the n-alkanes between C_6 and C_{20} are listed. As can be seen, the boiling points have a range of 350 °C. Table 1 records an abbreviated Hempel distillation report of the crude oil used in the spills (United States Bureau of Mines, 1951). The information obtained from this and similar distillations is helpful in refinery operations. Each fraction of this distillation was chromatographed on both types of SCOT columns. These chromatograms showed that many constituents were present in consecutive fractional cuts; for example, heptane was found in the first four cuts.

Some caution must be exercised in correlating the results of chromatograms of the aged oil with the data of the Hempel distillation. Generally there is a loss recorded in the Hempel distillation, in this instance, 3.1%, and this is usually explained as very light ends that did not condense. Accordingly values may be 3.1% higher by volume. Also the Hempel distillation conditions may not replicate the manner in which components evaporated from the crude oil used in this spill. The two modes of "distillation", however, are correlated, since it is realized that it is best to obtain a reasonable estimate of the residual oil. Chromatograms of several distillation cuts are shown in

Table 7. Boiling Points of N-Alkanes (°C)

Compound	Boiling point (°C)
n-hexane	67.0
n-heptane	98.4
n-octane	125.7
n-nonane	150.8
n-decane	174.1
n-undecane	195.9
n-dodecane	216.3
n-tridecane	235.4
n-tetradecane	253.7
n-pentadecane	270.6
n-hexadecane	287.0
n-heptadecane	301.8
n-octadecane	316.1
n-nonadecane	329.7
n-eicosane	343.0

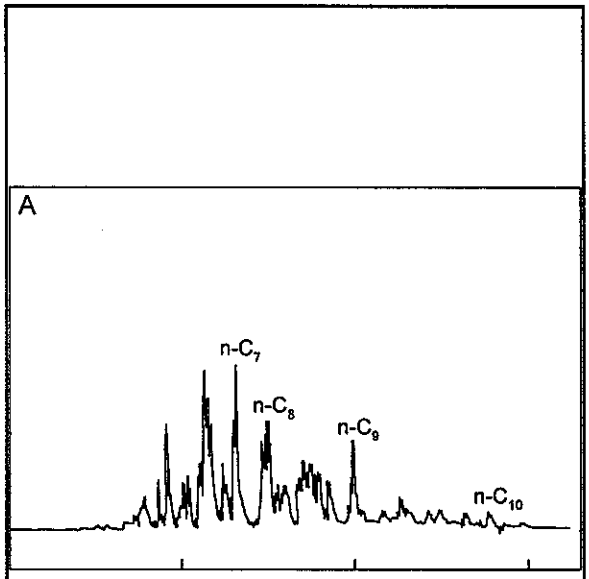

Figure 14. Chromatograms of fractions (a) no. 5 and (b) no. 8 of a Hempel distillation of Norman Wells crude oil.

Figure 14.

As apparent from the chromatograms, approximately 30% by volume or 27% by weight of the crude oil had evaporated within the first 24 hours because of the loss of the very volatile fractions, and by November 24 (93 hours), 41% by volume or 37% by weight of the oil had disappeared. On November 26, it was estimated that 46% by volume or 42% by weight had volatilized. By November 28, 48% by weight of the oil had gone. With only nominal differences of November 28, 29, and 30, it can be assumed that approximately 50% by weight of the oil had evaporated as determined by gas chromatography. The residue of the abbreviated Hempel distillation could still be poured at -5 °C (United States Bureau of Mines, 1951).

Table 8. Neutron Activation Analysis of Weathered Oil on Water under Ice-Forming Conditions

Sample	V (ppm)	Mn (ppb)	Cu (ppb)	Al (ppb)
original	6.5	19	570	90
Aged 1 hour	7.6	30	260	90
Aged 19 hours	10.2	42	320	300
Aged 24 hours	8.4	14	370	200
Aged 45 hours	8.4	12	180	80
Aged 71 hours	8.5	56	460	100
Aged 5 days	7.8	23	1,900	400
Aged 6 days	7.3	55	560	4,900
Aged 7 days	8.6	31	300	100
Aged 8 days	8.0	260	630	400
Aged 9 days	8.6	50	530	900
Aged 10 days	8.7	150	1,020	6,000

Neutron Activation Analysis

Neutron activation analysis is a technique that can be used to determine the concentration of heavy metals in an oil matrix. These metals are usually associated with components comprising the heavier ends of the oil, for example, the metal porphyrin complexes. In most systems, the metal in the complexes may exchange with other metals present in the vicinity. In the present experimental conditions such an exchange was not observed. This is not unexpected, since the water in the pond had low concentrations of other metals. Therefore any increase in the metal concentration of the oil primarily results from the evaporation losses of the lighter components.

Table 8 lists the concentrations of four metals initially present in the oil and their concentrations after definite periods of aging. Generally there is a concentrating effect. Three of the

elements, Mn, Cu, and Al, however, do not exhibit definite trends on aging. The variations in the values of these elements, given in Table 8, are considered to reflect the experimental difficulties because of the interferences of other trace metals present in small quantities. The spurious reactions of neutrons affecting Fe and Co nuclei give a higher reading for Mn. Similarly Zn interferes with Cu determination by undergoing the ($^{64}Zn + {}^{1}n \rightarrow {}^{64}Cu + {}^{1}p$) reaction. In light of the possible interferences and also because of the large statistical error during counting of the low activities, the values for Al, Cu, and Mn were not found to give any definite trends on weathering. The fourth element, vanadium, exhibits a well-defined behaviour. Indeed, in characterizing oils, vanadium and nickel are used extensively. From the vanadium values in Table 8, it is calculated that after 24 hours approximately 30% by weight of the oil had evaporated. After 11 days of exposure to the weather, the vanadium concentration indicates that 35% of the oil had disappeared. These neutron activation analyses confirm the estimate of the evaporative loss of the aged oil obtained from gas chromatographic techniques.

Ultraviolet Spectroscopy

It was not possible to obtain specific information from the UV/VIS spectra. It helped, however, in selecting the excitation wavelengths for the fluorescence measurements.

Infrared Spectroscopy

The samples were dissolved in chloroform, although this solvent has many interfering bands. It proved difficult to extract any valuable information, since very little difference could be seen in the spectra of samples of successive days.

Fluorescence Spectroscopy

Considerable effort was put into this method, as it is often used as an ancillary technique for determining the source of oil spills. The sensitivity of the technique, however, resulted in difficulties in comparing spectra. Samples were obtained below quenching concentrations (Parker, 1968), and Beer-Lambert plots were obtained using the unaged oil. Since this plot changed on successive days, calibration curves were determined daily and samples were run on the same day. No concentrating effect was found for this oil despite the loss of lighter components as indicated by other techniques. A typical fluorescence spectrum is shown in Figure 15."

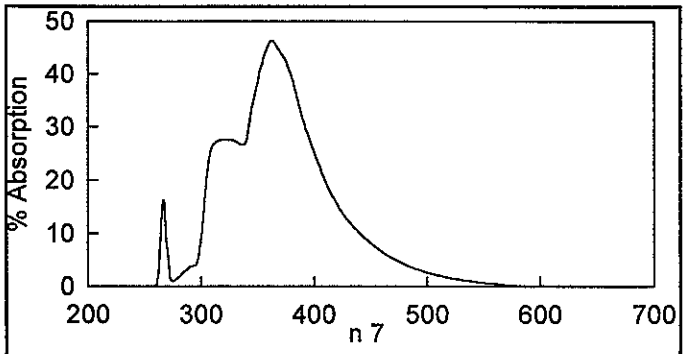

Figure 15. Fluorescence spectrum of Norman Wells crude oil.

BOSS Critique

The author does not discuss the error(s) in determining the loss of components, from weathering crude oil, when using gas chromatography.

There are several basic scientific errors in this work, such as % Absorption for the amplitude of a fluorescence spectrum and the x axis of the plot (Figure 15) should be labelled nm (nanometres). The excitation line that was chosen for the fluorescence spectra may have been the incorrect line to use. The UV/VIS absorption spectra of the aged oil may have had peak(s) that decreased as the oil was aged and the peak that decreased the most should have been used for the excitation line of the fluorescence spectra. This would then allow the authors to see a concentrating effect. The authors do not discuss the changes in the absorption spectra except to say that 256 was chosen as the excitation line since that feature had the largest absorption. The authors state that the UV/VIS did not change much, however, a small change in absorption may mean a large change in fluorescence. More detail needed to be presented describing the components that fluoresce.

The explanation of neutron activation analysis seemed also to have some misconceptions. For example, the half-life ($t_{1/2}$) of a component is based on a first-order rate constant, k, and the equation is $[A] = [A_0]\exp\{-kt\}$ where at $t_{1/2}$, $[A] = 1/2\ [A_0]$. Thus the concentration of the species decreases to one half of the original concentration at the half-life interval. This means that each passing segment of time that is in units of half-life, the concentration of the species decreases to 1/2 of the previous concentration. At $t=0$, $[A]=[A_0]$, at $t=t_{1/2}$, $[A]=1/2[A_0]$, at $t=2t_{1/2}$, $[A]=1/4[A_0]$ etc., with ever decreasing concentration. If two elements initially have identical concentrations but different half-lifes then after the same amount of time has passed each element will be at different concentrations. If there are two elements where one element has a $t_{1/2}$ that is one half of another element then if they start with identical concentrations the element with the largest half-life will be at the largest concentration after any time period is passed. In the manuscript the authors were trying to determine the concentration of ^{28}Al, $t_{1/2}$=2.3 min, with ^{51}V, $t_{1/2}$=3.8 min also present which would only be possible if the initial concentration of ^{28}Al is much greater than the initial concentration of ^{51}V. The authors do not discuss this.

Review of a manuscript by, Moir, J. and Y. Lau, *Some Observations of Oil Slick Containment by Simulated Ice Ridge Keels*, Environment Canada, Burlington, Ontario, 14 p, 1975.

Technical Summary

"1. The ice ridge keels will retain oil and conditions for containment are similar to oil slick retention in open water. However, slicks contained behind the sloping ridges are prone to long term leakage.

2. The presence of an ice-sheet upstream of the barrier does not significantly alter the slick profile or the maximum volume of oil containable, in comparison to the open water case."

Objective

The authors wanted to determine the effective oil containment of ice keels of different geometries.

Theory

The theory is presented along with the results in the results section.

Method

"The tilting flume was used with a test length of 15 metre, a reduced width of 0.6 metre and a variable depth of 0.06 metre to 0.6 metre. The bottom of the channel was artificially roughened with 1 mm. graded sand: the sides were smooth.

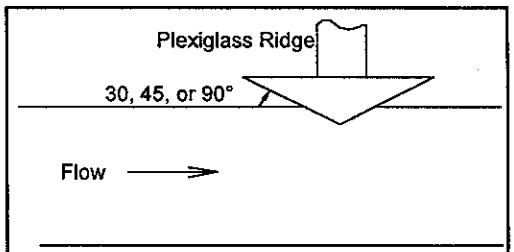

Figure 2. Cross-section Idealized Model Situation.

Three plexiglass barriers were used to model the ice ridges. The barriers were mounted perpendicular to the flow and at 90°, 45° and 30° respectively to the horizontal as in Figure 2. To simulate ice-cover, sheets of expanded foam wrapped in a vinyl covering were floated on top of the water. For a few of the tests a layer of coarse sand was glued top the bottom side of the vinyl covering to simulate roughness of the ice.

For each test the flow rate was established, and the downstream tailgate and slope were adjusted to obtain uniform flow at the required depth. Oil was injected on the surface of the water about 10 metre upstream of the barrier, or barrier and floating "ice".

For test for conditions under which the barriers would fail to contain oil, the flow was established initially at a discharge such that failure was certain to occur. The discharge was decreased, in steps, until some retention was observed; the depth being maintained at the initial setting. At the last discharge setting, with some oil retained, the depth was lowered a few millimetres until failure occurred. A significant change from uniform flow did not occur, and the failure depth and flow rate could be quite accurately determined.

For tests for volume containable and slick profile, the flow rate and depth were established with uniform flow and a known volume of oil was injected. Oil was added to the slick until quantities of oil passed under the barrier. ... The slick was allowed to stand for a period of time until

no change in the slick could be observed. This was taken as the maximum stable slick for the given flow conditions. ... The same test was performed for both open water condition and also with a top cover."

Results

"The tests for slick profile or volume change are tabulated in Table 1.

Table 1					
Test	Barrier	U, m/sec	d, cm	F_Ω	Note
1, 2	90°	0.205	16.84	0.40	comparison of profile for open water and smooth cover
3, 4	90°	0.145	16.20	0.29	same
5, 6	30°	0.240	25.38	0.38	comparison of smooth cover and rough cover

where U = average flow velocity,
d = depth of flow,
$F_\Omega = U/(gd\Omega)^{1/2}$,
$\Omega = (\rho_w - \rho_o)/\rho_w = 0.163$ for all tests,
g = gravitational constant,
ρ_w = water density,
ρ_o = oil density.

There was no observed change in the maximum volume of oil retainable or the profile of the slicks, behind sloping barriers, or a vertical barrier, because of the presence of the top cover. But because the sloping, barriers tended to leak droplets of oil at random intervals, the long term retention volume behind sloping barriers proved to be less than that for a vertical barrier. This effect was particularly acute at F_Ω near the failure limit. The degree of roughness of the underside of the ice sheet had no appreciable effect on the profile of the slick.

The results of the tests for maximum F_Ω, from this study, are listed below.

Table 2.							
Test	Barrier °	Open Water			Smooth Cover		
		U, m/sec	d, cm	Maximum F_Ω	U, m/sec	d, cm	Maximum F_Ω
1	90	0.234	15.0	0.477	0.249	13.95	0.527
2	45	0.227	16.9	0.437	0.243	15.7	0.487
3	30	0.225	17.0	0.431	0.242	15.8	0.480

Failure occurred as 1) droplets formed at the leading edge of the slick, or droplets formed at the barrier, and carried under the barrier, and 2) a "sheet" type failure ... .

Tests with multiple 45° barriers with "ice" were done at F_Ω near the failure limit to determine if the presence of an ice ridge upstream would interfere with the slick at a downstream ridge and whether it is possible to generate a "quiet" zone between two ridges at high F_Ω .

With the barriers spaced closely, at 10 times the draft, oil collected initially on both faces of the upstream barrier and on the downstream face of the downstream barrier. No oil ever collected at the upstream face of the downstream barrier. ...

With the barriers spaced at 21 drafts, oil collected initially at both faces of both barriers. A "separation point" about 5 barrier drafts downstream of the first barrier was noticed. A globule of oil that became detached from the slick and passed this point, was carried to the second barrier. Upstream of this point, the interfacial waves and detached droplets were carried upstream to the downstream face of the first barrier. On standing for a few hours at F_{Ω}, oil was retained downstream of the first barrier and upstream of the second barrier."

BOSS Critique

The authors do state that these tests were only qualitative, however, errors still should have been discussed for these cases. The authors state that failure depth and flow rate could be determined accurately but no ± value is stated for these measurements. The authors do not define the term draft (or barrier drafts) nor do they state the significance of this term in the context of the experiments.

Review of a manuscript by, McMinn, T.J. and P.C. Golden, "Behavioral Characteristics and Cleanup Techniques of North Slope Crude Oil in an Arctic Environment", in *Proceedings of the 1973 Joint Conference on Prevention and Control of Oil Spills,* American Petroleum Institute, Washington, D.C., pp 263-276, 1973.

The information is also presented in an identical format in a manuscript by McMinn, T.J., "Oil Spill Behaviour in a Winter Arctic Environment", in *Proceedings of the Fifth Offshore Technology Conference,* Vol. 1, OTC-1747, Offshore Technology Conference, Dallas, Texas, pp 233-248, 1973.

Technical Summary

"This paper deals with the physical fate and behaviour of crude oil when spilled on winter arctic ice and snow surfaces. The concepts and theories developed are a result of a series of experiments performed by Coast Guard personnel in the Alaskan arctic during January-February 1972. The paper will develop spreading and aging of oil on ice and snow, the unique interaction phenomena of snow and crude oil, and effectiveness of various cleanup techniques attempted on crude spilled on snow and ice. The paper will also briefly outline the Coast Guard's continuing research plans regarding arctic oil spills.

Investigations prove that oil spreading over ice and snow is largely unaffected by oil properties such as density, viscosity, and surface tension. Oil spreading rate is also believed not to be a function of ambient air temperatures. Terminal spreading limit, independent of oil properties, is a function of effective surface roughness and volume of oil spilled.

Oil was found to age on arctic ice. The winter aging rate was found to be significant although reduced from summer aging rates.

Migration of oil into the ice or snow surface is minimal. However, snow falling on the surface of a fresh spilled oil pool migrates into the oil forming a mixture that contains up to 80% snow (by volume). An array of sorbents, surfactants, and dispersants were tested with largely negative results."

Objective

"...to attempt to quantitize oil spreading on and under ice, oil aging on ice, unique interaction characteristics between snow and oil, ..."

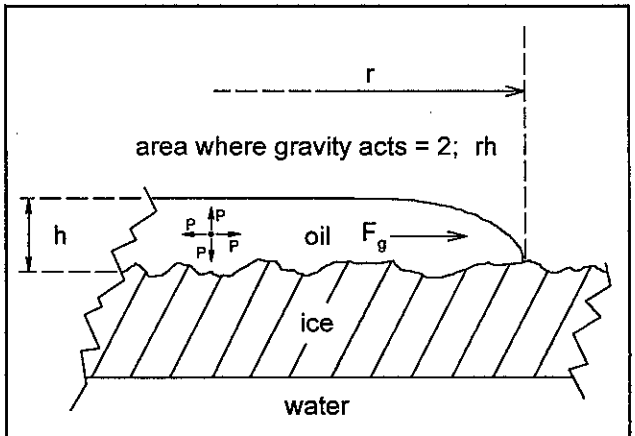

Figure 5: Gravity Forces Acting on Oil Spill on Ice.

Theory

"In an attempt to theoretically describe the spreading of oil on snow and ice a simplified theory was developed. This theory is based on the mechanics of oil spreading over water by Fay[4]. According to Fay, oil spreading on *water* is controlled by four physical phenomena: gravity, surface tension, inertia, and viscosity. Wind shear and current effects are neglected in

the analysis. It is obvious that water currents will not affect the experiments and that close to the ice surface, wind shear forces are negligible.

Initially, the oil driving force is due primarily to gravity generated pressure. Since pressure acts in all directions from a single point, forces due to this gravity pressure tend to force the oil outward from the center in all directions (Figure 5).

Hence the force due to gravity equals

$$F_g = \int_o^h P\,dA \qquad 1.1$$

$$\text{where } P = \rho g h \qquad 1.2$$

$$A = 2\pi r h \qquad 1.3$$

$$\text{and } dA = 2\pi r dh \qquad 1.3.1$$

Substituting in equation 1.1 we obtain

$$F_g = 2\pi\rho g r \int_o^h dh \qquad 1.4$$

Reducing equation 1.4 our relationship for force due to gravity becomes

$$F_g = \pi r g h^2 \qquad 1.5$$

As the oil continues to spread and the thickness (h) becomes very small, h^2 also becomes very small. Most oils have a surface tension value less than that of water or ice and therefore most oils "wet" these surfaces. Therefore as h^2 becomes small and F_g becomes small, forces due to surface tension begin to dominate positive oil spreading forces. The point at which surface tension forces begin to control spreading is the point where the force due to gravity equals the force due to surface tension. The spreading force due to surface tension F_s equals:

$$F_s = \sigma_r (2\pi r) \qquad 2.1$$

where σ_r is the resultant surface tension vector when oil interfaces an ice surface and $2\pi r$ is the circumference of the oil pool. Equating the surface tension force and the gravity forces

$$F_s = F_g$$

$$\text{we obtain} \quad \sigma_r (2\pi r) = \pi r \rho g h^2 \qquad 2.2$$

We now solve equation 2.2 for the thickness (h) of the oil at the instant $F_s = F_g$. We shall call this thickness the critical thickness (h_c). The critical thickness where surface tension forces begin to dominate spreading is therefore:

$$h_c = \sqrt{\frac{2\sigma_r}{\rho g}} \qquad 3.1$$

Hence in summarizing the positive oil spreading forces we find the following sequence:

(1) Gravity forces dominate spreading until $h = h_c$.

(2) At h_c, F_s F_g and surface tension forces dominate.

A similar situation is found when investigating the forces responsible for retarding the spreading of oil. The primary oil retarding forces are due to an inertial deceleration force and a viscous drag force.

Let us first consider the inertial forces. Inertia (F_i) is a retarding force that by definition equals mass x deceleration. For our purposes

$$F_i = \frac{m\,dv}{dt} \qquad 4.1$$

where $m = \pi r^2 h \rho$ 4.2

and $v = r/t$ 4.3

hence $F_i = \frac{\pi \rho r^3 h}{t^2}$ 4.4

The viscosity forces (F_u) are essentially friction forces due to the deformation of horizontal layers of the oil. The dynamic viscosity of the oil (u) is by definition the ratio of the shear intensity to the rate of deformation (dv/dh). We represent this by

represent this by $u = \frac{\tau}{dv/dh}$ 5.1

where $\tau = \frac{F_u}{\pi r^2}$ 5.2

and $\frac{dv}{dh} = \frac{v}{h}$ 5.3

for our purposes $v = r/t$

hence $\frac{v}{h} = \frac{r}{ht}$ 5.4

Our definition of viscosity now becomes

$$u = \frac{F_u h t}{\pi r^3} \qquad 5.5$$

Solving for viscous drag we obtain

$$F_u = \frac{\pi u r^3}{th} \qquad 5.6$$

If we examine the inertia to viscous force ratio $\rho h^2/ut$ we see that this ratio, for a particular oil, increases as h^2/t increases. It is evident from the 1/t relationship that initially, or when time is small, inertia forces dominate the retarding forces and as time increases and the inertial/viscous ratio becomes smaller, viscous forces dominate retarding forces.

Examining equation (3.1) it is apparent that the transition point from gravity to surface tension controlled spreading occurs when the oil diminishes to a critical thickness (h_c) of

$$h_c = \sqrt{\frac{2\sigma_r}{\rho g}} \qquad 3.1$$

(the surface tension σ_r is the resultant surface tension vector when oil is spreading on an ice surface).

We will now attempt to solve for h_c using representative values of ρ (density) and σ_r (surface

tension) obtained for the Prudhoe Bay test crude (See Appendix C). A density of 0.890 gm/cc will be substituted for ρ. The resultant surface tension σ_r is calculated as being

$$\sigma_r = \sigma_o (1 + \cos\theta) \qquad 6.1$$

where θ equals the oil/ice contact angle. For a contact angle of 45° (See Note) and an oil surface tension of 30 dynes/cm (measured value of Prudhoe Bay Crude):

$$\sigma_r = 30 (1 + \cos 45°) = 30(1.702)$$
$$\sigma_r = 51 \text{ dynes/cm}$$

(Note: No experimental data was available for the contact angle of oil on ice. For purposes of this discussion it is assumed that oil "wets" ice which indicates a contact angle of between 0° and 90°. A conservative value of 45° was assigned as the contact angle for determining the resultant surface tension. However, as the cosine of angles between 0° and 90° varies only from one to zero, we can see that by using the worst but impossible case of 0° contact angle, the cosine equals 1.0 resulting in a σ_r of 60 dynes/cm and an "h" of 0.371.)

Using the above mentioned values of ρ and σ_r and 980 gm/sec as the acceleration due to gravity (g),

$$h_c = \sqrt{\frac{2 \times 51}{0.89 \times 980}} = 0.342 \text{ cm}$$

From this calculation we can predict that gravity spreading forces will dominate positive spreading forces until an oil thickness of approximately one-third cm is reached.

From both field and laboratory oil spreading experiments it has been observed that terminal spreading thickness will never diminish to 0.342 cm.

It is believed that ice roughness and the subsequent pocketing of spilled oil within the ice roughness matrix is responsible for limiting the minimum thickness of oil spilled on ice.

Research is presently underway[6] to statistically determine the roughness of Arctic ice and tundra areas in terms of the most probable "average" pocket size. It has been shown[6] that average pocket size for a particular area can be calculated using data taken from airborne laser profilometer traces.

Assuming then, that the terminal spreading thickness of an oil spill will be greater that 0.342 cm, we can predict that oil spreading over ice will never enter into the surface tension controlled spreading regime.

Since the final thickness of an oil spill on ice is quite large when compared to an oil spill on water, and as previously discussed the ratio of inertia to viscous retarding forces vary as h^2 we can also make the assumption that viscous retarding forces are negligible contributions to the resultant retarding force.

Neglecting, then, the surface tension spreading forces and the viscous retarding forces, our discussion leaves us with only gravity spreading forces (Eq 1.5) and inertial retarding forces (Eq 4.4) affecting the spreading of oil on ice.

Equating the gravity spreading and inertial retarding forces we obtain

$$\pi r \rho g h^2 = \frac{\pi \rho r^3 h}{t^2} \qquad 7.1$$

Again depicting the volume (V) of spilled oil as

$$V = Qt = \pi r^2 h \qquad 7.2$$

and solving for thickness (h) to obtain:

$$h = \frac{Qt}{\pi r^2} \qquad 7.3$$

allows us to represent the oil thickness (h) in terms of average flow rate (Q) time (t) and spill radius (r).

Substituting h (Eq 7.3) in equation 7.1

$$\pi r \rho g (Qt/\pi r^2)^2 = \frac{\pi \rho r^3 (Qt/\pi r^2)}{t^2} \qquad 7.4$$

and solving for radius (r) we obtain:

$$r = 0.756\,(gQ)^{1/4}\, t^{3/4} \qquad 7.5$$

We conclude therefore, that oil spreading over ice will progress as a function of time and flow rate as described in equation 7.5 until spreading reaches the point where the volume of oil spilled equals the volume of the most probable pockets associated with the surface area vs. volume of pockets data for the particular area.

...

Oil Aging

Whenever crude oil is exposed to the atmosphere the more volatile components tend to evaporate. This process, sometimes referred to as aging, is dependent upon the partial vapour pressures of the individual components of the oil, the ambient air temperature, and the average wind velocity. This aging process, depending on the composition of the original oil, can quite drastically alter the oil's properties. The density, viscosity, and surface tension are three important properties of oil that increase in magnitude as aging processes.

In arctic areas, where ice is continually moving and an annual breakup occurs, alteration of the above mentioned properties may affect the procedures required to minimize oil contamination if and when a major spill occurs. Especially of concern is the density of oil. The density of undeformed sea ice, which depends upon its salinity and porosity, averages about 0.910 gm/cc. The density of underlying sea water is approximately 1.030 gm/cc. It is obvious that if aging is allowed to progress to the point where the oil density becomes equal to or greater that the density of sea ice or sea water the oil will be less buoyant than the ice or water and will tend to migrate under the ice (or water depending upon degree of aging).

...

APPENDIX A

List of Symbols					
A_t	total area	Φ_i	porosity of ice	σ_r	resultant surface tension
d	diameter of oil slick	Φ_s	porosity of snow	θ	contact angle
F_i	force due to inertia	Q	oil flow rate	t	time

List of Symbols					
F_g	force due to gravity	$\bar{Q}$	average oil flow rate	t_m	maximum time
F_s	force due to surface tension	ρ	density	V	volume
F_u	force due to viscosity	r	radius of oil slick	z_0	effective roughness height
h	thickness	r_m	maximum radius of oil slick	f(t)	is a function of t
h_c	critical thickness	σ	surface tension	$f(z_0)$	is a function of z_0
g	acceleration due to gravity				

...

APPENDIX B

Method of Non-Dimensionalizing Data

In order to depict the data in a non-dimensionalized form, the dimensionalized time and length data must be divided by the dimensionalized constants "Q" and "g" in such a way as to create a time (T_{na}) and length (L_{na}) without dimensions. Let us set $Q = L^3T^{-1}$ and $g = LT^{-2}$. To non-dimensionalize time and length Time(nd) = Time(data)/$Q^x g^y$ where

$$Q^x g^y = T \qquad \text{(B1)}$$

Length(nd) = Length(data)//$Q^a g^b$ where

$$Q^a g^b = L \qquad \text{(B2)}$$

Solving (B1) and (B2) we find that: x = 1/5; y = -3/5; a = 2/5; and b = -1/5. Hence: $T_{nd} = T_d/(Q/g^3)^{0.2}$ (B3) and $L_{nd} = L_d/(Q^2/g)^{0.2}$ (B4).

Substituting the values Q = 0.172 cuft/sec and g = 32.2 ft/sec^2 (which are the values that apply to the experimental procedures) into equations B3 and B4 we obtain: $T_{nd} = T_d/0.08758$ and $L_{nd} = L_d/0.24707$."

Method

"The winter tests were conducted on the Bering Sea and Port Clarence Bay during January and February 1972. The test party was based at the Coast Guard Loran Station, Port Clarence, located below the Arctic Circle at 65° 15' N, 166° 55' W. ... The weather and daylight characteristics of Port Clarence are depicted in Figures (1) and (2).

As crude oil will be the largest petroleum product transported in the arctic regions, a North Slope crude was chosen as test oil. ...

The temperature at which the crude was spilled on the ice ideally should have been the anticipated pipeline, tanker, or a typical well

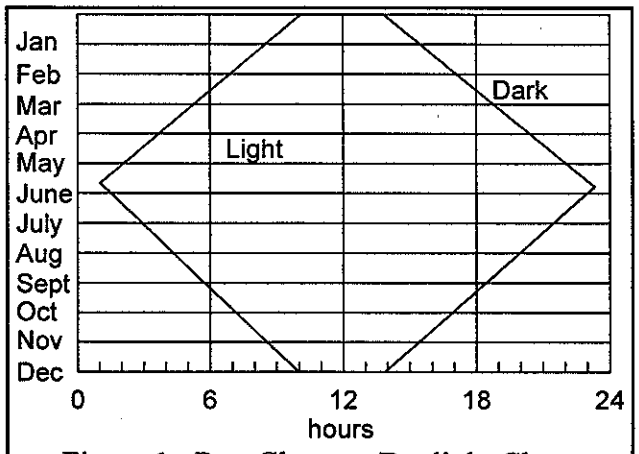

Figure 1: Port Clarence Daylight Chart.

head temperature. As neither the pipeline or tanker transit temperatures were known at the outset of the test operation, the oil was spilled onto the ice at ambient room temperature (+56° F).

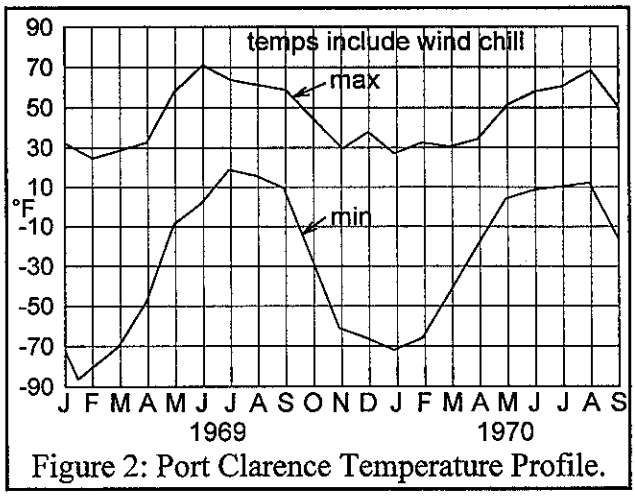

Figure 2: Port Clarence Temperature Profile.

Transporting the test crude from the base of operations to the test site was accomplished using an insulated tank sled (Figure 3)" Figure 3 has not been reproduced for this review. " designed specifically for this experiment. The sled was fabricated of aluminum to conserve weight. The sled body was mounted on two runners to facilitate movement over snow/ice surfaces. The forward half of the sled body consisted of an insulated test oil storage tank while the rear half provided space for operating personnel and a compressed air source for discharging oil from the test tank. The insulated tank consisted of an inner and outer shell, with three inches of insulation between the two shells. The inner shell, approximately 100 gallons in volume, was fitted with an oil discharge and an air inlet line. The rear half of sled was designed as open space for an operator to stand. A regulated compressed air bottle was installed in a portion of this open area. An air line, connecting the compressed air bottle to the tank air inlet line, was fitted with a fixed sonic orifice. Upon regulating the air flow into the oil tank, oil could be discharged at constant flow rate. A twelve foot pinned boom was attached to the oil discharge line allowing easy manipulation of the oil discharge point.

...

APPENDIX C

Routine Analysis of Prudhoe Bay Crude oil (Authors permitted to reprint from *OIL & GAS JOURNAL*)						
General Characteristics		Distillation, Bureau of Mines Routine Method, at atmospheric pressure, 741 mm Hg, first drop , 81 °F.				
		Approximate Summary	%	Sp gr	°API	Viscosity
Gravity, specific	0.893	Light gasoline	4.7	0.710	67.9	
Gravity, °API	27.0	Total gasoline and naphtha	19.0	0.762	54.2	
Pour point	15 °F	Kerosine distillate	4.3	0.818	41.5	
color	brownish black	Gas oil	18.4	0.860	33.1	
Sulfur	0.82 %	Nonviscous lubricating distillate	11.0	0.887-0.911	28.0-23.9	50-100
Nitrogen	0.230%	Medium lubricating distillate	8.1	0.911-0.922	23.9-22.0	100-200
Viscosity*	at 77 °F, 11 sec	Viscous lubricating distillate	1.8	0.922-0.924	22.0-21.6	Above 200
Viscosity*	at 100°F,84 sec	Residuum	36.3	0.990	11.4	

Routine Analysis of Prudhoe Bay Crude oil (Authors permitted to reprint from *OIL & GAS JOURNAL*)						
General Characteristics		Distillation, Bureau of Mines Routine Method, at atmospheric pressure, 741 mm Hg, first drop, 81 °F.				
		Approximate Summary	%	Sp gr	°API	Viscosity
		Distillation loss	1.1			

*Saybolt Universal

...

Spill Site Description

The spreading experiments were conducted on both a snow covered ice surface and a windswept ice surface (Figure 4)." Figure 4 is not reproduced here. "Surface (1), the snow covered ice surface was located approximately 1/4 mile east of the shoreline into Port Clarence Bay. The ice was stationary, averaging two to three feet in thickness and at the outset of the test was covered with 8" of snow. Surface (2), the wind swept ice surface, was the surface of a fresh water inland lake approximately 300 yards across and located 1/5 mile inland from the Bering Sea. The exact areas of the spilled oil were chosen such that the surface was as horizontal as possible. This hopefully would minimize error due to oil flowing down a gradient.

Aluminum stakes 1/2 inch in diameter were driven into the ice surface at fixed intervals to aid in calibrating the rate of spreading. The stakes were spaced every one foot along a radius extended from the point of release. The crude oil was poured on the ice in the center of the stake pattern at a known rate of flow. As the oil was being poured onto the snow/ice surface an 8 mm camera recorded the spreading. The film was later analyzed and spreading rate determined by recording the time interval required for the spreading oil to pass successive stakes.

A total of four spills were made for the purpose of analyzing oil spreading. Three of the spills were made on the snow surface with a total stake spacing of eight feet. The fourth spill was made on the lake ice surface with a total stake spacing of 14 feet. In each case the oil used was North Slope produced crude oil at a temperature of 56 °F.

...

Oil Aging Experimental Procedure

Two separate oil pools were poured on the ice for the purpose of determining the aging rate of crude oil. Each pool was 50 gallons in volume and approximately ten feet in diameter. Of the two spills tested for aging one spill was poured on a smooth ice surface while the other spill was on a snow covered ice surface. Once a day, beginning the day of the spill, two eight ounce samples of the oil were collected from each pool and stored in Teflon gasketed Nalgene sample bottles. Of the two samples the first sample was evaluated on station for viscosity using a Brookfield model LVF rotational viscometer. The remaining eight ounce samples were forwarded to the ESSO Research and Engineering Company, Baytown, Texas, for analysis of (1) density; (2) boiling point distribution, and (3) ratio of water to oil in sample."

Results

"As previously mentioned the spreading experiments were recorded on 8 mm film which was later analyzed for one dimensional time vs. distance. The data extracted from the film represents the time in seconds elapsed as the spilled oil passed stakes spaced at a known distance.

The raw data is tabulated in Table 1.

Table 1: Spreading Data plus the non-dimensionalized data (ND)									
Radius		Time — Sec.							
		Spill (1)		Spill (2)		Spill (3)		Spill (4)	
ft.	ND	Data	ND	Data	ND	Data	ND	Data	ND
1.0	4.1	0.7	8.0	0.7	8.0	0.9	10.3	0.7	8.0
2.0	8.1	2.3	26.3	4.2	50.	4.2	50.0	4.3	49.1
2.5	10.1	–	–	–	–	5.8	66.2	–	–
3.0	12.1	6.5	74.2	8.6	98.2	–	–	11.3	129.0
4.0	16.2	10.6	121.0	14.0	159.9	–	–	21.4	244.4
4.5	18.2	–	–	–	–	–	–	29.9	341.4
5.0	20.2	15.6	178.1	19.5	222.7	–	–	–	–
6.0	24.3	–	–	28.1	380.9	–	–	–	–

The experimental data is non dimensionalised as per Appendix (B) for comparison with the previously developed theory.

The non-dimensionalized data points are plotted in Figure (6). The data, as can be seen from Figure (6), plots in a straight line on log-log paper with very little scattering. The observation that oil spreading on ice is a single straight line relationship strengthens our assumption that only gravity and inertia forces are significant contributors to spreading and retarding forces. Had surface tension or viscous forces contributed significantly to spreading, the data plot would be expected to be composed of two straight lines of different slopes. Section (1), the gravity-inertia spreading, would appear as the data plot illustrated in Figure (6); however the plot would continue on a constant slope until where surface tension-viscosity forces would control spreading and the slope of the spreading curve would be reduced. Although the argument that only gravity and inertia forces are involved in the spreading of oil over ice is supported by the field data, the oil spread predicted by theory is not completely validated by the experimental results. As can be seen from Figure (6), the slope of the experimental data is less than that predicted by the simplified theory. The equation of the field data Figure (6) can be duplicated by the following equation:

$$r = 1.3\,(Q^2/g)^{0.1}\,t^{1/2}$$

The apparent discrepancy between the theory obtained spreading relationship and the data obtained relationship while interesting is

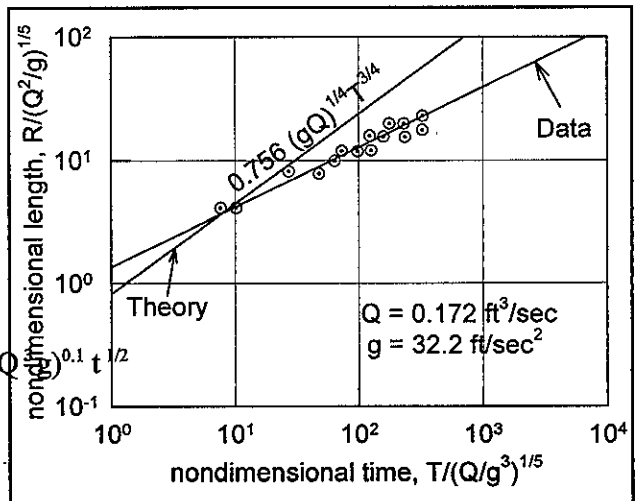

Figure 6: Spreading Rate — Winter Ice.

not considered significant. To some extent the discrepancy between theory and experiment is within the range of experimental error. Of greater significance is the fact that the experimental results validate the theoretical assumption that only gravity and inertia forces must be considered when predicting spread rate.

From a practical standpoint, ability to predict the ultimate size of a spill is of greatest importance. It is very probable that the response time for emplacement of spill cleanup equipment at an Arctic oil spill will be such that spreading will terminate before any significant action to control the movement of the oil can be initiated.

...

Temperature Effects

Examining the change in density of the oil and comparing it to data obtained by Glaeser and Vance, 1971, it becomes apparent that the aging rate of crude oil in the winter months is considerably less than the summer aging rate. This decrease in rate was expected. However, it is quite clear that oil *does* age in the winter months and that North Slope crudes will age to the density of sea ice (0.9010 gm/ml) and possible that of sea water (1.030 gm/ml) if left in place (note Figure 7).

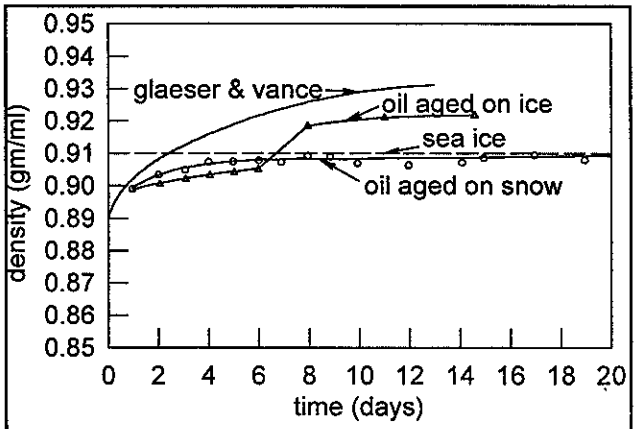

Figure 7: Oil Density vs. Time.

Further indications of the extent of winter aging are illustrated in Figures 7, 8, 9, 10, and 11. Although we see again that aging rate is decreased when ambient air temperature is decreased, the rate is significant and is not to be discounted.

Wind Effects

As illustrated in Figures 7 through 11, a substantial increase in density of the oil on ice is apparent after the sixth day. The density of the oil aged on snow shows no sudden increase. The aging rate is directly proportional to the rate of evaporation of the volatiles from the area adjacent to the oil-air interface. If a system of removing these vapours were not present, the area immediately adjacent to the interface would become saturated and an equilibrium condition would exist. Wind velocity, the chief mechanism for removal of these vapours, is the primary reason for the increase in aging rate after the sixth day. A severe storm, accompanied by high

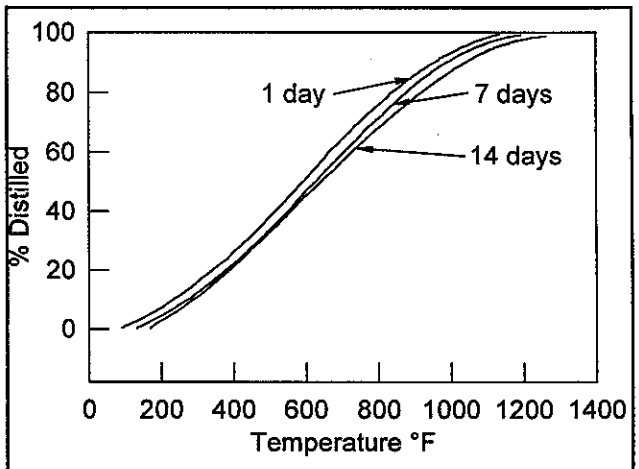

Figure 8: Distillation Curve — Oil With Heavy Snow.

winds (30-50 knots) passed through the spill area during the seventh day of the aging test. The increased aging rate during this time is believed to be a direct result of this increase in wind velocity. The "oil on snow" aging rate was unaffected primarily because the oil was protected by a eight to ten inch snow covering. The oil on ice, however, was clear of any snow covering at the storm's initiation.

The increased aging rate of the oil aged on ice is also apparent in Figure (8) and Figure (9). The eight (8) days distillation curve is much further advanced to the right on "ice aging" indicating a greater percentage of higher boiling point components comprising the sample aged on ice.

The oil that was protected from the wind by an eight to ten inch snow covering aged much slower than the oil exposed to the open wind despite a 20 °F to 30 °F increase in temperature in the snow protected oil. The explanation is that the snow effectively "capped" the oil, preventing volatile loss. We can conclude, therefore, that oil ages at a significant rate in the winter arctic until a now cover is effected. It is apparent that oil continues to age with a heavy snow covering, but it is not clear if this rate is significant.

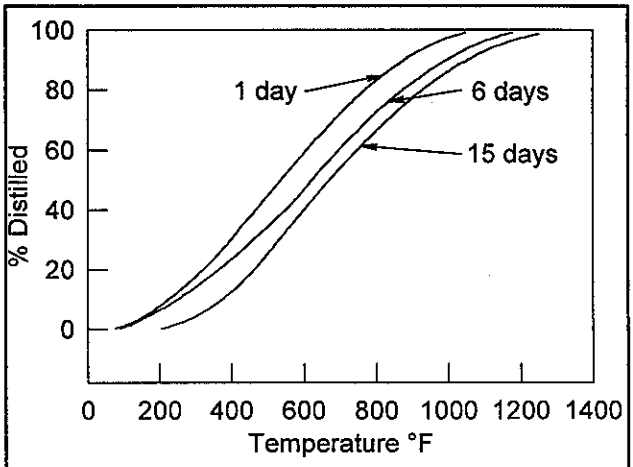

Figure 9: Distillation Curve — Oil with Blowing Snow.

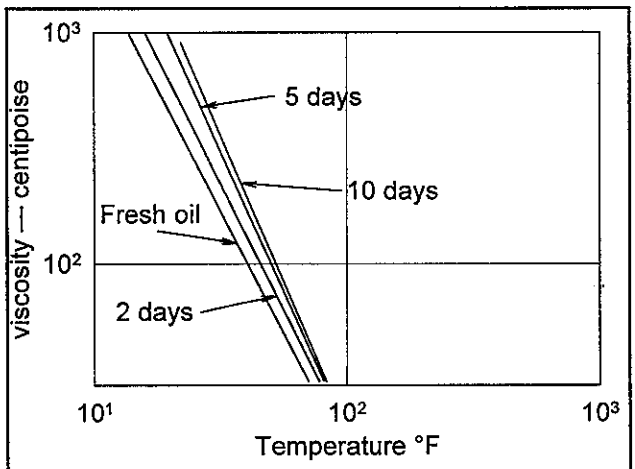

Figure 10: Oil Aged on Snow — Absolute Viscosity vs. Temperature.

Oil and Ice Interaction

Prior to the field tests, the anticipated interaction of warm oil (60 °F) poured on snow would be a movement of the oil by gravity and capillary forces down through the pore channels of the snow and ice. Penetration, however, of oil below the surface did not occur to any substantial degree. The temperature difference between the oil (56 °F) and the snow surface (+5 °F to -15 °F) caused the immediate melting of snow. The melted snow (water) moved by gravity and capillary action, down approximately 2 mm through the snow column where it refroze, blocking the pore channels and preventing the downward migration of oil. A similar effect was

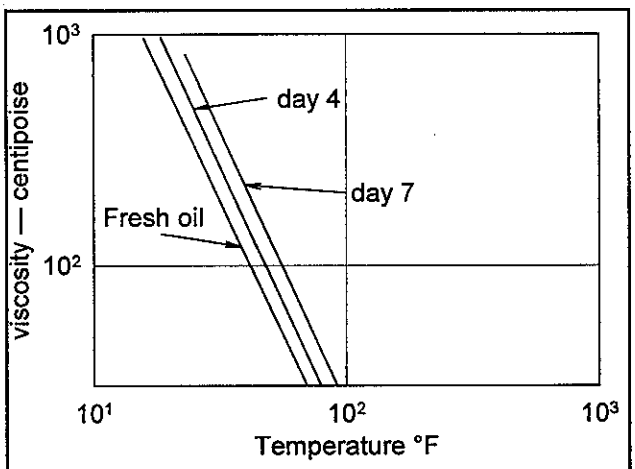

Figure 11: Oil on Ice — Absolute Viscosity vs. Temperature.

noted on ice when oil melted the surface layer of the ice and floated on this thin (1 mm) layer of water. Additionally, no clear downward migration of oil through the snow or ice columns was observed from oil spills up to 30 days old.

The layer of oil on the snow was quickly covered by wind blown snow. The snow cover tended to migrate downward into the oil forming an oil/snow crystalline mulch, Figure (12)." Figure 12 is not reproduced here. "This mulch was approximately 80% water by volume. The mulch had a firm cohesive consistency that could easily be recovered by mechanical means such as by shovelling or scraping. The mulch was dry in appearance with its temperature below the pour point (+15 °F) of the oil. However, as the temperature increased above the pour point, the oil became more fluid and began to separate out of the mulch.

The intensity of a snow fall, or blowing snow, effected the percentage of snow absorbed by the oil. Heavy snow falls resulted in the rapid accumulation of compacted snow on the surface of the oil. It is theorized that this compaction of the snow reduced the volume of the snow infiltrating into the oil."

BOSS Critique

The authors do not discuss the magnitude of the error involved in measuring the radius of the oil spill using a 8 mm camera to record the movement of spilled oil over a grid as discussed by the authors. The stakes on the grid were set at one foot intervals and therefore the error would be quite large at the initial phase of the spill and smaller towards the end of the spill depending upon the rate at which the oil moved over the grid and also at what angle the camera was to the oil spill. It is important to notice that the equations used to model the change of radius of the spill over time are largely dependent upon the volume of the oil spill and much less dependent upon other parameters of the oil.

Review of a manuscript by, Martin, S., P. Kauffman and P.E. Welander, "A Laboratory Study of the Dispersion of Crude Oil Within Sea Ice Grown in a Wave Field", in *Proceedings of the Twenty-Seventh Alaska Science Conference*, American Association For the Advancement of Science, Fairbanks, Alaska, 1977.

Technical Summary

"In a laboratory experiment, we studied the formation and growth of sea ice in a wave field, and the interaction with the sea ice of oil released under it. The kinds of ice which grew in the wave field were grease and pancake ice. Our experiments show that the grease ice, which generally grew to a thickness of 100 mm, had a porosity of about 60% and a surface temperature which was only of the order of 0.1 degrees below the sea water temperature. The presence of grease ice did not inhibit oil released beneath it, rather the oil rose through the ice and spread out on the surface. The pancake ice formed when the grease ice thickness reached about 100 mm; our experiments showed that the length scale of the pancakes was about one-fifth of the driving wavelength. The rims around the pancakes were built up from grease ice which the oscillating wave field pumped onto the ice surface where it would freeze. Petroleum spilled under the pancakes rose to the surface in the cracks around the pancakes, where the oscillating motion pumped the oil both laterally through the cracks and onto the ice surface. Once on the ice surface, the pancake rims contained the oil so that it did not re-enter the water."

Objective

To understand how grease ice and pancake ice form from salt water and then investigate the interaction of these ice types with spilled oil.

Theory

In the introduction of the report the authors use the ice glossary of the World Meteorological Organization and the Scott Polar Research Institute to define three types of ice.

"1. Frazil ice: "fine spicules or plates of ice in suspension in water".

2. Grease ice: "A later stage of freezing than frazil ice, when the spicules and plates of ice have coagulated to form a thick soupy layer on the surface of the water. Grease ice reflects little light, giving the sea a matt appearance".

3. Pancake ice: "Pieces of new ice usually approximately circular, about 30 cm to 3 m across, and with raised rims due to the pieces striking against each other. Formed from the freezing together of grease ice, slush or shuga, or the breaking up of ice rind or nilas".

Of these three kinds of ice, grease and frazil ice occur in all ice covered areas; ...

When grease ice solidifies, it forms sea ice with a random crystal structure which is called 'frazil' ice, as opposed to 'columnar' ice, which is made up of vertically-oriented parallel ice platelets. ... the oil absorption properties of columnar ice are well understood; the same properties for grease ice in either its liquid or solid form are not." The authors further state that pancake ice is formed from grease ice and that the pancake ice then goes on to form floes.

Method

"The experiment took place in a Plexiglas wave tank, which was surrounded by 52 mm thick sheets of polyurethane, and placed in a cold room. Figure 2, a schematic drawing of the tank, shows that the tank interior measured 2.2 m in length, 0.93 m in width, and about 0.6 in depth. The tank was filled with a 34‰ NaCl solution to a depth of 0.41 m. At one end of the tank, a wedge-shaped paddle drive by a Scotch Yoke coupled to a stepping motor generated waves. In order to keep the paddle free of ice, we placed a heating tape in the water behind the paddle. In running the experiment, we initially set the cold room temperature slightly below -2 °C until the water had cooled down to its freezing point of approximately -2.1 °C. We then covered the tank with a plywood lid and set the temperature to -20 °C. When the room reached this temperature we removed the lid and started the paddle. Typically, the paddle had a peak-to-peak amplitude of 50 mm, with a period which we set between 0.60 s and 1.0 s, which yielded wavelengths of 0.6 m to 1.3 m.

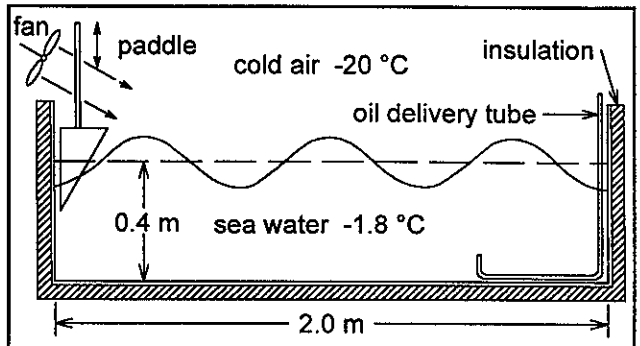

Figure 2. Schematic diagram of the apparatus.

We did a series of six experiments with the tank, namely a freshwater calibration experiment and five saltwater experiments. In one of the saltwater experiments we released diesel fuel into the tank; in another, we released Prudhoe Bay crude oil. Each experiment took about two weeks to set up, run, and clean. The oil spill experiments took an additional week for clean-up.

We recorded the physical appearance of the ice photographically, and the temperature structure with thermistors. In the photography, we illuminated the tank with three 650 watt Sun Gun movie lamps with a color temperature of 3400 °K, which matches that of Kodachrome Type A color movie and still film. Because these lights radiated a great deal of heat which could liquify the ice surface, we did most of our photography in short, 10 minute periods, followed by 40-50 minute periods of darkness. We also set up fans to blow over the water-ice surface, which generated capillary waves and advected away the heat.

We used the following cameras: a Nikon equipped with a Macro-Lens and loaded with Pan-X film; an additional Nikon with a wide angle lens and loaded with either Tri-X or Kodachrome Type A film; a Leica equipped with a Macro-Lens and generally loaded with Pan-X film. To prevent cold-soaking the cameras and condensation on the lenses, we kept the cameras in an adjacent cold room at a temperature of 0 °C and only brought them into the experimental room for short periods of time. We photographed the ice both from above the tank and through a side window measuring 0.3 m by 0.6 m. When we were not filming or observing, we covered this window with a polyurethane plug.

To measure the ice temperatures we used thermistors with an accuracy ±0.01 °C. For grease ice, we built a six-thermistor array to record the vertical temperature profile; for pancake ice, we used a single probe to explore the temperature variations around the cakes.

In most of our experiments, we began with a standing wave with a period of 0.63 s, which yielded a wavelength of 0.68 m, or a mode 6 oscillation in our tank. At the beginning of the experiment, we tuned this wave so that it was just at the breaking point; this generally yielded a peak-to-peak amplitude of about 200 mm. The first ice to form on this oscillating surface was small crystals of frazil ice; these quickly conglomerated into grease ice. After an additional 4-6 hours,

pancakes grew from the grease ice."

Results

"a. Grease Ice

We observed that the individual frazil ice crystals, which were plate-shaped with rough edges, had characteristic diameters of 1-3 mm and thicknesses of the order of 0.1 mm. When these crystals initially formed in the tank, they were transported away from the paddle, even if the fans were blowing toward the paddle, by the phenomenon of wave herding. From Figures 3a and b, which show two views of the tank at an early stages of the experiment, we see that because of wave herding, the surface is partially open and partially covered with grease ice." None of the photographs are reproduced in this review. "The figure also shows that grease ice damps out the small-scale waves.

Qualitatively, ..., the wave herding shown in Figure 3 occurs for the following reasons. Because the ice alters the free surface boundary condition, by either imposing a no-slip condition or forming a viscous slick, any ice formation tends to damp out the wave motion. For short capillary waves, the grease ice forms a no-slip surface boundary condition which rapidly damps out the waves. For longer gravity waves, the grease ice forms a viscous surface layer which imposes a stress condition and also causes wave attenuation. Therefore, for all scales of waves, the ice causes viscous decay which extracts energy from the waves. As the wave energy decreases, its momentum must also decrease. Because momentum must be conserved, momentum taken from the waves goes into mean drift current which sweeps the ice crystals away from the paddle. For standing waves, which consist of 180° out-of-phase progressive waves propagating both toward and away from the paddle, the argument still applies because when damping occurs, the wave propagating away has more energy than the wave propagating toward the paddle.

Grease ice has a number of interesting properties. First, it remained a fluid porous mass of frazil ice crystals up to a thickness of about 120 mm. Figures 4a and b show two sidewall photographs of the grease ice which were taken at times about one-half a wave period apart. Comparison of the two photographs shows that the grease ice is compressed at the wave crest, and stretched at the trough. This observation supports the idea that the layer of grease ice behaves as a buoyant viscous fluid floating on the sea water.

Second, we found from several measurements that the ratio of the volume of ice to the total volume of sea water and ice ranged from 35-40%, so that the grease ice shown in Figure 4 is about 60% sea water. We obtained this measurement by scooping up a sample of grease ice in a liter beaker, then quickly pouring off the sea water. We next allowed the remaining ice to melt, then measured the volume of both the sea water and the melted ice to obtain the porosity.

Third, the high grease ice porosity affected the heat transfer within the ice. Table 1 shows the distribution of temperature versus depth for grease ice of thickness 60 mm. To obtain this measurement, we placed our thermistor array within the fluid, stopped the paddle, then recorded the temperatures. The table shows that the temperature within the grease ice equals the sea water temperature except at the very surface, where the temperature is depressed by only 0.1° below the deep temperature. The reason for this very weak temperature gradient within the ice is that the heat

transfer very likely takes place by a combination of convection and mechanical stirring. The waves cause the stirring; the convection occurs because for a cooled salt water-ice mixture to remain in equilibrium, the solution salinity must increase by about 20‰ per degree of temperature depression. Therefore, cooling the grease ice surface creates a salinity increase and thereby a density increase so that heavy water forms at the grease ice surface. Because the grease ice is porous, this cold, heavy water sinks and is replaced by sea water, so that the surface remains warm. The waves, which both stretch and compress the ice field and wash water through the ice, add to the efficiency of the convection.

Because of this convection, on at least one occasion the grease ice thickness increased nearly linearly with time, rather than with time to the one-half power as occurs for solid ice (Carslaw and Jaeger (1959)). Figure 5 is a plot of grease ice thickness versus time, which we made by stopping the paddle at different times during the experiment, then letting the grease ice spread out to an average thickness which we measured. The graph suggests that the thickness increased nearly linearly up to the point at which pancake formed, at which time the total thickness increased more slowly. The rapid linear growth is probably caused by the convective heat transfer.

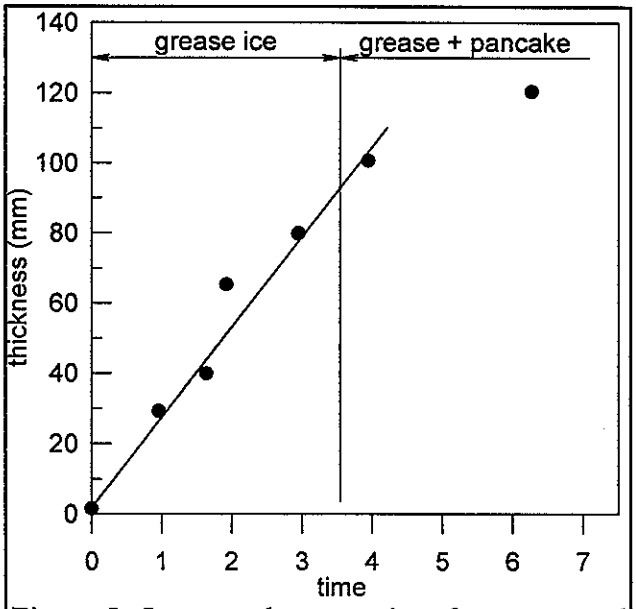

Figure 5. Ice growth versus time for grease and pancake ice.

Table 1. Temperature versus depth in 60 mm thick grease ice.

Height (mm)	Temperature (°C)	comments
+10	-18.8	(in air)
0	-2.33	(at grease ice surface, probe submerged)
-10	-2.23	
-20	-2.22	
-40	-2.22	
-90	-2.23	(in salt water below grease ice)

b. Pancake Ice

When the grease ice thickness reached 70-100 mm, the crystals at the surface began to join together into what we called 'proto'-pancakes. In Figure 6a, these proto-pancakes consist of clumps of crystals, measuring 50-100 mm in the cross tank direction, 50 mm wide, and 3-5 mm thick, which although they had a much lower porosity than the surrounding and underlying grease ice, were still so soft that we could not pick them up. The proto-pans apparently form when the grease ice thickness reduces the heat flux from the deep water and the grease ice buoyancy slows the washing

of the sea water through the ice surface, so that the surface cools and solidifies.

These proto-pans quickly evolve into pancake ice. Figures 6b and c are photographs of the ice field made one hour after 6a, where 6b and c are half a wave period out-of-phase. The two photographs show both the many small pans which make up the surface, and the presence of a large crack to the right of the thermometer which the waves periodically open and close. The photographs also shows that, particularly to the right of the large crack, grease ice has been pumped onto the ice surface by the convergent-divergent motion of the wave field. This pumping of grease ice onto the surface leads to the formation of the raised rims on the pancakes.

For the waves, the growth of pancakes from grease ice changes the surface boundary condition for waves with lengths of the order of the pancakes from that of a viscous slick to a solid, no-slip upper boundary condition. This greatly increases the wave damping for these short waves. For longer waves, the surface boundary condition remains mixed, with the gaps between cakes allowing some relative motion. The ice-induced decrease in wave amplitude permits the smaller pancakes to join together without being broken apart by the wave field, so that as the experiment progresses, small pans join up into larger cakes.

Figure 7a-7d is a photographic sequence showing the growth of pancakes from grease ice; the waves have a period of 0.81 s or a wavelength of 1 m. Near the paddle, the heat from the heating tape prevented the growth of pancakes; however, the photographs show that away from either end of the tank, the pancakes have an average width of 0.2 m or about one-fifth of the driving wavelength. Further, over the two hours covered by the sequence, the figure also shows that the rims around the cakes grow from virtually nothing to a height of 20-40 mm. As with the proto-pans, the rims in Figure 7 appear to grow from grease ice which is pumped up onto the pancake surface. In Figure 8, the two close-up photographs, which were taken immediately preceding Figure 7b and half a wave period apart, show both the opening and closing of the gaps between the pancakes and that the rims appear to be formed from grease ice which has flowed down the edges of the rims toward the pancake center and solidified. Our movie films further show, when the rims come together, that grease ice is pumped up between the rims to a height above the pancake surface. Because the pancakes oscillate together many times over their growth; for example the pancakes in the Figure 7 sequence oscillate together 9,000 times, the rims probably grow from the slow incremental pumping of grease ice up over the rims.

In the experiment, the pancakes floated in a much thicker layer of grease ice, which as Figure 5 shows, continued to increase in thickness even after the formation of pancakes. Beside supplying material for the rims, the grease ice affected the pancakes in three other ways; namely, it helped yield the dish-shaped bottom profile of the pancakes, determined the frazil crystal structure of the pancakes, and caused the ice to float such that the pancake center was below the water line. We next discuss these three effects in detail.

First, the combination of the oscillating grease ice and the cracks around the pancakes caused the pancakes to grow with a dish-shaped bottom profile. This occurred because although the pancakes grew by conduction, within the grease ice, the heat transfer was still convectively driven by heat loss to the air through the cracks around the pancakes. Within the cracks, we observed with the thermistors that the grease ice surface temperature was only 0.1 - 0.4 degrees colder than the deep sea water temperature. At the same time, the surface temperature at the center

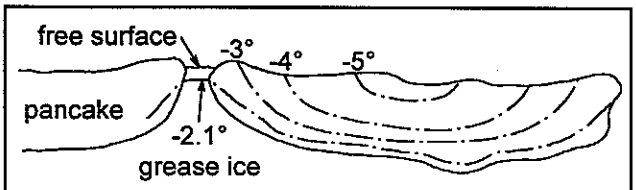

Figure 9. Schematic diagram of the isotherms within a pancake.

of the pancake was 3-5 degrees colder. Because the sides of the pancakes up to and above the water line were washed in warm grease ice, the temperature isotherms within the pancakes were curved as shown in Figure 9. This isotherm curvature means that the pancakes grow in thickness fastest at the center, which yields a dish-shaped cross-section. As an example, Figure 10 shows the cross-section of a typical piece of pancake ice. To take this photograph, we cut a piece of pancake ice in half, rubbed the surface first with alcohol, then with an oil-soluble dye to bring out the crystal structure. The photograph shows both the dish-shaped profile and that most of the small crystals which make up the pancake lie parallel to the surface.

Second, as Figure 10 suggests, the growth of the pancakes from a much thicker layer of grease ice determines the pancake crystal structure. To illustrate, Figure 11 and Figures 12a and b show both a full view and close-up photographs of a pancake cross-section taken in the following way. After running an experiment during which the pancakes grew to a thickness of 10-20 mm, we stopped the paddle, elevated the room temperature to -14 °C, then left the experiment overnight. On the following day, we cut a block of ice out of the tank which stretched across two pancakes from rim to rim, so that the center of the ice shown in Figure 11 is the boundary between two pancakes. We cut this block into a section about 30 cm thick, rubbed the surface with alcohol and dye, then photographed the ice with a flash from behind the ice. Because this ice continued to grow after we turned off the paddle, the shape of the ice in Figures 11 and 12 is not that of a pancake; however, the small arrow on the photograph in Figure 11 marks the bottom of a cavity between the two cakes, which is the water surface level at the time we turned off the paddle. Examination of the detailed photographs in Figures 12a and b show that the pancakes are made up of many small frazil ice crystals. In Figure 12, the crystals have no particular orientation, although Figure 10 suggests that for small pancakes the platelets are initially oriented horizontally. Our oil experiments suggest that these small crystal platelets, which are either randomly or horizontally-oriented, are less likely to capture oil flowing along the ice bottom than the parallel vertical crystals of columnar sea ice shown in Figure 1. The combination of the dish-shaped bottom profiles of the pancakes and their crystal structure means that oil spilled under the pancakes is likely to come to the grease ice surface in the cracks between the cakes.

Third, the low buoyancy of the grease ice combined with the raised pancake rim means that the pancakes float so low in the water that the ice surface at the pancake center is slightly below the water line. There are two reasons for this: first, the grease ice in which the pancakes float has a density less than sea water; second, the build-up of the rims on the pancakes adds weight above the water line. To look at the grease ice effect, we assume that the grease ice consists of 40% freshwater ice with a density of 920 kg m^{-3} and 60% sea water with a density of 1030 kg m^{-3}, so that the grease ice density is 990 kg m^{-3}. Therefore, if the pancakes, which have a salinity of about 20‰ or ... a density of about 930 kg m^{-3}, float in grease ice, and if for the moment we neglect the weight of the rims, then pancakes with an average thickness of 20 mm will have a freeboard of 1.2 mm as opposed to 2 mm if they were floating in pure sea water. The grease ice then, causes a 40% reduction in the pancake freeboard.

The additional weight of the rims is even more important. Figure 13 is a schematic diagram

of a pancake based on the cakes shown in Figure 5. If we assume that the pancakes are two-dimensional bodies measuring 200 mm in width by 20 mm in depth and with rims measuring 10 x 20 mm^2, then the effect of this additional mass above the water line is that the pancake now floats such that the mean water level is 0.7 mm above the ice surface at the pancake center. As an example of this low freeboard, examination of the waterline marked in Figure 11 shows that the water level around the cake is higher than the ice surface height at the pancake center.

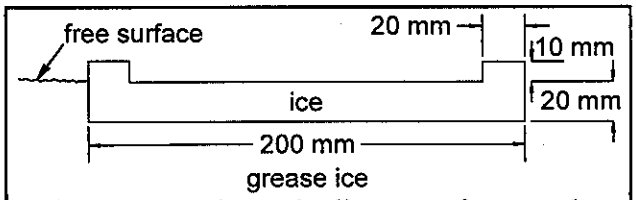

Figure 13. Schematic diagram of a pancake cross-section.

Because of the lowered freeboard and the raised rims, we observed in all of our pancake experiments that the pancake surface was covered with a thin layer of highly-saline brine, which was probably formed from the water pumped over the rims and onto the ice. Once on the surface, because of the lowered freeboard, the brine remained there. This lowered freeboard may also occur for much larger pancakes. W.J. Campbell (private communication, 1976) observed from low-level overflights of the Bering Sea during February and March, 1974 that pancake-like floes with diameters of the order of 2 m also had wetted surfaces. As we show later, this lowered freeboard makes the pancakes more vulnerable to oil spilled under the ice being pumped onto the surface.

3. The Oil Spills

We did two separate oil spills during our experiments. The first was a #2 diesel oil spill of 250 ml; the second, a Prudhoe Bay crude oil spill of 500 ml. The diesel oil spill was done just after the pancakes started to form; the Prudhoe spill was later in the growth of the pancakes.

a. The Diesel Spill

At the time of the spill, the grease ice thickness was about 100 mm, with the small ice pans of thickness 5-10 mm at the growth stage of those shown in Figure 6b. We discharged the oil through a small J-shaped tube which extended under the ice, so that the oil flowed out vertically in a turbulent jet at a depth of about 200 mm below the bottom of the grease ice. The combination of the high porosity grease ice and the buoyancy of the diesel oil meant that the grease ice did not absorb the oil, rather the oil quickly appeared on the grease ice surface in the cracks surrounding the pancakes. The oscillatory motion of the pancakes then pumped the oil laterally from its original discharge point. Figure 14, a photograph of the spill taken about 30 minutes after the discharge, shows that the oil affected an area measuring about 0.4 x 0.4 m^2, so that the average thickness of the slick is about 1 mm. An unmeasured amount of oil was pumped up onto the ice, where the combination of the raised rims and the low freeboard prevented its return to the cracks.

b. The Prudhoe Bay Crude Oil Spill

For this experiment, we used 500 ml of Prudhoe Bay crude oil, which the Atlantic Richfield Company (ARCO) donated to our laboratory. ... The oil has a pour point of -9.5 °C, and a specific gravity of 0.893. We measured the following viscosities at different temperatures for this oil, at 0° C, 19 centipoise (cp); at -2 °C, 175 cp, and at -8 °C, 10^3 cp. For comparison, fresh water at 4 °C has a viscosity of 1.6 cp. For the experiment, the crude oil although very viscous remained fluid.

During the discharge, the total ice thickness was 120-130 mm, and the pancakes were 10-30 mm thick. Preceding the discharge by about one hour, we increased the period of the paddle from 0.63 s to 0.94 s, or to a wavelength of 1.3 m. This had the desired effect of increasing the amplitude

of the convergent-divergent motion between the cakes from virtually nothing to 10-20 mm, but also allowed the smaller pancakes to join together into bigger cakes.

We discharged the oil through a fixed tube of 10 mm inner diameter shown schematically in Figure 2 which ran from one corner of the tank down along the bottom to terminate in a vertical tube pointing up under the ice. The top of this vertical tube was about 300 mm below the water surface. This tube was kept filled with air until just before the discharge, when we simultaneously released the air and pour the oil into a funnel attached to the tube. At the time of pouring the oil, its temperature was +7.5 °C; however, since it took about four minutes for the oil to flow completely through the tube into the tank, we suspect that it entered the water at a temperature very close to -2 °C. Visually, the oil flowed up out of the discharge tube in viscous slugs resembling poured molasses, rather than in a turbulent jet such as occurred in the diesel spill. After the oil left the discharge tube, we observed the oil to disappear up into the grease ice, which showed no signs of either inhibiting or capturing the released oil.

Five minutes after we began to pour the oil into the funnel, the oil appeared on the grease ice surface in a crack between two pancakes. Figure 15a shows the ice appearance immediately preceding the spill, and 15b shows the first appearance of the oil at the surface. Figures 15b-15e are taken at intervals of about 15 s, so that the entire sequence lasts no longer than two minutes. Within this time, the oil spread nearly all the way across the tank within the crack. The figure also shows that some of the oil was pumped onto the ice surface. Because the oil floated on top of the grease ice within the cracks and the low freeboard of the pancake ice, the oil was easily pumped onto the ice surface.

Figures 16a-16c, which are photographs of the ice surface 30 minutes after the discharge, show that a large amount of oil has been pumped up onto the ice by the combination of the oscillating pancake motion and the confinement of the spilled oil by the tank walls. Figure 16a and b, which were taken about one-half wave period apart, show when the pancakes come together, the volume decrease in the space between the cakes pumps the oil either laterally or onto the ice. By scraping up the oil on the ice surface after the experiment, we determined that 290 ml of the 500 ml of oil spilled had been pumped onto the ice.

Figure 17 is a sketch of the location of the oil both under and on the ice which we made for our observations in cutting up the oiled ice in the cold room at -14 °C on the day following the spill. Most of the oil appeared either to go to the ice surface or remain in the crack; however, there was a very light skim of oil on parts of the underside of the pancake. Because the flow of the oil within the crack was limited by the tank walls, the amount of oil on top of the ice is probably exaggerated in our experiment. As Figure 15 shows, however, the pancake oscillations drive the spilled oil both laterally and onto the ice surface.

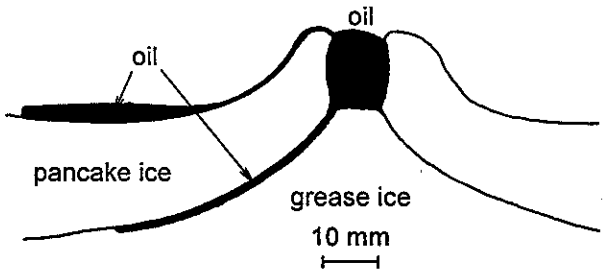

Figure 17. Schematic drawing of the pancake cross-section showing the location of the spilled oil.

4. Other Properties of Pancake Ice: The Formation of Brine Drainage Channels

In spite of the frazil crystal structure of pancake ice, we still observed the formation of the brine drainage channels similar to those which occur in columnar ice. The importance of these channels is that they provide an additional pathway of bringing oil from under the ice to the ice surface.

To study the formation of these channels, which are most prominent when cold sea ice is warmed up, at the end of the first day following the Prudhoe spill described above, we raised the room temperature from -14 °C to -6 °C, then let the room sit overnight. In the morning of the following day, or two days after the spill, we observed brine drainage from the ice at several locations; and at two locations away from the oil, we observed the formation of small ice stalactites with lengths of about 50 mm. We then cut out and removed from the tank one of the pancakes from which a stalactite grew. Upon removal, the stalactite disintegrated and a volume of water estimated at 250 ml poured out of the ice in a period of about 15 s. To examine the brine drainage system inside the ice, we marked the drainage channel which from the ice bottom was a 3 mm diameter hole, with a small piece of wire, then set the pancake into the cold room at a temperature of -20 °C. After the ice had cooled down, we cut the block into a 30 mm thick section with one cut through the line of the drainage tube.

Figure 18a and b shows two views of the pancake cross-section, which extends from rim to rim of the pancake. The first photograph, Figure 18a, is taken by transmitted light without any dye spread on the ice. The photograph clearly shows a cone-shaped dark region, funnelling into the lower protuberance on the pancake bottom around which the stalactite grew. The lower photograph, 18b, shows the same piece of the ice with dye rubbed on the surface to bring out the topography. This picture shows the large central drainage channel and pancake crystal structure. Comparison of this photograph to Figure 12 where the ice was not warmed up shows that warming the ice modified the top 20 mm of the ice, and presumably caused both the downward movement of the surface brine and the formation of the brine channels.

The significance of this observation is that brine drainage channels form as easily in frazil ice as in columnar ice. If an oil spill took place in the spring, these channels could serve as additional conduits of oil to the ice surface."

BOSS Critique

The manuscript is a descriptive presentation of the formation of grease and pancake ice. The authors then use a qualitative approach in evaluating the interaction of spilled oil with the grease and pancake ice. The is a short discussion of the tank size influencing (over estimating) the amount of the spilled oil ending up on top of the pancake ice. Outside of the temperature measurements, no errors are discussed and no mention is made about the whether these results can be scaled up to a real oil spill situation.

Review of a manuscript by, Chen, E.C., *Arctic Winter Oil Spill Test,* Technical Bulletin No. 68, Environment Canada, Ottawa, Ontario, 20 p, 1972.

Technical Summary

"As a result of the present test, the behaviour of Prudhoe Bay crude oil in an Arctic winter environment may be summarised as follows:

(1) The oil does not spread on a snow or ice surface except when warm and under influence of the forces caused by dumping.
(2) The oil, when spilled on a snow surface, penetrates only a small distance.
(3) When spilled on the surface of lake ice, the oil shows no visible signs of penetration.
(4) The rate of aging for spilled oil is extremely slow.
(5) The oil burns easily on snow or ice creating heavy black smoke and leaving a tar-like substance."

Objective

The author states that his objective was "to investigate the physical properties of crude oil spilled in an Arctic winter environment."

Theory

No theory was discussed by the author.

Method

"The general areas of investigation were similar to those of the summer test, namely:

(1) the spreading of crude oil on snow and ice,
(2) the change of the crude oil as a result of aging,
(3) absorption of oil by the ice and,
(4) the effectiveness of burning and use of absorbents as a method of oil removal.

The oil used for this winter test was Prudhoe Bay crude. An analysis of the crude oil is given in Table 1.

Table 1. Physical and Chemical Properties of Prudhoe Bay Crude Oil

Physical and Chemical Properties		Approximate Composition (Percent by Volume)	
Specific Gravity	0.893	Light gasoline	4.7
Sulphur	0.82%	Total gasoline and naphtha	19.0
Viscosity, Saybolt Universal		Kerosene distillate	4.3
at 77 °F	111		
at 100 °F	84	Gas oil	18.4
API Gravity	27.0	Nonviscous lubricating distillate	11.0
Pour Point	15 °F	Medium lubricating distillate	8.1

Table 1. Physical and Chemical Properties of Prudhoe Bay Crude Oil			
Physical and Chemical Properties		Approximate Composition (Percent by Volume)	
Nitrogen	0.188%	Viscous lubricating distillate	1.8
Color	brownish black	Residuum	36.3
		Distillation loss	1.1

A specially designed apparatus was used in the present test to spill the oil. The apparatus was essentially a welded aluminum sled with dimensions 8' x 3'5" x 2'10". ... The sled contained an oil storage tanker and a bottle of compressed air. Both were heavily insulated to keep their contents at 70 °F - 75 °F during the mission. The oil tanker had a capacity of 100 gallons; the air in the bottle was maintained at a constant pressure with a mass-flow rate independent of downstream conditions. When the air was allowed to flow into the tanker, the oil was forced out through a hose and on to the snow or ice surface at a rate determined by the pressure of the air. ...

For the spreading experiment, the sled was towed at a known speed over the snow- or ice-covered ground. When it reached the area marked by stakes to provide a length scale, the dump mechanism was activated pouring oil on the snow or ice surface. The motion of the spilled oil was followed by a movie camera to obtain a one-dimensional spreading rate.

The oil patches created by the spreading experiment were used for the other tests. The aging rate of spilled oil was determined by collecting oil samples from the pitch at regular intervals and analyzing the changes in physical properties. The test for absorption of oil by ice was carried out by taking ice cores from oil-contaminated ice and determining the oil content at different depths. The oil patches were also used to test the efficiency of burning and the use of various oil absorbents.

The designated test site was the sea bay area at Port Clarence and the tests were planned originally on the sea ice. However, during the test period, and in fact, during the winter time, snow cover was complete so that the tests had to be conducted on snow rather than ice surfaces. The spreading experiment was carried out on January 16. The temperature was -2 °F and the wind speed 12 knots. Six to nine inches of snow were on top of the sea ice while porosity of the snow was 55%. The spill was made at a dumping rate of 0.17 cubic feet per second with a total volume of 60 gallons. It was observed that the oil did not spread on the snow surface except at the very beginning when in addition to being warm, the oil was pushed by the outward pressure forces caused by pouring. This was not unexpected since the viscous force, the force retarding the spreading, was great at low temperatures; as soon as the oil temperature drops to 15 °F (the pour point of Prudhoe Bay crude oil) no spreading should occur. The spilled oil formed a slick 3/8 inches thick and penetrated half an inch into the snow. The oil slick was buried under 3 to 5 inches of fresh fallen snow the following day as the temperature on January 17 rose to 16 °F with snow, and a wind speed of 22 knots. The oil temperature under the snow was found to be 6-10 °F higher that the surrounding air temperature.
...

On January 19, a spill was made on a small snow-free ice surface which had been located on a lake. The temperature on that day was 7 °F and the wind speed 5 knots. About 57 gallons of oil was poured on the ice at a rate of 0.17 cubic feet per second. The oil, when it was warm, spread at a rate of about 0.2 feet per second and formed a slick of approximately 12 feet x 14 feet with a thickness of 5/16 inches. The slick remained free of snow for one day and then was covered by

blowing snow. Tests for the absorption of oil by ice were not made due to the breaking down of the ice-coring device. However, the oil showed no visible sign of penetration of the ice.

... No observation was made on the test of oil absorbents since the test was conducted after the author left Port Clarence. However, quantitative results of all the tests mentioned above will be available from a U.S. Coast Guard report."

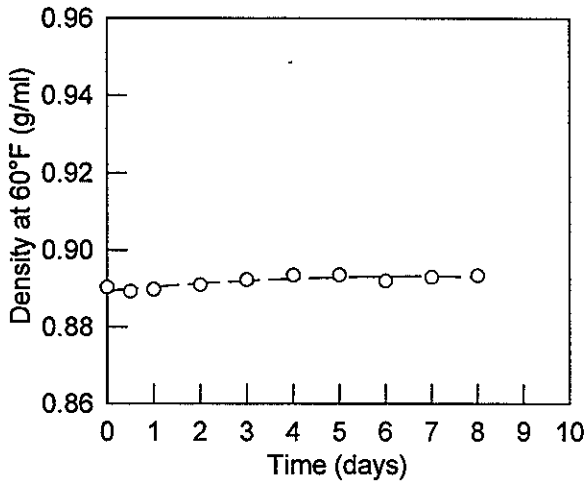

Figure 12. Density of Prudhoe Bay crude oil aged on snow.

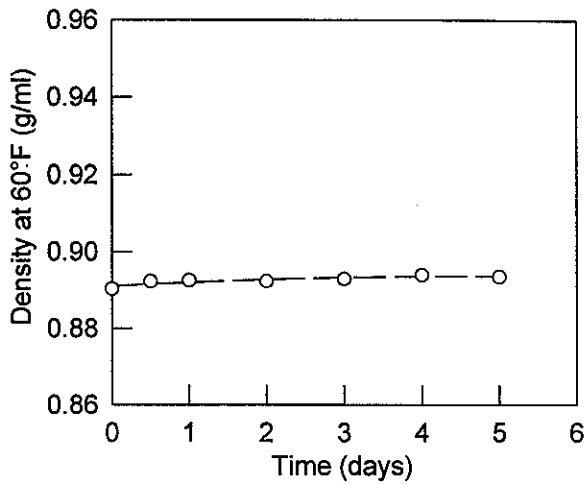

Figure 13. Density of Prudhoe Bay crude oil aged on ice.

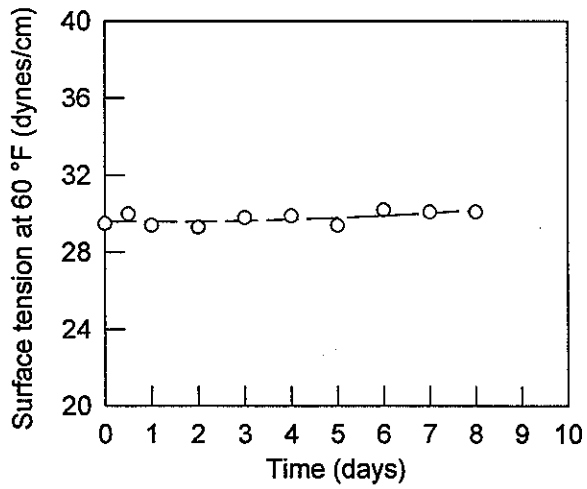

Figure 14. Surface tension of Prudhoe Bay crude oil aged on snow.

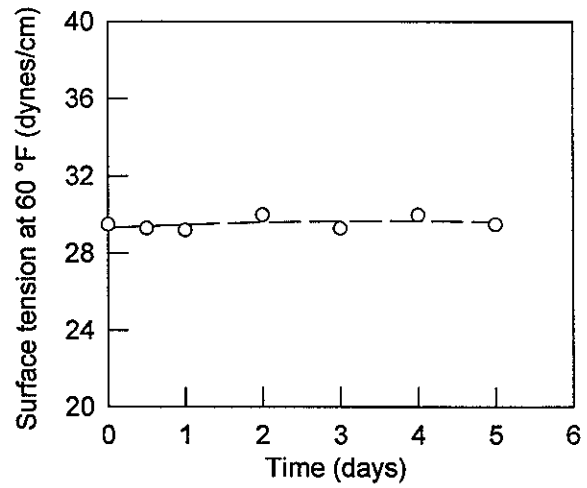

Figure 15. Surface tension of Prudhoe Bay crude oil aged on ice.

Results

"Samples of the spilled oil were collected daily from snow and ice and brought back to Ottawa. They were analyzed for density, surface tension, and viscosity. The densities were measured with a pycnometer, the surface tensions with a du Nouy-type tensiometer and the viscosisties with a Haake Rotovisko. All the measurements were made in a room with a constant

temperature of 60 °F. Results are given in Table 2 and shown in Figures 12 to 16.

Table 2. Oil Aging Experiment

Prudhoe Bay Crude Oil on Ice						Prudhoe Bay Crude Oil on Snow					
Age of Sample, days	Weather Condition		Surface Tension Dynes/cm	Density g/ml	Viscosity c.p.	Age of Sample, days	Weather Condition		Surface Tension Dynes/cm	Density g/ml	Viscosity c.p.
	Temp. °F	Wind Speed, knots					Temp. °F	Wind Speed, knots			
Fresh	-	-	29.5	0.8903	50.2	Fresh	-	-	29.5	0.8903	50.2
0.5	7	5	29.3	0.8922	60.2	0.5	-2	12	30.0	0.8892	65.5
1	-12	12	29.2	0.8925	59.9	1	16	22	29.4	0.8897	79.5
2	-1	10	30.0	0.8923	71.6	2	15	20	29.3	0.8909	83.7
3	-2	14	29.3	0.8929	72.2	3	4	5	29.8	0.8922	85.0
4	2	10	30.0	0.8939	66.1	4	-12	12	29.9	0.8935	84.8
5	9	12	29.5	0.8935	70.0	5	-1	10	29.4	0.8936	83.4
						6	-3	14	30.2	0.8920	84.5
						7	0	15	30.1	0.8930	88.9
						8	9	12	30.1	0.8934	95.4

All of the measurements were made at 60 °F (±2 °F)

As seen from these Figures, the oil aged at an extremely slow rate. The increase in density after five days of aging on snow or ice accounts only for 0.4%, whereas the corresponding increase in the summer test is 4.5%. The change in surface tension, as shown in Figures 14 and 15, is insignificant while a definite increase was found for the summer test. The difference in aging rate between the present test and summer test is most apparent (see Figure 16). As mentioned previously, the spilled oil on both snow and ice was buried under as much as 5 inches of snow. This cover plus the fact that the oils were "frozen" (as most temperatures were much below the pour point) is the obvious reason for a very slow rate of aging. In fact, the aging rate in the present test is negligible as compared with the aging rate in the summer test. Data of the summer test are given in

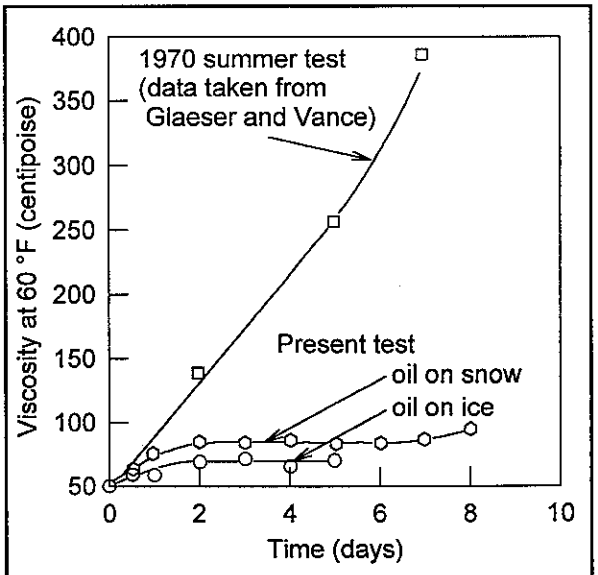

Figure 16. Viscosity of aged Prudhoe Bay crude oil.

the Appendix." The summer tests were reported in Glaeser, J.L. and G. Vance, *A Study of the Behaviour of Oil Spills in the Arctic,* 714/08/A/001,002, United States Coast Guard, Washington, D.C., 53 p, 1971, which was reviewed earlier.

BOSS Critique

The author does not report any errors for the measurements discussed in this report. There is no clear discussion of the camera type used to record the oil spill movement. Nor is there a discussion of the angle the camera was at in reference to the spilled oil. Photographs taken at an angle will cause a distortion of the field of view of the oil causing the oil slick to appear to be a different length or width, than it really is, depending upon the distortion. There is no statement about the spacing of the wooden stakes placed in the snow (ice) surface as a reference grid for scaling purposes in the photographs.

Oil-in-Ice Bibliography

Only the manuscripts listed in the table of contents, and at the beginning of each review, have been reviewed.

Al'khimenko, A.I., "Effect of Hydrometeorology Factors on Spreading of Oil Products in Reservoirs", in *Hydrotechnical Construction (Godrotekhnicheskoe Stroitel'stvo),* Vol. 4, pp 28-32, 1989.

Allen, A.A., "Case Study: Oil Recovery Beneath Ice", in *Proceedings of the Tenth Annual Offshore Technology Conference*, Vol. 1, Offshore Technology Conference, Dallas, Texas, OTC 3078, pp 261-266, 1978.

ARCTEC Canada Ltd., *Site Visit of Oil Spill Under Multi-Year Ice at Griper Bay, N.W.T.*, EE-42, Environment Canada, Ottawa, Ontario, 34 p, 1983.

Ayers, R.C., H.O. Jahns and J.L. Glaeser, "Oil Spills in the Arctic Ocean: Extent of Spreading and Possibility of Large-Scale Thermal Effects", *Science*, Vol. 186, pp 843-846, 1974.

Barber, F.G., "Oil Spilled With Ice: Some Qualitative Aspects", in *Proceedings of a Joint Conference on Prevention and Control of Oil Spills*, American Petroleum Institute, Washington, D.C., pp 133-137, 1971.

Barnes, P.W., E. Reimnitz, L. Toimil and H. Hill, *Fast Ice Thickness and Snow Depth in Relation to Oil Entrapment Potential, Prudhoe Bay, Alaska,* Open File Report 79-539, United States Department of the Interior, Geological Survey, Menlo Park, California, 30 p, 1979.

Barnes, P.W., E. Reimnitz, L. Toimil and H. Hill, "Fast Ice Thickness and Snow Depth in Relation to Oil Entrapment Potential, Prudhoe Bay, Alaska", in *Proceedings of the Fifth International Conference on Port and Ocean Engineering Under Arctic Conditions(POAC),* Norwegian Institute of Technology, Trondheim, Norway, pp 1205-1225, 1979.

Bar-Ziv, R. and S.A. Safran, "Surface Melting of Ice Induced by Hydrocarbon Films", *Langmuir*, Vol. 9, pp 2786-2788, 1993.

Bech, C. and P. Sveum, "Spreading of Oil in Snow", in *Proceedings of the Fourteenth Arctic Marine Oilspill Program Technical Seminar*, Environment Canada, Ottawa, Ontario, pp 57-71, 1991.

Belaskas, D.P. and P.D. Yapa, "An Experimental Study of Oil Spreading in Ice Covered Waters", in *Proceedings of the 1990 National Conference on Hydraulic Engineering*, American Society of Civil Engineers, New York, pp 26-31, 1990.

Belaskas, D.P. and P.D. Yapa, *Oil Spreading in Broken Ice*, Report No. 91-6, Clarkson University, Department of Civil and Environmental Engineering, Potsdam, New York, 101 p, 1991.

Belicek, J. and J. Overall, *Some Aspects of Weathering and Burning of Crude Oil in a Water-and-Ice Environment*, APOA 107-1, Arctic Petroleum Operators Association, Calgary, Alberta, 34 p, 1976.

Beljaars, A.C.M. and P. Viterbo, "The Sensitivity of Winter Evaporation to the Formulation of Aerodynamic Resistance in the ECMWF Model", *Boundary-Layer Meteorology*, Vol. 71, pp 135-149, 1994.

Belyayeva, A.N. and S.B. Tambiyev, "Role of Lipids and Alkanes in the Formation of Sea Snow", *Oceanology of the Academy of Sciences of the USSR*, Vol. 27, pp 49-52, 1987.

Berry, B.A. and N. Rajaratnam, "Oil Slicks in Ice Covered River", *Journal of Hydraulic Engineering*, Vol. 111, pp 369-379, 1985.

Belore, R.C. and I.A. Buist, "Modelling of Oil Spills in Snow", in *Proceedings of the Eleventh Arctic Marine Oilspill Program Technical Seminar*, Environment Canada, Ottawa, Ontario, pp 9-29, 1988.

Blackall, P.J., "Missiles or Parachutes: How to Track Oiled Ice", *Spill Technology Newsletter*, Vol. 3, pp 25-26, 1978.

Bobra, A.M. and M.F. Fingas, "The Behaviour and Fate of Arctic Oil Spills", *Water Science and Technology*, Vol. 18, pp 13-23, 1986.

Britch, R.P., N.C. Shi and R.V. Shafer, "An Interactive Oil Spill Trajectory Model For Alaskan Arctic Waters", in *Proceedings of the Thirteenth Arctic Marine Oil Spill Program Technical Seminar*, Environment Canada, Ottawa, Ontario, pp 157-171, 1990.

Buist, I.A., "Measured Behaviour of an Oil/Gas Plume Under Ice", in *Proceedings of a Workshop on In-Water-Large Drops Sub-Sea Containment of Oil*, EE-18, University of Toronto, Institute For Environmental Studies, Toronto, Ontario, pp 55-62, 1981.

Buist, I.A., R.C. Belore and L.B. Solsberg, "Behaviour of and Response to a Major Oil Spill From a Tanker in Arctic Waters", *Spill Technology Newsletter*, Vol. 8, pp 50-77, 1983.

Buist, I.A. and I. Bjerkelund, "Oil in Pack Ice: Preliminary Results of Three Experimental Spills", in *Proceedings of the Ninth Arctic Marine Oilspill Program Technical Seminar*, Environment Canada, Ottawa, Ontario, pp 379-397, 1986.

Buist, I. and D. Dickins, *Fate and Behaviour of Water-in-Oil Emulsions in Ice*, Report No. CS 11, Canadian Offshore Oil Spill Research Association (COOSRA), Calgary, Alberta, 121 p, 1983.

Buist, I.A. and D.F. Dickins, "Experimental Spills of Crude Oil in Pack Ice", in *Proceedings of the 1987 International Oil Spill Conference*, American Petroleum Institute, Washington, D.C., pp 373-381, 1987.

Buist, I., S. Joyce and D.F. Dickins, *Oil Spills in Leads: Tank Tests and Modelling*, EE-95, Environment Canada, Ottawa, Ontario, 126 p, 1987.

Buist, I., S. Joyce and S.L. Ross, "Modelling Oil Spills in Leads: Winds/Wave Tank Testing and Preliminary Results", in *Proceedings of the Tenth Arctic Marine Oilspill Program Technical Seminar*, Environment Canada, Ottawa, Ontario, pp 131-148, 1987.

Buist, I., W.M. Pistruzak and D.F. Dickins, "Dome Petroleum's Oil and Gas Undersea Ice Study", in *Proceedings of the Fourth Arctic Marine Oilspill Program Technical Seminar*, Environment Canada, Ottawa, Ontario, pp 647-686, 1981.

Buist, I.A., S.G. Potter and D.F. Dickins. "Fate and Behaviour of Water-in-Oil-Emulsions in Ice", in *Proceedings of the Sixth Arctic Marine Oilspill Program Technical Seminar*, Environment Canada, Ottawa, Ontario, pp 263-279, 1983.

Cammaert, A.B., *Oil and Gas Under Ice Laboratory Study*, Beaufort Environmental Impact Statement RWC17, Environment Canada, Ottawa, Ontario, 38 p, 1980.

Campbell, W.J. and S. Martin, "Oil and Ice in the Arctic Ocean: Possible Large-Scale Interactions", *Science*, Vol. 181, pp 56-58, 1973.

Carstens, T. and E. Sendstad, "Oil Spill on the Shore of an Ice-Covered Fjord in Spitsbergen", in *Proceedings of the Fifth International Conference on Port and Ocean Engineering Under Arctic Conditions (POAC),* Norwegian Institute of Technology, Trondheim, Norway, pp 1227-1242, 1979.

C-CORE (Centre For Cold Ocean Resources Engineering), *An Oilspill in Pack Ice*, EE-15, Environment Canada, Ottawa, Ontario, 231 p, 1980.

Chen, E.C., *Arctic Winter Oil Spill Test,* Technical Bulletin No. 68, Environment Canada, Ottawa, Ontario, 20 p, 1972.

Chen, E.C., B.E. Keevil and R.O. Ramseier, *Behaviour of Oil Spilled in Ice-Covered Rivers*, Scientific Series No. 61, Environment Canada, Ottawa, Ontario, 26 p, 1976.

Chen, E.C., B.E. Keevil and R.O. Ramseier, "Behaviour of Crude Oil Under Fresh-Water Ice", *Journal of Canadian Petroleum Technology*, Vol. 15, pp 79-83, 1976.

Chen, E.C., C.K. Overall and C.R. Phillips, "Spreading of Crude Oil on an Ice Surface", *Canadian Journal of Chemical Engineering*, Vol. 52, pp 71-74, 1974.

Chowdhury, T., *Spreading of Oil Spilled Under Ice*, M.Sc., Clarkson University, Department of Civil and Environmental Engineering, Potsdam, New York, 113 p, 1989.

Colony, R., "The Random Transport of Oil by Sea Ice", *Water Science and Technology*, Vol. 18,

pp 25-39, 1986.

Comfort, G., *Under-Ice Roughness Measurements*, ESRF File No. 265-26-04, Environmental Studies Research Fund, National Energy Board, Calgary, Alberta, 90 p, 1986.

Comfort, G., *Analytical Modelling of Oil and Gas Spreading Under Ice*, Report No. 077, Environmental Studies Research Fund, National Energy Board, Calgary, Alberta, 57 p, 1987.

Comfort, G. and W.F. Purves, *An Investigation of the Behaviour of Crude Oil Spilled Under Multi-Year Ice at Griper Bay, N.W.T.*, Environment Canada, Ottawa, Ontario, 87 p, 1978.

Comfort, G. and F. Purves, "An Investigation of the Behaviour of Crude Oil Spilled Under Multi-Year Ice at Griper Bay", in *Proceedings of the Third Arctic Marine Oilspill Program Technical Seminar*, Environment Canada, Ottawa, Ontario, pp 62-86, 1980.

Comfort, G. and W. Purves, *The Behaviour of Crude Oil Spilled Under Multi-Year Ice,* EPS 4-EC-82-4, Environment Canada, Ottawa, Ontario, 76 p, 1982.

Comfort, G., T. Roots, L. Chabot and F. Abbott, "Oil Behaviour Under Multi-Year Ice at Griper Bay, N.W.T.", in *Proceedings of the Sixth Arctic Marine Oilspill Program Technical Seminar*, Environment Canada, Ottawa, Ontario, pp 14-19, 1983.

Coon, M.D. and R. Pritchard, "The Transport and Behaviour of Oil Spilled In and Under Sea Ice", in *Environmental Assessment of the Alaskan Continental Shelf: Annual Reports of Principal Investigators For the Year Ending March 1980, Vol. VII: Transport Data Management*, Outer Continental Shelf Environmental Assessment Program, Ocean Assessment Division, National Oceanic and Atmospheric Administration, Alaska, pp 341-347, 1980.

Cox, J.C. and L.A. Schultz, "The Transport and Behaviour of Oil Spilled Under Ice", in *Proceedings of the Third Arctic Marine Oilspill Program Technical Seminar*, Environment Canada, Ottawa, Ontario, pp 45-61, 1980.

Cox, J.C. and L.A. Schultz, "The Containment of Oil Spilled Under Rough Ice", in *Proceedings of the 1981 International Oil Spill Conference*, American Petroleum Institute, Washington, D.C., pp 203-208, 1981.

Cox, J.C. and L.A. Schultz, "The Mechanics of Oil Containment Beneath Rough Ice.", in *Proceedings of the Fourth Arctic Marine Oilspill Program Technical Seminar*, Environment Canada, Ottawa, Ontario, pp 3-44, 1981.

Cox, C., L.A. Schultz, R.P. Johnson and R.A. Shelsby, "The Transport and Behaviour of Oil Spilled In and Under Sea Ice", in *Environmental Assessment of the Alaskan Continental Shelf: Final Report of Principal Investigators, Vol. 3, Physical Science Studies*, National Oceanic and Atmospheric Administration, Marine Pollution Assessment, pp 427-597, 1980.

Deslauriers, P.C., "Oil Spill Behaviour in Ice During the 1977 Buzzards Bay Oil Spill", *Proceedings of the Conference on Assessment of Ecological Impacts of Oil Spills,* American Institute of Biological Sciences, Washington, D.C. pp 197-215, 1978.

Deslauriers, P.C., "Observations of Oil Behaviour in Ice Floes and the 1977 Ethel H Spill", in *Proceedings of a Workshop on Oil, Ice and Gas,* EE-14, University of Toronto, Institute For Environmental Studies, Toronto, Ontario, pp 87-94, 1979.

Deslauriers, P.C. and S. Martin,"Behaviour of the Bouchard No. 65 Oil Spill in the Ice Covered Waters of Buzzards Bay", in *Proceedings of the Tenth Annual Offshore Technology Conference,* OTC 3079, Offshore Technology Conference, Dallas, Texas, pp 267-276, 1978.

Deslauriers, P.C., S. Martin, B. Morson and B. Baxter, *The Physical and Chemical Behaviour of the Bouchard No. 65 Oil Spill in the Ice Covered Waters of Buzzards Bay,* National Oceanic and Atmospheric Administration, Environmental Research Laboratory, Boulder, Colorado, 185 p, 1977.

Dethier, M.N., The Effects of an Oil Spill and Freeze Event on Intertidal Community Structure in Washington, MMS 91-0002, U.S. Department of the Interior, Minerals Management Service, Pacific OCS Region, Camarillo, California, 167 p, 1991.

Dickins, D.F., A. Dickinson and B. Humphrey, *Pack Ice in Canadian Waters: Dimensions and Dynamics of Leads and Floes,* EE-82, Environment Canada, Ottawa, Ontario, 136 p, 1986.

Dickins, D.F., I. Buist and W.M. Pistruzak, "Dome Petroleum's Study of Oil and Gas Under Sea Ice", in *Proceedings of the 1981 International Oil Spill Conference,* American Petroleum Institute, Washington, D.C., pp 183-189, 1981.

Dmitriev, F.A. and S.V. Pivovarov, "Hydrocarbons in the Snow-Ice Cover and Water of the Kara Sea", *Meteorologiia i Gidrologiia,* Vol. 5, pp 87-91, 1983.

Doerffer, J.W., *Oil Spill Response in the Marine Environment,* Pergamon Press, Oxford, pp 268-271, 1992.

Dome Petroleum Ltd., *Oil and Gas Under Sea Ice,* Report CV-1, Canadian Offshore Oil Spill Research Association (COOSRA), Vol. I and II, 286 p & appendices, Calgary, Alberta, 1981.

Dome Petroleum Ltd., Esso Resources Canada Ltd. and Gulf Canada Resources Inc., "Behaviour of Spilled Oil in the Arctic Environment", in *Hydrocarbon Development in the Beaufort Sea - MacKenzie Delta Region, Vol. 6: Accidental Spills,* Environment Canada, Ottawa, Ontario, Chapter 3, pp 31-39, 1982.

Duerden, F.C. and J.J. Swiss, "Kurdistan: An Unusual Spill Successfully Handled", in *Proceedings of the 1981 International Oil Spill Conference,* American Petroleum Institute, Washington, D.C., pp 215-219, 1981.

El-Tahan, H. and S. Venkatesh, "Behaviour of Oil Spills in Cold and Ice-Infested Waters: Analysis of Experimental Data on Oil Spreading", in *Proceedings of the Seventeenth Arctic Marine Oilspill Program Technical Seminar,* Environment Canada, Ottawa, Ontario, pp 337-354, 1994.

El-Tahan, H., G. Comfort and R. Abdelnour, *Development of a Methodology For Computing Oil Spill Motion in Ice-Infested Waters*, B73224-FR, Environment Canada, Downsview, Ontario, 108 p, 1988.

El-Tahan, M. and G. Warbanski, "Prediction of Short-Term Ice Edge Drift", in *Proceedings of the Sixth Conference on Offshore Mechanics and Arctic Engineering*, Vol. IV, The American Society of Mechanical Engineers, New York, pp 393-400, 1987.

Erickson, P., B. Fowler and D.J. Thomas, "The Fate of Oil-Based Drilling Muds at Two Artificial Island Sites in the Beaufort Sea", in *Drilling Wastes,* Eds F.R. Engelhardt, J.P. Ray and A.H. Gillam, Elsevier Applied Science, London, pp 23-58, 1989.

Erickson, P., B. Fowler and D.J. Thomas, *Oil-Based Drilling Muds: Off Structure Monitoring - Beaufort Sea*, Report No. 101, Environmental Studies Research Fund, National Energy Board, Calgary, Alberta, 188 p, 1988.

Fay, J.A., *The Spreading of Oil Slicks on a Calm Sea*, Massachusetts Institute of Technology, Department of Mechanical Engineering, Fluid Mechanics Laboratory, Boston, Massachusetts, 14 p, 1969.

Fay, J.A. and D.P. Hoult, *Physical Processes in the Spread of Oil on a Water Surface*, AD-726 281, United States Coast Guard, Washington, D.C., 16 p, 1971.

Fingas, M.F., "The Behaviour of Oil in Ice", in *Combatting Marine Oil Spills in Ice and Cold Conditions*, National Board of Waters and the Environment, Helsinki, Finland, pp 5-22, 1993.

Free, A.P., J.C. Cox and L.A. Schultz, *Laboratory Studies of Oil Spill Behaviour in Broken ice Fields,* DTCG39-80-C-80138, United States Coast Guard, Washington, D.C., 58 p, 1981.

Free, A.P., J.C. Cox and L.A. Schultz, "Laboratory Studies of Oil Spill Behaviour in Broken Ice Fields", in *Proceedings of the Fifth Arctic Marine Oilspill Program Technical Seminar*, Environment Canada, Ottawa, Ontario, pp 3-14, 1982.

Gavrilo, V.P. and V.N. Tarashkevich, "Study of Oil Intrusion Influence on Physical Properties of Sea Ice", in *Proceedings of the Second International Offshore and Polar Engineering Conference*, The International Society of Offshore and Polar Engineers, Golden, Colorado, pp 666-669, 1992.

Glaeser, J.L. and G. Vance, *A Study of the Behaviour of Oil Spills in the Arctic,* 714/08/A/001,002, United States Coast Guard, Washington, D.C., 53 p, 1971.

Goodman, R.H., A.G. Holoboff, T.W. Daley, P. Waddell, L.D. Murdock and M. Fingas, "A Technique For the Measurement of Under-Ice Roughness to Determine Oil Storage Volumes", in *Proceedings of the 1987 International Oil Spill Conference,* American Petroleum Institute, Washington, D.C., pp 395-398, 1987.

Goss, K., "Adsorption of Organic Vapours on Ice and Quartz Sand at Temperatures Below 0°C", *Environmental Science and Technology*, Vol. 27, pp 2826-2830, 1993.

Greene, G.D., P.J. Leinonen and D. Mackay, "An Exploratory Study of the Behaviour of Crude Oil Spills Under Ice", Canadian Journal of Chemical Engineering, Vol. 55, pp 696-700, 1977.

Hirvi, J-P., "Summary of the Environmental Effects of the Antonio Gramsci Oil Spill in the Gulf of Finland in 1987", in *Proceedings of the Thirteenth Arctic Marine Oil Spill Program Technical Seminar*, Environment Canada, Ottawa, Ontario, pp 179-195, 1990.

Hirvi, J-P., "The Oil Spill in the Gulf of Finland in 1987", in *International Association For Hydraulic Research (IAHR) Symposium on Ice 1990*, Vol. 3, Espoo, Finland, pp 127-141, 1990.

Hirvi, J.-P., J. Koponen and H. Vepsa, "A Case Study of m/t Antonio Gramsci Oil Accident in Ice Infested Waters: Comparison Between the Observations and Results From a Coupled 3D-Hydrodynamic-Oil Spill Model", in *Combatting Marine Oil Spills in Ice and Cold Conditions*, National Board of Waters and the Environment, Helsinki, Finland, 163-173, 1993.

Hoult, D.P., "The Aging of Oil Spilled in the Arctic", in *Literature Survey on the Behaviour of Oil Under Ice*, Environment Canada, Ottawa, Ontario, pp 1-24, 1974.

Hoult, D.P., S. Wolfe, S. O'Dea and J.P. Patureau, *Oil in the Arctic*, CG-D-96-75, United States Coast Guard, Washington, D.C., 218 p, 1975.

Humphrey, B., G. Sergy and E.H. Owens, "Stranded Oil Persistence in Cold Climates", in *Proceedings of the Thirteenth Arctic Marine Oilspill Program Technical Seminar*, Environment Canada, Ottawa, Ontario, pp 401-410, 1990.

Izmaylov, V.V., "Effect of Petroleum Products on the Snow-Ice Cover of the Arctic", *Polar Geography and Geology*, Vol. 5, pp 235-241, 1980.

Jayko, K., M.L. Spaulding, E. Howlett, W. Knauss, T. Isaji, E. Anderson, R. Goodman and B. McKenzie, "Personal Computer Oil Spill Response Model: Canadian Beaufort Sea", in *Proceedings of the 1991 International Oil Spill Conference*, American Petroleum Institute, Washington, D.C., pp 607-618, 1991.

Jerbo, A., "Two Types of Oil Spills in Swedish Inland Waters - Tests of New Materials, Ideas and Methods", in *Proceedings of the 1973 Joint Conference on Prevention and Control of Oil Spills*, American Petroleum Institute, Washington, D.C., pp 559-567, 1973.

Johansen, O., "Oil Spill in Ice Simulation Model Development", in *Proceedings of the 1989 Conference on Port and Ocean Engineering Under Arctic Conditions Conference (POAC)*, pp 1130-1141, 1989.

Johnson, W.R. and T. Paluszkiewicz, "Risk Assessment Initiatives in the U.S. Beaufort Sea", in *Proceedings of the Fifteenth Arctic Marine Oilspill Program Technical Seminar*, Environment Canada, Ottawa, Ontario, pp 197-210, 1992.

Jordan, R.E. and J.R. Payne, "Oil Released in Arctic Environments, Oil and Ice/Snow Interactions", in *Fate and Weathering of Petroleum Spills in the Marine Environment: A Literature Review and Synopsis*, Ann Arbor Science Publishers, Ann Arbor, Michigan, pp 108-114, 1980.

Kawamura, P., D. Mackay and M. Goral, *Spreading of Chemicals on Ice and Snow,* EE-79, Environment Canada, Ottawa, Ontario, 106 p, 1986.

Keevil, B.E., *Literature Survey on the Behaviour of Oil Under Ice*, Environment Canada, Ottawa, Ontario, 10 p, 1974.

Keevil, B.E. and R. Ramseier, "Behaviour of Oil Spilled Under Floating Ice", in *Proceedings of the 1975 Conference on Prevention and Control of Oil Pollution*, American Petroleum Institute, Washington, D.C., pp 497-501, 1975.

Kirstein, B.E. and R.T. Redding, "Ocean-Ice Oil-Weathering Computer Program Users Manual", in *Outer Continental Shelf Environmental Assessment Program*, Vol. 59, National Oceanic and Atmospheric Administration, Ocean Assessment Division, Alaska, 83 p, 1988.

Kovacs, A., "Sea Ice Thickness Profiling and Under-Ice Oil Entrapment", in *Proceedings of the Ninth Annual Offshore Technology Conference*, OTC 2949, Offshore Technology Conference, Dallas, Texas, pp 547-554, 1977.

Kovacs, A., "Oil Pooling Under Sea Ice", in *Outer Continental Shelf Environmental Assessment Program, Vol. VIII: Transport*, RK-8-0065, National Oceanic and Atmospheric Administration, Ocean Assessment Division, Alaska, pp 310-353, 1979.

Kovacs, A., R.M. Morey and D. Cundy, "Oil Pooling Under Sea Ice", in *Outer Continental Shelf Environmental Assessment Program, Vol. VII: Transport*, National Oceanic and Atmospheric Administration, Ocean Assessment Division, Alaska, pp 333-339,1980.

Kovacs, A., R.M. Morey, D.F. Cundy and G. Decoff, "Pooling of Oil Under Sea Ice", in *Proceedings of the Sixth International Conference on Port and Ocean Engineering Under Arctic Conditions (POAC)*, Vol. II, pp 912-922, 1981.

Kuroiwa, D., "Liquid Permeability of Snow", *Low Temperature Science Series*, Vol. 26 A, pp 29-52, 1968.

Leinonen, P.J. and D. Mackay, "A Mathematical Model of Evaporation and Dissolution From Oil Spills on Ice, Land, Water and Under Ice", *Water Pollution Research in Canada*, Vol. 10, pp 132-141, 1975.

Lepparanta, M., "The Problem of Sea Ice Dynamics in Oil Drift Modelling", in *Combatting Marine Oil Spills in Ice and Cold Conditions*, National Board of Waters and the Environment, Helsinki, Finland, pp 175-184, 1993.

Lewbel, G.S. and B.J. Gallaway, "Transport and Fate of Spilled Oil", in *Proceedings of a Synthesis Meeting: The Barrow Arch Environment and Possible Consequences of Planned Offshore Oil and Gas Development*, National Oceanic and Atmospheric Administration, Anchorage, Alaska, pp 7-29, 1983.

Lissauer, I.M. and D.A. Baird, *Aerial Photographic Surveys Analyzed to Deduce Oil Spill Movement During the Decay and Breakup of Fast Ice, Prudhoe Bay, Alaska*, CG-D-51-82, United States Coast Guard, Washington, D.C., 21 p, 1982.

Liu, S.K. and J.J. Leendertse, "A 3-D Oil Spill Model With and Without Ice Cover", in *1981 Workshop on the Mechanics of Oil Slicks*, l'Association Internationale de Recherches Hydrauliques, Paris, pp 249-261, 1981.

Liukkonen, S., R. Koskivaara and K. Lampela, "Adhesion of Oil To Plastic, Stianless Steel and Ice", in *Proceedings of the Eighteenth Arctic Marine Oil Spill Program Technical Seminar*, Environment Canada, Ottawa, Ontario, pp 69-90, 1995.

Loset, S., T. Carstens and H. Jensen, "Deflection of Open Pack Ice in an Oil Spill Recovery Area", in *Proceedings of the Fourteenth Arctic Marine Oil Spill Program Technical Seminar*, Environment Canada, Ottawa, Ontario, pp 495-507, 1991.

Mackay, D., *The Fate and Behaviour of Oil in Cold Climates*, Unpublished Document, Environment Canada, Ottawa, Ontario, 126 p., 1984.

Mackay, D., "The Physical and Chemical Fate of Spilled Oil", in *Petroleum Effects in the Arctic Environment*, Ed F.R. Engelhardt, Elsevier Applied Science Publishers, London, pp 37-61, 1985.

Mackay, D., M.E. Charles and C.R. Phillips, *The Physical Aspects of Crude Oil Spills on Northern Terrain (Final Report)*, Report No. 73-42, Department of Indian and Northern Affairs, Ottawa, Ontario, 213 p, 1974.

Mackay, D., K. Hossain and A. Kisil, "Research in Oil, Gas and Ice at the University of Toronto", in *Proceedings of a Workshop on Oil, Ice and Gas*, EE-14, Institute of Environmental Studies, University of Toronto, Toronto, Ontario, pp 27-31, 1979.

Mackay, D., A. Kisil, I. Buist, K. Hossain, R. Mascarenhas and S. Paterson, "A Laboratory Study

of the Behaviour of Oil and Gas Under Ice", in *Proceedings of the Arctic Marine Oilspill Program Technical Seminar*, Environment Canada, Ottawa, Ontario, pp 101-109, 1979.

Mackay, D., P.J. Leinonen, J.C.K. Overall and B.R. Wood, "The Behaviour of Crude Oil Spill on Snow", *Arctic*, Vol. 28, pp 9-20, 1975.

Mackay, D., M. Medir and D.E. Thornton, "Interfacial Behaviour of Oil Under Ice", *Canadian Journal of Chemical Engineering*, Vol. 54, pp 72-74, 1976.

MacLeod, Jr., M.Y. Uyeda, A.J. Friedman and P.G. Prohaska, "Weathering Estimations For Spilled Oil From Bouchard No. 65", in *Proceedings of the Conference on Assessment of Ecological Impacts of Oil Spills*, American Institute of Biological Sciences, Washington, D.C. pp 216-228, 1978.

MacNeill, M.R. and R.H. Goodman, "Motion of Oil in Leads", in *Proceedings of the Eighth Arctic Marine Oilspill Program Technical Seminar*, Environment Canada, Ottawa, Ontario, pp 42-52, 1985.

MacNeill, M.R. and R.H. Goodman, *Oil Motion During Lead Closure,* Report No. 053, Environmental Studies Research Fund, National Energy Board, Calgary, Alberta, 13 p, 1987.

Malcolm, J.D., "Studies of Oil Spill Behaviour Under Ice", in *Proceedings of a Workshop on Oil, Ice and Gas*, EE-14, Institute For Environmental Studies, University of Toronto, Toronto, Ontario, pp 47-53, 1979.

Malcolm, J.D. and A.B. Cammaert, "Movement of Oil and Gas Spills Under Sea Ice", in *Proceedings of the Sixth International Conference on Port and Ocean Engineering Under Arctic Conditions (POAC)*, pp 923-936, 1981.

Malcolm, J.D. and A.B. Cammaert, "Transport and Deposition of Oil and Gas Under Sea Ice", in *Proceedings of the Fourth Arctic Marine Oilspill Program Technical Seminar*, Environment Canada, Ottawa, Ontario, pp 45-73, 1981.

Malcolm, J.D. and C. Dutton, "The Interfacial Tension and Contact Angle of Crude Oil Under Ice", in *Proceedings of the Fifth International Conference on Port and Ocean Engineering Under Arctic Conditions (POAC)*, pp 771-778, 1979.

Martin, S., "A Field Study of Brine Drainage and Oil Entrainment in First-Year Sea Ice", *Journal of Glaciology*, Vol. 22, pp 473-502, 1979.

Martin, S., "Anticipated Oil-Ice Interactions in the Bering Sea", in *The Eastern Bering Sea Shelf: Oceanography and Resources*, Vol. I, Eds D.W. Hood and J.A. Calder, National Oceanic and Atmospheric Administration, Marine Pollution Assessment, pp 233-243, 1981.

Martin, S., "The Interaction of Oil With Sea Ice in the Arctic Ocean", in *Environmental Assessment*

of the Alaskan Continental Shelf: Annual Reports of Principal Investigators For the Year Ending March 1979, Vol. VII: Transport, National Oceanic and Atmospheric Administration, Ocean Assessment Division, Alaska, pp 171-180, 1979.

Martin, S. "The Interaction of Oil With Sea Ice in the Arctic Ocean", in *Environmental Assessment of the Alaskan Continental Shelf: Annual Reports of Principal Investigators for the Year Ending March 1980, Vol. VI: Transport*, National Oceanic and Atmospheric Administration, Ocean Assessment Division, Alaska, pp 1-8, 1980.

Martin, S. "The Interaction of Oil with Sea Ice in the Arctic Ocean", in *Environmental Assessment of the Alaskan Continental Shelf: Annual Reports of Principal Investigators for the Year Ending March 1981, Vol. V: Transport,* National Oceanic and Atmospheric Administration, Ocean Assessment Division, Alaska, 27 p, 1981.

Martin, S., P. Kauffman and P.E. Welander, "A Laboratory Study of the Dispersion of Crude Oil Within Sea Ice Grown in a Wave Field", in *Proceedings of the Twenty-Seventh Alaska Science Conference*, American Association For the Advancement of Science, Fairbanks, Alaska, 18 p, 1977.

McLean, A.Y., "The Behaviour of Oil Spilled in a Cold Water Environment", in *Proceedings of the Fourth Annual Offshore Technology Conference*, OTC 1522, Offshore Technology Conference, Dallas, Texas, pp 229-233, 1972.

McMinn, T.J., *Crude Oil Behaviour on Arctic Winter Ice,* Project 734108, United States Coast Guard, Washington, D.C., 75 p, 1972.

McMinn, T.J., "Oil Spill Behaviour in a Winter Arctic Environment", in *Proceedings of the Fifth Offshore Technology Conference,* Vol. 1, OTC-1747, Offshore Technology Conference, Dallas, Texas, pp 233-248, 1973.

McMinn, T.J. and P.C. Golden, "Behavioral Characteristics and Cleanup Techniques of North Slope Crude Oil in an Arctic Environment", in *Proceedings of the 1973 Joint Conference on Prevention and Control of Oil Spills,* American Petroleum Institute, Washington, D.C., pp 263-276, 1973.

Metge, M., *Oil in Pack Ice Coldroom Tests,* IPRT-16-78, Imperial Oil Limited, Calgary, Alberta, 30 p, 1978.

Metge, M. and A.S. Telford, "Oil in Moving Pack Ice-Laboratory Study", in *Proceedings of the Fifth International Conference on Port and Ocean Engineering Under Arctic Conditions (POAC),* pp 255-264, 1979.

Miller, M.C., J.R. Stout and V. Alexander, "Effects of a Controlled Under-Ice Oil Spill on Invertebrates of an Arctic and Subarctic Stream", *Environmental Pollution*, Vol. 42A, pp 99-132, 1986.

Milne, A.R., "The Physical Environment of the Beaufort Sea Related to Oil, Ice and Water Interactions", in *Proceedings of the Sixth Arctic Environmental Workshop*, EE-6, Institute For Environmental Studies, University of Toronto, Toronto, Ontario, pp 43-53, 1977.

Milne, A.R., R.H. Herlinveaux and G.R. Wilton, *A Field Study of the Permeability of Multiyear Ice to Sea Water With Implications on Its Permeability to Oil,* EPS-4-EC-77-11, Environment Canada, Ottawa, Ontario, 33 p, 1977.

Moir, J. and Y. Lau, *Some Observations of Oil Slick Containment by Simulated Ice Ridge Keels*, Environment Canada, Burlington, Ontario, 14 p, 1975.

Muir, D.C.G., R. Wagemann, B.T. Hargrave, D.J. Thomas, D.B. Peakall and R.J. Norstrom, "Arctic Marine Ecosystem Contamination", *The Science of the Total Environment,* Vol. 122, pp 75-134, 1992.

Narayanan, S., J.R. Marko and D.B. Fissel, *Movement of Oil Slicks in Northwestern Baffin Bay, SLIKTRAK Simulations,* Petro-Canada Ltd., Calgary, Alberta, 67 p, 1979.

National Oceanic and Atmospheric Administration/Ministry For Greenland, *USNS Potomac Oil Spill-Melville Bay, Greenland*, United States Department of Commerce/Greenland Fisheries Investigations, Washington, D.C., 136 p, 1977.

Nelson, W.G. and A. Allen, "Oil Migration and Modification Processes in Solid Sea Ice", in *Proceedings of the 1981 International Oil Spill Conference*, American Petroleum Institute, Washington, D.C., pp 191-198, 1981.

Nelson, W.G. and A.A. Allen, "The Physical Interaction and Cleanup of Crude Oil With Slush and Solid First Year Ice", in *Proceedings of the Fifth Arctic Marine Oil Spill Program Technical Seminar*, Environment Canada, Ottawa, Ontario, pp 37-59, 1982.

Neu, H.A., "Assessment of Tanker and Slick Drift Following Break-Up of the Tanker Kurdistan", in *The Kurdistan Oil Spill of March 16-17, 1979: Activities and Observations of the Bedford Institute of Oceanography Response Team*, Eds J.H. Vandermeulen and D.E. Buckle, Canadian Technical Report of Hydrography and Ocean Sciences, Department of Fisheries and Oceans, Dartmouth, Nova Scotia, pp 34-37, 1985.

NORCOR Engineering and Research Ltd., *The Interaction of Crude Oil With Arctic Sea Ice*, Beaufort Sea Technical Report, No. 27, Beaufort Sea Project, Department of the Environment, Victoria, B.C., 201 p, 1975.

NORCOR Engineering and Research Ltd., *Probable Behaviour and Fate of a Winter Spill in the Beaufort Sea.*, EPS 4-EC-77-5, Environment Canada, Ottawa, Ontario, 111 p, 1977.

Ormerod, R., Ed, "Long Term Monitoring of Bahia Paraiso Spill", *Antarctic*, Vol. 11, pp 476-478,

1990.

Payne, J.R., J.R. Clayton, G.D. McNabb, Jr., B.E. Kirstein, C.L. Clary, R.T. Redding, J.S. Evans, E. Reinmitz and E.W. Kepema, *Oil-Ice Sediment Interactions During Freezeup and Breakup*, Outer Continental Shelf Environmental Assessment Program, National Oceanic and Atmospheric Administration, Ocean Assessment Division, Anchorage, Alaska, 358 p, 1989.

Payne, J.R., L.E. Hachmeister, G.D. McNabb, H.E. Sharpe, G.S. Smith and C.A. Manen, "Brine-Induced Advection of Dissolved Aromatic Hydrocarbons to Arctic Bottom Waters", *Environmental Science and Technology*, Vol. 25, pp 940-951, 1991.

Payne, J.R., B.E. Kirstein, G.D. McNabb, Jr., J.L. Lambach, R.T. Redding, R.E. Jordan, W. Hom, C. de Oliveira, G.S. Smith, D.M. Baxter and R. Geagel, "Multivariate Analysis of Petroleum Weathering in the Marine Environment -Subarctic Volume I - Technical Results", in *Final Reports of Principal Investigators, February 1984*, Outer Continental Shelf Environmental Assessment Program, National Oceanic and Atmospheric Administration, Ocean Assessment Division, Juneau, Alaska, Vol. 21, 690 p, 1984.

Payne, J.R., B.E. Kirstein, G.D. McNabb, Jr., J.L. Lambach, R.T. Redding, R.E. Jordan, W. Hom, C. de Oliveira, G.S. Smith, D.M. Baxter and R. Geagel, "Multivariate Analysis of Petroleum Weathering in the Marine Environment - Subarctic Volume II - Appendices", in *Final Reports of Principal Investigators, February 1984*, Outer Continental Shelf Environmental Assessment Program, National Oceanic and Atmospheric Administration, Ocean Assessment Division, Juneau, Alaska, Vol. 22, 81 p, 1984.

Payne, J.R., G.D. McNabb, Jr. and J.R. Clayton, Jr., "Oil-Weathering Behaviour In Arctic Environments", *Polar Research*, Vol. 10, pp 631-662, 1991.

Payne, J.R., G.D. NcNabb, L.E. Hachmeister, B.E. Kirstein, J.R. Clayton, C.R. Phillips, R.T. Redding, C.L. Clary, G.S. Smith and G.H. Farmer, *Development of a Predictive Model For the Weathering of Oil in the Presence of Sea Ice,* Outer Continental Shelf Environmental Assessment Program, National Oceanic and Atmospheric Administration, Ocean Assessment Division, Anchorage, Alaska, Vol. 59, 63 p, 1987.

Payne, J.R., G.D. NcNabb, B.E. Kirstein, R. Redding, J.L. Lambach, C.R. Phillips, L.E. Hachmeister and S. Martin, *Development of a Predictive Model For the Weathering of Oil in the Presence of Sea Ice*, Contract No. 83-ABC-00062, Outer Continental Shelf Environmental Assessment Program, National Oceanic and Atmospheric Administration, Ocean Assessment Division, Anchorage, Alaska, pp 80-90, 117-132,143-158 and 247-249, 1984.

Pelletier, E. and C. Brochu, *Prototype, Mesoscale Simulator For the Study of Oil Weathering Under Severe Conditions*, Report 086, Environmental Studies Research Fund, National Energy Board, Calgary, Alberta, 55 p, 1987.

Pimlott, D., D. Brown and K. Sam, *Oil Under the Ice*, Canadian Arctic Resources Committee, Ottawa, Ontario, pp 93-111, 1976.

Pritchard, R.S., "Transport and Behaviour of a Prudhoe Bay Oil Spill", in *Proceedings of a Workshop on Oil, Ice and Gas,* EE-14, Institute For Environmental Studies, University of Toronto, Toronto, Ontario, pp 103-109, 1979.

Pritchard, R.S., "Pollutant Behaviour, Trajectories and Issues Analyses", in *Proceeding of a Synthesis Meeting*, Beaufort Sea Sale 71, Outer Continental Shelf Environmental Assessment Program, National Oceanic and Atmospheric Administration, Ocean Assessment Division, Alaska, pp 137-154, 1981.

Purves, F., *The Interaction of Crude Oil and Natural Gas With Laboratory-Grown Saline Ice*, EPS-4-EC-78-9, Environment Canada, Ottawa, Ontario, 18 p, 1978.

Puskas, J.K. and E.A. McBean, "The Transport of Crude Oil Under Saline Ice", in *Proceedings of the Fourth International Conference on Cold Region Engineering*, American Society of Civil Engineers, New York, pp 670-684, 1986.

Puskas, J. E. McBean and N. Kouwen, "Behaviour and Transport of Oil Under Smooth Ice", *Canadian Journal of Civil Engineering*, Vol. 14, pp 510-518, 1987.

Quam, H.A., "Oil Recovery From Under River Ice", *Spill Technology Newsletter*, Vol. 3, pp 51-73, 1978.

Raisbeck, J.M and M.F. Mohtadi, "The Environmental Impacts of Oil Spills on Land in the Arctic Regions", *Water, Air and Soil Pollution*, Vol. 3, pp 195-208, 1974.

Ramseier, R.O., "Oil Pollution in Ice-Infested Waters", in *International Symposium on Identification and Measurement of Environmental Pollutants*, National Research Council, Ottawa, Ontario, pp 271-276, 1971.

Ramseier, R.O., G.A. Gantcheff and L. Colby, *Oil Spill at Deception Bay, Hudson Strait*, Scientific Series No. 29, Environment Canada, Burlington, Ontario, 60 p, 1973.

Reed, M., "State of the Art and Future Directions Physical Processes in Oil Spill Fates: Advection, Spreading, Entrainment, Shoreline and Ice Interactions", in *Proceeding of a Workshop on Oil Spill Modelling: State of the Art and Future Directions*, Charleston, South Carolina, 15 p, 1992.

Reimer, E.M., "Aspects of Oil-Ice Interactions Subsequent to the Kurdistan Spill", in *Proceedings of a Workshop on Oil, Ice and Gas,* Institute For Environmental Studies, University of Toronto, Toronto, Ontario, pp 75-86, 1979.

Reimer, E.M., "Oil in Pack Ice: The Kurdistan Spill", in *Proceedings of the Third Arctic Marine*

Oilspill Program Technical Seminar, Environment Canada, Ottawa, Ontario, pp 529-544, 1980.

Reimer, E.M., "Anticipated Oil Dispersion Rates in Pack Ice", in *Proceedings of the 1981 International Oil Spill Conference*, American Petroleum Institute, Washington, D.C., pp 199-201, 1981.

Richardson, P., "ABSORB Tests Oil/Ice Interaction", *Alaska Construction and Oil*, Vol. 21, pp 18-20, 1980.

Rosenegger, L.W., *The Movement of Oil Under Sea Ice*, Technical Report No. 28, Beaufort Sea Project, Environment Canada, Victoria, B.C., 81 p, 1975.

Ruby, C.H., L.G. Ward, I.A. Fischer and P.J. Brown, "Buzzards Bay Oil Spill-An Arctic Analogue", in *Proceedings of the 1977 International Conference on Port and Ocean Engineering Under Arctic Conditions* , pp 844-854, 1977.

Sandkvist, J., "Oil Spills in Arctic Regions-Environmental Hazards and Recovery Techniques", in *Proceedings of the 1989 International Conference on Port and Ocean Engineering Under Arctic Offshore and Polar Engineering Conditions (POAC)*, Vol. 3, pp 1281-1296, 1989.

Sayed, M. and R. Abdelnour, *Oil Movement Under Ice*, Unpublished Document, Environment Canada, Downsview, Ontario, 49 p, 1982.

Sayed, M., L.S. Kotlyar, and B.D. Sparks, "Spreading of Crude Petroleum in Brash Ice: Effects of Oil's Physical Properties and Water Current", *International Journal of Offshore and Polar Engineering*, Vol. 5, pp 127-133, 1995.

Sayed, M. and S. Loeset, "Laboratory Experiments of Oil Spreading in Brash Ice", in *Proceedings of the Third International Offshore and Polar Engineering Conference*, International Society of Offshore and Polar Engineers, Golden, Colorado, pp 224-231, 1993.

Sayed, M. and S. Loeset, "Laboratory Experiments of Oil Spreading in Brash Ice", *International Journal of Offshore and Polar Engineering*, Vol. 3, pp 306-312, 1993.

Schulze, R., *A Field Guide For Arctic Oil Spill Behaviour*, CG-D-2-85, United States Coast Guard, Washington, D.C., 322 p, 1984.

Schulze, R., "Oil Spreading in Broken Ice", in *Proceedings of the Eighth Arctic Marine Oilspill Program Technical Seminar*, Environment Canada, Ottawa, Ontario, pp 1-4, 1985.

Schultz, L.A. and J.C. Cox, "The Transport and Behaviour of Oil Spilled In and Under Sea Ice: Phase II of Physical Processes", in *Environmental Assessment of the Alaskan Continental Shelf: Annual Reports of Principal Investigators For the Year Ending March 1980, Vol. VII: Transport Data Management*, Outer Continental Shelf Environmental Assessment Program, National Oceanic

and Atmospheric Administration, Ocean Assessment Division, Alaska, pp 349-360, 1980.

Scott, B.F., *Investigation of the Weathering of a Selected Crude Oil in a Cold Environment*, Environment Canada, Ottawa, Ontario, 22 p, 1973. Also published in Water Quality Parameters, ASTM STP 573, American Society For Testing and Materials, pp 514-525, 1975.

Scott, B.F. and R.M. Chatterjee, *Behaviour of Oil Under Canadian Climatic Conditions: Part 1.Oil on Water Under Ice-Forming Conditions*, Scientific Series No. 50, Environment Canada, Ottawa, Ontario, 21 p, 1975.

Shen, H.T., P.D. Yapa and M.E. Petroski, *Simulation of Oil Slick Transport in Great Lakes Connecting Channels: Theory and Model Formulation,* CRREL Report 90-1, United States Army Corps of Engineers, Detroit, Michigan, 35 p, 1990.

Shen, H.T., P.D. Yapa, D.S. Wang and X.Q. Yang, *A Mathematical Model For Oil Slick Transport and Mixing in Rivers,* CRREL Report 93-21, Cold Region Research and Engineering Laboratory, Hanover, New Hampshire, 78 p, 1993.

Shimizu, H., "Air Permeability of Deposited Snow", *Contributions From the Institute of Low Temperature Science,* Series A, No. 22, pp 1-32, 1969.

Singsaas, I., P.J. Brandvik, P.S. Daling, M. Reed and A. Lewis, "Fate and Behaviour of Oils Spilled in the Presence of Ice: A Comparison of the Results From Recent Laboratory, Meso-scale Flume and Field Tests", in *Proceedings of the Seventeenth Arctic Marine Oilspill Program Technical Seminar*, Environment Canada, Ottawa, Ontario, pp 355-370, 1994.

Siu, S.K., C.R. Phillips and E.C. Chen, "The Continuous Spilling of Hot Oil on Ice", *Canadian Journal of Petroleum Technology,* Vol. 16, pp 31-34, 1977.

S.L. Ross Environmental Research Ltd., *Testing of an Oil Recovery Concept For Use in Brash and Mulched Ice*, Environmental Studies Research Fund, Report No. 018, National Energy Board, Calgary, Alberta, 43 p, 1986.

S.L. Ross Environmental Research Ltd. and D.F. Dickins Associates Ltd., *Field Research Spills to Investigate the Physical and Chemical Fate of Oil in Pack Ice,* Environmental Studies Research Fund, Report No. 062, National Energy Board, Calgary, Alberta, 116 p, 1987.

S.L. Ross Environmental Research Ltd. and D.F. Dickins Associates Ltd., *Modelling of Oil Spills in Snow*, EE-109, Environment Canada, Ottawa, Ontario, 71 p, 1988.

Spaulding, M., T. Isaji, K. Jayko, E. Anderson, C. Turner and D. Mendelsohn, "An Oil Spill Model System For Arctic Waters", in *Proceedings of the 1989 International Oil Spill Conference,* American Petroleum Institute, Washington, D.C., pp 517-523, 1989.

Stiver, W. and D. Mackay, *Evaporation Rates of Hydrocarbon and Petroleum Mixtures*, EE-49, Environment Canada, Ottawa, Ontario, 34 p, 1983.

Stochmal, W., H. Gurgul, Z.F. Morza, K. Fizyki and U. Szczecinski, "The Crude Oil-Water Emulsion in the Polar Conditions", in *Combatting Marine Oil Spills in Ice and Cold Conditions*, National Board of Waters and the Environment, Helsinki, Finland, pp 61-80, 1993.

Stringer, W. and G. Weller, "Studies of the Behaviour of Oil in Ice", in *Proceedings of the Third Arctic Marine Oilspill Program Technical Seminar*, Environment Canada, Ottawa, Ontario, pp 31-44, 1980.

Svoma, J. and V. Houzim, "Protection of Groundwater From Oil Pollution in the Vicinity of Airports", *Environmental Geology and Water Sciences*, Vol. 6, pp 21-30, 1984.

Sydnes, L.K., "Oil, Water, Ice and Light", *Polar Research*, Vol. 10, pp 609-618, 1990.

Sydnes, L.K., T.H. Hemmingsen, S. Skare, S.H. Hansen, I. Falk-Pettersen, S. Lonning and K. Ostgaard, "Seasonal Variations in Weathering and Toxicity of Crude Oil on Seawater Under Arctic Conditions", *Environmental Science and Technology*, Vol. 19, pp 1076-1081, 1985.

Tebeau, P.A., D. Mackay, W.Y. Shiu, W. Stiver, K. Hossain, D. McCurdy and S. Paterson, "Oil Weathering Under Arctic Conditions", in *Proceedings of the Fifth Arctic Marine Oil Spill Program Technical Seminar*, Environment Canada, Ottawa, Ontario, pp 15-24, 1982.

Tebeau, P.A., T.M. Meehan and S.A. Saepoff, *A Laboratory Study of Oil Spreading Under Arctic Conditions,* Unpublished Report, United States Coast Guard, Groton, Connecticut, 58 p, 1984.

Tebeau, P.A., T.M. Meehan and J.C. Myers, *A Laboratory Experiment on Oil Weathering Under Arctic Conditions*, CG-D-34-82, United States Coast Guard, Washington, D.C., 112 p, 1982.

Thomas, D.R., "Interaction of Oil With Arctic Sea Ice", in *Outer Continental Shelf Environmental Assessment Program*, Vol. 40, National Oceanic and Atmospheric Administration, Ocean Assessment Division, 403-436, 1983.

Thomas, D.R., "Interaction of Oil and Arctic Sea Ice", in *The Alaskan Beaufort Sea: Ecosystems and Environments*, Eds P.W. Barnes, D.M. Schnell and E. Reimnitz, Academic Press, Toronto, Ontario, pp 441-460, 1984.

Thomas, D.R. and R.S. Pritchard, "Oil Movement in the Ice Covered Beaufort and Chukchi Seas", in *1979 Workshop on the Physical Behaviour of Oil in the Marine Environment*, Princeton University, Princeton, New Jersey, pp 5.17-5.31, 1979.

Topham, D.R., "The Deflection of an Ice Sheet by a Submerged Gas Source", *Journal of Applied Mechanics*, Vol. 44, pp 279-284, 1977.

Topham, D.R., "The Disposition of Gas/Oil Mixtures Trapped Under Ice", in *Proceedings of a Workshop on Oil, Ice and Gas*, EE-14, Institute For Environmental Studies, University of Toronto, Toronto, Ontario, pp 55-65, 1979.

Topham, D.R., "The Disposition of Gas/Oil Mixtures Trapped Under Ice", *Canadian Journal of Physics*, Vol. 58, pp 1183-1190, 1980.

Topham, D.R., "The Interaction of Oil With Sea Ice in an Offshore Environment", in *Proceedings of Offshore Environment in the 80's*, 24 p, 1980.

Topham, D.R., and P.R. Bishnoi, "Deep Water Blowouts" in *Proceedings of the Third Arctic Marine Oilspill Program Technical Seminar,* Environment Canada, Ottawa, pp 87-95, 1980.

Topham, D.R., P.R. Bishnoi, and B.B. Maini, "Laboratory Study of Behaviour of Oil and Gas Particles in Salt Water Relating to Deep Oil Well Blowouts" in *Proceedings of the Second Arctic Marine Oilspill Program Technical Seminar,* Environment Canada, Ottawa, pp 20-36, 1979.

Trites, R.W., J.H. Vandermeulen and D.J. Lawrence, "Modelling the Movement of Bunker C Oil Spills in Colder Waters", in *1981 Workshop on the Mechanics of Oil Slicks*, l'Association Internationale de Recherches Hydrauliques, Paris, Paper 1.a.4, 9 p, 1981.

Trites, R.W., D.J. Lawrence and J.H. Vandermeulen, "Modelling Oil Movements From the Kurdistan Spill in Cabot Strait, Nova Scotia", *Journal of Atmospheric Ocean*, Vol. 24, pp 253-264, 1986.

Tsang, G., "Recovery of Oil Spilled Under River Ice Cover", in *Proceedings of the 1979 International Oil Spill Conference*, American Petroleum Institute, Washington, D.C., pp 387-396, 1979.

Tsang, G. and E.C. Chen, *Laboratory Study of Diversion of Oil Spilled Under Ice Cover*, Environment Canada, Burlington, Ontario, 42 p, 1978.

Tsang, G., E.C. Chen and R. Carson, *Laboratory Study of Recovering Spilled Oil From Slots Cut on River Ice Cover*, Environment Canada, Burlington, Ontario, 61 p, 1978.

Tumeo, M.A. and B. Davidson, "Hydrocarbon Exclusion From Ground Water During Freezing", *Journal of Environmental Engineering*, Vol. 119, pp 715-725, 1993.

Uzuner, M.S., F.B. Weiskopf, J.C. Cox and L.A. Schultz, *Transport of Oil Under Smooth Ice*, EPA-600/3-79-041, Environmental Protection Agency, Corvallis, Oregon, 62 p, 1979.

Vance, G., "Control of Arctic Oil Spills", *Ocean Industry*, Vol. 6, pp 14-18, 1971.

Vandermeulen, J.H., "Oil-in-Ice and Oil-Stranding Observations", in *The Kurdistan Oil Spill of*

March 16-17, 1979: Activities and Observations of the Bedford Institute of Oceanography Response Team, Canadian Technical Report of Hydrography and Ocean Sciences, No. 35, pp 49-61, 1985.

Vandermeulen, J.H., B. Amero and T.P. Ahern, "Physical Weathering of Kurdistan Oil: Droplet Formation and Effect on Shore-Ice Melting", in *Proceedings of a Workshop on Scientific Studies During the Kurdistan Tanker Incident*, Bedford Institute of Oceanography, Dartmouth, Nova Scotia, pp 105-119, 1980.

Vandermeulen, J.H. and D.E. Buckley, Eds, *The Kurdistan Oil Spill of March 16-17, 1979: Activities and Observations of the Bedford Institute of Oceanography Response Team*, Canadian Technical Report of Hydrography and Ocean Sciences, No. 35, 190 p, 1985.

Vandermeulen, J.H. and D.E. Buckley, "BIO Spill Response", in *The Kurdistan Oil Spill of March 16-17, 1979: Activities and Observations of the Bedford Institute of Oceanography Response Team*, Canadian Technical Report of Hydrography and Ocean Sciences, No. 35, pp 20-29, 1985.

Vefsnmo, S. and B.O. Johannsessen, "Experimental Oil Spill in the Barents Sea: Drift and Spread of Oil in Broken Ice", in *Proceedings of the Seventeenth Arctic Marine Oilspill Program Technical Seminar,* Environment Canada, Ottawa, pp 1331-1343, 1994.

Venkatesh, S., "The Oil Spill Behaviour Model of the Canadian Atmospheric Environment Service, Part I: Theory and Model Evaluation", *Journal of Atmospheric Oceans*, Vol. 26, pp 93-108, 1988.

Venkatesh, S., "Oil Spill Trajectory Modelling: Prediction Accuracies For Open Water Spills and Oil Spills in Broken Ice, a Concern For Canada", *Canadian Technical Report of Hydrography and Ocean Sciences*, No. 140, pp 151-153, 1992.

Venkatesh, S. and H. El-Tahan, "On the Role of Viscosity in the Spreading of Oil on Water at Near-Freezing Temperatures", in *Combatting Marine Oil Spills in Ice and Cold Conditions*, National Board of Waters and the Environment, Helsinki, Finland, pp 35-45, 1993.

Venkatesh, S., H. El-Tahan, G. Comfort and R. Abdelnour, "Modelling the Behaviour of Oil Spills in Ice-Infested Waters", *Atmosphere-Ocean*, Vol. 28, pp 303-329, 1990.

Venkatesh, S., H. El-Tahan, G. Comfort and R. Abdelnour, "Modelling the Spread of Oil Spills in Ice-Infested Waters", in *Proceedings of the Thirteenth Arctic Marine Oilspill Program,* Environment Canada, Ottawa, Ontario, pp 139-156, 1990.

Venkatesh, S., H.S. Sahota and A.S. Rizkalla, "Prediction of the Motion of Oil Spills in Canadian Arctic Waters", in *Proceedings of the 1979 International Oil Spill Conference,* American Petroleum Institute, Washington, D.C., pp 677-683, 1979.

Wadhams, P., "Oil and Ice in the Beaufort Sea: The Physical Effects of a Hypothetical Blowout", *Canadian Shipping and Marine Engineering*, Vol. 51, pp 23-35, 1980.

Walker, E.R., Oil, Ice and Climate in the Beaufort Sea, Beaufort Sea Technical Report No. 35, Environment Canada, Victoria, B.C., 40 p, 1975.

Weerasuriya, S.A. and P.D. Yapa, "Unidirectional Spreading of Oil Under Solid Ice", *Canadian Journal of Engineering*, Vol. 20, pp 50-56, 1993.

Weiskopf, F.B. and M.S. Uzuner, "Oil Slick Spreading Beneath a Uniform Ice Cover in the Presence of a Current", in *Proceedings of the 1977 International Oil Spill Conference*, American Petroleum Institute, Washington, D.C., pp 297-300, 1977.

Weller, G., "Oil Pollution in Ice-Covered Arctic Waters", in *Proceedings of the Fifth International Conference on Port and Ocean Engineering Under Arctic Conditions (POAC)*, pp 393-406, 1979.

Welsh, J.P., I.M. Lissauer, G.L. Hufford, T.S. Ellis, B.D. Thompson, L.D. Farmer and R.T. Hiltabrand, "Some Dynamics of Spilled Oil in a Fractured Ice Field in Buzzards Bay, Massachusetts", *Ocean Engineering*, Vol. 4, pp 197-203, 1977.

Wessels, E. "Research on Oil Spills in Ice at HSVA's New Environmental Test Basin For Cold Regions", in *Proceedings of Combatting Marine Oil Spills in Ice and Cold Conditions*, National Board of Waters and the Environment, Helsinki, Finland, pp 82-97, 1993.

Wessels, E., "New Test Basin For Experimental Studies on Oil Spill in Ice", in *Proceedings of the Fifteenth Arctic Marine Oilspill Program Technical Seminar*, Environment Canada, Ottawa, Ontario, pp 271-279, 1992.

Wilson, D.G. and D. Mackay, "The Behaviour of Oil in Freezing Situations", in *Proceedings of the Ninth Arctic Marine Oilspill Program Technical Seminar*, Environment Canada, Ottawa, Ontario, pp 51-63, 1986.

Wilson, D.G. and D. Mackay, *The Behaviour of Oil in Freezing Situations*, EE-92, Environment Canada, Ottawa, Ontario, 65 p, 1987.

Wolfe, L.S. and D.P. Hoult, *Effects of Oil Under Sea Ice*, Publication No. 72-10, Massachusetts Institute of Technology, Department of Mechanical Engineering, Fluid Mechanics Laboratory, Cambridge, Massachusetts, 66 p, 1972.

Wolfe, L.S. and D.P. Hoult, "Effects of Oil Under Ice", *Journal of Glaciology*, Vol. 13, pp 473-488, 1974.

Wotherspoon, P.D. and J.J. Swiss, "Oil in Ice Computer Simulation Model", *Water Science and Technology,* Vol. 18, pp 41-46, 1986.

Wotherspoon, P., J. Swiss, R. Kowalchuk and J. Armstrong, *Oil in Ice Computer Model*, Report No. 019, Environmental Studies Research Fund, National Energy Board, Calgary, Alberta, 129 p, 1985.

Yapa, P.D. and D.P. Belaskas, "Radial Spreading of Oil Under and Over Broken Ice: An Experimental Study", *Canadian Journal of Civil Engineering*, Vol. 20 , pp 910-922, 1993.

Yapa, P.D. and T. Chowdhury, "Oil Spreading Under Ice Covers", in *Proceedings of the 1989 International Oil Spill Conference*, American Petroleum Institute, Washington, D.C., pp 161-166, 1989.

Yapa, P.D. and T. Chowdhury, *Spreading of Oil Spilled Under Ice*, Report No. 89-10, Clarkson University, Potsdam, New York, 98 p, 1989.

Yapa, P.D. and T. Chowdhury, "Spreading of Oil Under Ice", *Journal of Hydraulic Engineering*, Vol. 116, pp 1468-1483, 1990.

Yapa, P.D. and H.T. Shen, "Modelling River Oil Spills: A Review", *Journal of Hydraulic Research*, Vol. 32, pp 765-782, 1994.

Yapa, P.D., S.A. Weerasuriya, D.P. Belaskas and T. Chowdhury, *Oil Spreading in Surface Waters With an Ice Cover*, Report No. 93-3, Clarkson University, Potsdam, New York, 84 p, 1993.

Zatsepa, S., A. Ivchenko and S. Ovsienko, "Mathematical Modelling of Oil Behaviour in Ice", in *Proceedings of Combatting Marine Oil Spills in Ice and Cold Conditions*, National Board of Waters and the Environment, Helsinki, Finland, pp 175-184, 1993.